IAEA-TECDOC-1677

Natural Circulation Phenomena and Modelling for Advanced Water Cooled Reactors

IAEA
International Atomic Energy Agency

Natural Circulation Phenomena and Modelling For Advanced Water Cooled Reactors

The following States are Members of the International Atomic Energy Agency:

AFGHANISTAN
ALBANIA
ALGERIA
ANGOLA
ARGENTINA
ARMENIA
AUSTRALIA
AUSTRIA
AZERBAIJAN
BAHRAIN
BANGLADESH
BELARUS
BELGIUM
BELIZE
BENIN
BOLIVIA
BOSNIA AND HERZEGOVINA
BOTSWANA
BRAZIL
BULGARIA
BURKINA FASO
BURUNDI
CAMBODIA
CAMEROON
CANADA
CENTRAL AFRICAN REPUBLIC
CHAD
CHILE
CHINA
COLOMBIA
CONGO
COSTA RICA
CÔTE D'IVOIRE
CROATIA
CUBA
CYPRUS
CZECH REPUBLIC
DEMOCRATIC REPUBLIC OF THE CONGO
DENMARK
DOMINICA
DOMINICAN REPUBLIC
ECUADOR
EGYPT
EL SALVADOR
ERITREA
ESTONIA
ETHIOPIA
FINLAND
FRANCE
GABON
GEORGIA
GERMANY
GHANA
GREECE
GUATEMALA
HAITI
HOLY SEE
HONDURAS
HUNGARY
ICELAND
INDIA
INDONESIA
IRAN, ISLAMIC REPUBLIC OF
IRAQ
IRELAND
ISRAEL
ITALY
JAMAICA
JAPAN
JORDAN
KAZAKHSTAN
KENYA
KOREA, REPUBLIC OF
KUWAIT
KYRGYZSTAN
LAO PEOPLE'S DEMOCRATIC REPUBLIC
LATVIA
LEBANON
LESOTHO
LIBERIA
LIBYA
LIECHTENSTEIN
LITHUANIA
LUXEMBOURG
MADAGASCAR
MALAWI
MALAYSIA
MALI
MALTA
MARSHALL ISLANDS
MAURITANIA
MAURITIUS
MEXICO
MONACO
MONGOLIA
MONTENEGRO
MOROCCO
MOZAMBIQUE
MYANMAR
NAMIBIA
NEPAL
NETHERLANDS
NEW ZEALAND
NICARAGUA
NIGER
NIGERIA
NORWAY
OMAN
PAKISTAN
PALAU
PANAMA
PAPUA NEW GUINEA
PARAGUAY
PERU
PHILIPPINES
POLAND
PORTUGAL
QATAR
REPUBLIC OF MOLDOVA
ROMANIA
RUSSIAN FEDERATION
SAUDI ARABIA
SENEGAL
SERBIA
SEYCHELLES
SIERRA LEONE
SINGAPORE
SLOVAKIA
SLOVENIA
SOUTH AFRICA
SPAIN
SRI LANKA
SUDAN
SWEDEN
SWITZERLAND
SYRIAN ARAB REPUBLIC
TAJIKISTAN
THAILAND
THE FORMER YUGOSLAV REPUBLIC OF MACEDONIA
TUNISIA
TURKEY
UGANDA
UKRAINE
UNITED ARAB EMIRATES
UNITED KINGDOM OF GREAT BRITAIN AND NORTHERN IRELAND
UNITED REPUBLIC OF TANZANIA
UNITED STATES OF AMERICA
URUGUAY
UZBEKISTAN
VENEZUELA
VIETNAM
YEMEN
ZAMBIA
ZIMBABWE

The Agency's Statute was approved on 23 October 1956 by the Conference on the Statute of the IAEA held at United Nations Headquarters, New York; it entered into force on 29 July 1957. The Headquarters of the Agency are situated in Vienna. Its principal objective is "to accelerate and enlarge the contribution of atomic energy to peace, health and prosperity throughout the world''.

IAEA-TECDOC-1677

NATURAL CIRCULATION PHENOMENA AND MODELLING FOR ADVANCED WATER COOLED REACTORS

INTERNATIONAL ATOMIC ENERGY AGENCY
VIENNA, 2012

For further information on this publication, please contact:

Nuclear Power and Technology Development Section
International Atomic Energy Agency
Vienna International Centre
PO Box 100
1400 Vienna, Austria
Email: Official.Mail@iaea.org

Printed by the IAEA in Austria
March 2012

IAEA Library Cataloguing in Publication Data

Natural circulation phenomena and modelling for advanced water cooled reactors. – Vienna : International Atomic Energy Agency, 2012.
p. ; 30 cm. – (IAEA-TECDOC series, ISSN 1011-4289 ; no. 1677)
ISBN 978-92-0-127410-6
Includes bibliographical references.

1. Water cooled reactors – Cooling. 2. Water cooled reactors – Mathematical models. 3. Heat – Convection, Natural. I. International Atomic Energy Agency. II. Series.

IAEAL 12-00731

FOREWORD

The role of natural circulation in advanced water cooled reactor design has been extended with the adoption of passive safety systems. Some designs utilize natural circulation to remove core heat during normal operation. Most passive safety systems used in evolutionary and innovative water cooled reactor designs are driven by natural circulation. The use of passive systems based on natural circulation can eliminate the costs associated with the installation, maintenance and operation of active systems that require multiple pumps with independent and redundant electric power supplies. However, considering the weak driving forces of passive systems based on natural circulation, careful design and analysis methods must be employed to ensure that the systems perform their intended functions.

Several IAEA Member States with advanced reactor development programmes are actively conducting investigations of natural circulation to support the development of advanced water cooled reactor designs with passive safety systems. To foster international collaboration on the enabling technology of passive systems that utilize natural circulation, in 2004 the IAEA initiated a coordinated research project (CRP) on Natural Circulation Phenomena, Modelling and Reliability of Passive Systems that Utilize Natural Circulation. Three reports were published within the framework of this CRP. The first report (IAEA-TECDOC-1474) contains the material developed for the first IAEA training course on natural circulation in water cooled nuclear power plants. The second report (IAEA-TECDOC-1624) describes passive safety systems in a wide range of advanced water cooled nuclear power plant designs, with the goal of gaining insights into system design, operation and reliability. This third, and last, report summarizes the research studies completed by participating institutes during the CRP period.

The IAEA appreciates the contributions of N. Aksan, chairperson of the CRP, and of the chief scientific investigators from all CRP participating institutes. The IAEA officer responsible for this publication was J.H. Choi of the Division of Nuclear Power.

EDITORIAL NOTE

The papers in these Proceedings (including the figures, tables and references) have undergone only the minimum copy editing considered necessary for the reader's assistance. The views expressed remain, however, the responsibility of the named authors or participants. In addition, the views are not necessarily those of the governments of the nominating Member States or of the nominating organizations.

Although great care has been taken to maintain the accuracy of information contained in this publication, neither the IAEA nor its Member States assume any responsibility for consequences which may arise from its use.

The use of particular designations of countries or territories does not imply any judgement by the publisher, the IAEA, as to the legal status of such countries or territories, of their authorities and institutions or of the delimitation of their boundaries.

The mention of names of specific companies or products (whether or not indicated as registered) does not imply any intention to infringe proprietary rights, nor should it be construed as an endorsement or recommendation on the part of the IAEA.

The authors are responsible for having obtained the necessary permission for the IAEA to reproduce, translate or use material from sources already protected by copyrights.

Material prepared by authors who are in contractual relation with governments is copyrighted by the IAEA, as publisher, only to the extent permitted by the appropriate national regulations.

CONTENTS

1. INTRODUCTION

As part of the IAEA's overall effort to foster international collaborations that strive to improve the economics and safety of future water cooled nuclear power plants, an IAEA Coordinated Research Project (CRP) was started in early 2004. This CRP, entitled Natural Circulation Phenomena, Modelling and Reliability of Passive Safety Systems that Utilize Natural Circulation, focuses on the use of passive safety systems to help meet the safety and economic goals of a new generation of nuclear power plants. This CRP has been organized within the framework of the IAEA Department of Nuclear Energy's Technical Working Groups for Advanced Technologies for Light Water Reactors and Heavy Water Reactors (the TWG-LWR and the TWG-HWR) and has provided an international cooperation on research work underway at the national level in several IAEA Member States.

The use of passive safety systems was addressed in 1991 at the IAEA Conference on "The Safety of Nuclear Power: Strategy for the Future" [1-1]. Subsequently, experts in research institutes and nuclear plant design organizations from several IAEA Member States collaboratively presented their common views in a paper entitled "Balancing passive and active systems for evolutionary water cooled reactors" in Ref. [1-2]. The experts noted that a designer's first consideration is to satisfy the required safety function with sufficient reliability, and the designer must also consider other aspects such as the impact on plant operation, design simplicity and costs.

The use of passive safety systems such as accumulators, condensation and evaporative heat exchangers, and gravity driven safety injection systems eliminates the costs associated with the installation, maintenance and operation of active safety systems that require multiple pumps with independent and redundant electric power supplies. As a result, passive safety systems are being considered for numerous reactor concepts (including in Generation III and III+ concepts) and are expected to find applications in the Generation-IV reactor concepts, as identified by the Generation IV International Forum (GIF). Another motivation for the use of passive safety systems is the potential for enhanced safety through increased safety system reliability.

The CRP benefits from earlier IAEA activities that include developing databases on physical processes of significant importance to water cooled reactor operations and safety [1-3, 1-4], technical information exchange meetings on recent technology advances [1-5–1-11], and status reports on advanced water cooled reactors [1-12, 1-13]. In the area of thermohydraulic phenomena in advanced water cooled reactors, recent IAEA activities have assimilated data internationally on heat transfer coefficients and pressure drop [1-3]; and have shared information on natural circulation data and analytical methods [1-5], and on experimental tests and qualification of analytical methods [1-6]. This CRP also benefits from a recent report issued by IAEA [1-14] on the status of innovative small and medium sized reactor designs.

In order to establish the progress of work in this CRP, an Integrated Research Plan with description of the tasks addressing the objectives of the CRP was defined. These tasks are:

- Establish the state of the art on natural circulation
- Identify and describe reference systems
- Identify and characterize phenomena that influence natural circulation
- Examine application of data and codes to design and safety
- Examine the reliability of passive systems that utilize natural circulation

The results of the CRP work have been planned to be published in three consecutive IAEA-TECDOC reports. The activity under the first task is aimed at summarizing the current understanding of natural circulation system phenomena and the methods used experimentally to investigate and model such phenomena. In November 2005, the IAEA issued a technical document as first publication [1-15] in three TECDOC report series of this CRP on natural circulation, developed by the collaborative effort of the CRP participants and with major contributions from some selected experts in the CRP, aimed at

documenting the present knowledge in six specific areas; advantages and challenges of natural circulation systems in advanced designs, local transport phenomena and models, integral system phenomena and models, natural circulation experiments, advanced computation methods, and reliability assessment methodology.

The activity for the third task is aimed at identifying and categorizing the natural circulation phenomena of importance to advanced reactors and passive safety system operations and reliability. This task is the major link between the second and the fourth tasks. The activities related to the second task and the fourth task including the fifth task are agreed to be published in two different TECDOCs by the CRP participants. Since the third task is the backbone for both tasks, inclusion of this task in both TECDOCs in an appropriate form is a logical consequence.

The aim of the second publication in this series of TECDOCs [1-16] was to describe passive safety systems in a wide range of advanced water cooled nuclear power plant designs with the goal of gaining insights into the system design, operation, and reliability without endorsement of the performance. This second publication has a unique feature which includes plant design descriptions with a strong emphasis on passive safety systems of the specific designs. These descriptions of the passive safety systems together with the phenomena identification (including the definitions of the phenomenon to describe in some detail the titles of the phenomenon considered) are also given in the Annexes and Appendix of the report [1-16], respectively. Based on the passive systems and phenomena, which are considered, a cross-reference matrix has been established and also presented in this second report. As basis for the phenomenon identification, earlier works performed within the OECD/NEA framework during 1983–1997 were considered. These are:

- Code validation matrix of thermohydraulic codes for LWR loss of coolant accident (LOCA) and transients [1-17]
- State of the art report (SOAR) on thermohydraulic of emergency core cooling in light water reactors [1-18]
- Separate Effects Test (SET) Validation Matrix for Light Water Reactors [1-19]
- Integral Facility Tests Validation Matrix for Light Water Reactors [1-20]
- Status report on relevant thermohydraulic aspects of advanced reactor designs [1-21]

Since the Generation III and III+ reactor designs contain technological features that are common to the current generation reactors, the phenomena identified during the work performed for first item to fourth item can be used as base knowledge. The fifth item provides the important and relevant thermohydraulic phenomena for advanced reactor designs in addition to the relevant thermohydraulic phenomena identified for the current generation of light water reactors (LWR). The list of relevant phenomena established in Ref. 1-21 has been taken as basis for the CRP work and has been modified according to the reactor types and passive safety systems considered in TECDOC-1624 [1-16]. It is to be noted that in identifying the relevant thermohydraulic phenomena in the list which is provided in this report, expert judgement is the main contributor.

The two TECDOCs (the present TECDOC and TECDOC-1624) have been produced as consequent volumes independent of each other in their use and contents. The present TECDOC is the third publication in this series of TECDOC reports and its contents are described below.

The identification and definition of the phenomena for advanced water cooled reactors with emphasis to passive safety systems is also presented in the second chapter of this TECDOC. Phenomena have been classified into two categories. These are phenomena occurring during interaction between primary system and containment; and phenomena caused by the presence of new components and systems or special reactor configurations. These descriptions are supplement to the definitions of phenomena which are developed for the current operational water cooled nuclear power plants [1-19, 1-20].

Twelve phenomena have been identified as key outcome of the process in Chapter 2 and the characterization of these additional phenomena for advanced water cooled reactors are provided in Chapter 3. The characterization of these additional phenomena includes exhaustive description of

phenomena considering a comprehensive picture of the transient performance of the class of innovative reactors which are described in Ref. 1-16. Each of these descriptions includes outlines of models and an overview of the experimental data base that support the characterization of phenomena. The capabilities of thermohydraulics transient system codes or computational fluid dynamics (CFD) codes in predicting the same phenomena are evaluated and the results from the application of the codes to the analysis of experimental data are provided, as applicable to the case.

After providing an overview on the phenomena and their characterization, Chapter 4 includes example cases for integral test facilities which simulate the prototypical plant design, some analysis of the experimental data obtained, use of these experimental data to help assess the predictive capabilities of the computer codes to model the phenomena that are occurring in the experimental test facilities, and application to the nuclear power plant analysis. In this chapter, a wide variety of prototypical plant designs, integral test facilities and thermohydraulics transient system codes, which are used in the analysis of plants and integral test facilities, are included. The collected and summarized information makes this chapter an excellent resource for providing understanding on the general capabilities of the integral test facilities and computer codes used for the examination of the natural circulation phenomena.

As it has already been mentioned, the passive safety systems in their designs rely on natural forces to perform their accident prevention and mitigation functions once actuated and started. These driving forces are not generated by external power sources (e.g., pumped systems), as is the case in operating and some evolutionary reactor designs. Because the magnitude of the natural forces, which drive the operation of passive systems, is relatively small, counterforces (e.g. friction) can be of comparable magnitude and cannot be ignored as it is generally the case of systems including pumps. Moreover, there are considerable uncertainties associated with factors on which the magnitude of these forces and counter forces depends (e.g. values of heat transfer coefficients and pressure losses). In addition, the magnitude of such natural driving forces depends on specific plant conditions and configurations which could exist at the time a system is called upon to perform its safety function. All these uncertainties affect the thermohydraulic performance of the passive system. This particular aspect, inherent to the passive systems, has been dealt with in Chapter 5 and the methodology, which was developed within the framework of a project called Reliability Methods for Passive Safety Functions (RMPS) and performed under the auspices of the European Commission's 5th Framework Programme, has been presented in some detail in that chapter. To assess the impact of uncertainties on the predicted performance of the passive system, a large number of calculations with best estimate thermohydraulic codes are needed. If all the sequences where the passive system studied is involved are considered, the number of calculations can be prohibitive. For all these reasons, it is necessary to create a specific methodology to assess the reliability of passive systems. The methodology addresses the following problems:

- Identification and quantification of the sources of uncertainties and determination of the important variables;
- Propagation of the uncertainties through thermohydraulic models and assessment of thermohydraulic passive system unreliability;
- Introduction of passive system unreliability in the accident sequence analysis.

In Section 1 of Chapter 5 (Section 5.1), each step of the methodology is described and commented and a diagram of the methodology is presented. Some improvements of this methodology, proposed after the end of the RMPS project (in early 2004) are highlighted in Section 5.2. Alternative methodologies, which have been developed by other institutions in parallel, are presented in Section 5.3. These methodologies are the ENEA methodology (developed by ENEA, Bologna, Italy) and Assessment of Passive System Reliability (ASPRA) (developed by BARC, India). Finally the application of the RMPS methodology, as an example, to a Passive Residual Heat Removal System (PRHRS) of a "CAREM-like" reactor has been performed within the present IAEA CRP and this application is described in Section 5.4. The major aim of this work is to quantify the failure probability of the passive safety function associated with the system under analysis.

The last chapter of this TECDOC (Chapter 6) is devoted to summarize the detailed conclusions and recommendations, which were already provided in the contents of the various chapters. These conclusions and recommendations are given in a concise form for use of further needs in research, development, and technology areas.

REFERENCES FOR CHAPTER 1

[1-1] INTERNATIONAL ATOMIC ENERGY AGENCY, The Safety of Nuclear Power: Strategy for the Future (Proc. of a Conf., Vienna), IAEA, Vienna (1991).

[1-2] INTERNATIONAL ATOMIC ENERGY AGENCY, Evolutionary Water cooled Reactors: Strategic Issues, Technologies and Economic Viability, IAEA-TECDOC-1117, IAEA, Vienna (1999).

[1-3] INTERNATIONAL ATOMIC ENERGY AGENCY, Thermohydraulic Relationships for Advanced Water Cooled Reactors, IAEA-TECDOC-1203, IAEA, Vienna (2001).

[1-4] INTERNATIONAL ATOMIC ENERGY AGENCY, Thermo-physical Properties of Materials for Water Cooled Reactors, IAEA-TECDOC-949, IAEA, Vienna (1997).

[1-5] INTERNATIONAL ATOMIC ENERGY AGENCY, Natural Circulation Data and Methods for Advanced Nuclear Power Plant Design, IAEA-TECDOC-1281, IAEA, Vienna (2002).

[1-6] INTERNATIONAL ATOMIC ENERGY AGENCY, Experimental Tests and Qualification of Analytical Methods to Address Thermohydraulic Phenomena in Advanced Water Cooled Reactors, IAEA-TECDOC-1149, IAEA, Vienna (2000).

[1-7] INTERNATIONAL ATOMIC ENERGY AGENCY, Improving Economics and Safety of Water Cooled Reactors: Proven Means and New Approaches, IAEA-TECDOC-1290, IAEA, Vienna (2002).

[1-8] INTERNATIONAL ATOMIC ENERGY AGENCY, Performance of Operating and Advanced LWR Designs, IAEA-TECDOC-1245, IAEA, Vienna (2001).

[1-9] INTERNATIONAL ATOMIC ENERGY AGENCY, Technologies for Improving Current and Future Light Water Reactor Operations and Maintenance: Development on the Basis of Experience, IAEA-TECDOC-1175, IAEA, Vienna (2000).

[1-10] INTERNATIONAL ATOMIC ENERGY AGENCY, Fuel Cycle Options for LWRs and HWRs, IAEA-TECDOC-1122, IAEA, Vienna, (1999).

[1-11] INTERNATIONAL ATOMIC ENERGY AGENCY, Technical Feasibility and Reliability of Passive Safety Systems for Nuclear Power Plants, IAEA-TECDOC-920, IAEA, Vienna (1996).

[1-12] INTERNATIONAL ATOMIC ENERGY AGENCY, Status of Advanced Light Water Cooled Reactor Designs, IAEA-TECDOC-1391, Vienna (2004).

[1-13] INTERNATIONAL ATOMIC ENERGY AGENCY, HWRs — Status and Projected Development, Technical Reports Series No. 407, IAEA, Vienna (2002).

[1-14] INTERNATIONAL ATOMIC ENERGY AGENCY, Status of innovative small and medium sized reactor designs: 2005, IAEA-TECDOC-1485, IAEA, Vienna (2006).

[1-15] INTERNATIONAL ATOMIC ENERGY AGENCY, Natural Circulation in water cooled nuclear power plants: Phenomena, models, and methodology for system reliability assessments, IAEA-TECDOC-1474, IAEA, Vienna (2005).

[1-16] INTERNATIONAL ATOMIC ENERGY AGENCY, Passive Safety Systems and Natural Circulation in Water Cooled Nuclear Power Plants, IAEA-TECDOC-1624, IAEA, Vienna (2009).

[1-17] OECD/NEA, CSNI Code Validation Matrix of Thermohydraulic codes for LWR LOCA and transients, OECD-NEA-CSNI report no.132 (1987).

[1-18] OECD/NEA, State of the art report (SOAR) on Thermal-hydraulics of Emergency Core Cooling in Light Water .Reactors, OECD-NEA-CSNI report no. 161 (1989).

[1-19] AKSAN, N., et al., Separate Effects Test Matrix for Thermal-Hydraulic Code Validation,
a) Volume I: Phenomena Characterisation and Selection of Facilities and Tests,
b) Volume II: Facility and Experiment Characteristics.
OECD/NEA Report, NEA/CSNI/R(93)14/Part 1 and Part 2, Paris (1994).

[1-20] ANNUNZIATO, A., et al., CSNI Integral Test Facility Validation Matrix for the Assessment of Thermohydraulic Codes for LWR LOCA and Transients, OECD/NEA Report NEA/CSNI/R(96)17 (1996).

[1-21] AKSAN, N., D'AURIA, F., Relevant Thermal Hydraulic Aspects of Advanced Reactor Design — Status Report, OECD/NEA Report NEA/CSNI/R(96)22 (1996).

2. IDENTIFICATION AND DEFINITION OF PHENOMENA[1]

Phenomena have been classified into two categories (Table 2-1): (a) phenomena occurring during interaction between the primary cooling system and containment; and (b) phenomena occurring due to the presence of new components and systems or special reactor configurations. This classification takes into consideration of the information provided in the CSNI Report [2-1] which was developed for the primary cooling system, and is intended to provide complementary aspects that are relevant to advanced water cooled nuclear power plant designs, including containment designs. Therefore the descriptions given below are intended to supplement those in the CSNI Report. Tables 2-2–2-10, reproduced from IAEA-TECDOC-1474 [2-2], provide the definitions developed by the CSNI for phenomena applicable to current plants. These phenomena are also applicable to plants with passive systems, except the phenomena associated with pump behaviour.

2.1. BEHAVIOUR IN LARGE POOLS OF LIQUID

Large pools of water (e.g. up to several thousand cubic meters) at near atmospheric pressure are incorporated into several advanced designs. These large pools provide a heat sink for heat removal from the reactor or the containment by natural circulation, as well as a source of water for core cooling. Examples include the pressure suppression pool (wet well) of the ESBWR, the in-containment refuelling water storage tank of the AP-1000, the pool of the emergency condenser of the SWR-1000 and the gravity driven water pool of the AHWR.

Large pools may have a very wide spectrum of geometric configurations. Heat transfer often occurs in a limited volume (e.g. by condensing injected steam or by heat transfer from an isolation condenser) which results in non-homogeneous temperature distribution in the pool. Three dimensional convection flows develop, affecting the heat transfer process and resulting in temperature stratification.

Steam generated by heat transfer, or following injection, may be released from the pool into the containment causing increase in containment pressure. Compared to a homogeneous temperature distribution, the fluid at the top of the pool may reach the saturation temperature while the bulk fluid is subcooled. The evaporation from the top of the pool results in a pressure increase in the containment. Therefore the temperature stratification influences plant design. The three dimensional nature of the temperature stratification requires appropriate modelling.

2.2. EFFECTS OF NON-CONDENSABLE GASES ON CONDENSATION HEAT TRANSFER

Condensation occurs when the temperature of vapour is reduced below its saturation temperature. Presence of even a small amount of non-condensable gas (e.g. air, N_2, H_2, He, etc.) in the condensing vapour leads to a significant reduction in heat transfer during condensation. The buildup of non-condensable gases near the condensate film inhibits the diffusion of vapour from the bulk mixture to the liquid film. The net effect is to reduce the effective driving force for heat and mass transfer. This phenomenon is of concern in industrial applications and nuclear reactor systems.

In nuclear plants, the condensation of steam in the presence of non-condensable gas becomes an important phenomenon during LOCA when steam released from the coolant system mixes with the containment air. Besides this, nitrogen gas in accumulators is a source of non-condensable gas, which can affect the condensation heat transfer inside the steam generator tubes of nuclear power plants, and may affect the core make-up tank performance. The effect of non-condensable gases on condensation heat transfer is also relevant to certain decay heat removal systems in advanced reactor designs, such as passive containment cooling systems.

[1] The starting point for identification of phenomena associated with natural circulation was the OECD-CSNI report "Status of relevant thermo-hydraulic aspects of advanced reactors"[2-1].

The effect of non-condensable gases on the condensation of steam has been extensively studied for both natural and forced convection flows. In each of them, geometries of interest (e.g. tubes, plates, annuli, etc.) and the flow orientation (horizontal, vertical) can be different for various applications. The condensation heat transfer is affected by parameters such as mass fraction of non-condensable gas, system pressure, gas/vapour mixture Reynolds number, orientations of surface, interfacial shear, Prandtl number of condensate, etc. Multicomponent non-condensable gases can be present.

2.3. CONDENSATION ON CONTAINMENT STRUCTURES

This phenomenon involves heat and mass transfer from the containment atmosphere towards the surrounding structures. This phenomenon would occur in existing reactors in case of a coolant release into the containment. It also occurs in advanced designs where containment surfaces are cooled externally, usually by natural mechanisms. Good examples are the nuclear reactor designs of the "AP" series by Westinghouse, where the steel containment is cooled externally by water flowing on its exterior surface from a reservoir above the containment, and by ascending air driven by buoyancy.

Steam condensation is largely affected by conditions which can be split into two groups depending on the relevance of the physical dimensions of the system. The "scale-independent factors" are variables like the fraction of non-condensables, the pressure, the gas composition and so on, the effect of which could be well investigated through Separate Effect Tests. The "scale-dependent factors" are those phenomena that require to be investigated in actual or scaled geometries (i.e., Integral Effect Tests) since physical dimensions largely influence their quantitative effect. Examples of this kind are the natural convection process at both sides of the metallic structures and the potential gas stratification.

2.4. BEHAVIOUR OF CONTAINMENT EMERGENCY SYSTEMS

Nuclear power reactor containments are equipped with safety systems which protect the containment integrity under various accident conditions. The focus of this phenomenon is the natural circulation cooling and heat transfer in various containment passive cooling systems under accident conditions to remove the energy out of the containment by natural circulation and condensation heat transfer. Typical systems are the tube condensers such as the passive containment cooling system (PCCS) and external air cooling system or external liquid film cooling and internal condensation of steam in the containment by natural circulation. The major purpose of these containment systems is to protect the containment under both design basis accidents and severe accidents involving serious core damages and to prevent the significant release of radioactive materials to the atmosphere. These systems are required to remove the load on the containment from the LOCAs and other accidents by removing the heat but containing the mass within the structure. Most of the load comes from the released steam from the primary coolant system due to the LOCA or venting of the pressure relief valves. The major part of the non-condensable gases consists of the original containment atmosphere such as air or nitrogen; however, if core damage occurs, hydrogen or fission gases can be also released into the containment atmosphere. The thermohydraulic phenomena of importance are tube surface condensation with non-condensable gases, natural circulation of steam and non-condensable gases, degradation of condensation by the accumulation of non-condensable gases and purging of non-condensable gases from condenser systems. The passive containment cooling system can be vertical or horizontal tube condensers in external water pool, exposed condenser tube system in the containment cooled by natural circulation water through the tubes from the external pool or by external air circulation and others.

2.5. THERMO-FLUID DYNAMICS AND PRESSURE DROPS IN VARIOUS GEOMETRICAL CONFIGURATIONS

Pressure drop is the difference in pressure between two points of interest in a fluid system. In general, pressure drop can be caused by resistance to flow, changes in elevation, density, flow area and flow direction. Pressure drops in natural circulation systems play a vital role in their steady state, transient and stability performance.

It is customary to express the total pressure drop in a flowing system as the sum of its individual components such as distributed pressure loss due to friction, local pressure losses due to sudden variations of shape, flow area, direction, etc. and pressure losses (reversible losses) due to acceleration (induced by flow area variation or by density change in the fluid) and elevation (gravity effect). An important factor affecting the pressure loss is geometry. In a nuclear reactor, we have to deal with several basic geometrical shapes (circular pipes, annuli, etc.) and a number of special devices like rod bundles, heat exchangers, valves, headers, plenums, pumps, large pools, etc. Other factors are concerned with the fluid status (single or two phase/one component, two component or multicomponent), the flow nature (laminar or turbulent), the flow pattern (bubbly, slug, annular, etc.), the flow direction (vertical upflow, downflow, inclined flow, horizontal flow, countercurrent flow, etc.), flow type (separated and mixed), flow paths (one dimensional or multidimensional, open or closed paths, distributor or collector), and the operating conditions (steady state or transient).

An important focus of this phenomenon is the geometric conditions that hinder the establishment of fully developed flow especially when the fluid in question is a mixture of steam, air and water. This complex thermo-fluid dynamic phenomenon warrants special attention. However, it is worth mentioning here that though in many systems like the primary system of a nuclear power plant, flow is mostly not fully developed, pressure drop relationships used in these systems are invariably those obtained for developed flow. This practice is also experimentally proved to be more than adequate in most of the cases. However, in some specific cases like containment internal geometry, it is necessary to consider thermo fluid dynamics in the developing region.

A final, very important issue, is concerned with the driving force depending on whether the flow is sustained by a density difference in the fluid (natural circulation) or by a pump (forced convection), or whether there will be feedback between the pressure loss and the extracted power or not. Normally the pressure loss inside a device depends on the nature of flow through the device and not on the nature of driving head causing the flow. However, under some circumstances, because of local effects, the pressure loss may get influenced by the nature of the driving force.

2.6. NATURAL CIRCULATION IN CLOSED LOOP

The complex set of thermohydraulic phenomena that occur in a gravity environment when geometrically or materially distinct heat sinks and heat sources are connected by a fluid can be identified as Natural Circulation (NC). No external sources of mechanical energy for the fluid motion are involved when NC is established.

The above definition includes the situations of a heater immersed into a fluid, of an open flame in the air, of a chimney driven fire, of insurge of hot fluid into a pool of cold liquid, and of a heat source and sink (e.g. heater and cooler) consisting of separated mechanical components connected by piping and situated at different gravity elevations. Natural circulation also drives the occurrence of stratification in horizontal pipes.

Within the scope of this document, this phenomenon involves the following system configurations:

- Heat source and sink of primary loop constituted, respectively, by core and steam generator, or boiler, or primary side of heat exchanger, with core located at a lower elevation;
- Heat source and sink inside the pressure vessel, constituted, respectively, by core and (typically annular-like region of) vessel downcomer. ‘Steady state’ NC between core and downcomer occurs owing to continuous cooling of the downcomer fluid by a heat exchanger (boiler or steam generator) or by continuous inlet of feed-water liquid at a temperature lower than core outlet temperature;
- Cooling of the containment atmosphere by a closed loop.

In the current generation of nuclear plants, the NC core power removal capability is exploited for accident situations to demonstrate the inherent safety features of the plant (with the noticeable

exception of the Dodewaard commercial BWR unit, shut down in 1997). The natural circulation is also occurring during various phases of the refuelling.

In future generation of nuclear plants, NC is planned to be used for ensuring the nominal operating conditions and for achieving safe cooling following accidents in a wider spectrum than foreseen for current generation reactors.

2.7. STEAM–LIQUID INTERACTIONS

Large pools may have a very wide spectrum of geometric configurations. Heat transfer in one very limited zone in terms of volume (e.g. by condensing injected steam or by heat transfer from a passive containment cooler) does not imply homogeneous or nearly homogeneous temperature in the pool. Many containment phenomena involve steam–liquid interface. Steam discharge into a suppression pool of boiling water reactor is a good example of this case. After break-up of the originally created bubbles in the suppression pool, the subsequent formation of bubble plumes takes place. Consequently, complete condensation occurs and this induces mixing in the pool, the process is being determined by single and two phase natural circulation. It is important to understand the break-up and plume-stirring process and mechanisms, because the system pressure is ultimately controlled by the pressure in the vapour space above the water surface in the suppression chamber. This pressure is the sum of the partial pressures of steam and gas, the former controlled by the temperature at the pool surface. In turn, the pool surface temperature depends on the efficiency of steam condensation in the pool, and the degree of mixing in the pool.

The following is a listing of the steam–liquid interactions related phenomena:

- Direct contact condensation of steam in pool water;
- Bubble formation and break-up and the subsequent formation of bubble plumes;
- Break-up and plume-stirring process and mechanisms inducing mixing in the pool.

An example of steam–liquid interaction is a passive containment cooling (PCC) system venting into the suppression pool of ESBWR and also injection of steam-gas mixture through a downcomer vent line into the suppression pool.

2.8. GRAVITY DRIVEN COOLING AND ACCUMULATOR BEHAVIOUR

Gravity driven cooling provides emergency core cooling water by gravity draining, in events with loss of coolant. This system requires a large volume of water above the core, plus additional depressurization capacity, so that the primary coolant system can be depressurized to allow for gravity flow from the elevated suppression pool. Since there are no large reactor vessel pipes at or below the core elevation, this design ensures that the core will remain covered by water during all design basis accidents. In general, gravity driven cooling concept is mainly based on the depressurization of the reactor pressure vessel to sufficiently low pressures to enable reflooding of the core by gravity feed from an elevated pool. When the gravity driven cooling begins, the gravity drain flow rate to the reactor pressure vessel depends on the piping geometry, the state of the fluid, and the pressure in both the water pool and the reactor pressure vessel. Flow entering the reactor pressure vessel during the later stages of blowdown following a postulated LOCA must be sufficient to keep the nuclear core flooded. The system which provides gravity driven cooling is a simple and economic safety system.

The following is a listing of the gravity driven cooling related phenomena:

- Depressurization of the reactor pressure vessel by discharging through depressurization valves into the drywell and increase of pressure in the upper part of containment;
- Evaporation in the reactor pressure vessel due to depressurization;
- Friction in the gravity driven cooling system and injection lines including the valves in these lines;

- Large amounts of cold water immediately floods the lower parts of the reactor pressure vessel causing:
  - Collapse of void;
  - Condensation of steam;
  - Suppression of boiling;
  - Increase of water level inside the reactor pressure vessel;
- Condensing of steam out of the reactor pressure vessel and drywell gas space until air accumulates on the primary sides of the passive containment cooling system, resulting in termination of steam condensation.

Examples of gravity driven cooling systems include gravity driven cooling system (GDCS) of ESBWR and passive core flooding system (HA-2 hydraulic accumulators of the second stage) of WWER-1000/392 and passive core flooding systems (ECCS tank) of WWER 640/407.

2.9. LIQUID TEMPERATURE STRATIFICATION

Nuclear reactors that implement natural circulation passive safety systems may produce large temperature gradients in their working fluid as a result of local cooling caused by emergency core coolant (ECC) injection or local heating caused by steam condensation or heat exchanger heat transfer. Thermal stratification arises because the low flow condition typically encountered in a natural circulation system greatly reduces the amount of fluid mixing that can occur. Examples of thermal stratification during ECC injection include the formation of cold plumes in the downcomer, and liquid thermal stratification in the lower plenum, cold legs and loop seals.

ECC injection into horizontal piping partially filled with steam also results in liquid temperature stratification. The cooler liquid condenses the steam forming a saturated layer of liquid water on top of the subcooled liquid layer. This saturated layer is at a higher temperature than the subcooled layer, resulting in a stratified temperature condition. The formation of the saturated layer may mitigate occurrences of condensation-induced water hammer (CIWH) events.

Liquid temperature stratification can also arise in passive safety systems such as the natural circulation driven Core Make-up Tanks (CMT) and the large liquid-filled tanks that serve as the heat sink for reactor core or containment passive cooling systems. Steam vented into the large safety tanks condenses in the cold liquid producing hot rising plumes that form thermal layers at the free surface of the tank. Thermal layers having different temperatures grow with time to create a large temperature gradient in the liquid.

2.10. BEHAVIOUR OF EMERGENCY HEAT EXCHANGERS AND ISOLATION CONDENSERS

The removal of decay heat from a nuclear core can be accomplished by passive means using either an emergency heat exchanger or an isolation condenser (IC), depending on the system design. In some advanced pressurized water reactors (PWR), the emergency heat exchanger decay heat removal system consists of a closed loop that includes a shell and tube heat exchanger immersed in a large liquid pool that is elevated above the core. The relative elevation between the heat source and heat sink creates a buoyancy-driven natural circulation flow that eliminates the need for a pump. Decay heat is removed from the core by convective heat transfer from the fuel to the single phase liquid in the reactor vessel. The heat stored in the liquid is carried by natural circulation to the emergency heat exchanger. Heat is transferred from the fluid through the emergency heat exchanger tubes into the pool by three mechanisms; single phase convective heat transfer at the tube inside surface, heat conduction through the tube walls, and nucleate boiling at the tube outside surface. Some advanced PWRs use the steam generator as an intermediate emergency heat exchanger with a passively cooled, natural circulation feedwater loop.

Some advanced Boiling Water Reactors (BWR) use isolation condensers as the means of removing core decay heat. The IC consists of a shell and tube heat exchanger immersed in a large liquid pool

elevated above the core. In a BWR, core decay heat is removed by nucleate boiling. The steam generated by this process is condensed inside the IC tubes creating a low pressure region inside the tubes which draws in additional steam. Thus the driving mechanism for the flow is steam condensation. Heat is transferred through the IC tubes into the pool by three mechanisms; single phase steam condensation (phase change) at the tube inside surface, heat conduction through the tube walls, and convective heat transfer at the tube outside surface. The condensate is returned as a single phase liquid to the reactor vessel by gravity draining. Performance of the IC can be affected by the presence of non-condensable gases.

The following is a listing of the emergency heat exchanger related local phenomena:

- Emergency heat exchanger loop flow resistance;
- Buoyancy force;
- Single phase convective heat transfer;
- Shell-side nucleate boiling heat transfer.

The following is a listing of the IC related local phenomena:

- IC loop flow resistance;
- Low pressure steam condensation;
- Condensation heat transfer in the presence of non-condensable gases;
- Shell-side convection heat transfer;
- Condensate/steam countercurrent flow limitations.

2.11. STRATIFICATION AND MIXING OF BORON

Boric acid is introduced into the reactor coolant to control long term reactivity. Forced coolant circulation during normal operation ensures that the boric acid is homogeneously distributed in the reactor coolant system (RCS) so that the boron concentration is practically uniform. Decrease of the boron concentration results in an increase of the reactivity. Causes for decreasing of boron concentration are injection of coolant with less boron content from interfacing systems (external dilution) or separation of the borated reactor coolant into highly concentrated and diluted fractions (inherent dilution). Examples of external dilution are the injection of coolant of reduced boron concentration by the make-up system, and injection of low-boron pump sealing water into the primary system. Inherent dilution can occur after reflux condenser heat transfer or back flow from the secondary system in case of primary-to-secondary leakage accidents.

Operation in the reflux condenser mode over a lengthy period of time could occur in the event of small-break loss of coolant accidents (SB-LOCA) concurrent with limited operability of the emergency core cooling (ECC) systems. In such an event the condensate descending down the cold-leg steam generator (SG) tubing into the SG outlet plenum and from there into the pump seal could form slugs of low-boron water. On restoration of natural circulation after refilling of the reactor coolant system such slugs would be transported towards the reactor core. However, on their way to the core, they would be mixed in the cold-leg piping, the reactor pressure vessel (RPV) downcomer and the lower plenum and thus cause increase in boron concentration.

Restarting of a reactor coolant pump (RCP) after a SBLOCA or a SG tube rupture (SGTR) is very unlikely to occur as such events can be clearly identified on the basis of measured data and starting of a RCP is an action which involves several individual actions and therefore requires some time. Assuming that an inadvertent demineralized water injection into one loop were to occur before starting of the RCP in this loop in spite of the monitoring and measurement of the boron concentration of the water injected into the RCS, a slug of demineralized water moves towards the core inlet after pump start. Mixing of the diluted slug with the ambient coolant of higher boron content provides the only mitigation mechanism before the slug enters the core.

The main mixing mechanism in case of the low-boron water slug accelerated by the RCP start is turbulent mixing between the fluid flows having different velocities whereas in case of re-establishing the natural circulation after a reflux condensation phase the main mixing mechanism is buoyancy driven turbulent mixing. The density differences between the fluids are due to the temperature and the boron concentration differences.

2.12. CORE MAKE-UP TANK BEHAVIOUR

Several advanced reactor designs implement core make-up tanks (CMTs) to provide natural circulation cooling to the core. CMTs are elevated tanks connected to the reactor vessel and primary loop at the top and bottom of the tank. Special lines connect the bottom of the tank with the vessel, and are termed direct vessel injection (DVI). In connection to this, an important interaction occurs between the CMT, the accumulator and the incontainment refuelling water storage tank (IRWST) also considering the actuation signal for automatic depressurization. The tanks are filled with cold borated water and can provide coolant injection at system pressure. The tanks are normally isolated from the reactor vessel by an isolation valve located at the bottom of the vessel. The fluid is always sensing full system pressure through the top connection line. In the event of an emergency, the bottom isolation valve is opened to complete the natural circulation loop and permitting cold borated water to flow into the core. The relative elevation between the core and the CMT and the density difference between the hot primary system water and the cold CMT water creates a buoyancy-driven natural circulation flow that eliminates the need for a pump. Decay heat is removed from the core by convective heat transfer from the fuel to the single phase liquid in the reactor vessel. CMT behaviour includes natural circulation, liquid thermal stratification in the tank, and liquid flashing during plant depressurization.

TABLE 2-1. IDENTIFICATION AND CHARACTERIZATION OF PHENOMENA

Phenomena Identification		Characterizing Thermohydraulic Aspect
1	Behaviour in large pools of liquid	Thermal stratification Natural/forced convection and circulation Steam condensation (e.g. chugging, etc.) Heat and mass transfer at the upper interface (e.g. vaporization) Liquid draining from small openings (steam and gas transport)
2	Effects of non-condensable gases on condensation heat transfer	Effect on mixture to wall heat transfer coefficient Mixing with liquid phase Mixing with steam phase Stratification in large volumes at very low velocities
3	Condensation on containment structures	Coupling with conduction in larger structures
4	Behaviour of containment emergency systems (PCCS, external air cooling, etc.)	Interaction with primary cooling loops
5	Thermo-fluid dynamics and pressure drops in various geometrical configurations	3-D large flow paths e.g. around open doors and stair wells, connection of big pipes with pools, etc. Gas liquid phase separation at low Re and in laminar flow Local pressure drops
6	Natural circulation in closed loop	Interaction among parallel circulation loops — inside and outside the vessel Influence of non-condensable gases Stability Reflux condensation
7	Steam–liquid interaction	Direct condensation Pressure waves due to condensation
8	Gravity driven cooling and accumulator behaviour	Core cooling and core flooding
9	Liquid temperature stratification	Lower plenum of vessel Down-comer of vessel Horizontal/vertical piping
13	Behaviour of emergency heat exchangers and isolation condensers	Low pressure phenomena
14	Stratification and mixing of boron	Interaction between chemical and thermohydraulic problems Time delay for the boron to become effective in the core
15	Core make-up tank behaviour	Thermal stratification Natural circulation

TABLE 2-2. LIST OF PHENOMENA [2-2]

0	BASIC PHENOMENA	1	Evaporation due to Depressurization
		2	Evaporation due to Heat Input
		3	Condensation due to Pressurization
		4	Condensation due to Heat Removal
		5	Interfacial Friction in Vertical Flow
		6	Interfacial Friction in Horizontal Flow
		7	Wall to Fluid Friction
		8	Pressure Drops at Geometric Discontinuities
		9	Pressure Wave Propagation
1	CRITICAL FLOW	1	Breaks
		2	Valves
		3	Pipes
2	PHASE SEPARATION/VERTICAL FLOW WITH AND WITHOUT MIXTURE LEVEL	1	Pipes/Plena
		2	Core
		3	Downcomer
3	STRATIFICATION IN HORIZONTAL FLOW	1	Pipes
4	PHASE SEPARATION AT BRANCHES	1	Branches
5	ENTRAINMENT/DEENTRAINMENT	1	Core
		2	Upper Plenum
		3	Downcomer
		4	Steam Generator Tube
		5	Steam Generator Mixing Chamber (PWR)
		6	Hot Leg with ECCI (PWR)
6	LIQUID-VAPOUR MIXING WITH CONDENSATION	1	Core
		2	Downcomer
		3	Upper Plenum
		4	Lower Plenum
		5	Steam Generator Mixing Chamber (PWR)
		6	ECCI in Hot and Cold Leg (PWR)
7	CONDENSATION IN STRATIFIED CONDITIONS	1	Pressurizer (PWR)
		2	Steam Generator Primary Side (PWR)
		3	Steam Generator Secondary Side (PWR)
		4	Horizontal Pipes
8	SPRAY EFFECTS	1	Core (BWR)
		2	Pressuriser (PWR)
		3	Once-Through Steam Generator Secondary Side (PWR)
9	COUNTERCURRENT FLOW / COUNTERCURRENT FLOW LIMITATION	1	Upper Tie Plate
		2	Channel Inlet Orifices (BWR)
		3	Hot and Cold Leg
		4	Steam Generator Tube (PWR)
		5	Downcomer
		6	Surgeline (PWR)
10	GLOBAL MULTIDIMENSIONAL FLUID TEMPERATURE, VOID AND FLOW DISTRIBUTION	1	Upper Plenum
		2	Core
		3	Downcomer
		4	Steam Generator Secondary Side
11	HEAT TRANSFER: NATURAL OR FORCED CONVECTION	1	Core, Steam Generator, Structures
	SUBCOOLED/NUCLEATE BOILING	2	Core, Steam Generator, Structures
	DNB/DRYOUT	3	Core, Steam Generator, Structures
	POST CRITICAL HEAT FLUX	4	Core, Steam Generator, Structures
	RADIATION	5	Core
	CONDENSATION	6	Steam Generator, Structures
12	QUENCH FRONT PROPAGATION/REWET	1	Fuel Rods
		2	Channel Walls and Water Rods (BWR)
13	LOWER PLENUM FLASHING		
14	GUIDE TUBE FLASHING (BWR)		
15	ONE AND TWO PHASE IMPELLER-PUMP BEHAVIOUR		
16	ONE AND TWO PHASE JET-PUMP BEHAVIOUR (BWR)		
17	SEPARATOR BEHAVIOUR		
18	STEAM DRYER BEHAVIOUR		
19	ACCUMULATOR BEHAVIOUR		
20	LOOP SEAL FILLING AND CLEARANCE (PWR)		
21	ECC BYPASS/DOWNCOMER PENETRATION		
22	PARALLEL CHANNEL INSTABILITIES (BWR)		
23	BORON MIXING AND TRANSPORT		
24	NON-CONDENSABLE GAS EFFECT (PWR)		
25	LOWER PLENUM ENTRAINMENT		

TABLE 2-3. SEPARATE EFFECTS TEST FACILITY-CROSS-REFERENCE MATRIX [2-2]

LEGEND

x suitable for model validation
o limited suitability for model validation
- not suitable for model validation

Phenomena		Separate Effects Test Facilities																												
																														3. France
		MOBY-DICK	SUPER MOBY-DICK	CANON and SUPER CANON (Horiz.)	VERTICAL CANON		TAPIOCA (Vertical)	DADINE (Vertical Tube, Inside)	PERICLES Rectangular	PERICLES Cylindrical	PATRICIA GV 1	PATRICIA GV 2	ERSEC Tube (Inside)	ERSEC Rod-Bundle	OMEGA Tube (Inside)	OMEGA Rod-Bundle	ECTHOR Loop Seal (Air/Water)	COSI	SUPER MOBY-DICK TEE	PIERO (Air/Water)	EPOPEE	EVA								
	Facility No.	1	2	3	4	5	6	7	8	9	10	11	12	13	14	15	16	17	18	19	20	21								
	Info Sheet available	x	x	x	x		x	x	x	x	x	x	x	x	o	o	x	x	x	x	o	x								
BASIC PHENOMENA	1 Evaporation due to Depressurization	-	-	-	-		-	-	-	-	-	-	-	-	-	-	-	-	-	-	-	-								
	2 Evaporation due to Heat Input	-	x	-	-		o	-	-	-	-	-	o	-	-	-	-	-	-	-	-	-								
	3 Condensation due to Pressurization	-	-	-	-		-	-	-	-	-	-	-	-	-	-	-	-	-	-	-	-								
	4 Condensation due to Heat Removal	-	-	-	-		-	-	-	-	o	-	-	-	-	-	-	-	-	-	-	-								
	5 Interfac. Frict. Vertic. Flow	-	-	-	o		o	x	-	-	-	o	-	-	-	-	o	o	-	-	-	-								
	6 Interfac. Frict. Horiz. Flow	-	-	o	-		-	-	-	-	-	-	-	-	-	-	-	o	o	-	-	-								
	7 Wall to Fluid Friction	x	x	-	-		-	-	-	-	-	-	-	-	-	-	-	-	-	x	-	-								
	8 Press. Drops at Geometr. Discontinuities	-	x	x	o		o	-	-	-	-	-	-	-	-	-	-	-	-	-	-	-								
	9 Pressure Wave Propagation																													
1 CRITICAL FLOW	1 Breaks	-	x	x	x		x	-	-	-	-	-	-	-	-	x	-	-	x	-	-	-								
	2 Valves	-	-	-	-		-	-	-	-	-	-	-	-	-	-	-	-	-	-	-	-								
	3 Pipes	x	x	-	-		-	-	-	-	-	-	-	-	-	-	-	-	-	-	-	-								
2 PHASE SEPARATION /VERTICAL FLOW WITH AND W/OUT MIXTURE LEVEL	1 Pipes/Plena	-	-	-	x		x	o	-	-	o	x	-	-	-	-	-	-	-	-	o	-								
	2 Core	-	-	-	-		-	-	x	x	-	-	-	-	-	-	-	-	-	-	-	-								
	3 Downcomer	-	-	-	-		-	-	-	-	-	-	-	-	-	-	-	-	-	-	-	-								
3 STRATIFICATION IN HORIZ.FLOW	1 Pipes	-	-	-	-		-	-	-	-	-	-	-	-	-	-	o	o	x	-	-	-								
4 PHASE SEPARATION AT BRANCHES	1 Branches	-	-	-	-		-	-	-	-	-	-	-	-	-	-	-	-	x	-	-	-								
5 ENTRAINMENT/DEENTRAINMENT	1 Core	-	-	-	-		-	o	x	x	-	-	-	x	-	x	-	-	-	-	-	-								
	2 Upper Plenum	-	-	-	-		-	-	o	x	-	-	-	-	-	-	-	-	-	-	-	-								
	3 Downcomer	-	-	-	-		-	-	-	-	-	-	-	-	-	-	-	-	-	-	-	-								
	4 SG-Tube	-	-	-	-		-	-	-	-	x	-	-	-	-	-	-	-	-	-	-	-								
	5 SG-Mix. Chamber (PWR)	-	-	-	-		-	-	-	-	-	-	-	-	-	-	-	-	-	-	-	-								
	6 Hot Leg with ECCI (PWR)	-	-	-	-		-	-	-	-	-	-	-	-	-	-	-	-	-	-	-	-								
6 LIQUID–VAPOUR MIXING WITH CONDENSATION	1 Core	-	-	-	-		-	-	-	-	-	-	-	-	-	-	-	-	-	-	-	-								
	2 Downcomer	-	-	-	-		-	-	-	-	-	-	-	-	-	-	-	-	-	-	-	-								
	3 Upper Plenum	-	-	-	-		-	-	-	-	-	-	-	-	-	-	-	-	-	-	-	-								
	4 Lower Plenum	-	-	-	-		-	-	-	-	-	-	-	-	-	-	-	-	-	-	-	-								
	5 SG-Mix. Chamb. (PWR)	-	-	-	-		-	-	-	-	-	-	-	-	-	-	-	-	-	-	-	-								
	6 ECCI in Hot and Cold Leg (PWR)	-	-	-	-		-	-	-	-	-	-	-	-	-	-	-	x	-	-	-	-								
7 CONDENSATION IN STRATIFIED CONDITIONS	1 Pressurizer (PWR)	-	-	-	-		-	-	-	-	-	-	-	-	-	-	-	-	-	-	-	-								
	2 SG-Primary Side (PWR)	-	-	-	-		-	-	-	-	x	-	-	-	-	-	-	-	-	-	-	-								
	3 SG-Secondary Side (PWR)	-	-	-	-		-	-	-	-	-	x	-	-	-	-	-	-	-	-	-	-								
	4 Horizontal Pipes	-	-	-	-		-	-	-	-	-	-	-	-	-	-	-	x	-	-	-	-								
8 SPRAY EFFECTS	1 Core (BWR)	-	-	-	-		-	-	-	-	-	-	-	-	-	-	-	-	-	-	-	-								
	2 Pressurizer (PWR)	-	-	-	-		-	-	-	-	-	-	-	-	-	-	-	-	-	-	-	-								
	3 OTSG Second. Side (PWR)	-	-	-	-		-	-	-	-	-	-	-	-	-	-	-	-	-	-	-	-								
9 CCF/CCFL	1 Upper Tie Plate	-	-	-	-		-	-	o	o	-	-	-	-	-	-	-	-	-	-	-	-								
	2 Channel Inlet Orifices (BWR)	-	-	-	-		-	-	-	-	-	-	-	-	-	-	-	-	-	-	-	-								
	3 Hot and Cold Leg	-	-	-	-		-	-	-	-	-	-	-	-	-	-	o	-	-	-	-	-								
	4 SG-Tube (PWR)	-	-	-	-		-	-	-	-	x	-	-	-	-	-	-	-	-	-	-	-								
	5 Downcomer	-	-	-	-		-	-	-	-	-	-	-	-	-	-	-	-	-	-	-	-								
	6 Surgeline (PWR)	-	-	-	-		-	-	-	-	-	-	-	-	-	-	-	-	-	-	-	-								
10 GLOBAL MULTIDIMENSIONAL FLUID TEMPERATURE, VOID AND FLOW DISTRIBUTION	1 Upper Plenum	-	-	-	-		-	-	o	-	-	-	-	-	-	-	-	-	-	-	-	-								
	2 Core	-	-	-	-		-	-	x	-	-	-	-	-	-	-	-	-	-	-	-	-								
	3 Downcomer	-	-	-	-		-	-	-	-	-	-	-	-	-	-	-	-	-	-	-	-								
	4 SG-Secondary Side	-	-	-	-		-	-	-	-	-	-	-	-	-	-	-	-	-	-	-	-								
11 HEAT TRANSF. NAT.FORC.CONV	1 Core, SG, Structures	-	-	-	-		-	x	x	-	-	-	-	-	-	-	-	-	-	-	-	-								
SUBC./NUCL.BOIL	2 Core, SG, Structures	-	-	-	-		-	x	x	-	-	-	x	-	-	-	-	-	-	-	-	-								
DNB/DRYOUT	3 Core, SG, Structures	-	-	-	-		-	x	-	-	-	-	x	x	-	x	x	-	-	-	-	-								
POST CHF	4 Core, SG, Structures	-	-	-	-		-	x	-	-	-	-	-	x	-	x	x	-	-	-	-	-								
RADIATION	5 Core	-	-	-	-		-	-	-	-	-	-	-	-	-	-	-	-	-	-	-	-								
CONDENSATION	6 SG, Structures	-	-	-	-		-	-	-	-	x	-	-	-	-	-	-	-	-	-	-	-								
12 QUENCH FRONT PROPAG./REWET	1 Fuel Rods	-	-	-	-		-	-	x	x	-	-	o	x	-	-	-	-	-	-	-	-								
	2 Channel Walls and Water Rods (BWR)	-	-	-	-		-	-	-	-	-	-	-	-	-	-	-	-	-	-	-	-								
13 LOWER PLENUM FLASHING		-	-	-	-		o	-	-	-	-	-	-	-	x	x	-	-	-	-	-	-								
14 GUIDE TUBE FLASHING (BWR)		-	-	-	-		-	-	-	-	-	-	-	-	-	-	-	x	-	-	-	-								
15 ONE AND TWO PHASE IMPELLER PUMP BEHAVIOUR		-	-	-	-		-	-	-	-	-	-	-	-	-	-	-	-	-	-	x	x								
16 ONE AND TWO PHASE JET-PUMP BEHAVIOUR (BWR)		-	-	-	-		-	-	-	-	-	-	-	-	-	-	-	-	-	-	-	-								
17 SEPARATOR BEHAVIOUR		-	-	-	-		-	-	-	-	-	-	-	-	-	-	-	-	-	-	-	-								
18 STEAM DRYER BEHAVIOUR		-	-	-	-		-	-	-	-	-	-	-	-	-	-	-	-	-	-	-	-								
19 ACCUMULATOR BEHAVIOUR		-	-	-	-		-	-	-	-	-	-	-	-	-	-	-	-	-	-	-	-								
20 LOOP SEAL FILLING AND CLEARANCE (PWR)		-	-	-	-		-	-	-	-	-	-	-	-	-	-	-	x	-	-	-	-								
21 ECC BYPASS/DC PENETRATION		-	-	-	-		-	-	-	-	-	-	-	-	-	-	-	-	-	-	-	-								
22 PARALLEL CHANNEL INSTABILITIES (BWR)		-	-	-	-		-	-	-	-	-	-	-	-	-	-	-	-	-	-	-	-								
23 BORON MIXING AND TRANSPORT		-	-	-	-		-	-	-	-	-	-	-	-	-	-	-	-	-	-	-	-								
24 NON-CONDENSABLE GAS EFFECT (PWR)		-	-	-	-		-	-	-	-	x	-	-	-	-	-	-	-	x	-	-	-								
25 POWER PLENUM ENTRAINMENT		-	-	-	-		-	-	-	-	-	-	-	-	-	-	-	-	-	-	x	-								

TABLE 2-4. CROSS-REFERENCE MATRIX FOR LARGE BREAKS IN PWRS [2-2]

Matrix I CROSS-REFERENCE MATRIX FOR LARGE BREAKS IN PWRs		Test Type			Test Facility and Volumetric Scaling						
- Phenomena versus test type + occurring o partially occurring - not occurring - Test facility versus phenomenon + suitable for code assessment o limited suitability - not suitable - Test type versus test facility + performed o performed but of limited use - not performed or planned		Blowdown	Refill	Reflood	CCTF 1:25	LOFT 1 : 50	BETHSY 1 : 100	PKL 1 : 145	LOBI 1 : 712	SEMISCALE 1 : 1600	UPTF 1 : 1 (a)
Phenomena	Break flow	+	+	+	o	o	o	o	o	o	o
	Phase separation (condition or transition)	o	+	+	+	+	+	+	+	+	+
	Mixing and condensation during injection	o	+	+	o	o	o	o	o	o	+
	Core wide void + flow distribution	o	+	+	o	o	o	o	o	-	o
	ECC bypass and penetration	o	+	o	+	+	-	o	o	-	+
	CCFL (UCSP)	o	+	+	o	o	o	o	o	-	+
	Steam binding (liquid carry over, ect.)	-	o	+	o	o	-	o	o	o	o
	Pool formation in UP	-	+	+	o	o	o	o	o	o	+
	Core heat transfer incl. DNB, dryout, RNB	+	+	+	o	+	+	+	o	o	-
	Quench front propagation	o	o	+	+	+	+	+	-	+	-
	Entrainment (Core, UP)	o	o	+	o	o	+	o	o	o	+
	De-entrainment (Core, UP)	o	o	+	o	o	o	o	o	o	+
	1 - and 2-phase pump behaviour	+	o	o	-	o	-	o	+	+	-
	Non-condensable gas effects	-	o	o	-	-	o	-	-	-	o
Test Facility	CCTF	-	o	+	Important test parameter						
	LOFT	+	+	+							
	BETHSY	-	-	+	- break location/break size - pumps off/pumps on						
	PKL	o	+	+	- cold leg injection/combined injection						
	LOBI	+	+	-	(a) UPTF integral tests						
	SEMISCALE	+	+	+							
	UPTF	o	+	+							

TABLE 2-5. CROSS-REFERENCE MATRIX
FOR SMALL AND INTERMEDIATE BREAKS IN PWRS [2-2]

Matrix II CROSS-REFERENCE MATRIX FOR SMALL AND INTERMEDIATE BREAKS		Test Type							Test Facility and Volumetric Scaling								
- Phenomenon versus test type + occurring o partially occurring - not occurring - Test facility versus phenomenon + suitable for code assessment o limited suitability - not suitable - Test type versus test facility + performed o performed but of limited use - not performed or planned		Stationary test addressing energy transport on primary side	Stationary test addressing energy transport on secondary side	Small leak overfeed by HPIS,secondary side necessary	Small leak without HPIS overfeeding, secondary side necessary	Intermediate leak, secondary side not necessary	Pressurizer leak	U-tube rupture	PWR 1 : 1	LOFT 1 : 50	LSTF 1 : 50	BETHSY 1 : 100	PKL-III 1 : 145	SPES 1 : 430	LOBI-II 1 : 712	SEMISCALE 1 : 1600	UPTF, TRAM 1 : 1 (2)
Phenomena (3)	Natural circulation in 1-phase flow, primary side	+	+	+	o	-	+	+	+	+	+	+	+	+	+	+	-
	Natural circulation in 2-phase flow, primary side	+	-	o	+	+	o	-	-	+	+	+	+	+	+	+	o
	Reflux condenser mode and CCFL	+	-	-	+	+	-	-	-	o	+	+	o	o	o	o	+
	Asymmetric loop behaviour	-	-	+	+	-	o	+	-	-	o	+	+	+	o	o	+
	Break flow	-	-	+	+	+	+	+	-	+	+	+	+	+	+	+	o
	Phase separation without mixture level formation	+	-	o	+	+	+	o	-	o	+	+	+	+	+	o	+
	Mixture level and entraiment in SG second side	-	+	+	+	+	+	+	-	-	+	+	+	o	o	-	-
	Mixture level and entraiment in the core	+	-	-	+	+	+	-	-	o	+	+	+	o	o	o	o
	Stratification in horizontal pipes	+	-	-	+	+	-	-	-	+	+	o	o	+	o	o	+
	Phase separation in T-junct. and effect on breakflow	-	-	-	+	+	-	-	-	o	o	o	o	o	o	-	+
	ECC-mixing and condensation	-	-	o	+	+	+	+	-	o	o	o	o	o	o	o	+
	Loop seal clearing	-	-	-	+	+	o	-	-	+	+	+	+	+	+	+	+
	Pool formation in UP/CCFL (UCSP)	+	-	-	o	+	+	-	-	o	o	o	o	o	-	o	+
	Core wide void and flow distribution	+	-	-	o	+	+	-	-	o	o	o	o	-	-	-	o
	Heat transfer in covered core	+	+	+	+	+	+	+	o	+	+	+	+	+	+	+	-
	Heat transfer in partly uncovered core	+	-	-	o	+	-	-	-	+	+	+	+	o	o	o	-
	Heat transfer in SG primary side	+	o	o	+	+	o	o	-	o	+	+	+	+	+	o	-
	Heat transfer in SG secondary side	o	+	+	+	+	+	+	-	o	+	+	+	o	+	o	-
	Pressurizer thermohydraulics	o	-	o	o	+	+	+	o	o	o	o	o	o	o	-	+
	Surgeline hydraulics	o	-	-	o	+	+	o	-	o	o	o	o	o	o	o	+
	1- and 2-phase pump behaviour	-	-	-	o	+	-	-	o	o	o	o	o	o	+	+	-
	Structural heat and heat losses (1)	+	-	o	+	+	o	o	-	o	o	o	o	o	o	o	o
	Non-condensable gas effects	+	-	-	-	-	-	-	-	-	o	o	o	-	-	o	+
	Boron mixing and transport	+	-	+	+	+	+	+	-	-	-	-	-	-	-	-	o
Test Facility	PWR	-	-	o	-	-	+	+	(1) problem for scaled test facilities (2) UPTF integral tests (3) for intermediate breaks phenomena included in large break reference matrix may be also important								
	LOFT	-	-	+	+	+	+	-									
	LSTF	+	+	+	+	+	+	+									
	BETHSY	+	+	+	+	+	+	+									
	PKL-III	+	+	+	+	+	+	+									
	SPES	+	+	+	+	-	-	-									
	LOBI-II	+	+	+	+	+	+	+									
	SEMISCALE	o	o	+	+	+	+	+									
	UPTF, TRAM	-	-	-	-	+	+	-									

TABLE 2-6. CROSS-REFERENCE MATRIX FOR TRANSIENTS IN PWRS [2-2]

- Phenomenon versus test type + occurring o partially occurring - Test facility versus phenomenon + suitable for code assessment o limited suitability - not suitable - Test type versus test facility + performed o performed but of limited use - not performed or planned		ATWS	Loss of feedwater, non ATWS	Loss of heat sink, non ATWS (c)	Station blackout	Steam line break	Feed line break	Reactivity disturbance	Overcooling	PWR 1 : 1	LOFT 1 : 50	LSTF 1 : 50	BETHSY 1 : 100	PKL-III 1 : 134	SPES 1 : 430	LOBI-II 1 : 712	SEMISCALE 1 : 1000
Phenomena	Natural circulation in 1-phase flow	+	+	+	+	+	+	o	o	+	o	+	+	+	+	+	+
	Natural circulation in 2-phase flow	+	+	+	+	-	-	o	-	-	o	+	+	+	+	+	+
	Core thermohydraulics	+	+	+	+	o	o	+	o	o	+	+	+	+	+	+	+
	Thermohydraulics on primary side of SG	+	o	o	+	o	o	o	+	o	o	+	+	+	+	+	o
	Thermohydraulics on secondary side of SG	+	+	+	+	+	+	o	+	o	o	+	+	+	o	+	o
	Pressurizer thermohydraulics	+	+	+	+	o	o	o	+	o	o	o	o	o	o	o	o
	Surgeline hydraulics (CCFL, choking)	+	+	+	+	o	o	o	o	o	o	o	o	o	o	o	o
	Valve leak flow (a)	+	+	+	+	+	+	+	+	-	o	o	o	o	o	o	o
	1- and 2-phase pump behaviour	+	+	+	+	o	o	o	+	o	o	+	o	o	o	+	+
	Thermohydraulic-nuclear feedback	+	-	-	-	-	-	+	-	+	+	-	-	-	-	-	-
	Structural heat and heat losses (b)	o	o	o	o	o	o	o	o	-	o	o	o	o	o	o	o
	Boron mixing and transport	-	-	-	-	o	-	-	o	-	-	-	-	-	-	-	-
	Separator behaviour	o	-	-	-	+	-	-	-	-	-	-	-	-	o	o	-
Test Facility	PWR	-	-	-	-	-	-	-	o	(a) valve flow behaviour will be strongly design-dependent, specific experimental data should be used if possible (b) problem for scaled test facilities							
	LOFT	+	+	+	o	-	-	+	+								
	LSTF	-	+	-	+	+	+	-	+								
	BETHSY	-	+	+	-	+	+	-	-								
	PKL-III	-	+	+	+	+	+	-	+								
	SPES	-	+	-	+	-	-	-	-								
	LOBI-II	+	+	+	+	+	+	-	-								
	SEMISCALE	-	+	+	+	+	+	-	+								

TABLE 2-7. CROSS-REFERENCE MATRIX FOR TRANSIENTS AT SHUTDOWN CONDITIONS IN PWRS [2-2]

Matrix V CROSS-REFERENCE MATRIX FOR TRANSIENTS AT SHUTDOWN CONDITIONS IN PWRS		Test Type				Test Facility and Volumetric Scaling		
- Phenomenon versus test type + occurring o partially occurring - not occurring - Test facility versus phenomenon + suitable for code assessment o limited suitability - not suitable - Test type versus test facility + performed o performed but of limited use - not performed or planned		Loss of RHR with no opening	Loss of RHR with openings	Loss of RHR with dam in HL	Boron dilution at shutdown	LSTF	BETHSY	PKL III
Phenomena	Pressurization due to boiling	+	+	+	-	+	+	+
	Reflux condenser mode and CCFL	+	+	o	-	+	+	o
	Asymmetric loop behaviour	-	o	+	-	+	+	+
	Flow through openings (manways, vents)	-	+	+	-	+	+	-
	Mixture level formation in upper plenum and hot legs	+	+	+	-	+	+	+
	Mixture level and entrainment in the core	+	+	+	-	+	+	+
	SG syphon draining	-	-	+	-	+	-	-
	Asymmetry due to the presence of a dam	-	-	+	-	+	-	-
	Stratification in horizontal pipes	+	+	+	-	+	o	+
	Phase separation in T-junctions and effect on flow	-	+	+	-	o	o	o
	ECC mixing and condensation	+	+	+	-	o	o	o
	Loop seal clearing and filling	+	+	+	-	+	+	-
	Pool formation in UP/CCFL (UCSP)	-	-	-	-	-	-	-
	Core 3D thermohydraulics	+	+	+	+	o	o	o
	Heat transfer in covered core	+	+	+	-	+	+	+
	Heat transfer in partially uncovered core	+	+	+	-	o	o	-
	Heat transfer in SG primary side	+	+	+	-	+	+	+
	Heat transfer in SG secondary side	+	+	+	-	+	+	+
	Pressurizer thermohydraulics a)	-	x	x	-	o	o	o
	Surge line thermohydraulics a)	-	x	x	-	o	o	o
	Structural heat and heat losses	-	-	-	-	-	-	o
	Non-condensable gas effects	+	+	+	-	+	+	+
	Boron mixing and transport	-	-	-	+	-	-	-
	Thermohydraulics-nuclear feedback	-	-	-	+	-	-	-
Test Facility	LSTF	+	+	+	-			
	BETHSY	-	+	-	-			
	PKL III	+	-	-	-			

a) x is dependent on opening location
+ pressurizer manway open
- pressurizer manway shut

TABLE 2-8. CROSS-REFERENCE MATRIX FOR ACCIDENT MANAGEMENT FOR NON-DEGRADED CORE IN PWRS [2-2]

Matrix VI Cross-reference Matrix for Accident Management for a non-Degraded Core in PWRs		Test Type					Test Facility and Volumetric Scaling						
- Phenomenon versus test type + occurring o partially occurring - not occurring - Test facility versus phenomenon + suitable for code assessment o limited suitability - not suitable - Test type versus test facility + performed o performed but of limited use - not performed or planned		High pressure primary side feed and bleed	Low pressure, primary side feed and bleed	Secondary side, feed and bleed	RCP-Restart in a highly, voided PCS	Primary to secondary break with multiple failures	LOFT 1 : 50	LSTF 1 : 50	BETHSY 1 : 100	PKL-III 1 : 1 : 145	SPES 1 : 430	LOBI-II 1 : 712	UPTF, TRAM 1 : 1 (2)
Phenomena	Natural circulation in 1-phase flow, primary side	+	-	+	-	+	+	+	+	+	+	+	-
	Natural circulation in 2-phase flow, primary side	+	+	+	-	+	+	+	+	+	+	+	o
	Reflux condenser mode and CCFL	-	-	+	-	+	o	+	o	o	o	o	+
	Asymmetric loop behaviour	+	+	+	+	+	-	o	+	+	+	o	+
	Break flow	+	+	o	+	+	+	+	+	+	o	+	o
	Phase separation without mixture level formation	+	+	+	+	+	o	+	+	+	+	+	+
	Mixture level and entrainment in SG secondary side	-	-	+	-	+	-	+	+	+	o	o	-
	Mixture level and entrainment in the core	+	+	+	o	+	o	+	+	+	o	o	o
	Stratification in horizontal pipes	+	+	+	o	+	+	+	o	o	o	o	+
	Phase separation in T-junct. and effect on breakflow	+	+	o	-	+	o	o	o	o	o	o	+
	ECC-mixing and condensation	+	+	+	-	+	o	o	o	o	o	o	+
	Loop seal clearing (3)	o	o	+	o	+	+	+	o	o	+	+	+
	Pool formation in UP/CCFL (UCSP)	+	+	+	-	+	o	o	o	o	o	-	+
	Core wide void and flow distribution	+	+	+	+	+	o	o	o	o	-	-	o
	Heat transfer in covered core	o	o	+	-	+	+	+	+	+	+	+	-
	Heat transfer in partly uncovered core	+	+	+	+	+	+	+	+	+	o	o	-
	Heat transfer in SG primary side	-	-	+	o	+	o	+	+	+	+	+	-
	Heat transfer in SG secondary side	-	-	+	o	+	o	+	+	+	o	+	-
	Pressurizer thermohydraulics	+	+	o	o	+	o	o	o	o	o	o	+
	Surgeline hydraulics	+	+	o	o	+	o	o	o	o	o	o	+
	1- and 2-phase pump behaviour	o	o	+	+	+	o	o	o	o	o	+	-
	Structural heat and heat losses (1)	+	+	+	+	+	o	o	o	o	o	o	o
	Non-condensable gas effects	o	+	+	+	+	-	o	o	+	-	-	+
	Accumulator behaviour	-	+	+	-	o	o	+	+	+	+	+	+
	Boron mixing and transport	+	+	+	+	+	-	-	-	-	-	-	o
	Thermohydraulic-nuclear feed back	-	-	-	+	-	-	-	-	-	-	-	-
	Separator behaviour	-	-	-	-	-	-	-	-	-	-	-	-
Test Facility	LOFT	-	-	+	-	-	(1) problem for scaled test facilities (2) UPTF integral tests (3) long term cooling not included						
	LSTF	+	+	+	-	o							
	BETHSY	+	+	+	-	+							
	PKL-III	o	+	+	+	-							
	SPES	+	+	+	-	+							
	LOBI-II	+	+	+	-	+							
	UPTF, TRAM	o	+	-	-	-							

TABLE 2-9. CROSS-REFERENCE MATRIX FOR LOCA IN BWRS [2-2]

Matrix VII CROSS-REFERENCE MATRIX FOR LOCA IN BWRs		Test Type						Test Facility and Volumetric Scaling						
- Phenomena versus test type + occurring o partially occurring - not occurring - Test facility versus phenomenon + suitable for code assessment o limited suitability - not suitable - Test type versus test facility + performed o performed but of limited use - not performed or planned		Large Steam Line Break with Fast Depressurization	Large Break Below Water Level with Fast Depress.	Small Break without Depress. before ADS Actuation	Intermediate Break with Slow Depress.	Spray Line Break	Refill - Reflood	BWR 1 : 1 (a)	TBL, 1 : 382, 2 Chan., Full Pow., Full Height	ROSA III, 1 : 424, 4 Channels	TLTA, 1 : 624, 1 Chan., Full Power	FIST, 1 : 624, 1 Chan., Full Pow., Full Height	FIX 2, 1 : 777, 1 Chan., Full Pow., Full Height	PIPER 1, 1 : 2200, 1 Chan., Full Height
Phenomena	Break flow	+	+	+	+	+	o	-	o	o	o	o	o	+
	Channel and bypass axial flow and void distribution	+	+	+	+	+	+	o	+	o	+	+	+	+
	Corewide radial void distribution	o	o	+	+	+	+	o	o	+	o	o	o	-
	Parallel channel effects-instabilities	-	-	+	+	+	+	-	o	+	-	-	-	o
	ECC Bypass	-	-	o	o	o	+	-	o	o	o	o	-	+
	CCFL at UCSP and channel inlet orifice	o	+	-	+	+	+	-	o	o	-	o	o	o
	Core heat transf. incl. DNB, dryout, RNB. surf. to surf radiation	+	+	o	+	o	+	-	+	+	+	+	+	+
	Quench front propagation for both fuel rods and channel walls	-	-	-	-	-	+	-	+	+	+	+	-	+
	Entrainment and de-entrainment in core and upper plenum	+	+	o	o	o	+	-	-	o	o	o	-	o
	Separator behaviour incl. flooding, steam penetration and carryover	+	+	o	o	o	-	o	+	o	o	+	o	o
	Spray cooling	-	-	o	o	o	+	-	o	o	o	o	-	+
	Spray distribution	-	-	o	o	o	+	-	-	o	-	-	-	-
	Steam dryer - hydraulic behaviour	+	-	o	o	-	-	o	o	o	o	o	-	o
	One and two phase pump recirc. behaviour incl. jet pumps	o	o	+	+	+	o	o	o	o	o	o	o	-
	Phase separation and mixture level behaviour	+	+	+	+	+	+	-	o	+	o	+	+	o
	Guide tube and lower plenum flashing	+	+	-	o	o	-	-	+	+	+	+	+	+
	Natural circulation- core and downcomer	-	-	+	o	o	+	+	+	o	o	+	+	+
	Natural circulation core bypass, hot and cold bundles	-	-	+	o	o	+	-	o	o	o	o	o	o
	Mixture level in core	-	-	+	o	o	+	-	+	+	+	+	+	o
	Mixture level in downcomer	+	+	+	+	+	+	-	+	o	o	+	+	o
	ECC mixing and condensation	-	-	+	o	+	+	-	o	o	o	o	-	o
	Pool formation in upper plenum	o	o	-	o	o	+	-	o	o	o	o	o	o
	Structural heat and heat losses	o	o	o	+	+	+	-	+	o	o	o	o	o
	Phase separ. in T - junction and effect on break flow	-	-	+	o	+	-	-	-	-	-	-	-	+
Test Facility	BWR	-	-	-	-	-	-	(a) These are non-LOCA data but may be used for assessment						
	TBL	+	+	+	+	-	+							
	ROSA III	+	+	+	+	-	+							
	TLTA	+	+	-	+	-	+							
	FIST	+	+	+	+	-	+							
	FIX 2	-	+	-	+	-	-							
	PIPER 1	-	+	+	+	-	+							

TABLE 2-10. CROSS-REFERENCE MATRIX FOR TRANSIENTS IN BWRS [2-2]

Matrix VIII CROSS-REFERENCE MATRIX FOR TRANSIENTS IN BWRs		Test Type									Test Facility and Volumetric Scaling			
Phenomenon versus test type + occurring o partially occurring - not occurring **Test facility versus phenomenon** + suitable for code assessment o limited suitability - not suitable **Test type versus test facility** + performed o performed but of limited use - not performed or planned		Stationary Test Measuring Power Flow Map	Recirculation Pump Trip	Core Stability	Loss of Main Heat Sink	Feedwater Flow or Temperature Disturbance e. g. LOFW	Loss of Feedwater (LOFW) up to time of Const. Pressure	Inadvertent Increase in Steam Flow	ATWS	Station Blackout (Loss-of-Offsite Power)	BWR 1 : 1	ROSA III, 1 : 424, 4 Channels	FIST, 1 : 642, 1 Channel, Full Power, Full Height	FIX 2, 1 : 777, 1 Channel, Full Power, Full Height
Phenomena	Natural circulation in one- and two phase flow	+	+	+	+	-	-	-	+	+	+	o	+	o
	Collapsed level behaviour in downcomer	-	+	o	+	+	+	+	+	+	+	o	+	+
	Core thermohydraulics	o	+	+	+	o	o	o	+	+	o	+	+	+
	Valve leak flow	-	-	-	+	-	-	-	+	+	o	o	o	-
	Single phase pump behaviour (a)	o	+	o	+	o	o	+	+	+	o	o	o	o
	Parallel channel effects and instabilities	-	+	+	o	-	-	-	+	+	o	+	-	-
	Nuclear thermohydraulic feedback including spatial effects	o	o	+	-	o	o	o	+	-	+	-	-	-
	Nuclear thermohydraulic instabilities	-	o	+	-	-	-	o	+	-	+	-	-	-
	Downcomer mixing	-	-	-	-	+	+	-	+	+	o	o	-	-
	Boron mixing and distribution	-	-	-	-	-	-	-	+	-	-	-	-	-
	Steam line dynamics	-	-	-	+	-	-	+	+	+	o	-	o	-
	Void collapse and temp. distribution during pressurization	-	-	-	+	-	-	-	+	+	o	+	+	+
	Critical power ratio	-	+	+	+	+	+	+	+	+	o	+	+	+
	Rewet after DNB at high press. and high power incl. high core flow	-	+	-	+	-	-	o	+	o	-	o	+	+
	Structural Heat and Heat Losses	-	o	-	o	-	o	o	o	o	-	o	o	o
Test Facility	BWR	+	+	+	+	+	+	+	-	o				
	ROSA III	-	+	+	+	-	+	-	-	+				
	FIST	-	o	-	+	-	+	+	o	+				
	FIX 2	-	+	-	+	-	-	-	-	-				

(a) Two phase pump behaviour is of interest for certain special ATWS and inadvertent increase of steam flow transients.

REFERENCES FOR CHAPTER 2

[2-1] AKSAN, N., D'AURIA, F., Relevant Thermohydraulic Aspects of Advanced Reactor Design — Status Report, OECD/NEA Report NEA/CSNI/R(96)22 (1996).

[2-2] INTERNATIONAL ATOMIC ENERGY AGENCY, Natural Circulation in Water Cooled Nuclear Power Plants, IAEA-TECDOC-1474, Annex 21, IAEA, Vienna (2005).

3. CHARACTERIZATION OF PHENOMENA

The origin of the phenomena considered in the present report is outlined at the beginning of Chapter 2 (dealing with phenomena identification). Namely, phenomena have been classified into two categories: (a) phenomena occurring during interaction between primary system and containment; and (b) phenomena originated by the presence of new components and systems or special reactor configurations. In the same headlines statement of Chapter 2, it is clarified that the descriptions given below are intended to supplement those in the previous international reports on the same subject (e.g. the OECD/NEA-CSNI Reports mentioned in the list of references in Chapter 2) and that most of the phenomena applicable to current plants are also applicable to plants with passive systems.

Twelve phenomena have been identified as key outcome of the process outlined in Chapter 2.

The present chapter deals with the characterization of these identified phenomena. These should be considered as 'additional' related to the phenomena that were the object of consideration in previous international reports (e.g. OECD/NEA-CSNI reports, above mentioned). The characterization of 'additional' phenomena consists of an exhaustive description of phenomena, as far as possible. This has been done having in mind three key guidelines:

- To distinguish the 'additional' phenomena from the phenomena occurring or expected following transient behaviour in current generation of reactors (limited use of passive systems),
- To distinguish among each other the 'additional' phenomena,
- To contribute in providing a comprehensive picture of the transient performance of the class of innovative reactors (i.e. focus of present report) where passive system features are exploited.

Furthermore, each description includes outlines of models and an overview of the experimental data base that support the characterization of phenomena. The capabilities of system codes or of Computational Fluid Dynamics codes in predicting the same phenomena are evaluated and results from the application of the codes to the analysis of experimental data are also provided.

The scope of the description is typically bounded by the material discussed in the IAEA CRP meetings and by the expertise of the authors of the individual sections. Owing to this, the content of the sections below shall not be considered as state of the art for the individual phenomena, notwithstanding the attempt of the various authors and contributors to provide general surveys on the subject.

3.1. BEHAVIOUR IN LARGE POOLS OF LIQUID

3.1.1. Introduction

Large pools of water at near atmospheric pressure provide a heat sink for heat removal from the reactor or the containment by natural circulation, as well as a source of water for core cooling. Heat transfer in a limited zone in terms of volume results in non-homogeneous temperature distribution in the pool. Three dimensional convection flows develop, affecting the heat transfer process, which results in a temperature stratification. Temperature stratification can compromise the heat transfer process. Generation of steam might increase the flow velocities, mix liquids having different temperatures and destroy again the temperature stratification. Furthermore steam is released from the pool into the containment and increases containment pressure. Under conditions of strong temperature stratification compared to a homogeneous temperature distribution, the fluid at the top of the pool reaches the saturation temperature first. The evaporation starts much earlier (than if the pool temperature was uniform) resulting in an earlier pressure increase in the containment.

Usually the heat is transferred via horizontally oriented U-tubes into the pool. Sloshing might occur in the pool depending on the geometric construction of the pool and the thermohydraulic events in the facility. Under unfavourable conditions dependent on the location of the U-tubes this might cause uncovering of the tubes with adverse consequences on the heat transfer capability.

In some reactor systems steam discharge and heat exchanger are interconnected. In these cases the flow conditions at the heat exchanger tubes are influenced by the thermohydraulic event with corresponding influence on the heat transfer capability.

The different temperature stratification phenomena are discussed in detail in the following chapters. These processes are three dimensional in nature. Their adequate simulation requires a Computational Fluids Dynamics (CFD) approach. In Section 3.1.4 the state of the art of the modelling and the expected problems simulating heating up of a liquid in large pools are described.

CFD simulations reduce the reliance on experimentally derived correlations by predicting local turbulence effects rather than predicting integral quantities like pressure drop and heat transfer coefficients. As a consequence, simpler separate effects experiments, which capture the turbulence effects but not necessarily the integral effects within a specific component of a system, can be utilized as the primary validation basis for the CFD codes. However, while the need for large carefully scaled integral experiments is reduced, the high spatial and temporal resolution of these codes requires that experimental data be collected at similar spatial and temporal resolutions.

3.1.2. Example cases

Examples of heating up phenomena in large pool include the pressure suppression pool (wet well) of the ESBWR, the suppression pool of the GE's SBWR-600, the in-containment refuelling water storage tank of the AP-1000, the pool of the emergency condenser of the SWR-1000 and the gravity driven water pool of the AHWR.

Figure 3.1-1 presents the operation scheme for an emergency condenser. At normal conditions of reactor operation, the U-tubes of the emergency condenser are filled with water (see Fig. 3.1-1, left side for the normal operation case) while almost no heat is transferred. In case of an accident, with a decreasing water level in the reactor core, the water in the U-tubes of the emergency condenser is replaced by steam. The steam in the tubes condenses and the heat is transferred to the secondary side (see Fig. 3.1-1, right side for the emergency case). Under these conditions the condenser acts as an effective passive heat sink.

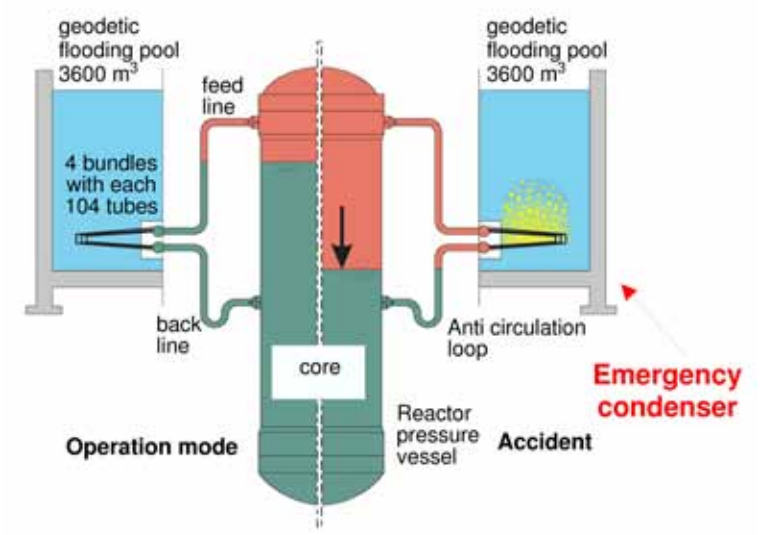

FIG. 3.1-1. Operation schema of the SWR-1000 emergency condenser.

3.1.3. Experimental basis

Several experiments were designed to investigate the phenomena in large pools namely the temperature stratification processes and their influence on the heat transfer capability. In these experiments, the temperature field is measured by a 3D arrangement of thermocouples. In some experiments, additional information on local void fractions was provided.

Depending on the phenomenon to be investigated the scaling of the test facility has to be considered. For density driven natural circulation phenomena geodetic height differences play an important role.

3.1.3.1. ISP-42 at PANDA test facility

PANDA is a large scale facility, which has been constructed at the Paul Scherrer Institute (PSI) for the investigation of both overall dynamic response and the key phenomena of passive containment systems during the long term heat removal phase for Advanced Light Water Reactors (ALWRs). The facility has been configured to simulate the containment of a passive BWR, but the phenomena, which are taking place, are of a more generic character and of interest to LWR containment's in general. The facility is described in detail in Section 4.6.

The ISP-42 PANDA test scenario was established to cover many typical LWR and ALWR containment and primary system phenomena. The test procedure and a summary of the numerical results are described by Lübbesmeyer and Aksan [3.1-1, 3.1-2]. The following short overview and the statements concerning code capabilities are quoted from these reports.

The main issues and phenomena covered in the ISP-42 PANDA test were the following:

- Transient and quasi steady state operation of a passive containment cooling system (condenser immersed in pool),
- Coupled primary system and containment behaviour and phenomena,
- Reactor Pressure Vessel (RPV) operation at low power and low pressure under natural circulation conditions,
- Gravity driven ECCS injection in an initially saturated RPV,
- Venting of a steam/non-condensable gas mixture (through an immersed vent pipe into a wet well compartment),
- Steam condensation in the presence of non-condensable gases in tubes,
- Mixing and stratification of light (helium) and/or heavy (air) gases with steam in large volumes (3D effects, steam jets, air or helium release),
- Mixing and stratification in large water pools.

The configuration used for ISP-42 simulated the European Simplified Boiling Water Reactor (ESBWR) containment and passive decay heat removal system at about 1:40 volumetric and power scale, and full scale for time and thermodynamic state. The ISP-42 PANDA test consisted of six phases:

- Phase A: Passive Containment Cooling System Startup
- Phase B: Gravity-Driven Cooling System Discharge
- Phase C: Long Term Passive Decay Heat Removal
- Phase D: Overload at Pure-Steam Conditions
- Phase E: Release of Hidden Air

- Phase F: Release of Light Gas in Reactor Pressure Vessel

Some of the major conclusions drawn on the basis of the six phases of the ISP-42 post test cases and also covering the "blind" phase results can be summarized as follows (more detailed information is given by Lübbesmeyer and Aksan [3.1-1, 3.1-2]):

- The most important parameter relevant to reactor safety, the containment pressure history, has been calculated sufficiently accurately for most of the ISP-42 participants for all six phases of ISP-42.
- The overall best results were obtained by the lumped parameter code SPECTRA.
- Although system codes like CATHARE or RELAP5 were not designed to calculate typical containment problems in low pressure environments in the presence of large amounts of non-condensable gases, they produced acceptable results. Containment code COCOSYS also produced globally acceptable results.
- Some codes (like GOTHIC) had problems to model specific equipment (e.g. PCCs) properly, some tuning of physical models, which needed some knowledge of the facility behaviour, were introduced. The RELAP5 or CATHARE codes were superior with respect to the higher flexibility to simulate special components and, in this case, specifically the modelling of the PCCs.
- Most of the major deviations could be attributed to problems with the nodalization or simply input errors rather than deficiencies of the specific codes. For example, in the case of RELAP5 and CATHARE, the same code used by different organizations produced quite different results ("user effect", including different level of experience of the code users).
- It was observed that major attention should be given to provide the appropriate input parameters, which are used in the analysis. As an example, use of loss coefficients and their distribution, especially for low power, low pressure transients as in ISP-42, is a very important factor. Even though experimentally measured data are provided to the code users, due to modelling necessities specific to the computer code used, there could be substantial deviations in the input data. In order to ensure the appropriateness of these types of parameters, every input model should be reviewed as carefully as possible. An important factor is the computer code user's discipline. This discipline cannot be forced, or substituted by Quality Assurance (QA) procedures. However, appropriate QA procedures may help reduce inappropriate use of some input parameters.
- For simple physical situations (e.g., well-mixed conditions in phase A), choice of a lumped parameter approach is justified. In such cases, little gain in predictive capability is achieved at the cost of very large computation time for 3-D simulation and detailed nodalizations. Sensitivity studies can help to select the appropriate detailed nodalization and needed sophistication of physical models, and determine criteria for reasonable compromises between accuracy and computing time or costs.
- 3-D models incorporated in codes such as GOTHIC include correct physical representation of phenomena but a number of difficulties currently prevent the user from taking full advantage of these capabilities, e.g., accurate calculation of stratified conditions and its effect on system pressure (global parameter). Consequently, further assessment of 3-D models and advanced modelling features (e.g., turbulence) are necessary using well defined separate effects experiments for specific phenomena related to containment multicompartment geometries.
- The use of CFD codes is still exploratory, as they usually lack built-in physical models, have difficulties defining interfaces (boundary conditions) with other components, and occasionally encounter difficulties with convergence. Consequently, no simulations with CFD codes were submitted as part of this project.
- The knowledge gained in ISP-42 and other PANDA tests indicated the need to improve and upgrade some of the instrumentation, e.g., improved measurement of injected medium,

improved measurement of local concentration of air, helium and steam in the gas spaces of the different PANDA compartments.

- The data set produced for the six phases of the ISP-42 PANDA tests will be used as the basis of assessment of computer codes in relation to the passive containment cooling systems for at least the next ten years. These data will be available to the requesting organizations through the NEA-Data Bank and European Community Project CERTA.

3.1.3.2. Suppression pool mixing and condensation tests in PUMA facility

The Purdue University Multi-Dimensional Integral Test Assembly (PUMA) facility was used to perform suppression pool mixing and condensation test [3.1-3, 3.1-4]. The facility and experimental results are described in detail in Sections 3.7 and 4.7, respectively.

3.1.3.3. Experiments at Oregon State University

Experiments were conducted at the Oregon State University to investigate the passive systems of AP600 and AP1000 [3.1-5]. The passive residual heat removal (PRHR) system consists of a C-Tube type heat exchanger that resides in the water-filled in-containment refuelling water storage tank (IRWST). The tank was equipped with thermocouples (see Fig. 3.1-2) and video observations were made. The facility is also referenced in Section 3.10.

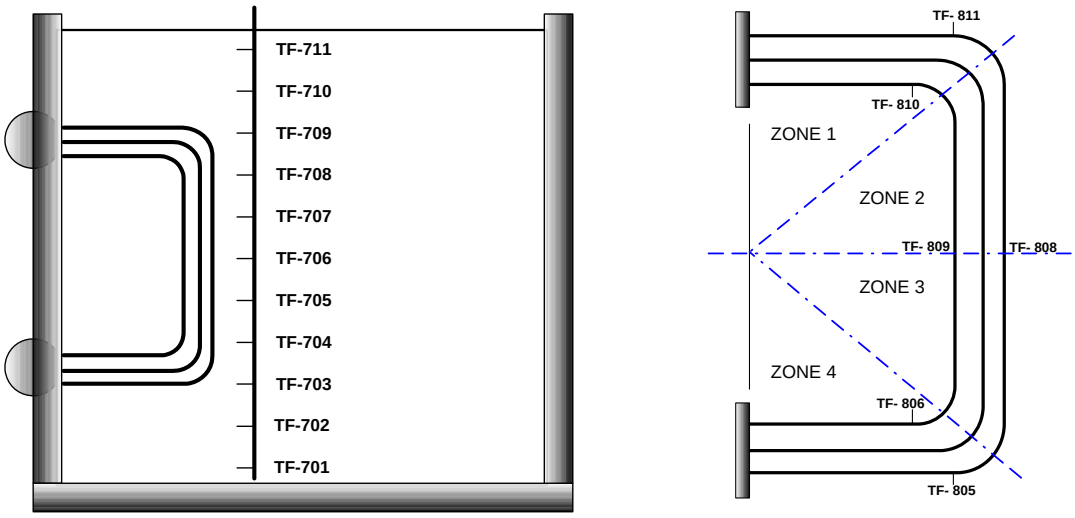

FIG. 3.1-2. Fluid temperature measurements in IRWST and PRHR tubes.

During the tests a strong temperature stratification followed by a destruction of the stratification in the IRWST was observed (see Fig. 3.1-3). The consequences for the distribution of heat removal over the different zones of the IRWST are shown in Fig. 3.1-4.

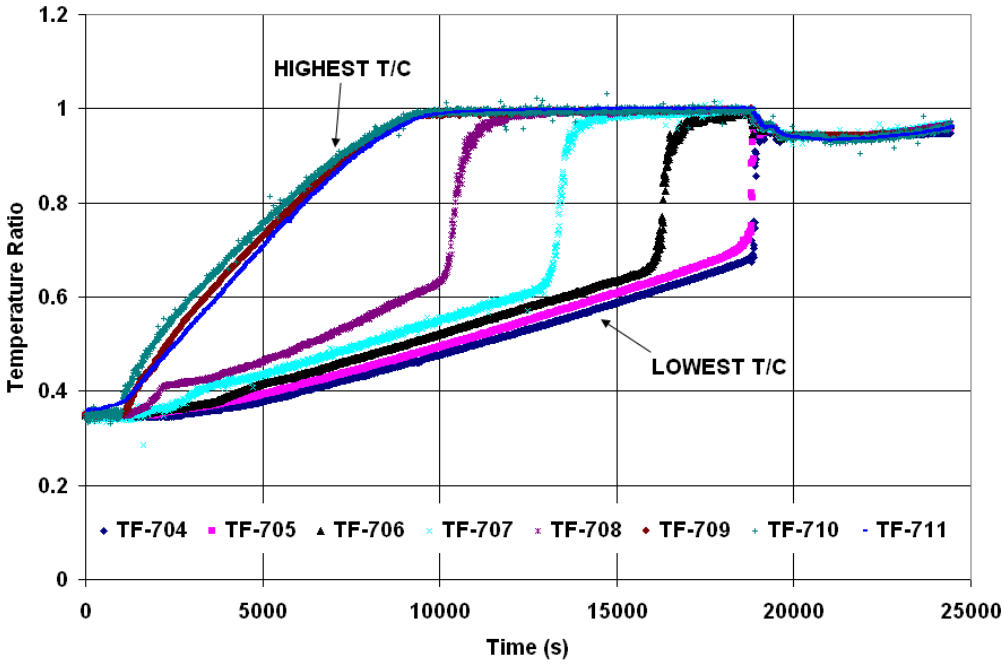

FIG. 3.1-3. Temperature courses at different vertical locations in the IRWST.

Figure 3.1-4 shows that the top horizontal bundle in the PRHR (Zone 1) serves to transfer a major portion of the heat load throughout the transient. As the saturation layer grows, the top zone becomes less effective and Zones 2 and 3 become more effective. Recirculation patterns were observed at the free surface of the IRWST.

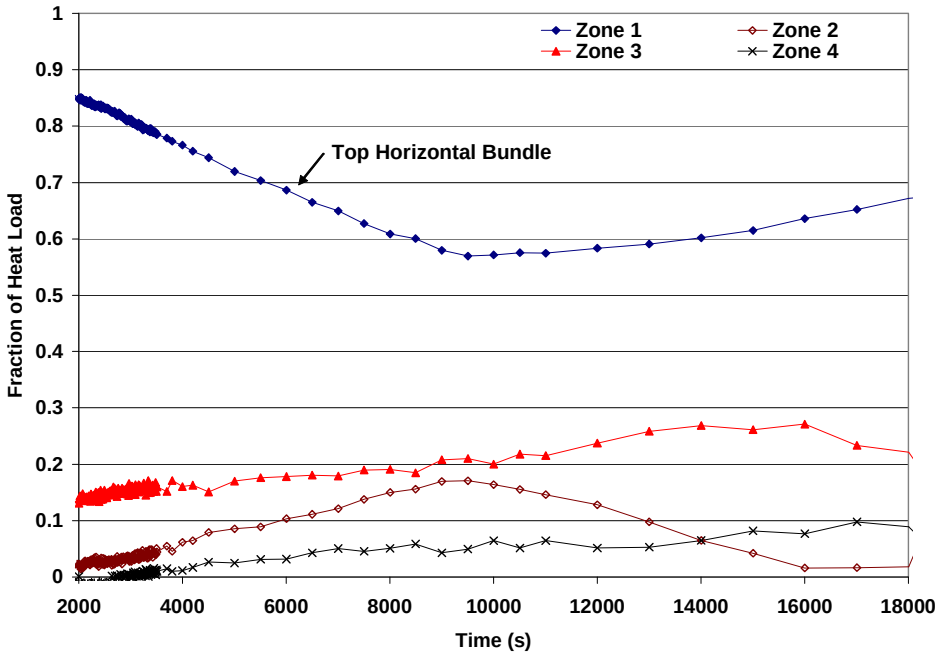

FIG 3.1-4. Fraction of heat load transferred in each zone.

3.1.3.4. Experiments at NOKO (FZK Jülich)

To investigate the heat removal capacity of an emergency condenser, comprehensive experiments were performed in the test facility NOKO at the Forschungszentrum Jülich [3.1-6, 3.1-7]. In 1998, tests were performed to investigate the heating up process in the secondary pool [3.1-8].

During the operation of the emergency condenser both on the primary and on the secondary side, natural circulation is observed. For the present purpose the processes on the secondary side are of particular interest. Initially, single phase and later two phase natural circulation was established. In the tests detailed temperature measurements on the secondary side of NOKO was realized with a number of thermocouples (175 thermocouples were arranged in five cross section planes). Various tests with different primary and secondary pressure and different startup temperatures were performed. In the case under consideration, a test with atmospheric pressure and a startup temperature of 293 K on the secondary side was completed. During this test, only the upper legs of three condensation tubes were active and were filled with steam to induce temperature stratification. The water level in the primary reactor vessel was adjusted to ensure that the boundary between steam and condensed water in these condensation tubes is fixed at the bent of the tubes. This might correspond to an early stage of the simulated accident.

The primary pressure in the test under consideration was 1 MPa. An overall power of 0.6 MW was transferred to the secondary side by condensation of steam from the upper legs of the three tubes. Heat transfer may be assumed to be equally distributed along the whole length of the upper tube. The heating up test was continued until the onset of boiling in the secondary tank.

The temperature distribution in the measuring planes after a heat-up time of 2000 sec showed strong vertical temperature stratification [3.1-8]. An essential portion of the fluid in the lower region is not involved in the heating up process. Moreover, the measurement showed the temperature field in the tank having almost no axial profile. Each measuring plane shows almost the same temperature distribution.

The experiments were analysed by using a 2D representation in the CFD code CFX-4 and the results of this analysis were published in [3.1-9, 3.1-10].

3.1.3.5. Heating up tests at TOPFLOW (FZ Dresden-Rossendorf)

The heating up tests were repeated in 2005 at the “Transient Two Phase Flow Test Facility” TOPFLOW. The facility went into operation in 2002 and consisted mainly of a heater and a cooler. Different experimental arrangements enabled the investigation of different aspects of two phase flow [3.1-11]. Particularly the equipment with modern two phase measurement techniques enabled the generation of data which are also suited for CFD code validation.

The main components of the facility are the pressure vessel (height 12.6 m, diameter 0.448 m) simulating the reactor vessel and the laterally connected emergency condenser bundle. The bundle of condensation tubes consists of eight inclined tubes having a length of 8.5 to 10 metres and an inner diameter of 44.5 millimetres and was arranged in the condenser tank (see Fig. 3.1-5). The bundle is arranged in a pool, which is a horizontal cylindrical tank with an inner diameter of 2 m and a length of 6 m. The condenser volume consisted of 17.7 m^3. The steam was produced by an electrical heater with a maximum power of 4 MW. The maximum steam mass flow is 2.5 kg/s.

The tubes were designed for a maximum pressure of 7 MPa and a maximum temperature of 560 K. The tank was designed for a maximum pressure of 1 MPa and a maximum temperature of 450 K. Eighty-eight thermocouples were arranged in 8 measuring planes (Fig. 3.1-5).

During different tests steam was injected in the tubes at primary pressures of 1, 3, 5 and 6.5 MPa, respectively. The water in the condensation tank was heated up by the tubes starting at normal temperature of 300 K and at 0.1 MPa while the steam in the tube bundle condensed. The mass flow and pressure of the condensate at the bundle outlet indicated the energy transferred from the primary to the secondary side. The differential pressure between tube in- and outlet represented the water level in the reactor pressure vessel.

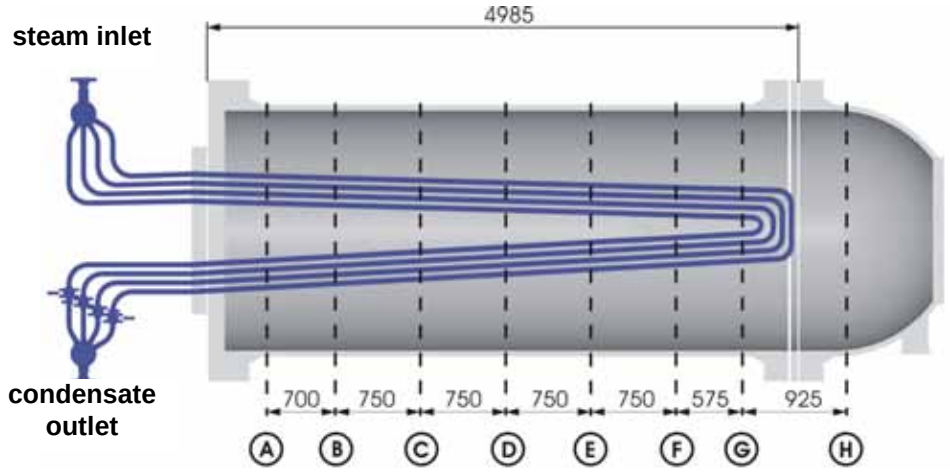

FIG. 3.1-5. Arrangement of thermocouples in the condenser tank.

The main purpose of the test was the investigation of the heat transfer capability by condensation in slightly inclined tubes. The result is the bundle characteristic for different primary pressures shown in Fig. 3.1-6. The nonlinear behaviour can be explained by the nonlinear dependency of the surface covered by steam in the inner of the exchanger tubes on the differential pressure between inlet and outlet.

As a second result, the three dimensional heating up characteristic of the secondary side in the condenser was obtained. Figure 3.1-7 shows the temperature distribution on the secondary side after 1300 s heating up time. Compared to the NOKO heating up tests, the temperatures on the secondary side were recorded until steam was found also in the condenser volume. One example for a primary pressure of 6.5 MPa is shown in Fig. 3.1-8. The figure shows temperatures taken from points arranged in a vertical line. The establishment of temperature stratification can be seen from the results. At about 1500 s steam is produced and the fluid becomes well mixed until all temperatures increase to nearly saturation temperature.

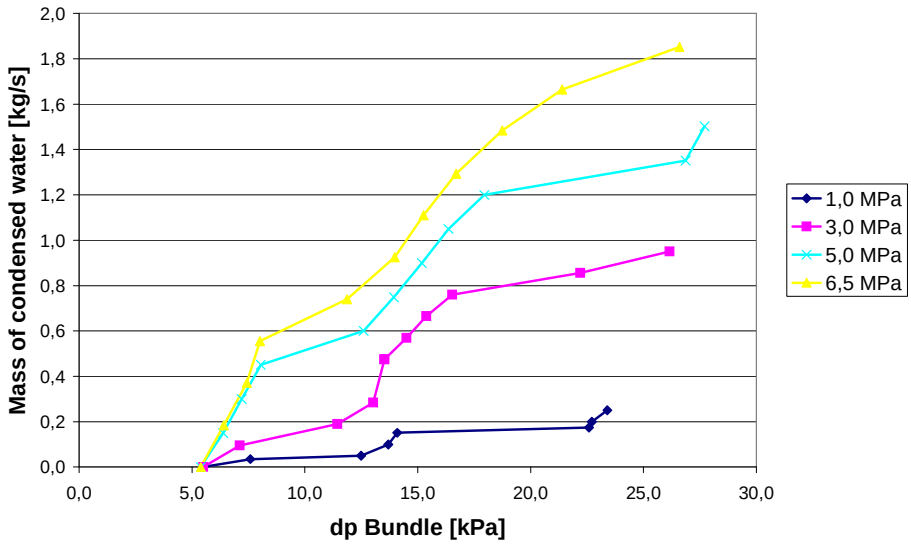

FIG.3.1-6. Characteristic curves of the bundle.

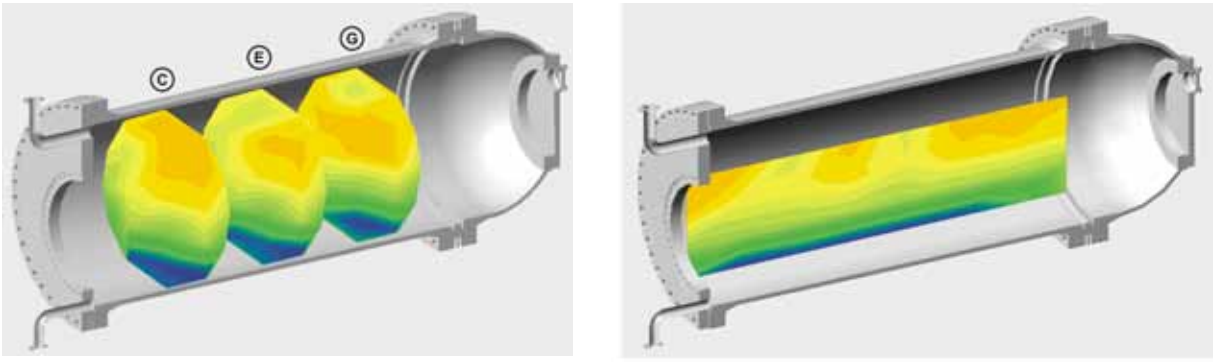

FIG. 3.1-7. Temperature distribution after a heating up time of 1300 s (primary pressure 6.5 MPa, compare Fig. 3.1-8).

Numerical analyses were performed using the CFD code CFX-11. To limit the computational grid a 2D representation was simulated. This procedure was justified by the similar axial cross sectional temperature distributions shown in the upper part of Fig. 3.1-7. A test performed 1998 in the FZ Jülich was selected for comparison. To cause temperature stratification, only the upper tubes were assumed to be filled with steam and contribute to the heat transfer. This corresponds to an early state of an accident which results in decrease of reactor water level. The heating power of these tubes was estimated to be $2.32 \cdot 10^{+5}$ W/m^2. At the heated tube walls, a wall boiling model was applied. The steam was modelled leaving the tank at the upper surface.

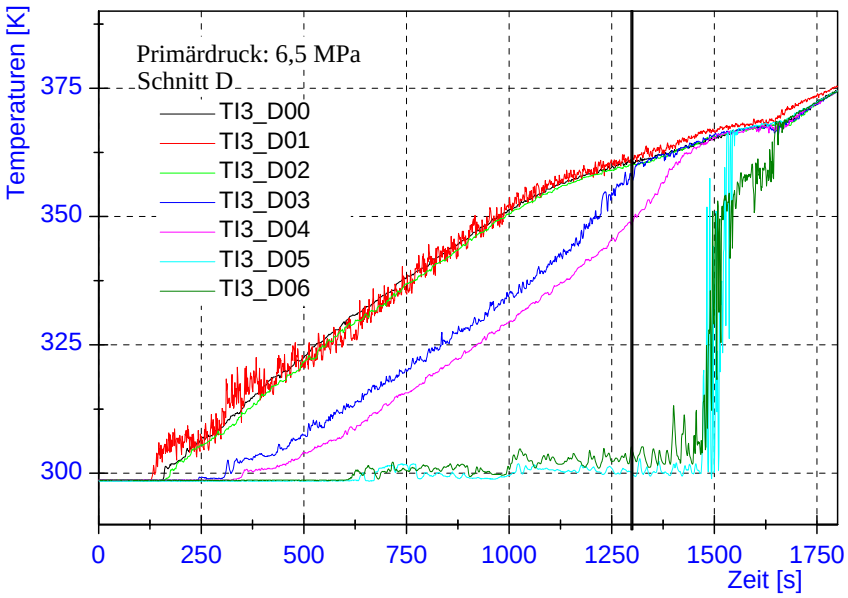

FIG. 3.1-8. Time development of temperatures in the tank, the points D00 to D06 are vertically arranged in plane D.

Figure 3.1-9 shows the locations of the thermocouples. In Fig. 3.1-10 temperatures at the different vertical positions are shown. Firstly, the simulations were performed considering only heating up of single phase water. The results are presented in Fig 3.1-10 by dotted lines where strong temperature stratification is observed. A simulation with two phase flow shows insignificant stratification for this case (see solid lines in Fig. 3.1-10). At the heated tube walls a wall boiling model was applied. For the two phase case, Fig. 3.1-10 shows maximum stratification after about 2000 s followed by a destruction of the stratification by increased steam production.

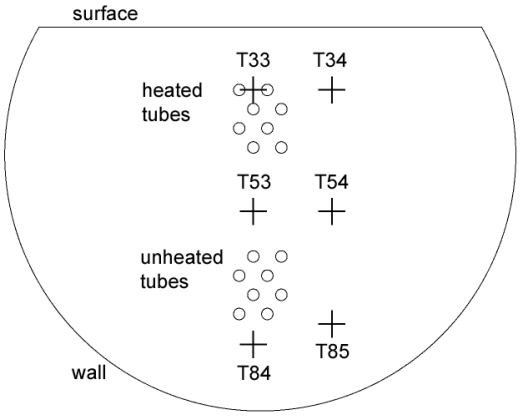

FIG. 3.1-9. Arrangement of the thermocouples in the tank.

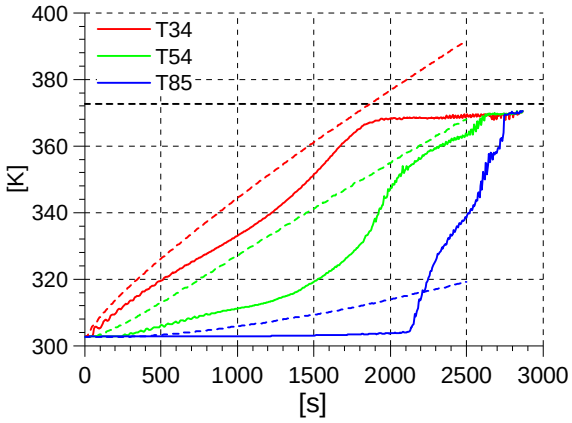

FIG. 3.1-10. Temperatures at different vertical positions in the tank centre.
(dotted lines: single phase calculation, solid lines two phase calculation)

The calculated water velocities as a function of time are presented in Fig. 3.1-11. While the velocities are limited to less than 0.1 m/s during the first 1000 s, they later increase by the generated steam to typical bubble rising velocities of more than 0.3 m/s.

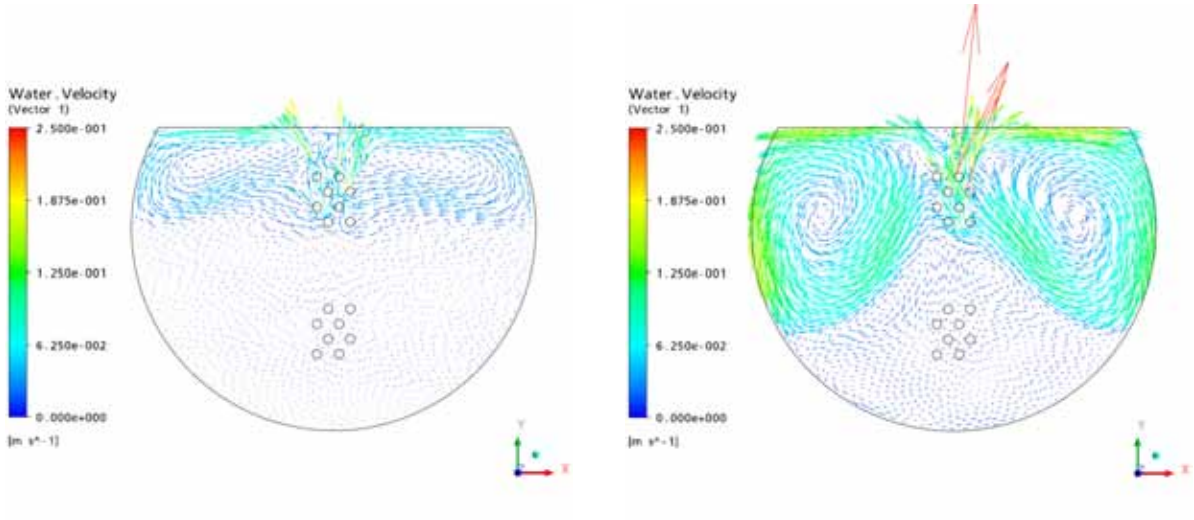

a) 1800 s b) 2500 s

FIG. 3.1-11. Water velocities depending on the heating up time.

3.1.3.6. Side wall heated tank

The small scale test is capable of explaining the mechanisms of creating temperature stratification and their subsequent destruction. The test was performed in FZ Dresden-Rossendorf and comprises transient heating up of water in a cylindrical tank from the side walls. Temperatures and local volume fractions were measured.

The experimental test arrangement consisted of a tank with a diameter of 0.25 m and a height of 0.25 m. The initial water inventory was about 10 kg. On the side walls, heating elements with an overall power of 4 kW are arranged so that the heat power was equally distributed over the wall.

During the tests, the tank was equipped with thermocouples and with conductivity probes for measuring the local void fractions at different locations (see Fig. 3.1-12). The measuring devices were

arranged in certain heights over the bottom in the centre of the tank and at the walls having a distance of 1 mm (thermocouples and void fraction measurements) and 10 mm (thermocouples only).

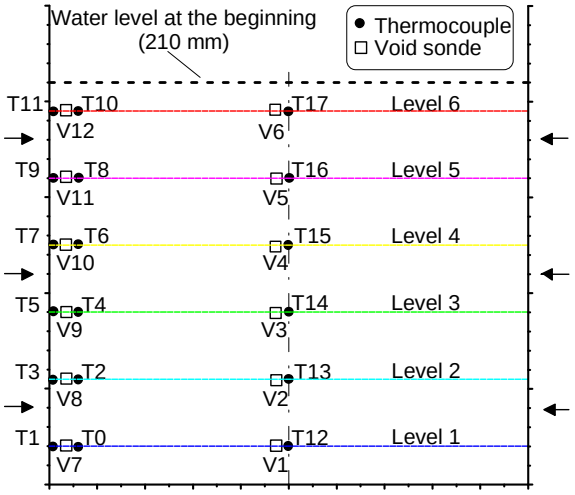

FIG. 3.1-12. Location of the temperature and void fraction measurements.

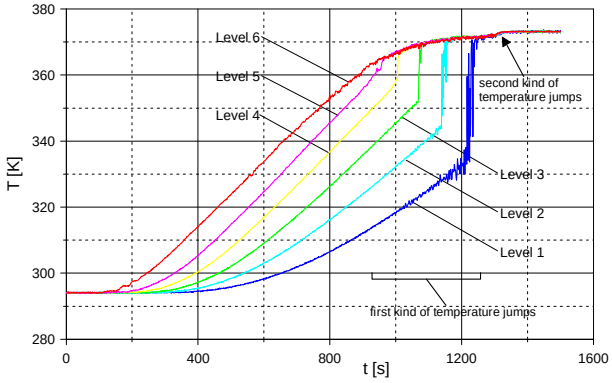

FIG. 3.1-13. Temperature courses in the centre of the tank.

After starting the test by switching the power supply on, the construction material was heated up. Since the temperature at the heated wall was also measured, the time dependence of the real heat transfer from the wall into the water during the test could be reconstructed. The experimental results were published by Aszodi et al. [3.1-12].

Different experiments were performed which showed qualitatively the same behaviour of the fluid during the heating up process. The time dependence of the temperatures measured at different heights from the tank bottom is shown in Fig. 3.1-13 for the thermocouples in the centre.

A few hundred seconds after the beginning of heating, strong temperature stratification occur. Temperature differences up to 50 degrees between the 1st and the 6th height levels are observed (see Fig. 3.1-13 after about 1000 s). The different temperatures of the thermocouples at 1 mm and at 10 mm distance from the wall show that shortly after starting the test a small boundary layer of only some millimetres was established with up to 10 degrees higher fluid temperature.

The CFD simulations by an in-house model [3.1-13] and CFX-4 [3.1-14] showed that during this test period the fluid in a very thin layer near the heated side wall moves rapidly upward. Almost in the whole tank volume, the fluid moves very slowly downward. This is the key phenomenon for establishing a strong temperature stratification.

After about 1100 s, the first boiling is detected by the void probes at the upper region of the wall for levels 6–3. During the time period from 900 to 1200 s, the temperature jumps to about 370 K, which should be denoted here as first kind of temperature jumps (see Fig. 3.1-13).

The phenomena occurring during the heat up of the tank, especially the observed temperature jumps, was not initially obvious, but could be explained by the CFD simulations. The CFD simulations showed that during this period the upper region of the tank becomes well mixed by steam whereas in the lower region the temperature stratification remains quite stable. The horizontal boundary between these regions moves gradually downwards. When the boundary meets a thermocouple, the measured temperature jumps upward to saturation temperature (see Fig. 3.1-14, Fig. 3.1-15)

During this period no steam is detected in the centre of the tank. Shortly after the last jump of level 1, a second temperature jump from 370 K to 373 K was observed for all thermocouples at about 1300 s,

which are denoted here as second kind of temperature jumps (see Fig. 3.1-13, Fig. 3.1-15). The downward velocity in the centre subsequently exceeds the steam bubble rising velocity and pool boiling is observed in the vessel.

Simultaneously with the second temperature jumps, a clear increase of the void fraction was indicated by the needle probes V9–V12 near the wall. Only after that, steam was detected at levels 6–3 in the centre of the tank.

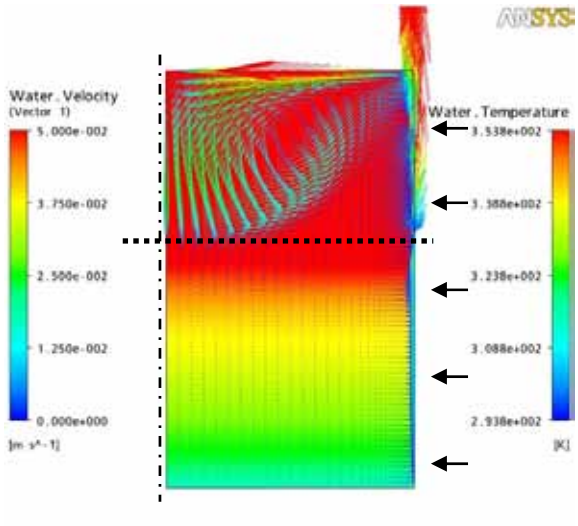

FIG. 3.1-14. CFX-11 results of the side wall heated tank experiment, heating form the right side after 1000 s heating up.

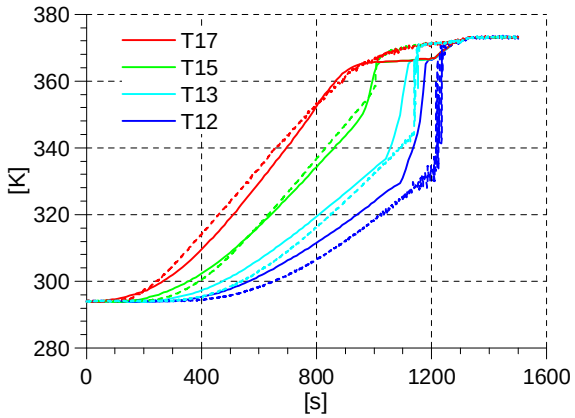

FIG. 3.1-15. Measured and calculated temperature courses (for the locations of the thermocouples see Fig. 3.1-12).

3.1.3.7. Experiments performed in the Reactor engineering division of BARC

In the Reactor engineering division of Bhabha Atomic Research Centre (BARC) in Trombay, Mumbai India different tests were performed to investigate the phenomenon of thermal stratification [3.1-15]. The experiments were directed on aspects of the passive decay heat removal system of AHWR. The tests were accompanied by CFD simulations.

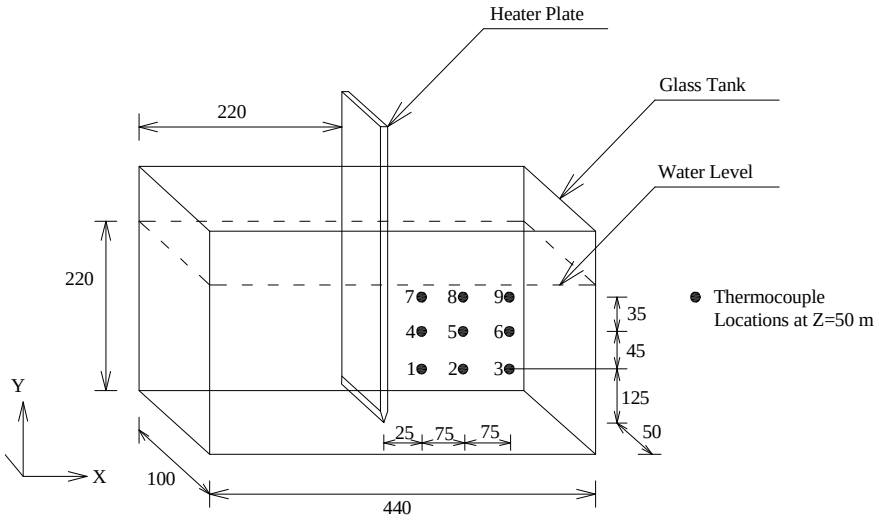

FIG. 3.1-16. Schematic of experimental set-up at BARC.

To understand the basic flow behaviour near an immersed heater, phenomenological experiments were carried out with visualization to obtain flow pattern around a single strip heater immersed in a rectangular water tank. The set-up was instrumented with nine thermocouples located at different locations in the tank. (see Fig. 3.1-16).

For visualization, Aluminum particles, Tellurium dye and fluorescent Rhodamine dye were used.

When power is applied to the heater, the particles clinging to the heater move up along the surface of the heater and to the top free surface. At the free surface, the detaching boundary layer is reflected downwards as shown in left side of Fig. 3.1-17). However, due to its higher temperature (lower density), it is observed to rise back to the free surface and flows along the free surface horizontally towards the wall of the container (see right side of Fig. 3.1-17). Also, it was seen that at higher heating rates, a vortex is formed as the boundary layer rebounds at the free surface. The visualization was also done using Tellurium dye and fluorescent Rhodamine dye. Similar flow patterns were observed.

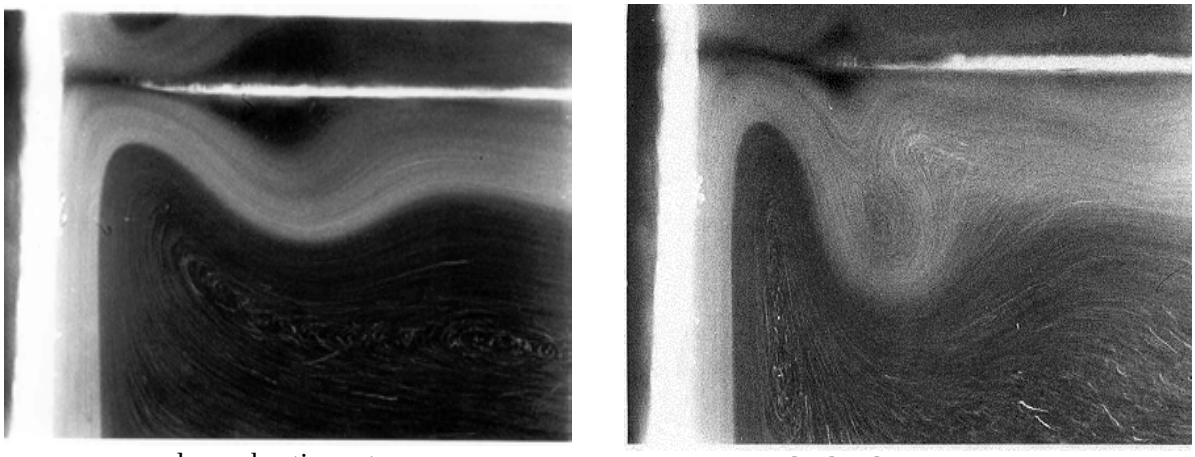

lower heating rates higher heating rates

FIG. 3.1-17. Flow pattern in the vicinity of heater near the top free surface using aluminium particles.

Numerical simulations [3.1-16] were carried out using CFD code PHOENICS 3.6 for this case for a period of 30 minutes. The temperature field predictions after 30 minutes of transient run show predominant stratification in the tank. The flow pattern predictions at the end of 30 minutes show comparatively high velocities near the heater zone and nearly static fluid in other parts of the tank.

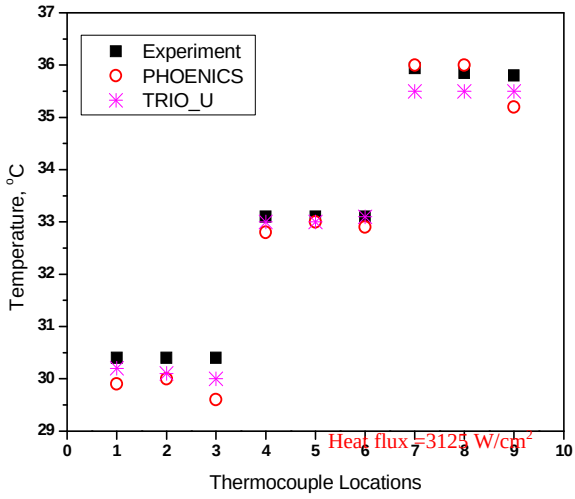

FIG. 3.1-18. Temperature readings after 1800 s.

The numerical predictions for this case were compared with the data generated in the experiment (see Fig. 3.1-18). At 1800 s, the temperatures measured by thermocouples at specific locations were compared with the code predictions and the agreement between the two is reasonably good. The comparison was also made in the time domain by selecting a particular thermocouple location and comparing the time variation of the measurement with the code prediction and good agreement was found except towards the end of the transient where the unaccounted heat losses in the experiment might have caused the difference.

To simulate the 2-D behaviour in the zone between two heaters, a particular case for which experimental data has been reported was selected. The case consisted of two equally heated plates on either of their sides. The bottom wall is adiabatic while at the top, convective heat transfer is allowed. For this specific case, a 2-D CFD code has been developed. Numerical simulations were then performed with and compared with the reported data. The comparison also shows predictions of one more in-house code which is based on 1-D approach. The comparison shows the time variation of temperatures at specific locations where test data is available with the predictions of 1-D and 2-D codes.

This case has also been numerically simulated using CFD package TRIO-U. The results generated by the code are very similar to those obtained using the 1-D & 2-D codes [3.1-15]. The similarities of results from CFD package reiterate the capability of the two in-house codes for such geometry. Few results generated by using TRIO-U are given in Fig. 3.1-19.

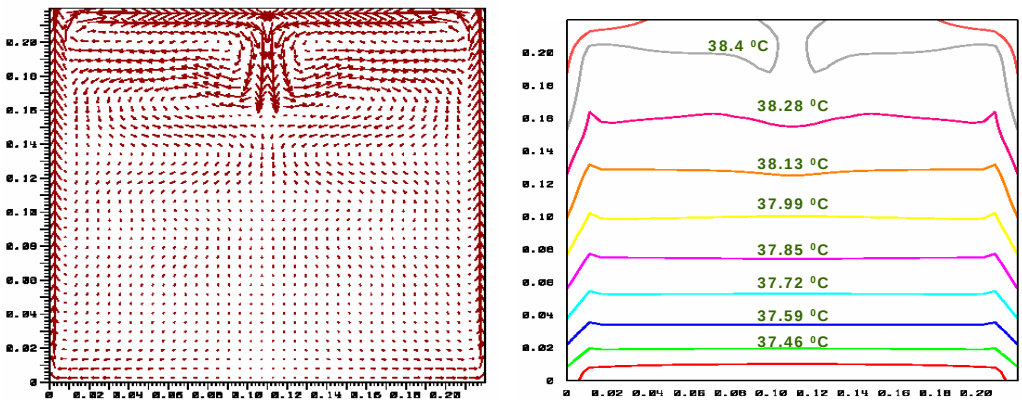

Velocity vectors after 15000 s Temperature Contours after 15000 s

FIG. 3.1-19. Numerical simulations using CFD Package TRIO-U.

Numerical simulations for this case using CFD package TRIO-U are also checked for possible modeling inaccuracies by comparing the results against the reported data. The results generated by the code for two different heat flux values (and hence, two different Rayleigh numbers) were found to be in reasonable agreement with the reported data for respective tests.

To simulate the 3-D behaviour in the zone between two cylindrical heaters, another case for which experimental data has been reported was selected. The case consisted of two equally heated cylindrical rods located inside the domain while all the enclosing walls were maintained adiabatic. For simulating this case, both the CFD packages PHOENICS (3.6) & TRIO-U were used. The results are in general very similar.

3.1.4. Theoretical basics of the simulations

3.1.4.1. Single phase flow

a) Governing equations

The governing equations for a CFD simulation are for the mass:

$$\frac{\partial \rho}{\partial t} + \frac{\partial}{\partial x_i}\left(\rho U_i\right) = 0 \tag{3.1-1}$$

for the momentum:

$$\frac{\partial}{\partial t}\left(\rho U_i\right) + \frac{\partial}{\partial x_j}\left(\rho U_i U_j\right) = B_i - \frac{\partial P}{\partial x_i} + \frac{\partial \tau_{ij}}{\partial x_j} \tag{3.1-2}$$

whereby B_i are body forces e.g. $B_i = \rho g_i$ for the gravity,

and for the energy:

$$\frac{\partial}{\partial t}\left(\rho H\right) + \frac{\partial}{\partial x_j}\left(\rho U_j H\right) = \frac{\partial}{\partial x_j}\left(\Gamma \frac{\partial H}{\partial x_i}\right) + S \tag{3.1-3}$$

b) Bossinesq approximation

For many practical applications, the dependency of the density ρ on the pressure P can be neglected and the dependency on the temperature can be expressed as

$$\rho = \rho_0\left(1 + \beta \Delta T\right) \tag{3.1-4}$$

$\beta\Delta T << 1$ is a precondition for the validity of this approach known as the Boussinesq-Approximation. β is the heat expansion coefficient.

c) Turbulence

The relation between buoyancy and flow resistance is described by the Rayleigh Number

$$Ra = \frac{g\beta}{\nu a}\Delta T L^3 \tag{3.1-5}$$

For flow conditions exceeding a Rayleigh Number of 10^{10} the flow is assumed to be turbulent.

The decomposition of all instantaneous flow quantities in their mean and fluctuating part according to $a = \overline{a} + a'$ and applying it to the basic conservation equations results in a set of equations similar for laminar flow. The variables are replaced by the mean part of the flow quantities. The fluctuating parts are either averaged to zero or their products yield new terms, namely the Reynolds stress $-\overline{\rho U_i' U_j'}$ and the Reynolds flux $-\overline{\rho U_i' H'}$. The Reynolds stress is calculated according to the eddy viscosity hypothesis as a linear function of the rate of the deformation tensor:

$$-\overline{\rho U_i' U'}_j = \mu_T\left(\frac{\partial \overline{U}_i}{\partial x_j} + \frac{\partial \overline{U}_j}{\partial x_i}\right) - \frac{2}{3}\rho k \delta_{ij} \tag{3.1-6}$$

with the eddy viscosity μ_T. The Reynolds flux is calculated as linearly dependent on the mean total enthalpy gradient:

$$-\overline{\rho U_i' H'} = \Gamma_T \frac{\partial \overline{H}}{\partial x_i} \tag{3.1-7}$$

Γ_T is the turbulent heat diffusivity:

$$\Gamma_T = \frac{\mu_T}{\sigma_T} \tag{3.1-8}$$

σ_T is the turbulent Prandtl Number.

The very often used K-Epsilon Turbulence model relates the eddy viscosity to the turbulent kinetic energy k and the turbulent dissipation ε by:

$$\mu_T = C_\mu \rho \frac{k^2}{\varepsilon} \tag{3.1-9}$$

Additional transport equations for k and ε have to be solved. This model has a large validation database and yields adequate results for many industrial applications.

d) Problems of CFD simulation of natural circulation in large pools

For the case of simulating natural circulation in large pools the following problems arise, which have to be solved and requires additional model development:

Depending on the flow situation for higher Rayleigh Numbers (see Eq. 3.1-5) the range of validity of the Boussinesq approximation (see Eq. 3.1-4) might be exceeded.

The calculation of the Reynolds stress and the Reynolds flux is based on isotropic approaches. According to the eddy viscosity hypothesis, values which are tensors are modelled by scalars (see Eq. 3.1-6 and 3.1-7). For natural circulation, however, the gravity plays an important role which requires an anisotropic simulation. The following different solutions are possible:

- The K-Epsilon Turbulence model is extended by additional components considering the isotropic nature of gravity. Whereas the computational effort remains reasonable, this modelling approach requires additional validations for different flow situations.
- The Reynolds stresses are not approximated as a scalar but simulated as a tensor. Different approaches of Reynolds stress models are known. The computational effort is increased but might be accepted, keeping in mind the increased power of modern computers. Additional model validation is necessary.
- Whereas the Reynolds averaging is extended over the full range of turbulent scales, the Large Eddy Simulation (LES) approach allows only small scales to be averaged by filtering whereas large turbulent scales are simulated directly. Meeting the requirements of mesh size and time step resolution the additional computational effort is remarkable and limits the application to industrial problems.
- Direct Numerical Simulation (DNS) requires no averaging approximation. The computational effort increases remarkably. The method is successfully applied to calculate benchmark solutions for limited well specified problems. These can be used for validation of the model extensions mentioned above.

3.1.4.2. Two phase flow

In the case of higher heat fluxes, a phase transition by boiling occurs and the flow has to be simulated as two phase. For lower gas content, the application of the Euler/Eulerian multifluid model is very

popular. The phases are considered interpenetrating each other. For each phase the full set of equations (see Eq. 3.1-1–3.1-3) is solved. In each computational cell the volume fractions of all phases is summarized to 1. For the governing equations, exchange terms between the phases have to be considered:

The flow resistance of bubbles in a fluid is considered as additional source in the momentum equation. Besides these drag forces, the so called non-drag forces, which are acting perpendicular to the flow direction, play an important role for the flow regime. The lift force is the interaction of the bubbles with the liquid flow gradient. The action of turbulence structures on the gas is expressed by the turbulence dispersion force. In near wall regions, the wall force pushes the bubbles away from the wall. The influence of bubbles on the turbulent liquid flow is considered in an increase of the eddy viscosity.

Dependent on the difference of the liquid from the saturation temperature either evaporation or condensation has to be considered. These mass transfer rates depend on the interfacial area which is determined by the bubble size.

Dependent on the flow situation, the bubble size can be simulated using a constant size. More realistic simulations model considers the bubble size as a function of liquid temperature. For higher gas content, the application of a bubble population balance model is necessary, particularly when additional dependence of the bubble forces on the bubble size has to be considered. An alternative approach, the momentum method, considers the size distribution with a distribution function.

When the heat is transferred via a wall, considering the heat transfer by single phase convection only underestimates the vapour generation. Instead a wall boiling model has to be applied that considers , in addition to single phase convection, heat transfer by evaporation and, when a vapour bubble leaves the wall, heat transfer by quenching.

3.1.5. Comments on code capabilities

Because of the three dimensional nature, the simulation of the phenomena in large pools requires the application of a CFD code. In recent years the capability of CFD codes was demonstrated for single phase problems (e.g. simulating mixing phenomena in the primary circuit of a nuclear reactor; see also Section 3.11 Boron mixing). Significant progress was made in the field of multiphase CFD. This includes experiments, applying new measurement techniques to gain the necessary data for CFD model development and validation (e.g. at TOPFLOW [3.1-11, 3.1-17]) and in the field of CFD simulations [3.1-18] (e.g., work done in the European Project NURESIM).

The competiveness of CFD is continuously growing due to the rapid development in computer technology. However, computer capacity is still, and will be for the foreseeable future, a limiting factor for CFD calculations to produce completely accurate results. Simplified models for describing turbulence have to be used and current computer capacity places restrictions on the resolution (in space and time) that one can use in a CFD calculation. This leads to modelling errors and numerical errors that contribute to inaccurate results. Validation of the quality and confidence in different approaches in CFD calculations are therefore needed. The so-called best practice guidelines (BPG) have to be used for quality assurance of the validation calculations [3.1-19]. The BPG are based on the concept of error hierarchy. The different types of errors in CFD simulations are divided into two main categories:

- Numerical errors, caused by the discretization of the flow geometry and the model equations, and by their numerical solution
- Model errors, which arise from the approximation of physical processes by empirical mathematical models

This concept implies that numerical errors can be quantified and reduced to an acceptable level, before comparison with experimental data is made. That means the CFD solution has to be shown to be grid-

independent, i.e. the results do not change significantly when the grid is further refined. A grid-independent solution can be defined as a solution that has an error that is within a range that can be accepted by the end-user, depending on of the purpose of the calculations.

The state and limits of CFD simulation of natural circulating phenomena was described in Section 3.1.4. A grid independent CFD solution simulating containment phenomena in a fully three dimensional representation can only be achieved by a significant computational effort. Dependent on the problem to be solved, however, the effort can be reduced by focusing on the description of the main physical mechanisms. For the case of temperature stratification phenomena, circulating fluid flows play an important role. In certain cases these circulating flows can be described considering only a two dimensional plane of the fluid domain. This procedure was demonstrated for the NOKO facility and TOPFLOW facility simulations for the heating up processes in a horizontally oriented cylinder (see Sections 3.1.3.4 and 3.1.3.5). The simulation in a 2D representation yields good agreement with the measurements (see Fig. 3.1-10). The same was shown for the example of a side wall heated tank (see Section 3.1.3.6).

In cases where turbulence plays no role, the circulating flow processes can be described by lumped parameter codes. The limited numerical effort enables faster solutions respective to the investigation of variations of the boundary conditions.

In recent developments, efforts have been made to couple codes of different scale resolution such as coupling CFD with system codes (e.g. lumped parameter system codes). In these cases, the advantage of an overall system description is combined with the advantage of the detailed CFD description of the most important phenomena.

REFERENCES FOR SECTION 3.1

[3.1-1] LUEBBESMEYER, D., AKSAN, N., ISP-42 PANDA Tests: Behaviour of Passive Containment Systems During the Long term Heat Removal Phase In Advanced Light Water Reactors; Blind Phase Comparison Report, OECD/NEA Report, NEA/CSNI/R(2003)6 (2003), CD-ROM.

[3.1-2] LUEBBESMEYER, D., AKSAN, N., ISP-42 PANDA Tests: Behaviour of Passive Containment Systems During the Long term Heat Removal Phase In Advanced Light Water Reactors; Open Phase Comparison Report, OECD/NEA Report, NEA/CSNI/R(2003)7 (2003), CD-ROM.

[3.1-3] ISHII, M., et al., Scientific Design of Purdue University Multi-Dimensional Integral Test Assembly (PUMA) for GE SBWR, NUREG/CR-6309, PU-NE 94/1 (1996).

[3.1-4] CHENG, L., WOO, K.S., ISHII, M., LIM, J., HAN, J., Suppression pool mixing and condensation tests in PUMA facility, Int. Conf. on Nuclear Engineering ICONE14, July 2006, Miami, Florida, USA, paper ICONE14-89348 (2006).

[3.1-5] WOODS, B., NELSON, K., REYES, Jr., J.N., Phenomena 13: Behaviour of Emergency Heat Exchangers and Isolation Condensers, 4th RCM on the IAEA CRP on Natural Circulation Phenomena, Modeling and Reliability of Passive Safety Systems that Utilize Natural Circulation, September 10-13, 2007, IAEA, Vienna (2007).

[3.1-6] HICKEN, E.F., VERFONDERN, K., Investigation of the Effectiveness of Innovative Passive Safety Systems for Boiling Water Reactors, Forschungszentrum Jülich, Series Energy Technology Vol. 11, ISBN 3-89336-263-0 (2000).

[3.1-7] JAEGERS, H., European BWR R&D Cluster for Innovative Passive Safety Systems-WP2: NOKO Experiments for Code Calculations, INNO-IPPS(907)-D-0, Forschungszentrum Jülich (1997).

[3.1-8] HICKEN, E.F., JAEGERS, H., KOSCHMIEDER, R., VERFONDERN, K., Pool Heat-Up Experiments: Experimental Results from NOKO-EC Tests, INNO-IPSS(99)-D-2.1.9. (2000).

[3.1-9] KREPPER, E., HICKEN, E.F., JAEGERS, H., Investigation of Natural Convection in Large Pools, International Journal of Heat and Fluid Flow **23** (2002) 359–365.
[3.1-10] KREPPER, E., SCHAFFRATH, A., ASZODI, A., Numerical simulation of the emergency condenser of the SWR-1000, Nuclear Science and Engineering **135** (2000) 267–279.
[3.1-11] PRASSER, H.-M., et al., The multipurpose thermalhydraulic test facility TOPFLOW: an overview on experimental capabilities, instrumentation and results, Kerntechnik **71** No. 4 (2006) 163–173.
[3.1-12] ASZÓDI, A., KREPPER, E., PRASSER, H.-M., Experimental and numerical investigations of one and two phase natural convection in storage tanks, Heat and Mass Transfer **36** (2000) 497–504.
[3.1-13] ASZÓDI, A., Modelling of transient natural convection – Thermal-hydraulic analysis for an accident of dangerous fluid storage tanks, PhD. Thesis, Technical University Budapest (1997).
[3.1-14] KREPPER, E., ASZODI, A., PRASSER, H.-M., Experimental and numerical investigations of one and two phase natural convection in storage tanks, 4th International Conference on Multiphase Flow, New Orleans (2001) paper 515.
[3.1-15] SHATISH KUMAR, N.V., et al., Theoretical Studies on Thermal Stratification in a Side Heated Cavity, Kerntechnik **70** (2005) 3.
[3.1-16] SAHA, D., SINHA, R.K., Thermal Hydraulic Studies on the Passive Systems of Advanced Heavy Water Reactor, Global Conference 2005, Tsukuba, Japan, Oct. 9-13, 2005.
[3.1-17] PRASSER, H.-M., et al., Influence of the pipe diameter on the structure of the gas/liquid interface in a vertical two-phase pipe flow, Nuclear Technology **152** (2005) 3–22.
[3.1-18] LUCAS, D., TISELJ, I., HASSAN, Y. A., MORETTI, F., Computational fluid dynamics for gas–liquid flows, Science and Technology of Nuclear Installations, Vol. 2009 (1).
[3.1-19] MAHAFFY, J., et al., Best Practice Guidelines for the Use of CFD in Nuclear Reactor Safety Applications, NEA/CSNI/R(2007)5, May 2007.

3.2. EFFECT OF NON-CONDENSABLE GASES ON CONDENSATION HEAT TRANSFER

Condensation plays a key role in removing heat in many industrial applications. The presence of even a small amount of non-condensable gas in the condensing vapour leads to a significant reduction in heat transfer during condensation. In nuclear plants, the condensation of steam in the presence of non-condensable gas becomes an important phenomenon during LOCA when steam released from the coolant system mixes with the containment air. In addition, ingress of small amount of air affects the performance of the power plant condensers. The effect of non-condensable gases on the condensation of steam has been studied for various geometries (e.g. tubes, plates, annulus, etc.) for these applications. The phenomena have been investigated experimentally and theoretically. A number of correlations have been developed and incorporated in the computer codes available for thermohydraulic analysis of the various systems.

3.2.1. Introduction

Condensation on cooling surfaces is a phenomenon of great importance for a number of passive safety systems to reject heat to a sink. It is one of the most effective passive cooling mechanisms of containments of advanced water cooled reactors. Containment of a nuclear reactor is a key component of the mitigation part of the defence in depth philosophy, since it is the last barrier designed to prevent large radioactive releases to the environment. To provide safety-grade heat sink for preventing the containment from exceeding its design pressure, passive systems with condensing steam are utilized. The presence of non-condensable gas in containment affects the steam condensation. The other important system encountering condensation in the presence of non-condensable gas is the condenser. The presence of non-condensable gas greatly influences the condensation process warranting in-depth study of the phenomena.

3.2.2. Scenario

In this brief outline of the scenario, the condensation mechanism followed by the effect of non-condensable gases is presented.

The phenomenon takes place during LOCA or a main-steam-line-break (MSLB) accident, or any other accident that causes a coolant release into the containment. During such accidents, large amount of steam is released into the containment which mixes with the non-condensable gases. There are cooling surfaces provided for condensing the steam from steam/non-condensable gas mixture. During the condensation process, the steam condenses on the surfaces, while the non-condensable gases are accumulated on the film condensate layer creating an additional thermal resistance. This gas layer acts like a barrier resulting in a degradation of the heat transfer to the wall.

In the design and operation of a steam turbine the exit temperature of the process fluid is kept as low as possible so that a maximum change in enthalpy occurs during the conversion of heat into work. The presence of small proportion of air in the vapour can reduce heat transfer performance in a marked manner which increases the condenser pressure.

Two distinct forms of condensation on surfaces are observed: film condensation and dropwise condensation as shown in Fig. 3.2-1.

In film condensation the condensate wets the surface and forms a liquid film on the surface while in dropwise condensation the condensed vapour forms droplets on the surface instead of a continuous film and the surface is covered by countless droplets of varying diameters.

In film condensation the surface is blanketed by a liquid film of increasing thickness and this “liquid wall” between solid surface and the vapour serves as a resistance to heat transfer. The heat of vaporization released, as the vapour condenses, must pass through this resistance before it can reach the solid surface and be transferred to the medium on the other side. In dropwise condensation part of the surface is in contact with vapour leading to higher heat transfer rates.

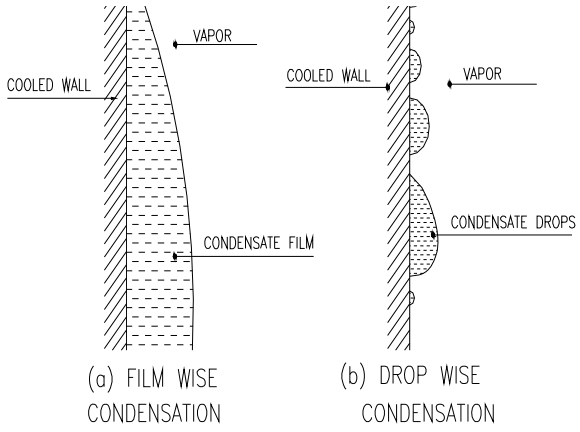

FIG. 3.2-1. Filmwise and dropwise condensation.

However, attempts to achieve sustained dropwise condensation have not been very successful in most of the industrial applications. Therefore the common practice is to assume filmwise condensation in heat transfer equipments for conservatism. Hence, further discussions will be related to filmwise condensation. The influence of non-condensable gas which acts as a barrier between the vapour and the condensate layer is shown in Fig. 3.2-2.

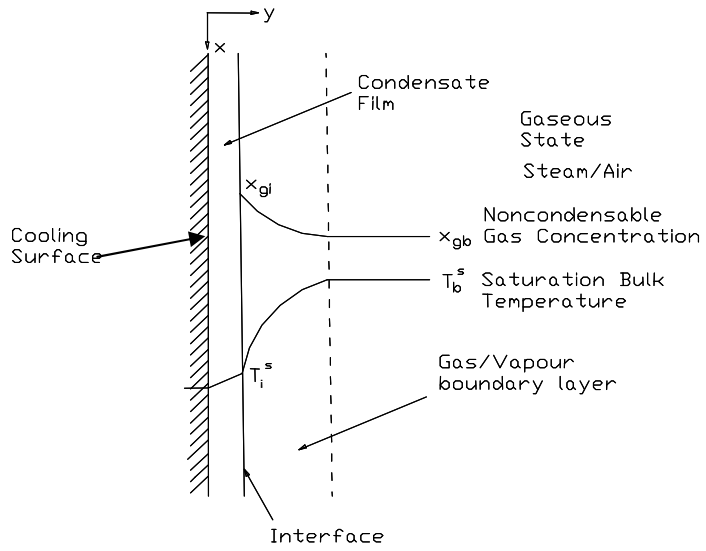

FIG. 3.2-2. Schematic illustration of the present filmwise condensation model.

The most important factor affecting the condensation is the amount of non-condensable gas present in the steam/non-condensable gas mixture. An air mass fraction of 1% can reduce heat transfer to 50% in static conditions [3.2-1]. After a typical postulated LOCA, the steam released from the primary coolant circuit mixes with reactor containment air which inhibits the condensation process. The release of additional air may occur from instrument lines. During a severe accident, hydrogen, a non-condensable gas, may be generated due to metal–steam reaction and radiolysis of water. If hydrogen is released into the containment, there will be a shift in the composition that will affect both locally and globally the condensation phenomenon; locally, due to the change in the diffusion coefficient and in the driving buoyancy force from the bulk to the interface and globally, due to the hydrogen lower density, that can cause a barrier that will produce a strong decrease in the heat transfer coefficient. The other sources of non-condensable gases are accumulator nitrogen, fission gases, etc., but their effect is very small.

The effect of non-condensable gases on the condensation of steam depends on flow regime for both natural and forced convection flows. In addition, the geometries (e.g. tubes, plates, annulus, etc.) and the flow orientation (horizontal, vertical) can be different for various natural and forced circulation applications. Other phenomena affecting condensation are suction effect, waviness of the film, and mist formation in the vapour.

3.2.3. Examples of hardware

A drastic reduction in the condensation heat transfer coefficient is observed in the presence of non-condensable gas and is a concern in industrial applications. A few examples are given below.

3.2.3.1. Passive containment cooling system

The most important hardware related to this phenomenon is the Passive Containment Cooling System (PCCS). PCCS provides a passive means for post-accident decay heat removal from containment during a long term cooling period. The purpose of the PCCS is to limit the containment pressure to a value below a predetermined level and to achieve a grace period without operator action. There are several PCCS concepts that evolved in recent years. In these systems, the transfer of heat from the containment building to the environment is affected by employing either evaporation of water from

water pools or natural draft cooling of containment structures. Some of the design concepts of PCCS are given below.

3.2.3.1.1. PCCS with passive containment coolers

The isolation condenser (IC) was originally designed for early BWRs to prevent reactor overpressurization and to remove decay heat during reactor isolation transient events, without losing coolant from RPV. A similar concept [3.2-2] has been adopted in the simplified BWR (SBWR) for passive containment cooling. The PCCS consists of steam/non-condensable gas inlet line from the dry well, the PCC, condensate return lines to the RPV, and non-condensable gases vent line to the suppression pool, which are used to purge non-condensable gas from the PCCs. The PCC pool is located above the main steam lines to allow the condensed water to flow down by gravity to the vessel. The condensate return line and non-condensable gas vent line have no valves.

3.2.3.1.2. PCCS with building condenser

For the long term decay heat removal from the containment of the SWR-1000 [3.2-3], building condensers are provided above each of the four flooding pools. At later stages in an accident transient, generation of steam can lead to a rise in temperature and pressure inside the drywell. Steam then starts condensing on the finned tubes of the condenser which limits the containment pressure and temperature. The secondary side of the building condenser is permanently connected to the dryer-separator storage pool located above the containment by feed and return lines. Consequently, the primary side steam condensation initiates the development of secondary side natural circulation. A purge line is also provided from dry well to wet well to avoid accumulation of non-condensable gas close to building condensers. In the Indian AHWR, the PCCS [3.2-4] consists of passive external condensers (PECs) which are connected to a gravity driven water pool above it. The steam condenses on the outer surface and water flows by natural circulation inside the condenser tubes.

3.2.3.2. Power plant condenser

The condenser has long been known as an important integral component of the steam heat engine cycle. The first and most vital objective arises directly from heat engine theory and calls for providing the lowest possible temperature at heat rejection or exhaust end of the cycle. Hence, these condensers are designed to operate at the highest possible vacuum to get maximum cycle efficiency. The major part of heat rejection is achieved under saturated conditions. Ingress of air causes rise in condenser pressure and thereby reduction in condenser efficiency.

3.2.4. Literature review

In general, condensation of steam is important with stagnant and flowing steam/non-condensable gas mixture. In case of stagnant steam/non-condensable gas mixture, the steam condensation is caused by free convective heat transfer. On the other hand, for condensation with flowing steam/non-condensable gas mixture, forced convection plays an important role. The effect of non-condensable gas is much less in case of moving steam–gas mixture compared to stagnant mixture. This is because of the motion of the mixture, which causes sweeping of the non-condensable gas from the zone next to the interface, thereby resulting in a reduction of its concentration in the boundary layer.

The heat transfer rate increases with the Reynolds number and vapour concentration. The enhancement effect of various parameters like suction, film roughness, development length and calculation of mixture properties by various methods were considered by the researchers.

Apart from experimental technique, the researchers generally employ two approaches to the analysis. The first approach solves the governing equations in the boundary layer. The second approach considers the mass and energy balance at the interface and application of heat and mass transfer analogy. The thermal resistances in condensate film and gas/vapour boundary layer are estimated by

correlations along with heat and mass transfer analogy. A literature survey based on most of the methods is given in the following sections.

3.2.4.1. Experimental studies on condensation in presence of non-condensable gases

3.2.4.1.1. Condensation of steam in a stagnant environment

Othmer [3.2-1] carried out one of the earliest experiments and measured the heat transfer rate for a 76.2 mm (3″) diameter and 1.22 m long copper tube placed in a stagnant air/steam environment. An empirical correlation was derived relating the heat transfer coefficient to air/steam partial pressure ratio and temperature difference between the cooled surface and stagnant air/steam mixture. Othmer found that the heat transfer coefficient would decrease by 50% when a little amount of air (0.5%) was added to the steam chamber.

Al-Diwani and Rose [3.2-5] used a small glass chamber in which a stagnant mixture of steam and non-condensable gases was allowed to come in contact with a cooled vertical plate (size 97 mm × 97 mm). The gases used included air, argon, neon and helium. The reported results pertain to a natural convection flow regime and show good agreement with other published data.

The effect of surface orientation on steam condensation in the presence of air has been studied by Huhtiniemi et al. [3.2-6]. The orientation of the condensing surface was varied from 0 to 90° (plate surface facing down at 0°). The authors observed that by tilting the condensing surface from the horizontal to vertical position, the heat transfer coefficient decreased by 15–25% depending on the mass fraction.

Dehbi et al. [3.2-7] conducted experiments with steam/air mixture under turbulent natural convection conditions. Their condensing section consisted of a 3.5 m long, 38 mm diameter copper cylinder located concentrically inside a 5 m long, 0.45 m diameter stainless vessel. The authors observed that the heat transfer coefficient increased significantly with the total pressure of the mixture. The wall subcooling and length effects were found to be of secondary importance.

Liu et al. [3.2-8] performed experiments in the presence of air and helium to evaluate the heat removal capacity of a passive cooling unit. Condensation heat transfer coefficient on a vertically mounted smooth tube (40 mm diameter and 2 m long) was determined for the pressure range from 0.248 to 0.455 MPa and air mass fraction from 0.3 to 0.65. An empirical correlation for heat transfer coefficient was developed in terms of a steam mole fraction, total pressure and wall subcooling. They compared experimental data with the Peterson's diffusion layer model and found that experimental data are in good agreement with the model. They also compared with the Uchida correlation and found that the experimental heat transfer coefficient is 2.2 times higher than estimated by Uchida heat transfer correlation. Experiments with an axial shroud around the test section tube to model restriction on the radial flow showed a reduction in the heat transfer coefficient by a factor of about 0.6. In all the experiments the cooling water inside the tube was kept near saturation. Heat was transferred from the non-condensable gas/vapour mixture outside the tube to the two phase cooling water, which maintained natural convection between the tank and tube. The heat transfer rate was obtained by measuring the liquid level change in the tank by gravity separation of the steam water mixture.

Anderson et al [3.2-9] performed experiments on condensation onto the internal surfaces of two scaled vessels with similar aspect ratios to the actual AP600. The heat transfer rate in the presence of non-condensable gas was analysed for different non-condensable mixtures of air and helium. The effect of orientation of condensing surface (0.91 m characteristic length) was found to be small.

Maheshwari et al. [3.2-10] performed experiments on a horizontal tube of diameter 21.3 mm and length 0.75 m to study the effect of non-condensable gas on steam condensation. The characteristic length (diameter) of the tube was maintained similar to that of the passive external condenser of the AHWR. The tube was installed horizontally in a cylindrical vessel which was partially filled with water. The water was heated electrically to produce steam which mixed with the air present in the

tank. The cooling water was flowing inside the condensing tube. The effect of pressure, air mass fraction and wall subcooling was studied.

Abdullah [3.2-11] performed experiments on condensation on a bank of horizontal tubes in the presence of a non-condensable gas. The reduction in heat transfer was attributed to the accumulation of non-condensable gas towards the bottom of the tube bank in place of expected reduction in heat transfer due to condensate falling on tubes in case of pure steam condensation.

3.2.4.1.2. Condensation of steam inside vertical tubes

Recently a number of forced convection in-tube condensation experiments in the presence of a non-condensable gas have been performed. The reported results are in the form of very simple empirical correlations, which relate the reduction in the overall pure vapour heat transfer coefficient to the amount of non-condensable gas present at the inlet to the tube.

Votta and Walker [3.2-12] performed experiments for forced convection flow down a vertical tube with 25.4 mm inner diameter (ID) and 1 m long. All tests were conducted at atmospheric pressure with vapour flowing downward. The experiments were conducted for Steam-air, steam-carbon dioxide, steam-helium, etc. Morgan and Rush [3.2-13] measured average heat transfer coefficients for forced convection condensation of air/steam and helium/steam mixtures inside a vertical tube (14.1 mm ID, 1.52 m condensing length) at pressures ranging between 11 and 133.8 atmospheres. They found that at these high pressures the non-condensable gas also diffused into the condensate layer. They also found that for a laminar vapour flow with inlet non-condensable gas mass fraction of less than 0.7% by mole fraction, non-condensable gas caused severe degradation in heat transfer. About more than 15% reduction in heat transfer coefficient was found as compared to heat transfer coefficient calculated for the pure vapour Nusselt analysis. In turbulent vapour flow with mole fraction up to 3.5%, a small to moderate degradation in heat transfer coefficient was found (<15% reduction compared to heat transfer coefficient calculated for pure vapour by Nusselt analysis).

Nagasaka et al. [3.2-14] and Kataoka et al. [3.2-15] performed experiments in GIRAFFE (a full-height test facility simulating SBWR containment with PCCS at Toshiba Ukishima Site) as well as theoretical analysis to study the effect of non-condensable gases (nitrogen and helium). The passive containment cooler of the facility consisted of three full scale tubes (47.5 mm ID, 2.54 m long) of SBWR. The non-condensable gas effect was defined in terms of degradation coefficient (ratio of heat transfer coefficient when non-condensable gas is present to that of pure steam) as a function of nitrogen or helium partial pressure. Masoni et al. [3.2-16] conducted experiments in the PANTHERS test facilities using a full scale prototype of PCC of SBWR. The thermohydraulic performance in terms of condenser efficiency (ratio of condensate flow rate to inlet steam flow rate) as a function of inlet pressure and air mass fraction was presented. Steady state tests (B series) [3.2-17] were conducted in the PANDA test facility to determine the condenser efficiency affected by the presence of non-condensable gas.

Information about local heat transfer is needed when the heat transfer coefficient decreases drastically down the tube length. The overall heat transfer correlations derived from the above tests are suitable only for the systems used in deriving them. Extrapolation to other situations where the tube diameter, the tube length, or the flow velocity is different is not valid because these correlations do not address these variables. The effects of non-condensables on the local condensation heat transfer coefficient inside vertical tubes have been investigated by many researchers. The correlations developed for the calculation of local heat transfer coefficient inside vertical tubes are expressed in terms of non-dimensional parameters such as Nusselt number, film Reynolds number, gas/vapour Reynolds number, Prandtl number, Jakob number, air mass fraction, etc.

Ogg [3.2-18] measured local heat transfer coefficients in a vertical circular metallic tube having cooling length of 2.44 m. The inner diameter (ID) of the tube was 49 mm. The tube was surrounded by annular jacket through which liquid coolant flowed upward. The experiments were performed with air/steam and helium/steam mixture. A correlation for heat transfer coefficient was developed based

on the experiment in term of Nusselt's pure steam heat transfer coefficient and a degradation factor consisting of two separate factors which involve mixture Reynolds number and air mass fraction.

Vierow [3.2-19] performed experiments to investigate the effects of air on local steam condensation rates in natural circulation in a vertical tube. Experiments were performed with inlet air mass fraction varying from 0.0 to 0.14 and vapour mass flow rate from 13 to 55 lb/hr in a vertical condenser tube (22 mm ID and 2.13 m long). The authors found that at an air inlet mass fraction of 14%, the heat transfer coefficients were reduced to one-seventh the values of pure steam. Instabilities were observed at high air contents. Vierow developed a correlation for local heat transfer coefficient in terms of a correction factor and local heat transfer coefficient based on Nusselt theory. The correction factor is obtained as a function of local condensate Reynolds number and air mass fraction. Vierow and Schrock [3.2-20] developed another correlation, which includes the effects of non-condensable gas and interface shear on condensation.

Hasanein et al. [3.2-21] carried out experiments on steam condensation in a vertical tube (46.0 mm ID and 2.54 m long) under forced flow conditions in the presence of non-condensable gas. They developed correlations for estimating the local heat transfer coefficient. The local Nusselt number was correlated as a function of local mixture Reynolds number, Jakob number and gas mass fraction and Schmidt number.

Siddique et al. [3.2-22] performed experiments using steam-air and steam-helium mixture under forced flow condition in a vertical tube (46.0 mm ID and 2.44 m condensing length) and developed their own correlations for both mixtures. They correlated Nusselt number as a function of mixture Reynolds number, Jakob number and air mass fraction. A comparison of air/steam results with the predictions of University of California-Berkeley (UCB) correlation [3.2-19] was made and it was found that UCB correlation is conservative at high values of mixture Reynolds number and low air mass fractions and non-conservative at low values of mixture Reynolds number and high bulk air mass fractions. Siddique et al. concluded that for the same mole fraction, compared with helium, air has more inhibiting effect on condensation heat transfer, but for the same mass ratio, helium is found to be more inhibiting.

Araki et al. [3.2-23] studied heat transfer coefficient experimentally in a vertical tube and correlated it as a function of mixture Reynolds number and air partial pressure ratio. The experimental studies were carried out for air partial pressure ratio of 0.0 to 0.24 in a 49.5 mm ID and 1.21 m long stainless steel tube. The local heat flux was estimated by using the measured inner and outer wall temperatures and the thermal conductivity of the tube [3.2-24].

Kuhn [3.2-25] performed experiments on steam condensation in the presence of non-condensable gases in a vertical tube of 47.5 mm ID and 2.4 m long (full scaled tube of SBWR PCC). The tube was jacketed in a similar manner as in the experiments carried out by Vierow [3.2-19] and Siddique et al. [3.2-22], but the calculation of cooling water axial profile was different. They measured the cooling water axial temperatures by measuring the condensing tube wall outer surface and jacketed tube wall inner surface temperatures. The results were correlated by a new correlation.

Park et al. [3.2-26] carried out experiments in a vertical tube (47.5 mm ID and 2.4 m long) in a range similar to that of Siddique et al. and correlated heat transfer coefficient as a function of liquid film Reynolds number, Jakob number and air mass fraction. The effects of pressure, steam flow rate and air mass fraction at the inlet on steam condensation were studied. The range of validity for Jakob number in the correlation is smaller than that of the correlation developed by Siddique et al [3.2-22].

Maheshwari et al. [3.2-10, 3.2-27] carried out experiments in a full scaled vertical tube (42.8 mm ID and 1.6 m long) of immersed condenser of PCCS of AHWR. The experiments were performed with natural convection of water outside the tube and with forced flow of water flowing in a cooling jacket surrounding the tube. Both experiments were performed in separate experimental set-ups. The full scale tubes of immersed condenser of PCCS were used for both experiments. In the experiment with natural convection of water outside the condensing tube, the local heat flux was estimated based on

temperature readings taken on the inside and outside of the tube wall by thermocouples brazed to the surface. In the experiment with forced flow of water, the local heat flux was estimated based on the heat received by the cooling water flowing in the jacket. The effects of various parameters like air mass fraction, steam flow and wall subcooling were studied. It was found that the local heat transfer coefficient decreases throughout the length of the tube with increase in inlet air mass fraction due to high local air mass fraction inside the tube. The difference in local heat transfer coefficients between high and low air mass fraction was reduced while moving towards the outlet of the tube due to reduction in bulk mixture temperature difference. The local heat transfer coefficient decreased as the inlet saturated steam temperature (total pressure) increased due to higher wall subcooling. A strong dependency of heat transfer coefficient on Reynolds number of the inlet mixture was also found over the range of Reynolds number from 6000 to 24000. It increases with increase in steam/air mixture Reynolds number at the inlet. Results for local heat transfer coefficient were compared with the correlations available in the literature.

Oh and Revankar [3.2-28] performed experiments for film condensation with non-condensable gas in a vertical tube. The experiments were performed with steam-air mixture in a vertical tube (26.6 mm ID and 0.984 m condensing length) submerged in a water pool where the heat from the condenser tube was removed through boiling heat transfer. Degradation of the condensation with non-condensable gas was investigated.

3.2.4.2. Theoretical studies on condensation in the presence of non-condensable gas

For theoretical analysis of the heat and mass transfer during condensation of vapour in the presence of a non-condensable gas, two methodologies are mainly employed. The first methodology is based on boundary layer analysis and the other is based on heat and mass transfer analogy. The two adjacent interacting boundary layers, namely the vapour/gas and condensate boundary layers, are considered for the condensation process in both methods. In the boundary layer analysis, the simplified governing differential conservation equations for both boundary layers are solved simultaneously to predict the heat transfer rate. Many researchers have solved these equations by different methods, namely integral analysis, similarity solutions and finite difference methods. Sparrow and Lin [3.2-29], Mincowiycz and Sparrow [3.2-30] and Denny et al. [3.2-31] solved the conservation equations for the boundary layer method.

The heat and mass transfer analogy models follow the general methodology of Colburn and Hougen [3.2-32]. In 1934, Colburn and Hougen proposed the theory that condensation mass transfer is controlled by diffusion across a thin film at which the accumulation of non-condensable gas occurs. In their methodology the main equation involves the balance at the liquid–gas interface between the heat transfer through the vapour/gas boundary layer and the heat transfer through the condensate film. The transfer of heat through vapour/gas mixture is made up of two components, the sensible heat transfer because of temperature difference between bulk vapour/gas mixture and interface and the latent heat given up by the condensing vapour. Separate models for sensible and latent heat fluxes were used. Since the film model of Colburn and Hougen requires extensive iterations to match the condensation mass flux to heat transport through the condensate film and external thermal resistances, several attempts have been made to arrive at simpler methods. However, the basis of all these modifications is still the heat balance at the interface.

The boundary layer solutions, although insightful from a theoretical point of view, are not useful for containment analysis due to their complexity. The analogy based models can be easily implemented into the nodal system codes used in the containment accident analysis and they provide insight into the phenomena.

3.2.4.2.1. Condensation in stagnant environment

As stated earlier, a large number of experiments pertaining to stagnant conditions have been reported and a number of empirical correlations were developed. Most of these correlations are applicable only for the particular systems from which they were developed. Researchers, who found shortcomings in

these correlations, suggested more mechanistic simulations of in-containment heat removal, though they are approximate. These models could result in better and more reliable estimates of the gas pressure and temperature (Krotiuk et al. [3.2-33]). Corradini [3.2-34] extended the Reynolds-Colburn analogy for heat and momentum transfer to mass and momentum transfer for both natural and forced convection turbulent condensation in the presence of non-condensable gas. In the same direction, Bunker and Carey [3.2-35] developed a model based on heat and mass transfer analogy, which compared quite favourably with experimental observations for tests simulating loss of coolant accident conditions in the primary containment of a boiling water nuclear reactor.

More recently, Peterson et al. [3.2-36] used the Clapeyron equation to develop a more compact expression of condensation heat transfer, in which the condensation driving force, based on concentration differences, was formulated as a function of temperature differences (much more convenient in heat transfer problems). Herranz et al. [3.2-37] suggested an improved model of condensation heat transfer on surfaces based on Peterson's approach. They analysed the experimental data of Anderson et al. [3.2-38] and Dehbi [3.2-39] by the improved model.

Peterson [3.2-40] provided the theoretical basis for the Uchida correlation for condensation in reactor containment. The theory presented showed that the Uchida correlation can produce substantial error for bulk gas densities other than the constant gas density at one atmospheric air pressure. They concluded that the heat removal rate is under-predicted for bulk gas pressures greater than 1 atmosphere. When non-condensable gas becomes concentrated in containment sub-volumes, this under prediction generates a non-conservative error in the calculation in the heat removal rate.

Peterson [3.2-41] analysed condensation of steam in the presence of multicomponent non-condensable gases. He presented a fundamental analysis of the mass transport with multiple non-condensable species.

Maheshwari et al [3.2-42] developed a theoretical model for the condensation of steam in the presence of non-condensable gas in a stagnant atmosphere. The variations of wall subcooling, pressure, non-condensable gas mass fraction in the bulk, etc. were studied. Comparisons with the experimental data and correlations available in the literature were made.

The European designs for new generation of nuclear reactors (EPR and SWR-1000) incorporate passive systems to enhance heat removal by employing condensers having finned tubes. The researchers realized that condensation heat transfer is enhanced by using finned tube. However, a few researchers felt that heat transfer may be poor due to the accumulation of water between the fins. Herranz [3.2-43] et al. developed a model capable of predicting condensation of cross flow air-steam mixture onto a single horizontal fined tube. They performed a comparative study with the experimental data available in literature for heat transfer coefficient in presence of non-condensable gas.

Sun et al. [3.2-44] performed experiments on two phase annular flow at various pressures in a 9.5 mm vertical tube under conditions of evaporation and condensation. The main aim of the experiments was to understand the mechanism of heat transfer in annular flow by distinguishing between convective mechanism in high quality region and alternative hypothesis in which heat transfer is enhanced by secondary nucleation in the region. They concluded that secondary nucleation mechanism does not play a significant role in evaporation and condensation.

Hart et al. [3.2-45] performed experiments in the AIDA (Aerosol Impaction and Deposition Analysis) experimental facility of PSI to investigate the degradation of passive decay heat removal due to fission product aerosols deposited on the inside surfaces of the PCC (Passive Containment Cooler) heat exchanger tubes. The test performed revealed that the degradation of heat transfer in the PCC tubes due to the deposition of SnO2 aerosols reached about 20 %.

3.2.4.2.2. Condensation inside vertical tubes

For theoretical analysis of in-tube condensation of vapour in the presence of a non-condensable gas, the heat and mass transfer analogy models with the general methodology of Colburn and Hougen [3.2-32] is widely used.

Peterson et al. [3.2-36] developed a mechanistic model by combining the thermal resistance of the liquid and gas/vapour sides in series to evaluate the total heat transfer coefficient. The heat transfer coefficient of the liquid film was estimated using the Balangatti's correlation [3.2-46]. The mass transfer and the sensible heat transfer in the gas/vapour side were estimated by the Dittus-Boelter equation [3.2-47], using the heat and mass transfer analysis. They derived an empirical method for estimating condensation heat transfer based on equivalent thermal conductivity due to condensation, derived from thermodynamic relationships with several additional assumptions. Using this methodology, the mass transfer problem was recast as a heat transfer problem by defining the condensation thermal conductivity. The correlations, however, involve a large number of empirically adjusted parameters, which are attributed to the effects of mist formation, surface roughness due to film waviness and suction effect due to condensation. It involves an iterative multistep procedure and incorporates a search for the variation of the bulk and interface concentration. The predictions are compared with the experimental data from Ogg [3.2-18], Vierow [3.2-19] and Siddique [3.2-22].

A similar approach was employed by Siddique et at. [3.2-48] who analysed two phase heat transfer using an annular flow pattern with a liquid film at the wall and a turbulent gas/vapour core. The liquid-phase heat transfer was modelled by multiplying the value from the Nusselt's analysis by a factor of 1.28. Emphasis was also placed on the effects of developing flow, condensate film roughness and suction effect using the correlation given by Kays and Moffat [3.2-49] and property variation in the gas phase. The model was applied for helium/steam and air/steam mixtures separately and the theoretical results were compared with the experimental results from Siddique et al. [3.2-22].

Ghiaasiaan et al. [3.2-50] used a two-fluid model to analyse the condensation process in the presence of air as the non-condensable in a co-current two phase channel flow. The predicted results are also compared with the experimental data of Ogg [3.2-18], Vierow [3.2-19] and Siddique [3.2-22].

Hassan et al. [3.2-51] implemented the model for condensation in the presence of the non-condensable, proposed by Kageyama et al. [3.2-52] in RELAP5/MOD3, which is a computer code used for safety analysis of nuclear reactors. The theoretical results are compared with the experimental data of Siddique [3.2-22].

Herranz et al. [3.2-53] developed a model in which the new methods to estimate the film thickness were incorporated. They re-derived the effective condensation thermal conductivity by taking the Peterson's fundamental theory into account with new assumptions. In place of Dittus-Boelter correlation for heat transfer, the Ginielinsky correlation [3.2-54] was applied. The model considers the effects of high mass flux, mist and film roughness. Kuhn [3.2-55] developed a mechanistic model and the correlation for estimating the suction effect was modified based on their experiments. No et al. [3.2-56] developed a non-iterative method in which the unknown interfacial temperature needs not to be assumed beforehand. The Nusselt number for condensation heat transfer is expressed in terms of air mass fraction, Jakob number, Stanton number for mass transfer, gas mixture Reynolds number, gas Prandtl number and condensate film Nusselt number. The theoretical data are compared with experimental data of Siddique [3.2-22], Kuhn [3.2-25] and Park [3.2-26].

Maheshwari et al. [3.2-57] developed a theoretical model to study the condensation heat transfer when steam/non-condensable gas mixture is flowing in a vertical tube. The local heat transfer coefficient and local steam mass flow were calculated along the length of the tube and compared with the experimental data. The effects of the Reynolds number, interfacial shear, developing length, etc. were also studied. It was observed that the heat transfer coefficient decreased precipitously in the initial length and then slowly as the mass fraction of non-condensable gas increased along the length. The heat transfer coefficient depends strongly on the mixture Reynolds number, especially in the first part

of the condensing tube. The effect of film roughness and developing length was found to be negligible when the Moody correlation is used. Various models were used for calculating film heat transfer coefficient and interfacial friction and compared.

3.2.5. The mechanistic model

The diffusion layer model provides a convenient approach to predict the condensation rates in the presence of non-condensable gas species. During the condensation of vapour in the presence of non-condensable gas, the condensate liquid film forms near the cooled wall while at the liquid–vapour interface, the non-condensable gas accumulates. This reduces the interface saturation temperature, T_i below the bulk saturation temperature T_b. The heat flux through the condensate film, driven by the temperature difference (T_i-T_w), must be equal to the flux of latent and sensible heat to the interface from the gas/vapour mixture. The analysis of the condensation in the presence of non-condensable gas typically involves a heat balance at the liquid–gas interface. However separate models for the condensate film and gas/vapour are linked and simultaneously solved for the heat and mass transfer rates. Figure 3.2-2 shows the schematic illustration of the model.

3.2.5.1. Fundamentals of heat and mass transfer at gas/vapour boundary layer

The heat transfer through the gas/vapour boundary layer consists of the convective heat transfer and the latent heat given up by the condensing vapour. Hence, the heat transfer between the interface and the gas/vapour bulk can be written as,

$$dQ = dm_{cond} H_{fg,i} + h_g dA(T_b - T_i) \tag{3.2-1}$$

This must be equal to the rate of heat transfer from the condensate film to the tube wall, i.e.

$$dQ = h_{film} dA(T_i - T_w) \tag{3.2-2}$$

From Eqs (3.2-1) and (3.2-2)

$$q'' = h_{film}(T_i - T_w) = m''_{cond} H_{fg,i} + h_g (T_b - T_i) \tag{3.2-3}$$

where, h_g is the heat transfer coefficient for convective heat transfer from the gas phase to liquid film. The condensation heat transfer coefficient, h_{cond} can be defined as

$$h_{cond}(T_b - T_i) = m''_{cond} H_{fg,i} \tag{3.2-4}$$

From Eqs (3.2-3) and (3.2-4) we obtain,

$$q'' = h_{film}(T_i - T_w) = h_{cond}(T_b - T_i) + h_g (T_b - T_i) = (h_{cond} + h_g)(T_b - T_i) \tag{3.2-5}$$

From Eq.(3.2-5), the expression for interface temperature is given as,

$$T_i = \frac{h_{film} T_w + (h_g + h_{cond}) T_b}{h_{film} + h_g + h_{cond}} \tag{3.2-6}$$

The total heat flux from the gas to the coolant may be expressed by,

$$q'' = h_{tot}(T_b - T_w) \tag{3.2-7}$$

where h_{tot} is the total heat transfer coefficient, which is obtained from Eqs (3.2-5) and (3.2-7) as

$$h_{tot} = \left[\frac{1}{h_{film}} + \frac{1}{h_{cond} + h_g} \right]^{-1} \quad (3.2\text{-}8)$$

The convective heat transfer coefficient from gas phase to liquid film h_g is found as follows,

$$h_g = Nu \frac{k}{L} \quad (3.2\text{-}9)$$

To find m''_{cond} a mass balance at the interface is done to yield the following equation,

$$m''_{cond} = \left[-\rho D \frac{\partial W_{v,i}}{\partial y} \right]_i + W_{v,i} \left(m''_{tot} \right)_i \quad (3.2\text{-}10)$$

As the condensate surface is impermeable to the non-condensables, Eq.(3.2-9) can be simplified by putting $m''_{cond} = m''_{tot}$, as

$$m''_{cond} = \frac{\left(-\rho D \frac{\partial W_v}{\partial y} \right)_i}{1 - W_{v,i}} = h_m \frac{\left(W_{v,b} - W_{v,i} \right)}{\left(1 - W_{v,i} \right)} \quad (3.2\text{-}11)$$

where, h_m is the mass transfer coefficient. Sherwood number can be defined as

$$Sh_o = \left(\frac{h_m L}{\rho D} \right) \quad ` \quad (3.2\text{-}12)$$

replacing h_m in Eq.(3.2-11), using Eq.(3.2-10)

$$Sh_o = \frac{m''_{cond} L}{\rho D} \frac{W_{nc,i}}{(W_{nc,i} - W_{nc,b})} \text{ where, } W_{nc,i} = 1 - W_{v,i} \text{ and } W_{nc,b} = 1 - W_{v,b} \quad (3.2\text{-}13)$$

For the calculation of the various heat transfer coefficients defined above, various correlations [3.2-50, 3.2-52, 3.2-53, and 3.2-57] have been used. These correlations are based on free and forced convection phenomena to account for stagnant and moving vapour/non-condensable gas mixtures. Necessary modifications to take into account the condensate film roughness effect, suction and developing length effects for enhancing the heat and mass transfer have been taken into account [3.2-50, 3.2-52, 3.2-53, and 3.2-57].

3.2.6. Description of the experimental and theoretical studies carried out as part of the CRP

The following studies have been carried out for condensation of steam in the presence of non-condensable gas.

3.2.6.1. BARC experiments on condensation of steam in presence of air in stagnant atmosphere

The tubes of the passive external condenser (PEC) [3.2-42] of the Advanced Heavy Water Reactor (AHWR) are made up of stainless steel (SS) material of size 21.3 mm OD, 15.2 mm ID (15 NB pipe) and 3.0 m length. A stainless steel tube with the same ID and OD but with a smaller length of 750 mm was used as the condensing section for an experiment to simulate this system. The condensing section was fitted with the two elbows on both sides and connected with two pipes at right angle. These pipes

were enclosed by large diameter pipes and the annular gaps were filled with ceramic wool for insulation to avoid condensation on the side arm pipe sections of the model. The condenser model can be installed either horizontally or vertically in a vertical cylindrical vessel of size 1.0 m in inner diameter and 2.0 m in length. For horizontal installation, the condenser model was hanged from the nozzles provided in the top flange of the vessel. The condenser model can also be installed vertically through the nozzles provided in the cylindrical body of the vessel.

Figure 3.2-3 shows the schematic of the test set-up in which the condenser model is kept in horizontal orientation. A relief valve and a rupture disk were installed on the vessel to prevent overpressurization.

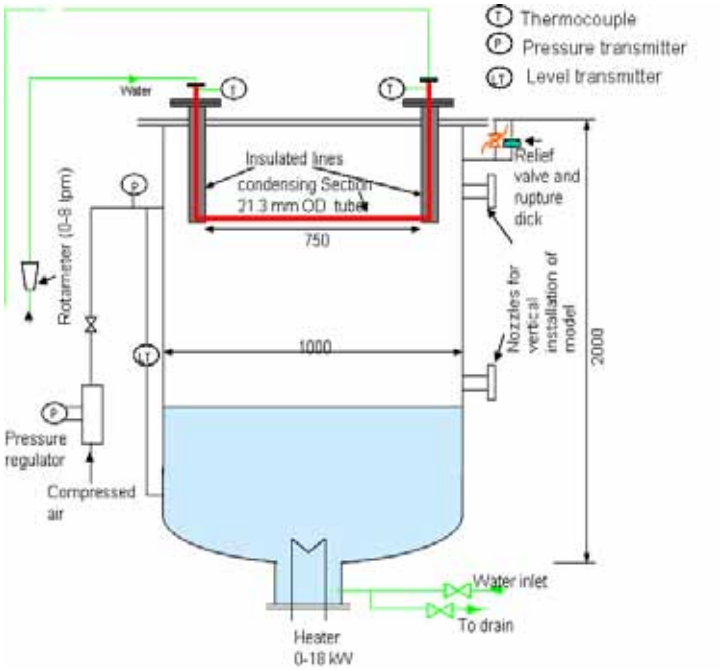

FIG. 3.2-3. Schematic of test set-up for steam condensation outside the tube.

Figure 3.2-4 shows the variation of heat transfer coefficient as a function of air mass fraction. The pressure and average wall subcooling were kept almost constant at 2.8 atm. and 55°C respectively. A comparison of theoretical heat transfer coefficient with experimental heat transfer coefficient is also given in Fig. 3.2-4. It can be seen that the prediction of heat transfer coefficient by the present model is in good agreement with experimental data. Figure 3.2-5 shows the comparison of experimental data with theoretical heat transfer coefficients.

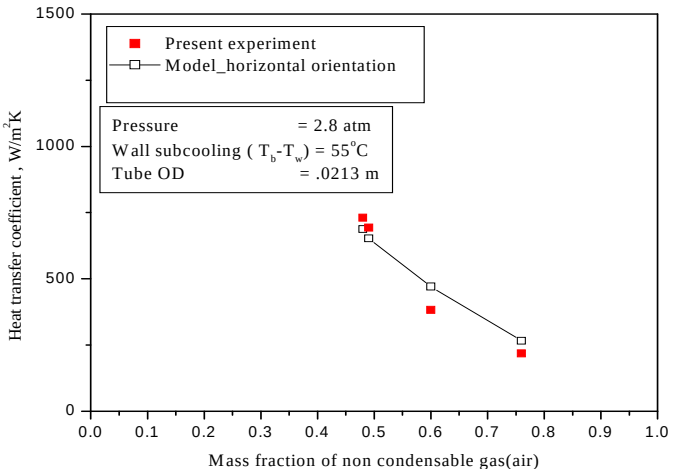

FIG. 3.2-4. Variation of heat transfer coefficient with air massfraction.

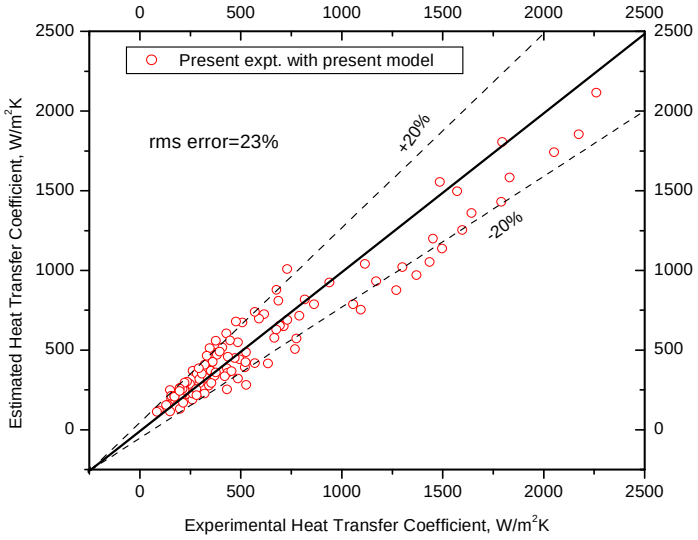

FIG. 3.2-5. Comparison between experimental and theoretical heat transfer coefficient.

3.2.6.2. BARC experiments on condensation of steam in the presence of air inside vertical tubes immersed in a water pool

Experiments [3.2-27] on condensation of steam inside the vertical tubes of a condenser have been carried out in presence of air. The condenser model consisted of 4 full-scale tubes of size 48.3 mm outer diameter, 42.76 mm inner diameter and 1.6 m length. The IC model is immersed in a pool of water. Figure 3.2-6 shows a schematic diagram of the test set-up. To determine local heat transfer coefficients and heat fluxes, the temperature differences between the inner and outer condenser tube wall was calculated from the measured temperatures of the thermocouples brazed to the tube wall.

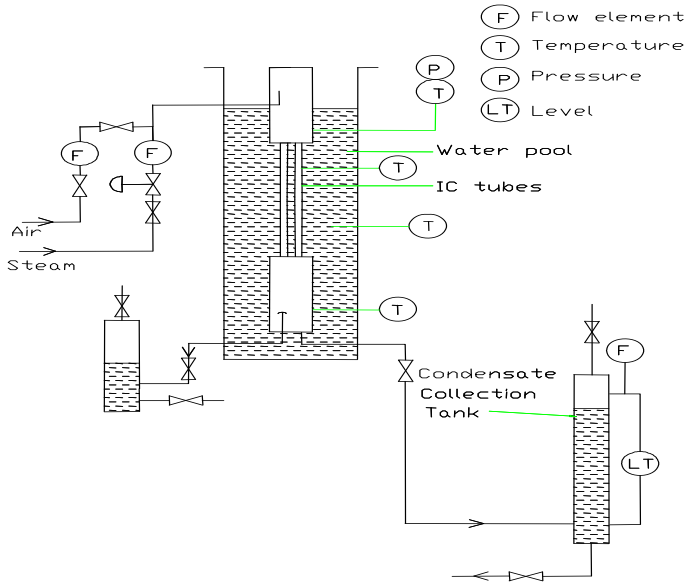

FIG. 3.2-6. Test set-up for condensation of steam in presence of non-condensable gas.

Figure 3.2-7 shows the local heat flux along the length of the tube for some of the cases analysed. The local heat flux decreases rapidly along the flow direction for all cases. This is mainly due to the increase in air mass fraction and decrease in steam/air mixture velocity along the flow direction due to steam condensation. The other reason for this can be given as the heat removal in the upper part of the tubes is through turbulent natural convection outside the tube and the heat removal in the lower part of the tubes near the exit is through laminar natural convection. During the analysis, it was found that the region for laminar heat transfer in the pool is small and it exists near the exit of the tube. The heat flux in the upper part is higher because the overall heat transfer coefficient comprising condensation of vapour in the tube and turbulent natural convection in the pool is higher than that of the lower region where the heat transfer due to condensation of steam decreases as the air content in the air-steam mixture flowing down the tube increases. Moreover, only the laminar natural convection heat transfer plays a role in the lower region of the pool (tube bottom). From Fig. 3.2-7, it can be seen that the local heat flux is higher throughout the length of the tube for the low air mass fraction due to the low local air mass fraction. For the low air mass fraction case, the wall temperature is higher due to the higher bulk mixture temperature and low local air mass fraction.

For a fixed steam inlet flow rate, Fig. 3.2-8 shows the axial variation of heat transfer coefficient at two different values of the inlet air mass fraction. Hence, in Fig. 3.2-8, the two cases having the same total pressure of $3.26 \cdot 10^5$ Pa and steam flow rate of 0.0043 kg/s in one tube with inlet air mass fractions of 0.128 and 0.248, are compared for their heat transfer coefficients. The steam flow is given in Fig. 3.2-8 as inlet mass flux of steam in kg/m^{2}s as the IC model is comprised of 4 tubes. The temperature of cooling water in the pool was nearly the same in both cases. The condensing heat transfer coefficient decreases down the length of the condensing tube because the condensation of steam decreases the total mixture flow rate and increases the air mass fraction. As shown in Fig. 3.2-8, the lower inlet mass fraction of air yields much higher local heat transfer coefficient near the inlet and higher values throughout the condensing tube. It has been observed that for lower inlet mass fraction, the local air mass fraction is maintained lower throughout the tube. Due to this local lower air mass fraction, the local heat transfer resistance through the mixture boundary layer adjacent to the condensate layer is low. As a result, the local heat transfer coefficient is higher for lower inlet mass fraction. Due to the higher value of this local heat transfer coefficient, more steam is removed from steam-air mixture flow through the condensing tube. Because of higher steam condensation, the condensate heat transfer is reduced towards the tube outlet. Hence, the difference between the heat

transfer coefficients towards the outlet of condensing tube reduces for different inlet air mass fraction cases.

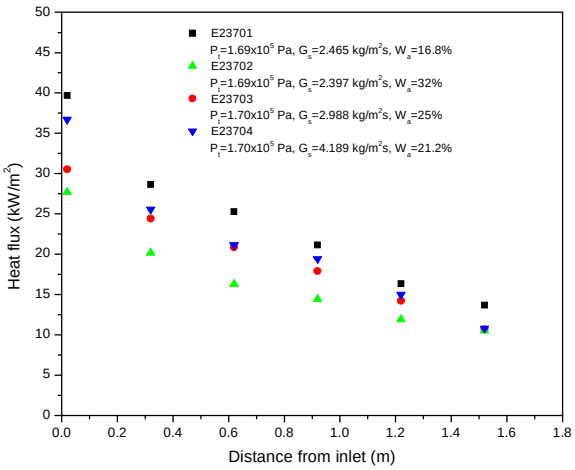

FIG. 3.2-7 Variation of heat flux with distance.

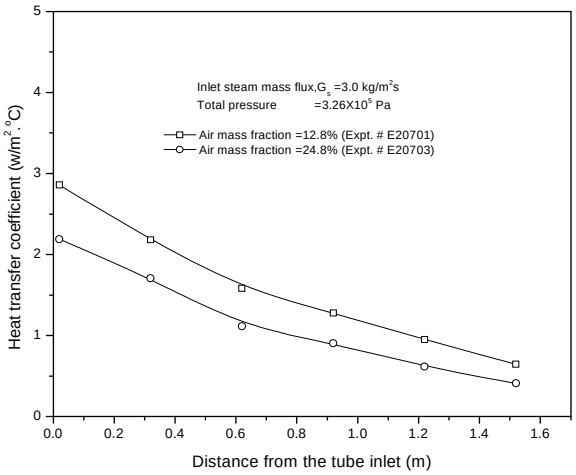

FIG. 3.2-8 Comparison of expt. heat transfer coeff. for different inlet air mass fraction.

The experiments were also performed for two different inlet pressures of $3.26 \cdot 10^5$ Pa and $1.7 \cdot 10^5$ and at about 25% inlet air mass fraction and 0.0043 kg/s inlet steam flow in one tube of IC (steam mass flux 3.0 kg/m^{2}s) and a comparison of heat transfer is given in Fig. 3.2-9. The local heat transfer coefficient for higher pressure (inlet saturation steam temperature) is always lower as compared to the case with lower saturation temperature because of higher accumulation of air in the mixture boundary layer (the vapour–liquid interface temperature is lower due to higher wall subcooling). Figure 3.2-10 shows the wall subcooling for the two cases mentioned above. The higher wall subcooling permits higher heat flux due to higher thermal driving force. In the case of pure steam condensation, the local heat transfer coefficient decreases with higher wall subcooling because of more steam condensation causing the film thickness to increase. However, in the case of steam-air mixture the resistances offered by the thicker condensate film does not cause reduction in local heat transfer coefficient because the condensation heat transfer coefficient in air-steam mixture case is much smaller as compared to the pure liquid film heat transfer coefficient. It can also be seen from Fig. 3.2-9 that the heat transfer coefficient in the initial portion of the tube is much higher for the case with lower pressure but reduces sharply due to the increase in subcooling and air mass fraction and reduction in mixture velocity.

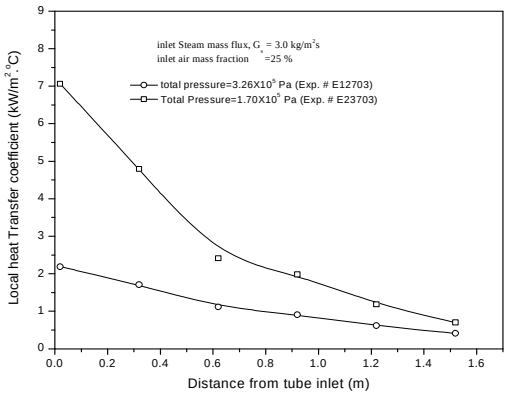

FIG. 3.2-9. Comparison of expt. heat transfer coefficients with variation of pressure.

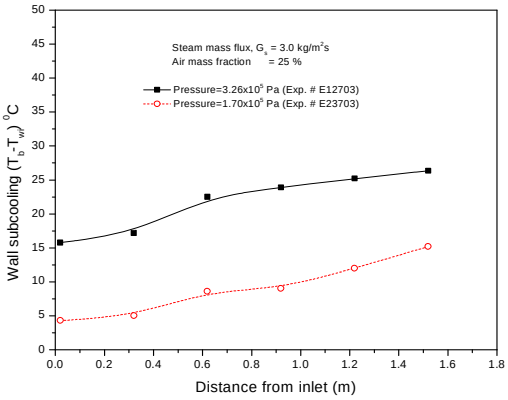

FIG. 3.2-10. Wall subcooling along the length of the tube.

3.2.6.3. Theoretical estimation of total heat transfer coefficient and its comparison with experimental data

Figure 3.2-11 shows the variation in the total heat transfer coefficient along the length of the tube. The total heat transfer coefficient was estimated using the theoretical model [3.2-57] with McAdams Modifier and Blangetti model for heat transfer in the condensate layer, and Moody and Wallis correlations to account for the condensate film roughness effect on the condensation and sensible heat transfer coefficients. It was found that the total heat transfer coefficient estimated with Blangetti model and Wallis correlation was higher as compared to that estimated with McAdams Modifier and Moody correlation and with Blangetti model and Moody correlation.

The calculations were performed from the inlet of the tube by reducing the bulk saturation temperature (ΔT_b) incrementally by 0.05°C for the first 0.5 m of the tube because of rapid change in heat transfer coefficients. The code calculates the differential axial length across which differential temperature of 0.05°C will be achieved. Beyond 0.5 m, a constant value of 0.1°C is used. Sensitivity analysis by reducing differential saturation temperatures (ΔT_b) by a factor of 10 has also been performed. Figure 3.2-12 shows the comparison of total heat transfer coefficients with different values of differential saturation temperatures (ΔT_b) along the length of the tube.

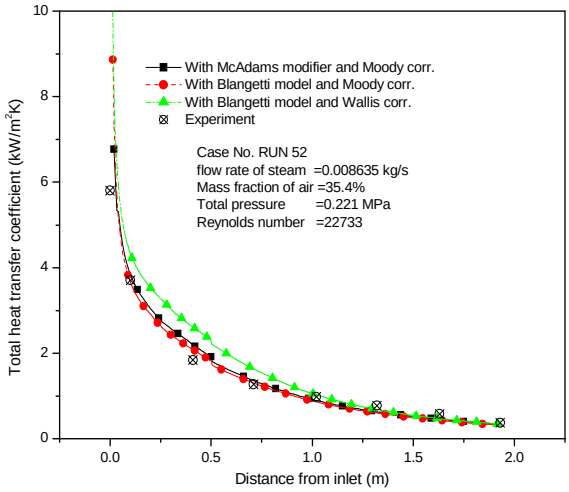

FIG.3.2-11. Variation of total heat transfer coefficient along the length of the tube.

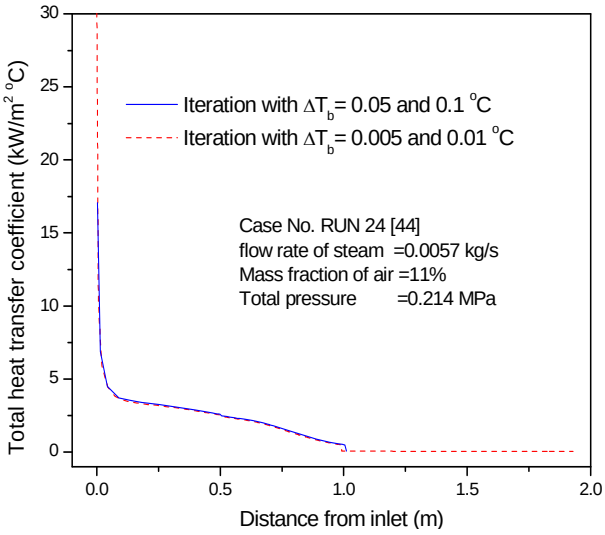

FIG. 3.2-12. Sensitivity analysis for heat transfer coefficient.

3.2.6.4. Experimental studies on steam condensation in presence of non-condensable gas at Middle East Technical University

A schematic of the METU_CTF test facility [3.2-58] is shown in Fig. 3.2-13. It consists of a boiler with an air inlet that produces a saturated steam/air mixture. This steam/air mixture flows downward through a vertical tube of 38.1 mm outer diameter and 2.6 m length. Cooling water flows upward through a jacket that surrounds the tube while steam/air mixture flows downwards. Axial temperature measurements of cooling water were used to determine the axial heat flux through the tube walls. The experiments were conducted for pressure range of 1.8–5.5 bars, mixture Reynolds number range of 45 000–94 000 and air mass fraction from 0 to 52%.

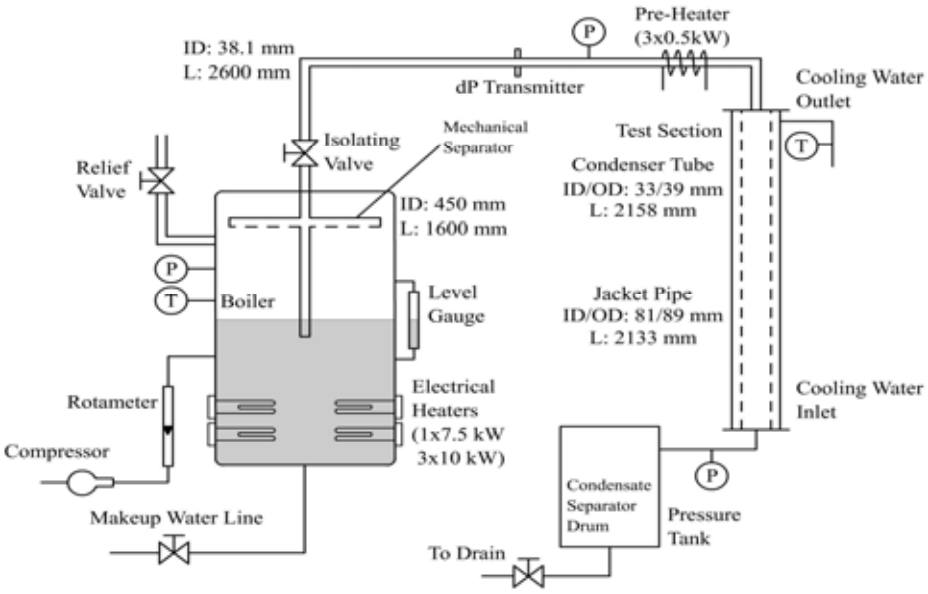

FIG. 3.2-13. Flow diagram of METU-CTF.

Figure 3.2-14 shows the variation of heat flux along the length of the tube. The heat flux corresponding to the air/vapour mixture gets closer to those of pure vapour towards the bottom of the condenser tube due to diminishing condensation rate as a result of dominating film and diffusion resistance. Furthermore, it can be seen from Fig. 3.2-14 that the local heat flux drastically decreases as inlet air mass fraction increases for the same pressure setting. Figure 3.2-15 shows variation of heat transfer coefficient along the length of the tube. Increase of inlet air mass fraction results in decrease of local HTCs and this is mainly governed by the local heat flux and inner wall temperature. Figure 3.2-16 shows comparison of experimental data with RELAP5 analysis.

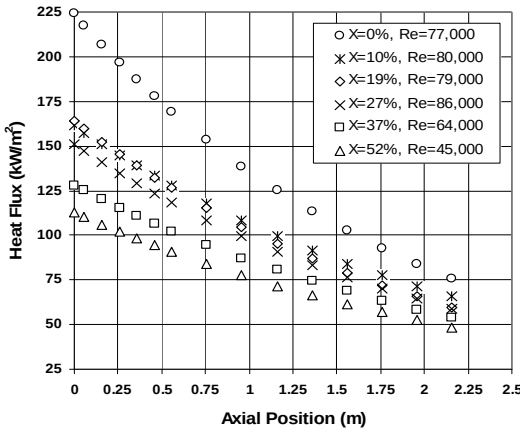

FIG. 3.2-14. Heat flux along the condenser tube (P_t=3 bar).

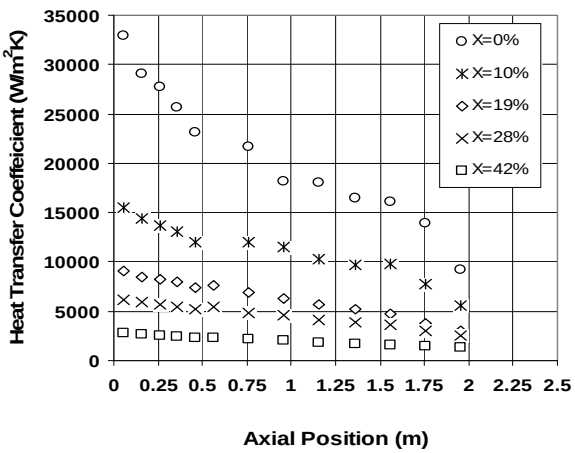

FIG. 3.2-15. Heat transfer along the condenser tube.

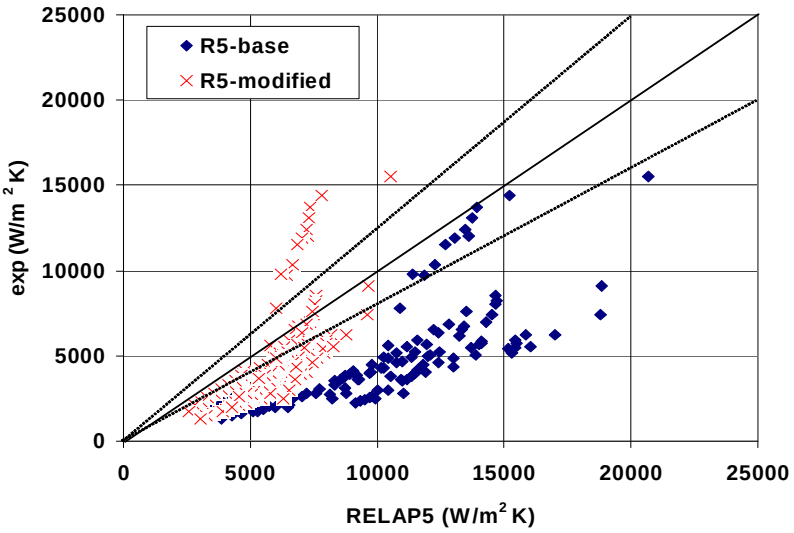

FIG. 3.2-16. Comparison of experimental and theoretical heat transfer coefficient.

3.2.6.5. Theoretical studies performed by UPV inside a vertical tube

The Polytechnic University of Valencia (UPV) has developed a non-iterative model for the condensation in the presence of non-condensable gases inside vertical tubes. A second degree equation for estimating condensation heat transfer coefficient is derived. A separate treatment for estimating the film heat transfer coefficient to account for the influence of non-condensable gas is considered. UPV has analysed the data of Vierow experiments [3.2-19] carried out in the University of California at Berkeley (UCB) using UPV empirical-correlation model implemented in TRAC-BF1 code. Figure 3.2-17 shows a comparison of heat transfer coefficient, steam mass flow rate and tube inner wall temperature with experimental data (Berkeley run no. 12).

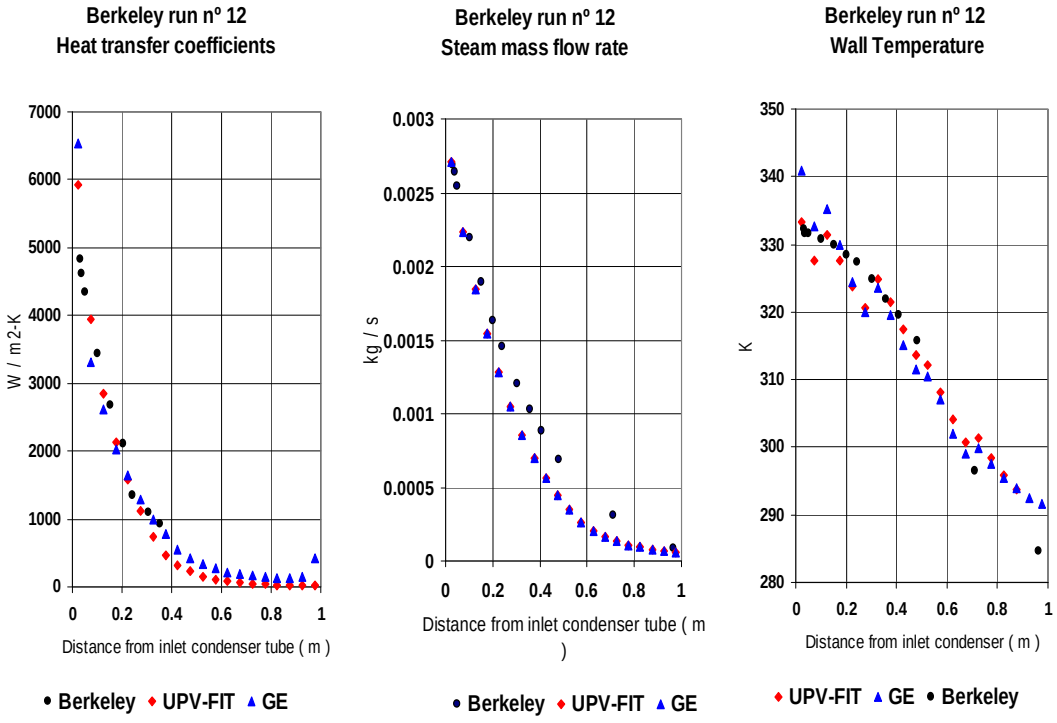

FIG. 3.2-17. Comparison of theoretical heat transfer coefficient, steam mass flow rate and tube inner wall temperature with experimental data (Berkeley run no. 12).

3.2.7. Some of the correlations available in the literature

There are number of correlations available in the literature. Some of the correlations developed are given in the following subsections below.

3.2.7.1. Correlations for condensation in stagnant atmosphere

The correlations given below are developed for condensation of stagnant vapour/non-condensable gas mixture.

The correlation developed by Uchida for vertical plate [3.2-59]

$$h_{tot} = 380\left(\frac{W_{nc}}{1-W_{nc}}\right)^{-0.7} \tag{3.2-14}$$

The Dehbi correlation [3.2-7]

$$h_{tot} = \frac{L^{0.05}\left[\left(3.7+28.7P_{tot}\right)-\left(2438+458.3P_{tot}\right)\log_{10}W_a\right]}{\left(T_b-T_w\right)^{0.25}} \tag{3.2-15}$$

This correlation is applicable for the following conditions

0.3 m < L < 3.5 m; 1.5 atm. < P_{tot} < 4.5 atm. and 10 ^{o}C < $T_b - T_w$ < 50°C

The condensation heat transfer coefficient in presence of air and helium [3.2-7]

$$h_{tot} = \frac{L^{0.05}\left[\left(3.7+28.7P_{tot}\right)-\left(2438+458.3P_{tot}\right)\log_{10}\left(W_{He}+W_a\right)\right]}{\left(T_b-T_w\right)^{0.25}}\cdot\left[0.948-8.67W_{He}+7.36W_{He}\left(W_{He}+W_a\right)\right] \tag{3.2-16}$$

The correlation developed by Liu et al. [3.2-8] is given as

$$h_{tot} = CX_s^{2.344}P_t^{0.252}dT^{0.307} \tag{3.2-17}$$

The heat transfer coefficient h_{tot}, is given in W/m^{2}K. C is the constant coefficient, equal to 55.635 W/m^2 Pa$^{0.252}$ ^{o}C$^{1.307}$, X_s is the steam mole fraction, dimensionless; P_t is the overall pressure (Pa); dT is the wall subcooling ($^{\circ}$C).; This equation is valid for the following range of parameters

2.533 X 10^5 Pa < P_t < 4.559 X 10^5 Pa; 4°C < dT < 25°C and 0.395 < X_s < 0.873

3.2.7.2. Correlations for condensation inside a vertical tube

There are two types of correlations for estimating the heat transfer coefficient inside a vertical tube. In the first type, the local heat transfer coefficient is expressed in the form of a degradation factor defined as the ratio of the experimental heat transfer coefficient, h_{tot} (when non-condensable gas is present) and pure steam heat transfer coefficient, h_{film}. The correlations in general are functions of local non-condensable gas mass fraction and mixture Reynolds number (or condensate Reynolds number). In the other type of correlation, the local heat transfer coefficient is expressed in the form of dimensionless numbers and does not require information of condensation heat transfer coefficient for pure steam. In these correlations, local Nusselt number is expressed as a function of mixture Reynolds number, Jacob number, non-condensable gas mass fraction and condensate Reynolds number, etc. Some of the correlations developed for condensation of vapour inside the vertical tube are given below.

3.2.7.2.1. Correlations based on degradation factor (f)

The degradation factor is defined as

$$f = \frac{h_{tot}}{h_{film}} \tag{3.2-18}$$

where, f may be the function of film Reynolds number (Re_f) , vapour/non-condensable gas mixture (Re_g), non-condensable gas mass fraction (W_a), Jakob number, Prandtl number (Pr_g).

Kuhn , Schrock, Peterson Correlation based on UCB-4 data [3.2-25]

For Air

$$f = f_1 f_2 \tag{3.2-19}$$

$$f_1 = f_{1shear}\left(1 + 7.32 \cdot 10^{-4}\,\mathrm{Re}_f\right) \tag{3.2-20}$$

$$f_2 = \left(1 - 2.601 W_a^{0.708}\right) \qquad \text{for } W_a < 0.1 \tag{3.2-21}$$

$$f_2 = \left(1 - W_a^{0.292}\right) \qquad \text{for } W_a > 0.1 \tag{3.2-22}$$

Where W_a is the air mass fraction & Re_f is the film Reynolds number

For Helium

$$f_1 = f_{1shear}\left(1 + 7.32 \cdot 10^{-4}\,\mathrm{Re}_f\right) \tag{3.2-23}$$

$$f_2 = \left(1 - 35.81 W_{He}^{1.04}\right) \qquad \text{for } 0.003 < W_{He} < 0.01 \tag{3.2-24}$$

$$f_2 = \left(1 - 2.09 W_{He}^{0.457}\right) \qquad \text{for } 0.01 < W_{He} < 0.1 \tag{3.2-25}$$

$$f_2 = \left(1 - W_{He}^{0.137}\right) \qquad \text{for } W_{He} > 0.1 \tag{3.2-26}$$

The parameter f_{1shear} is the ratio of liquid film thickness with interfacial shear to film thickness without interfacial shear.

Vierow correlation based on UCB data [3.2-19]

$$f = 0.0050\,\mathrm{Re}_{film}^{0.45} W_a^{-1.1} \tag{3.2-27}$$

Park correlation based on KAIST data [3.2-26]

$$f = 0.0012 W_a^{-1.4} Ja^{-0.63}\,\mathrm{Re}_{film}^{0.24} \tag{3.2-28}$$

Which is applicable in the following range

$1715 < Re_g < 21670$

$0.83 < Pr_g < 1.04$

$0.111 < W_a < 0.836$

$0.01654 < Ja < 0.07351$

UPV empirical-correlation based model

$$f = 1 - P_1 W_{nc}^{P2} + P_3 e^{-(P_4 W_{nc})} \tag{3.2-29}$$

Where the fitted parameters are given below

$$P_1 = 1.0266 ; P_2 = 0.12791 ; P_3 = 0.78074 ; P_4 = 29.122$$

3.2.7.2.2. Correlations based on non-dimensional numbers

Siddique Correlation based on MIT data [3.2-22]

For Air

$$Nu(x) = 1.137\,\mathrm{Re}_g^{0.404} W_a^{-1.105} Ja^{-0.741} \tag{3.2-30}$$

Which applies in the following range of experiments

$0.1 < W_a < 0.95$

$445 < Re_g < 22700$

$0.004 < Ja < 0.07$

For Helium, the correlation [3.2-22] is given below

$$Nu(x) = 0.537\,\mathrm{Re}_g^{0.433} W_{He}^{-1.249} Ja^{-0.624} \tag{3.2-31}$$

The above correlation is applicable within the following range,

$0.02 < W_{He} < 0.52$

$300 < Re_g < 11400$

$0.004 < Ja < 0.07$

Araki correlation for condensation heat transfer coefficient based on their experimental data [3.2-23].

Araki had correlated condensation heat transfer coefficient (h_{cond}) (in place of total heat transfer coefficient, h_{total}) with air partial pressure and mixture Reynolds number.

$$h_{cond} = \begin{cases} 0.33\left(\dfrac{P_a}{p_t}\right)^{-0.67} & \text{for } 650 < Re_g < 2300 \\ 2.11\times10^{-4}\,\mathrm{Re}_g^{0.8}\left(\dfrac{p_a}{p_t}\right)^{-0.99} & \text{for } 2300 < Re_g < 21000 \end{cases} \tag{3.2-32}$$

The condensation heat transfer coefficient, h_{cond}, given in eq. (3.2-32) is in kW/m^2K.

For estimating the convective and film heat transfer coefficient, separate correlations have to be used. The convection heat transfer coefficient was estimated using the well-known Colburn formula for turbulent and an analytically obtained constant value for laminar flow, as follows

$$\mathrm{Nu}_{\mathrm{conv}} = \begin{cases} 3.66 & \text{for } \mathrm{Re}_g < 2300 \\ 0.023\mathrm{Re}_g^{0.8}\mathrm{Pr}^{0.33} & \text{for } 2300 < \mathrm{Re}_g < 10^7 \end{cases} \quad (3.2\text{-}33)$$

The condensate film heat transfer coefficient, h_{film} can be calculated by Nusselt theory with McAdam modifier.

Maheshwari correlation based on BARC experiments [3.2-10]

$$Nu(x) = 0.15\,\mathrm{Re}_{film}^{0.15}(W_a)^{-0.85}\,Ja^{-0.8}\,\mathrm{Re}_g^{0.5} \quad (3.2\text{-}34)$$

This equation is valid in the following range

$0.1 < W_a < 0.6$

$8000 < Re_g < 22700$

$0.005 < Ja < 0.07$

The Hasanein et al. [3.2-21] correlations for condensation is given below

$$Nu(x) = 1.279\,\mathrm{Re}_g^{0.256}\,W_a^{-741}\,Ja^{-0.952} \quad (3.2\text{-}35)$$

and

$$Nu(x) = 2.244\,\mathrm{Re}_g^{0.161}\,Sc^{-1.652}\,Ja^{-1.038} \quad (3.2\text{-}36)$$

For condensation of steam in the presence of air and helium, Hasanein et al. [3.2-21] formulated the following correlation

$$Nu(x) = 1.279\,\mathrm{Re}_g^{0.256}(1-1.681W_a)W_{He}^{-0.741}\,Ja^{-0.952} \quad (3.2\text{-}37)$$

3.2.8. System and containment codes

A number of codes have been developed to analyse the various systems discussed above. Specific condensation models are implemented in these codes. The most comprehensive data collected from PANDA test facility for ESBWR PCCS performance testing was documented in ISP-42 (see Section 4.6). Dreier et. al. [3.2-60] performed BC4 test to simulate the behaviour of SWR-1000 containment with building condenser under accident conditions. These tests were simulated with various codes. In general, code predictions for overall PCCS [3.2-61] and SWR containment with building condenser [3.2-62] performance was reasonable. A few system and containment codes are described below.

The RELAP5/MOD3.2 code employs the two-fluid model to describe the thermohydraulic phenomenon of two phase flow. Finite differencing fluid cells (control volumes) are adopted for the fluid system. Six conservation equations are used to describe the conservation of mass, momentum and energy between the two phases. The constitutive relations used in RELAP5/MOD3.2 include models for determining flow regimes, and flow regime related models for interphase drag and shear, interphase heat and mass transfer, wall friction, wall heat transfer and the coefficient of virtual mass.

Faluomi and Aksan [3.2-17] and Lubbesmeyer [3.2-61] performed analysis for PANDA experimental data related to the condensation and concluded that the code condensation models can calculate the general trend of the experiments with sufficient accuracy.

GOTHIC (Generation Of Thermohydraulic Information in Containment) is a general purpose thermohydraulics code for design licensing safety and operation of nuclear containments. This code solves mass, momentum and energy balances for three separate phases (vapour, liquid and drops). The vapour phase can include both steam and non-condensable gases. Containment compartments can be modelled in 1, 2 and 3 dimensions. Three dimensional and lumped parameter modelling in different compartments can be connected to each other. The code is capable of modelling valves, pumps, pools, pressure suppression systems and metal water reactions. For solid structures, GOTHIC employs heat transfer correlations that account for the effects of condensing steam and the non-condensing gases that build up in the boundary layer, reducing the rate of condensation. The condensation options in GOTHIC include the empirical Uchida [3.2-59] correlation and the semi-empirical correlation developed by Gido and Koestel based on boundary layer theory with certain coefficients adjusted to give good agreement with experimental data including those obtained by Uchida. Bandurski et al. [3.2-63] performed analysis for containment cooling with building condenser for PANDA experimental facility.

MELCOR is an integrated code that can model a severe accident sequence from initiation through to release from the containment. The code is designed to be used in parametric studies. This code was used to analyse the PANDA experimental data [3.2-64].

FUMO is a lumped parameter code developed by the University of Pisa to perform thermohydraulics studies in containments following LOCA or severe accidents. Mass and energy is conserved at nodes and momentum balance is conserved at junctions. Six non-condensable gases (Ar, CO, CO_2, H_2, N_2 and O_2) can be modelled. Homogeneous gas/water mixture which may or may not be in thermal equilibrium with water pool can be modelled.

JERICO, developed by CEA, is a lumped parameter thermohydraulics code with nodes connected by flow paths and heat structures. Each node is split into two subnodes (liquid and gaseous). The gaseous subnode can contain 5 non-condensable gases namely N_2, O_2, H_2, CO and CO_2.

There are some other system and containment codes which are described in Ref. [3.2-65].

3.2.9. General remarks

Some limited view for condensation in the presence of non-condensable gases is presented above covering experimental and theoretical studies. A number of correlations are developed and incorporated in computer codes available for thermohydraulic analysis of various systems. In nuclear plant containments, a large number of non-condensable gases are present during LOCA and the work performed is not adequate to model scenarios where more than one non-condensable gas is present. Therefore, it is recommended that further studies in this area are performed for various relevant geometries.

NOMENCLATURE

A	surface area, m^2	Nu	Nusselt number, hL/k
C	molar concentration, mol/m^3	Pr	Prandtl number, $Cp\mu/k$
Cp	specific heat, J/kgK	P	pressure, Pa
d	diameter, m	Q	heat transferred, W
D	diffusion coefficient, m^2/s	q''	heat flux, J/m^2s
f	degradation factor	Re	Reynolds number
h	heat transfer coefficient, $J/m^2s\ ^oC$	Sc	Schmidt number, $\mu/\rho D$
h_m	mass transfer coefficient, kg/m^2s	Sh	Sherwood number, $h_m L/\rho D$
H_{fg}	latent heat of vaporization, J/kg	T	temperature, K
Ja	Jakob number	W	mass fraction
k	thermal conductivity, W/mK	X	molar fraction
L	characteristic length, m		
m	mass flow, kg/s		
m''	mass flux, kg/m^2s		

Greek symbols

ρ	density, kg/m^3
μ	dynamic viscosity, $kg/m\ s$

Subscript

a	air	nc	non-condensable gas
b	bulk	o	without suction
cond	condensate	s	steam
film	film	t, tot	total
g	gas phase	ref	reference
He	Helium	v	vapour
i	interface	w	wall
l	liquid phase, condensate	x	local
mix	mixture	y	distance

REFERENCES FOR SECTION 3.2

[3.2-1] OTHMER, D.F., The Condensation of Steam, Industrial and Engineering Chemistry 21, (1929).

[3.2-2] INTERNATIONAL ATOMIC ENERGY AGENCY, Status of Advanced Light Water Reactor Designs 2004, IAEA-TECDOC-1391, IAEA, Vienna (2004) 207–231.

[3.2-3] DREIER, J., et al., "SWR 1000 related containment cooling system tests in PANDA", Experimental Tests and Qualification of Analytical Methods to Address Thermohydraulic Phenomena in Advanced Water Cooled Reactors, IAEA-TECDOC-1149, IAEA, Vienna (2000) 277–286.

[3.2-4] SINHA, R.K., KAKODKAR, A., in Evolutionary Water Cooled Reactors: Strategic Issues, Technologies and Economic Viability, IAEA-TECDOC-1117, IAEA, Vienna (1999) 305-312.

[3.2-5] AL-DIWANI, H.K., ROSE, J.W., Free convection film condensing vapour, Int. J. Heat Mass Transfer **16**, 1359 (1973).

[3.2-6] HUHTINIEMI, I.K., CORRADINI, M.L., Condensation in the presence of non-condensable gases, Nuclear Engg. and Design **141** (1993) 429–446.

[3.2-7] DEHBI, A.A., The Effect of Non-condensable Gases on Steam Condensation under Turbulent Natural Convection Conditions, MIT Thesis, Dept. of Nucl. Engg., Massachusetts Institute of Technology (1991).
[3.2-8] LIU, H., TODREAS, N.E., DRISCOLL, M.J., An experimental investigation of a passive cooling unit for nuclear plant containment, Nuclear Engg. and Design **199** (2000) 243–255.
[3.2-9] ANDERSON, M.H., HERRANZ, L.E., CORRADINI, M.L., Experimental analysis of heat transfer within the AP600 containment under postulated accident conditions, Nucl. Eng. Des. **185** (1998) 153–1721.
[3.2-10] MAHESHWARI, N.K., Ph. D. Thesis on Studies on Passive Containment Cooling System of Indian Advanced Heavy Water Reactor, Tokyo Institute of Technology, Tokyo, Japan (2006).
[3.2-11] ABDULLAH, R., COOPER, J.R., BRIGGS, A., ROSE, J.W., Condensation of steam and r113 on a bank of horizontal tubes in the presence of a non-condensable gas, Experimental Thermal and Fluid Science **10** (1995) 298–306.
[3.2-12] VOTTA, F. JR., WALKER, C.A., Condensation of vapour in the presence of noncondensing gas, AICHE J. **4** (1958) 413.
[3.2-13] MORGAN, C.D., RUSH, G.C., "Experimental measurements of condensation heat transfer with non-condensable gases present in a vertical tube at high pressure", 21st National Heat Transfer Conf., Seattle, Washington, (ASME-HTD-27) (1983).
[3.2-14] NAGASAKA, N., YAMADA, K., KATOH, M., YOKOBORI, S., "Heat removal tests of isolation condenser applied as a passive containment cooling system", Proceeding of 1st JSME/ASME Int. Conf. On Nuclear Engineering (ICONE-1), Vol. 1, Tokyo (1991).
[3.2-15] KATAOKA, K., ARAI, A., YOKOBORI, S., "TRAC analysis and GIRAFFE tests for PCCS performance prediction", IAEA–TECDOC-1149, IAEA, Vienna (2000).
[3.2-16] MASONI, P., ACHILLI, A., BILLIG, P. F., BOTTI, S., CATTADORI, G., SILVERII SIET, R., "Tests on full-scale prototypical passive condensers for SBWR application," Progress in Design, Research and Development and Testing of Safety Systems for Advanced Water Cooled Reactors, IAEA-TECDOC-872, IAEA, Vienna (1996).
[3.2-17] FALUOMI, V., AKSAN, S.N., "RELAP5 capabilities in thermal-hydraulic prediction of SBWR containment behaviour: PANDA steady-state and transient tests evaluation", IAEA–TECDOC-1149, IAEA, Vienna (2000).
[3.2-18] OGG, D.G., Vertical Downflow Condensation Heat Transfer in Gas-Steam Mixtures, MS Thesis, University of California, Berkeley (1991).
[3.2-19] VIEROW, K.M., Behaviour of Steam-Air Systems Condensing in Concurrent Vertical Downflow, MS Thesis, University of California, Berkeley (1990).
[3.2-20] VIEROW, K.M., SCHROCK, V., "Condensation in a natural circulation loop with non-condensable gases, Part 1- heat transfer", Proc. Int. Conf. Multiphase Flows, Tsukaba, Japan (1991).
[3.2-21] HASSANEIN, H.A., KAZIMI, M.S., GOLAY, M.W., Forced convection in-tube steam condensation in presence of non-condensable gases, Int. Journal of Heat and Mass Transfer **39** (1996) 2625–2639.
[3.2-22] SIDDIQUE, M., GOLAY, M.W., KAZIMI, M. S., Local heat transfer coefficients for forced convection condensation of steam in a vertical tube in the presence of a non-condensable gas, Nucl. Technology **102** (1993).
[3.2-23] ARAKI, H., KATAOKA, Y., MURSE, M., Measurement of condensation heat transfer coefficient inside a vertical tube in the presence of non-condensable gas, Journal of Nuclear Science and Technology **32** (1995).
[3.2-24] NUSSELT, W.A., The surface condensation on water vapor, Zeitschrift Des Vereines Deutscher. Ing. **60** (1926) 541.
[3.2-25] KUHN, S.Z., Investigation of Heat Transfer from Condensing Steam-Gas Mixture and Turbulent Films Flowing Downward inside a Vertical Tubes, Ph.D. dissertation, University of California at Berkeley (1995).
[3.2-26] PARK, H. S., NO, H.C., A condensation experiment in the presence of non-condensables in a vertical tube of a passive containment cooling system and its assessment with RELAP5/MOD3.2, Nuclear Technology **127** (1999).

[3.2-27] MAHESHWARI, N.K., SAHA, D., SINHA, R.K., ARITOMI, M., Experimental studies on condensation of steam mixed with non-condensable gas inside vertical tubes in a pool filled with subcooled water, Kerntechnik **68** (2003) 5–6.
[3.2-28] OH, S., REVANKAR, T., Experimental and theoretical investigation of film condensation with non-condensable gas, Int. J. of Heat and Mass Transfer **49** (2006) 2523.
[3.2-29] SPARROW, E.M., LIN, S.H., Condensation heat transfer in the presence of a non-condensable gas, J. Heat Transfer **9** (1964) 430.
[3.2-30] MINKOWYCZ, W.J., SPARROW, E.M., Condensation heat transfer in the presence of non-condensables, interfacial resistance, superheating, variable properties and diffusion, Int. J. of Heat and Mass Transfer **9** (1966) 1125.
[3.2-31] DENNY, V.E., MILLS, A.F., JUSIONIS, V.J., Laminar film condensation from a steam-air mixture undergoing forced flow down a vertical surface, J. Heat Transfer, August (1971) 297-304.
[3.2-32] COLBURN, A.P., HOUGEN, O.A., Design of cooler condensers from a steam-air mixtures of vapours with noncondensing gas, Ind. Eng. Chem. **26**, (1934) 1178.
[3.2-33] KROTIUK, W.I, RUBIN, M.B., Condensing heat transfer following a loss-of-coolant-accident, Nucl. Technology **37** (1978) 118.
[3.2-34] CORRADINI, M.L., Turbulent condensation on a cold wall in the presence of a non-condensable gas, Nucl. Technology **64** (1984) 186.
[3.2-35] BUNKER, R.S., CAREY, V.P., Modeling of turbulent condensation heat transfer in the boiling water reactor primary containment, Nucl. Engg. Design **91** (1986) 297.
[3.2-36] PETERSON, P.F., SCHROCK, V.E., KAGEYAMA, T., Diffusion layer theory for turbulent vapor condensation with non-condensable gases, HTD197, Two Phase Flow and Heat Transfer, ASME (1992) 181188.
[3.2-37] HERRANZ, L.E., ANDERSON, M.H., CORRADINI, M.L., A diffusion layer model for steam condensation within the AP600 containment, Nucl. Engg. and Design **183** (1998) 133–150.
[3.2-38] ANDERSON, M.H., HERRANZ, L.E., CORRADINI, M.L., Experimental analysis of heat transfer within the AP600 containment under postulated accident conditions, Nucl. Engg.and Design **185** (1998) 153–172.
[3.2-39] DEHBI, A.A., The Effect of Non-condensable Gases on Steam Condensation under Turbulent Natural Convection Conditions, MIT Thesis, Dept. of Nucl. Engg., Massachusetts Institute of Technology (1991).
[3.2-40] PETERSON, P.F., Theoretical basis for the Uchida correlation for condensation in reactor containment, Nuclear Engg. And Design **162** (1996) 301–306.
[3.2-41] PETERSON, P.F, Diffusion layer modeling for condensation with multicomponent non-condensable gases, J. of Heat Transfer **122** (2000) 716–721.
[3.2-42] MAHESHWARI, N.K., PATEL, A.G, SAHA, D., ARITOMI, M., Heat transfer modeling on condensation from nonflowing steam-gas mixture, J. of Energy, Heat and Mass Transfer, **28** (2006)135–160.
[3.2-43] HERRANZ, L.E., MUNOZ-COBO, J.L., PALOMO, M.J., Modeling of condensation heat transfer on a horizontal finned tube in the presence of non-condensable gases, Nucl. Engg. and Design **201** (2000) 273–288.
[3.2-44] SUN, G., HEWITT, G.F., Evaporation and condensation of steam-water in a vertical tube, Nucl. Engg. and Design **207** (2001) 137–145.
[3.2-45] HART, J., et al., TEPSS — technology enhancement for passive safety systems, Nucl. Eng. and Design **209** (2001) 243–252.
[3.2-46] BALANGATTI, F., KREBS, R., SCHLUNDER, E.U., Condensation in vertical tubes-experimental results and modeling, Chemical Engineering Fundamentals, 1 (1982) 20–63.
[3.2-47] MCADAMS, W.H., Heat Transmission, 3rd ed. P329, McGraw-Hill Book Company New York (1954).
[3.2-48] SIDDIQUE, M., GOLAY, M.W., KAZIMI, M.S., Theoretical modeling of forced convection condensation of steam in a vertical tube in the presence of a non-condensable gas, Nucl. Technology **106** (1994).
[3.2-49] KAYS, W.M., MOFFAT, R.J., The behaviour of transpired turbulent boundary layers," Studies in Convection, pp. 223, Academic Press, New York (1975).

[3.2-50] GHIAASIAAN, S.M., KAMBOJ, B.K., ABDEL-KHALIK, S.I., Two fluid modeling of condensation in the presence of non-condensables in two phase cannel flows, Nucl. Sci. Eng. **119** (1995) 1.
[3.2-51] HASSAN, Y.A., BANERJEE, S., Implementation of a non-condensable model in RELAP5/MOD3, Nucl. Eng. Design **162** (1996) 281.
[3.2-52] KAGEYAMA, T., PETERSON, P.F., SCHROCK, V.E., Diffusion layer modeling for condensation in vertical tubes with non-condensable gases, Nucl. Eng. Design **41** (1993) 289.
[3.2-53] HERRANZ, L.E., MUNOZ-COBO, J.L., VERDU, G., Heat transfer modeling in the vertical tubes of the passive containment cooling system of the simplified boiling water reactor, Nuclear Engineering and Design **178** (1997) 29–44.
[3.2-54] GNIELINSKI, V., New equations for heat and mass transfer in turbulent pipe and channel flow, Int. Chem. E.g. **16** (1976) 359.
[3.2-55] KUHN, S.Z., SCHROCK, V.E., PETERSON, P.F., An investigation of condensation from steam-gas mixture flowing downward inside a vertical tube, Nuclear Engg. and Design **177** (1997) 53–69.
[3.2-56] NO, H.C., PARK, H.S., Non-iterative condensation modeling for steam condensation with non-condensable gas in a vertical tube, Int. J. of Heat and Mass Transfer **45** (2002) 845–854.
[3.2-57] MAHESHWARI, N.K., SAHA, D., SINHA, R.K., ARITOMI, M., Investigation on condensation in presence of a non-condensable gas for a wide range of reynolds number, Nuclear Engineering and Design **227** (2004) 219–238.
[3.2-58] TANRIKUT, A., YESIN, O., "Experimental research on in-tube condensation in the presence of air", Proceedings of a Technical Committee Meeting, IAEA-TECDOC-1149, IAEA, Vienna (2000).
[3.2-59] UCHIDA, H., OYAMA, A., TOGO, Y., "Evaluation of post-incident cooling systems of light-water power reactors", Proc. Int. Conf. on Peaceful Uses of Atomic Energy **13** (1965) 93–102.
[3.2-60] DREIER, J., AUBERT, C., HUGGENBERGER, M., STRASSBERGER, H.J., MESETH, J., YADIGAROGLU, G., "The PANDA tests for SWR1000 passive containment cooling system", 7th Int. Conf. on Nuclear Engineering (ICONE-7316), Tokyo, Japan (1999).
[3.2-61] LUEBBESMEYER, D., "Post test analysis of TEPSS tests-P2, P3, P5 and P7 using the system code RELAP5/MOD3.2", in IAEA-TECDOC-1149, IAEA, Vienna (2000).
[3.2-62] WICHERS, V.A., HUGGENBERGER, M., Testing and Enhanced Modelling of Passive Evolutionary Systems Technology for Containment Cooling-TEMPEST, European Commission, EVOL-TEMPEST-D16 (2004).
[3.2-63] BANDURSKI, T.H., PUTZ, F., ANDRENI, M., ANALYTIS, M., "Modelling of particular phenomena observed in PANDA with GOTHIC", in IAEA-TECDOC-1149, IAEA, Vienna (2000).
[3.2-64] HART, J., et al, "TEPSS-technology enhancement for passive safety systems", in IAEA-TECDOC-1149, IAEA, Vienna (2000).
[3.2-65] INTERNATIONAL ATOMIC ENERGY AGENCY, Status of Advanced Containment System for Next Generation Water Cooled Reactors, IAEA TECDOC-752, IAEA, Vienna (1994).

3.3. CONDENSATION ON THE CONTAINMENT STRUCTURES

3.3.1. Introduction

Condensation on the containment structures during an accident is one of the thermohydraulic phenomena that characterize the operation of passive emergency systems in the nuclear reactors of new generation. This phenomenon, together with the pressure suppression pool, and the condensation by means of an additional heat exchanger device, represents one of the three main mechanisms of containment cooling based on natural circulation.

In order to characterize this phenomenon, two main aspects must be taken into account: the natural circulation of the flow gas, and the high sensitivity to the boundary conditions, even more if the containment dimensions are considered. Both of them make that condensation, when its actual scenario is taken into account, has to be analysed locally and globally.

The design of the Generation III and III+ reactors foresees the presence of different safety systems, some of which are based on natural circulation. With respect to the containment, there are three ways to keep its integrity (i.e., to maintain containment pressure below the design threshold):

(1) Heat exchangers: Devices aimed to foster steam condensation and to transfer latent heat to a large water suppression pool located at a higher level.

(2) Suppression pools: The steam is eventually discharged into a pool where it condenses and releases latent heat.

(3) Containment structures: Containment is made of a metal which transport latent heat from the condensing steam to another fluid located out of the containment.

Because of the large sensitivity of condensation to the boundary conditions, an accurate simulation of steam condensation will require to have a suitable predictability of thermohydraulic variables influencing the phenomenon. In order to meet this requirement, analysts sometimes resort to 2D and 3D modelling of large scale facilities.

3.3.2. Models for the simulation of the condensation on plane wall in presence of non-condensable gases

Usually, many of the literature about condensation — related both with modelling and experimental evidence — is used for purposes where the geometrical and system configuration where the condensation occurs is different from what the study was carried out for. This is why some words have to be said about the possibility of using and extrapolating the models and experimental results of condensation not occurring in a vertical plate.

Actually, besides of a vertical plate, the following hardwares regarding condensation in the presence of non-condensables can be recognized in the literature:

a. Condensation inside small tubes: Some of the new passive containment safety mechanisms consist of a bundle of small section vertical tubes where condensation occurs inside them. These tubes are characterized by their small section (maximum diameter of one or two centimetres) and by their very different boundary conditions. One example is the PCCS of the ESBWR (Economic Simplified Boiling Water Reactor). The reasons for not using the models and experimental results taken from (and applied to) this configurations are the followings:

   - The interfacial shear is very sensitive to the area and geometry of the wall, becoming a relevant parameter that affects the gas and liquid velocity, contrary to the reference scenario (long vertical plate; natural circulation).

   - The gas moves because of the difference of pressure between the drywell and the wet well. This is why the circulation pattern that has to be considered in this case is forced

regime. This fact modifies the relative value of each thermal resistance, avoiding, for example, the non-consideration of the liquid film thermal resistance.

- Almost all the models implemented in the codes contain some correlations for the determination of the heat and mass transfer coefficients. Obviously, these correlations depend on the scale and geometry of the wall surface, as well as on the gas circulation pattern and fluid flow. This fact avoids us to use a model developed for this kind of configuration to a vertical plate condensation.

b. Condensation outside tubes: they can be with or without fins. Some examples are the PCCS of the SWR-1000, or of the AHWR. In this case, the mixture of gases flows within the containment atmosphere:

   - As the circulation pattern is similar from our case, the only difference will be related with the geometry of the tubes, and not with the boundary conditions of the source term.
   - If the tube is vertical-oriented, then the extrapolation can be carried out, because the phenomenology and boundary conditions are almost the same.
   - If the tube is horizontal-oriented, then the surface orientation will affect the liquid film thermal resistance, creating different specific zones along the cross section of the tube, according to the relative magnitude of the gravity and surface water tensional force. This new phenomenon will affect the heat flow, avoiding the direct extrapolation of a model (and experimental result) that have been addressed to this kind of configuration. At the same time, it is important to keep in mind that the condensate thermal resistance is often neglected when vertical plate and natural circulation is considered. Two conditions will have to be accomplished in order to use the models and experimental results[2] that have to do with this type of configuration:

     i. The tube has a very small flat cross section that avoids the storing of huge amounts of condensate in the lower part of the tube.

     ii. The configuration is not a matrix -so there are no tubes at a higher level in a way that the condensate accumulated on them can drop down to the lower rows.

3.3.2.1. Models obtained from a theoretical approach

This kind of models is characterized by the fact that their development is based on theoretical premises, although in many of them the model equations are empirical correlations that have been derived from experimental data.

The theoretical models can be classified into two main groups:

a. On one hand, there are models based on the numerical solution of the conservation equations. Their structure consists in the field equations (continuity, momentum, energy and conservation of vapour species) in combination with some thermodynamic relationships and empirical correlations (if required) related with the heat transfer. These models have usually one or two dimensional nature and include a specific approach for the interface and, therefore, they are iterative with respect to the interfacial temperature. These models, which will be named “integral models”, are able to simulate the phenomenon of condensation calculating the liquid and gas mass flows, updating the thermodynamic conditions for each phase, etc. Therefore, these models are thermohydraulic integral models applied to the condensation scenario.

[2] But not directly without certain reservations, that depend specifically on the facility configuration.

b. On the other hand, there are the models that directly (and only) solve the equations related to the fundamental parameters of condensation (condensation flow or HTC) and that will be termed as "separate models". These models need to be initialized from the boundary conditions for the phenomenon of condensation, whose calculation is conducted by means of the field equations or taken from experimental data, as the local velocity of steam or the non-condensables mass fraction. Since these models are not restricted in its use to a specific form of the field equations, their implementation is much more flexible and, therefore, can be easily employed in thermohydraulic codes.

In Table 3.3-1 the regime of the gas and the pattern of the trajectories for some of the main condensation models are reported (separate models and models based on the conservations equations).

TABLE 3.3-1. GAS REGIME AND CIRCULATION PATTERN OF SOME OF THE MAIN CONDENSATION MODELS

Model	Gas-regime	Circulation pattern	Year
Colburn-Hougen	Stagnant	Correlation not specified	1934
Sparrow & Minkowycz	Laminar	Natural / Forced	1966
Denny	Laminar	Forced	1971
Whitley	Turbulent	Forced	1976
Rose	Laminar	Forced	1979
Corradini	Turbulent	Natural/ Forced	1983
Kim	Laminar/turbulent	Natural/ Forced	1987
Herranz	Transition	Natural	1998

Both the integral and separate models present some problems when have to be implemented in a thermohydraulic containment code:

a. The implementation in a lumped-parameter (LP) code of an integral model is practically impossible, due to the necessity of dealing with large volumes, while the field equations require local values for the variables. Since the separate models deal with the variables of the bulk, their implementation will be also complicated in this type of codes, because the three dimensional distribution of the gaseous flow (temperature, mass fraction, etc.) will prevent the values for the bulk from being adequately averaged by means of the typical volumes of a LP code.

b. With respect to the Computational Fluid Dynamics (CFD) codes, the integral models are also difficult to be implemented, since the specific equations of condensation depend on the way the field equations are formulated. With respect to the separate models, their inclusion must take into account that the concept of "bulk" does not exist in CFD codes and therefore different nodalizations must be tested in order to obtain adequate values for the variables in the bulk. This is the option usually chosen in the implementation of a condensation model.

3.3.2.1.1. Models based on the field equations

Nusselt [3.3-1] conducted the first studies that deal with the problem of the heat and mass transfer in filmwise condensation. In his pioneering work, he considered the ideal situation of a saturated steam in steady state conditions condensing on an isothermal vertical plane plate.

Colburn and Hougen [3.3-2], on the contrary, studied the thermal resistance caused by a gaseous diffusive boundary layer. In this diffusive layer, the heat transfer coefficient is the sum of two different resistances in parallel: the contribution of the sensible heat and the contribution of the latent heat of the steam. The sensible heat is given by the sum of the conduction in the gaseous layer and an

additional term due to the energy of the condensation flow. The sensible (convective) energy transferred can be neglected, being counterbalanced, in addition, by the respective term of the non-condensables to the bulk.

During the 1960s, Sparrow and Minkowycz published many papers in which they solved the conservation equations applied to the phenomenon of condensation for a vertical flat plate in presence of non-condensables. These papers deal with different scenarios and they take into account several thermohydraulic phenomena.

In the following, our attention will be focused to the thermohydraulic aspects of the modelling, without considering the various numerical techniques employed for the solution of the system equations.

In those first papers [3.3-3–3.3-5], the authors considered an isothermal vertical plate adjacent to an amount of gas in quiescent conditions or in forced circulation (in this case, the heat flow was almost twice than in quiescent conditions). The additional phenomena to the Nusselt model considered, apart from the new diffusive thermal resistance of the gas, were the followings:

- Variability of the thermodynamic and transport properties,
- Interfacial resistance,
- Thermal diffusion and diffusion thermo,
- Overheating of the steam,
- The phenomenon that would be the inverse of the additional film thickness shrinkage due to the momentum transfer of the condensate vapour. The loss of part of the momentum by the liquid makes the condensate mass flux to decrease.

With respect to the interfacial shear forces, in those analyses where free convection or stagnant steam has been considered, the shear stress at the interface has been neglected and it has been taken into account only in the case of forced convection. Some of these phenomena, such as the interfacial resistance or the thermal diffusion, have been neglected in more recent analyses conducted by different authors. The same occurred with other phenomena related to the liquid phase, whose negligible importance was demonstrated by the analyses of Koh et al. [3.3-4] or Minkowycz and Sparrow [3.3-3]. These negligible phenomena were the inertial forces, the mass thermal diffusion (Soret effect), the diffusion thermo (Dufour effect), the axial transmission of conductive heat of the liquid parallel to the surface, and the convective transport of the condensate. Other phenomena, on the contrary, such as the subcooling of the steam or the inertia of the liquid layer, neglected in the previous works, have been reconsidered in recent papers. Since then, the liquid film heat transfer has always been considered one dimensional and conductive only. These simplifications and additions modify the conservation equations for natural circulation — without taking into account the possible turbulence — in the boundary layer of the condensate and gas.

This first large block of theoretical development concludes with the work of Sudhindra and Minkowycz [3.3-6]. In this paper, the equations of a model for liquid laminar flow and gaseous turbulent flow are reported. This model, although it is simple from a phenomenological point of view (it is based on the hypotheses of axial velocity equal to zero at the interface, interfacial temperature equal to the saturation temperature, thermal convection neglected), could be one of the last works (with some relevant exceptions) based on the field equations and, with the model proposed by Rohsenow, one of the first theoretical models referring to turbulent flow.

Another considerable contribution is the work conducted by Mori and Hijikata [3.3-7], where the theoretical implementation of the drop-formation in the gaseous layer is introduced, in other words, the anticipated condensation or mist. Usually, the phenomenon of mist is considered in a simple manner by means of the addition of a multiplication factor for the Nusselt number, which is a constant value. Afterwards, other authors demonstrated that the importance of this phenomenon, which is

responsible for an increase of the specific heat of the gas, is restricted only for low Reynolds number values (below 2300), as in the case considered by Mori and Hijikata where the gas in the bulk was quiescent.

The work proposed by Denny and Jusionis [3.3-8] reconsiders the case of laminar forced flow, where the employed equations are the same proposed by Minkowycz and Sparrow [3.3-3]. The innovation of this work consists of stressing the manner for decoupling the equations related to both phases by means of the direct solution of the linking variable between them: the interfacial temperature. Starting from the empirical adjustment of the Acrivos expression for the mass conductance [3.3-9], the authors determine iteratively the interfacial temperature using the expression of Denny et al. [3.3-10] for the heat flow through the liquid layer, setting the heat flow equal to the latent heat. In this last expression, the authors realized that if a mass conductance independent from the interfacial properties were found, after solving a system of two equations in two unknowns the interfacial temperature would be obtained.

3.3.2.1.2. Separate models

From now on, a 'nuclearization' tendency will guide the theoretical and experimental works related to the study of the thermohydraulic phenomena, and thus in the study of the condensation in presence of non-condensable gases:

a. In the theoretical field, the appearance of thermohydraulic codes in the nuclear industry moves the interest in modelling a phenomenon from a traditional general approach to a nuclear specific perspective. In this manner, the objectives are no more the calculation of all the relevant variables in the modelling and the emphasis on the numerical method for the system resolution. Instead of them, the tendency goes to a more specific approach of the phenomenon, where the objective is limited to the determination of the fundamental parameters of condensation.

b. In the experimental field, the analysis related to the condensation in presence of non-condensable gases focuses on what is peculiar in the phenomenon when it occurs in a reactor containment. The boundary conditions that characterize the phenomenon are taken into account. These boundary conditions are essentially related to the characterization of the gas flow in the containment, as well as its geometrical configuration and particular dimensions.

Collier was one of the first authors in resume the problem of condensation without considering the conservation equations. For that, Collier took up the Colburn and Hougen model [3.3-2] for the gas boundary layer, whose resolution for the condensation heat transfer is based on the kinetic theory of gases and considers the mass diffusion film's theory hypothesis which states that "the convective non-condensable gases term towards the interface is equal in magnitude to the non-condensable gases diffusion term towards the bulk" [3.3-11].

The Colburn and Hougen model for the mass transfer coefficient is the so called Collier-Stephan formulation, where the velocity has been obtained by means of an integration instead of a simple linearization. The hypothesis of net total non-condensable flux at the interface is admitted by each formulation.

With respect to the sensible contribution, Colburn and Hougen reduced the convective term to the conductivity contribution of the steam (so neglecting the convective transport of the gas and the conductivity transfer contribution of the non-condensable gases), plus the contribution due to the convective energy transport of the condensation flux (instead of restricting this contribution only to the convective term of the condensation flux, because the energy transport by the steam diffusive flux is counterbalanced with the energy carried by the non-condensable diffusive flux that flows in the contrary sense through the bulk). Together with this formulation, Collier and Thome developed a solution for the condensate film thermal resistance. Finally, in order to solve the gas mass transfer coefficient, Collier and Thome applied the HMTA (Heat and Mass Transfer Analogy).

In 1976, Whitley et al. [3.3-12] published a paper based on his doctoral thesis. In this work, he performed a survey of the various correlations used in the nuclear reactors for the prediction of the heat transfer towards the materials of the containment. In addition, Whitley compared the correlations of Uchida and Tagami with the results of the only available American experiments at that time, conducted in the CVTR (Corolinas Virginia Tube Reactor) facility [3.3-13]. In the same paper, Whitley developed his own model, again without considering the conservation equations. This model is a separate model that makes use of the Nusselt equation for the film thickness calculation, following the Colburn and Hougen analysis for the gas boundary layer. The model iterates on the interfacial temperature. In the same paper, together with this model, Whitley validates another one where the sensible heat contribution and the thermal resistance of the condensate film have been neglected.

Corradini conducted in 1984 [3.3-14] one of the first works where the phenomenon of condensation is analysed under the consideration of the real scenario where it would occur. As Whitley, Corradini observed that the dimensions of the wall (and of the containment in general) prevent the direct application of the equations that simulate the heat and mass transfer characterizing condensation as have been described by previous authors. Both Whitley and Corradini stress the turbulent character (and not laminar, as has been treated) of the flow in the containment, as well as its forced circulation pattern in the first instants of the transient, and subsequently natural convection. In fact, Corradini focuses both on the natural convection -present during most of the time of the accident that would produce the steam discharge and the onset of condensation-, and on the forced circulation -during the blowdown, approximately the first 15 or 20 s. As Whitley, Corradini developed his model neglecting the thermal resistance of the film, verifying that its contribution is actually not important.

Some years later, Kim and Corradini [3.3-15] published a new paper on condensation where the scenario assumes a fundamental importance. In this work, two circulation patterns have been considered — natural and forced convection — corresponding to the blowdown and to the subsequent temporal evolution of the accident that would cause the steam discharge in the containment. The main innovation consists of the correction of the heat transfer coefficients in the case in which the condensate film contains waves.

In addition, the relative importance of the thermal resistance that the condensate can assume is analysed in detail. In practice, the Nusselt theory has been reformulated, including the interfacial shear and the momentum drag caused by the gas. Two models for the liquid thermal resistance are proposed, distinguishing between laminar and turbulent film. Finally, by means of a comparison with experimental data obtained from the CVTR facility, it is demonstrated that in some situations the contribution of the film resistance is not negligible.

Considering what has been previously described in this section, we can draw the following conclusions:

a. Two pioneer works have constituted a guide for subsequent studies. These works are the Nusselt work on the condensate film in the 1910s, and the work of Colburn and Hougen in the 1930s, where the formulation of the resistance of the gaseous diffusive layer has been proposed based on the kinetic theory of gases and using the HMTA for its determination.

b. Next, the period from the beginning of the 1960s to the end of the 1980s is characterized by:

    - An in depth general study of the phenomenon of condensation starting from the rigorous application of the conservation equations.
    - The progressive considering of the phenomena that occur in condensation, with a study, analytical or experimental, that provides the evaluation of the relative importance of each phenomenon.
    - A progressive orientation towards the study and application of the phenomenon taking into account the boundary conditions and the scenario where it occurs.
    - A switch regarding the objective of modelling: instead of calculating all the variables related to condensation, the resolution of the two fundamental parameters (HTC and

condensation flow) is addressed, allowing implicitly the implementation of the equations in a code for determining the remaining variables. The only exceptions in which the problem of condensation is tackled starting from the conservation equations are usually represented by academic studies, for instance, in doctoral theses [3.3-16] [3.3-17–3.3-19].

From the 1990s, as Sudhindra and Minkowycz observed in the mid-1970s [3.3-6], the existing models are able to predict adequately the phenomenon of condensation in presence of non-condensable gases in the containment of a nuclear reactor. Therefore, in this new period of research, we will find efforts aimed to accomplish one of the following objectives:

a. Incidence in the experimentation. Until the 1990s, the only real databases available are limited (with the exceptions of the CVTR or the Battelle-Frankfurt) to small facilities, without considering the scale dependency, and reproducing only separate effects. Therefore, after the 1990s, strong efforts have been devoted to the attempt of extending the experimental data also to large facilities that simulate the containment. The main concern — owing to the fact that the models have a strong dependency on the gas conditions — moves from the condensation phenomenon to the thermo-hydrodynamic of the gaseous flow, as well as to its distribution and transport in the enclosure of the containment.

b. An attempt of reducing the calculations performed by the model, in order to reduce the computational burden of the thermohydraulic code where the model has to be implemented. Therefore, it is important to obtain concise formulations able to take into account the diversity of the relevant phenomena occurring during the condensation process.

As we will observe below, the improvements achieved from the 1990s do not imply new theoretical approaches: almost every new model is based on already existing approaches. The only theoretical innovation will be focused on a new simpler formulation or on the use of new correlations or multiplication factors able to take into account the phenomena with a better approximation, easier to be employed in a separate model and implemented in a containment thermohydraulic code.

Together with the formulation of Colburn-Hougen [3.3-2], one of the more employed formulations is that proposed by Peterson et al. [3.3-20], related to the heat transfer by means of condensation. The author used the integration mentioned above -in the film's mass diffusion form-, which is the so-called Collier and Stephan formulation, to obtain an average gas-vapour velocity, and with the use of the HMTA, yielded condensation conductivity. The difference with the Colburn and Hougen model lies in the particular form of Peterson's coefficient, based on both the use of kinetic theory of gases and the Clausius-Clapeyron equation to set the jump boundary pressures in a jump boundary temperatures, in such a way that it is simpler to implement it in an algorithm to compute the HTC. In this way, instead of solving the condensation flow using a heat transfer correlation -by means of the HMTA- for the mass transfer coefficient, Peterson defines a conductivity condensation coefficient, based on the definition of the Sherwood number:

$$k_{cond} = \frac{1}{\varphi}\left(\frac{h_{fg}^2 P_0 M_v^2 D_0}{R^2 T_0^2}\right) \tag{3.3-1}$$

Where φ is an average value of the steam concentrations in the bulk and in the interface, and the subscript *0* means a reference value.

In this way, the mass transfer coefficient is expressed as follows:

$$G = \frac{Sh \cdot k_{cond}}{D} \tag{3.3-2}$$

Therefore, the HMTA is applied to the Sherwood number and not directly to the mass transfer coefficient.

In 1998, Herranz et al. [3.3-21] published a model based on the formulation proposed by Peterson and on the use of HMTA, also known as Diffusion Layer Modeling. This model improves the formulation of the Peterson condensation conductivity, considering the convenience of keeping variable the gas density in the diffusive boundary layer that in Clausius-Clapeyron equation Peterson had kept constant. This model accomplishes both tendencies previously described: on one hand, it is restricted to the obtainment of the fundamental parameters of condensation and, in addition, it includes some of the most important parameters in a simplified manner, such as the waviness of the film (by means of a coefficient which is function of the Reynolds number) and the transport of the gaseous mixture due to the natural convection. This phenomenon is a function of the temperature difference and of the difference of the relative concentrations of the gas components between the bulk and the interface, which is formulated through the Grashof number. The model proposed by Herranz employs the correlation of McAdams and, therefore, it is suitable for regimes of natural convection in the containment, with values of the Rayleigh number (for the mass transfer) in the range between 10^8 and 10^{10}, that is, for transition regimes (the same range observed by Malet et al. in the TOSQAN facility [3.3-22]). Other modification of the Herranz model is the reformulation of the diffusion coefficient in order to take into account the existence of light gases (in the experiments for the model validation, helium was used):

$$D = \left(\frac{X_{He}}{X_{nc}\, D_{He,st}} + \frac{X_{air}}{X_{nc}\, D_{air,st}} \right)^{-1} \tag{3.3-3}$$

With respect to the other models published since then, usually related to the validation of an experimental work or to a doctoral thesis, they employ one of the integral model previously described, or a combination of heat and mass transfer coefficients coming from the different models.

Finally, it is very important to mention the importance gained by the empirical correlations for the convective heat transfer coefficient in the separate models, because they are in the basis of the mass transfer coefficient calculation, which can be seen as a real shortcoming of the separate models. Malet et al. [3.3-22] made a comparison for the condensation rate calculated by means of the Chilton and Bird formulation with the experimental results of the TOSQAN facility. In this study, different correlations for natural convection were compared, for both laminar and turbulent flow, observing that the best agreement was achieved by the correlations suitable for turbulent or transition flow, such as the correlation proposed by McAdams.

In Table 3.3-2 the value of some relevant parameters related with the more widespread separate models is indicated, together with some of the experimental databases that have been used for their validation.

TABLE 3.3-2. EXPRESSIONS OF SOME OF THE MAIN VARIABLES REGARDING SEPARATE CONDENSATION MODELS

Model	Regime	τ_i	δ	h_s	G	experiments
Denny	FC	$\dot{m}(u_b - u_i)$	Nusselt equation	–	$\dfrac{0.8\,\rho_{st,b} u_b Sc_b^{-1}\,\mathrm{Re}^{-1/2}\,\zeta_1(W_{nc,b})}{\left[(1+\zeta_2(W_{st,b}, W_{st,i}))(1+Sc_b^{-1})\right]^{1/2}}$	–
Corradini	NC	$\dfrac{\rho v_g^2 0.045}{2}\left(\dfrac{v_g}{\Gamma_x \delta_x}\right)^{1/4}$	Neglected	$0.0295\left(\dfrac{k}{L}\right)\mathrm{Gr}^{2/5}\,\mathrm{Pr}^{7/15}$	$0.0188\Gamma\theta\,\mathrm{Re}^{-0.25}\,\mathrm{Sc}^{-2/3}$	Uchida Tagami
	FC	$\dfrac{\rho v_g^2 0.0592}{2}\mathrm{Re}_x^{-0.2}$		$0.037\left(\dfrac{k}{L}\right)\mathrm{Re}^{0.8}\,\mathrm{Pr}^{1/3}$	$0.037 v_g\,\mathrm{Re}^{-0.2}\,\mathrm{Sc}^{-2/3}$	
Kim	NC	-	$\dfrac{d\delta}{dx} = \dfrac{\rho_l^2 g h_{fg}}{\mu k_l (T_i - T_w)}\delta^3 + \dfrac{\rho_l \tau_i h_{fg}}{\mu k_l (T_i - T_w)}\delta^2 + \dfrac{\rho_l (u_g - u_i)}{\mu}\dfrac{\delta}{2}$	$\mathrm{Nu} = A\cdot(\mathrm{Gr}\,\mathrm{Pr})^b$	$\mathrm{Sh} = A\cdot(\mathrm{Gr}\,\mathrm{Sc})^b$	Goodykoontz and Dorsh Asano Dallmeyer CVTR
	FC	$\rho v_g^2 \cdot 0.0296\,\mathrm{Re}_x^{-0.2}$		$C_p \rho_g u_g f/2\,\mathrm{Pr}_t^{-1}$	$\rho_g u_g f/2 \mathrm{Sc}_t^{-1}$	
	Wavy	$\rho v_g^2 \dfrac{0.168}{\ln(864\delta_m/k_s)^2}$		$\mathrm{Nu} = \dfrac{f/2\,\mathrm{Re}\,\mathrm{Pr}}{\mathrm{Pr}_t + (f/2)/\mathrm{St}}$	$\mathrm{Sh} = \dfrac{f/2\,\mathrm{Re}\,\mathrm{Sc}}{\mathrm{Sc}_t + (f/2)/\mathrm{St}}$	
Collier (Colburn-Hougen	FC	No data	$\dfrac{4\Gamma_z}{\mu_l} = \dfrac{4}{3}(\delta_z^*)^3 + 2\tau_i^*(\delta_z^*)^2$	Appropriate correlation	$\left(\dfrac{h_s}{C_{p,st}}\right)\left(\dfrac{\mathrm{Pr}}{\mathrm{Sc}}\right)^{2/3}\dfrac{\ln\left(X_{nc,i}/X_{nc,b}\right)}{(X_{nc,i} - X_{nc,b})}$	–
Whitley	FC	Neglected	Nusselt equation	$0.037\left(\dfrac{k_g}{L}\right)\mathrm{Re}^{0.8}\,\mathrm{Pr}^{0.6}$	$0.037\,\theta\,\rho_b u_g\,\mathrm{Re}^{-0.2}\,\mathrm{Sc}^{-0.4}$	Uchida Tagami CVTR
Herranz	NC	Neglected	Nusselt equation, adding a waving factor ($\mathrm{Re}_l^{0.04}$)	$0.13\left(\dfrac{k_g}{L}\right)\mathrm{Gr}^{1/3}\,\mathrm{Pr}^{1/3}$	$\dfrac{0.13(Gr\,Sc)^{1/3} k_{cond,\mathrm{mod}}(T_b - T_i) X_{nc,avg}}{(X_{nc,i} - X_{nc,b})L}$	Anderson Dehbi

3.3.2.2. Models obtained from experimental results

Unlike other thermohydraulic phenomena, the modelling of wall condensation in presence of non-condensable gases has been developed more theoretically than experimentally. Nevertheless, the use of empirical correlations in the modelling of the phenomenon has become predominant since the beginning, especially for two reasons:

a. A correlation-based model (as Uchida's), compared to a model based on a system of differential equations (as Sparrow or Minkowycz's), is more simple to be solved.

b. The lack of knowledge of the phenomenon required the use of the empirical correlations in the evaluation models in order to be conservative.

Due to these reasons, the major part of the licensing activities aimed to the calculation of the conservative condition for pressure and temperature in the containment [3.3-23], and to the determination of the conservative scenario for the effectiveness of the Emergency Core Cooling System (ECCS[3]) [3.3-24] will employ very conservative empirical correlations, sometimes unknown origin for the modelling of the HTC from the atmosphere towards the surroundings of the containment. In a large number of cases, the HTC assumed was the following [3.3-12]:

a. For the design of the containment (maximum value of the pressure), during the blowdown the HTC is a linear function of the time, from 0 to the value given by the Tagami correlation. After the blowdown, the HTC is given by the Uchida correlation.

b. For the evaluation of the ECCS (low value of the pressure), during the blowdown the HTC is a linear function from 45.4 W/m^2K to a value which is 4 times the maximum value of the Tagami correlation at the end of the blowdown. During the long term stagnation phase, the HTC is 1.2 times the value obtained by the Uchida correlation. Between the end of the blowdown and the previous period -transient stage- the HTC is given by:

$$h = 1.2h_{uchida} + \left(h_{tagami} - 1.2h_{uchida}\right)e^{-0.025(t-t_{EOB})} \qquad (3.3\text{-}4)$$

Before the publication of the Code of Federal Regulations (CFR), the correlations employed for the HTC were constant values that conservatively (from the point of view of the peak value for the pressure) calculated the heat transfer in the containment, where the most used value was 227 W/m^2K [3.3-12].

The empirical correlations have been used not only for licensing activities, but also in the majority of the thermohydraulic codes used for modelling the containment.

The two first published correlations -of known origin- that have been more extensively used are the correlations of Uchida [3.3-25] and Tagami [3.3-26]. Since their publication until the 1990s, almost no empirical correlations have been published for modelling the heat transfer in the containment. The most important difference that we can observe between these correlations and others more recent [3.3-27] [3.3-28] regards the consideration of other phenomena and parameters whose importance has been stated since the analysis had been focused on the phenomenon as it would occur in the containment of a nuclear reactor, according to the evolution in the treatment of the condensation phenomenon as has been mentioned above.

Uchida correlation is essentially a fit of the experimental results of the HTC obtained by Sagawa [3.3-29] when they are expressed as a function of η. The experimental facility consists of a steel containment containing a condenser surface of 140 × 300 mm. The non-condensable pressure in the bulk was always 0.1 MPa in saturation conditions and low atmospheric turbulence. Although natural circulation conditions have been supposed — in the experiments, the velocity was not measured,

[3]The conservative values in the calculation of the peak values for pressure and temperature are the contrary for the scenario of the effectiveness of the ECCS: in the first case, the peak value will be a maximum, while in the second case, due to the worse performance of the emergency system at low pressure, it will be a minimum.

Almenas [3.3-30] and other authors supposed that in reality there was a forced convection component, due to the fact that the validation results with the experimental data of Al-Diwany and Rose [3.3-31], obtained in natural circulation in the same conditions of pressure, temperature and mass fractions, showed a significant difference, being almost twice the experimental value. Other authors, as Peterson [3.3-32], assumes that the correlation could have been obtained in natural circulation conditions; this would imply that in the real conditions of the containment the negative effect of a pressure below the atmospheric value could result in an overestimating calculation of the HTC. Actually, the confusion can be explained assuming a slight high velocity for natural circulation conditions in the Sagawa experiments. In fact, many authors have observed that the velocity that provides the best agreement with the correlations of Uchida and Tagami is around 2 m/s for the gaseous mixture, being 2–3 m/s the highest value usually found in the natural circulation large scale facility tests recently carried out, as will be shown below.

Tagami used the same facility, but with a cylindrical condensation surface of bigger size than the one used by Uchida. The thermodynamic conditions of the mixture were not determined — the pressure in the enclosure was not measured — and the gas velocity was not monitored. The steam injection rate, in an attempt to simulate a real scenario of a LOCA, were in the range from $2.2 \cdot 10^4$ to $57 \cdot 10^4$ J/m^{3}s, being the average injection in a LBLOCA around $15 \cdot 10^4$ J/m^{3}s. The experiments were conducted in a turbulent atmosphere where η was increased. The correlation, therefore, distinguishes between the initial stage of the LOCA and the remaining part of the transient.

Kataoka et al. [3.3-33] proposed another correlation that, although quite recent, depends only on η. The facility consisted of a vertical wall 4.2 m high.

Another correlation has been proposed by Murase et al. [3.3-34] for the simulation of one of the first passive configurations of cooling of the containment, by means of an external pool which acts as a heat sink through the wall of the primary containment of the vessel (PCV). The peculiarity of this correlation stands on the even higher importance of η, whose exponent takes a value of unity.

One of the correlations currently used is the one proposed by Dehbi [3.3-27]. The reason lies in the fact that, unlike the previous correlations, Dehbi includes not only the dependence on the mass fractions of the gases, but also some of the main important variables that the experimental literature has identified as particularly relevant. The experiment of Dehbi looked specifically at the effect of the containment variables at a small scale. The experimental work was performed on a 3.5 m long and 0.038 m diameter tubular geometry (PCC tube geometry) with different pressures and mass fractions of vapour and non-condensable gases (helium as a hydrogen simulant).

Liu, with Todreas and Driscoll from MIT [3.3-28], and with Byun et al. [3.3-35] from Korea Electric Power Research Institute, published some papers where they defined the theoretical basis for a possible new design for a passive cooling system for the containment. Its validation is performed using a GOTHIC simulation of a next generation Korean nuclear plant (KNGR), where the new cooling system has been virtually installed. The facility consisted of a carbon-steel U-tube in one loop, feed by water (secondary side) that moves upwards once evaporated, going back to the pool where homogeneous condensation is produced. This natural circulation loop is immersed in a cylindrical enclosure (0.4 m diameter, 3.35 m high), where 3 electrical heaters have been mounted in the lower part to produce the boiling in the liquid pool (primary side). The correlation, although it provides very good agreement with the experimental results of the facility, was compared by Maheshwari et al.- [3.3-36] with the results of an experimental facility of BARC, whose configuration was very similar to the facility of Liu, with the significant difference represented by the fact that the condensation is occurring on a horizontal tube instead of vertical-oriented pipe. According to what has been previously stated, this fact should produce lower values for the calculated HTC with respect the experimental values (an average experimental value up to 20%). However, the results provided by Maheswari et al. [3.3-36] showed that the correlation of Liu yields values of the HTC to about 100% greater than the values obtained by Uchida and Dehbi. In this validation, the Uchida and the Dehbi correlation has also been compared, showing in this case that Dehbi's correlation is slightly lower than that proposed by Maheshwari for horizontal tubes, being coherent with what has been previously

stated. On the other hand, Uchida correlation always predicts very conservative values, except when the pressure of the facility is lower than 0.15 MPa, which confirms that the experimental database from which the Uchida correlation has been derived, was taken under some influence of forced convection, or at least under conditions where the gas velocity was considerably high (2 m/s).

In Table 3.3-3 the main models based on empirical correlations are reported with the boundary conditions from which they have been obtained.

TABLE 3.3-3. MAIN CORRELATION-BASED MODELS AND BOUNDARY CONDITIONS OF THE EXPERIMENTAL SOURCE DATA

Author	Correlation	Conditions
Uchida	$h = 380 \cdot \eta^{-0.7}$	$0.1 \le \eta \le 13$ NC=air, N_2, Ar $0.1 \le P \le 0.287$ MPa T_w=322 K $0.3 \le L \le 0.9$ m
Tagami	$h_{steady\_state} = 11.4 + 284\left(\frac{X_{st}}{X_{air}}\right)$ for $0 < m_v / m_g < 1.4$ $h_{tot\_max} = 426\left(\frac{E_A}{t_A V_c}\right)^{0.6}$ $h_{tot} = h_{tot\_max}\left(\frac{t}{t_A}\right)^{0.5}$ for $t \le t_A$ $h_{tot} = h_{steady\_state} + (h_{tot\_max} - h_{steady\_state}) \exp(-0.5(t - t_A))$ for $t > t_A$	$0.6 \le \eta \le 5$ T_w=322 K L=0.3 m
Dehbi	$h = \frac{L^{0.05}\left[(3.7 + 28.7P) - (2438 + 458.3P)\log X_{air}\right]}{(T_b - T_w)^{0.25}}$	NC=air, He $0.15 \le P \le 0.45$ MPa $10 \le (T_b - T_w) \le 50$ K 0.3 m < L < 3.5 m
Kataoka	$h = 430 \cdot \eta^{-0.8}$	No data
Murase	$0.47 \cdot \eta^{-1}$	$0.8 \le \eta \le 30$ $0.10 \le P \le 0.35$ MPa $295 \le T_b \le 383$ K 0.9 m < L < 4.2 m
Liu	$55.635 \cdot X_{st}^{2.344} \cdot P^{0.252} \cdot (T_b - T_w)^{0.307}$	$0.395 < W_{st} < 0.873$ $0.25 \le P \le 0.45$ MPa $4 \le (T_b - T_w) \le 25$ K

3.3.3. Scenario

During a Design Basis Accident (DBA), large amount of steam is released to the containment. As the wall temperature is lower than its saturated temperature, the steam starts condensing on the containment walls, while the non-condensable gases are accumulated beside the film condensate layer creating an additional thermal resistance. This gas layer acts like a barrier resulting in a degradation of the heat transfer to the wall, making that the interface temperature takes a lower value as a consequence of the diffusion mass process through the non-condensable gases layer, which brings on a lower condensate mass flux.

Throughout the transient we can distinguish two different phases, both logically corresponding to the phases registered in the vessel of the reactor during a LOCA regarding the vapour generated, and the difference of pressures between the vessel and the containment:

a. The first phase corresponding to the blowdown is the stage where the major part of the steam which will remain in the containment is injected. With respect to the phenomenon of condensation, it is very important to realize that during the blowdown the trajectory of the flux will be characterized by the pressure difference between vessel and containment; therefore the condensation model must employ equations and correlations typical of forced circulation regime. This first phase usually lasts less than one minute, being very often around 20–30 s.

b. During the remaining part of the accident, the pressure difference between the vessel and the containment decreases until the effect of the inertial forces is negligible compared with the buoyancy force. This is responsible for a reduction in the injection of steam (with possible presence of light gases). Since then, the predominant regime will be natural circulation, with low values of the Froude number. Consequently the equations and correlations employed by the condensation model must be conveniently modified.

The scenario is characterized by a continuous injection of steam with possible presence of light gases in a large area where a mixture of air and steam is present, where the latter will be condensing on the walls. Since the possible position of the steam injection will always be at a relatively low height in the containment — depending on the position of the reactor in the enclosure — there will be a main vortex due to the combination of an ascending flow of the jet in a radial position close to the centre of the containment, and a successive descending flow on the walls of the enclosure, where the density of the gas increases due to an increase of the ratio air/steam and to a reduction in temperature. Afterwards, some of the less humid gas will mix with the ascending gas rich in steam, and the other part will stratify in the lower part of the enclosure. Three dimensional theoretical study and experimental studies usually distinguish radial vortices between the jet and the walls.

In the containment there will be a double stratification (could be triple, if there were light gases coming from the nuclear reactor). The less humid and cooler air, produced by the condensation process occupies the lower axial levels and the more humid air at higher temperature, due to buoyancy will be in the higher part of the containment.

With respect to the dynamic regime of the gas, both theoretical and experimental results for three dimensional simulation show a velocity profile very heterogeneous typical of turbulent regimes, with many vortices of different scales set along the containment. In addition, the following driving forces with different directions and magnitudes are observed:

a. The buoyancy due to the difference of temperature between the steam jet and the containment atmosphere at a relatively lower axial level.

b. A force caused by the different composition of the gas between the higher and lower parts of the atmosphere and the jet.

c. The air-steam mixture is also influenced by the buoyancy towards the interface due to the strong density difference between the bulk and the interface. This is why the pressure difference term in the momentum equation in our scenario is expressed as a buoyancy force

resulting from the density difference between the bulk and the wall, and not an axial level density difference, as usually.

d. Gravity next to the enclosure walls.

e. Inertial forces near the jet.

The relative contribution and combination of each one of these forces makes the gas regime one of the most difficult problems to be solved, even though for the problem of condensation only boundary conditions are required. In other words, is fundamental to know the regime of the gas and its main parameters (velocity, temperature, pressure, etc.). Usually, with the exception of the first instants after the break, it is possible to assume that the interaction between inertial forces and buoyancy forces is sufficiently low — which means low Froude numbers — and, therefore, the major part of the transient will be characterized by natural circulation. Many authors propose a transient regime that in a separate model means the use of a correlation similar to the one suggested by McAdams for the heat and mass transfer coefficient [3.3-15] [3.3-20] [3.3-21].

In addition to the complexity of the scenario just described, in the case in which the light gases enters into the containment, the effect of the presence of these gases on the different forces must be taken into account, as well as the existence of an additional stratification from a mass fraction relative to the air that the different researches stands at a minimum of 30%. From then, the mixture of non-condensable gases, which will be lighter than the steam, will start to ascend, creating a barrier in the dome of the containment, blocking almost completely the steam flow preventing the superior walls of the containment from acting as condensers, thus being at a lower temperature than the rest of the surface area [3.3-37]. Moreover, since this layer of light gases will have a lower temperature than the steam and the ascending air, the temperature profile will be modified, specifically when the gaseous mixture will cool down in contact with the light gas and will start to descend and, as a consequence, the main vortex will be shorter, appearing an additional one limited to the layer of light gases situated on the top axial level.

3.3.4. Experiments

3.3.4.1. Classification

The experimental studies related with the condensation problem can address different objectives:

a. To reproduce the real scenario of the condensation phenomenon as it would occur in the containment of a nuclear reactor, stressing the performance and evolution of the boundary conditions.

b. To validate a model able to predict the condensation phenomenon.

The real scenario, even when is limited only to the phenomenon of condensation, is very complex because its boundary conditions are two or three dimensional and have a global nature, since the dimension of the system affects the development of the phenomenon.

According to what previously described, from a point of view that we could define as “experiment-to-reality”, we can classify the experimental facilities in three different ways:

I. The experiment[4] is able to reproduce nothing or only partially the existing phenomena related to the condensation in the real scenario of the containment[5].

[4] By the term ‘experiment’ we indicate the separate effects test (set) facility, which means that not only the configuration and dimensions of the facility must be characterized the containment, but also the type of test must be able to simulate our scenario. For instance, if in the sequence of events of the test, an increase in pressure must be achieved through an increase in the amount of steam introduced, then the real effect of the pressure is lost (in this case, it is overestimated), measuring a different HTC as if the new higher level of pressure would have been obtained by means of an increase of the initial amount of air.

II. The experiment is able to separately reproduce the existing phenomena and boundary conditions in the real scenario of the containment related to condensation (II.1, or simply II). If the experiment has a difference in the hardware configuration or some relevant phenomenon regarding the boundary conditions is altered, then it will be classified as II.2.

III. The experiment reproduces totally the phenomena and boundary conditions related to the condensation in both the case when almost all the boundary conditions are situated in real ranges (III.1, or simply III), and the case when they are not (III.2). If a large scale experiment is able to reproduce (integrally) the condensation phenomenon, but at the same time lacks some important phenomenon related to the boundary conditions[6], then the experiment will be classified as II.2.

From the point of view "reality-to-experiment", we can classify the experimental facilities as follows:

I. The experiment is only able to measure (indirectly) the fundamental parameter of condensation locally, or another important parameter, such as η, but not all the relevant parameters (temperatures, pressure, axial and radial velocities, and mass fractions).

II. The experiment is able to measure some or all the important parameters of the condensation, but only in a global fashion, in lumped-volumes.

III. In addition to the fundamental parameter of condensation, the experiment is able to measure locally also the remaining fundamental parameters.

Bearing in mind the previous double classification, we can draw the following conclusions:

a. An experiment will accomplish the objective 1 when it belongs to the group III in experiment-to-reality.

b. An experiment will accomplish the objective 2 when it belongs to the group III in experiment-to-reality, and in addition it belongs to the type III in reality-to-experiment (III/III).

c. If the experiment belongs to the type II or III.2 in experiment-to-reality, the use of another experimental database will be required to support the obtained results, and more precisely to be able to reproduce the missing phenomena and to verify that the validated model is in the real range of values.

As it has been shown above, the main problem in the experimentation on the phenomenon of condensation is represented by the fact that the magnitudes of the dimensions of the enclosure, and the strong dependence of the phenomenon on its boundary conditions, make that the simulation-validation of the model must be linked to the real simulation of the flow conditions in the containment. The main phenomena and parameters related to the boundary conditions that have to be adequately reproduced are the followings:

a. Turbulence

b. Natural or transitory circulation

c. Triple stratification of steam, temperature, and light gases (if exist)

d. Thermo-hydrodynamic conditions of the flow:

- Velocity
- Pressure
- Temperature
- Ratio of mass fractions

---

[5] The expression "related to the condensation" means that the phenomena to be reproduced are limited to those that constitute the phenomenon of condensation and its boundary conditions. The boundary conditions will be listed below.

[6] This is the case for the CVTR when, although reproducing the condensation phenomenon globally, the forced circulation regime of the gas makes the test carried out far from the major part of the condensation scenario.

e. Wall inclination (less important)

f. Heat sink represented by the wall, or control temperature of the wall

g. Temperature difference between wall and flow

h. Presence of light gases

i. Characteristics of the jet: velocity, temperature, inclination

The previous distinction between experiments reproducing integrally or only separately all the existing phenomena in the containment, is aimed to highlight that very often the experimental facilities are able to simulate a phenomenon without considering another one, or at the expense of neglecting other phenomena. For instance, in their facility, Huhtiniemi and Corradini [3.3-16], in order to reproduce the velocities achieved in the containment, had to generate a forced circulation, modifying the lines of flow (and the equations and correlations in the models) through the process of condensation. A more common situation is the capability of simulating different ratios of mass fraction: it is possible to determine how the condensation develops from the knowledge of this parameter, but it will not be possible to reproduce the mass stratification in the containment. Therefore, it is convenient to distinguish the facilities able to reproduce the phenomena occurring in the containment, also in the corresponding real ranges in an integral -simultaneously- fashion, and the facilities where the only way to reproduce a phenomenon is to cause the phenomenon artificially in a way that the containment scenario will not occur in the facility. This would not allow, obviously, to extend the results of the simulation-validation to the containment even if it were a large scale facility.

In the following, we will briefly describe some of the most important experimental facilities proposed in the literature that can be used whether for the validation of models or for the characterization of the phenomenon of condensation into the containment, indicating the corresponding type of the facility from the previous classification that has been addressed. Subsequently, the ranges of the fundamental parameters of condensation will be summarized for each facility in Table 3.3-4. In Table 3.3-5 the approximate real conditions for some of the main parameters in the reactor containment are presented.

TABLE 3.3-4. DIMENSIONS AND VARIABLE RANGES OF SOME OF HE MAIN EXPERIMENTAL FACILITIES

EXPERIMENT	TYPE	DIMENSIONS (m)**		FLOW	P (bar)	T_b (°C)	T_w (°C)	W_{nc} (%)	v_g (m/s)	W_{He} (%)	HTC (W/m^2K)
Dehbi	II.2/III	Ø0.45/5	Ø0.038/3.5	NC	1.5-4.5	79-137	60-100	25-90	-	1.7-8.3	200-1200
Anderson	II/III	2.8/1.7/0.32	2 x 0.91*0.91	NC	1-3	60-120	25-100	24-83	-	0-30	75-750
Uchida/Tagami	I/I	Ø0.15/0.45	0.14*0.30	FC	1-2.75	No data	322	η=1-13	-	NO	80-1100
CVTR	II.2/II	Ø17.66/32		FC	0-1.72	57-116	No data	No data	10 máx.	NO	100-1500
Fox & Peterson	II/III	1.9/0.15/0.15	0.152*1.066	NC/FC	1	50-90	30	13-90	-	NO	30-300
Kang & Kim	II.2/III	1.72/0.15/0.0984	0.15*1.52	FC	~1	70-96	20-40	0-78	<3	NO	100-2000
Al-Diwany & Rose	I/III	Ø0.46	0.097*0.097	NC	~1	40-90	10-85	η=0-25	~0	0-30	No data
Huhtiniemi	II.2/III	1.9/0.152/0.152	0.152*1.066	FC	1-1.65	70-95	30	η=0-87	1-3	NO	100-1500
Liu	II.2/III	Ø0.4/3.35	Ø0.04/2.0	NC	2.4-4.5	104-125	100	30-60.5	-	6-42	500-1500
TOSQAN	III.2/III	Ø1.5/4.8	9.4 (2 m high)	NC	1-6	60-153	52-149	15-75	0-6	NO	100-1000
MISTRA	III/II	Ø4.25/7.3	26.2, 2x21.4 (5 m high)	NC	3-5.5	120-135	115	No data	0-3.5	0-32	No data
ThAI	III/III	Ø3.2/9.2		FC	1-1.5	20-65	No data	80-95	-	0-30	No data
NUPEC	III[7]/III	Ø10.8/14.4	No data	NC/FC	1-1.6	20-105	15-70	No data	0-2	0-65	No data
COPAIN	II/III	2/0.6/0.5	2*0.6	FC	1-7	70-165	32-136	0-100	0-3	0-69	37-1100

** See explanation given at the end of Section 3.3.4.2

TABLE 3.3-5. APPROXIMATE REAL CONDITIONS IN THE CONTAINMENT

P (bar)	W_{nc} (%)	v_g (m/s)	HTC (W/m^2K)
2.48-4.55	30-60	0.3 - 3	100-1500

[7] The only difference regarding the real scenario is that it is not wall temperature-controlled.

3.3.4.2. Survey

The first experiments related with the condensation of steam in presence of non-condensable gases are attributed to Uchida and Tagami[8] [3.3-25] [3.3-26]. Starting from their experiments, two empirical correlations have been obtained for the direct calculation of the HTC, only from the ratio of mass fractions. This is just the main shortcoming: since they do not depend on other variables, whose importance has been demonstrated by successive analytical and experimental studies — as has been shown above, the correlations of Uchida and Tagami are applicable only under some kind of boundary conditions in a very small range. Therefore, this experiment can be classified as type I/I, because it cannot be used neither for the simulation of the scenario of the containment, nor for the adequate validation of a model[9].

The experiments conducted in the CVTR (Carolinas Virginia Tube Reactor) [3.3-13] at the end of 1960s have been the only integral experiments of large scale in USA before the 1990s. The results are only partially exploitable, essentially because of the following three reasons:

a. There was a lack of measured data: only few measuring points and only few measured variables.

b. The particular geometric configuration of the enclosure: the injection is placed just on the top of a tray which restricts the passage in the axial zone of the enclosure to a small radial gap.

c. The simulated scenario is different from the real one (the regime of the fluid is always forced convection), so the major part of the LOCA scenario in the containment is not exactly reproduced.

In this test, the HTC was measured in 5 different ways and in different positions. The values for the temperature of bulk and wall, together with the pressure and the velocity, were also obtained. With respect to the data for the velocity, the results are not very reliable due to the lack of a large database and some errors during the acquisition of the data [3.3-12] [3.3-15], as well as due to the particular geometric configuration of the enclosure: the high velocity measured near to the wall was the result of a tray which was limiting the passage from the Operating Region towards the Intermediate Region (placed at a lower level). This tray forms a peripheral ring, in a way that the connection between the two regions is very small. This narrowing causes high velocities in the gas flow from a zone to the other.

One of the most important aspects was the deduction of the existence of a stratification in the distribution of η: the saturation pressure calculated from the measured temperature was significantly higher then the value expected from the difference between the total pressure and the partial pressure of the air. Therefore, it was possible to deduct that the hypotheses of homogeneity and/or thermodynamic equilibrium were not satisfied. It is important to remark that the regime was strongly turbulent, and in the simulation conducted by Kim and Corradini [3.3-15] with the code K-FIX, the velocity profiles obtained were very complex, strongly affected by the high injection velocity and by the narrow connection between the Operating and the Intermediate Regions. It was observed how the axial velocities close to the wall could be positive or negative — in proximities of the gap, the radial velocities were negative, indicating flow going far from the wall — and, therefore, in the simulation with K-FIX the countercurrent model showed values for the HTC sufficiently similar than in the parallel flows model, under the assumption that one of the two laminar layer is completely developed. In the case that countercurrent flows actually exist, in axial levels where the thickness of the film were high, the possible effect of its resistance should be taken into account because the not-developed gas layer, together with a large thickness of the film, could be responsible for a liquid and gas thermal

[8] Five years before, in 1959, Alf Kolflat [3.3-40] obtained HTC experimental values between 142 and 6520 $W/m^2 K$. The authors of the present section only could find out that the facility consisted of a 22 m^3 stainless steel enclosure.

[9] In what follows, the validation will be referred to a *best-estimate* model.

resistances of almost the same magnitude order. In any event, the velocity profile obtained by Kim and Corradini in the simulation of the test of the CVTR is not exhaustive for two main reasons: on one hand the particular configuration of the facility due to the narrowing in the axial zone close to the measuring region is responsible for high axial velocities with modifications in the flow direction and for radial negative velocity components; in addition, the existence of the forced circulation (the velocities obtained by the simulation of Kim and Corradini confirm the magnitude of the experimental value and therefore ensure the forced character of the flow) modifies significantly the flow trajectory in the containment, characterized in almost all the transient by natural driving forces and by values for the velocity in the range between 0.3 and 3 m/s.

From what previously described, we can say that this experiment belongs to the group II.2/II, being useful to confirm the existence of important stratifications in the gas composition, or the importance and complexity of the velocity with respect to the condensation, but not to simulate the real scenario of the containment, neither to adequately validate a model.

Another recent facility is the Fox and Peterson at the University of Berkeley, California [3.3-17]. It is a separate-effect test (SET) of small section, but 2 m high in order to achieve natural driving forces not far from those of the containment, although the pressures are usually lower than the real pressure in the containment (around 1 bar). In this kind of facility, as in the Anderson facility [3.3-37], the visual analysis is fundamental because it helps to easily understand the distribution patterns of the flow, fact much more difficult to understand mathematically[10]. As usual in this type of SET configurations, the condensation surface is limited to only one side of the enclosure, based on the existence of an axial symmetry (in this way, it is possible to reduce the size of the base of the prism without losing phenomena). Once the steady state had been achieved, the gaseous flow showed an intermittent turbulence in time (the turbulence was observed sometimes) and in space (turbulence was not present in all the enclosure). The flow showed several vortices, whose size was almost inversely proportional to the values of the convective forces, both natural and inertial. A large vortex extended to all the enclosure was observed, constituted by the central rise caused by the steam injection at high temperature, coming down from the periphery after being cooled in the proximities of the wall, whose velocity was only a very small fraction compared to the values in the intermediate and low levels. In the axial levels closer to the injection, the fluid accelerated due to the cooling and it encountered with the ascending steam at higher velocity, causing multiple vortices of smaller size, characterized by sufficient stability. The fluid, as in the CVTR, undergoes a force towards the condensation surface. In this way, the visual observation indicated that the flow was essentially two dimensional. Other important phenomenon was the generation of mist, whose higher density caused a negative acceleration, increasing significantly its proportion in the lower part of the enclosure.

A similar facility with respect to the possible use for validation and for reproducing a real scenario is the one proposed by Kang and Kim [3.3-39]. The main difference is represented by the fact that the velocity is imposed as a boundary condition and the condenser tube is horizontal-oriented. The value of the pressure is around the experimental value. An important difference in the results between this experiment and the experiment conducted by Fox and Peterson is represented by the fact that some values of the HTC arrived up to 3000 W/m^2K, significantly higher than the values measured by Fox and Peterson. The reason is not very clear because the authors do not report the value of η. However, the major part of the values of the HTC is in the range 100–1000 W/m^2K.

The experiments conducted by Anderson et al. [3.3-37] constitute a recent attempt of simulating the behaviour of the PCCS system of a Westinghouse AP600. In addition, the authors aimed to produce a parametric study of the phenomenon of condensation. Two facilities in scale 1:12 were built in order to observe both by visual inspection and data analysis the dependence of the most important parameters of condensation, as well as the established scenario from a phenomenological point of view. This experiment is classified in the type II/III.

[10] Which justifies the importance of CFD codes, not only for their capability of predicting three dimensional nature scenarios, but also for their interface which allows the determination of results that otherwise would not be achievable at the moment of understanding the phenomena occurring in the containment.

The experiments of Al-Diwany and Rose [3.3-31] contribute with some interesting results about the appearance of thermal and mass stratifications. The authors noticed that when light gases (e.g. helium) were introduced, the higher temperatures were observed on the lower axial levels of the enclosure, whereas the contrary occurred when heavy gases (e.g. Argon) were introduced; this is related to the axial distribution of the hot steam, dependent on the buoyancy force in the gaseous mixture. Another important result was the measure of the temperature profiles both axial and radial, where a strong gradient is observed in the gaseous laminar boundary layer than in the different axial levels; however, the small height of the facility must be taken into account. This demonstrates the convenience of considering the driving forces due to the difference of the densities between the interface and the bulk under conditions of natural circulation: by means of the Grashof formulation (in a separate model), or in the pressure differential term in the momentum equation (in an integral model based on field equations). Finally, Al-Diwany and Rose observed that the experimental results showed values of the HTC lower than those obtained in previous experiments; this fact was attributed to the existence of convective forces in those experiments, deduction confirmed from the assumption made in the use of the model of Sparrow and Minkowycz [3.3-3] for natural circulation. In this way, the importance of the regime of the fluid was further demonstrated. The experiment belongs to the type I/III, because the reduced axial dimensions prevent from reproducing the phenomena of the condensation.

The experiment of Huhtiniemi and Corradini [3.3-16] is among the first ones investigating the effect of the inclination of the surface in the condensation, as we observed in the parametric study. The ranges of the main variables are similar to those obtained by Kang and Kim [3.3-40] (100–1000 W/m^2K), being the peak value of the HTC equal to 6200 W/m^2K for horizontal pipe with pure steam at the maximum velocity. The experiments belong to the type II.2/III, because the velocities that are achieved in the containment are taken under forced convection.

In the experiment conducted by Murase et al. [3.3-34], although the dimensions are similar to other SET (height equal to 4.2 m; small section), due to the fact of simulating the behaviour of a suppression pool, the phenomena observed are very different from those that would take place in the containment, such as homogeneous condensation, evaporation in the surface of the pool, heating and stratification of the liquid in the pool, etc. The published data are highly restricted to the evolution of pressure and temperature in the wet well and in the drywell. Therefore, it is not recommendable to employ it with the purpose of studying the scenario of the containment, or for model validation.

The experiment of Liu et al. [3.3-28] consists in an enclosure, where a horizontal condenser tube is placed, partially filled by water where three electrical heaters have been installed, with a total power of 27 kW, in order to produce the continuous evaporation of the liquid. Although the total height of the enclosure is 3.5 m, part of it is occupied by liquid and part by the gaseous atmosphere; the mean level of the pool has not been indicated by the authors. Although this inconvenient, the ranges of the main variables have been adjusted to the reality. Since the objective of the experiment is to propose a new PCCS for an ABWR and not the simulation of the PCCS of a reactor like the AP 600, the configuration of the facility does not suit the reality of our scenario and therefore the reproduced phenomena will not be useful for a better understanding of it. Therefore, the experiment is classified as type II.2/III: it is not useful for understanding the behaviour of the flow in the containment with respect to the condensation, but it is useful for validating a theoretical model although with reservations, because the condenser is a horizontal tube. Although the total range of values of the HTC is from 200 to 2500 W/m^2K, again the more usual values are in the range from 500 to 1500 W/m^2K. Essentially, the restrictions regarding the condensation scenario are the flow distribution (in this experiment there is not a particular jet in the lower part of the enclosure, far from the surface of condensation, but a uniform steam flow arising all through the volume of the enclosure), and mostly the fact that the tube is horizontally oriented, which modifies substantially the possibility of the condensate film to develop, also avoiding the influence of the wall side condensation on the axial and radial gas flow paths.

The experiment of Dehbi [3.3-27] exhibits almost the same configuration of Liu experiment but being the tube vertically oriented. The objective of the work of Dehbi, conducted at the MIT, is the same as Liu: the study of an alternative PCCS for an ABWR. Therefore, the measurements are the same

obtained by Liu, with a gap between the surface of the pool and the pipe equal to only 0.4 m; the only difference is that in this case the pipe does not have the shape of a U-loop, but its section shows the longer length in the central part, which is in vertical position (U-shape rotated by 90 degrees), then allowing the condensate film to develop, although the gas flow distribution will not have anything to do with respect to that of the reality. This is why this experiment is II.2/III.

Before the 1990s, beyond the CVTR there are three main facilities of large scale (LST) for simulating the configuration of the containment: the Battelle Model Containment (BMC), the Heissdampfreaktor (HDR), and the Marviken.

To the best of our knowledge, no tests have been conducted in the BMC and in the Marviken that address condensation on the surface of a wall.

Starting from the 1990s, important international projects for the simulation of accidents in the containment started to be developed. The main objectives are tackling the problem of the present survey, characterized by the lack of data regarding large scale of the containment, and to validate a set of thermohydraulic codes able to simulate a priori the containment in a three dimensional fashion (CFD), whose validity has not already been rigorously demonstrated. In order to accomplish these tasks, a double line of investigation has been established: on one hand, the construction of experimental facilities with many monitoring points for the main variables that characterize the scenario of the containment (flow velocity, temperatures, gas composition and pressure); on the other hand, employing the generated data in order to verify the effective capability of the CFD codes, determining their advantages and limitations with the aim of elaborating a Best Practice Guideline (BPG), able to ensure "high-quality results and for the formalized judgement of CFD calculations and experimental data" [3.3-41].

The predominant phenomenon in the containment is the gas distribution, composed by air and steam (with the possibility of light gases) coming from the reactor. Therefore, these large projects do not give priority to the condensation produced on the walls of the containment. In addition, it must be considered that the different passive configurations existing for the condensation of the steam injected in the containment are very specific, which means that the experimental simulation could not be easily generalized as in the case of the transport and distribution of the gaseous flow in the containment.

Even this, in the majority of the facilities developed in these projects, local measurements of temperatures have been considered in the gas, in the bulk, and on the internal and external surfaces of the wall, in order to calculate the heat flux and the HTC. As it has stated above, one of the fundamental problems to be tackled regarding validation, is the possibility of assuming an error in the estimation of the HTC as it were caused by the inaccuracy of the condensation model, whereas the error has been produced by a deviation in the calculation of the boundary conditions.

One important experimental activity was performed under the International Standard Problem ISP-47 [3.3-42], which has the objective of demonstrate the actual capability of CFD and LP codes in the field of containment thermohydraulics, mainly related with the hydrogen distribution. To achieve this objective, a two-step strategy was proposed: in the first step, the validation of refined models in the separate effect facility TOSQAN (7 m^3) and at larger scale in MISTRA (~ 100 m^3) would be carried out, where a study of the different phenomena that take place in the containment — including their interactions — is performed; and in the second step a more real validation of the codes in a complex and more realistic compartmented geometry ThAI (60 m^3) would be addressed.

In the TOSQAN facility (an enclosure of low-intermediate size without compartmentalization) it was possible to distinguish different zones with respect to the flow patterns, besides of two axial zones clearly delimited by the height where the injection is placed. In the lower one (thermal natural convection zone), convective rising flows are observed, with a higher velocity in the centre of the enclosure. Again, in the upper axial zone, a vortex is formed by the plume of hot steam (injection zone) which goes down on the periphery (condensation zone) while it is cooling down. When it starts to be heated close to the lower axial zone (rising convective flow), it is decelerated, then the drag due

to the plume in the centre is reinforced, moving upwards again. The tendency of the steam in moving towards the high layers of the enclosure producing stratification in the gas composition has been confirmed, and differences in the corresponding mass fraction were about 10%. This experiment belongs to the type III.2/III, because although the boundary conditions of the condensation have been completely reproduced, due to the small dimensions of the enclosure it is difficult to reproduce the values of the stratification of the flow that would be observed in the real configuration of the containment.

With respect to the MISTRA facility, Studer et al. [3.3-43] have recently published the results related both with the experimental data and with the simulation carried out with different thermohydraulic codes. The conclusions with respect to the experiments are the followings:

A main pattern in the flow was observed, consisting in a vortex extended to the entire enclosure, formed by an upflow in the central part of the facility and a downflow on the sides, once heat is exchanged with the condensers. Unfortunately, to the best of our knowledge, radial velocities were not measured.

Among the three condensers, the one placed at the highest level recorded the highest heat transfer, certainly due to the major concentration of steam in the proximities of the wall at the higher axial levels. The fact that the lowest condenser has a lower rate of heat transfer is responsible for its lower temperature which causes a higher concentration of non-condensable gases in proximity of the wall. This fact has been also demonstrated by the experiments.

The experiment in which helium was injected did not exhibit any stratification with respect to the distribution of the light gas in the enclosure.

The facility ThAI [3.3-44], with a larger size than TOSQAN, is composed by two concentric steel cylinders with a closure between the two cylinders situated at a medium axial level. The test conducted consisted in the injection at a high level in the annulus (inner cylinder) of steam and helium at 293 K; subsequently, after 2700 s, steam only at 383 K and finally, at 4700 s, the position of the injection was moved at a lower height of the enclosure (in the lower compartment). Unfortunately, the authors were able to find only general results related to the temporal evolution of pressure, temperature, and mass fraction. The experimental values measured in the experiment showed a strong double thermal stratification: the first one between the upper plenum and the annulus with differences of 30 K; the second one between the two axial compartments where the closure made by 4 trays limits to 1/3 (120°) the total available space of the connection between them. Since the injection of the hot steam increases the temperature in the upper plenum and the annulus, the corresponding lower plenum and lower annulus are not affected by the injection, and consequently their temperature remains almost equal to 293 K as before — increasing only when the injection is placed at a lower level; therefore, the temperature difference between the two axial levels is greater than 45 K. This means that the axial zone below the injection constitutes a limit to the vortex formed by the injection (or plume), the condensing walls, and the drag-heating of the cold gas descending in contact with the injection (or plume). With respect to the gas composition, the corresponding distribution follows the same guidelines of the temperature: in the internal cylinder and in the annulus a difference not greater than 10% is observed, whereas in the two axial levels this difference is twice (around 20%). The same occurs with the mass fraction of the helium.

The Nuclear Power Institute of China (NPIC) has developed some preliminary experiment research and relative theoretical analysis for passive characteristics of advanced PWR nuclear power plant AC600/1000 [3.3-45]. This experimental research plan has been divided into three steps. In the third step, NPIC has constructed (or is nearly constructed) an integral containment cooling test facility in order to simulate and research comprehensive characteristics of passive containment cooling system for AC600/1000. The facility is 1:10 in scale.

Another recent experimental program has been carried out under the joint research project of DABASCO (acronym for ‘common experimental database for development of physical models and

correlations for thermohydraulic containment analysis'), which is supported by the European Community [3.3-46]. The DABASCO project deals with several important phenomena involved in the containment thermohydraulic analysis, among others, with the influence of non-condensable gases on condensation. One of the carried out program was the COPAIN separate-effect test (SET). The general aim of the COPAIN work package at CEA (Commissariat à l'Énergie Atomique) is to investigate steam condensation on vertical walls in the presence of non-condensable gases. The facility is provided with a water cooler which permits to control the wall temperature. During the experiments, the heat flux through the plate (at 20 locations), liquid film thickness (at four locations), gas temperature, gas velocity and vapour-gas mixture composition have been measured.

The NUPEC (Nuclear Power Engineering Corporation) facility represents a LST multicompartment containment. It includes the main rooms of any actual 4-Loop PWR plant, but metallic components such as Steam Generators, pumps, etc., are excluded. Two tests have been performed without activating the sprays.

The PHEBUS-FP program is performed by the French Institut de Protection et de Sûreté Nucléaire (IPSN) with contributions of the CEC, EDF, Japan, Korea, and USA [3.3-47]. This program has been mainly designed to obtain experimental reference data to check and qualify the code systems used in the safety analysis of source term evaluation. The containment houses a 10 m^3 volume. It consists of a 4.5 m high and 1.8 m diameter cylinder closed at the top and at the bottom by ellipsoidal surfaces. The floor of the vessel is equipped with a 0.5 m depth and 0.528 m diameter sump, respect to a representative PWR containment one. In order to achieve a representative ratio, the internal facing surfaces of the vessel were "neutralized" by heating them up to a thermal state slightly over the one of the containment atmosphere. Three cylindrical structures (2.6 m high, 0.15 m diameter) were attached to the containment ceiling to provide a total surface area of around 2.3 m^2 for heat transfer. Each of them was divided in two parts: an upper one called "wet" or cold zone (0.775 m^2), designed to control steam condensation; a lower part called "dry" or hot zone (0.336 m^2) where sliding condensate from the wet section is collected and then drained to the sump. On the condensing surface, the temperature can be controlled by the use of an organic liquid coolant system inside the cylinder. This system regulates the condenser surface temperature and maintains it at an almost uniform temperature for all condensing surfaces. They are instrumented with level sensors that measure condensed mass. The containment instrumentation measure H_2 and O_2 concentrations (1 point), gas temperature (25 points), sump temperature (4 points), structure temperatures and condensation rates. The condensation flow rate is deduced from the information given by the level sensors located inside the water collection bottles, which are periodically emptied by returning the collected water to the sump.

In Table 3.3-4 the ranges of some of the main variables regarding the different experimental facilities that have been analysed were presented. With respect to the third column, the right subcolumn deals with the dimensions of the enclosure where condensation is occurred. If this is a cylinder, then its diameter and height is written; if it is a prism, the height, wide and depth are given in this order. If only a measure is given, then this is the total volume of the enclosure. Regarding the left subcolumn, the dimensions of the condensers placed inside the enclosure are given. The criteria follow the same meaning than for the right subcolumn. When the condensation surface is a plate, then only two dimensions are given, and when the number of condensations is two, then a '2 x' is found. The fourth column deals with the circulation pattern that rules in the tests performed in the facility, where 'NC' and 'FC' mean natural and forced circulation.

3.3.5. Validation of codes

One of the main problems to be tackled in the simulation of the phenomenon of condensation is represented by the choice of a suitable model for the scenario of the containment: An a priori error in the stage of modelling could be the choice of a condensation model in natural convection for the blowdown, or a model in forced convection or laminar regime for the remaining part of the accident.

An a posteriori error to be taken into account is the possibility of attributing the disagreement between the calculated value and the experimental value of an important parameter for the condensation (HTC;

condensate rate) to an error in the condensation model, whereas actually the error has been caused by a deviation in the boundary conditions. The boundary conditions that have to be addressed are those nominated at the beginning of Section 3.3.4 (experiments).

Since the validation of the condensation phenomenon belongs to the more general objective of validating the behaviour of the PCCS in the reactor containment, the validation of a condensation model must be achieved from the validation of the thermohydraulic code simulation where the model is implemented. In order to analyse adequately the validation exercises present in the literature regarding condensation models, it has to be clear the meaning of deriving the conclusions of the validation from the results of a code simulation. The point is to keep in mind that the link between the thermohydraulic code and the condensation model lies in the calculation of the boundary conditions. So when a noticeable deviation is produced in the calculus of any relevant variable of the atmosphere containment (relevant condensation boundary conditions), the error will be derived to the calculation of the HTC or the condensate rate, avoiding us to draw any conclusions regarding the validation of the condensation model implemented in the code.

Nowadays, a large number of numerical codes for the simulation of the accident conditions in the containment of a reactor are available (see Table 3.3-6).

TABLE 3.3-6. CONDENSATION MODELS IMPLEMENTED IN SOME OF THE MAIN THERMOHYDRAULIC CODES

Code	Type of code	Nature of the code	Condensation model
GOTHIC	Nuclear	LP / Field code	Uchida correlation and Gido and Koestel correlation
COMMIX-1D	Nuclear	Field code	Collier's model (HMTA[11])
PCCSAC	Nuclear	Field code	Collier's model (HMTA)
CFX4	Commercial	Field code	Non implemented
FLUENT	Commercial	Field code	Non implemented
MAAP-DBA	Nuclear	LP	Uchida and Tagami correlations
CONTAIN	Nuclear	LP	Collier's model (HMTA)
CONTEMPT-LT	Nuclear	LP	Collier's model (HMTA)
CONTEMPT-4/MOD5	Nuclear	LP	Tagami correlation and others
MELCOR	Nuclear	LP	Collier's mass flux and Chilton-Colburn correlation (HMTA)
COMPACT	Nuclear	LP	Uchida and Tagami correlations
TONUS	Nuclear	LP / Field code	Chilton/Bird condensate rate formulation with McAdams correlation (HMTA)

[11] 'HMTA' means *Heat and Mass Transfer Analogy*.

Since the phenomenon of condensation is strongly affected by the boundary conditions, especially for the flow thermodynamics (regime, flow patterns, velocity, composition, temperature and pressure), but also for the subcooling grade of the wall and the length of the condensing surface, the code capability in simulating the condensation phenomenon will be strongly affected by the capability of simulating the flow conditions. Therefore, although a theoretical model of condensation implemented in a thermohydraulic code yielded good results in a SET facility, the validation performed in an IET facility could call the code capability into question. For instance, the contribution of each condenser to the total heat transfer in the MISTRA facility was not adequately predicted when helium was introduced [3.3-48]. This inconvenient does not mean that the implemented model was not working properly, but that the boundary conditions used for the local initialization of the model were different from the experimental ones: the code did not predict correctly the stratification of the gas composition in the containment.

In the following, we examine the conclusions of the validations related to the phenomenon of condensation. These conclusions, although deriving from the general validation related to the simulation of the scenario of the containment, will attempt to be restricted to the capability of simulating the condensation heat and mass transfer.

Due to the commercial nature of many CFD codes, a condensation model is usually not included and must be implemented by the user. The implementation of a condensation model based on the conservation Eqs [3.3-49] [3.3-50] [3.3-51] consists in the introduction of the sink terms in the gas energy equation and in the equations of mass conservation for the gas and the steam for the cells contiguous to the wall, being these terms function of quantities calculated by the code.

Another more extended manner of implementing a condensation model [3.3-22] [3.3-52] is based on the introduction of the sink terms which can be an empirical correlation or a separate model previously calculated by means of a subroutine introduced by the user, as an additional term of the conservation equations. In the case of the separate models, since they depend on the average values (values in the bulk) whereas the CFD codes are based on the calculation of local properties, the definition of the bulk in the code is not trivial, because the required separation of the wall that is just the bulk, can reduce the precision of calculation, making it difficult to observe phenomena whose scale is smaller than the size of the cell contiguous to the wall. This problem prevents from considering the evolution of the variables all along the different boundary layers. As a condition, the size of the cell contiguous to the wall must be at least greater than the largest thickness of the different boundary layers (kinetic, thermal, mass):

$$s_{wall-atm} \geq \delta_i \qquad i = v, T, W_{st} \tag{3.3-5}$$

Therefore, since the model is implemented by the sink terms in the gaseous atmosphere, the possible influence of the liquid on the gaseous phase is neglected, because the thickness of the liquid is considered negligible compared to the volume occupied by the gas. Since the difference between the interface and wall temperature is usually small (less than 1 ºC), both temperatures are set equal in many codes, which means that the condensate film thermal resistance is neglected.

Another aspect to be considered in relation to the validation exercise from a code simulation is represented by the fact that in almost all the analyses reported in literature, the different authors only show the evolution and spatial distribution of the different variables that characterize the scenario of the containment in two dimensions with respect to the condensation phenomenon. In other words, only in few situations the flow will require a three dimensional scenario for the adequate simulation of condensation. The works of Andreani et al. [3.3-51] and Wolf et al. [3.3-53] show how the three dimensional character of the flow is very important when the temporal evolution of the flow is to be analysed, because it can affect the time evolution of the distribution and transport of the mixture in the different compartments and connections of the containment.

The condensation models implemented in the LP codes are based whether on empirical correlations or separate models. Both methods have been validated extensively using many experiments, including

large scale tests. The ISP-47 [3.3-42] exercise results showed that all LP models calculate similar heat transfer coefficients with a spread of 30%. Based on overall indicators such as the measured system pressure and total measured condensate masses (as it is the case of MELCOR validation with TOSQAN, and on local indicators for a Westinghouse AP600 large scale tests in GOTHIC validation), it can be generally concluded that the total condensation can be predicted using LP codes with the same approximation than CFD codes.

In their study based on the validation of the FLUENT 6 code with the experimental results of TOSQAN, Forgione and Paci [3.3-50] consider directly the conservation equations without any implementation of a separate model or an empirical correlation able to take into account the condensate mass flow or the corresponding transferred enthalpy. In this case, the sink term referred to the condensation is not a pointer passed to the subroutine where the field equations are implemented. For instance, the condensation mass flow will be:

$$\dot{m}_c = -\frac{\rho D}{1 - W_{st,i}} \cdot \left. \frac{\partial W_{st}}{\partial y} \right|_i \tag{3.3-6}$$

where the differential term and the flow properties are calculated by the code (the mass fraction is calculated from the pressure and temperature). It is convenient in these cases to conduct an analysis on the sensitivity of the cell thickness adjacent to the wall, because this parameter constitutes a limit on the study of the wall, in terms of the development of the boundary layers generated. This dependence will be more significant than in the case in which a separate model is to be implemented in the sink terms of the field equations, since in the last case the thickness of the cells adjacent to the wall will only modify the value of the properties of the bulk appearing in the model, usually temperature and density (mass fraction).

It is important to consider that the CFD code will not calculate the latent heat, but the sensible heat. Therefore, when the heat transfer will be implemented, only the term due to the phase change must be taken into account. This is the reason why in many works [3.3-22] [3.3-43] the condensate rate is the variable used for the validation instead of the local HTC. It also happens that the sink term in the energy equation is expressed by means of the steam enthalpy at the temperature considered as bulk:

$$Q = \dot{m}_c \cdot A_w \cdot \left(C_{p,st}\, T_b - C_{p,bg}\, T_{ref} \right) \tag{3.3-7}$$

Where ‘bg’ means the conditions of the background gas taken as a reference. In this equation, the transfer of latent heat has been calculated at the bulk temperature and not at the saturation temperature of the steam, once that the phase change occurs. The total energy transmitted to the wall in reality would be given by the sum of the contribution due to the phase change and the sensible contribution (neglecting the thermal resistance of the condensate):

$$Q = \dot{m}_c \cdot A_w \cdot \left[\left(C_{p,st}\, T_w - C_{p,bg}\, T_{ref} \right) + \frac{h_s \left(T_{cell} - T_w \right)}{\dot{m}_c} \right] \tag{3.3-8}$$

In this manner, the sensible heat coefficient has made equal to the heat capacity of the condensate steam:

$$h_s = \dot{m}_c \cdot C_{p,st} \tag{3.3-9}$$

Malet et al. [3.3-22] managed to calculate experimentally the sensible HTC (by means of a theoretical approximation to the definition of the sensible HTC, where the heat flux at the wall was considered by means of Fourier’s law), finding values around 5 W/m^2 K. In turn, the previous equation provides higher values for the calculated HTC. In addition, since the CFX code calculates by itself the sensible heat transfer, we would obtain a result calculated *a priori* significantly greater than the real value,

except for the fact that the condensate mass flow could have been underestimated and all the phenomena that improve the mass and energy transfer towards the wall could have not been taken into account.

Other general aspect related to the implementation of the condensation model in a commercial CFD code is the consideration of the mist formation: since the homogenous condensation by thermal disequilibrium is not calculated in the code, the user must introduce a suitable model. The used models are in general in-house, simple models based whether on the non-equilibrium of pressures of steam, or on an Algebraic Slip Model.

A possible improvement in the implementation of a condensation model in a commercial CFD code could be to reconsider the resolution of the Fick's equation for the wall in order to obtain the mass flow, parameter of interest for condensation. As suggested by Houkema (in press), different meshes should be analysed for the cells adjacent to the wall to allow a better calculation of the different profiles defining the boundary layers. This type of implementation is based on operating directly the conservation equations, as we have previously observed in the work conducted by Forgione and Paci [3.3-50].

In a recent paper [3.3-22], a condensation model based on the Uchida correlation has been implemented in the CFX 4.4 code. The experiments used for the validation had been conducted in the TOSQAN and ThAI facilities. The authors introduced two degrees of freedom in the sink terms implemented to allow a better agreement of the obtained results related to the pressure average temperature of the gas atmosphere: the constant in the Uchida correlation, and the width of the cell contiguous to the wall (the objective of the study was not the validation of the condensation model, but the verification of the capability of CFX in simulating the transport and the stratification of the flow). In the calculation of the condensation mass flow, an error is introduced by neglecting the sensible term. Although this is taken into account by the code, it is not possible to compute the condensation flow neglecting the sensible term:

$$q = h_{uchida} \cdot A_w \cdot (T_b - T_w) = \dot{m}_c \, h_{fg} + h_s \cdot (T_b - T_i) \tag{3.3-10}$$

Defining the condensation mass flow as follows:

$$\frac{h_{uchida} \cdot A_w \cdot (T_b - T_w)}{h_{fg}} = \dot{m}_c \tag{3.3-11}$$

introduces an error in the calculation of the transferred mass. The same would happen in the energy equation, where although it has been considered only an enthalpy sink due to the condensate (the term due to the sensible contribution has not been adequately added), the mass flow is still not correctly calculated. This would produce, a priori, calculated values of temperature and pressure lower than the real ones (consequently overestimating the mass and heat transfer), but due to the fact that the authors tuned the Uchida correlation, besides of adjusting the width of the cell contiguous to the wall (then the bulk temperature in the correlation), this overestimation is lost in the calculations. More important than the overestimation of the mass flow is the fact that the Uchida correlation has been used as the condensation model. Since the boundary conditions in the experiments conducted by Uchida were very close to a pressure of 1 bar and to a steam injection at 290 K, values situated at the lower part of the range of the TOSQAN facility boundary conditions, the assumed correlation will underestimate the heat transfer, as it can be confirmed in the Malet et al. [3.3-22] study, where the Uchida correlation is the model that predicts the lower results when the pressure in the facility is greater than 1 bar.

Malet et al. [3.3-22] conducted a very interesting theoretical study where they validate not only some models related to condensation, but also the importance of different relevant parameters. In this study, the results obtained by means of the correlations of Uchida, Tagami, Kataoka and Dehbi have been compared, observing that the first one overestimates the HTC when the heat transfer is low (low pressure and temperature), whereas when the HTC is high an underestimation of the condensation rate

is observed, which is coherent with Peterson's theoretical analysis of the Uchida correlation [3.3-32]. The errors of the correlations proposed by Uchida, Tagami and Kataoka were below 30% in many cases, whereas for Dehbi's correlation the errors oscillate between 63% and 202% (always below the real value). The correlation which yielded better results was Uchida's. Nevertheless, the mass flow is significantly underestimated for the case of high heat transfers. On the contrary, this did not occur in the condensation model employing the Chilton and Bird formulation for the mass transfer coefficient, and the McAdams correlation. For this model, the calculated condensation rates yielded errors below 20% almost in the whole cases.

The numerical TONUS code [3.3-55], developed by CEA and IRSN, in the same way as GOTHIC [3.3-56], is able to simulate the containment by a lumped volumes approach or by means of a CFD approach. The code contains a model for the condensation in presence of non-condensable gases based on the McAdams correlation (for natural circulation), assuming the HMTA for the formulation of the mass transfer coefficient. TONUS has been validated by means of a comparison with the experimental data obtained from the facilities TOSQAN, MISTRA, PHEBUS, ThAI and PANDA. One of the main results achieved from the comparison with the MISTRA facility is that a simplified mesh, exploiting a 180^{o} degrees symmetry in the enclosure, is enough for the computation. All the results have been obtained by means of simplified models that make use of the various symmetries in the facility, considering all the phenomena occurring in the experiment. In general, the code predicts adequately the main variables of the enclosure (pressure and temperature), as well as the fundamental parameters of condensation (condensation rate; data regarding the HTC are not shown) both in LP and CFD modalities.

Houkema [3.3-57] performed a validation exercise with the CFX4 code using the experiments of Kuhn, PHEBUS, PANDA and the facilities of the ISP47 (TOSQAN, MISTRA and ThAI). As usual, Houkema implemented the model by means of sinks linked to user subroutines (mass, steam and enthalpy), but in addition, he introduced a sink for the turbulence. The model starts from the formulation of Chilton and Bird for the condensation mass flow. The steam mass fraction at the interface is calculated from the wall temperature (again, the condensate thermal resistance is neglected) and from the equation of Antoine for the saturation pressure. In the same work, Houkema confirmed the importance of the value of y^{+} (dimensionless distance to the wall) with respect to the different models of turbulence employed, and with respect to the calculated condensate rate.

In the comparison with the PHEBUS database, Houkema employed the low Reynolds number k-ω model for turbulence, because the flow was almost laminar in free convection. The comparison of the calculated condensate rate with the PHEBUS experimental values yielded small errors, as well as in the estimation of the pressure and temperature evolution.

Finally, although data supporting the conclusion have not been presented, Houkama affirms that the condensation has been adequately predicted in the major part of the cases employed for the validation, being the main deviations associated with the wall treatment -the type of regime assumed for the solution of the boundary layers-, without mentioning the possible errors due to the calculation of the boundary conditions.

Sha et al. [3.3-58] took the 1/8 large scale test facility of Westinghouse [3.3-56] that simulate an AP600 reactor, but using the COMMIX-1D code [3.3-59], which uses a single phase flow with multicomponents. In order to simulate the PCCS performance of the AP600, Sha divided the containment model into three domains, namely a bulk gaseous mixture inside the containment vessel, bulk moist air in an annulus between the outside containment shell and the inside shielding building wall, and a thermal coupling domain linking the other domains. The thermal coupling domain consists of a condensate film inside the containment vessel wall, the containment vessel wall itself, the evaporating liquid film outside the containment vessel wall, and paint on both sides of the vessel wall. COMMIX-1D code solves mass, momentum and energy equations for a mixture of N components, based on the porous-medium formulation through local volume averaging. In the analytical model, it is assumed that the volume occupied by the thin liquid film in the first two domains is very small relative to the corresponding volume of the domains, and can be neglected without affecting overall results,

and both the evaporation and condensation rate at the interface between the liquid film and the bulk gaseous mixture can be computed iteratively and treated as boundary conditions for the first two domains. For the closure relations, it is used the transport equations for k−ε two-equation turbulence model, turbulent transport properties, and a liquid-film tracking model, both for the condensate and evaporative film. The liquid films are considered in the thermal coupling between flow domains inside and outside the containment vessel. The tracking models compute the liquid film thickness, its mean velocity and temperature on both sides of the steel containment vessel. The local convective heat transfer coefficients, as well the mass transfer rate and coefficients, are obtained from the CONTAIN code [3.3-60], which employs the Collier model (Colburn and Hougen model).

PCCSAC-2D, 3D, [3.3-61] are respectively two and three dimensional computer codes developed by the Nuclear Power Institute of China (NPIC). PCCAC-2D is a two dimensional computer code already used in the design of AC600/1000 passive containment cooling system. PCCAC-3D is a three dimensional computer code finished in September 2000. Both codes can predict the pressure and temperature of mixing gas inside the containment in a design-basis-accident (DBA). The heat removal characteristics from inside containment to atmosphere through the water film on the out surface of steel shell and natural circulation flow of air can be also simulated in the codes. The general structure of the code, together with the implemented condensation model, is very similar to COMMIX-1D code. The condensation model uses the Colburn and Hougen formulation for solving the condensate mass flux. The results have also been compared with those obtained in the Westinghouse's test facility for the AP600 [3.3-56], showing a good agreement with them.

Martín-Valdepeñas et al. [3.3-52] implemented in the CFX4 code a model which considered the condensate thermal resistance, calculated from the Nusselt formulation, conveniently corrected in order to take into account the waviness and the possibility of a horizontal wall. For the computation of the gas resistance, Martín-Valdepeñas started from the Nusselt formulation applying to this equation a so-called degradation factor[12] [3.3-63]. In addition, this factor was increased to take into account the effect of the pressure, not included because the database used for deriving the Terasaka factor were taken from the experiments conducted by Uchida and the PHEBUS facility at 1 bar. By means of an iterative process, the correct temperature at the interface has been calculated. The experimental data for the validation were taken from the tests MICOCO and NUPEC and from the experiments of Anderson and Dehbi. In another paper, Martín-Valdepeñas et al. [3.3-64] pointed out how this model works adequately, except in the case of high pressures or low concentrations of air (in other words, in those regions far from the experiments used for the determination of the degradation factor). Another validated model in the same paper is the one proposed by Herranz et al. [3.3-21], the Diffusion Layer Modelling, which provided better results at the expense of a significant increase of the computational burden. In the comparison with the experiments of Dehbi and Anderson, the model calculated the HTC with a deviation of approximately 25%, except for the tests with helium conducted by Anderson where the helium concentration was higher than 15%, which yielded an error up to 60%, although, as reported by the authors, the test boundary conditions were not reproduced adequately by the code, which can cause large deviations in the calculation of the HTC. The model was also validated with the MICOCO test conducted in the MISTRA facility. In this case, the code was also able to adequately predict the pressure field -which is indicative of a correct prediction of the total condensate mass-, as well as the condensate in the two upper condensers, whereas in the lower one, the corresponding rate was overestimated, essentially due to an overestimation of temperature for assuming adiabatic the walls of the enclosure, and for obtaining a more homogenous distribution in the gas composition. The NUPEC facility was also simulated, obtaining good results for the pressure field (relative error approximately around 3% for the test M-4-3). Again, the larger error in the calculation of the pressure (6% at the end of the transient in the test M-8-1) is related to the calculation of the boundary conditions, because the code does not predict adequately the stratification in the enclosure (as in the

[12] This factor was first introduced by Vierow [3.3-64], who derived an empirical correlation between the Nusselt theoretical film heat transfer and the experimental value, taken from a facility that simulated the condensation inside vertical tubes. This correlation was a function of the Reynolds number and η. After Vierow, some other authors have published their own correlations.

Anderson experiment). Martín-Valdepeñas pointed out that a larger deviation for the pressure was obtained with the MELCOR code, in particular around 13% at the end of the transient.

3.3.6. General remarks

Condensation on the containment structures in presence of non-condensables constitutes one of the passive safety systems for some of the new generation reactors. Although many publications have been devoted to this subject, there is still a lack of clarity in order to know which models and experimental databases are suitable for simulating and having a better understanding of this phenomenon as it occurs in the containment.

Regarding the modelling of the condensation phenomenon, we have distinguished between the models that start from the continuity equations, those which are restricted to the solution of the fundamental parameters of condensation (HTC and heat and mass flux), and the models that consist of an empirical correlation derived from experimental data, usually taken from a SET facility. The theoretical models, both 'integral' and 'separate' models, present problems when have to be implemented in a thermohydraulic containment code, both LP and CFD codes. If gas flow mixing and distribution, together with condensation on the containment, has to be modelled, the only combination that can be tackled is a separate model in a CFD code.

With respect to the experimental evidence existing in the open literature, we have analysed and classified the main studies that have been carried out. Each experiment (facility and tests) has been classified according to its physical configuration and dimensions (which falls into the 'experiment-to-reality' category), and the associated instrumentation (which falls into the 'reality-to-experiment' category).

Last part of the section is devoted to the model validation and code capability. The phenomenon of condensation has a 1D nature; therefore in practical applications codes solving the accident scenario in a three dimensional way would not be required. The only limitation to the simulation with no CFD codes (where the simulation is 1D) is represented by the coupling between the condensation and the gaseous flow, since this has a 3D nature, being 2D with respect to condensation. The phenomena where the codes usually show more difficulties in the simulation related with condensation are the transport and flow distribution. In addition, the variation of temperature caused by the formation of mist, not considered in the major part of the thermohydraulic codes (present only in GOTHIC and GASFLOW), can affect the thermodynamic properties of the flow, and thus the condensation rate. The LP codes are able to adequately simulate the condensation phenomenon when they can employ an adequate nodalization that could reproduce the relevant phenomena, both along the axial and radial axis, and especially in the proximities of the wall.

NOMENCLATURE

A	Van Driest constant
A_w	wall area
C_p	specific heat [J/g·K]
D	diffusion coefficient [m^2/s]
E_A	primary coolant energy
f	friction factor
G	mass conductance
Gr	Grashof number [-]
h	heat transfer coefficient [$W/m^2 K$]
h_{fg}	latent heat of evaporation of water [J/kg]
k	thermal conductivity [W/m K]
L	flat plate length [m]
M	molar mass [kg/mol]
$\dot{m}$	mass flux [kg/m^2s]
Nu	Nusselt number

P	pressure [Pa]
Pr	Prandtl number [-]
Q	heat transfer [W]
q	heat flux [W/m^2]
Re	Reynolds number [-]
$s_{wall-atm}$	size of the cell contiguous to the wall
Sc	Schmidt number [-]
Sh	Sherwood number [-]
St	Stanton number [-]
T	temperature [K]
t	time
t_A	time
u,v	axial and normal component velocities [m/s]
W	mass fraction [-]
X	molar fraction [-]
x,y	Cartesian coordinates

Greek letters

δ	boundary layer thickness or condensate film thickness [m]
Γ	condensation mass flux per unit of circumferential length [kg/m s]
θ	Bird suction factor
μ	dynamic viscosity [kg/m s]
ν	kinematic viscosity [m^2/s]
ρ	density [kg/m^3]
τ	shear stress
τ_i^*	dimensionless interfacial shear stress
ζ_1, ζ_2	mathematical functions
φ	Average steam concentration between interface and bulk
η	W_{nc}/W_{st}

Subscripts

air	air
avg	average
b	bulk
bg	conditions of the background gas
c, cond	condensation
EOB	end of blowdown
g	gas mixture
He	Helium
i	interface
l	liquid
m	mass
mod	modified
nc	non-condensable
ref	reference
s	sensible
st	steam
t	turbulent or total
v	steam
w	wall
z	axial coordinate
0	reference value
*	condensation scenario

REFERENCES FOR SECTION 3.3

[3.3-1] NUSSELT, W., Die Oberflaechenkondensation des Wasserdampfes, Z. VDI, Frankfurt, 60 (1916) 541–546 and 569–575.

[3.3-2] COLBURN, A.P., HOUGEN, O.A., Design of cooler condensers for mixture of vapors with noncondensing gases. Ind. Eng. Chem. **26** (1934) 1178–1182.

[3.3-3] MINKOWYCZ, W., SPARROW, E., Condensation heat transfer in the presence of non-condensables, interfacial resistance, superheating, variable properties, and diffusion, Int. J. Heat Mass Transfer **9** (1966) 1125–1144.

[3.3-4] KOH, J.C.Y., SPARROW, E.M., HARTNETT, J.P., The two phase boundary layer in laminar film condensation, Int. J. Heat Mass Transfer **2 (**1961) 69–82.

[3.3-5] MINKOWYCZ, W., SPARROW, E., The effect of superheating on condensation heat transfer in a forced convection boundary layer, Int. J. Heat Transfer **12** (1968) 147–154.

[3.3-6] SUDHINDRA, P.V., MINKOWYCZ, W.J., Forced convection condensation with turbulent vapor flow over a horizontal surface, Letters Heat Mass Transfer 1 (1974) 37–42.

[3.3-7] MORI, Y., HIJIKATA, K., Free convection condensation heat transfer with non-condensable gas on a vertical surface, Int. J. Heat Mass Transfer **16** (1973) 2229–2240.

[3.3-8] DENNY, V.E., JUSIONIS, V.J., Effects of non-condensable gas and forced flow on laminar film condensation, Int. J. Heat Mass Transfer **15** (1972) 315–326.

[3.3-9] ACRIVOS, A., Mass transfer in laminar-boundary-layer flows with finite interfacial velocities, AIChE **6** (1960) 410–414.

[3.3-10] DENNY, V.E., MILLS, A.F., JUSIONIS, V.J., Laminar film condensation from a steam-air mixture undergoing forced flow down a vertical surface, J. Heat Transfer **93** (1971) 297-304.

[3.3-11] COLLIER, J.G., THOME, J.R., Convective boiling and condensation, Third Ed., Oxford: Clarendon Press (1994).

[3.3-12] WHITLEY, R., CHAN, C., OKRENT, D., On the analysis of containment heat transfer following on LOCA, Ann. Nucl. Eng. **3** (1976) 515–525.

[3.3-13] SCHMITT, R.C., BINGHAM, G.F., NORBERG, J.A., Simulated Design Basis Accident Test of Carolinas Virginia Tube Reactor Containment-Final Report, Idaho Nuclear Corp, IN-1403 (1970).

[3.3-14] CORRADINI, M.L., Turbulent condensation on a cold wall in the presence of a non-condensable gas, Nucl. Technol. **64** (1984) 186–195.

[3.3-15] KIM, M.H., CORRADINI, M.L., Modeling of condensation heat transfer in a reactor containment, Nucl. Eng. Des. **118** (1990) 193–212.

[3.3-16] HUHTINIEMI, I.K., CORRADINI, M.L., Condensation in the presence of non-condensable gases, Nucl. Eng. Des. **141** (1993) 429–446.

[3.3-17] FOX, R.J., PETERSON, P.F., CORRADINI, M.L., PERTENSTEINER, A.P., Free convective condensation in a vertical enclosure. Nucl. Eng. Des. **177** (1997) 71–89.

[3.3-18] GHIAASIAAN, S.M., KAMBOJ, B.K., ABDEL-KHALIK, S.I., Two fluid modeling of condensation in the presence of non-condensables in two phase channel flows. Nuc. Sci. Engin. **119** (1995) 1–17.

[3.3-19] GROFF, M.K., ORMISTON, S.J., SOLIMAN, H.M., Numerical solution of film condensation from turbulent flow of vapor–gas mixtures in vertical tubes. Int. J. Heat Mass Transfer **50** (2007) 3899–3912.

[3.3-20] PETERSON, P.F., SHROCK, V.E., KAGEYAMA, T., Diffusion layer theory for turbulent vapour condensation with non-condensable gases. J. Heat Transf. **115** (1993) 998–1003.

[3.3-21] HERRANZ, L.E., ANDERSON, M.H., CORRADINI, M.L., A diffusion layer model for steam condensation within the AP600 containment. Nucl. Eng. Des. **183** (1998) 133–150.

[3.3-22] MALET, J., PORCHERON, E., VENDEL, J., Filmwise Condensation applied to containment studies: conclusions of the TOSQAN air-steam condensation tests. NURETH-11 (11th International Topical Meeting on Nuclear Reactor Thermohydraulics), Avignon, France (2005).

[3.3-23] NUCLER REGULATORY COMMISSION, United States Code of Federal Regulations 10 CFR Part 50, Appendix A, General Design Criteria for Nuclear Power Plants, General Design Criterion 2 (1976).

[3.3-24] NUCLER REGULATORY COMMISION, United States Code of Federal Regulations 10 CFR Part 50, Appendix K, ECCS Evaluation Models (1976).
[3.3-25] UCHIDA, H., OYAMA, A., TOGO, Y., Evaluation of Post-Incident Cooling Systems of Light-Water Power Reactors. Proceedings of International Conference on Peaceful Uses of Atomic Energy, 13 (1965) 93–102.
[3.3-26] TAGAMI, T., Interim Report on Safety Assessments and Facilities Establishment Project for June 1965, No. 1. Japanese Atomic Energy Research Agency (1965).
[3.3-27] DEHBI, A.A., Analytical and experimental investigation of the effects of non-condensable gases on steam condensation under turbulent natural convection conditions. Ph.D. dissertation, M.I.T. Department Nuclear Engineering (1990).
[3.3-28] LIU, H., TODREAS, N.E., DRISCOLL, M.J., An experimental investigation of a passive cooling unit for nuclear plant containment, Nucl. Eng. Des. **199** (2000) 243–255.
[3.3-29] SAGAWA, N., An experimental determination of transient condensing heat transfer with heat absorption in circular cylinders, Bull. JSME **11** 44 (1968) 294.
[3.3-30] ALMENAS, K., Heat transfer from saturated and superheated atmospheres for containment analysis. Nucl. Eng. Des. **71** (1982) 1–14.
[3.3-31] AL-DIWANY, H.K., ROSE, J.W., Free convection film condensation of steam in the presence of non-condensing gases. Int. J. Heat Mass Transfer 16 (1973) 1359–1369.
[3.3-32] PETERSON, P.F., Theoretical basis for the Uchida correlation for condensation in reactor Containments. Nucl. Eng. Des. **162** (1996) 301–306.
[3.3-33] KATAOKA, Y., et al., Experiments on convection heat transfer along a vertical flat between pools with different temperatures. Nucl. Technol. **99** (1992) 386–396.
[3.3-34] MURASE, M., KATAOKA, Y., FUJII, T., Evaporation and condensation heat transfer with non-condensable gas present. Nucl. Eng. Des. **141** (1993) 135–143.
[3.3-35] BYUN, C.S., JERNG, D.W., TODREAS, N.E., DRISCOLL, M.J., Conceptual design and analysis of a semi-passive containment cooling system for a large concrete containment. Nucl. Eng. Des. **199** (2000) 227–242.
[3.3-36] MAHESHWARI, N.K., VIJAYAN, P.K., SAHA, D., Tracking of non-condensables. 3rd RCM on the IAEA CRP on Natural Circulation Phenomena, Modelling and Reliability of Passive Safety Systems that Utilize Natural Circulation. Cadarache, France (2004).
[3.3-37] ANDERSON, M.H., HERRANZ, L.E., CORRADINI, M.L., Experimental analysis of heat transfer within the AP600 containment under postulated accident conditions. Nucl. Eng. Des. **185** (1998) 153–172.
[3.3-38] KOLFLAT, A., Results of 1959 Nuclear Power Plant Containment Tests. SL-1800 (1960).
[3.3-39] KANG, H.C., KIM, M.H., Effect of non-condensable gas and wavy interface on the condensation heat transfer in a nearly horizontal plate, Nucl. Eng. Des. **149** (1994) 313–321.
[3.3-40] KANG, H.C., KIM, M.H., Characteristic of film condensation of supersaturated steam-air mixture on a flat plate, Int. J. Multiphase Flow **18** (1992) 423–437.
[3.3-41] SCHEUERER, M., et al., Evaluation of computational fluid dynamic methods for reactor safety analysis (ECORA), Nucl. Eng. Des. **235** (2005) 359–368.
[3.3-42] FISCHER, K., et al., International Standard Problem ISP-47 on containment thermohydraulics. OECD (2005).
[3.3-43] STUDER, E., MAGNAUD, J.P., DABBENE, F., TKATSCHENKO, I., International standard problem on containment thermal-hydraulics ISP47 Step 1—Results from the MISTRA exercise, Nucl, Eng. Des. **237** (2007) 536–551.
[3.3-44] FISCHER, K., et al., Containment code comparison exercise on experiment ThAI TH7. NURETH-10, Seoul, Republic of Korea (2003).
[3.3-45] ZHANG, S., "Experiment research and calculation method of natural circulation flow for AC600/1000", Natural Circulation Data and Methods for Advanced Water Cooled Nuclear Power Plant Designs, IAEA-TECDOC-1281, IAEA, Vienna (2000).
[3.3-46] CHENG, X., et al., Experimental data base for containment thermohydraulic analysis. Nucl. Eng. Des. **204** (2001) 267–284.
[3.3-47] SHEPERD, I., JONES, A.V., Thermohydraulics testing of the PHEBUS-FP containment. International Centre of Heat and Mass Transfer (1995).

[3.3-48] CARON-CHARLES, M., QUILLICO, J.J., BRINSTER, J., The MISTRA facility for field containment code validation: steam condensation experiments. ICONE10 (Proceedings, 10th International Conference on Nuclear Engineering), Arlington, Virginia, USA (2002).
[3.3-49] SMITH, B.L., MILELLI, M., SHEPEL, S., "Aspects of nuclear reactor simulation requiring the use of advanced CFD models", Technical meeting on Use of Computational Fluid Dynamics (CFD) Codes for Safety Analysis of Reactor Systems, including Containment, Pisa (2002).
[3.3-50] FORGIONE, N., PACI, S., "Computational analysis of vapour condensation in presence of air in the TOSQAN facility", NURETH-11 (11th International Topical Meeting on Nuclear Reactor Thermohydraulics), Avignon France (2005).
[3.3-51] ANDREANI, M., et al., A benchmark exercise on the use of CFD codes for containment issues using best practice guidelines: A computational challenge, Nucl. Eng. Des. **238** (2008) 502–513.
[3.3-52] MARTÍN-VALDEPEÑAS, J.M., et al., Improvements in a CFD code for analysis of hydrogen behaviour within containments, Nucl. Eng. Des. **237** (2007) 627–647.
[3.3-53] WOLF, L., HOLZBAUER, H., SCHALL, M., Comparisons between multidimensional and lumped-parameter GOTHIC containment analyses with data, Nucl. Tech. **125** (1999) 155-165.
[3.3-54] BABIC, M., KLJENAK, I., MAVKO, B., Prediction of light gas distribution in experimental containment facilities using the CFX4 code, Nucl. Eng. Des. 239 (2009) 708–721.
[3.3-55] BENET, L.V., et al., TONUS: A Code for Severe Accidents Containment Atmosphere Analysis. Heat and Mass Transfer in Severe Nuclear Reactor Accidents, J.T. Rogers (editor), Begell House, Inc., New York (1996) 419–435.
[3.3-56] SPENCER, D.R., WOODCOCK, J., WRIGHT, R.F., GRESHAM, J.A., Westinghouse — GOTHIC comparision with passive containment cooling system tests scaling evaluation and analysis, ASME/JSME Nuclear Engineering Conference, 1, ASME (1993).
[3.3-57] HOUKEMA, M., et al., Validation of the CFX4 CFD code for containment thermal-hydraulics, Nucl. Eng. Des. **238** (2008) 590–599.
[3.3-58] SHA, W.T., CHIEN, T.H., SUN, J.G., CHAO, B.T., Analysis of large-scale tests for AP-600 passive containment cooling system, Nucl. Eng. Des. **232** (2004) 197–216.
[3.3-59] SHA, W.T., DOMANUS, H.M., SCHMITT, R.C., ORAS, J.J., LIN, E.I.H., COMMIX-1: a three-dimensional transient single-phase computer program for thermal-hydraulic analysis, NUREG/CR-0785, Argonne National Laboratory Report ANL-77-96 (1978).
[3.3-60] TILLS, J., GRIFFITH, R.O., MURATA, K.K., STAMPS, D.W., User Guidance on the CONTAIN Code for Advanced Light Water Reactors, SAND96-0947, Sandia National Laboratories. Albuquerque (1996).
[3.3-61] YU, J., JIA, B., PCCSAC: A three dimensional code for AC600 passive containment cooling system analysis, Nucl. Sci. Eng. **142** (2002) 230–236.
[3.3-62] VIEROW, K.M., Behaviour of steam-air systems condensing in cocurrent downflow. Master Thesis, University of California at Berkeley (1990).
[3.3-63] TERASAKA, H., MAKITA, A., Numerical analysis of the PHEBUS containment thermohydraulics, J. Nucl. Sci. Technol. **34** 7 (1997) 666–678.
[3.3-64] MARTÍN-VALDEPEÑAS, J.M., JIMÉNEZ, M.A., MARTÍN-FUERTES, F., FERNÁNDEZ, J.A., Comparison of film condensation models in presence of non-condensable gases implemented in a CFD code, Heat Mass Transfer **41** (2005) 961–976.

3.4. BEHAVIOUR OF CONTAINMENT EMERGENCY SYSTEMS

3.4.1. Major function of the containment and passive safety systems for the containment

The containment of a nuclear power plant is the ultimate barrier against the release of radioactive materials into the environment. Therefore the integrity of the containment system should be maintained during any postulated accident. This is done mainly by suppressing the pressure and temperature of the containment atmosphere below the design limits. Thus the development of a reliable containment cooling system is one of the key areas in advanced reactor development. The major load to the containment comes from the steam or two phase flow discharge from the accidents such as loss of coolant accidents (LOCAs) and activation of the automatic depressurization system (ADS) to reduce the pressure of the primary coolant system. In order to reduce the load, the steam in the containment must be condensed by the containment emergency systems. Since the initial atmosphere of the containment is consisted of typically air or nitrogen gas, it acts as a non-condensable (NC) gas during the condensation process. This also implies that the distribution of the steam and NC gas in the containment is an important issue. Since the steam is lighter than the original containment gas, the stratification of the NC gas relative to the intake of the containment emergency systems can be also important. For the containment cooling, several phases can be considered. The first phase is the blowdown phase where a large amount of steam is rapidly discharged into containment and mixed with the original containment atmosphere. The blowdown phase ends when the emergency core cooling system (ECCS) water is injected into RPV where the steam generation is suppressed by the cold injected water. The next phase called cyclic venting phase starts with the reboiling of RPV water by the decay heat in reactor and pressurization of the containment due to the steam generated from RPV. The last phase is a long term containment cooling period of which the containment atmosphere has almost pure steam condition.

The containment emergency systems play the key role in maintaining the containment pressure below the design maximum pressure. In general, the effectiveness of the containment emergency systems strongly depends on the condensation process, steam stratification and NC gas distribution. Some of the condenser systems for containment cooling require passive purging of the NC gases, however other systems work without purging.

3.4.1.1. Vertical PCCS condenser (GE's SBWR/ESBWR) [3.4-1]

The simplified boiling water reactor (SBWR) and economic SBWR (ESBWR) developed by General Electric (GE) were designed to employ a passive containment cooling system (PCCS) as shown in FIG. 3.4-1. The PCCS is a passive heat exchanger system that transfers heat from the containment to the liquid pool surrounding the PCCS heat exchangers by condensation [3.4-2–3.4-4]. The application of the PCCS to the nuclear power plant design was first proposed by GE for the SBWR design, where the PCCS is used not only to cool the containment but also to provide condensed water to the core through the gravity-driven cooling system (GDCS). The GE's PCCS utilizes the heat exchanger that consists of straight vertical heat transfer tubes having a relatively large diameter of 50 mm, and large header pipes at the inlet and outlet of the tubes. The inlet header of the heat exchanger is connected to the Drywell (DW), and the outlet header is connected to the GDCS for the PCCS condensate water return to RPV, and the SP for the NC gas vent. This configuration enables the passive long term core cooling without depending on the active components and thus establishes a very reliable containment cooling system. This system requires the existence of the SP and vacuum breakers (VBs) to properly purge the NC gases which can accumulate in the PCCS condensers.

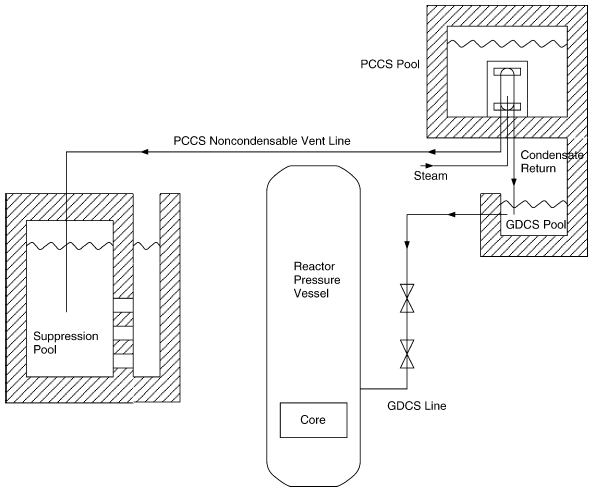

FIG. 3.4-1. Schematic of SBWR safety components.

3.4.1.2. Horizontal PCCS condenser [3.4-5]

The other type of the PCCS was proposed by the Japanese industries for the ABWR-II. For this design concept, the PCCS has only a function of the heat removal from the containment during severe accidents with failures of the active safety systems. This system concept is illustrated in FIG. 3.4-2: the PCCS heat exchanger is connected to the DW as the inlet and to the SP as the outlet. Liquid water is supplied to the containment bottom region from the suppression chamber by using some accident management measures in case that the core melt is ejected from the pressure vessel.

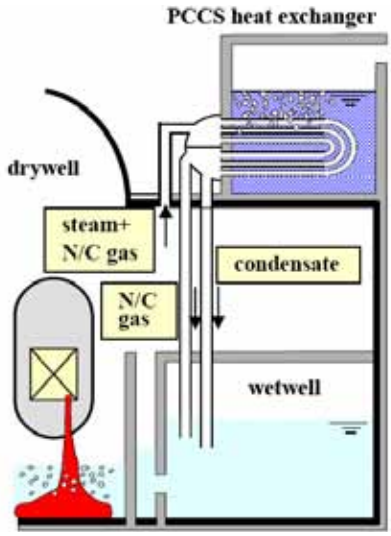

FIG. 3.4-2. Schematic of PCCS with horizontal heat exchanger.

3.4.1.3. External air cooling system (Westinghouse's AP600/AP1000) [3.4-6]

The AP600 and AP1000, advanced pressurized water reactors developed by Westinghouse, utilize a PCCS to remove the decay heat released inside the containment vessel following postulated DBA. During a DBA, heat released to the interior of the steel containment vessel is removed by evaporation of a continuously flowing thin liquid film on the outside surface of the vessel, which lowers the temperature of the steel vessel wall so that steam condenses on the containment inside surface. Consequently, the pressure and temperature of the gaseous mixture inside the containment vessel is decreased. The thin liquid film outside the steel vessel wall is formed by applying water at the top of the ellipsoidal containment dome. Evaporation of the falling liquid film is enhanced by buoyancy-driven flows of moist air in an annular space between the outside of the steel containment shell wall and the inside of a baffle suspended from the shield building wall. Air inlets are provided at the top of the shield building. The AP600 PCCS is designed to maintain containment pressure below the design limit for 72 hours without operator action during a DBA (IAEA-TECDOC-1624 [3.4-7]).

3.4.1.4. Containment cooling condenser (AREVA's SWR-1000) [3.4-8]

The SWR-1000, an advanced BWR developed by AREVA, utilizes the containment cooling condensers (CCCs) to remove residual heat passively from the containment atmosphere to the shielding/storage pool located above the containment. The containment concept of high performance light water reactor (HPLWR: super-critical water reactor -SCWR-) is based also on the SWR-1000 and similar CCCs are foreseen in the design of the HPLWR (Aksan et al. [3.4-9]). The SWR-1000 has four CCCs [3.4-7]. Each condenser consists of tubes at a slight angle to horizontal. The condensers are connected to the shielding/storage pool via an inlet to the lower end elevation and a discharge line at the higher end elevation. The feed line and discharge line as well as the condenser tubes are filled with water from the shielding/storage pool. All connecting lines to the shielding/storage pool are open during plant operation. Since the system functions entirely passively as a function of the thermal gradients, no actuation is necessary for startup. In the event of an accident accompanied by postulated failure of the active residual heat removal system, the temperature of the water in the core flooding pools may increase to such an extent (due to the heat input via the emergency condensers or the safety-relief valves) that the pool water starts to evaporate, releasing steam into the DW atmosphere. The function of the CCC system is to passively remove the decay heat released to the DW and to transfer this heat to the water of the shielding/storage pool located above the containment, as this heat is not able to be accommodated by the SP or the core flooding pools. Hence the system is provided for long term, passive heat removal from the containment. The objective of the CCC system is to keep the pressure level inside the containment as low as possible. Since the condenser tubes are exposed directly to the containment atmosphere, no purging of the NC gases is required. The accumulating gases are moved away by the natural convection due to the difference in densities.

In general, the boiling water reactors such as BWR, ABWR-II, SBWR, ESBWR and LSBWR have a large suppression pool within the containment. The steam coming into the containment due to the LOCA or other accident is passively injected into SP through the vent pipes by the pressure difference between the DW and SP. This particular containment cooling system takes the initial load of the LOCA. However, since the heat sink of SP is within the containment, it is not designed for the long term cooling of the containment.

Other containment emergency systems include, for example, the containment passive heat removal system (C-PHRS) of WWER-640/407 [3.4-7]. It ejects the energy in the containment through the cooler of the primary containment to the emergency heat removal tank.

3.4.2. Key phenomena influencing the performance and reliability of PCCS

The PCCS performance can be deteriorated by NC gases that come from the containment atmosphere and from the gases produced by the damaged fuel or during a severe accident. These NC gases degrade the heat transfer capability of the condensers in the PCCS since they provide a heat transfer resistance to the condensation process by acting as resistances to the steam condensation to the tube

walls (Upton et al. [3.4-10]). Therefore, the effect of the NC gases should be taken into account in the PCCS designs.

3.4.3. Relevant test facilities

The GIRAFFE [3.4-11] test facility with a full-height and 1/400 reduced-volume was used by the Toshiba Corporation to investigate the thermohydraulic characteristics of the SBWR passive heat removal safety systems, support SBWR design certification in the U.S., and support TRACG code qualifications. Both separate effects and system response tests were performed in order to investigate the ability of the PCCS heat exchanger to condense steam in the presence of NC gases, demonstrate venting of the NC gases from the PCCS venting tube to the SP, and simulate the main steam line break (MSLB), bottom drain line break (BDLB), and GDCS drain line break (GDLB) events. There was also a test to demonstrate the operation of the PCCS in the presence of lighter-than-steam NC gas.

The PANDA [3.4-12, and 3.4-13] test facility is located at the Paul Scherrer Institute (PSI) in Switzerland and it is used to study the long term SBWR and ESBWR PCCS performance. It is a full height and 1/25 volume and power scale for SBWR and 1/40 volume and power scale for ESBWR. A series of steady state tests were conducted using one of the PANDA PCC condensers with variations in air flow with a constant steam flow. Three tests were performed to investigate the effects of the PCCS pool inventory on the PCCS system performance. Additional tests were run to investigate the PCCS startup and long term heat removal capabilities for SBWR and ESBWR configurations.

PANTHERS [3.4-14] is a test facility located at SIET (Societ`a Informazioni Esperienze Termoidrauliche) in Italy, to provide data for TRACG qualification and to demonstrate testing of the performance of prototypic PCCS heat exchangers. The facility had full-size prototypic heat exchangers which including a single condenser unit with two modules, each module having 248 tubes. Steam and NC gas were supplied to prototype heat exchangers over the complete range of SBWR conditions. A series of experiments were performed at the same thermohydraulic conditions as in GIRAFFE and PANDA. The tests were conducted with low and high NC gas concentrations.

The PUMA [3.4-15] test facility was built to simulate SBWR safety systems and obtain confirmatory integral test data for the U.S. Nuclear Regulatory Commission (NRC). The U.S. NRC identified a need to develop independent confirmatory data from a well-scaled integral test facility built to reproduce the major thermohydraulic phenomena at low pressure (<1033 kPa). The PUMA facility has a scale of 1/4 in height, 1/400 in volume, and a time scale of 1/2. The power is scaled by 1/200 of the prototype and the pressure is scaled at 1:1. The facility contains all of the important safety and non-safety systems of the SBWR that are pertinent to the postulated LOCA transients. The system response tests were performed such as MSLB, BDLB and GDLB and separate effect test has been carried out in order to investigate the ability of the PCCS heat exchanger tubes to condense steam in the presence of NC gases during the three operational modes of the PCCS, namely bypass, cyclic venting, and long term cooling modes.

LSTF [3.4-16] is an integral test facility located at Japan Atomic Energy Agency (JAEA) in Japan, to simulate thermohydraulic phenomena peculiar to SBLOCA of a typical Westinghouse-type 3424-MWt pressurized water reactor (PWR). It is characterized by the use of prototypically scaled components with full-height, 1/48 volume scale and full-pressure conditions to the reference PWR. LSTF steam generators and accumulator tanks which have a function to generate steam are used to supply large amount of steam to the PCCS test sections. The capability of the saturated steam supply is up to 10 MW. The capability of NC gas supply of LSTF is enough to keep 1% concentration at the reference steam supply condition even if the heat exchanger is employed as the test section.

3.4.4. Condensation heat transfer models

Nusselt [3.4-17] developed a theoretical model to calculate the filmwise condensation rate for a vertical flat plate in stagnant steam. Several assumptions were made by Nusselt such as thermal equilibrium between liquid film and vapour, constant wall temperature, no interfacial shear effect

(vapour is stagnant) and negligible heat and momentum transfer in the liquid film. Other researchers considered the effect of interfacial shear but typically assumed a constant interfacial shear along the axial direction. Sparrow et al. [3.4-18] included the role of subcooling, the interface and mass diffusion based on Nusselt's research. Chen and Ke [3.4-19] included the effect of surface waves and turbulence. For film condensation without shear stress at the interface and with concurrent down-flow, numerous research studies exist with considerable deviations in methods and assumptions among researchers. The topics of the NC gas effects on the condensation heat transfer and the condensation on the containment structures are discussed in Section 3.2 and 3.3 in details.

Vierow [3.4-20] performed experiments to obtain the local condensation heat transfer coefficient along a vertical tube. A natural circulation loop was used to simulate the passive condenser with a 22 mm diameter tube and a 2.1 m active heat transfer length. Steam was injected into the lower plenum and condensation occurred in the top most part of the loop. The experimental data were correlated using a correction factor to the heat transfer coefficient obtained by Nusselt's theory. This correlation has been one of the bases for other research studies on single-tube steam condensation. The correction factor is defined as the ratio of the experimental heat transfer coefficient to the theoretical Nusselt heat transfer coefficient.

Vierow and Schrock [3.4-21] developed an empirical degradation factor that contains two factors for the theoretical Nusselt value, considering the effect of the interfacial shear stress on the condensation rate and the NC gas effect. This correlation is used as an "alternative model" in RELAP5/MOD3.2 and RELAP5/MOD3.3 to evaluate wall film condensation.

Siddique [3.4-22] conducted an experiment to obtain the local heat transfer coefficient in the presence of air or helium with downward flow conditions. The condenser tube had a 22 mm diameter and a length of 2.1 m. An empirical correlation was developed by starting with the governing equations of the air-vapour boundary layer which are used for producing the appropriate non-dimensional groups.

Kuhn [3.4-23] performed condensation experiments in a vertical tube 2.4 m in length and 47.5 mm in diameter. The venting flow rate was not measured and the effect of venting was not considered, but the results showed that the mixture should be vented to maintain a steady state condition along the condenser tube. Kuhn evaluated the degradation factor by taking into account the interfacial shear thinning and waviness effect instead of using the mixture Reynolds number as in Vierow and Schrock [3.4-21].

Kim and No's [3.4-24] PCCS experiments were conducted with high pressure steam at a maximum pressure of 7.5 MPa in a single vertical tube with an inner diameter of 46 mm. However, although pool boiling was simulated, the test conditions were restricted to high pressure steam condensation with a turbulent film.

Leonardi [3.4-25] developed an empirical model of condensation heat transfer in the downward concurrent steam-air mixture flow through a condenser tube, taking into account the accumulation of NC gas in the PCCS. The model depends solely on the condenser inlet conditions including the mixture Reynolds number and NC gas concentration.

Oh [3.4-26] performed experiments for three PCCS flow conditions which were bypass, cyclic venting, and long term cooling modes. The secondary-side pool experienced pool boiling. Oh developed a boundary layer model which suggests the possibility of combining all three PCCS operation modes into one universal condensation heat transfer model. In addition, an empirical correlation was suggested for calculating laminar and turbulent film thicknesses. However, the prototypic PCCS NC gas venting boundary condition was not simulated due to the limit of NC gas cyclic venting system.

In the following sections, the relevant experiments and analyses for Phenomena 4, "Behaviour of containment emergency systems," are summarized. The scaling basis of the experiments and correlations should be carefully evaluated. Some experiments had a prototypic tube size but the

boundary conditions might not represent the most typical conditions. It can be said that most separate effect experimental conditions correspond to the blowdown phase while some steam and NC gas leave the exit under quasi-steady state condition. Section 3.4.5 addresses three different phases for PCCS performance. The cyclic venting phase is the most difficult phase to simulate in separate effect tests because it requires both the DW and WW. The PUMA separate effect test used the integral test facility, thus all of three phases could be simulated. Most correlations use the NC gas concentration and steam-gas mixture Reynolds number as correlating variables for the condensation Nusselt number.

3.4.5. PUMA-PCCS separate effect test [3.4-27]

The development of a reliable PCCS is one of the key areas in the design of advanced nuclear reactors. Many experiments were performed to study the PCCS capability for heat exchange. The existing models are mainly for the “bypass mode”, in which the steam-air mixture may vent directly to the wet well (WW) gas space. These models may not be applicable when there is no open passage for the steam and NC gas to escape.

The PCCS uses natural circulation to passively provide long term cooling and no active devices are required for the PCCS to function. The driving force of the flow through the PCCS is the pressure difference between the DW and the WW. The cooling capacity of the PCCS must be sufficient to maintain the containment pressure below 0.48 MPa during any postulated DBA by removing the decay heat for at least 72 hours. A good understanding of the condensation of the steam-air mixture inside vertical tubes is necessary to evaluate the performance of the PCCS. Of particular importance are the condensation heat transfer characteristics of the PCCS in the presence of NC gas. Since the condensation heat transfer rate can be significantly reduced by NC gases, it is important to study this effect with consideration of the PCCS as a primary containment cooling system in the long term mode.

A series of experiments have been conducted in this study to obtain experimental data for the downward co-current flow of a steam-air mixture through the condenser tube bundles during the three operational modes of the PCCS: the bypass mode during the initial blowdown phase, the cyclic venting mode with the periodic venting of NC gas through the PCCS venting line which is submerged into the WW water, and the long term cooling mode with a very low NC gas concentration in the DW. A total of 42 data sets for the bypass, cyclic venting, and long term cooling modes were obtained from the Purdue University multi-dimensional integral test assembly (PUMA) under a task sponsored by the U.S. NRC.

3.4.5.1. Test facility

The PUMA facility was built to simulate the safety systems for the SBWR (GE [3.4-28]) and to obtain confirmatory integral test data for the U.S. NRC (see Chapter 4). As shown in FIG. 3.4-3, steam is supplied from the reactor pressure vessel (RPV) to the DW and the NC gas concentration is controlled by injecting preheated NC gas into the MSL-B upstream at a pre-determined flow rate. The DW and WW pressures determine the pressure boundary conditions for the PCCS tests. The air injection and venting valves are used in the WW gas space to control the WW initial test pressure condition.

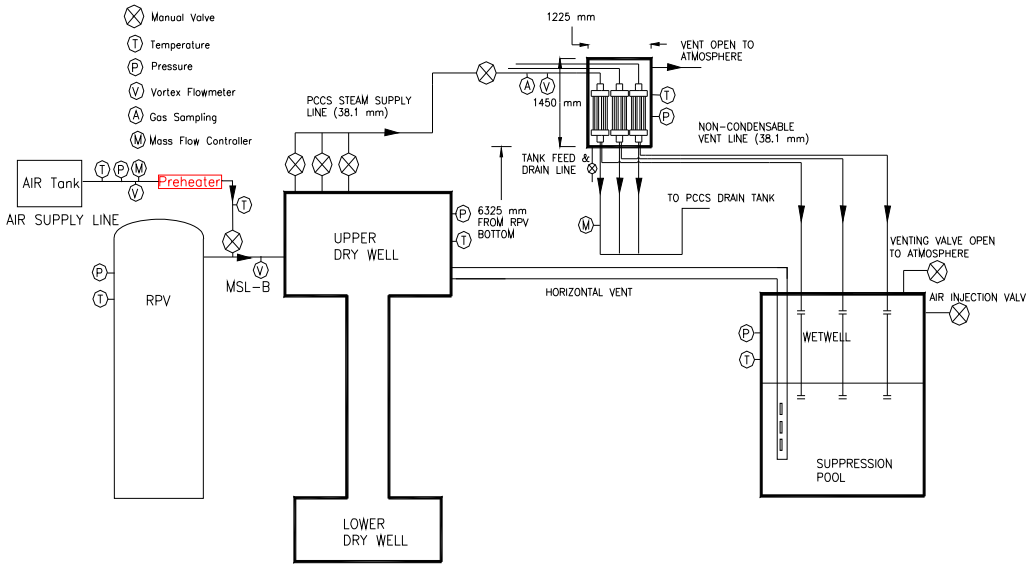

FIG. 3.4-3. Schematic of PUMA-PCCS separate effect test facility.

Three PCCS units, each having 10 active tubes, are submerged in a common pool that is partitioned into three sections. Each PCCS unit is equipped with measurements of pool-side water temperature and water level. One of condenser tubes in each unit has three thermocouples on the outer tube wall and tube centerline placed along the tube length direction at approximately equal distances. To obtain the overall heat transfer coefficient, the temperature, pressure, and flow rate are also measured at the inlet and outlet of the PCCS condenser..

3.4.5.2. Test matrix

To obtain a comprehensive data set, the following were referred for choosing the pressure, NC gas, and steam flow rate conditions:

(1) PUMA integral test results to obtain the steam flow rate for MSLB, BDLB, and GDLB according to the bypass, cyclic venting, and long term cooling modes.

(2) RELAP5 calculation results to predict the pressure and NC gas trend in the DW during the bypass mode.

(3) Experimental conditions for other integral test such as PANTHERS [3.4-14], PANDA [3.4-12], and GIRAFFE [3.4-11] to obtain appropriate data such as the pressure, steam flow rate, and NC gas concentration from.

In Table 3.4-1, test conditions are summarized for the bypass, cyclic venting, and long term cooling modes for the PUMA-PCCS separate effect tests [3.4-29].

For the bypass mode, the PCCS condenser inlet and outlet have continuous flow because a large amount of steam comes from the RPV before the GDCS injection into the RPV. In this mode, the NC gas is continuously vented through the vent lines. Pressure conditions are selected from RELAP5 code calculations, and the steam flow rate and NC gas concentration in the DW are based on the PUMA integral test results.

TABLE 3.4-1. TEST MATRIX FOR PUMA-PCCS SEPARATE EFFECT TESTS

Test Mode	Steam Flow Rate (kg/s)	Pressure (kPa)	PCCS Pool Water Level (m)	NC Gas Mass Fraction (%)
Long term Cooling (LT)	0.018~0.028	200 230 260	0.92 0.60	< 0.5
Cyclic Venting (CY)	0.031~0.042	220 240 260	0.92 0.60	0.3, 2, 4
Bypass (BY)	0.060~0.075	220 260 300	0.92	0, 10, 15

For the cyclic venting mode, the periodic venting of NC gas to the WW was simulated. For this operation the PCCS vent lines are submerged in the WW water to a depth of 200 mm. The venting behaviour varies depending on the inlet NC gas concentration. As the NC gas accumulates in the tube, the condensation is inhibited because the NC gas acts as a resistance to the condensation.

The long term cooling mode simulates the continuous cooling mode that happens at the final stage of an accident. There is a very low NC gas concentration in the DW because most of the NC gas has been vented into the WW. The PCCS pool water temperature was at the saturation temperature, about 101 ℃, during the experiments. The PCCS pool water level is a parameter to be considered due to evaporation of water.

3.4.5.3. Data analysis procedure

The PCCS condensers provide decay heat removal by condensing steam from the DW and supplying condensate water to the RPV. The scaling of the heat transfer rate through the condenser is given by Ishii et al. [3.4-15] as:

$$\dot{Q}_{pccs} = N_{units} N_{tubes} \overline{U} A_i \left(\overline{T}_g - \overline{T}_p \right) \approx \dot{m}_{con} h_{fg} \tag{3.4-1}$$

where N_{units} is the number of PCCS units; N_{tubes} is the number of PCCS condenser tubes per unit; $\overline{U}$ is the overall heat transfer coefficient; A_i is the inner surface area of a condenser tube; $\overline{T}_g$ and $\overline{T}_p$ are the average steam and PCCS pool temperatures, respectively; $\dot{m}_{con}$ is the outlet condensate mass flow rate; and h_{fg} is the latent heat of condensation. The overall heat transfer coefficient $\overline{U}$ can be obtained from Eq. (3.4-1) and can also be expressed as

$$\overline{U} = \left[\frac{1}{\overline{h}_c} + \frac{\ln\left(D_o / D_i\right) D_i}{2k_w} + \frac{D_i}{\overline{h}_p D_o} \right]^{-1} \tag{3.4-2}$$

where D_i and D_o are the inner and outer diameters of the condenser tube, respectively; k_w is the thermal conductivity of the tube wall; and $\overline{h}_c$ and $\overline{h}_p$ are the heat transfer coefficients for the tube inside and outside (pool), respectively. In the brackets on the right hand side of Eq. (3.4-2), the first term represents the tube-inside condensation heat transfer resistance; the second term represents the tube-wall conduction heat transfer resistance; and the third term represents the tube-outside pool heat transfer resistance. The average condensation heat transfer coefficient $\overline{h}_c$ corresponds to the

condensation of the steam-air mixture in a vertical tube, and can be obtained by using Eq. (3.4-2) as

$$\bar{h}_c = \left[\frac{1}{\bar{U}} - \frac{\ln(D_o/D_i)D_i}{2k_w} - \frac{D_i}{\bar{h}_p D_o} \right]^{-1} \tag{3.4-3}$$

where the heat transfer coefficient for the pool $\bar{h}_p$ can be obtained by

$$\bar{h}_p = \frac{\dot{Q}_{pccs}}{A_o(\bar{T}_w - \bar{T}_p)} \tag{3.4-4}$$

where A_o is the total outer surface area of the condenser tubes and $\bar{T}_w$ is the tube outer wall temperature. This method provides an average total heat transfer coefficient for the PCCS, which can determine the average Nusselt number:

$$Nu = \frac{\bar{h}_c L}{k_g} \tag{3.4-5}$$

where L is the tube length and k_g is the steam thermal conductivity.

3.4.5.4. Results and discussion

3.4.5.4.1. Mass and energy balances

To check the mass balance in the PCCS, the steam mass flow rate from the RPV to the DW and the sum of the condensate mass flow rates from the three PCCS units were compared. The total steam mass flow rate varies between 0.017 and 0.063 kg/s as determined by the steam flow rate measurement from the vortex flow meter installed on the MSL. The discrepancy between the PCCS inlet and outlet mass flow rates increases for the cyclic venting and bypass modes, while the long term cooling mode shows a good agreement. FIG. 3.4-4 shows the same trend for the energy balance between the PCCS inlet and outlet. The discrepancy can be explained by the increase of NC gas purging with steam when the inlet NC gas fraction is increased. Therefore, the larger differences in mass and energy between the PCCS inlet and outlet were observed at higher mixture inlet flows with higher NC gas fraction conditions for the bypass and cyclic venting modes.

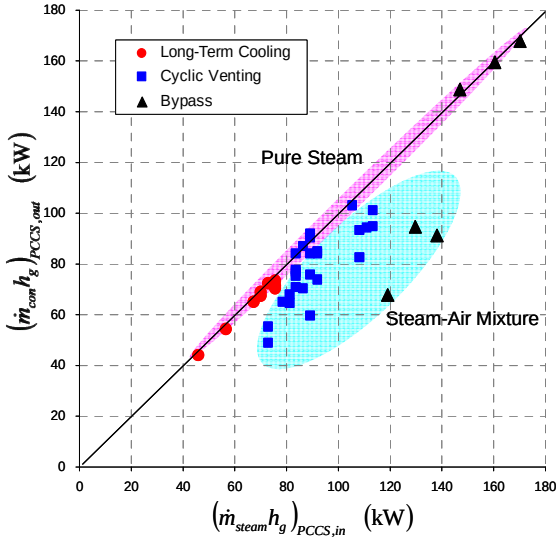

FIG. 3.4-4. Energy balance in PUMA-PCCS separate effect tests.

3.4.5.4.2. Long term cooling mode

For the long term cooling mode, the test control parameters were the DW pressure and the PCCS pool water level. The experiments were conducted with NC gas concentrations less than 1%. The experimental data showed the effects of the DW pressure and the water level of the PCCS pool. As the DW pressure increases, the average heat removal rate also increases, while the average condensation heat transfer coefficient decreases. The decreased PCCS pool water level provides a lower heat removal rate due to the decrease of heat transfer area between PCCS pool water and condenser tubes.

3.4.5.4.3. Bypass mode

For the bypass mode, the experimental results demonstrated the effects of the DW pressure and NC gas concentration. As the DW pressure increases, the average heat removal rate increases, while the average heat transfer coefficient decreases. Test results also showed that the average heat transfer coefficient decreases as the NC gas concentration increases in the DW.

3.4.5.4.4. Cyclic venting mode

For the cyclic venting mode, a wide range of tests were performed with the parameters of the DW pressure, steam flow rate, and inlet NC gas concentration. The parametric effects on the heat transfer rate and heat transfer coefficient are the same as the long term cooling and bypass modes. The PUMA-PCCS condensation heat transfer coefficients were compared with Kuhn's [3.4-23] and Vierow's [3.4-21] models. Generally, the two models overpredicted the heat transfer coefficient compared with the PUMA data. This can be explained by different NC gas venting conditions which affect the degree of NC gas accumulation inside the condenser tubes and oscillation of NC gas fraction along the condenser tubes due to cyclic venting effects. As shown in Fig. 3.4-5, this explanation can be supported by the fact that the discrepancy in the heat transfer coefficient decreases as the NC gas fraction increases due to the increased similarity in the NC gas venting frequency.

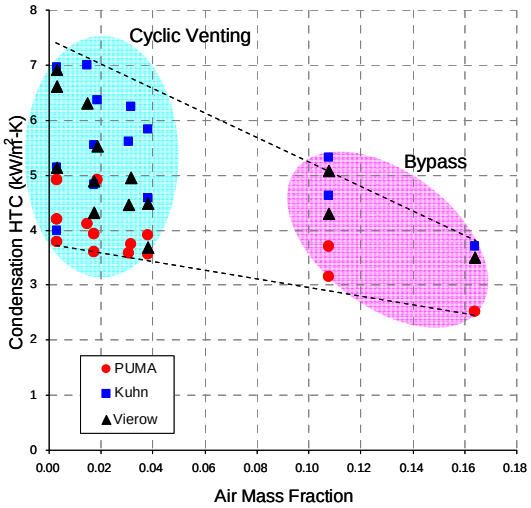

FIG. 3.4-5. Effect of NC gas mass fraction on PCCS condensation heat transfer coefficient for bypass and cyclic venting modes.

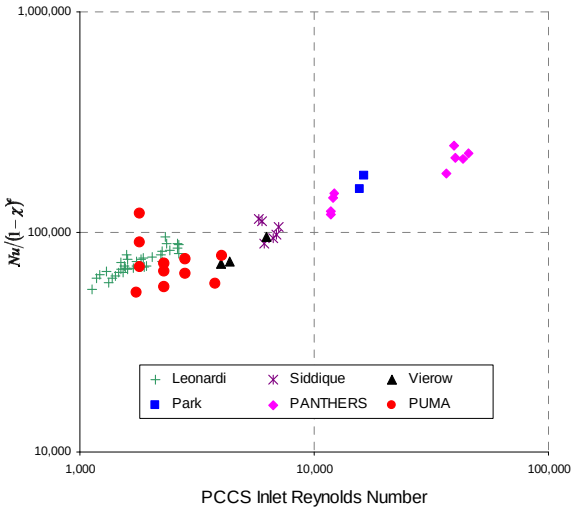

FIG. 3.4-6. Combined correlated test results for different experiments.

To further validate the experimental data, combined correlated test results were compared with other experimental data as shown in Fig. 3.4-6. The data are plotted as $Nu/(1-\chi)^c$, where χ is the NC gas mass fraction, to isolate the flow rate (Re) dependency. The constants were determined to be $c = 2.5 \pm 0.05$. The data sets for this comparison are from Vierow et al. [3.4-21], Siddique [3.4-22], Park [3.4-30], Leonardi [3.4-25], and PANTHERS (Parlatan et al. [3.4-14]). As shown in Fig. 3.4-6, both the cyclic venting and bypass with continuous venting follow the same trends as other research results. Especially, this data comparisons is showing that the PUMA-PCCS and PANTHERS data fall on the same trend line which verify the quality of well scaled down PUMA-PCCS data.

3.4.5.5. Summary of PUMA-PCCS tests

A total of 42 data sets have been obtained from the PUMA-PCCS separate effect tests. These tests were carried out to confirm the performance of the PCCS in the bypass, cyclic venting, and long term cooling modes. Three parallel PCCS units were used in the tests. To check the data quality, mass and energy balances in the PCCS were evaluated by using the inlet steam flow rates from the RPV to the DW measured by vortex flow meters and the condensate flow rates measured by magnetic flow meters and water level changes in the PCCS drain tank. Through redundant measurement cross checking, reliable data can be obtained.

The experimental results showed that as the PCCS inlet pressure increases, the heat removal rate increases while the average condensation heat transfer coefficient decreases. For the effect of the PCCS pool inventory in the long term cooling mode, the heat removal rates for the case of the PCCS pool water level at middle of the condenser tube are lower than those for the case of the normal PCCS pool water level. This shows that the PCCS pool inventory is one of the key parameters that determine the PCCS cooling capability. The condensation heat transfer characteristics of the PCCS in the presence of NC gas have also been investigated. As the PCCS inlet NC gas concentration increases, the average condensation heat transfer coefficient decreases. Compared with Kuhn's and Vierow's models among others, the heat transfer coefficients and heat removal rates from the PUMA data have the same trends as those from the two models, however the average heat transfer coefficients from the PUMA data were overpredicted by the two models. This discrepancy can be explained by continuous NC gas venting conditions for the existing models, which cannot simulate prototype conditions such as the NC gas accumulation in the PCCS vent line and its cyclic venting, and pool boiling conditions.

3.4.6. Overview on PANDA test facility and ISP-42 PANDA tests data base [3.4-13]

The PCCS is the preferred means of decay heat removal following a LOCA for ESBWR and SBWR. The system is a unique ESBWR engineered safety feature (similar to the SBWR PCCS). Containment heat removal is provided by the PCC system, consisting of four low-pressure loops, which is a safety related system. Each loop consists of a heat exchanger, which opens to the containment, a condensate drain line that returns the PCCS condensate to a PCCS condensate tank, which is connected to the RPV via its own nozzle, and a vent discharge line submerged in the SP. The four heat exchangers, similar to the isolation condensers (ICs), are located in cooling pools external to the containment. Once PCCS operation is initiated following RPV depressurization, the condensate return line to the vessel is opened permanently. The PCCS uses natural convection to passively provide long term containment cooling capability. The PCCS pool is sized to remove post-LOCA decay heat at least 72 hours without requiring the addition of pool inventory.

The PCCS heat exchangers are extensions of containment. The lines entering and leaving the PCCS from the DW do not have containment isolation valves. No sensing, control, logic or power operated devices are required for the PCCS to initiate. Flow through the PCCS loop is driven by the pressure difference created between the containment DW and the SP that exists following a LOCA and the pressure drop through the PCCS tubes. The PCCS condensate is returned to the RPV under the force of gravity.

3.4.6.1. PANDA facility

PANDA is a large scale facility constructed at PSI (in Switzerland) for the investigation of both overall dynamic response and the key phenomena of passive containment systems during the long term heat removal phase for advanced light water reactors (ALWRs). Using a modular concept with a basic set of cylindrical vessels which are interconnected by piping, the facility can be adapted to simulate different passive containment designs. The facility configuration used for International Standard Problem number 42 (ISP-42) tests is a scaled down model of ESBWR containment and safety systems. After a detailed scaling analysis, power and volumes are scaled 1:40, and pressure, relevant heights and pressure drops are 1:1.

The RPV is connected to the PANDA facility via the two MSLs (steam supply to the system), the PCC drain line (liquid return of the condensed steam in the PCCs) and the GDCS drain line. The details of PANDA facility is given in Section 4.6. The reactor pressure vessel acts as a steam source. Two large cylindrical vessels of an inner height 8.0 m and an inner volume of 89.9 m^3 each, represent the DW, connected each other with a large diameter DW connection pipe (outer diameter of 1.0 m). The DW as a whole is connected to the rest of the system via the two MSLs (steam supply to the system and input from RPV), the PCC feed lines (output of DW), the main vent lines (output of DW) and the vacuum breaker lines (input to DW, in case the WW pressure exceeds the DW pressure). The other two large cylindrical vessels, of inner volume of 115.9 m^3 each and an inner height of 10.11 m, filled with water at a level of approximately 4m, represent the WW (also called suppression chamber). The two WW vessels are connected each other by two large diameter pipes of 4m length each, one in the liquid section of the WW (1.5 m diameter), and the other one in the gas space of the WW (1.0 m diameter). The WW as a whole is connected to the PANDA facility via the two main vent lines (input), the three PCC vent lines (input), the two pressure equalization lines and the vacuum breaker lines (output, in case the WW pressure exceeds the DW pressure significantly). The last vessel primarily represents a GDCS pool with a volume of 17.6 m^3 and inner height of 6.06m, and it can function as additional containment volume for WW gas space. The GDCS tank is connected to the rest of the facility via the GDCS drain line to RPV (output) and the pressure equalization line to the WW vessels. GDCS drain line connects the inside bottom of the GDCS tank with the lower part of the downcomer of the RPV. A check valve allows only one directional flow from the tank to the RPV. To establish similar pressure in the gas spaces of GDCS tank and WW, the pressure equalization line connects GDCS tank with the gas space of the two WWs. Three PCCS heat exchanger units are submerged in the pool outside of the containment.

3.4.6.2. ISP-42 PANDA test overview

The overview of ISP-42 PANDA tests is given in Section 4.6. The main interest for this ISP-42 is code validation in relation to a range of LWR and ALWR (mainly) containment issues that have been designated as important and involving thermohydraulic phenomena.

The main issues and phenomena covered in the ISP-42 PANDA test are the following:

(1) Transient and quasi steady state operation of a PCCS,

(2) Coupled primary system and containment behaviour and phenomena,

(3) RPV operation at low power and low pressure under natural circulation conditions,

(4) Gravity driven ECCS injection in an initially saturated RPV,

(5) Venting of a steam/NC gas mixture through an immersed vent pipe into a WW compartment,

(6) Steam condensation in the presence of NC gases in tubes,

(7) Mixing and stratification of light (helium) and/or heavy (air) gases with steam in large volumes to see 3D effects, steam jets, air or helium release,

(8) Mixing and stratification in large water pools.

The ISP-42 PANDA test consists of six phases, A through F. These phases represent a sequence of concatenated operating modes or processes as used for the simulation and study of the behaviour of ALWR containment with passive safety systems. In fact, each of these phases is a separate experiment, with its own initial and boundary conditions. These six different test phases are listed as below:

Phase A : PCCS Startup
Phase B : GDCS Discharge
Phase C : Long Term Passive Decay Heat Removal
Phase D : Overload at Pure-Steam Conditions
Phase E : Release of Hidden Air
Phase F : Release of Light Gas in RPV

The ISP-42 participants in the exercise chose the number of test phases they wished to calculate. Ten organizations from nine countries did participate in the "blind" phase pretest calculations. Forty-nine submitted calculation results are included in the "blind" phase comparisons report [3.4-31]. A large number of physical parameters were selected for comparison. In general, most of the predicted results were in quite good agreement with the test results; however, some prediction cases differed significantly and the reasons for these differences were discussed.

3.4.6.3. Some results of ISP-42 Phase-A test and code predictions

The objective of the first test phase (Phase A) of ISP-42 was to investigate the startup of a passive cooling system when steam is injected into a cold vessel filled with air and to observe the resulting gas mixing and system behaviour.

During this Phase A test, all three PCCs are operational, and there is no interconnection between the different PCC pools. The GDCS is filled with water whereas the water level in the RPV is much below the downcomer entrance/riser exit. The main vent lines and the vacuum breaker lines are not operational for this test.

At zero second, RPV power has been switched on thus allowing steam to flow into the two DW vessels. Therefore, the steam slowly diluted the gas content of the DW and partially condensed at the cold vessel walls. Due to the inflow of additional gas (steam) into the DW, pressure in the DW as well as in the PCCs increased until it exceeded WW pressure by approximately 10 kPa, the hydrostatic head at the outlet of the PCC vent lines. Then, DW content partially was pushed through the PCC primary sides into the two WW pools via the PCC vent lines; the rest of the steam was stored in the DWs or condensed on the DW walls. As long as the feed flow is small because of a high condensation rate at the DW walls or/and the steam content of the flow mixture is low, no condensation has taken place in the PCCs. Instead, the mixture has been vented into the WWs where the steam content has been condensed and the air content was separated into the gas space. Here, the separated air increased the amount of gas in the gas space thus increasing the system pressure. After some time, the dilution of the initial air content by the steam has been progressed and steam condensation started in the PCC tubes removing significant amounts of steam out of the vent flow, thus decreasing the inflow of air into the WW gas space, which resulted in a decrease of the pressure increase. The condensed steam has flown through the drain lines back into the RPV whereas a reduced gas flow was vented into the WWs. During the final stationary part of the experiment, nearly the whole gas flow consisted of steam, which was condensed in the PCC tubes removing steam in the same order of magnitude as produced in the RPV, which resulted in ceasing the inflow of air into the WW gas space and consequently the pressure increase in the primary system.

The time behaviour of the pressures defines the response of the whole system to the specific transient and it is the first item of the phenomena to be investigated as well as the main parameter with respect to safety issues. Fig. 3.4-7 shows all ISP-42 Phase-A test participants predicted the right time behaviour for the system pressure except one.

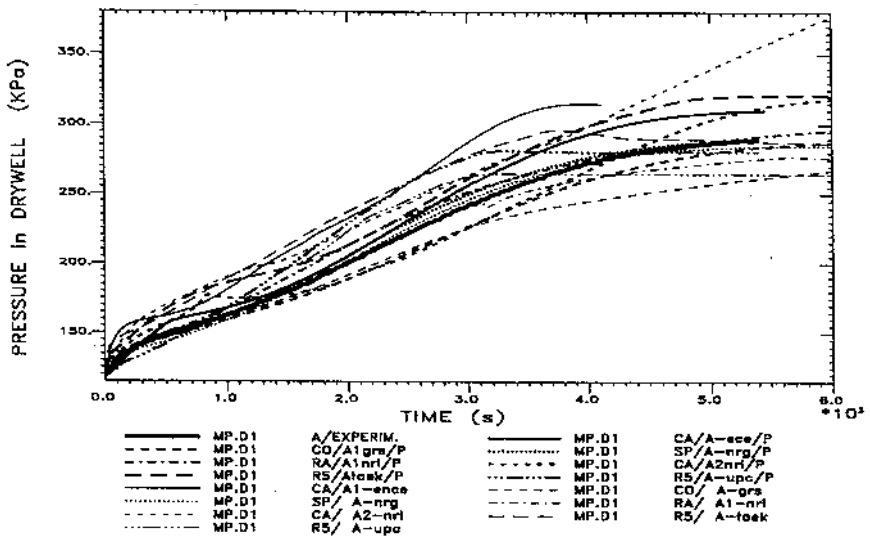

FIG. 3.4-7. Comparison of DW pressure calculations (blind and open phases) with experimental data for Phase A of ISP-42.

The decrease of the liquid mass inventory in the RPV determines the production of steam, which is injected into the two DWs. The injected steam partly condenses in the DWs (at least at the beginning of the transient) and afterwards mostly condenses on the primary sides of the PCCs. FIG. 3.4-8 shows the comparison of the liquid mass inventory predictions in the RPV to the experimental data.

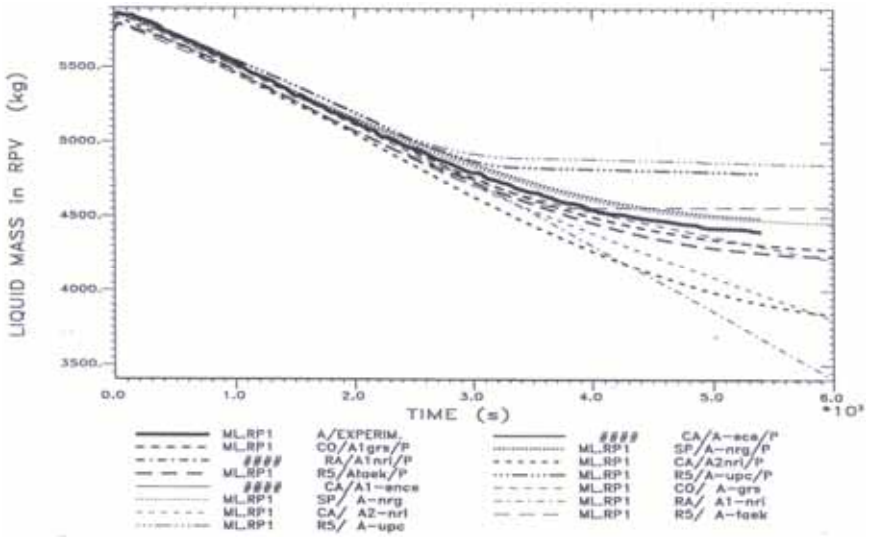

FIG. 3.4-8. Comparison of liquid mass inventory predictions (blind and open phases) with experimental data (RPV) for Phase A of ISP-42.

Figure 3.4-9 for the DW pressure provides some indication of the "User Effect." The same code used by different organizations, in this case RELAP5 and CATHARE codes, produced quite different results as seen in this figure. For further detailed analysis of the comparisons of the calculated and experimental data for ISP-42 Phase-A, interested reader can refer to the references (Luebbesmeyer and Aksan [3.4-31]; Luebbesmeyer and Aksan [3.4-32]).

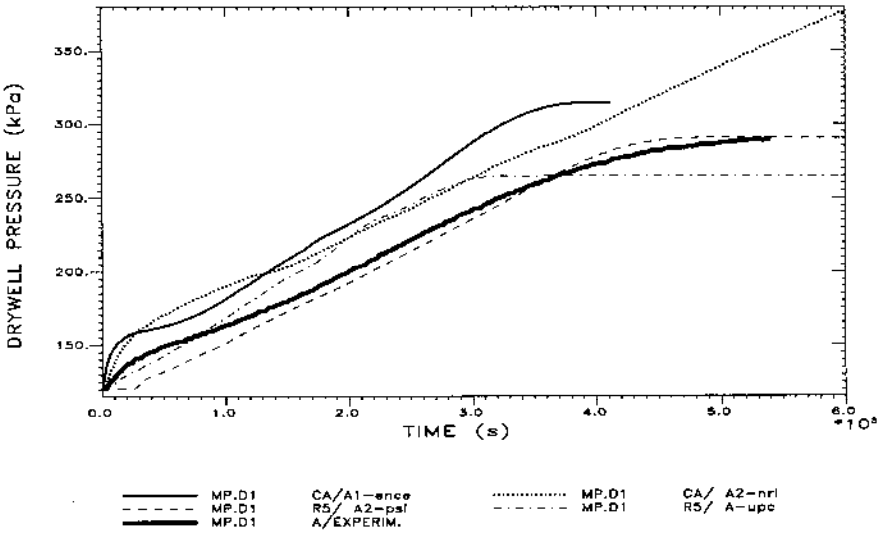

FIG. 3.4-9. DW pressure RELAP5/Mod3 and CATHARE code calculations compared to experimental data for Phase A of ISP–42.

3.4.6.4. Summary of the major conclusions from ISP-42 PANDA test and code predictions

Some of the major conclusions drawn on the basis of the six phases of the ISP-42 post test cases and the "blind" phase results can be summarized as follows (Interested readers should refer to the Refs [3.4-31], [3.4-32] for more detailed information):

(1) Objectives set at the beginning of this ISP-42 activity have been achieved.

(2) As the most important parameter in relation to reactor safety, the containment pressure history has been calculated sufficiently correct for most of the ISP-42 participants for all six phases.

(3) The overall best results were obtained by the lumped parameter code SPECTRA.

(4) Although system codes like CATHARE or RELAP5 were not designed to calculate typical containment problems in low pressure environments in the presence of large amounts of NC, they produced acceptable results. Containment code COCOSYS also produced globally acceptable results.

(5) Some codes (like GOTHIC) had problems to model specific equipment (e.g., PCCs) properly. Some tuning of physical models, which needed knowledge of the facility behaviour, were introduced. The RELAP5 or CATHARE codes were superior with respect to the higher flexibility to simulate special components and, in this case, specifically the modeling of the PCCs.

(6) Most of the major deviations could be attributed to problems with the nodalization or simply input errors rather than deficiencies of the specific codes.

(7) It was observed that major attention should be given to provide the appropriate input parameters, which are used in the analysis.

(8) For simple physical situations (e.g. well-mixed conditions in Phase A), choice of a lumped parameter approach is permitted. In such cases, little gain in predictive capability is achieved at the cost of very large computation time for 3-D simulation and detailed nodalization. Sensitivity studies can help to select the appropriate detailed nodalization and needed sophistication of physical models, and determine criteria for reasonable compromises between accuracy and computing time or costs.

(9) 3-D models such as in GOTHIC code include right physical representation of phenomena but number of difficulties currently prevents to take full advantage of these capabilities, e.g., accurate calculation of stratified conditions and its effect on system pressure (global parameter). Consequently, further assessment of 3-D models and advanced modeling features (e.g., turbulence) are necessary using well defined separate effects experiments for specific phenomena related to containment multicompartment geometries.

(10) The use of CFD codes is still exploratory, as they usually lack built-in physical models, interfaces (boundary conditions) with other components are difficult to set, and they occasionally show problems with respect to convergence. Consequently, there was no submission with CFD codes.

(11) The data set produced for the six phases of the ISP-42 PANDA tests will be used as the basis of assessment of computer codes in relation to the PCCSs in the next future, at least next ten years. These data will be available to the requesting organizations through NEA-Data Bank and European Community Project CERTA.

3.4.7. JAEA's research project on horizontal heat exchanger for PCCS [3.4-33]

The research project on the PCCS started in 1998 at JAEA with collaboration from the Japanese industry. In this project, the use of the horizontal heat exchanger was proposed for the PCCS because of the following advantages over the vertical one:

(1) The heat exchanger's geometry such as tube diameter, pitch, and length can be optimized based solely on the heat transfer performance. For the vertical heat exchanger, the tube length is limited by the water level in the PCCS pool, and the tube diameter is limited by the requirement for the earthquake resistance because the tubes also have a function of the structure support for the large and heavy inlet header pipe locating above the tube bundle. These advantages enable the horizontal heat exchanger to be more compact.

(2) The horizontal heat exchanger can be submerged in the PCCS pool with lower liquid level compared to that for the vertical one, which enables the more efficient use of the pool water inventory.

(3) The maintenance and inspection of the PCCS components can be much easier because the inlet and outlet plenums can be placed outside the PCCS pool.

The design condition of the PCCS is determined from the required function to maintain the containment integrity for at least one day during severe accidents with failures of the active safety systems. Since it is well known that the containment failure due to the overpressurization occurs at pressure of much higher than the design pressure, the pressure of 0.7 MPa is used as the reference pressure for the PCCS design, which is a relatively conservative value as a threshold of the containment failure. The reference inlet steam flow rate represents the 1% of the nominal core power, which is a typical decay heat level during the long term core cooling phase. Furthermore, the PCCS of this concept should be functional even under the presence of some degree of the NC gas because the NC gas is likely to be generated through various chemical processes during severe accidents. The reference inlet NC-gas quality of 1% is determined from this requirement. These requirements constitute both the PCCS design specification and the reference conditions for the experiments.

The program consisted of experiments using two facilities for fundamental thermohydraulic investigation and integral confirmation, the validation and modification of the analysis codes, and the system analysis for the BWR severe accidents. Those are described in the followings in this report.

3.4.7.1. Fundamental thermohydraulic experiment

The fundamental thermohydraulic experiments were conducted to obtain better understandings on heat transfer and condensing two phase flow in a U-shaped horizontal tube (Nakamura et al. [3.4-34]]; Nakamura et al. [3.4-35]) as shown in Fig. 3.4-10. The tested tube geometry is a U-tube that can be placed in the vertical plane; the flow direction inside the U-tube is horizontal for the straight sections and downward for the bend section. The tube is contained in the outer tube to cool the outer surface of the tested tube by single phase liquid flow. The outer tube is divided into several sections having an instrumented water supply system so that the local heat transfer rate can be measured for each section. The tested thermohydraulic parameters include the velocity of vapour and gas mixture at the inlet, the system pressure, and the NC gas quality.

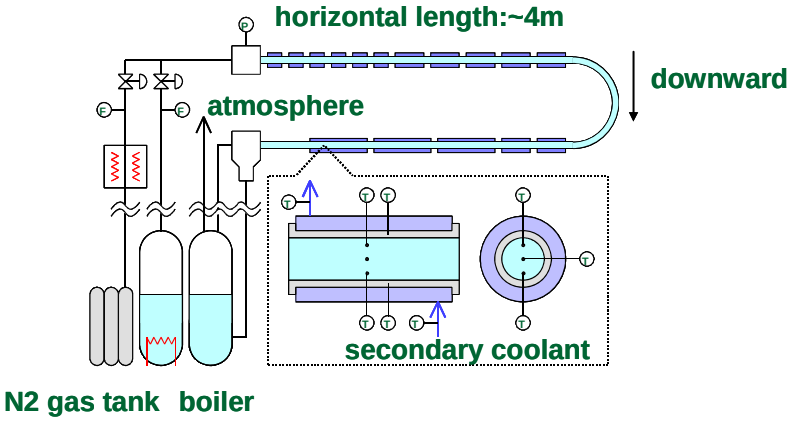

FIG. 3.4-10. Single U-tube test facility.

The measured heat transfer coefficients were compared with existing heat transfer correlations. In general, the correlations showed poor agreements especially for the condensation heat transfer in the annular flow regime and the heat transfer deterioration by the presence of NC gas. Fig. 3.4-11 shows the comparison of the predictions with existing and newly developed correlations, and the experimental data for the annular flow regime at pressure of 0.7 MPa. Fig. 3.4-11 shows that the Shah model used in the RELAP5 code underpredicts the heat transfer coefficients. The newly developed condensation correlation is based on the measured linear relationship between the heat transfer coefficient and the roll wave passing frequency along the inner surface of the tube, which shows better agreements [3.4-36]. From those investigations, a heat transfer package consisting of newly-developed and validated correlations was established for the improvement of the RELAP5 code [3.4-37].

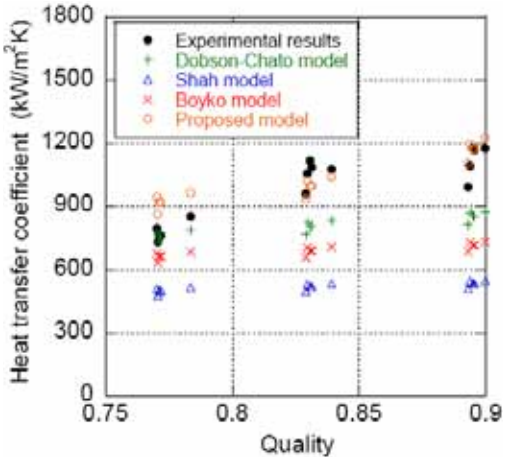

FIG. 3.4-11. Comparison of the experimental data and predictions with existing and proposed.

3.4.7.2. Large scale experiment

The purposes of the large scale experiment were to 1) confirm the performance of the horizontal heat exchanger under the reference conditions mentioned previously, 2) investigate effects of the multichannel tubes in the primary side and the multidimensional boiling flow in the secondary side, and 3) validate the analysis codes ([3.4-38]–[3.4-40]). The test section consisted of a tube bundle which was a halved, full height, prototypical-scale bundle, and a secondary pool as shown in Fig. 3.4-12. The tube length was typically 8 m from the inlet to the outlet. The electric power of up to 10 MW was used for the steam supply to the facility. The water supply to the PCCS pool was controlled to keep the collapsed level above the tube bundle. The pool gas phase was connected to atmosphere through several large nozzles so that the pressure was kept approximately at atmospheric level. The void fraction distribution in the secondary side was measured by traversing optical void probes between the middle and top elevation of the bundle.

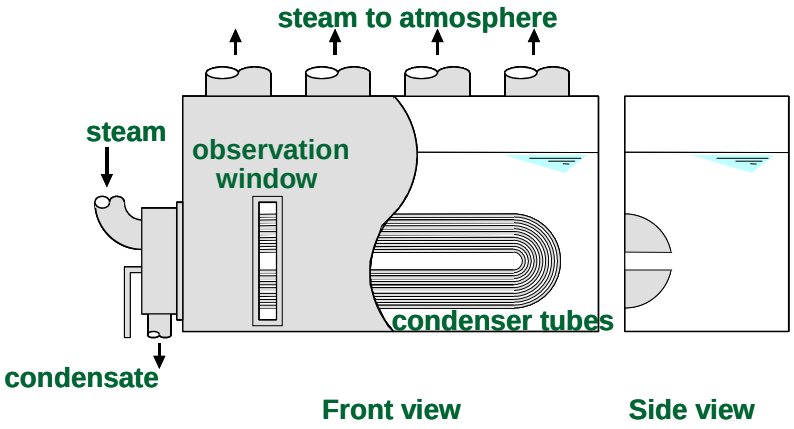

FIG. 3.4-12. U-tube bundle test facility.

The onset of boiling was observed in the lowest tubes of the upper tube bundle, that is, the lower tube bundle was cooled only by single phase liquid flow for typical test conditions. The flow regime transition from bubbly to churn flow occurred in the upper bundle with increase of elevation. The measured heat transfer coefficient for the tube outer surface increased with the increase in the void fraction in the upward direction. The magnitude of the increase, however, was not enough to differentiate the total heat transfer rate among the tubes, because the other heat transfer resistances at the tube inner surface and through the wall were not affected by the flow regime transition in the secondary side. Heat transfer deterioration due to the formation of vapour blanket around the tubes was not observed for the present test conditions.

Although the primary side steam flow is perfectly condensed at the reference pressure condition, uncondensed steam is discharged to the outlet plenum at relatively low pressure conditions due to small temperature difference between the primary and secondary sides. Since the uncondensed steam and NC gas flow from the outlet plenum was directly discharged to facility outside through the vent line for the present test configuration, such insufficient condensation did not affect the pressure response, which would have increased the primary pressure if the system consisted of a closed loop as for the actual reactor. The effect, however, is insignificant because the primary pressure increase is suppressed by the increase of the condensation rate, establishing a new balanced condition at a higher pressure. The present experimental data have indicated that the entire vapour is condensed in the tubes before the pressure reaches the reference pressure of 0.7 MPa.

3.4.7.3. Code development for horizontal heat exchanger analysis

A new code for the detailed analysis was developed using two codes: RELAP5 and ACE-3D that is an analysis code for the multidimensional two phase flow developed at JAERI (Ohnuki et al. [3.4-41]). The RELAP5 code calculates the primary side behaviour; the ACE-3D calculates the secondary side. Both codes are thermally coupled at the condenser tube surface. Typical validation results for the code are shown in Fig. 3.4-13 and Fig. 3.4-14, where the prediction results are compared with the measured distribution of the quality in the condenser tubes and the void fractions in the bundle side. The calculation successfully predicted the uniform quality distribution inside the tubes with the multidimensional boiling behaviour in the secondary side as it was observed in the experiments.

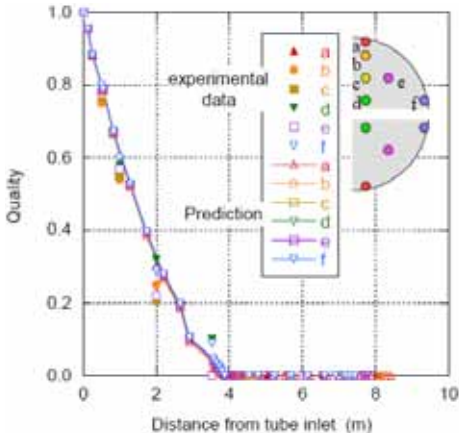

FIG. 3.4-13. Quality distribution in condenser tube.

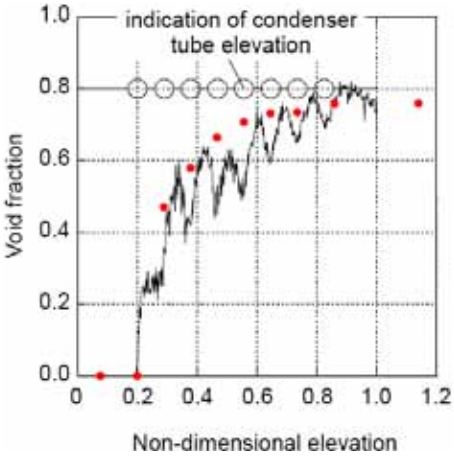

FIG. 3.4-14. Void fraction distribution in tube bundle.

Since this code takes a relatively long calculation time, a simplified RELAP5 noding model of the horizontal heat exchanger was developed for efficient and economical system analysis, where the RELAP5 was modified using the heat transfer package developed in this study. In this analysis, the heat exchanger is modelled with a single tube based on the experimental result of uniform condensation behaviour among the tubes. The evaluation results showed that the simplified model predicted well the total heat removal rate and pressure drop across the heat exchanger for all the tested conditions.

3.4.7.4. System analysis

The system analysis was performed using the simple node model and the RELAP5 code modified using the heat transfer package developed in Ref. [3.4-42]. The objective of this analysis was to confirm the performance of the PCCS with the horizontal heat exchanger in preventing the containment failure for at least one day. Since the RELAP5 cannot predict the generation of NC gas by the chemical reactions such as molten core concrete interaction (MCCI) during severe accidents, the MELCOR code (version 1.8.5) was used to evaluate the gas generation rate. The MELCOR results were imposed by using the time dependent volumes and junctions components in the RELAP5 code. The RELAP5 calculation started at the onset time of ejection of the core melt from the RPV bottom. It is conservatively assumed that the containment is filled completely with NC gas at this time.

The two calculated DW pressures are shown in Fig. 3.4-15 for the scenario of the transient without the ECCS injection (TQUV), where two cases corresponded to the calculations with and without the PCCS. The Fig. 3.4-15 clearly indicates the effects of the PCCS heat removal; the containment pressure increased beyond the reference pressure of 0.7 MPa for the case without the PCCS

at 50,000sec, and was kept below the pressure limit for more than 100,000 sec for the case with the PCCS. This result confirms the effectiveness of the PCCS to prevent the containment failure for at least 1 day for this scenario (= 86,400 s).

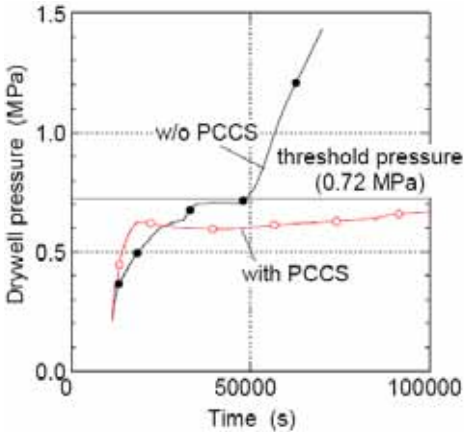

FIG. 3.4-15. DW pressure behaviour with and without PCCS.

The research project was conducted at JAEA to clarify the applicability of the PCCS with horizontal heat exchangers to a next-generation BWR. The design requirement of the PCCS of this concept is to prevent the containment damage due to pressurization for at least one day during severe accidents with failures of the active safety systems. The research program consisted of the fundamental thermohydraulic experiments, the bundle experiments, the code validation and modification, and the reactor analyses with the modified code.

The fundamental thermohydraulic experiments were performed first to investigate the performance of a horizontal condenser tube under wide ranges of experimental conditions. Experimental results have shown that the condensation heat transfer coefficients for the annular flow regime are underpredicted by existing correlations. A new model was developed, which was based on the measured relationship between roll wave passing frequencies and the heat transfer rates. The new correlation predicted well the experimental data.

The large scale experiments were performed secondly to confirm the total performance of the horizontal heat exchanger and to validate analysis codes to predict overall thermohydraulic behaviour of the horizontal heat exchanger. Various flow regimes were observed in the secondary side of the tube bundle including single phase liquid, bubbly, and churn flows with the increase in the elevation in the tube bundle. Effects of such flow regime transition, however, were not large enough to differentiate the heat transfer rates among tubes. No instability was observed for the present test conditions.

A code to predict the detail behaviour at the PCCS heat exchanger was newly developed by using the RELAP5 code for the primary side calculation and the ACE-3D for the bundle side calculation. The RELAP5 code was modified by adding the heat transfer package developed in this study. The developed code agreed well with the measured quality distribution inside the tube and void distribution in the tube bundle.

The BWR severe accidents were analysed assuming failures of all the active safety systems by using the modified RELAP5 code. The results has confirmed that the design target of the PCCS is clearly satisfied; that is, the containment pressure is kept below the reference pressure of 0.7 MPa, and the containment is not damaged at a large scale by pressurization during severe accidents for at least one day even when all the active safety systems failed.

3.4.8. Summary

A state of the art review of the studies on the behaviour of containment emergency systems is presented in the experimental and analytical aspects. Since the containment of a nuclear power plant is the ultimate barrier against the release of radioactive materials into the environment, the integrity of the containment should be maintained during any postulated accident by suppressing the pressure and temperature of the containment atmosphere below the design limits. In view of the importance of the containment protection, there have been a number of studies on reliable containment cooling systems especially for the development of advanced nuclear power reactors. Among them, in this report are introduced four passive safety systems for the containment: (1) vertical PCCS condenser employed in the GE's SBWR/ESBWR, (2) horizontal PCCS condenser proposed for the Japanese ABWR-II, (3) external air cooling system used in the Westinghouse's AP600/AP1000, and (4) containment cooling condenser developed for the AREVA's SWR-1000. Also the relevant test facilities such as GIRAFFE, PANDA, PANTHERS, PUMA, and LSTF are briefly described, and several condensation heat transfer models are reviewed. Among the recent studies on the containment cooling systems, in this report are summarized four of the relevant researches: (1) Purdue's PUMA-PCCS separate effect tests, (2) PSI's ISP-42 PANDA tests, (3) JAEA's study on the horizontal PCCS heat exchanger, and (4) Purdue's modular SBWR design with passive safety systems. For each study, both experimental and analytical aspects are highlighted. Overall, the system analysis codes produced acceptable results for the containment thermohydraulic behaviour. However, for better simulations of the containment behaviour under the low pressure conditions in the presence of large amounts of NC gases, it is recommended that the relevant physical models need to be improved based on the experimental data.

ABBREVIATIONS

ABWR	Advanced boiling water reactor
AC	Alternating current
ADS	Automatic depressurization system
ALWR	Advanced light water reactor
BDLB	Bottom drain line break
BWR	Boiling water reactor
CCC	Containment cooling condenser
C-PHRS	Containment passive heat removal system
CRP	Coordinated research project
CSNI	Committee on the Safety of Nuclear Installations
DBA	Design basis accident
DPV	Depressurization valve
DW	Drywell
ECCS	Emergency core cooling system
ESBWR	Economic simplified boiling water reactor
GDCS	Gravity-driven cooling system
GDLB	GDCS Drain line break
GE	General electric
HPLWR	High performance light water reactor
ICS	Isolation condenser system
ISP	International standard problem
JAEA	Japan Atomic Energy Agency
JAERI	Japan Atomic Energy Research Institute
LOCA	Loss of coolant accident
LPCI	Low pressure coolant injection
LSBWR	Long operating cycle simplified boiling water reactor
LSTF	Large scale test facility
LWR	Light water reactor
MCCI	Molten core concrete interaction
MSLB	Main steam line break
NC	Non-condensable

PCCS	Passive containment cooling system
PSI	Paul Scherrer Institute
PUMA	Purdue University Multi-Dimensional Integral Test Assembly
PWG	Principal working group
PWR	Pressurized water reactor
RHR	Residual heat removal
ROSA	Rig of safety assessment
RPV	Reactor pressure vessel
RWCU	Reactor water clean up
SBWR	Simplified boiling water reactor
SCWR	Super-critical water reactor
SDC	Shutdown cooling
SIET	Societ`a Informazioni Esperienze Termoidrauliche
SP	Suppression pool (Wet well, WW)
SRV	Safety relief valve
SWR	Siedewasserreaktor
TAF	Top of the active fuel
USNRC	United States Nuclear Regulatory Commission
VB	Vacuum breaker
WW	Wet well (Suppression pool, SP)

NOMENCLATURE

A_i	Inner surface area of a condenser tube, m^2
A_o	Total outer surface area of the condenser tubes, m^2
D_i	Inner diameter of the condenser tube, m
D_o	Outer diameter of the condenser tube, m
$\overline{h}_c$	Average heat transfer coefficient for the condenser tube inside, kW/m^2-K
h_{fg}	Latent heat of condensation, kJ/kg
h_g	Specific enthalpy of steam, kJ/kg
$\overline{h}_p$	Average heat transfer coefficient for the condenser tube outside (pool), kW/m^2-K
k_g	Steam thermal conductivity, kW/m-K
k_w	Thermal conductivity of the condenser tube wall, kW/m-K
L	Condenser tube length, m
$\dot{m}_{con}$	PCCS condensate mass flow rate, kg/s
$\dot{m}_{steam}$	PCCS steam mass flow rate, kg/s
N_{tubes}	Number of PCCS condenser tubes per unit
N_{units}	Number of PCCS units
Nu	Average Nusselt number
$\dot{Q}_{pccs}$	Heat transfer rate through the PCCS condenser, kW
$\overline{T}_g$	Average steam temperature, K
$\overline{T}_p$	Average PCCS pool temperature, K
$\overline{T}_w$	Condenser tube outer wall temperature, K
$\overline{U}$	Overall heat transfer coefficient, kW/m^2-K
χ	NC gas mass fraction

REFERENCES FOR SECTION 3.4

[3.4-1] LEONARDI, T., ISHII, M., Condensation heat transfer with non-condensable gas for passive containment cooling of nuclear reactors, Nuclear Engineering and Design **236** (2006) 1789-1799.

[3.4-2] MASONI, P., et al., "Tests on full-scale prototypical passive containment condenser for SBWR's application," ICONE-3, Vol. 2, 1023, Kyoto, Japan, April (1995).

[3.4-3] DREIER, J., et al., "The PANDA tests for the SWR 1000 passive containment cooling system", ICONE-7, ICONE-7316, Tokyo, Japan, April 19–23 (1999).

[3.4-4] HUGGENBERGER, M., et al., "ESBWR related passive decay heat removal tests in PANDA", ICONE-7, ICONE-7322, Tokyo, Japan, April 19–23 (1999).

[3.4-5] KONDO, M., et al., "Primary-side two phase flow and heat transfer characteristics of a horizontal-tube PCCS condenser," ICONE-14, ICONE14-89652, Miami, FL, USA, July 17-20 (2006).

[3.4-6] SHA, W.T., CHIEN, T.H., SUN, J.G., CHAO, B.T., Analysis of large scale tests for AP-600 passive containment cooling system, Nuclear Engineering and Design **232** (2004) 197-216.

[3.4-7] INTERNATIONAL ATOMIC ENERGY AGENCY, Passive Safety Systems in Water Cooled Nuclear Power Plants: The Use of Natural Circulation, IAEA-TECDOC-1624, IAEA, Vienna (2009).

[3.4-8] PASLER, D., "The safety concept of the SWR 1000", ICAPP'04, Paper 4207, Pittsburgh, PA, USA, June 13–17 (2004).

[3.4-9] AKSAN, N., et al., "Potential safety features and safety analysis aspects for high performance light water reactor (HPLWR)", International Conference on Global Environment and Advanced Nuclear Power Plants, GENES4/ANP2003, Kyoto, Japan, September 15–19 (2003).

[3.4-10] UPTON, H.A., COOKE, F.E., SAWABE, J.K., "Simplified boiling water reactor passive safety features", Second ASME/JSME Nuclear Engineering Joint Conference, Vol. 1, New York, NY, USA (1993) 705–712.

[3.4-11] VIEROW, K.M., "GIRAFFE passive heat removal testing program", Technical Report NEDC-32215P, GE Proprietary Information (1993).

[3.4-12] YADIGAROGLU, G., "The PANDA tests for the SBWR", 25th Water Reactor Safety Information Meeting, Bethesda, MD, USA (1997).

[3.4-13] AKSAN, N., "Overview on PANDA test facility and ISP-42 PANDA tests data base", 2nd RCM of IAEA's CRP on Natural Circulation Phenomena, Modeling, and Reliability of Passive Systems that Utilize Natural Circulation, Oregon State University, Corvallis, Oregon, USA, Aug. 29–Sep. 2 (2005).

[3.4-14] PARLATAN, Y., BOYER, B.D., JO, J., ROHATGI, U.S., "Analysis of PANTHERS full-scale heat transfer tests with RELAP5", ICONE-4, New Orleans, LA, USA, March 10-13 (1996).

[3.4-15] ISHII, M., et al., "Scientific design of Purdue University multi-dimensional integral test assembly (PUMA) for GE SBWR", NUREG/CR-6309, PU-NE 94/1, Purdue University (1996).

[3.4-16] The ROSA-V Group, ROSA-V Large Scale Test Facility (LSTF) System Description for the Third and Fourth Simulated Fuel Assemblies, JAERI-Tech 2003-037 (2003).

[3.4-17] NUSSELT, W., Die Oberflachenkondensation des Wasserdampfes (The surface condensation of water vapor), Zeit. D. Ver. Deut. Ing. **60** (1916) 541–575.

[3.4-18] SPARROW, E.M., MINKOWYCZ, W.J., SADDY, M., Forced convection condensation in the presence of non-condensables and interfacial resistance, International Journal of Heat and Mass Transfer **10** (1967) 1829–1845.

[3.4-19] CHEN, S.L., KE, M.T., Forced convective film condensation inside vertical tubes, International Journal of Multiphase Flow **19** (1993) 1045–1060.

[3.4-20] VIEROW, K.M., Behaviour of Steam-Air Systems Condensing in Concurrent Vertical Downflow, Master's Thesis, Department of Nuclear Engineering, University of California, Berkeley (1990).

[3.4-21] VIEROW, K.M., SCHROCK, V.E., "Condensation in a natural circulation loop with non-

condensable gases, Part I - heat transfer", International Conference on Multiphase Flows, Tsukuba, Japan, September 24–27 (1991) 183–186.
[3.4-22] SIDDIQUE, M., The Effects of Non-condensable Gases on Steam Condensation under Forced Convection Conditions, Ph.D. Thesis, MIT (1992).
[3.4-23] KUHN, S.Z., Investigation of Heat Transfer from Condensing Steam-Gas Mixtures and Turbulent Films Flowing Downward Inside a Vertical Tube, Ph.D. Thesis, University of California, Berkeley (1995).
[3.4-24] KIM, S.J., No, H.C., Turbulent film condensation of high pressure steam in a vertical tube, International Journal of Heat and Mass Transfer **43** (2000) 4031–4042.
[3.4-25] LEONARDI, T.L.W., Condensation Heat Transfer Analysis of the Passive Containment Cooling System of the Purdue University Multi-Dimensional Integral Test Assembly, Ph.D Thesis, Purdue University (2000).
[3.4-26] OH, S., Experimental and Analytical Study of the Effects of Non-condensable Gas in a Passive Condenser System, Ph.D Thesis, Purdue University (2004).
[3.4-27] ISHII, M., CHOI, S.W., YANG, J., YOO, Y.-J., "PUMA-PCCS Separate Effect Tests", 3rd RCM of IAEA's CRP on Natural Circulation Phenomena, Modeling, and Reliability of Passive Systems that Utilize Natural Circulation, CEA, Cadarache, France, September 11-15 (2006).
[3.4-28] GE NUCLEAR ENERGY, SBWR Standard Safety Analysis Report, Report 25A5113, Rev. A, August (1992).
[3.4-29] ISHII, M., CHOI, S.W., YANG, J., VIEROW, K., WANG, W., HAN, J., PCCS Separate Effect Tests in the PUMA Facility, PU/NE-05-17, Purdue University (2006).
[3.4-30] PARK, H.S., Steam Condensation Heat Transfer in the Presence of Non-condensables in a Vertical Tube of Passive Containment Cooling System, Ph.D. Thesis, KAIST (1999).
[3.4-31] LUEBBESMEYER, D., AKSAN, N., "ISP-42 PANDA tests: behaviour of passive containment systems during the long term heat removal phase in advanced light water reactors; blind phase comparison report", OECD/NEA Report, NEA/CSNI/R(2003)6, May (2003).
[3.4-32] LUEBBESMEYER, D., AKSAN, N., "ISP-42 PANDA tests: behaviour of passive containment systems during the long term heat removal phase in advanced light water reactors; open phase comparison report", OECD/NEA Report, NEA/CSNI/R(2003)7, May (2003).
[3.4-33] KONDO, M., NAKAMURA, H., YONOMOTO, T., "Summary of the Research Project on Horizontal Heat Exchanger for PCCS", 2nd RCM of IAEA's CRP on Natural Circulation Phenomena, Modeling, and Reliability of Passive Systems that Utilize Natural Circulation, Oregon State University, Corvallis, Oregon, USA, Aug. 29 – Sep. 2 (2005).
[3.4-34] NAKAMURA, H., et al., "Experimental investigation of thermal-hydraulic performance of PCCS with horizontal tube heat exchangers: single U-tube test", Severe Accident Research Japan 99 (SARJ-99), JAERI-Conf 2000-015, Tokyo, Japan, November 8–10 (1999).
[3.4-35] NAKAMURA, H., et al., "Single U-tube testing and RELAP5 code analysis of PCCS with horizontal heat exchanger", 2nd Japan-Korea Symposium on Nucl. Thermal Hydraulics and Safety (NTHAS2), 336, Fukuoka, Japan, October 15–18 (2000).
[3.4-36] KONDO, M., et al., "Roll wave effects on annular condensing heat transfer in horizontal PCCS condenser tube", ICONE-10, ICONE10-22403, Arlington, VA, USA, April 14-18 (2002).
[3.4-37] KAWAI, H., et al., "RELAP5 code improvement for horizontal passive containment cooling system (PCCS) thermal hydraulic performance evaluation", NUTHOS-6, Paper N6P362, Nara, Japan, October 4–8 (2004).
[3.4-38] ARAI, K., et al., "Multi-dimensional thermal-hydraulic analysis for horizontal tube type PCCS," ICONE-10, ICONE10-22442, Arlington, VA, USA, April 14-18 (2002).
[3.4-39] KONDO, M., et al., "Experimental observation of thermal hydraulic behavior in PCCS horizontal heat exchanger", GENES4/ANP2003, Paper 1173, Kyoto, Japan, September 15-19 (2003).
[3.4-40] ARAI, K., KURITA, T., YAMAMOTO, K., FUKUDA, T., "Post-test analysis of thermal-hydraulic test using full-scale horizontal PCCS condenser", ICAPP'03, Paper 3133, Cordoba, Spain, May 4–7 (2003).

[3.4-41] OHNUKI, A., NAKAMURA, H., ANODA, Y., OBATA, H., SAISHU, S., "ACE-3D code analyses of multi-dimensional boiling flow in horizontal PCCS water pool", ICONE-9, Nice, France, April 8–12 (2001).
[3.4-42] KONDO, M., et al., "Confirmation of effectiveness of horizontal heat exchanger for PCCS", ICONE-13, ICONE13-50691, Beijing, China, May 16–20 (2005).

3.5. THERMO-FLUID DYNAMICS AND PRESSURE DROPS IN VARIOUS GEOMETRICAL CONFIGURATIONS

Pressure drop is an important parameter for design and analysis of many systems and components. Particularly in natural circulation systems, the mass flux and the driving heads are low compared to those of forced circulation systems. Therefore, it is necessary to determine the pressure loss components very accurately. Though it is widely believed that the pressure loss inside a device does not depend on whether the flow is sustained by a pump or by a density difference, under some circumstances, because of local effects the pressure loss may get influenced by the nature of the driving force. In the present report, an attempt has been made to assess pressure drop correlations for its application in natural circulation loops. The pressure drop phenomenon is defined and various scenarios and hardware related to the pressure drop phenomena are explained. Important aspects like transition region, diabatic boundary condition are addressed. A comparison of flow characteristics under forced and natural circulation conditions has been given. The effect of friction factor correlation on steady state flow and stability prediction for both single phase as well as two phase natural circulation has been discussed. The effect of two phase friction multiplier on steady state and stability of two phase natural circulation loop is also presented The two phase pressure drop correlations recommended by different authors for pipe flow have been included.

3.5.1. Introduction

Pressure drop can be defined as the difference in pressure between two points of interest in a fluid system. A large number of single phase and two phase flow pressure drop correlations can be found in the literature. Some important pressure drop relationships can be found in the IAEA technical document on "Thermohydraulic relationships for advanced water cooled reactors" (IAEA-TECDOC-1203 [3.5-1]).

Though the effect of natural circulation (or flow developed due to heating) on pressure drops is not well established, it should be noted that most of the pressure drop correlations are developed from data generated in forced circulation systems. The mechanism of flow in natural circulation loop may be complex due to buoyancy effect and formation of secondary flows. Also, natural circulation flows are characterized by low driving head and low mass flux along with potential instabilities under certain operating conditions. On the other hand, natural circulation as a mode of heat removal is gaining momentum in many advanced water reactors due to its passive nature and seemingly higher reliability. Therefore, there is a need to take a closer look at pressure drop phenomena under natural circulation, which is both complex and important.

To deal with pressure drop, it is advisable not only to define it, but also to examine it in the backdrop of a particular scenario (*when* it occurs) and in a particular hardware (*where* it occurs), which will enable us to understand and judge its applicability in a particular situation.

3.5.1.1. Definition

Pressure drop is the difference in pressures between two points of interest in a fluid system. In general, pressure drop can be caused by resistance to flow, changes in elevation, density, flow area and flow direction. Pressure drops in natural circulation systems play a vital role in their steady state, transient and stability performance.

It is customary to express the total pressure drop in a flowing system as the sum of its individual components such as distributed pressure loss due to friction, local pressure losses due to sudden variations of shape, flow area, direction, etc. and pressure drops (the reversible ones) due to acceleration (induced by flow area variation or by density change in the fluid) and elevation (gravity effect). An important factor affecting the pressure loss is the geometry. In a nuclear reactor, we have to deal with several basic geometrical shapes (circular pipes, annuli, etc.) and a number of special devices of complex shapes like rod bundles, heat exchangers, valves, headers, plenums, pumps, large pools, etc. Other factors are concerned with the fluid status (single or two phase/one component, two component or multicomponent), the flow nature (laminar or turbulent), the flow pattern (bubbly, slug, annular, etc.), the flow direction (vertical upflow, downflow, inclined flow, horizontal flow, countercurrent flow, etc.), flow type (separated and mixed), flow paths (one dimensional or multidimensional, open or closed paths, distributor or collector), and the operating conditions (steady state or transient).

An important focus of this phenomenon is the geometric conditions that hinder the establishment of fully developed flow especially when the fluid in question is a mixture of steam, air and water. This complex thermo-fluid dynamic phenomenon warrants special attention. However, it is worth mentioning here that though in many systems like the primary system of a nuclear power plant, flow is mostly not fully developed, pressure drop relationships used in these systems are invariably those obtained for developed flow. This practice is experimentally proved to be more than adequate in most of the cases. However, in some specific cases like containment internal geometry, it is necessary to consider thermo fluid dynamics in the developing region.

A final, very important issue, is concerned with the driving force depending on whether the flow is sustained by a density difference in the fluid (natural circulation) or by a pump (forced convection), or whether there will be feedback between the pressure loss and the extracted power. Normally, the pressure loss inside a device depends on the nature of flow through the device and not on the nature of the driving head causing the flow. However, under some circumstances, because of local effects, the pressure loss may get influenced by the nature of the driving force.

3.5.1.2. Scenario

For a given system or network, a portion of the total pressure that is spent to overcome the resistance forces arising from the flow of real (viscous) fluids through pipes and channels is irretrievably lost. This loss of total pressure (or pressure drop) is due to irreversible conversion of mechanical energy (the work of resistance force) into heat. Therefore, the term loss due to fluid resistance or hydraulic loss, represents the irreversible loss of total pressure over a given system length. There are also reversible component of pressure drop such as elevation pressure drop and acceleration pressure drop.

As stated earlier, the total pressure drop comprises of distributed pressure loss due to friction, local pressure loss due to sudden variations of shape, flow area, direction, etc. and pressure drops (the reversible ones) due to acceleration (induced by flow area variation or by density change in the fluid) and elevation (gravity effect). Various components of pressure drop are further elaborated below.

a. The fluid friction loss is due to the viscosity (both molecular and turbulent) of real liquid and gases in motion, and results from momentum transfer between the molecules (in laminar flow) and between individual particles (in turbulent flow) of adjacent fluid layers moving at different velocities. For two phase flow, an additional frictional pressure drop may be due to the interphase friction between gas–liquid or steam–liquid phases.

b. The local losses of total pressure are caused by the following: local disturbance of the flow; separation of flow from the walls; formation of vortices and strong turbulent agitation of the flow at locations where the configuration of pipeline changes or fluid streams meet or flow past obstructions (e.g. entrance of a fluid into pipeline, expansion, contraction, bending and branching of the flow, flow through orifices, grids or valves, filtration through porous bodies, flow past different bluff bodies etc.).

c. The energy spent in accelerating the molecules of the fluid is manifested as acceleration pressure drop. This reversible component of pressure drop is caused by a change in flow area or density. Fluid flowing through an expansion, contraction or a heated section are some of the examples where acceleration pressure drop can occur.

d. Some work needs to be done against the gravity to raise the fluid molecules to a certain height. This energy spent is the reason behind the elevation pressure drop. This reversible component of pressure drop is caused by the difference in elevation. In many instances with vertical test sections, the elevation pressure drop is the largest component.

The pressure loss components in any complex flow situation are inseparable. However, for ease of calculation they are artificially subdivided into components like local losses, frictional losses etc. It is also assumed that the local losses are concentrated in one section, although they can occur virtually over a considerable length, except, of course, for the case of flow leaving the system, when its dynamic pressure becomes immediately lost. This paper mainly deals with irreversible pressure drops.

It should be noted that most of the pressure drop correlations are generated from data obtained from fully developed flow, whereas flow in nuclear reactors are generally not fully developed except in some cases like the steam generator (SG) section and feeder section of PHWR etc. Further, most of the pressure drop correlations reported in literature had been developed from steady state experimental data and mostly under adiabatic conditions.

3.5.1.3. Hardware

The geometries of interest to Nuclear Power Plants (NPPs) will only be considered here. Virtually every component of NPPs comes under the purview of pressure drop. However, emphasis is on geometric conditions that are relevant to the primary loop of NPPs. The secondary loop of NPPs (the steam generator and the piping up to the Main Steam Isolation Valve (MSIV) and the feedwater valves in case of PWRs and PHWRs) is also important and needs to be considered. In addition, the Emergency Core Cooling (ECC) lines from the ECC pumps to the injection point along with the different types of valves may also be considered. A list of locations where local and distributed pressure losses are important is given below. Further, particular emphasis is put to deal with locations for local and distributed pressure losses in some of the advanced designs such as AHWR, SWR-1000, AP-600, APWR, ABWR, CAREM etc. Finally, for easy reference, the important locations for pressure drop are described in two categories: channel type reactors and vessel type reactors.

TABLE 3.5-1. LOCATIONS WHERE LOCAL PRESSURE DROP AND DISTRIBUTED PRESSURE DROP ARE IMPORTANT

	Channel type	Vessel type
Distributed pressure drop: (RPV & Primary Loop)	- Feeder and tail pipe - Bare bundle - SG Tubes - Fuel assembly	- Core and core bypasses - Downcomer - Upper plenum - Surge line - Steam Generator (SG) tubes
Local pressure drop: (RPV & Primary Loop)	- Spacers, tie plate & bundle junction - Header connections - Fuel locator, liner tube, grayloc	- Pump - Pressurizer and surge line connections - Spacers & tie plates - SG inlet / outlet
Safety system pressure drop:(Local & distributed)	- Accumulator connection - Check valve, ruptured disc - Gravity injection line	- Accumulator connections - Advanced fluidic device, check valve, ruptured disc - Gravity injection line

3.5.2. Single phase pressure drop relationships

Pressure drop relationships for all the components of pressure drop covering important configurations are given in IAEA-TECDOC-1203 [3.5-1]. A few important aspects are discussed below.

3.5.2.1. Flow under transition regime

Most of the single phase pressure drop correlations are applicable to steady state fully developed flow. Fully developed flow conditions are expected to occur in long components like the steam generator U-tubes, feeder pipes etc. A large number of correlations valid for laminar and turbulent flow regimes can be found in literature. It may be noted that well established correlations for friction factor do not exist in the transition region between $2000 \leq Re \leq 3000$. Furthermore, in many transients, the flow may change from laminar to turbulent, or vice versa, necessitating a switch-over of correlations. Numerical calculations often encounter convergence problems when such switching takes place due to the discontinuity in the friction factor values predicted by the laminar flow and turbulent flow equations. A simple way to overcome this problem is to use the following criterion for switch over from laminar to turbulent flow equation.

$$\text{If } f_t > f_l \text{ then } f = f_t \tag{3.5-1}$$

where f_t and f_l are friction factors calculated by turbulent and laminar flow equations respectively. This procedure, however, causes the switch over from laminar to turbulent flow equation at $Re \approx 1100$. Solbrig's [3.5-2] suggestion to overcome the same problem is to use friction factor as equal to the greater of $(f_t)_{4000}$ and f_l below Reynolds number of 4000. $(f_t)_{4000}$ is the friction factor calculated by the turbulent flow equation at Re = 4000. Effectively this leads to

$$f = (f_t)_{4000} \text{ for } 2000 \leq Re \leq 4000 \tag{3.5-2}$$

In addition, a condition to avoid infinite friction factor is required to take care of flow stagnation (i.e. $Re \approx 0$).

3.5.2.2. Flow under diabatic condition

Another special kind of pressure drop calculation is that occurring under diabatic single phase flow conditions. In general, isothermal friction factor correlations are used with properties evaluated at the film temperature $T_f = 0.4 (T_W - T_b) + T_b$, where T_W and T_b are the wall and bulk fluid temperatures [3.5-3]. Sometimes the friction factor for non-isothermal flow is obtained by multiplying the isothermal friction factor with a correction coefficient, F. The correction coefficient accounts for the temperature gradient in the laminar layer and the consequent variation in physical properties of the fluid. The correction coefficient can be expressed as a function of the temperature drop in the laminar layer, ΔT_f as given below:

$$F = 1 \pm C\Delta T_f \tag{3.5-3}$$

The negative sign shall be used for heat transfer from wall to the fluid, and

$$\Delta T_f = q''/h' \tag{3.5-4}$$

Different values of the constant C are given by different investigators. El-Wakil [3.5-4] gives a value of 0.0025, while Marinelli and Pastori [3.5-5] give a value of 0.001.

An alternative approach is to express the correction factor in terms of the viscosity ratio. This approach is more widely used and the following empirical equation proposed by Leung and Groeneveld [3.5-6] is recommended.

$$F = (\mu_b / \mu_w)^{-0.28} \tag{3.5-5}$$

where the subscripts “b” and “w” refer to the bulk fluid and wall, respectively.

3.5.3. Two phase pressure drop relationships

3.5.3.1. Flow under adiabatic condition

A large number of two phase flow pressure drop correlations developed from adiabatic experimental data can be found in literature. These correlations can be classified into the following four general categories.

(1) Empirical correlations based on the homogeneous model,

(2) Empirical correlations based on the two phase friction multiplier concept,

(3) Direct empirical models,

(4) Flow pattern specific models.

These pressure drop correlations are comprehensively covered in the CRP on Thermohydraulic relationships for Advanced Water Cooled Reactors [3.5-1]. A few important aspects are discussed below.

3.5.3.2. Models using interfacial friction

Another form of two phase pressure drop correlations uses interfacial friction models. The two-fluid model used in many of the advanced system codes requires correlations for interfacial friction in addition to wall friction. Complete description of the models used in computer codes like TRAC-PFI/MOD1 Liles and Mahaffy [3.5-7] and RELAP5/MOD3.2 the RELAP5/MOD3 development team [3.5-8] are readily available in the open literature. For specific flow patterns, models are proposed by Wallis [3.5-9], Coutris [3.5-10] and Stevanovic and Studovic [3.5-11]. For use in computer codes, it is also essential that such correlations for the various flow patterns be consistent. For example, when the

flow pattern changes from bubbly to slug, the interface force predicted at the transition point by correlations for the bubbly and slug flow should be the same. A consistent set of interfacial and wall friction correlations for vertical upward flow has been proposed by Solbrig [3.5-2] along with a flow pattern map for use in two-fluid models.

3.5.3.3. Flow under diabatic condition

The correlations discussed so far are applicable to adiabatic two phase flow. The effect of heat flux on two phase pressure drop has been studied by Leung and Groeneveld [3.5-6], Tarasova [3.5-12] and Koehler and Kastner [3.5-13]. Tarasova [3.5-12] observed that two phase friction pressure drop is higher in a heated channel compared to that in an unheated channel for the same flow conditions. However, Koehler and Kastner [3.5-13] concluded that two phase pressure drops are the same for heated and unheated channels. Studies conducted by Leung and Groeneveld [3.5-6] indicate that the surface condition is significantly influenced by heat flux. Effective surface roughness increases due to the formation of bubbles at the heated surface leading to larger pressure drop. They concluded that for the same flow conditions, the two phase multiplier is larger for low heat flux than high heat flux. They further observed that the maximum value of the two phase multiplier is obtained when heat flux approaches the Critical Heat Flux value. In the absence of established procedure to take the affect of heat flux into account, the following procedure for calculation of two phase diabatic pressure drop is generally followed.

For diabatic two phase flow, the quality, void fraction, flow pattern, etc. change along the heated section. To calculate the pressure drop in such cases, two approaches are usually followed. In the first approach, the average ϕ_{LO}^2 is calculated as:

$$\phi_{LO}^2 = \frac{1}{L}\int_0^L [\phi_{LO}^2(z)]dz \qquad (3.5\text{-}6)$$

The approach can be used in cases where the $\phi_{LO}^2(z)$ is an integrable function. Numerical integration is resorted to in other cases. An example of such an approach is proposed by Thom [3.5-14]. Thom has derived average values of $\phi_{LO}^2(z)$. Similar integrated multiplication factors for diabatic flow as a function of outlet quality are also available for the Martinelli-Nelson [3.5-15] method. Thom has also obtained multiplication factors for calculating the acceleration and elevation pressure drops for diabatic flow in this way.

In the second approach the heated section is subdivided into a large number of small segments. Based on average conditions (i.e. x_i, α_i and flow pattern) in that segment, the pressure drop is calculated as in adiabatic two phase flow using one of the models described previously.

3.5.3.4. Void fraction relationships

Void fraction plays an important role, not only in pressure drop calculation, but also in flow pattern determination and neutron kinetics. All the four components of pressure drop (skin friction, local, acceleration and elevation) directly or indirectly depend on the void fraction. For certain situations of practical interest, accurate prediction of all the components is required. For example, steady state flow prevails in a natural circulation loop when the driving pressure differential due to buoyancy (i.e. the elevation pressure drop) balances the opposing pressure differential due to friction, acceleration and local effects. For such cases, accurate estimation of each component of pressure drop is required. All these pressure drop components are highly dependent on void fraction in two phase flow. Therefore, it is very important to have a reliable relationship for the mean void fraction. In general, the published void fraction correlations can be grouped into three, viz., (a) slip ratio models, (b) $K-\beta$ models, and (c) correlation based on drift flux models. In addition, there are some empirical correlations, which do not fall under any of the three categories. Detailed void fraction relationships can be found in IAEA-TECDOC-1203 [3.5-1].

3.5.3.5. Assessment of two phase pressure drop correlations

Table 3.5-2 gives the assessment of pressure drop correlations by various authors and their recommendation.

3.5.4. Natural and forced circulation pressure drop

A final, very important issue is concerned with the driving force. Driving force may be due to buoyancy caused by a density difference in the fluid (natural circulation) or due to a pump (forced convection). There may be feedback between the pressure loss and the extracted power. The flow transition from laminar to turbulent for a heated pipe occurs much earlier than for an unheated pipe due to the effect of secondary flow. There is a fundamental difference between a forced circulation loop and a natural circulation loop. For forced circulation loops, the driving force is due to the pressure developed by the pump which is generally far greater than the buoyancy driving head. For natural circulation loops, however, the buoyancy pressure differential, being the driving force, is always the largest component of pressure drop. Further, the buoyancy pressure differential is essentially the elevation pressure difference over the closed loop and is directly proportional to the elevation difference. Usually the elevation difference in natural circulation loops is limited to a few meters. Thus, all the pressure loss terms are generally one to two orders of magnitude less than that under forced flow. Therefore, natural circulation flows are characterized by low driving head and low mass flux. Hence, pressure drop correlations with greater accuracy at low mass flux conditions are required for the analysis of natural circulation loops.

There is a need to reassess the existing correlations and to develop new correlations, if required for natural circulation loops as the existing correlations are mainly applicable for forced circulation loops. The mechanism of flow in natural circulation loops can be different from that of forced circulation loops. For example, due to buoyancy effect and presence of secondary flows, the velocity profile in a heated pipe may get modified which also depends on the orientation of the pipe (horizontal, vertical upward or downward). This was observed experimentally by Bau and Torrance [3.5-38]. These secondary flows are driven by transverse temperature variations within the fluid which, in turn, cause localized natural convection circulations within the duct. The time required to establish these circulations is small compared to the time required to initiate flow through the loop. The authors also speculated that secondary flows may arise from centrifugal effects in the curved sections of the duct. The secondary flow may, in turn, affect the friction factor for the pipe, as the friction factor is mainly dependent upon the velocity gradient. For a natural circulation loop, due to low velocities and improper mixing, thermal stratification may occur during single phase conditions especially in horizontal pipes. There is also a concern about flow separation during two phase flow in a horizontal pipe. The pressure drop under these conditions has to be predicted accurately. Some of the important characteristics of natural circulation flows in comparison to forced circulation flows are as follows. The driving head for forced circulation flows are generally large as compared to natural circulation flows. The thermally induced secondary flow has little effect on the forced circulation flow owing to its large driving head, whereas it may significantly affect the natural circulation flow. Also, the transition from laminar to turbulent flow may occur at lower Reynolds number in natural circulation flows (Creveling et al. [3.5-39]; Hallinan and Viskanta [3.5-40]) than that for forced circulation due to the presence of secondary flow in natural circulation. Also the velocity profile in a natural circulation fully developed flow may not follow the classical profile shape (parabolic for laminar, logarithmic for turbulent) because of secondary flows. As the natural circulation systems are characterized by low driving head, the pressure drop correlations should be highly accurate particularly at low mass flux conditions. Further, owing to the large driving head in forced circulation systems, the associated transients are also relatively fast as compared to that of natural circulation systems. The potential occurrence of instabilities, especially at low pressure, is relatively higher in natural circulation systems as compared to forced circulation systems. Finally, under oscillatory flow conditions, the critical heat flux (CHF) for natural circulation systems are generally lower than steady forced circulation CHF (Kim et al. [3.5-41]).

TABLE 3.5-2. ASSESSMENT OF PRESSURE DROP CORRELATIONS

Authors	*Categories*	*No. of correlations tested*	*No. of data points*	*Recommended correlation*
Weisman-Choe [3.5-16]	Homogeneous model	---	---	McAdams [3.5-17] and Dukler et al. [3.5-18]
Idsinga et al. [3.5-19]	Homogeneous model	18	3500	Owens [3.5-20] and Cicchitti [3.5-21]
Beattie-Whalley [3.5-22]	Homogeneous model	12	13500	Beattie and Whalley [3.5-22]
Dukler et al. [3.5-18]	Multiplier concept	5	9000	Lockhart and Martinelli [3.5-23]
Idsinga et al. [3.5-19]	Multiplier concept	14	3500	Baroczy [3.5-24] and Thom [3.5-14]
Friedel [3.5-25]	Multiplier concept	14	12868	Chisholm [3.5-26] and Lombardi-Pedrocchi [3.5-27]
Snoek-Leung [3.5-28]	---	9	1217	Friedel [3.5-29]
Vijayan et al. [3.5-30]	---	14	424	Lockhart and Martinelli [3.5-23] with Chexal et al. [3.5-31] for void fraction.
Weisman-Choe [3.5-16]	Flow pattern specific	11		*Separated flow*: Agrawal et al. [3.5-32] and Hoogendoorn [3.5-33]
		10		*Homogeneous flow* : McAdams [3.5-17], Dukler et al. [3.5-18] and Chisholm [3.5-26]
		7		*Intermittent flow*: Dukler [3.5-18], Lockhart-Martinelli [3.5-23] and Hughmark [3.5-34]
		6		*Annular flow*: Dukler [3.5-18] and Lockhart-Martinelli [3.5-23]
Mandhane et al. [3.5-35]	Flow pattern specific	14	10500	*Bubbly*: Chenoweth and Martin [3.5-36]
				Stratified: Agrawal et al. [3.5-32]
				Stratified wavy: Dukler et al [3.5-18]
				Slug: Mandhane et al. [3.5-37]
				Annular, annular mist: Chenoweth and Martin [3.5-36]
				Dispersed bubble : Mandhane et al. [3.5-37]

3.5.4.1. Pressure drop under low mass flux, low pressure conditions

Natural circulation reactors are characterized by relatively low mass flux and low driving pressure differential compared to forced circulation systems. Therefore, correlations chosen for the analysis of natural circulation systems require improved accuracy at low mass fluxes. For the analysis of critical flow, following a break in high pressure systems, pressure drop correlations valid for very high mass fluxes (10–20 Mg/m^2s) are required. For investigations on the startup procedure for natural circulation boiling water reactors, correlations valid over a wide range of pressures starting from atmospheric pressure are required. At the startup, the flow is very low and hence the low flow pressure drop correlations are important. Further, for a natural circulation loop the flow builds up virtually from zero

flow conditions. Hence the friction factor and loss coefficient correlations should cover the whole range from very low flow to very high flow conditions. Low flows are also important due to the fact that natural circulation loops are particularly susceptible to instabilities at low power and low flow conditions. These flow instabilities may be characterized by repetitive flow reversals. Hence even for a simple circular pipe flow may vary from negative to very high positive values which again calls for a pressure drop correlation applicable for all flow regimes (laminar, transition and turbulent). In addition, flow regime transition criteria are important as they are used in computer codes to select the friction factor/ loss coefficient correlation used for the component. In fact, in some cases these correlations can greatly affect the prediction (e.g. during the prediction of the stability boundary in a natural circulation system).

Figure 3.5-1 shows the comparison of measured and calculated pressure drop (Chisholm model) under low mass flux condition in a vertical pipe of diameter 26.64 mm with diabatic flow. The experimental results are in good agreement with the calculated pressure drop. Furthermore, the experiments were conducted at various system pressures and heat fluxes for the low mass flux region. The measured pressure drops were compared with pressure drops calculated using the CNEN [3.5-5] correlation. The CNEN correlation was able to predict the measured pressure drop with an error of $\pm$ 30% as shown Figure 3.5-2.

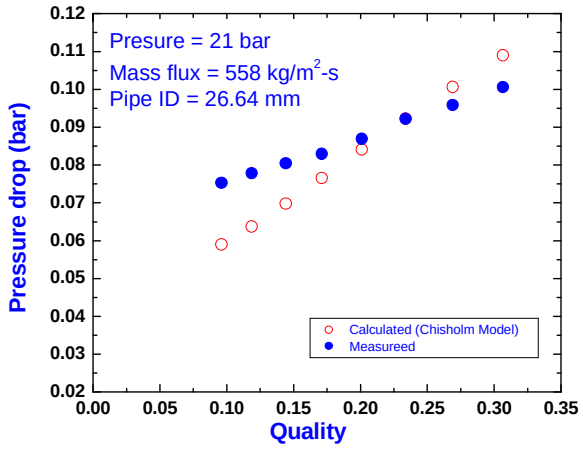

FIG. 3.5-1. Comparison of measured and calculated pressure drop in a vertical pipe with diabatic flow.

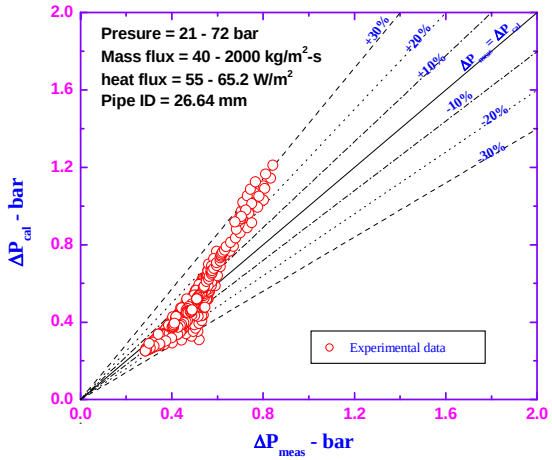

FIG. 3.5-2. Comparison of measured and predicted pressure drop using CNEN [3.5-5] correlation for vertical upward diabatic flow in a tube.

3.5.4.2. Generalized flow correlation

3.5.4.2.1. Single phase natural circulation

The generalized flow correlation for single phase loops (Vijayan and Austregesilo [3.5-42]) is given by,

$$\mathrm{Re}_{ss} = C\left(Gr_m \frac{D}{L_{eff}}\right)^r \tag{3.5-7}$$

where the constants C and r depend on the constants of the friction factor correlation as shown below. The above correlation suggest that if we plot Re vs $Gr_m\, D/L_{eff}$ on a log-log plot, the constants C and r can be obtained as the intercept and exponent, respectively. From the values of C and r, the p and b values applicable to the friction factor correlations can be obtained as

$C = (2/p)^r$ and $r = (1/3 - b)$

where p and b are given by the friction factor correlation of the form $f = p/\mathrm{Re}^b$. Depending on the value of the components p and b, the flow correlation is given as

$$\mathrm{Re}_{ss} = 0.1768\left(\frac{Gr_m}{N_G}\right)^{0.5} \quad \text{laminar flow } (p = 64, b = 1) \tag{3.5-8}$$

$$\mathrm{Re}_{ss} = 1.96\left(\frac{Gr_m}{N_G}\right)^{0.364} \quad \text{turbulent flow } (p = 0.316, b = 0.25\text{; Blasius correlation[3.5-43]}) \tag{3.5-9}$$

$$\text{where } Gr_m = \frac{D_r^3 \rho_0^2 \beta_T g Q_h H}{A_r \mu^3 C_p},\ N_G = \frac{L_t}{D_r}\sum_{i=1}^{N}\left(\frac{l_{eff}}{d^{1+b} a^{2-b}}\right)_i \text{ and } \mathrm{Re}_{ss} = \frac{D_r W_{ss}}{A_r \mu} \tag{3.5-10}$$

Experimental results obtained from a natural circulation loop are compared with results obtained from the above relationships in Fig. 3.5-3(a). Good agreement is obtained although a forced flow correlation (Blasius) is used. The results obtained with other forced flow correlations are also compared with experimental result in Fig. 3.5-3(a). In addition, an extensive comparison of single phase natural circulation data reported in literature has been carried out with Eqs (3.5-8) and (3.5-9), as shown in Fig. 3.5-3(b). Subsequently, data from a non-uniform diameter loop were also compared with the generalized correlation neglecting effect of local losses (Fig. 3.5-3(c)). In general, a reasonably good agreement is obtained with all reported data. However, in experiments where complex geometries are involved, the friction factor correlation used may be insufficient to obtain reasonable agreement. In such cases, it may be required to determine the pressure drop experimentally.

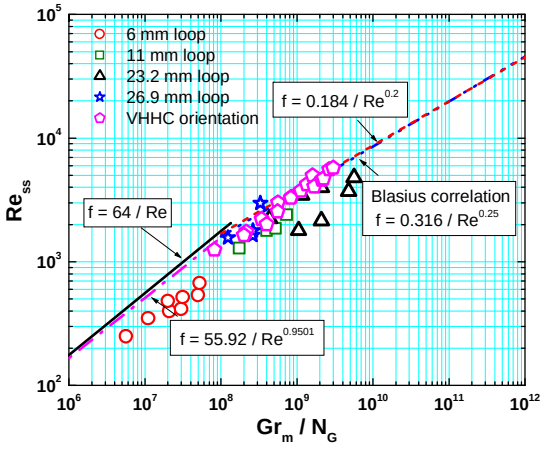

FIG. 3.5-3(a). Effect of friction factor on steady state flow rate in a single phase natural circulation loop as predicted by generalized flow correlation and comparison with experimental results (Vijayan and Austregesilo [3.5-42]).

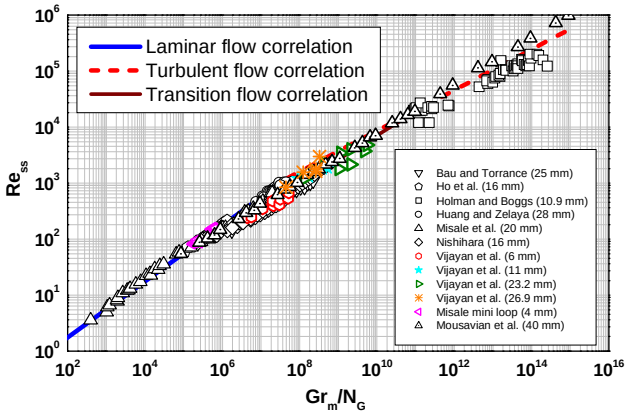

FIG. 3.5-3(b). Steady state performance of single phase loops differing in diameter.

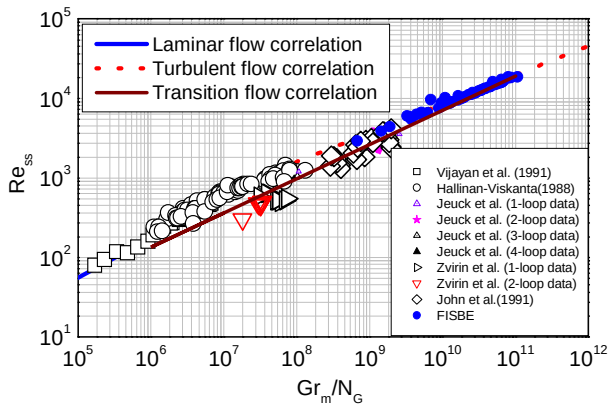

FIG. 3.5-3(c). Steady state performance of non-uniform diameter single phase natural circulation loop neglecting local losses.

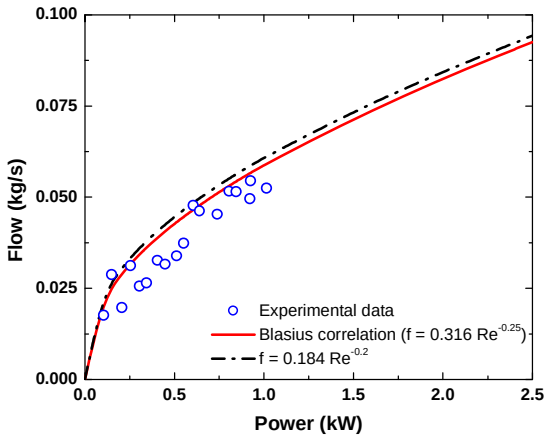

FIG. 3.5-4. Effect of friction factor on steady state flow rate in a single phase natural circulation loop.

3.5.4.2.2. Flow dependency on power in single phase natural circulation loop

The steady state flow rate can be obtained from the generalized correlation as

$$W_{ss} = \left[\frac{2\, g\, \rho_0^2\, \beta_T\, H\, Q_h}{R\, Cp} \right]^{\frac{1}{3}} \tag{3.5-11}$$

where the total hydraulic resistance of the loop is given by, $R = \sum_{i=1}^{N_t} \left(\frac{f_i L_i}{D_i} + K_i \right) \frac{1}{A_i^2}$

Steady state flow rate in a single phase natural circulation loop was predicted using two different turbulent forced flow correlations. The variation of flow for different powers using different friction factor correlations along with the experimental data obtained from 23.2 mm single phase natural circulation loop is shown in Fig. 3.5-4.

3.5.4.2.3. Two phase natural circulation

A generalized flow correlation of the same form as that for single phase has been developed (Gartia et al. [3.5-44]) to estimate the steady state flow rate in two phase natural circulation loops which is given by,

$$\mathrm{Re}_{ss} = C\left(Gr_m / N_G\right)^r \tag{3.5-12}$$

where, Re_{ss} is the Reynolds Number, Gr_m is the Modified Grashoff Number, N_G is the contribution of loop geometry to the friction number. The value of C is 0.1768 and 1.96 for laminar and turbulent flow, respectively and corresponding values for 'r' are 0.5 and 0.3636, respectively. For laminar flow $f = 64/\mathrm{Re}$ and for turbulent flow the Blasius equation, both formulation based on forced flow, have been used. The above correlation shows that it is possible to simulate the steady state behaviour with just one non-dimensional parameter. To account for the density variation in the buoyancy term, a new parameter $\beta_{tp} = \frac{1}{v_m}\left(\partial v / \partial h\right)_p$ has been used in Gr_m, where, v_m is the mean specific volume and h is the enthalpy.

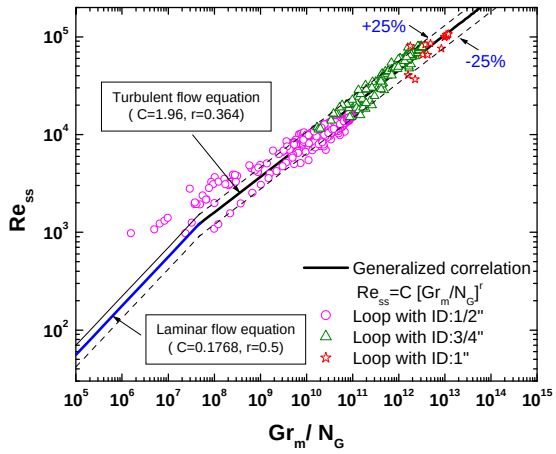

FIG. 3.5-5(a). Effect of friction factor on steady state flow rate in a two phase natural circulation loop (Gartia et al. [3.5-44]).

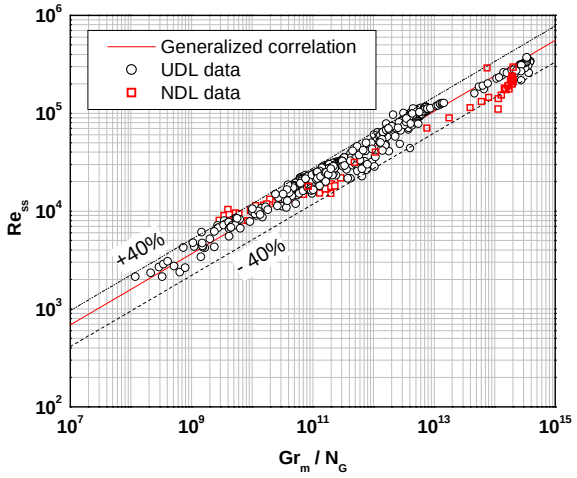

FIG. 3.5-5(b). Steady state performance of uniform and non-uniform diameter two phase natural circulation loops.

In Fig. 3.5-5(a), experimental result obtained from three different natural circulation loops are compared with theoretical results based on the above relationships. As can be seen, reasonably good agreement is obtained. Further, data from both uniform diameter loop (UDL) and non-uniform diameter loop (NDL) were compared with the two phase generalized correlation (Fig. 3.5-5(b)). In general, a reasonably good agreement is obtained with all reported data. However, in experiments where complex geometries are involved (e.g. in NDL), the friction factor correlation used may be insufficient to obtain reasonable agreement. Hence, large deviations are found in case of non-uniform diameter loop data as shown in Fig. 3.5-5(b). In such cases, it may be required to determine the pressure drop experimentally and then the flow rate can be calculated as suggested in Eq. (3.5-13).

3.5.4.2.4. Effect of friction factor on two phase flow prediction

The steady state flow rate in a two phase natural circulation loop can be obtained from the generalized correlation as

$$W_{ss} = \left[\frac{2}{p} \frac{g\, \rho_r\, \beta_{tp}\, H\, Q\, D_r^b\, A_r^{2-b}\, \rho_l}{\mu_r^b\, N_G} \right]^{\frac{1}{3-b}} \tag{3.5-13}$$

The variation of two phase steady state flow rate with power using different single phase friction factor correlations is shown in Fig. 3.5-6. Figure 3.5-6 shows that the steady state flow prediction can differ with different single phase friction factor models.

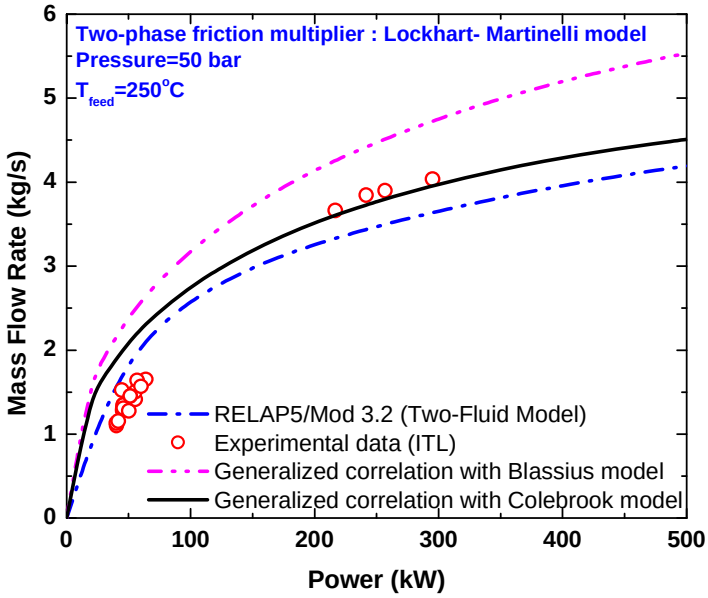

FIG. 3.5-6. Effect of friction factor on steady state flow rate in a two phase natural circulation loop as predicted by generalized flow correlation.

3.5.4.3. Effect of two phase friction multiplier on the flow prediction

3.5.4.3.1. Flow dependency on power

The effect of changing the two phase friction multiplier (ϕ_{LO}^2) correlation in two phase generalized correlation is shown in Fig. 3.5-7. It is clear from the figure that even at the same power the steady state flow may change depending on the friction multiplier correlation used in the analysis.

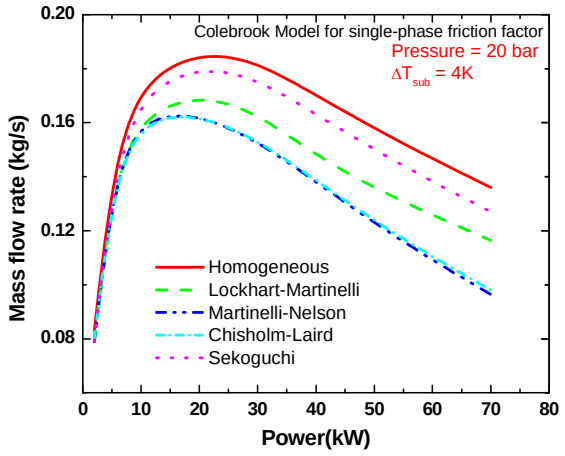

FIG. 3.5-7. Effect of two phase friction factor multiplier on steady state flow rate in a two phase natural circulation loop using generalized correlation (Nayak et al.[3.5-45]).

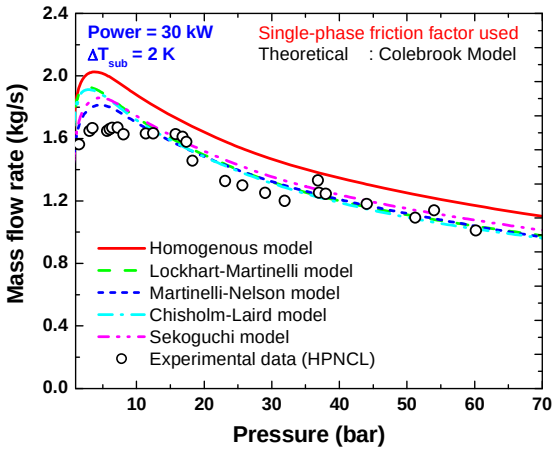

FIG. 3.5-8. Effect of pressure on steady state flow rate in a two phase natural circulation loop.

3.5.4.3.2. Flow dependency on pressure

The variation of steady state flow rate with pressure at different two phase friction multiplier (ϕ_{LO}^2) correlation is shown in Fig. 3.5-8.

3.5.4.4. Effect of pressure drop on stability

Natural circulation (NC) systems are susceptible to several kinds of instabilities. Following a perturbation, a system is considered to be stable if it returns back to the original steady state. If on the other hand, the system continues to oscillate with the same amplitude, then the system is neutrally stable. If the system stabilizes to a new steady state or oscillates with increasing amplitude, then the system is considered to be unstable. There are two main types of instabilities, static and dynamic instability. Static instability can be fully described by the steady state governing equations. Examples of this type of instability are Ledinegg (flow excursion), flow pattern transition instability, flashing instability, etc. In the case of dynamic instability, the feedback effects (due to mass flow rate, pressure drop, density and void fraction) in two phase systems are important. Typical example is the density wave oscillations (DWO) observed in two phase systems. Generally, two unstable regions are observed for two phase NCSs. The first unstable zone occurs at low power and hence at low quality and is named Type-I instability (Fukuda and Kobori [3.5-46]). Similarly, the second unstable zone in the two phase region occurs at high powers and hence at high qualities and is named Type-II instability. The gravitational pressure drop plays a dominant role in Type-I instability whereas frictional pressure drop is dominant in Type-II instability. Both single phase and two phase natural circulation system instabilities are affected significantly by the pressure drop model chosen.

3.5.4.4.1. Single phase natural circulation

Figure 3.5-9 shows the stability map for a single phase natural circulation loop with HHHC (Horizontal-Heater and Horizontal-Cooler) orientation (Vijayan [3.5-47]). This figure shows that the stability boundary changes with the choice of friction factor correlation even in single phase loops. The change is even more significant when stability maps for laminar and turbulent flow are compared (Vijayan et.al. [3.5-48]).

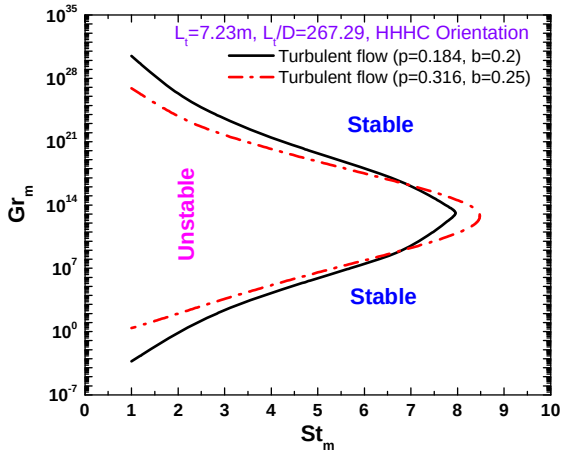

FIG. 3.5-9. Effect of friction factor on stability in a single phase natural circulation loop (Vijayan [3.5-47]).

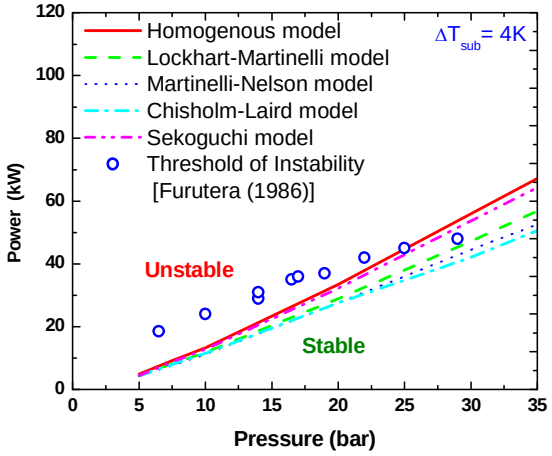

FIG. 3.5-10. Effect of two phase friction factor multiplier on the stability of a two phase natural circulation loop (Nayak et al. [3.5-45]).

3.5.4.4.2. Two phase natural circulation

Figure 3.5-10 (Nayak et al. [3.5-45]) shows the stability map for a two phase natural circulation loop along with the threshold of instability obtained experimentally. It is clear that the threshold of instability predicted by the code may vary with the choice of two phase friction factor multiplier in a two phase natural circulation loop.

While instability is common to both forced and natural circulation systems, the latter is inherently less stable than forced circulation systems. This is attributable to the regenerative feedback inherent

in the natural circulation phenomenon, where any change in the driving force affects the flow which in turn affects the driving force that may lead to a sustained oscillatory behaviour for certain operating conditions.

3.5.4.5. Effect of large flow areas on pressure drops

Although large diameter pipes, large manifolds such as headers, plena, water boxes in steam generators etc. are widely used in PHWRs, PWRs, BWRs or even in new generation advanced reactors (AHWR, SBWR, ABWR etc.), there is still no valid correlation for such geometries. Simpson et al. [3.5-49] compared six pressure drop correlations with data from large diameter (127 and 216 mm) horizontal pipes. None of the pressure gradient correlations studied predicted the measured pressure drops adequately. In particular, measured pressure gradients for stratified flow differed by an order of magnitude from those predicted by the various correlations. In view of this, the validity of the existing correlations which are generally developed from experiments conducted at scaled experimental set up needs to be checked. However, this is not unique to only natural circulation systems. Also there is a need to generate correlations for loss coefficients for such geometries under both single and two phase conditions. Furthermore, there is lack of experimental data on 3-D large flow paths (e.g. around open doors and stair wells) in the open literature. These flow configurations are particularly relevant to containment studies and flow between compartments of large water pools meant for long term heat removal. Therefore, attention must be given for generating such experimental data owing to the greater importance for the reliability of such systems in advanced reactors.

3.5.4.6. Pressure drop at the entrance of geometric discontinuity

Flow does not develop at the upstream and downstream of geometric discontinuities. Examples are flow into/out of the header (converging or diverging flow), sharp bends, sudden expansion/contraction, etc. Correlations are available in literature for fully developed flow cases. One should be very careful to apply such correlations (fully developed) to the actual cases of geometric discontinuities.

3.5.4.7. Pressure drop in consecutive geometric discontinuity

In cases of consecutive geometric discontinuities, such as fuel spacers in fuel bundle of nuclear reactors, one should take into account the combined effect of all the discontinuities. This will be sum of the individual effects.

3.5.4.8. Uncertainties in measurement

Use of experimental pressure drop database for the above situations will be more helpful in the prediction of pressure drop. However, the measurement inaccuracies in the experiments should be taken into account.

3.5.4.9. Local pressure drops in 3D situation

Local pressure drop measurement in 3D situations, specifically in the presence of phase change (in the upper plenum and lower plenum of PWR) is complicated. The static pressure measurement is difficult as velocity components may cause error.

3.5.5. General remarks

Within the range of parameters studied so far, relationships for forced circulation as given in TECDOC-1203 [3.5-1] were found to be adequate for studying natural circulation and stability of natural circulation. More accurate prediction capability is required at low mass fluxes and for large area flow paths. However, this issue is not unique to only natural circulation systems. Applicability of existing correlations to natural circulation needs to be assessed covering a wider range of parameters. More attention should be given to geometries for which pressure drop correlations are not readily available, such as advanced fluidic devices, large geometries relevant to containment, large flow paths, etc.

NOMENCLATURE

A	flow area, m^2
a	dimensionless flow area, A/A_r
b	constant in friction factor correlation, $f = p / Re^b$
C_p	specific heat, $J / kg\,K$
D	hydraulic diameter, m
d	dimensionless hydraulic diameter, D/D_r
f	Darcy-Weisbach friction factor
g	gravitational acceleration, m/s^2
Gr_m	modified Grashof number
h	enthalpy, J/kg
h'	heat transfer coefficient, $W/m^2\,K$
H	loop height, m
l	dimensionless length, L_i/L_t
L	length, m
N	total number of pipe segments
N_G	dimensionless parameter defined by equation (3.5-10)
p	constant in friction factor correlation, $f = p / Re^b$
q''	heat flux, W/m^2
Q	total heat input rate, W
Re	Reynolds number, $DW/A\mu$
v	specific volume, m^3/kg
W	mass flow rate, kg/s

Greek symbols

β_T	single phase thermal expansion coefficient, kg/J
β_{tp}	two phase thermal expansion coefficient, kg/J
μ	dynamic viscosity, $N\,s/m^2$
ϕ_{LO}^2	two phase friction multiplier
ρ	density, kg/m^3
ρ_r	reference density, kg/m^3

Subscripts

eff	effective
i	Ith segment
l	liquid
LO	liquid only
m	mean
r	reference value
ss	steady state
t	total
tp	two phase

REFERENCES FOR SECTION 3.5

[3.5-1] INTERNATIONAL ATOMIC ENERGY AGENCY, Thermohydraulic Relationships for Advanced Water Cooled Reactors, IAEA-TECDOC-1203, IAEA, Vienna (2001), Chapter 5,109–162.

[3.5-2] SOLBRIG, C.W., Consistent flow regime map and friction factors for two phase flow, AIChE Annual meeting, Miami Beach, Florida (1986).

[3.5-3] KNUDSEN, J.G., KATZ, D.L., Fluid Dynamics and Heat Transfer, McGraw-Hill Book Company, Inc.; New York (1958) 178.

[3.5-4] EL-WAKIL, M.M., Nuclear Heat Transport, International text book company (1971) 233–234.

[3.5-5] MARINELLI, V., PASTORI, L., AMLETO, A pressure drop computer code for LWR fuel bundles, RT/ING (73)11, Comitato Nazionale Energia Nucleare (CNEN) (1973).

[3.5-6] LEUNG, L.K.H., GROENEVELD, D.C., AUBE, F., TAPUCU, A., New studies of the effect of surface heating on frictional pressure drop in single-phase and two-phase flow, NURETH-3, Grenoble, France (1993).

[3.5-7] LILES, D.R., MAHAFFY, J.H., TRAC PF1-MOD1: An advanced best-estimate computer program for pressurised reactor thermal-hydraulic analysis, Los Alamos National Laboratory (1984).

[3.5-8] THE RELAP5 DEVELOPMENT TEAM, RELAP5/MOD3 Code Manual, Vol.1 code structure, system models and solution methods, NUREG/CR-5535 or INEL-95/0174, Idaho National Engineering Laboratory, Idaho Falls, Idaho (1995).

[3.5-9] WALLIS, G.B., J. Basic Engg. Trans ASME Ser. D. 92, 59 (1970).

[3.5-10] COUTRIS, N., DELHAYE, J.M., NAKACH, R., Two-phase flow modelling: the closure issue for a two-layer flow, Int. J. Multiphase Flow **15** (1989) 977–983.

[3.5-11] STEVANOVIC, V., STUDOVIC, M., A simple model for vertical annular and horizontal stratified two phase flows with liquid entrainment and phase transitions: one dimensional steady state conditions, Nuclear Engineering Design **154** (1995) 357–379.

[3.5-12] TARASOVA, N.V., et al., "Pressure drop of boiling subcooled water and steam water mixture flowing in heated channels", Proceedings of 3rd Int. Heat Transfer Conf. 178, ASME (1966).

[3.5-13] KOEHLER, W., KASTNER, W., Two Phase Pressure Drop in Boiler Tubes, Two phase Flow Heat Exchangers: Thermalhydraulic Fundamentals and Design, Editors: S. Kakac, A.E. Bergles E.O. Fernandes, Kluwer Academic Publishers (1988).

[3.5-14] THOM, J.R.S., Prediction of pressure drop during forced circulation boiling of water, Int. J. Heat Mass Transfer **7** (1964) 709–724.

[3.5-15] MARTINELLI, R.C., NELSON, D.B., Prediction of pressure drop during forced circulation boiling of water, Trans. ASME **70** (1948) 695–702.

[3.5-16] WEISMAN, J., CHOE, W.G., "Methods for calculation of pressure drop in cocurrent gas-liquid flow", Proceedings of the Two phase Flow and Heat Transfer Symposium Workshop, 18–20, Fort Lauderdale, Florida, U.S.A., Two phase Transport and Reactor Safety Vol. 1 (1976).

[3.5-17] MCADAMS, W.H., WOODS, W.K., HEROMAN, JR., R.H., Vaporization inside horizontal tubes, II. Benzene oil mixtures, Trans ASME **64** 193 (1942).

[3.5-18] DUKLER, A.E., WICKS, M., CLEVELAND, R.G., Frictional pressure drop and holdup in two phase flow, Part A, A Comparison of existing correlations for pressure drop and holdup, Part B An approach through similarity analysis, AIChE J **10** (1964) 38–43 and 44–51.

[3.5-19] IDSINGA, W, TODREAS, N., BOWRING, R., An assessment of two phase pressure drop correlations for steam–water mixtures, Int. J. Multiphase Flow **3** (1977) 401–413.

[3.5-20] OWENS, W.S., Two phase pressure gradient, Int. Developments in Heat Transfer, Part II, ASME (1961).

[3.5-21] CICCHITTI, A., LOMBARDI, C., SILVESTRI, M., SOLDAINI, G., ZAVATTARELLI, R., Two phase cooling experiments: pressure drop, heat transfer and burnout experiments, Energia Nucleare **7** (1960) 407–425.

[3.5-22] BEATTIE, D.R.H., WHALLEY, P.B., A simple two phase frictional pressure drop calculation method, Int. J. Multiphase Flow **8** (1982) 83–87.

[3.5-23] LOCKHART, R.W., MARTINELLI, R.C., Proposed correlation of data for isothermal two phase, two-component flow in pipes, Chem. Engg. Prog. **45** (1949) 39–48.
[3.5-24] BAROCZY, C.J., A systematic correlation for two phase pressure drop, Chem. Eng. Progr. Symp. Ser., 62 (1966) 232–249.
[3.5-25] FRIEDEL, L., Pressure drop during gas / vapor liquid flow in pipes, Int. Chemical Engineering **20** (1980) 352–367.
[3.5-26] CHISHOLM, D., Pressure gradients due to friction during the flow of evaporating two phase mixtures in smooth tubes and channels, Int. J. Heat Mass Transfer **16** (1973) 347–358.
[3.5-27] LOMBARDI, C., PEDROCCHI, E., A pressure crop correlation in two phase flow, Energia Nucleare **19**(2) (1972) 91–99.
[3.5-28] SNOEK, C.W., LEUNG, L.K.H., A model for predicting diabatic pressure drops in multi-element fuel channels, Nuclear Engineering and Design **110** (1989) 299–312.
[3.5-29] FRIEDEL, L., Improved friction pressure drop correlations for horizontal and vertical two phase flow, European two phase flow group meeting, Ispra (1979).
[3.5-30] VIJAYAN, P.K., Experimental observations on the general trends of the steady state and stability behaviour of single phase natural circulation loop, Nuclear Engineering and Design **215** (2002) 139–152.
[3.5-31] CHEXAL, B., MAULBETSCH, J., SANTUCCI, J., HARRISON, J., JENSEN, P., PETERSON, C., LELLOUCHE, G., HOROWITZ, J., Understanding void fraction in steady and dynamic environments, TR-106326 / RP-8034-14, Electric Power Research Institute, 3412 Hillview Avenue, Palo Alto, California (1996).
[3.5-32] AGRAWAL, S.S., GREGORY, G.A., GOVIER, G.W., An analysis of stratified two phase flow in pipes, Canadian J. Chem. Engg. **51** (1973) 280–286.
[3.5-33] HOOGENDOORN, C.J., Gas liquid flow in horizontal pipes, Chemical Eng. Science **9** (1959) 205–217.
[3.5-34] HUGHMARK, G.A., Holdup and heat transfer in horizontal slug gas-liquid flow, Chemical Engineering Science **20** (1965) 1007–1010.
[3.5-35] MANDHANE, J.M., GREGORY, G.A., AZIZ, K., Critical evaluation of friction pressure drop prediction methods for gas liquid flow in horizontal pipes, J. Petroleum Technology **29** (1977) 1348–1358.
[3.5-36] CHENOWETH, J.M., MARTIN, M.W., Pressure drop of gas liquid mixtures in horizontal pipes, Petroleum Engr. **28** (1956) C 42–45.
[3.5-37] MANDHANE, J.M., GREGORY, G.A., AZIZ, K., A flow pattern map for gas liquid flow in horizontal pipes, Int. J. of Multiphase flow **1** (1974) 537.
[3.5-38] BAU, H.H., TORRANCE, K.E., Transient and steady behaviour of an open, symmetrically-heated, free convection loop, International Journal of Heat Mass Transfer **24**, No. 4 (1981) 597–609.
[3.5-39] CREVELING, H.F., DE PAZ, J.F., BALADI, J.Y., SCHOENHALS, R.J., Stability characteristics of a single phase free convection loop, Journal of Fluid Mechanics **67** part 1 (1975) 65–84.
[3.5-40] HALLINAN, K.P., VISKANTA, R., Heat transfer from a vertical tube bundle under natural circulation conditions, International Journal of Heat and Fluid Flow **6** (1985) 256–264.
[3.5-41] KIM, Y.I., BAEK, W.P., CHANG, S.H., Critical heat flux under flow oscillation of water at low-pressure, low-flow conditions, Nuclear Engineering and Design **193** (1999) 131–143.
[3.5-42] VIJAYAN, P.K., AUSTREGESILO, H., Scaling laws for single phase natural circulation loops, Nuclear Engineering and Design **152** (1994) 331–347.
[3.5-43] BLASIUS, H., Mitt. Forsch. Geb. Ing.-Wesen, 131 (1913).
[3.5-44] GARTIA, M.R., VIJAYAN, P.K., PILKHWAL, D.S., A generalized flow correlation for two phase natural circulation loops, Nuclear Engineering and Design **236** Issue 17 (2006) 1800–1809.
[3.5-45] NAYAK, A.K., DUBEY, P., CHAVAN, D.N., VIJAYAN, P.K., Study on the stability behaviour of two phase natural circulation systems using a four-equation drift flux model, Nuclear Engineering and Design, Nuclear Engineering and Design **237** Issue 4 (2007) 386–398.
[3.5-46] FUKUDA, K, KOBORI, T., Classification of two phase flow stability by density-wave oscillation model, J. Nuclear Science and Technology **16** (1979) 95–108.

[3.5-47] VIJAYAN, P.K., Experimental observations on the general trends of the steady state and stability behaviour of single phase natural circulation loop, Nuclear Engineering and Design **215** (2002) 139–152.
[3.5-48] VIJAYAN, P.K., SHARMA, M., SAHA, D., Steady state and stability characteristics of single phase natural circulation in a rectangular loop with different heater and cooler orientations, Experimental Thermal and Fluid Science **31** (2007) 925–945.
[3.5-49] SIMPSON, H.C., et al., Two phase flow in large diameter horizontal lines, Paper A6, European Two Phase Flow Group Meeting, Grenoble (1977).

3.6. NATURAL CIRCULATION IN CLOSED LOOP

An overview of the current understanding in relation to natural circulation in existing nuclear energy systems is provided in this section. The scope of the investigation comprises the natural circulation performance of primary loop of water cooled reactors such as PWR, VVER (both 440 and 1000 types), CANDU, BWR and RBMK as well as the performance of horizontal and vertical tube steam generators.

The objective of the investigation is covered in Section 3.6.1 and more details about its scope, experiments and fundamental modelling are discussed in Sections 3.6.2 and 3.6.3, respectively.

A key issue in natural circulation is flow stability, especially when two phase conditions are encountered and when feedback with neutron kinetics is possible. This is discussed in Section 3.6.4.

Existing computational tools are capable of investigating natural circulation including stability in the mentioned reactor types and related conditions for industrial purposes. Thus, an overview is given of the features of those tools in Section 3.6.5.
The activity documented hereafter constitutes the follow-up and the consequence of wide investigations on the subject carried out world-wide in the last 30–40 years. Direct benefit is taken from, and suitable consideration is given to, the following three groups (and types) of documents/activities:

- IAEA TECDOC reports 1281 and 1474 [3.6-1, 3.6-2],
- Research activities discussed within the present CRP [3.6-3–3.6-8],
- Journal papers and other international documents [3.6-9–3.6-26].

Namely, the two IAEA reports [3.6-1, 3.6-2] consist of 252 and 638 pages, respectively and only focus on natural circulation. Thus, also in order to avoid duplication of efforts and inconsistencies with other IAEA documents, large parts of the writing below are taken from the Refs [3.6-1–3.6-26] and elaborated in order to account for the road-map of the present report.

As key conclusions, it is found that natural circulation is a ‘living’ phenomenon for the technology in the sense that it was of interest for the design of existing reactors and it is of interest for the innovative-future reactors and that improvements and development of tools constitute the subject of relevant research.

3.6.1. Introduction

The complex set of physical phenomena that occur in a gravity environment where a geometrically distinct heat sink and heat source are connected by a fluid flow path can be identified as natural circulation (NC). No external sources of mechanical energy for the fluid motion are involved when NC is established. In a number of publications, including textbooks, the term natural convection is used as a synonym of NC. Within the present context, natural convection is used to identify the

phenomena that occur when a heat source is put in contact with a fluid. Therefore, natural convection characterizes a heat transfer regime that constitutes a subset of NC phenomena.
This report provides the presented papers and summarizes the discussions within the framework of the IAEA CRP on Natural Circulation Phenomena, Modelling, and Reliability of Passive Systems that Utilize Natural Circulation. The presented papers and the discussion addressed both evolutionary and innovative water cooled reactors, as defined by the IAEA. NC principles are of fundamental interest to the designers of nuclear power plant systems and components. Making reference to the existing water cooled reactors, the consideration of NC is brought to the design of the layout of the primary circuit. The core is located at a lower elevation with respect to the steam generators and the feed-water inlet location, in the cases of pressurized and boiling water reactors, respectively. In all of the adopted geometrical configurations, NC allows the removal of the decay heat produced by the core, should the forced circulation driven by centrifugal pumps become unavailable. Furthermore, NC is the working mode for the secondary side of most steam generators in existing pressurized heavy and light water reactors. It is essential as well for the core cooling in the unlikely event of loss of primary coolant. Reactors based on natural circulation during normal operation (e.g. the Dodewaard Reactor in the Netherlands and the VK-50 in Russia) operated for an extended period of time. Most boiling water reactors can operate in the natural circulation mode for power levels below about 40% of full power. Some newly developed designs are based on natural circulation core cooling for normal operation and on the use of natural convection heat transfer for some safety systems. Reliance on natural circulation can result in simplified systems, reduced costs and, most importantly, a relatively higher safety level.

The accomplishment of the objectives of achieving a high safety level and reducing the cost through utilization of the NC mechanism, requires a thorough understanding of those mechanisms. Natural circulation systems are usually characterized by smaller driving forces with respect to the systems that use an external source of energy for the fluid motion. For instance, pressure drops caused by vertical bends and siphons in a given piping configuration, or heat losses to environment are a secondary design consideration when a pump is installed and drives the flow. On the other hand, a significant influence upon the overall system performance may be expected due to the same pressure drops and thermal power release to the environment when natural circulation produces the coolant flow. Therefore, the level of knowledge for the thermohydraulic phenomena for the specific geometric conditions and governing heat transfer conditions should be deeper when NC is involved. In addition, the lower driving forces for natural circulation systems might lead to quite large equipment for which the role of 3D phenomena could be significant.

Within nuclear technology the renewed interest in NC is a consequence of the above, in combination with the potential for cost savings from increased use of NC mechanisms in plant designs. Relevant experiments directed to the characterization of NC have been carried out in the past because of the importance of the related mechanisms to the safety of existing reactors. Similarly, thermohydraulic system codes have been developed and qualified through the comparison of predicted results and experimental data. The quality of recorded experimental data and the precision level of the available system codes, or the expected uncertainty in these predictions, are generally evaluated as satisfactory for the needs of the current reactors.

However, the exigencies posed by the more extensive use of the NC in the design of evolutionary and innovative water cooled reactors require a re-evaluation of the experimental data and of the code capabilities considering the new phenomena and conditions involved. Recent activities completed under the IAEA umbrella and other institutions, such as the U.S. Nuclear Regulatory Commission (U.S. NRC), the OECD/NEA/CSNI (Organization for Economic Cooperation and Development/Nuclear Energy Agency/Committee on the Safety of Nuclear Installations) and the European Commission (EC), show the importance of the subject and constitute the basis for future activities in the area of NC.

Potential future international activities could be directed toward:

- Identification of still unresolved issues from evolutionary and innovative water reactor, designs,

- Enhancing the quality levels of the available computational tools and experimental databases in relation to design needs.

This section provides an overview of the current state of the art of natural circulation data and methods. The main attention in this section is paid to the design basis accident phenomena.

3.6.1.1. Scope

Within the scope of this document, the natural circulation phenomenon involves the following system configurations:

a) Heat source and sink of primary loop constituted, respectively, by core and steam generator, or boiler, or primary side of heat exchanger, with core located at a lower elevation.

b) Heat source and sink inside the pressure vessel, constituted, respectively, by core and (typically annular-like region of) vessel downcomer. 'Steady state' NC between core and downcomer occurs owing to continuous cooling of the downcomer fluid by a heat exchanger (boiler or steam generator) or by continuous inlet of feed-water liquid at a temperature lower than core outlet temperature.

c) Cooling of the containment atmosphere by a closed loop.

In the current generation of nuclear plants, the NC core power removal capability is exploited for accident situations to demonstrate the inherent safety features of the plant (with the noticeable exception of the Dodewaard commercial BWR unit, shut down in 1997). Natural circulation also occurs during various phases of refuelling.

In future generation of nuclear plants, NC is planned to be used for ensuring the nominal operating conditions and for achieving safe cooling following accidents in a wider spectrum than foreseen for current generation reactors.

3.6.1.2. Scenario

Nominal and off-nominal NC conditions shall be distinguished within the present framework. Within the former category, the operational conditions of steam generators (primarily U-Tube types) and the startup or shutdown conditions of BWR shall be considered. Within the latter category, several SBLOCA events in all reactors listed in the scope, involve phenomenological windows more or less long in terms of time duration, where NC is relevant. The final period of a LBLOCA in all reactor systems also involves the occurrence of NC.

An overview of NC scenarios relevant within the present context can be derived from Table 3.6-1.

TABLE 3.6-1. RELEVANT NC SCENARIOS

Reference condition / Reference system	Nominal		Off-nominal	
	1Φ	2Φ	LBLOCA (end phase)	SBLOCA, MCP trip, Other
BWR & RBMK		x	x	x
SG (secondary side)		x		x
PWR, VVER, CANDU (primary system)	x		x	x

An excellent description of one of the scenarios listed in Table 3.6-1, i.e. NC in PWR following SBLOCA constitutes part of Annex 17 of ref. [3.6-2] (author N. Aksan) and is partially reported hereafter.

The March 1979 accident at TMI-2 brought into question the capability of natural circulation cooling to remove core decay heat, especially during accident conditions. Because natural circulation is expected to be an essential core heat removal mechanism during certain kinds of accidents or transients in a PWR (e.g., SBLOCA or operational transients involving loss of pumped circulation), a thorough understanding of natural circulation processes and factors that influence the natural circulation response of the reactor system is necessary. Characterization of the natural circulation cooling processes requires:

- Identifying conditions under which natural circulation will occur,
- Determining the effectiveness of natural circulation in removing core decay heat and recovering the plant (i.e. what are natural circulation cooling limitations),
- Identifying how changing plant conditions affect natural circulation cooling.

Natural circulation will occur in a PWR primary loop (in the absence of pumped flow) whenever buoyant forces caused by differences in loop fluid densities are sufficient to overcome the flow resistance of loop components (steam generators, primary coolant pumps, etc.). The fluid density differences occur as a result of fluid heating in the core region (causing the liquid to become less dense) and cooling fluid in the steam generators (causing the fluid to become more dense). The buoyancy forces resulting from those density differences cause fluid to circulate through the primary loops, providing a means of removing the core decay heat. Depending on the primary loop fluid inventory, natural circulation consists of three distinct modes of cooling:

- Single phase,
- Two phase (liquid continuous),
- Reflux condensation (or boiler-condenser mode for once-through steam generators).

Progression from the single phase mode through the two phase and reflux condensation modes occurs as primary system liquid inventory decreases (Fig. 3.6-1). Natural circulation flow in PWR is driven by temperature induced density gradients, enhanced by a thermal centre elevation difference between the hot (core) and cold (steam generator) regions in the primary loop. This density gradient produces a buoyancy force that drives the natural circulation flow. Thus, single phase natural circulation is the flow of an essentially subcooled primary liquid driven by liquid density differences within the primary loop.

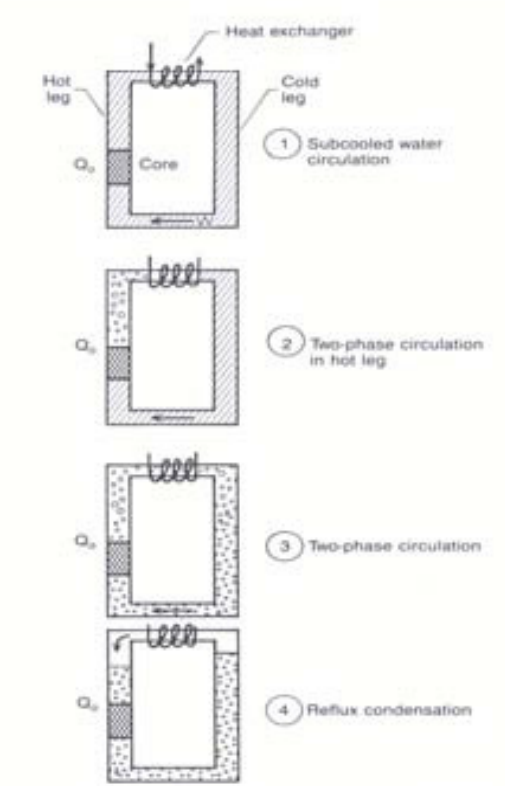

FIG. 3.6-1. Different modes of natural circulation cooling in a PWR.

Two phase natural circulation is normally defined as the continuous flow of fluid and vapour. In this mode of natural circulation, vapour generated in the core enters the hot leg and flows along with the saturated liquid to the steam generator, where at least some of the vapour is condensed. Hence, density gradients are affected in two phase mode not only by temperature differences, but also mainly by the voids in the primary loop. In both single phase and two phase natural circulation, the mass flow rate is the most important heat removal parameter.

In the reflux condensation, the vapour generated in the core flows through the hot leg, is condensed in the steam generator, and flows back to the core as a liquid. In this mode, the loop mass flow rate has a negligible effect because the primary mechanism of heat removal is vapour condensation.

In summary, the three modes of natural circulation are distinguishable based upon characteristic mass flow rates, loop temperature difference, and basic phenomenological differences. The dominant heat transfer mechanism in single phase natural circulation cooling is convection, making the loop flow rate the most important parameter governing heat removal. Heat generated by the core is transported away from the reactor vessel through the hot leg to steam generators (heat sink) via the subcooled primary liquid. Heat is transferred from the primary side to the secondary side in the steam generator.

The cooling cycle is completed when the cooled primary fluid flows back to the reactor vessel. The amount of heat removed from the core through single phase natural circulation cooling is normally the amount produced by decay heat power levels (about 5% core power). Since the study of natural circulation cooling in PWR systems became of interest, work on the characterization of natural circulation has been focused in several areas, including effects of both primary and secondary liquid inventory and distribution on natural circulation effectiveness, the stability of the various natural circulation modes and transitions between modes as well as the possibilities of natural circulation flow interruption due to instabilities, countercurrent-flow limiting in the hot leg and steam generator tubes, and the effect of non-condensable gases on natural circulation process.

With respect to the primary side liquid inventory issue, natural circulation will provide decay heat removal at significantly reduced primary side inventory. The concern here is identifying the minimum primary side liquid inventory at which natural circulation will continue to provide adequate cooling of the core. Similarly, the steam generator secondary side will continue to act as a heat sink for the primary at significantly reduced secondary liquid inventories. Again, the concern is identifying the minimum secondary inventory that will ensure continued natural circulation flow in the primary loop.

An additional concern with respect to the secondary inventory is the instabilities in primary side natural circulation flow caused by severely reduced secondary side liquid levels. These secondary side induced flow instabilities could reduce the effectiveness of natural circulation cooling. Generally, the stability of the different modes of natural circulation cooling, as well as the stability of transients between the modes, is of concern because natural circulation will be the primary mechanism for core decay heat rejection for certain kinds of PWR accidents or transients, and instabilities in natural circulation process could lead to an interruption of natural circulation flow with a corresponding reduction in the removal of core decay heat. Thus an understanding of factors that influence the onset of flow instabilities as well as the effects of the instabilities on decay heat removal is necessary.

The presence of non-condensable gas in the primary side of a steam generator operating in the two phase or reflux condensation mode of natural circulation is of concern because the gas may have a large effect on the condensation process occurring in the steam generator. The non-condensable gas in the steam generator tubes can cause a redistribution of the condensation locations as well as influence the amount of liquid being carried to the down side of the U-tubes. Thus the potential exists for the non-condensable gas to have a considerable influence on the natural circulation process. The presence of non-condensable gas in the primary loop may impede or even stagnate the natural circulation flow, thereby significantly reducing or terminating the heat removal capability of the steam generators both for single phase and two phase natural circulation cooling. Non-condensable gases can be introduced into the primary system through safety injection and by fuel degradation. As examples, hydrogen from the pressurizer vapour space, air dissolved in the refuelling water, and nitrogen from accumulators (once they are depleted of water), are several sources of non-condensable gases. In addition, helium may enter the primary coolant system if breaching of cladding occurs.

Research has concentrated on determining whether non-condensable gases will migrate to and collect in the upper elevations of the primary loop. There, they may interrupt the natural circulation flow and jeopardize the effectiveness of single phase and two phase natural circulation cooling. In PWRs with U-tube SGs, reflux condensation occurs when single phase vapour generated in the core flows through the hot leg piping to the SG, and is condensed in both the up-flow and down-flow sides of the steam generator U-tubes. Condensate in the up-flow sides of the steam generator U-tubes drains back to the hot leg and eventually back to the vessel along the bottom of the hot leg. A countercurrent flow of liquid and vapour exists in the up-flow sides of the steam generator U-tubes and in the hot leg. Condensate in the down-flow sides flows into the cold leg pump suction piping co-currently with any uncondensed steam. The reflux condensation process is shown in Fig. 3.6-2. During reflux condensation, primary to secondary heat transfer is accomplished through vapour condensation in SG.

This heat transfer is very effective due to the high latent heat associated with condensation. Consequently, removal of decay heat from the core during reflux condensation does not require large mass flow rates or large primary to secondary temperature differences. Small mass flow rates and primary to secondary temperature differences are characteristic of the reflux condensation mode of natural circulation. The experiments carried in the PKL test facility, which simulates PWR plant with U-tube steam generators, shows the major modes of energy transport observed in this facility for natural circulation cooling (See also Section 3.6.3).

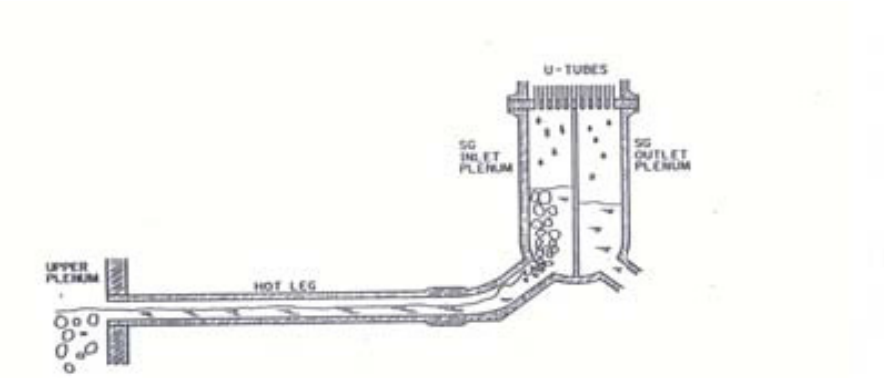

FIG. 3.6-2. Schematic of liquid distribution during reflux condensation in PWR.

3.6.1.3. Reference systems

The NC systems of interest to this section include the primary system and the steam generators, where applicable, of the following reactor types: PWR, VVER (both 440 and 1000 types), CANDU, BWR and RBMK. The remaining systems where NC is relevant that are dealt with by the broad definition above are considered in Sections 3.1, 3.3, 3.4, partly 3.8 and 3.9, 3.10, and 3.12.

3.6.2. Relevant models for natural circulation

Algebraic equations or field equations properly solved by simplified numerical models or by complex computer codes, respectively, can be used to predict NC performance in a wide variety of geometrical conditions and technological systems including those listed in Section 3.6.1.3. The two approaches are outlined hereafter.

3.6.2.1. Fundamental principles approach

Generalized algebraic equations valid for different geometric systems are derived in refs. [3.6-2, 3.6-21 and 3.6-24]. Derivations from Ref. [3.6-2] and [3.6-21] are summarized hereafter.

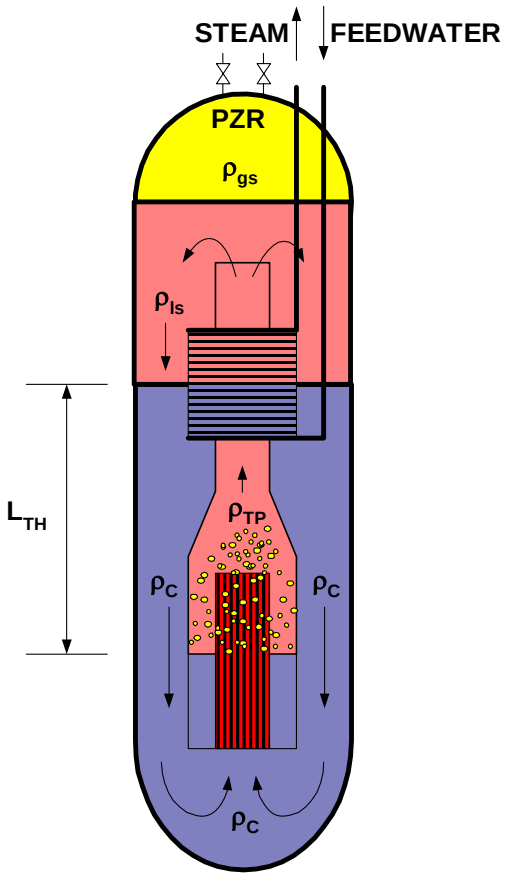

FIG. 3.6-3. Regions of single phase and two phase natural circulation within an integral reactor.

The loop in the sketch given in Fig. 3.6-3 is considered. This is divided into two regions: a two phase region with a fluid density ρ_{TP} and a single phase region with a fluid density ρ_l. The simplifying assumptions are as follows:

- Constant core inlet enthalpy,
- Uniform fluid properties at every cross-section,
- Homogeneous flow in the two phase region,
- Chemical Equilibrium — no chemical reactions,
- Thermal Equilibrium — both phases at the same temperature,
- The sum of convective accelerations due to vaporization and condensation are negligible,
- Viscous effects included in determination of form losses only,
- Form losses, primarily in the core and steam generator regions, dominate the loop resistance.

The assumptions listed above were applied to the mass, momentum, and energy equations for each component in the loop to obtain the conservation equations. The equations were then integrated over their respective single phase and two phase regions to obtain the following loop balance equations:

Loop momentum equation:

$$\sum_{i=1}^{N}\left(\frac{l_i}{a_i}\right)\cdot\frac{d\dot{m}}{dt}=g\left(\rho_l-\rho_{TP}\right)L_{th}$$

$$-\frac{\dot{m}^2}{\rho_l a_c^2}\left\{\sum_{SP}\left[\frac{1}{2}\left(\frac{fl}{d_h}+K\right)_i\left(\frac{a_c}{a_i}\right)^2\right]+\frac{\rho_l}{\rho_{TP}}\sum_{TP}\left[\frac{1}{2}\left(\frac{fl}{d_h}+K\right)_i\left(\frac{a_c}{a_i}\right)^2\right]\right\} \tag{3.6-1}$$

Loop energy balance equation:

$$M_{sys}\frac{d\left(e_M-e_l\right)}{dt}=\dot{m}\left(h_{TP}-h_l\right)-\dot{q}_{SG}-\dot{q}_{loss} \tag{3.6-2}$$

For two phase flow conditions, the equilibrium vapour quality and the mixture density are defined as follows.

Equilibrium vapour quality at core exit:

$$x_e=\frac{h_{TP}-h_f}{h_{fg}} \tag{3.6-3}$$

Homogeneous two phase fluid mixture density:

$$\rho_{TP}=\frac{\rho_f}{1+x_e\left(\frac{\rho_f-\rho_g}{\rho_g}\right)} \tag{3.6-4}$$

Unlike single phase natural circulation, a simple analytical expression for the velocity at the core inlet cannot be readily obtained from the steady state solution. This is due to the fact that the two phase mixture density is dependent on core flow rate (Annex 11 in ref. [3.6-2] by J. Reyes).

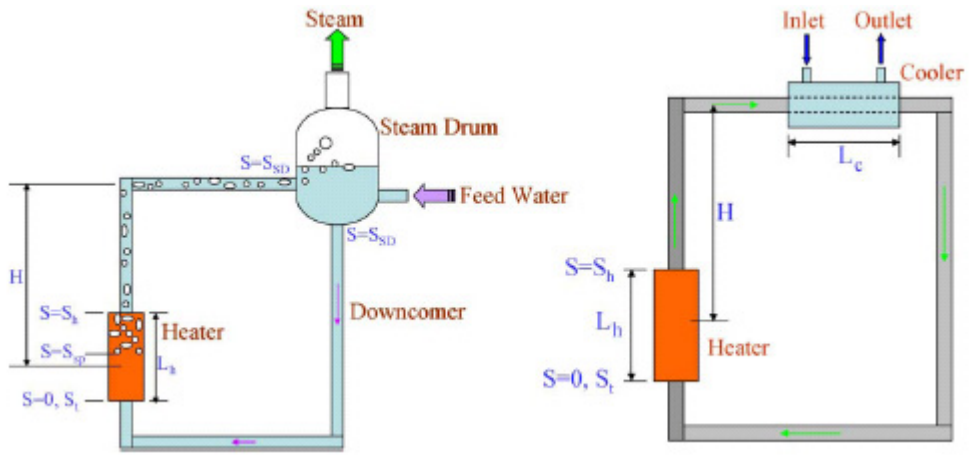

FIG. 3.6-4. Sketch for NC loop (to derive an algebraic model).

Making reference to the sketch in Fig. 3.6-4, Vijayan, ref. [3.6-21], proposes the following model, see also ref. [3.6-8].

Let us consider the following nomenclature:

$$\omega = \frac{W}{W_{ss}}, \quad \mathcal{H} = \frac{h - h_r}{(\Delta h)_{ss}}, \quad Z = \frac{z}{H}, \quad S = \frac{s}{H}, \quad a_i = \frac{A_i}{A_r}, \quad d_i = \frac{D_i}{D_r}, \quad l_i = \frac{L_i}{L_t}$$

$$A_r = \frac{\sum_{i=1}^{N_t} A_i L_i}{\sum_{i=1}^{N} L_i} = \frac{V_t}{L_t}, \quad D_r = \frac{1}{L_t}\sum_{i=1}^{N_t} D_i L_i, \quad (l_{eff})_i = \frac{(L_{eff})_i}{L_t}, \quad \rho_r = \rho_{in}, \quad h_r = h_{in}$$

$$f_i = \frac{p}{\mathrm{Re}_i^b} = \frac{p}{\mathrm{Re}_{ss}^b}\frac{\omega^{-b} a_i^b \mu_i^b}{d_i^b \mu_r^b}, \qquad \mathrm{Re}_{ss} = \frac{D_r W_{ss}}{A_r \mu_r}, \quad L_{eff} = L_i + L_{eq}, \quad \text{and} \quad \mu_r = \frac{\sum_i \mu_i L_i}{\sum_i L_i}$$

At steady state, putting $\omega = W/W_{ss} = 1$, $\mu_i = \mu_r$ and $q_c = q_h$, the balance equations will become

$$\frac{d}{dS}\left(\frac{\omega}{a}\right) = 0 \tag{3.6-5}$$

$$0 = \frac{g\rho_r \beta_{tp} H (\Delta h)_{ss} A_r V_t \rho_r}{L_t W_{ss}^2}\oint \mathcal{H}\, dZ - \frac{p}{2}\frac{\mathrm{Re}_{ss}^{2-b}\,\mu_r^2}{D_r^2 \rho_l}\frac{A_r V_t \rho_r}{L_t W_{ss}^2} N_G \tag{3.6-6}$$

where

$$N_G = \frac{L_t}{D_r}\left[\sum_{i=1}^{N_{sp}} \frac{(l_{eff})_i}{d_i^{1+b} a_i^{2-b}} + \bar{\phi}_{LO}^2 \sum_{i=N_{sp}}^{N_{he}} \frac{(l_{eff})_i}{d_i^{1+b} a_i^{2-b}} + \phi_{LO}^2 \sum_{i=N_{he}}^{N_t} \frac{(l_{eff})_i}{d_i^{1+b} a_i^{2-b}}\right] \tag{3.6-7}$$

In the case of uniform diameter loop, one obtains:

$$W_{ss} = \left[\frac{2}{p}\frac{g\,\rho_r\,\beta_{tp}\,H\,Q\,D_r^b\,A_r^{2-b}\,\rho_l}{\mu_r^b\,N_G}\right]^{\frac{1}{3-b}} \tag{3.6-8}$$

$$\mathrm{Re}_{ss} = 0.176776\left(\frac{Gr_m}{N_G}\right)^{0.5}; \qquad \text{laminar flow} \tag{3.6-9}$$

$$\mathrm{Re}_{ss} = 1.9561\left(\frac{Gr_m}{N_G}\right)^{0.36364}; \qquad \text{turbulent flow} \tag{3.6-10}$$

Where

$$Gr_m = \frac{D_r^3 \rho_r \rho_l \beta_{tp} gHQ}{A_r \mu_r^3} \tag{3.6-11}$$

3.6.2.2. Field equations

Accurately describing the transport of mass, momentum and energy in a two phase fluid flowing through a complex geometry, such as a nuclear reactor core, while undergoing phase change, is a formidable task. Nonetheless, this is only part of the challenge laid before the nuclear reactor safety analyst (the remaining parts being the qualification of the models and the development and the qualification of suitable nodalizations).

An example of field equations solved in each individual node that constitute a complex system is (Ref. [3.6-2], contribution by J. Reyes):

Mass:

$$\frac{\partial}{\partial t}\{\rho_k \alpha_k\} + \frac{\partial}{\partial z}\{\rho_k v_k \alpha_k\} = \Gamma_k \tag{3.6-12}$$

Momentum:

$$\frac{\partial}{\partial t}\{\rho_k v_k \alpha_k\} + \frac{\partial}{\partial z}\{\rho_k v_k^2 \alpha_k\} = \{\Gamma_k \vec{v}_{ks} \cdot \vec{n}_z\} + \sum_{i=1}^{N}\{\vec{F}_{wk} \cdot \vec{n}_z\}_i - \frac{\partial}{\partial z}\{p_k \alpha_k\} + \{\vec{F}_{sk} \cdot \vec{n}_z\} + \{\rho_k \alpha_k\}\vec{g} \cdot \vec{n}_z \tag{3.6-13}$$

Energy: (Neglecting axial heat conduction and axial shear effect)

$$\frac{\partial}{\partial t}\{\rho_k u_k^o \alpha_k\} + \frac{\partial}{\partial z}\{\rho_k h_k^o v_k \alpha_k\} = \Gamma_k h_{ks}^o - \left\{p_k \frac{\partial \alpha_k}{\partial t}\right\} + \sum_{i=1}^{N}\left\{q_k'' \alpha_k \frac{P}{A}\right\}_i - \{\rho_k g v_k \alpha_k\} + \{Q_{sk}\} \tag{3.6-14}$$

Consistent sets for the above equations are solved by system codes (see Section 3.6-5).

3.6.3. Experimental data and facilities

Reference is made hereafter to Integral Test Facilities (ITF) that have been used for NC investigations. An overview of the available experimental data base, i.e. geometric and operational features of ITF and boundary and initial conditions for NC experiments, can be obtained from refs. [3.6-13] and [3.6-24] (see also ref. [3.6-1]).

Because of the expense of conducting full-scale integral system tests, much of the thermohydraulic testing for advanced reactor designs is conducted in “reduced-scale” integral system test facilities. The design of such facilities requires performing a thorough thermohydraulic scaling analysis. The general objective of a scaling analysis is to obtain the physical dimensions and operating conditions of a reduced scale test facility capable of simulating the important flow and heat transfer behaviour of the system under investigation. To develop a properly scaled test facility, the following objectives must be met for each operational mode of interest. First, the thermohydraulic processes that should be modelled must be identified. Second, the similarity criteria that should be preserved between the test facility and the full-scale prototype must be obtained. Third, because all of the similarity criteria cannot be simultaneously preserved in a reduced scale facility, priorities for preserving the similarity criteria must be established. Fourth, based on satisfying the most important similarity criteria, the specifications for the test facility design are established. Fifth, biases due to scaling distortions can

then be quantified. Lastly, the critical attributes of the test facility that must be preserved to meet Quality Assurance requirements must be identified.

3.6.3.1. Relevant ITF

Key characteristics of selected ITF that simulate PWR systems can be found in Table 3.6-2. All the considered ITF include the main zones of the reference NPP and are designed following the full height, full linear power, and time preserving scaling laws.

TABLE 3.6-2. RELEVANT HARDWARE CHARACTERISTICS OF THE PWR SIMULTATORS CONSIDERED FOR NATURAL CIRCULATION

Item	1 Semiscale Mod2A	2 Lobi Mod2	3 Spes	4 PKL-III	5 Bethsy	6 Lstf
Reference Reactor	W-PWR	KWU-PWR	W-PWR	KWU-PWR	FRA-PWR	W-PWR
and power (MW)	3411	3900	2775	3900	2775	3423
No of fuel rods simulators	25	64	97	340	428	1064
No of U-tubes per SG	2/6	8/24	13/13/13	30/30/60	34/34/34	141/14
Internal diameter of U-tubes (mm)	19.7	19.6	15.4	10.0	19.7	19.6
Actual Kv	1/1957	1/589	1/611	1/159	1/132	1/48

3.6.3.2. The experimental database

The evaluation of the experimental data brought to the NC maps shown in Figs 3.6-5 and 3.6-6.

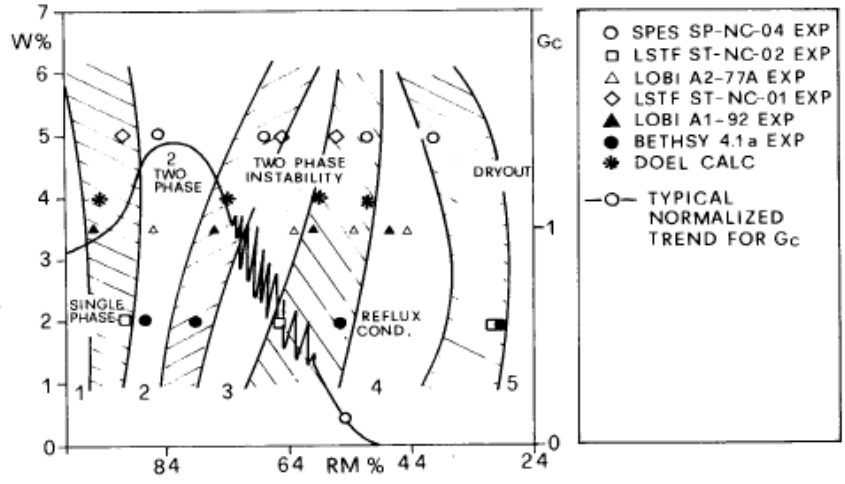

FIG. 3.6-5. Characterization of natural circulation flow regimes based on experimental data and system codes calculations.

The data in Fig. 3.6-6, were at the origin of the natural circulation flow map that was used for deriving the NC performance of various systems (e.g. refs. [3.6-1] and [3.6-13]). Information from ref. [3.6-4] can also be added to the database of Fig. 3.6-6.

The study of NC in the PKL test facility contributed to the understanding and the characterization of mechanisms that cause boron dilution in case of SBLOCA in PWR systems equipped with U-Tube steam generators, ref. [3.6-3]. Namely, diluted liquid accumulates in the loop seals during phases of the accident when break flow is almost equal to ECCS injection flow and mass inventory of the primary system ranges between 70% and 50% of the initial-nominal value. Once loop seal space is filled by boron diluted water there is the potential that such liquid is transported to the core following restart of NC, thus causing the potential for re-criticality.

A key feature of PWR primary circuit, including ITF, is constituted by the so called 'loop-seal'. This is the part of pipe connecting the outlet of the steam generator with the (bottom) inlet of the main coolant pump. The bottom of the resulting U-shaped pipe has an elevation lower (by about 1 m) than the Top of Active Fuel (TAF).

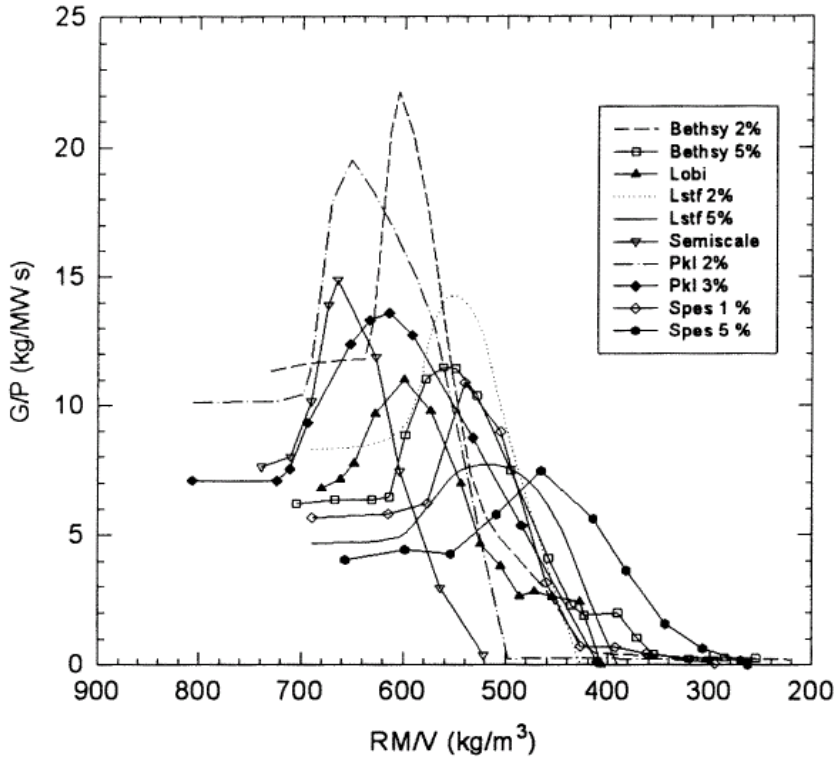

FIG. 3.6-6. Natural Circulation system behaviour measured in ten experiments performed in six PWR simulators.

In case of two phase natural circulation the loop seal may be liquid filled causing a gravity counter-pressure that pushes the 'collapsed' liquid level in the core below the TAF. Dry-out may result as a consequence of this. The clearing of the loop seal typically causes recovery from the CHF condition.

The cyclic filling and emptying of the loop seal also contributes to oscillations as outlined in the Section 3.6.4 below.

Finally, during the reflux condensation (a NC mode, as described in 3.6-5), boron diluted liquid may accumulate in the loop seal causing the potential for reactivity excursion. This may occur when and if the plug of de-borated water is transported into the core following restart of natural circulation. However the de-borated water plug mixes with borated water in the cold leg, down-comer and lower

plenum before entering the core. This phenomenon is strictly connected with the NPP geometry and with the area of the break.

3.6.4. Stability of natural circulation

The stability (or instability) constitutes a key feature of a natural circulation system. A wide variety of NC stability conditions are investigated in the literature and hundreds of journal papers address the related issues, see also refs. [3.6-1] and [3.6-2]. Thus classifications of stability conditions can be expected, an example being given by the list in Table 3.6-3 (D'Auria et al., in ref. [3.6-2]).

All the information given in this Section 3.6 relates or is directly applicable to natural circulation in NPP conditions (list in Table 3.6-1). However, in the case of stability (present section) a broader range of conditions are investigated in fundamental (NC related) research and related results are discussed.

TABLE 3.6-3. CLASSIFICATION OF STABILITY CONDITIONS (RELEVANT TO NC SYSTEMS)

Class	Type	Mechanism	Characteristic
Static instabilities			
Fundamental (or pure) static instabilities	Flow excursion or Ledinegg instabilities	$\left.\frac{\partial \Delta p}{\partial G}\right\|_{\text{int}} \leq \left.\frac{\partial \Delta p}{\partial G}\right\|_{ext}$	Flow undergoes sudden large amplitude excursion to a new, stable operating condition
	Boiling crisis	Ineffective removal of heat from heated surface	Wall temperature excursion and flow oscillation.
Fundamental relaxation instability	Flow pattern transition instability	Bubbly flow has less void but higher Δp than that of annular flow	Cyclic flow pattern transitions and flow rate variations
Compound relaxation instability	Bumping, geysering, or chugging	Periodic adjustment of metastable condition, usually due to lack of nucleation sites	Period process of super-heat and violent evaporation with possible expulsion and refilling
Dynamic instabilities Fundamental (or pure) dynamic stabilities	Acoustic oscillations	Resonance of pressure waves	High frequencies (10-100Hz) related to the time required for pressure wave propagation in system
	Density wave oscillations	Delay and feedback effects in relationship between flow rate, density, and pressure drop.	Low frequencies (1Hz) related to transit time of a continuity wave
Compound dynamic instabilities	Thermal oscillations	Interaction of variable heat transfer coefficient with flow dynamics	Occurs in film boiling
	BWR instability	Interaction of void reactivity coupling with flow dynamics and heat transfer	Strong only for small fuel time constant and under low pressures
	Parallel channel instability	Interaction among small number of parallel channels	Various modes of flow redistribution
Compound dynamic instability as secondary phenomena	Pressure drop oscillations	Flow excursion initiates dynamic interaction between channel and compressible volume.	Very low frequency periodic process (0.1Hz)

Stability related investigation can be subdivided into three broad categories:

a) related to physical model and/or system characteristics,

b) measured in experiments,

c) numerical method related.

In a number of cases the investigations at items a) and c) cannot be easily distinguished [3.6-9, 3.6-10, 3.6-12, 3.6-16, 3.6-18, 3.6-22 and 3.6-23].

It should be noted that the coupled thermohydraulics and neutron kinetics oscillations in case of natural circulation, investigated in ref. [3.6-18], might be considered as an additional category of instabilities. Sample results or findings related to each of the three groups are outlined below.

An established 'stability related' result is constituted by the effect of orificing of channel inlet to increase the stability of the system, item a). A typical result can be seen in Fig. 3.6-7, reported in the (classical) plane NPCH versus NSUB.

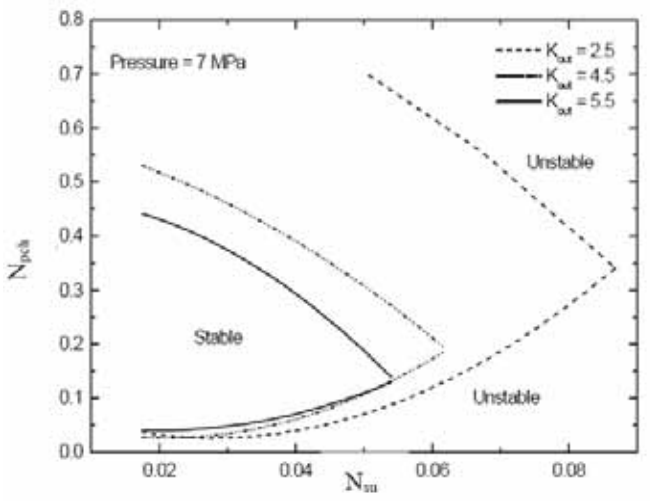

FIG. 3.6-7. Effect of orificing upon the system stability in case of DWI.

Oscillations measured in experiments are used to qualify the models, item b). An interesting set of data, taken from ref. [3.6-22], is reported in Figs 3.6-8a and 3.6-8b, where the system under investigation is a simple rectangular shaped closed loop.

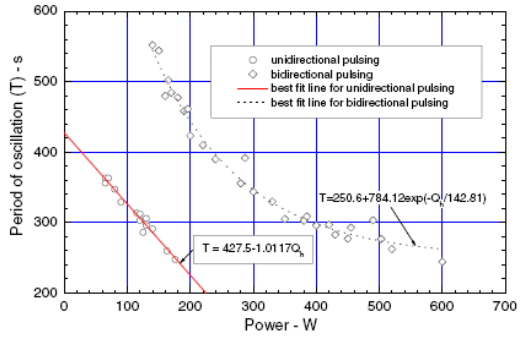

FIG. 3.6-8a. Variation of period of oscillation with power.

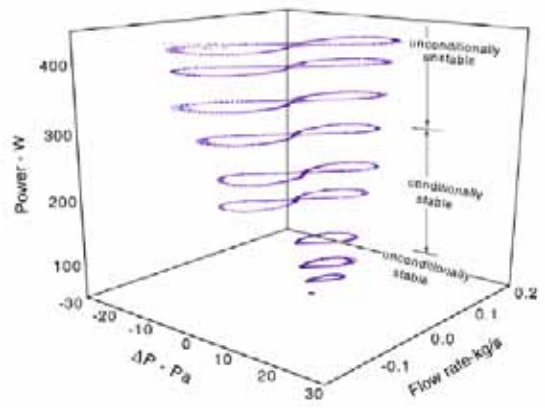

FIG. 3.6-8b. 3-D phase space of instability (plot for 2500 s for each power after neglecting initial transients).

An example of numerical method related oscillation can be seen in Fig. 3.6-9, as taken from ref. [3.6-9]. The influence of the number of nodes in the stability prediction can be derived in a condition where time step of integration is assigned.

Stability data measured in ITF at conditions simulating the PWR and the innovative reactor type MASLWR are discussed in Refs [3.6-4] and [3.6-5], respectively. Furthermore, the MASLWR facility, Ref. [3.6-5] is ready for fundamental investigations in the area of natural circulation.

A characteristic source of oscillation is the presence of parallel loops, i.e. multiloop facility or NPP, and the current design of U-Tube steam generators and of BWR cores involving the presence of several thousands ‘parallel’ tubes and of a few hundreds parallel channels, respectively. Parallel channel stability constitutes the related issue and a wide literature is associated with this, e.g. Refs [3.6-27] and [3.6-28], dealing with density wave stability in BWR and with siphon condensation in PWR.

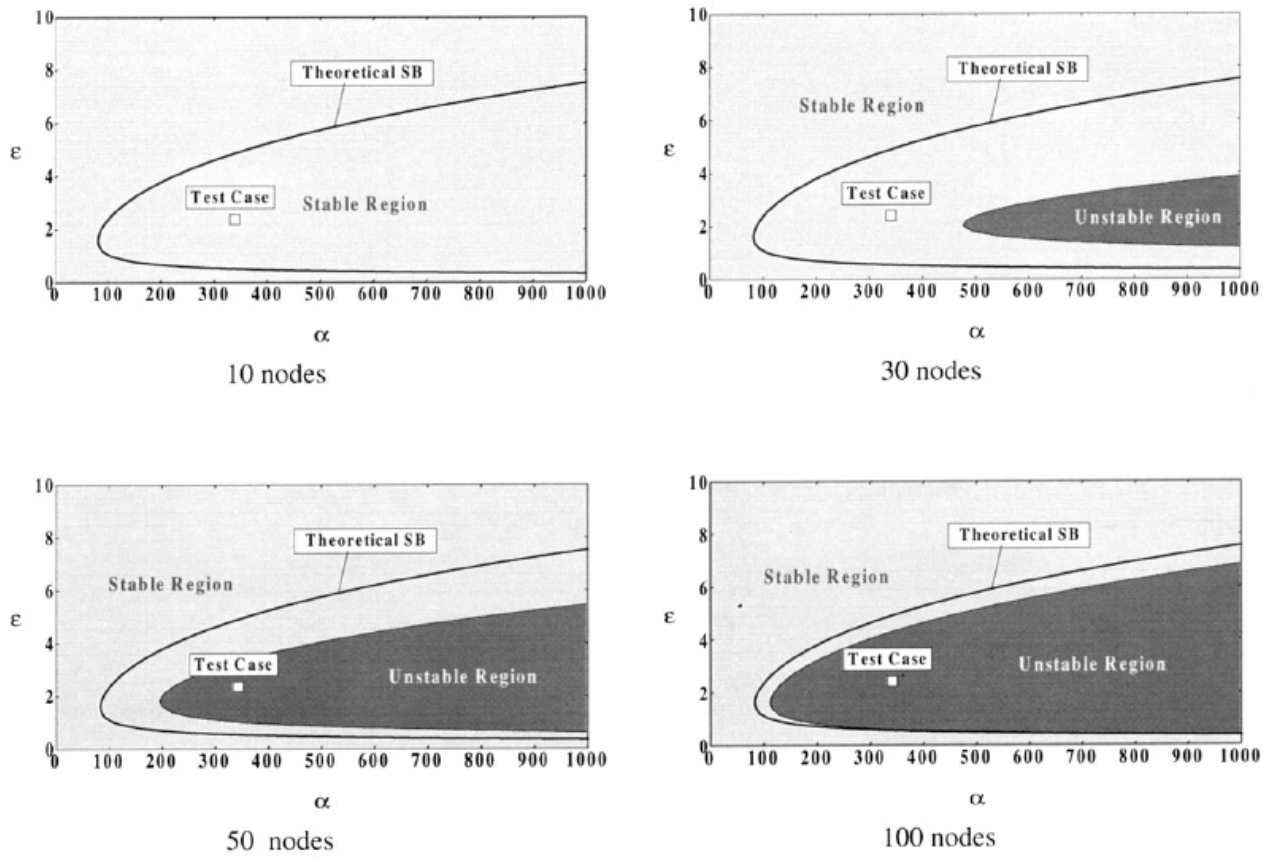

FIG. 3.6-9. Linear stability maps for the upwind explicit scheme with various numbers of nodes ($\xi = 1.75$, $Dt = 10^{-3}$, $C_{max} = 0.8$).

3.6.5. Computational tools

A variety of computational methods have been developed to predict thermohydraulic phenomena related to natural circulation. Analytical approaches to predict single phase and two phase natural circulation flow rates in simple loops are outlined in Section 3.6.2 (with the balance equations that are at the basis of codes briefly presented in Section 3.6.2.2), see also Refs. [3.6-1], [3.6-2], [3.6-13], [3.6-14] and [3.6-15] for more details. A summary of the many different formulations used in thermohydraulic safety analysis codes can be derived from Table 3.6-4 (contribution by J. Reyes in Ref. [3.6-2]). They range from very simple 3-equation homogeneous equilibrium models to advanced full non-equilibrium models using 6 balance equations. New codes, such as NRC's TRACE code are also under development.

As already mentioned, neutron kinetics can have a large impact on the stability of two phase natural circulation flows, particularly during BWR operations. A detailed list of the computer codes used for linear and non-linear stability analysis can be found in Ref. [3.6-2]. These codes have neutron kinetics models ranging from point kinetics to full 3-D kinetics.

Computational fluid dynamic (CFD) codes can also serve as valuable tools for the analysis of natural circulation flows. CFD codes are particularly well suited for analysing single phase fluid flow inside complex geometries; see also ref. [3.6-10] for applications of CFD codes to the analysis of NC and of related instabilities. An overview on the use of CFD codes in nuclear power plant applications is also given in ref. [3.6-2].

Consistently with the information provided in Table 3.6-4, attention is focused hereafter to system codes and to the nodalizations that represent the interface between those codes and the physical reality, e.g. the NPP systems. In relation to the application of system codes with main reference to NC studies,

it may be noted that the 'predictability' of the NC phenomenon, as compared to phenomena like CHF, CCFL, TPCF (two phase critical flow), is strongly influenced by the nodalization structure. In facts the information related to the 'other' listed phenomena is embedded into the constitutive equations part of the code and the phenomena can be predicted in a single node where the code equations are solved. This is not the case of NC whose predictability depends upon the existence (in numerical terms) of a closed loop, thus from the development/existence of several nodes (at least two nodes).

3.6.5.1. Numerical codes

System codes, like APROS, ATHLET, CATHARE, RELAP5 and TRAC, are based upon the solution of a system of six partial differential equations. Two main fields, one for each of the two phases liquid and steam are considered and coupling is available with the solution of the conduction heat transfer equations within solids interfaced with the fluid phases. A one dimensional solution for the characteristics of the fluid is achieved in the direction of the fluid motion in time dependent conditions. It should be emphasized that more sophisticate models are also available including three dimensional solutions and multifield approaches in two and multiphase fluids.

Suitable descriptions of those codes can be found in documents available in the public literature including the outcome of international cooperation, e.g. Refs. [3.6-1] and [3.6-25]. The relevance of code validation is stressed in Refs. [3.6-25] and [3.6-26] and an example of code validation in NC conditions can be found in Ref. [3.6-4].

3.6.5.2. Nodalizations and applications

The mentioned codes have been applied to the simulation of data measured in experimental facilities of different dimensions and complexity as well as to the prediction of the NC performance of existing nuclear power plants and of advanced reactor concepts, Ref. [3.6-1]. The application requires the development and the qualification of nodalizations, see also Ref. [3.6-6].

Criteria and road-maps for developing nodalizations and for qualifying the same nodalization including procedures for addressing the scaling issue for code and nodalizations can be found in Ref. [3.6-26].

The applications of system codes have been of help for interpreting the experimental scenarios, for optimizing the features of the nodalizations and for characterizing the code capabilities. A list of significant achievements from code applications is given below.

a) The codes have been used to distinguish five main NC flow patterns depending upon the value of the mass inventory of the primary loop, see also the analysis carried out in Ref. [3.6-4] and Fig. 3.6-10:

    - Single phase NC with no void in the primary system excluding the pressurizer and the upper head;
    - Stable co-current two phase NC with mass flow rate increasing when decreasing primary system fluid inventory;
    - Unstable two phase NC and occurrence of siphon condensation;
    - Stable reflux condensation with liquid flowing countercurrent to steam in the hot legs flow-rate is sufficient to remove core power till loop mass inventory achieves values as low as 30–40% of the nominal values;
    - Natural circulation with part of core rods in dry-out condition not favorable from the current technological and safety point of view.

TABLE 3.6-4. MAIN FEATURES OF SYSTEM CODES ADOPTED IN THE NC STUDIES

Conservation equations	Restrictions[1]	Constitutive Laws[2]	Calculated Parameters
6–Equation Models			
Two –Fluid Non-Equilibrium (2) Mass Phase Balance (2) Momentum Phase Balance (2) Energy Phase Balance		(2) Phase wall friction (2) Phase heat flux friction (1) Interfacial mass (1) Interfacial momentum (1) Interfacial energy	α, p,v_l v_v T_l T_v
5-Equation Models			
Two-Fluid Partial Non-Equilibrium (2) Mass Phase Balance (2) Momentum Phase Balance (1) Mixture Energy Balance	$T_l = T_{SAT}$ or $T_v = T_{SAT}$	(2) Phase wall friction (1) Mixture wall heat flux (1) Interfacial mass (1) Interfacial momentum	α, p,v_1, v_v (T_l or T_v)
Two-Fluid Partial Non-Equilibrium (1) Mixture Mass Balance (2) Momentum Phase Balance (2) Energy Phase Balance	$T_l = T_{SAT}$ or $T_v = T_{SAT}$	(2) Phase wall friction (2) Phase heat flux friction (1) Interfacial mass[3] (1) Interfacial momentum (1) Interfacial energy	α, p,v_1, v_v (T_l or T_v)
Slip or Drift Non-Equilibrium (2) Mass Phase Balance (1) Mixture Momentum Balance (2) Energy Phase Balance	Slip or Drift Velocity	(1) Mixture wall friction (2) Phase heat flux friction (1) Interfacial mass (1) Interfacial energy (1) Slip velocity or Drift flux	α, p,T_l T_v , v_m
Homogeneous Non-Equilibrium (2) Mass Phase Balance (1) Mixture Momentum Balance (2) Energy Phase Balance	Equal Velocity $v_l = v_v = v_m$	(1) Mixture wall friction (2) Phase heat flux friction (1) Interfacial mass[3] (1) Interfacial energy	α, p, T_l T_v , v_m
4-Equation Models			
Two-Fluid Equilibrium Model (1) Mixture Mass Balance (2) Momentum Phase Balance (1) Mixture Energy Balance	$T_l = T_v = T_{SAT}$	(2) Phase wall friction (1) Mixture heat flux friction (1) Interfacial mass[3] (1) Interfacial momentum	α, p,v_1 ,v_v
Drift Partial Non-Equilibrium (2) Mass Phase Balance (1) Mixture Momentum Balance (1) Mixture Energy Balance	Drift Velocity T_v or $T_l = T_{SAT}$	(1) Mixture wall friction (1) Mixture wall heat flux (1) Interfacial mass (1) Drift flux correlation	α, p, v_m, T_v or T_l
Slip Partial Non-Equilibrium (1) Mixture Mass Balance (1) Mixture Momentum Balance (2) Phase Energy Balance	Slip Ratio T_v or $T_l = T_{SAT}$	(1) Mixture wall friction (1) Mixture wall heat flux (1) Interfacial mass (1) Drift flux correlation	α, p, v_m T_v or T_l
Homogenous Partial Non-Equilibrium: (1) Mixture Mass Balance (1) Mixture Momentum Balance (2) Phase Energy Balance	$U_l = U_v = U_m$ T_v or $T_l = T_{SAT}$	(1) Mixture wall friction (2) Phase wall heat flux (3) Interfacial mass (1) Interfacial energy	α, p, v_m T_v or T_l
3-Equation Models			
Homogenous Equilibrium (HEM): (1) Mixture Mass Balance (1) Mixture Momentum Balance (1) Mixture Energy Balance	$u_l = u_v = u_m$ $T_l = T_v = T_{SAT}$	(1) Mixture wall friction (1) Mixture wall heat flux	α, p, u_m
Slip or Drift Equilibrium: (1) Mixture Mass Balance (1) Mixture Momentum Balance (1) Mixture Energy Balance	Slip or Drift Velocity $T_1 = T_v = T_{SAT}$	(1) Mixture wall friction (1) Mixture wall heat flu (1) Slip velocity or Drift flux	α, p, u_m

1. Restrictions imposed on fluid phase velocities or temperatures for enthalpies in lieu of temperatures).
2 Minimum number of constructive laws. For example for N structures in the flow N structure heat flux and N wall friction correlations may be required.
3. Interfacial mass transfer is required to determine interfacial momentum or interfacial energy transfer.

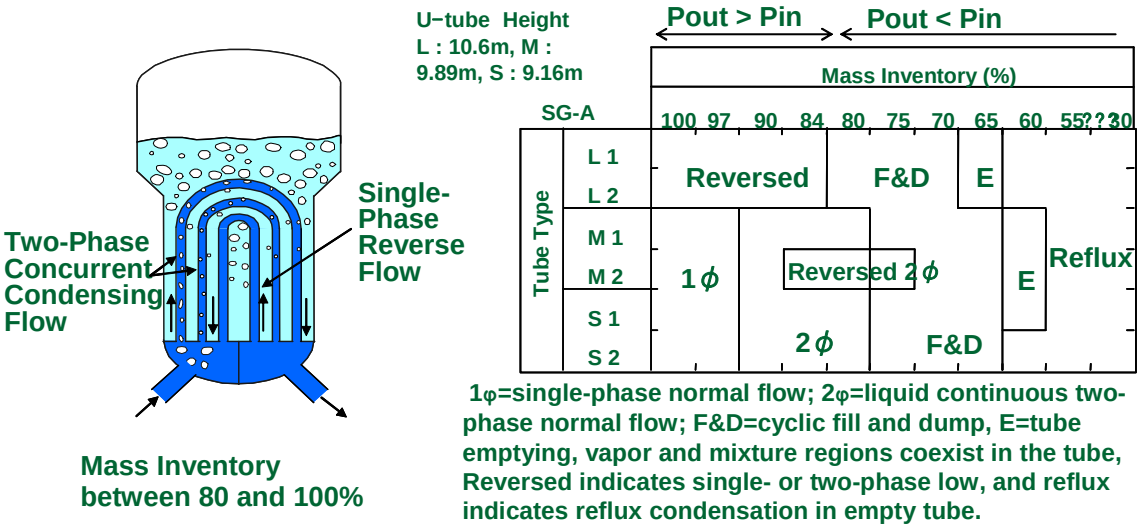

FIG. 3.6-10. Natural circulation flow regimes [3.6-4].

b) The code has been used for characterizing the oscillations showing the different role of the countercurrent flow limitation (CCFL) at the entrance of the U-tubes, the siphon effect and the steam condensation both in the rising part of the U-tubes. The flow reversal and the different behaviour of parallel groups of U-tubes could also be observed with the help of the code.

c) Different codes used by different European organizations have been applied to the comparative analysis of the A2-77 experiment carried out in the LOBI facility. Capabilities of the codes were characterized as well as the influence upon the results that are caused by the code-user effect. Deficiencies were observed in the predictions of pressure drops at low values of the Reynolds number.

d) The application to the study of NC in VVER-440 showed the code capability in predicting the flow stagnation and the consequent rise in system pressure caused by the loop sealing present in the hot leg of this reactor type (see also Ref. [3.6-6]). Clearing of loop seal occurs before dangerous situation for the system is reached and is also predicted by the code.

e) The code has been used to determine the maximum core power at which the PWR systems or PWR simulators can be operated in NC while maintaining a subcooled core. The limit was found close to 10% of the core nominal power. Higher limits were found with different thresholds for the system operation.

f) The code has been successfully used in predicting NC phenomena measured in systems that are relevant to the AP-600, including NC across the PRHR (pressurized residual heat removal), and the CMT (core make-up tank) systems.

g) The application of the MARS system thermohydraulics code to the design of the SMART reactor shows that the NC flow-rate expected following MCP stop is of the order of 10% of the initial-nominal value, Ref. [3.6-7].

3.6.6. General remarks

An overview has been given of the natural circulation phenomenon. Key summary remarks are:

- NC occurs in a gravity environment: single phase and two phase natural circulation should be distinguished. Single phase is relevant only when relatively large fluid density changes are associated with temperature changes.
- NC is important for the design of existing nuclear reactors. Its relevance is greater as far as new generation of reactors is concerned.
- Compared with forced circulation, where pumps are present in an assigned loop, in the case of NC smaller driving forces govern the fluid motion. This makes NC flow more prone to instability than forced circulation flow.
- Analytical models are available to predict the occurrence of instability. However, attention must be paid to the development or the application of numerical solution methods that may strongly affect the prediction of stability performance of a loop.

NOMENCLATURE

a	cross-section area
Cmax	Courant number
d or D	equivalent diameter
Dt	time step
e	internal energy
f	friction coefficient
Gr	Grashof number
h	enthalpy
K	local pressure drop coefficient
Kv	volume scaling factor
l	length
L	elevation difference
m	mass flow-rate
M	mass
n	vector
N	quantity defined in Section 2.1
p	pressure
q	heat transfer rate
q”	heat flux
Re	Reynolds number
S	entropy
t	time
V	velocity
W	power
x	quality
α	void fraction
β	thermal expansion coefficient
Γ	vaporization rate
Φ or ϕ	two phase flow multiplier
μ	viscosity
ν	velocity
ρ	density
ω	non-dimensional quantity defined in Section 2.1
ξ	friction factor

Subscripts

c	restriction
e	equilibrium
eff	effective
f	liquid phase
fg	g-f
g	vapour phase
h	hydraulic
k	f or g
i	generic index
in	initial value
l	liquid phase
loss	heat losses
LO	Liquid Only
M	mixture
out	outlet
SG or SS	across steam generator
sat or SAT	saturation
sys	system
TP	two phase
v	vapour (or steam)

ABBREVIATIONS

BWR	Boiling water reactor
CANDU	Canadian deuterium uranium
CCFL	Countercurrent flow limiting
CFD	Computational fluid dynamics
CHF	Critical heat flux
CMT	Core make-up tank
CRP	Coordinated research project
CSNI	Committee on the Safety of Nuclear Installations
DWI	Density wave instability
EC	European Commission
ECCS	Emergency core cooling system
IAEA	International Atomic Energy Agency
HEM	Homogeneous equilibrium model
ITF	Integral test facility
LBLOCA	Large break LOCA
LOCA	Loss of coolant accident
MCP	Main coolant pump
NC	Natural circulation
NEA	Nuclear Energy Agency
NPCH	Phase change number
NPSH	Net positive suction head
NPP	Nuclear power plant
NRC	Nuclear Regulatory Commission
NSUB	Subcooling number
OECD	Organization for Economic Cooperation and Development
PRHR	Pressurized residual heat removal
PWR	Pressurized water reactor
RBMK	Reactor Bolshoy Moshchnosty Kanalny
SB	Stability boundary

SBLOCA	Small break LOCA
SG	Steam generator
TPCF	Two phase critical flow
TAF	Top of active fuel
TMI	Three Mile Island
VVER	Water cooled water moderated energy reactor (see also WWER)

REFERENCES FOR SECTION 3.6

[3.6-1] INTERNATIONAL ATOMIC ENERGY AGENCY, Natural Circulation Data and Methods for Advanced Water Cooled Nuclear Power Plants Designs, IAEA-TECDOC-1281, IAEA, Vienna (2002).

[3.6-2] INTERNATIONAL ATOMIC ENERGY AGENCY, Natural Circulation in Water cooled Nuclear Power Plants Phenomena, Models, and Methodology for System Reliability Assessments, IAEA-TECDOC-1474, IAEA, Vienna (2005).

[3.6-3] D'AURIA, F., "Natural circulation and boron dilution process in PWR", 2nd CRP RCM, Corvallis, Oregon (US), Aug. 29–Sept. 2 (2005).

[3.6-4] YONOMOTO, T., "LOSA/LSTF experiments on PWR natural circulation and validation of RELAP5/MOD3.3", 2nd CRP RCM, Corvallis, Oregon (USA), Aug. 29–Sept. 2 (2005).

[3.6-5] REYES, J., "Testing of the multi-application small light water reactor (MASLWR) passive safety systems", 2nd CRP RCM, Corvallis, Oregon (USA), Aug. 29–Sept 2 (2005).

[3.6-6] MATEJOVIC, P., "Natural circulation and use of passive heat removal principles in VVER-440/V213 reactors", 2nd CRP RCM, Corvallis, Oregon (USA), Aug. 29–Sept. 2 (2005).

[3.6-7] CHUNG, Y. J., "Characteristics of a two phase natural circulation in the passive residual heat removal system of an integral type reactor", 2nd CRP RCM, Corvallis, Oregon (USA), Aug. 29–Sept. 2 (2005).

[3.6-8] VIJAYAN, P.K., "Steady state behaviour of single phase and two phase natural circulation loops", 2nd CRP RCM, Corvallis, Oregon (USA), Aug. 29–Sept. 2 (2005).

[3.6-9] AMBROSINI, W., FERRERI, J.C., The effect of truncation error on numerical prediction of stability boundaries in a natural circulation single phase loop, J. Nucl. Eng. Des. **183** (1998) 53–76.

[3.6-10] PILKHWAL, D.S., et al., Analysis of the unstable behaviour of a single phase natural circulation loop with one dimensional and computational fluid-dynamic models, J. Annals of Nuclear Energy **34** Issue 5 (2007) 339–347.

[3.6-11] DIMMICK, G.R., CHATOORGOON, V., KHARTABIL, H.F., DUFFEY, R.B., Natural-convection studies for advanced CANDU reactor concepts, J. Nuclear Engineering and Design **215** Issues 1-2, June (2002) 27–38.

[3.6-12] ROHATGI, U.S., DUFFEY, R.B., Stability, DNB and CHF in natural circulation two phase flow, J. Int. Communications in Heat and Mass Transfer **25** No 2 (1998) 161–174.

[3.6-13] D'AURIA, F., FROGHERI, M., Use of natural circulation map for assessing PWR performance, J. Nuclear Engineering & Design (Special Issue) **215** Nrs 1&2 (2002) 111–126.

[3.6-14] MOUSAVIAN, S.K., D'AURIA, F., SALEHI, M.A., Analysis of natural circulation phenomena in VVER-1000, J. Nuclear Engineering & Design **229** (2004) 25–46.

[3.6-15] GROUDEV, G.P., PAVLOVA, M.P., Sensitivity calculations of PRZ water level during the Natural Circulation test at Unit 6 of Kozloduy NPP, J. Progress in Nuclear Energy **49** Issue 2, March (2007) 130–141.

[3.6-16] KURAN, S., et al., Startup transient simulation for natural circulation boiling water reactors in PUMA facility, J. Nuclear Engineering and Design **236** Issue 22, November (2006) 2365–2375.

[3.6-17] LINZER, W., WALTER, H., Flow reversal in natural circulation systems, J. Applied Thermal Engineering **23** Issue 18, December (2003) 2363–2372.

[3.6-18] LEE, J.D., PAN, C., Nonlinear analysis for a nuclear-coupled two-phase natural circulation loop, J. Nuclear Engineering and Design **235** Issue 5, February (2005) 613–626.

[3.6-19] UMMINGER, K., MANDL, R., WEGNER, R., Restart of natural circulation in a PWR–PKL test results and 5 calculations, J. Nuclear Engineering and Design **215** Issues 1-2, June (2002) 39–50.
[3.6-20] SAMOILOV, O.B., KUUL, V.S., MALAMUD, V.A., TARASOV, G.I., Integral nuclear power reactor with natural coolant circulation. Investigation of passive RHR system, J. Nuclear Engineering and Design **165** Issues 1-2, 2 August (1996) 259–264.
[3.6-21] GARTIA, M.R., VIJAYAN, P.K., PILKHWAL, D.S., A generalized flow correlation for two -phase natural circulation loops, J. Nuclear Engineering and Design **236** Issue 17, September (2006) 1800–1809.
[3.6-22] VIJAYAN, P.K., SHARMA, M., SAHA, D., Steady state and stability characteristics of single phase natural circulation in a rectangular loop with different heater and cooler orientations, J. Experimental Thermal and Fluid Science **31** Issue 8, August (2007) 925–945.
[3.6-23] ZANOCCO, P., GIMÉNEZ, M., DELMASTRO, D., Modeling aspects in linear stability analysis of a self-pressurized, natural circulation integral reactor, J. Nuclear Engineering and Design **231** Issue 3, July (2004) 283–302.
[3.6-24] D'AURIA, F., GALASSI, G.M., VIGNI, P., Calastri A., Scaling of natural circulation in PWR systems, J. Nuclear Engineering & Design **132** No. 2 (1992) 187–206.
[3.6-25] D'AURIA, F., et al., Neutronics/Thermohydraulics Coupling in LWR Technology — CRISSUE-S WP1: Data Requirements and Databases Needed for Transient Simulations and Qualification, OECD/NEA Report No 4452, ISBN 92-64-02083-7, Paris, France (2004), (Vol. I, 103 pages, Vol II 293 pages, Vol III 65 pages).
[3.6-26] D'AURIA, F., GALASSI, G.M., Code Validation and uncertainties in system thermohydraulics, J. Progress in Nuclear Energy **33** (1998) 175–216.
[3.6-27] D'AURIA, F., et al., State of the Art Report on Boiling Water Reactor Stability (SOAR ON BWRS), OECD-CSNI Report OECD/GD (97) 13, Paris, France, Jan (1997).
[3.6-28] D'AURIA, F., GALASSI, G.M., Flow-rate and density oscillations during two-phase natural circulation in PWR typical conditions, J. Nuclear Engineering & Design **122** (1990).

3.7. STEAM–LIQUID INTERACTIONS

3.7.1. Introduction

The capacity to keep the containment pressure below a limiting value by means of a passive system relies basically on the condensation phenomenon in the primary loop after a LOCA has already taken place. Given that condensation will arise under passive conditions i.e. without outer electrical, mechanical or hydraulic component, its evolution will be strongly determined by the physical structure of the device on which the aforementioned condensation takes place.

This way, and taking into account the reference systems that stand for the main reactor designs of the III and III+ generations, the study of the process phenomenology must make a distinction between forced condensation (according to the existing pressure difference between drywell and wet well) on the one hand, which takes place inside the pipes of a heat exchanger immersed in a water pool (Type I, Section 3.2), then condensation under natural circulation conditions over the very containment walls (Type II, Section 3.3) and finally direct contact condensation between a steam jet and non-condensable gases coming from the containment (Type III; current section).

3.7.2. Hardware

There are two scenarios related to the III and III+ generation reactors that involve the phenomenon of direct condensation: on the one hand, relief of the primary loop through discharge of the safety valves and pressurizer relief in the in- containment Refuelling Water Storage Tank -IRWST-, and on the other hand the purging of non-condensed steam and non-condensable gases from the containment passive cooling system (PCCS) when in contact with the liquid stored in the suppression pool, which brings about a partial condensation of the steam, whereby a drop in the containment pressure takes place.

The first scenario turns out to be simpler than the second one, given that it is determined by fixed boundary pressure conditions, unrelated to the steam flow coming from the primary loop (primary loop pressure; IRWST pressure right out of the spargers). The mentioned flow is made out of pure steam (stemming from the vessel), belongs in the forced convection circulation regime and, on the grounds of its velocity, corresponds to the ’jet’ type.

The second scenario, in contrast, is more complex and in fact encompasses a set of scenarios made up of stages that unfold sequentially over time, given that venting will flow depending on changing pressure conditions (transient phases) [3.7-1]: on the one hand, pressure in the containment dry well, which undergoes cyclic modifications, in accordance with the different stages of the loss of coolant accident and the venting of non-condensables accumulated in the wet well, and on the other hand pressure in the wet well, which depends likewise on the accumulation of non-condensable gases dragged along with the steam flow from the dry well, but also on the liquid surface temperature which determines the value of the partial pressure of steam saturation, thus conditioning pressure in the wet well gas-filled zone, and therefore in the suppression pool vent opening.

In this case, the flow regime will depend on variables such as the gas speed or the liquid subcooling, the latter being conditioned by actual condensation and thermal stratification. This way, a multiplicity of steam/non-condensables combinations will arise whose features regarding heat transfer and interfacial area will be equally modified.

As an example, thermal stratification will depend on the flow pathway after exiting the vent opening, and characterized by Richardson’s number. It will also depend on the liquid drag brought about by buoyancy or on the amount of non-condensable matter flowing from the dry well. Due to its greater complexity, and assuming therefore that the first scenario can be understood as a subcase of this one, we will focus on the discharge of steam/non-condensables past the venting of the containment passive cooling system.

The suppression pool liquid inventory stands as a separate department of the containment dry well and is connected to it by means of a venting pipe through which the gas mixture is discharged. It is the case that in all the settings that passively cool down the containment, direct condensation, in sharp contrast with condensation brought about by means of heat exchangers (either immersed in water or on the containment walls), is never the sole device bearing the responsibility of producing an eventually necessary containment cooling.

Thus, from an all-embracing viewpoint accounting for the relationship between the direct condensation system and the other containment cooling systems, it would be possible to make a distinction between those containment configurations whose pressure is limited to values akin to the ones in 2nd generation reactors, and those other ones, smaller in size, that withstand much higher pressures.

In the former case (target reactors: ESBWR, ABWR, RMWR), the suppression pool is coupled to an in-water, submerged heat exchanger, by means of a venting pipe. In this case, direct condensation of steam — not condensed on the exchanger pipe — in the face of air dragged along by gas flow stemming from the dry well is not as much the containment cooling system as the determination of the pressure boundary condition necessitated so that steam will flow towards the heat exchanger pipes.

In the latter case, the containment compact design (integral reactors) allows for a containment pressure of a value far higher than that in current designs. This way, it is not necessary anymore to have an auxiliary system geared towards the evacuation of great amounts of containment heat, be it an immersed heat exchanger or an oversized outer surface for the containment. It is due to this that the condensation rate is lower than the one attained in type I/II devices.

In this case, direct condensation in the suppression pool, together with condensation on the containment walls (target reactors: MASLWR, LSBWR) or backed by the heat removal emergency system (target reactor: IRIS), permit that the in-containment pressure be equal to — or even higher than — in-vessel pressure, so that the reactor itself relieves containment pressure, keeping it steadily well below the safety limit.

Therefore, direct condensation does not stand as a key mechanism for containment cooling, but as a secondary one, be it because it only establishes a pressure boundary condition or else because it is backed by other cooling systems in those containment designs in which the required condensation rate is lower.

From a phenomenological standpoint, direct condensation in the suppression pool is characterized by its being a flow regime of the vapour/non-condensables jet type in the venting system, which will thereafter become an upward bubble plume in the liquid zone. Once the jet comes into contact with the liquid past the vent exit, high temperature steam condensation is immediate. A rising plume is formed out of heated-up high temperature liquid and non-condensable gas.

The surrounding pool liquid is put in motion not only by the hot liquid plume brought about the by the liquid temperature difference, but also by the rising gas bubble plume caused by the gas-liquid density difference. Due to the strong drag effect of the bubble plume (produced by the buoyancy of non-condensable gases), thermal stratification will be reduced, and as a result the mass of liquid acting as a sink for the gas jet heat will stay at a threshold under that of the vent exit (as opposed to the theoretical situation for pure steam), essentially depending on the jet's Richardson number and on the non-condensable gases fraction.

3.7.3. Theoretical basis

The mass and energy transfer that is characteristic of a steam and non-condensable gases flow introduced in the suppression pool through a venting pipe is a three dimensional phenomenon.

The difficulty of modelling direct condensation for great volumes of liquid[13] is essentially due to the fact that the transferred heat flux depends on the geometrical configuration adopted by the gas flow. This way, and similarly to what happens in two phase regimes, it is necessary right off from the start to determine which is the extant regime type, so that thereafter its heat transfer coefficient and the associated interfacial area can be elucidated.

Normally, authors assume a jet or plume regime type depending on the balance of buoyancy and inertial forces derived from Richardson's or Froude's numbers, in order to calculate the distribution of each regime in the mass of liquid after that, and then apply an empirical interfacial heat transfer correlation (Nusselt's number), which is usually a function of Reynolds', Prandtl and Jacob's numbers. For the sake of an example, this is how authors such as [3.7-2], [3.7-3], [3.7-4], and others proceed.

There are literatures available regarding the direct contact condensation of steam jet in a subcooled pool. Some researchers defined three general idealized shapes of the pure steam jet plume in a subcooled pool of water [3.7-5–3.7-7]. These are ideal conical, ellipsoidal and divergent shapes. The justifications for defining these idealized shapes were based on experimental observations, where the plume shape and length were found to depend on the injection diameter, injection orientation and pool subcooling, with combination of three well defined shapes occurring within specified ranges of steam mass flux.

The condensation regime map for direct contact condensation is characterized by two parameters: the rate of vapour injection (steam mass flux) and the degree of liquid subcooling (pool temperature). The steam mass flux provides a measure of the driving force exerted on the liquid side (driving mechanism), whereas the pool temperature represents the magnitude of the thermal driving potential (condensation).

In the Table 3.7-1 we include some authors that have studied the direct contact condensation. The mass fluxes used in the experiments vary from 0 to 600 kg/m^2s and the pool temperatures from 0°C to 100°C. The experimental injection directions studied are downward, upward and lateral vent pipe, and multihole sparger.

[13] The opposite scenario is not considered herein, i.e. the one in which liquid is injected in a steam atmosphere. This would be the case of the condensation caused in the vicinity of an injection aiming at the cooling of the containment or the core in a steam environment in 2nd generation reactors.

TABLE 3.7-1. LITERATURE SURVEY ON DIRECT CONTACT CONDENSATION

Author	Diameter (mm)	Water temp **(°C)**	Steam mass flux (kg s^{-1} cm^{-2}**)**	Direction exit	Regime
Chan & Lee [3.7-8]	51	40-90	1-175	Downward Vent Pipe	Chugging Oscillatory bubble Ellipsoidal oscillatory bubble Ellipsoidal jet Oscillatory cone jet
Fukuda & Saito [3.7-10]	8 16.1 27.6	25-90	0-350	Downward Vent Pipe	Type A: chugging Type B: transition Type C: subsonic jet Type D: oscillatory bubble Type E: sonic jet
Nariai & Aya [3.7-11]		0-100	0-200	Downward Vent Pipe	Chugging Condensation oscillation Transition Bubbling
Aya & Nariai [3.7-4]	9-38	0-100	0-40	Downward Vent Pipe	Chugging Condensation oscillation Bubbling
Liang [3.7-12]	19.1	50-100	0-50	Upward Rectangular Channel	Chugging Bubbling Subsonic jet Sonic jet
Lahey & Moody [3.7-13]		0-100	0-125		*Internal Condensation* Chugging Condensation oscillation Quasi-steady condensation Transition Incomplete condensation
Lee & No [3.7-14]	13 - 14	31-91	20-80	Lateral Vent pipe	Sonic jet Subsonic jet Steam cavity
Cho et al. [3.7-15]	5-20	20-95	44-450	Single hole	Chugging Transient chugging Condensation oscillation Stable condensation Bubble condensation oscillation Interfacial oscillation condensation
Youn et al. [3.7-16]	5/8 inch 6/8 inch	30-80	10-80	Lateral Single hole	Chugging Transient chugging Bubble condensation oscillation
Cho et al. [3.7-17]	20-21x5	30-95	70-215	Multihole Sparger	Condensation oscillation
Park et al. [3.7-18]	64x10 Lateral	20-95	100-550	Multihole Sparger	Condensation oscillation Stable condensation
Park et al. [3.7-19]	144x10 Lateral 17.6 Bottom	20-95	190-600	Multihole Sparger with a bottom hole	Condensation oscillation Transition Stable condensation
Petrovic de With et al. [3.7-9]	0-50	0-90	0-150		15 regimes Chugging Interfacial condensation oscillation Jetting: conical, ellipsoidal and divergent shape Bubbling

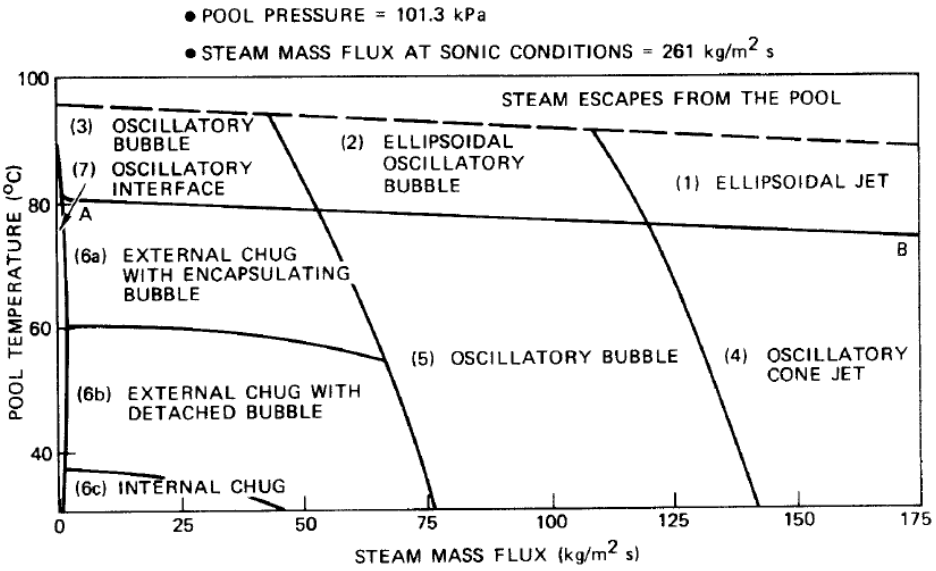

FIG. 3.7-1. Condensation regime map for DCC downward vent pipe.

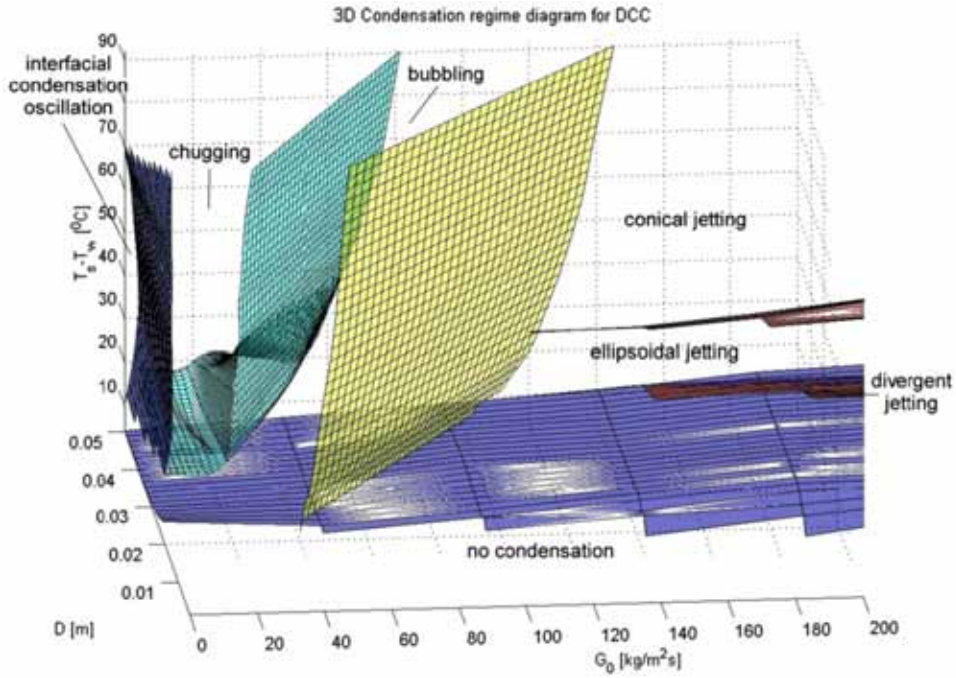

FIG. 3.7-2. Three dimensional regime map for small steam inflow rates.

In Fig. 3.7-1 we show the condensation regime map obtained by Chan [3.7-8]. The classification proposed by the authors is made by two simple criteria: the location of the steam region relative to the injection pipe exit and the position of the bubble detachment. The classification is based on a specific geometry (downward vent pipe) and the boundaries of this condensation regime map are only approximate and are system dependent. The main regimes of this map are the following:

- Internal chugging occurs at small steam mass flux and low water temperature. It is characterized by a back flow of pool water sucked up into vent tubes, a large pressure spike followed by pressure oscillation with high frequency during each chugging.

- Small chugging is characterized by the movement of the steam–water interface around the vent tube exit. From the wave shape of the pressure oscillation, it can be deduced that the small chugging is a transitional state between internal chugging and condensation oscillation.
- Condensation oscillation occurs at a larger steam mass flux than chugging. It is characterized by the growth and shrinking of a steam bubble attached to the vent tube exit, where the pressure oscillates with the same high frequencies as those of the interface movement.
- Bubbling at high water temperature is characterized by slow growth and detachment of the steam bubbles, the period of this detachment is consistent with that of the pressure changes without the high frequency component.
- At very high water temperatures, no pressure oscillation occurs and a part of the steam escapes from the pool to the atmosphere.
- For high steam flow rates, steam forms a plume. The shape of the plume is conical or ellipsoidal.

The comparison of the above regime map with the other maps of Table 3.7-1 shows that all maps hold similar features. However, steam and water conditions as well as the regime pattern can vary significantly. This is due to injector sizes that are different. This implies that the regime map varies depending on the injector size.

Petrovic de With et al. [3.7-9] propose a three dimensional condensation regime map. They use the classical dependency of steam mass flux and the water subcooling instead of the pool temperature. The third dependency selected by the authors is the injector diameter. The data used to make the map was obtained from a large number of experimental studies. Figures 3.7-2 and 3.7-3 show the three dimensional regime maps obtained by the authors for small inflow steam mass flux (G_0 from 0 to 200 kg/m^{2}s) and large inflow steam mass flux (G_0 from 0 to 1500 kg/m^{2}s).

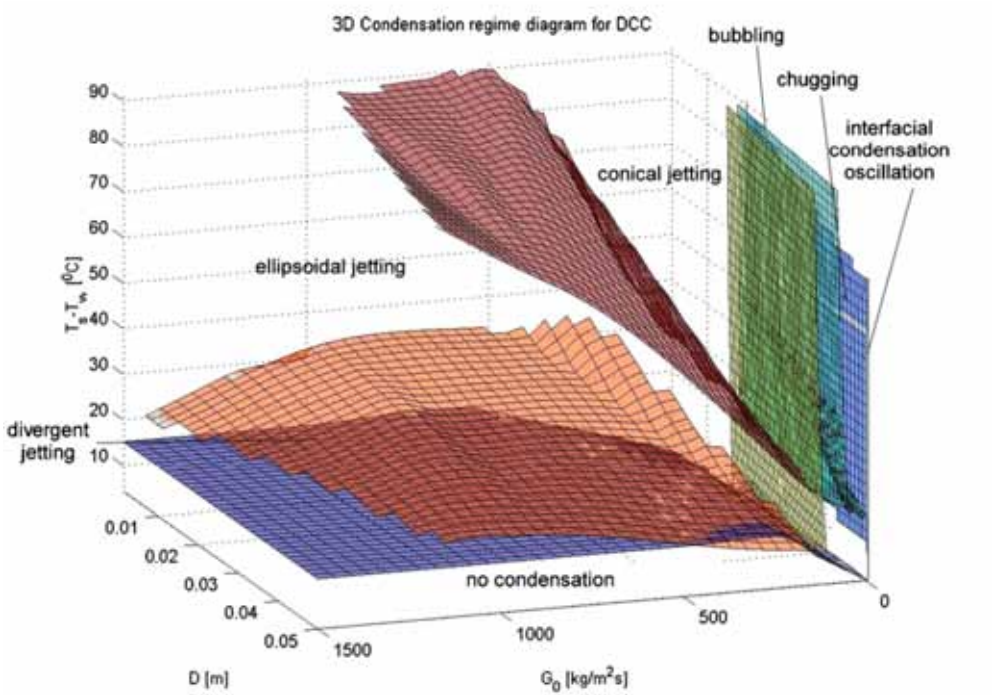

FIG. 3.7-3. Three dimensional regime map for large steam inflow rates.

3.7.4. Experimental evidence

3.7.4.1. Suppression pool mixing and condensation tests in PUMA facility

Condensation of steam with non-condensables in the form of jet flow or bubbly flow inside the suppression pool is an important phenomenon for determining the containment pressure of a passively safe boiling water reactor. 32 cases of pool mixing and condensation tests have been performed in Purdue University Multi-Dimensional Integral Test Assembly (PUMA) to investigate thermal stratification and pool mixing during the reactor blowdown period [3.7-20]. The test boundary conditions cover a wide range of prototype (SBWR-600) conditions during a LOCA that were obtained from the RELAP5 calculation.

Significant features of a suppression pool are passive steam condensation in the pool, lower maximum pressures and rapid pressure reduction, higher capacity for blowdown energy discharge, and insensitivity to the initiation time of heat exchangers for energy removal. The PUMA facility was used to perform suppression pool mixing and condensation tests. The PUMA facility is a scaled down facility from the GE's SBWR-600. It was designed to simulate the reactor blow-down transient during a loss of coolant accident event after the reactor primary vessel depressurizes below 1.03 MPa (see Fig. 3.7-4).

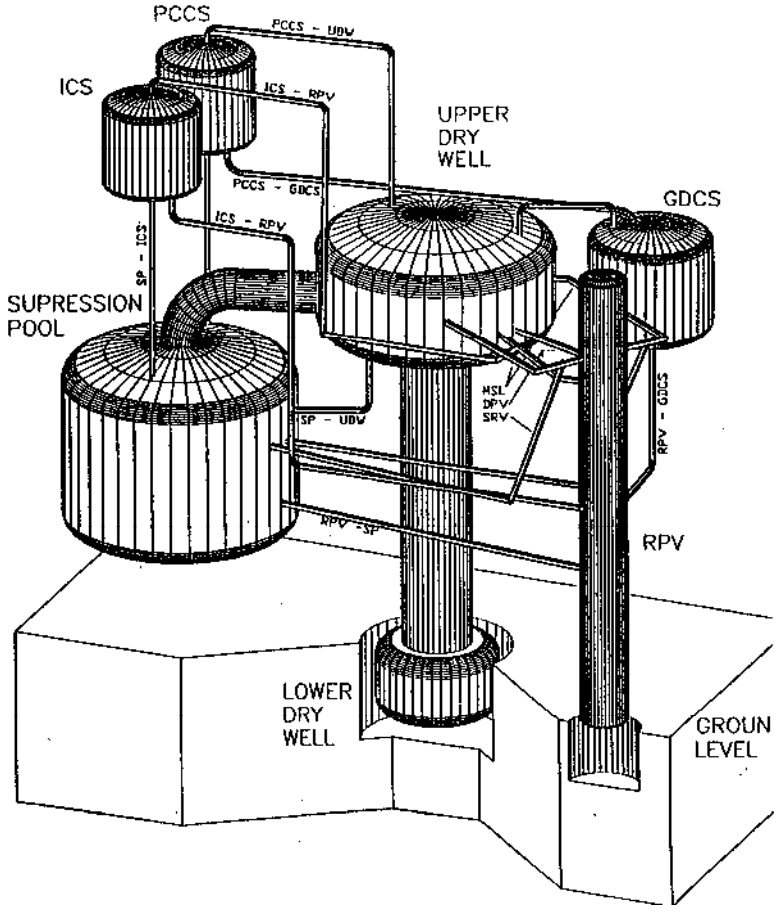

FIG. 3.7-4. PUMA-test facility.

The design of the PUMA facility was based on scaling methods from the integral response function, from the boundary flow of mass and energy between the components and on the key local phenomena and constitutive relations. The scaling ratios of the PUMA facility to SBWR-600 are summarized in Table 3.7-2.

TABLE 3.7-2. SCALING RATIOS OF THE PUMA FACILITY TO SBWR-600

Parameter	Scaling Ratio
Diameter	1:10
Area	1:100
Volume	1:400
Pressure	1:1
Power	1:200
Time	1:2

During several experiments the operation of the suppression pool during a main steam line break and bottom drain line break have been analysed. Non-condensable gas concentration in the air-steam mixture discharging flow was an important test parameter. The suppression pool was equipped with thermocouples for the observation of temperature stratification effects. A high speed camera was used to capture the jet interfacial area structure during the direct condensation in a short time period. A digital camcorder was used to record the jet surface structure during the entire test.

The test matrix was obtained by using RELAP5 simulation for the blowdown phase of the SBWR-600. Values obtained from the RELAP5 simulation were scaled down according to the PUMA to SBWR scaling ratios. During the tests the steam flow rate, air flow rate, the drywell pressure, initial water level in the suppression pool, and the bulk water initial temperature of suppression pool were controlled.

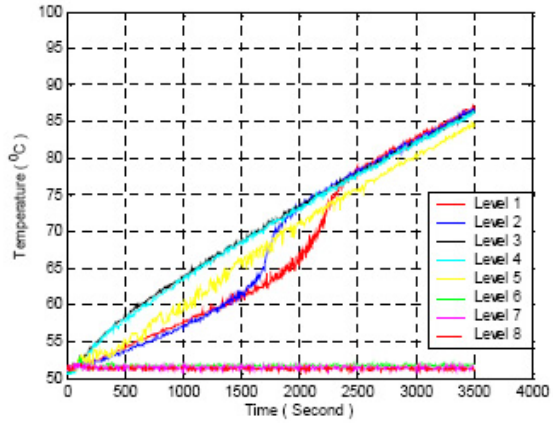

FIG. 3.7-5. Temperature distributions at R = 106 cm for 0.07 kg/s pure steam injection case.

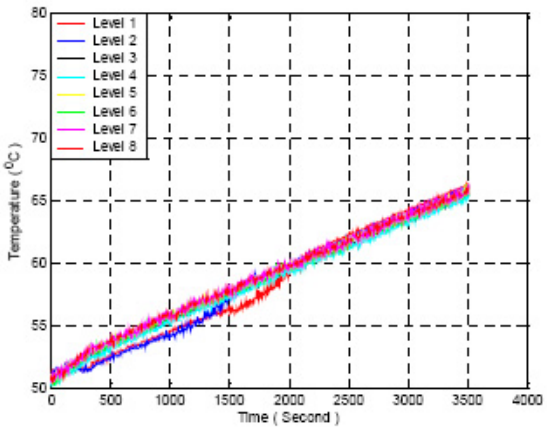

FIG. 3.7-6. Temperature distributions at R = 106 cm for 0.07 kg/s steam, 3.684 g/sec air injection case.

Several tests were performed to investigate the thermal stratification[14], direct contact condensation, and the pool circulation by plume and jet in the suppression pool. The axial temperature distribution for pure steam injection at R = 106 cm is plotted in Fig. 3.7-5. This figure shows that the pool region above the vent opening mixes homogeneously, while the pool region below the vent opening stays at the initial temperature. This means that heat is accumulated only in the upper high temperature region, which is above the elevation of vent opening. In other words, thermal stratification decreases the effective pool inventory available for energy storage. The axial temperature distribution at R = 106 cm for steam air mixture injection is shown in Fig. 3.7-6. This figure shows that complete pool mixing has been achieved in the high non-condensable gas injection rate case. In the pure steam test, the pool circulation driven by the rising hot water plume is weak, restricting the mixing to

[14] This experimental evidence is deeply connected with section 3.1, 'behaviour in large pools of liquid'.

the upper portion of the pool above the elevation of the vent opening. In turn, in the steam/air mixture injection, the surrounding pool liquid is circulated not only by the hot liquid plume caused by the liquid temperature difference (see Figs 3.7-7 and 3.7-8), but also by the rising gas bubble plume caused by the gas-liquid density difference. Due to the strong entrainment effect of the bubble plume, the whole pool is homogenously mixed and the thermal stratification in the pool is destroyed.

In the experiments, it was found that the degree of thermal stratification in the suppression pool is strongly affected by the non-condensable gas injection flow rate. It is also affected by the vent opening depth, the pool pressure and the steam flow rate. Further influences by the pool water initial temperature were observed.

Cheng et al. [3.7-20] concluded, that a mechanistic model is needed which can evaluate the pool mixing/recirculation velocity induced by the air bubble plume and hot liquid plume in order to utilize these results in reactor system code (RELAP5, TRACE, etc.). To evaluate this model, the pool mixing/recirculation velocity and the void fraction distribution in the air bubble plume should be acquired in future experiments.

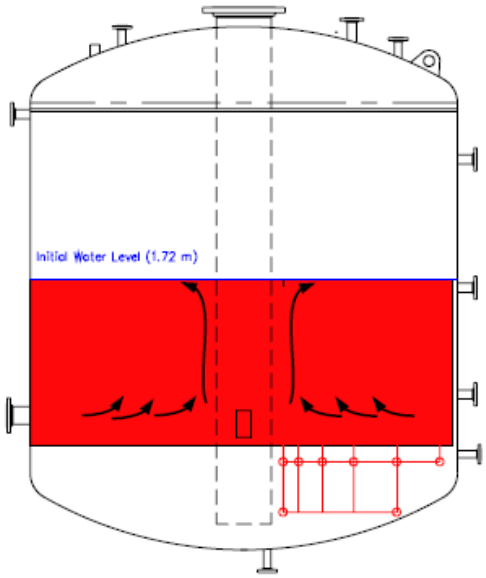

FIG. 3.7-7. Schematic of pool circulation during pure Steam Injection.

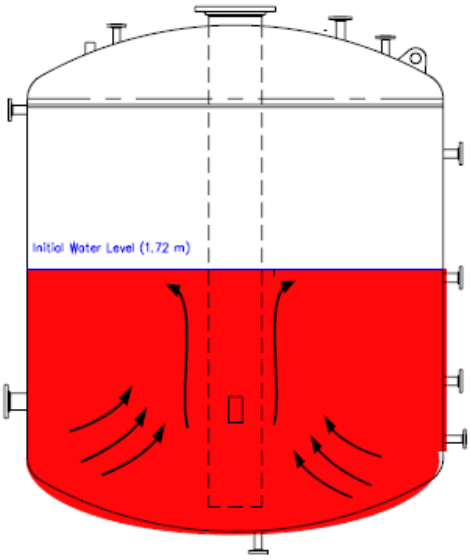

FIG. 3.7-8. Schematic of pool circulation during steam and high non-condensable gas injection.

3.7.4.2. Experimental survey

Given that the studied scenario is direct condensation produced in the suppression pool, as has already been mentioned in the hardware-related section, the phenomenon of thermal stratification will always be experimentally linked to that of direct condensation. Moreover, and still in the line of what was commented in Section 3.7.3, one of the keys to adequately solve for direct condensation is to obtain a regime flow map that enables us to properly apply the heat transfer and interfacial area coefficients. Because of that, great part of the experimental survey consisted of working out those maps, alongside with the study of direct condensation.

One of the first studies of the interaction of an upward venting system with steam flow submerged in a pool of liquid is the one performed by Fukuda and Saito [3.7-10], in which five different types of

condensation regimes were identified (on the basis of the diverse geometrical configurations of the flow in its interaction with the liquid).

General Electric [3.7-21–3.7-23] carried out during the 70's a series of tests in the Pressure Suppression Test Facility (PSTF) whose goal was the validation of the wet well configuration in its conjoint functioning with the dry well. Later on, Gamble et al. [3.7-24] utilized the data to validate a model that simulates the influence of a jet-type steam flow on thermal stratification, by means of a model implementation in TRACG.

Still intent on establishing a flow regime map, Liang and Griffith [3.7-2] experimentally analysed the effect of non-condensable gases, aiming at acting over the condensation rate (in its relationship with the flow rate of the steam injected through the venting duct), and this way being able to avoid chugging and thereby the violent pressure oscillations that arise in this regime type. If the classical formula to establish a chugging-type flow ($\frac{\rho_s v_s A_v h_{fg}}{h_i A_i \Delta T_{sub}} \leq 1$) is used, it is sufficient to modify the energy transferred to the liquid through its interfacial heat transfer coefficient in order to avoid entering the chugging flow regime. The existence of even a low fraction of non-condensable gases will alter the condensation process, making it diffusion-controlled, and this way, as a positive effect, the chugging zone will be averted. Therefore, the violent pressure oscillations can be avoided.

Liang and Griffith [3.7-2] developed a transient conduction-diffusion model for the onset of chugging in the presence of non-condensable gases. Given the importance of buoyancy on turbulent mixing, this model is only applicable to upward steam flow.

Still other authors [3.7-25, 3.7-26] experimentally investigated turbulent direct condensation, deriving from the gathered data an empirical correlation for the calculation of the interfacial heat transfer coefficient as a function of Stanton's number. It is important to stress the resemblance between the different derived correlations.

But as Kim et al. [3.7-6] duly underline, the problem posed by the use of a correlation based on dimensionless numbers is that these are a function of the amount of interfacial transfer, which is the reason why they will be highly dependent on the type of regime and specific shape of the extant gaseous flow — whether it is jet, plume, etc. It is because of this that they will only be of possible application to specific types of extant two phase flow. This situation is aggravated in the case of turbulent regime, for in this case other prevailing factors such as the instability of the interfacial area through the two phase interface break-up, eddy diffusivities, specific structure of the turbulence field and others will show up.

It is very important to point out the different influence of non-condensable gases on direct condensation, regarding condensation in the inside/outside of pipelines (Section 3.2) and on the condensation in the case of natural free flow on containment structures (Section 3.3). Although in all cases the phenomenon of condensation undergoes a heavy decrease[15] because of its being controlled by the mechanism of mass diffusion of steam through the diffusive layer, in direct condensation the presence of a steady gas glow contributes to a better mixing up of the liquid stock, which results in a greater heat transfer between the fractions of liquid over and under the vent opening level.

Likewise, the presence of non-condensable gases may also result in chugging suppression [3.7-12], which would hinder an eventual steady inflow and outflow of liquid into and from the venting pipe, thereby reducing violent pressure oscillations but making it hard at the same time to achieve a better mixing (large scale motion) [3.7-24].

[15] A mass concentration of circa 2% in non-condensable gases may result in the transferred heat power dropping by as much as 50%.

Many authors point to the reduction in the condensation rate caused by the presence of non-condensable gases in the steam injected into a pool [3.7-2, 3.7-3], indicating strong degradations even with the presence of low amounts of non-condensable gases. Even so, it is necessary to bear in mind that the role of condensation in the suppression pool is secondary, the setting of a pressure condition downstream from the dry well being the true determining factor of this phenomenon.

Therefore, if it were required to study the effect of non-condensable gases on direct condensation over the containment of III/III+ generation reactors, it would be necessary to compare the evolution of pressure at the vent opening over the suppression pool in the case of a pure steam injection, against a mixture of steam and non-condensable gases. From the data offered by Cheng [3.7-20], we can only know this pressure evolution for the LSF1 test (pure steam), and hence the comparison cannot be carried out. But on the other hand, it is indeed possible to compare the different temperature evolution in the case of pure steam and air admixture.

In Figs 3.7-9 and 3.7-10 it is shown that (aside from the mixing and non-stratification for the case of a gas mixture) the value attained after 1000 s in the case of pure steam injection is higher by more than 10ºC, which entails a greater partial steam pressure. Even this, a greater value of the steam pressure does not mean a greater pressure in the gas zone, because of the fact that the existence of non-condensable gases will cause the total pressure in the gas zone to be certainly higher. This way, the existence of non-condensables, even eliminating the liquid stratification, involves a decrease in the driving force that causes the gas mixture to flow from the drywell to the wet well.

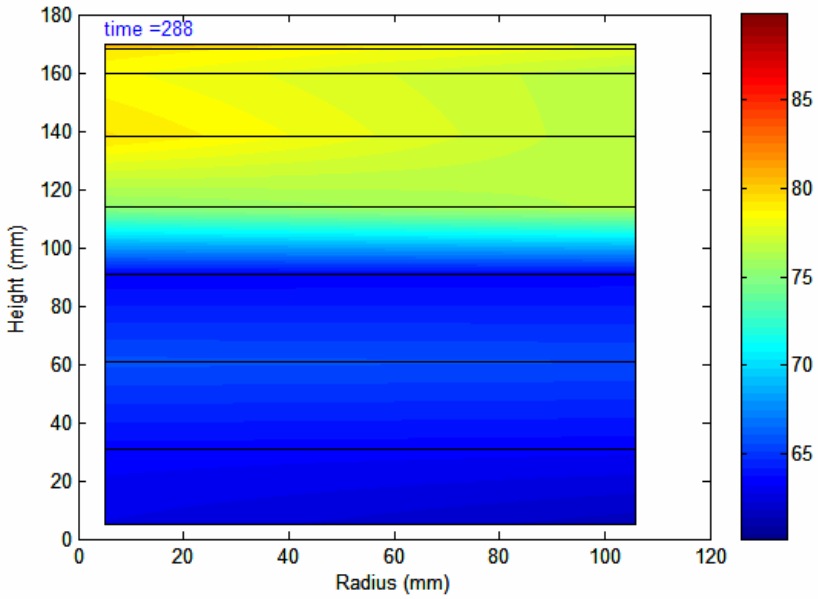

FIG. 3.7-9. 2-D Temperature distributions during pure steam injection at t=1000 s.

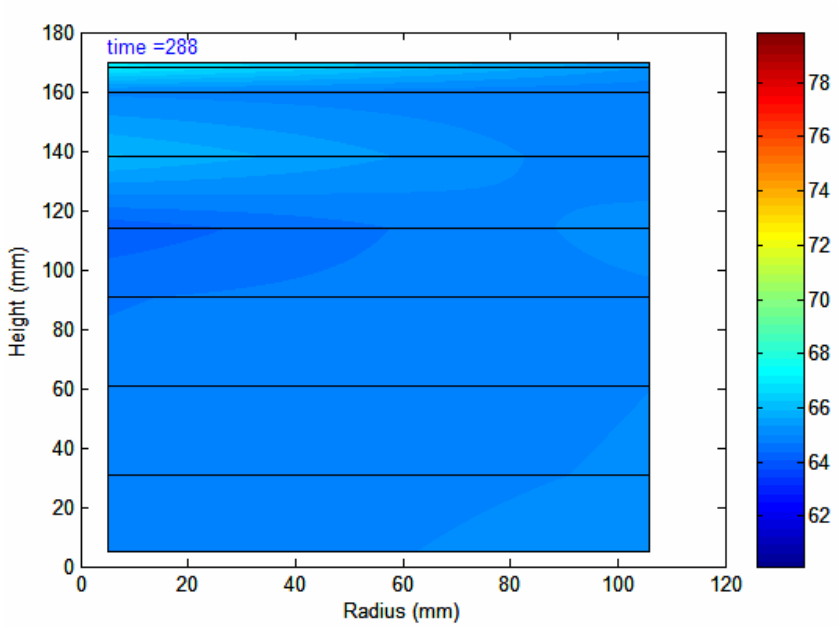

FIG. 3.7-10. 2-D temperature distributions during steam/air injection at t=1000 s.

3.7.5. Computer codes

Gamble et al. [3.7-24] implemented in the TRACG code a system of equations for the calculation of the mixing-up and thermal stratification of a jet-type flow in the suppression pool. This implementation was performed through calculating the size and shape of the gas flow, which also included the introduction of the corresponding sources and sinks for both mass and energy. The results showed good agreement between predictions and test data, though the scarcity of experimental data prevented a good assessment of the precision of the calculations.

The RELAP5/MOD3.1 code has been assessed by Lee and No [3.7-27], in an experiment involving small scale gravity injection simulating direct-contact condensation in the CMT of the PHPIS. The aim is to assess the predictive capability of the code regarding direct contact-condensation in the core make-up tank (CMT) of the passive high-pressure injection system (PHPIS) in the CARR passive reactor (CP-1300).

In the base case study, RELAP5/MOD3.1 did not properly predict the water level arrived at experimentally. The reason is thought to be the uncertainty regarding knowledge of the heat transfer coefficients at the interface. Furthermore, sensitivity studies were carried out with two RELAP5 code versions, namely MOD3.0 and MOD3.1. None of these code versions predicted accurately the experimental data. However, the results produced by RELAP5/MOD3.1 are in better agreement with the experimental results than is the case with the predictions of RELAP5/MOD3.0. Both MOD3.0 and MOD3.1 identify the flow regime in the test section as vertical stratification, whereas the experimentally found flow regimes were either sonic jet or subsonic jet, depending on the steam flow. A nodalization study of RELAP5/MOD3.1 has shown that the 1-node model matches the experimental data better than other multinode models. However, considering the depth to which jets penetrate, the appropriate number of nodes that should be considered in the CMT is still to be determined.

The reproduction of direct-contact condensation in the CMT by means of RELAP5/MOD3.1 requires that new correlations accounting for the interfacial heat transfer coefficients be developed. These prospective correlations should somehow encapsulate the physical processes underway during direct-contact condensation in the CMT.

Regarding commercial Computational Fluid Dynamics (CFD) codes, a simplified model accounting for direct-contact condensation was implemented into the Volume of a Fluid (VOF) model of the Fluent code by Timperi et al. [3.7-28]. Computer tests were run for the POOLEX experiments, involving 3-D transients: steam is blown into a water pool. The STB142 POOLEX experiment performed, was conforming to the parameters described as follows: The simulations were performed with Fluent version 6.3.26, and the direct-contact condensation model was implemented by means of the user-defined functions provided by Fluent. The numerical mesh encompassed circa 94 000 hexahedral cells. The Volume of Fluid (VOF) model of Fluent was used with an explicit interpolation scheme. The discretization of mass, momentum, turbulence and energy equations was carried out by means of a second order, upwind method. The volume fraction was accounted for by resorting to the modified HRIC method. The PRESTO method was utilized to discretize pressure, and PISO was used for pressure velocity coupling. The modelling of turbulence was performed by means of the standard k-ε model of Fluent, resorting to wall functions. The time step used in the simulation was $5 \cdot 10\text{-}4$ s. The obtained numerical data are clearly different from the experimental results: On one hand, the condensation rate of steam is too low; on the other hand, the interface between steam and water remains outside the pipe all the time throughout the simulation, whereas in the experiment, chugging does occur as expected, and the steam–water interface moves periodically into the blowndown pipe — when quick condensation of a steam bubble takes place. This may be attributed to a rapid increase in the steam–water interface area, which would bring about a fast increase of heat transfer and thereby ensuing condensation. It has also to be mentioned that the shape of the bubble arrived at analytically and the one actually observed during the experiments are also different: the vertical axis of the calculated bubble is too large. Conversely, the calculated diameter of the bubble in the horizontal direction is too small.

Therefore, improvements of the numerical methods must be achieved to accurately predict heat transfer around the bubble. Heat transfer should be larger below the bubble and smaller in other directions.

The utilized numerical model has been found to be quite robust. The discrepancies that have arisen during the experiments, such as very low condensation rates, could be ameliorated through improving the condensation model itself. Moreover, using a finer mesh past the blowndown pipe outlet would improve numerical results to some extent. Use of an Euler-Euler multiphase method with full transport equations for both phases would also be convenient given that this model includes separate energy equations for the steam and water phases. However, apparently only a limited subset of versatile experimental situations can be accurately simulated with such models.

Thermal mixing experiments were carried out by [3.7-29] with the aim of clarifying the phenomena arising when a steam discharge is injected into subcooled water within the APR1400 IRWST, seeking to forestall unstable steam condensation due to locally higher water temperature. State of the art commercial CFD codes do not have an in-built model enabling them to cope with direct contact condensation, and only very recently a numerical model trying to capture the features of direct contact condensation was tried out for the case of ideal flow [3.7-30]. In the study at hand, a steam condensation region model was developed based on the data for water temperature in the vicinity of a steam jet, with the aim of simulating direct contact condensation. In the frame of this approach, the speed and temperature calculated for the condensed water and the entrained water in the condensation region or nearby were used as the boundary conditions in order to perform a CFD analysis of the ensuing thermal mixing. The thermal mixing test was carried out in the so-called Blowdown and Condensation (B&C) facility [3.7-29].

The B&C test facility consists of a pressurizer, a steam discharge pipeline, a tank containing the mass of subcooled water, a steam sparger inside the tank and a steam generator. The pressurizer furthers saturated steam at a pressure of 150 bars down the discharge pipeline and into the subcooled water tank, with the sparger being located at the end of the discharge duct and inside the tank. This sparger is a specially modified one, with the purpose of better capturing the features that are of importance if the IRWST of the APR1400 is to be simulated. Specifically, the sparger is made out of 40S 6 inch pipe. In its outer casing, there are 4 rows of punched holes, there being 16 holes per row and thus

totalling 64 holes. Each of these holes is 1 cm across. From the lower part of the sparger to the very bottom of the tank there is a stretch of 90 cm, with the tank itself having a height of 4 m and a diameter of 3 m. Eight thermocouples were placed around the sparger. Their purpose was to measure the temperature of the steam and the entrained water flowing into the steam jet zone. Outwards from the sparger, contained in vertical planes and intent on getting quantitative measures characteristic of the unfolding overall thermal mixing pattern, there were two additional groups of thermocouples, each including 27 devices. The thermocouples in the second group — the one whose plane does not contain the geometrical axe of the sparger — is rigged so as to measure thermal mixing along a circumferential direction in the tank.

From the series of tests performed, the one chosen for the CFD calculation assessment is a case of transient steam discharge stretching over 60 s. The pressurizer started at 150 bar, and the initial temperature in the water tank was 26ºC. The thermal mixing test involved saturated steam at a pressure of about 10 bar within the sparger being delivered into the tank water, which was at 26ºC and a pressure of 1 bar. Choking may have momentarily taken place at the sparger openings during this process.

After progressing through the tank liquid to some extent, the steam jet quickly condensed by virtue of the DCC mechanism. Numerically modelling this process of condensation is difficult, and a concept termed “steam condensation region model” is resorted to. This entails assuming that the steam jet perfectly condenses into the surrounding water mass within the penetration length distance. The penetration length of the steam jet is supposed to be a definite function of the steam mass flow, the diameter of the discharge holes (holes punched in the sparger casing) and the temperature and pressure of the water in the tank. The thickness of the jet at the end of the penetration stage can be worked out on the grounds of the boundary layer theory. This jet width and the penetration length are used as intervening constant values in the CFD calculations. The obtained mass flow rate and the assumed enthalpy based on the test results are plugged into equations to work out the enthalpy of condensed water. The value arrived at for this enthalpy can then be compared with the value assumed at the start. If the difference between these two values is less than 5%, then the values assumed for the enthalpies of the condensed and entrained water are taken as boundary condition values in the CFD analysis.

CFX4.4 uses these values to calculate the thermal mixing of condensed water and subcooled water already present in the tank. This is made by using a suitable turbulence model, together with other concurrent physical models.

The selected locations were expected to be representative of the typical thermal mixing pattern in the tank. It is apparent that the profiles of temperature variations arrived at experimentally and through the use of CFD are very similar.

The CFD-predicted results are typically higher than those obtained in the tests by 1–3ºC. The reason may well be that the condensation region model in the CFD analysis resorts to the concept of average area, but thermocouples measure strictly local values. On the other hand, CFD results sometimes show that the code overestimates temperature peaks at around t = 6 s. This can partly be attributed to CFD not being able to simulate complicated local thermal mixing phenomena arising when condensed water flows upwards and over the tank wall.

The predictions for other temperature peaks however are accurate, notwithstanding that three dimensional effects may also play a role in the settling of the temperature distribution in the uppermost layer.

The experimentally obtained data and the CFD-calculated results agree to within 7–8%. The reason for this discrepancy may be that the temperature and speed of the condensed water — calculated in the frame of the condensation region model — are higher than the real, experimental value. Another cause may be the use of the average area concept, still in the mindset of the condensation region model.

In addition, this concept inherently entails ignoring three dimensional flow features taking place in the tank, whereas CFX calculations are carried out under the assumption that the processes exhibit axial symmetry –aiming at saving computation time-.

As a final note, commercial CFD-type codes such as CFX4.4 alongside with the condensation region model named in this text can simulate thermal mixing behaviour well provided that the mesh structure selected for the computation is appropriate and that the choice of numerical methods is correct.

NOMENCLATURE

ρ_s	steam density
v_s	steam velocity at the exit of the vent pipe
A_v	vent pipe area
h_{fg}	phase change enthalpy
h_i	interfacial heat transfer coefficient
A_i	interfacial area
ΔT_{sub}	liquid subcooling

REFERENCES FOR SECTION 3.7

[3.7-1] OH, S., REVANKAR, T., Effect of non-condensable gas in a vertical tube condenser, Nuclear Engineering and Design **235** (2005) 1699–1712.

[3.7-2] LIANG, K.-S., GRIFFITH, P., Experimental and analytical study of direct contact condensation of steam in water, Nuclear Engineering and Design **147** (1994) 425–435.

[3.7-3] JANICOT, A., BESTION, D., Condensation modelling for ECC injection, Nuclear Engineering and Design **145** (1999) 37–45.

[3.7-4] AYA, I., NARIAI., H., Boundaries between regimes of pressure oscillation induced by steam condensation in pressure suppression containment, Nuclear Engineering and Design **99** (1987) 31–40.

[3.7-5] CHUN, M.H., KIM, Y.S., PARK, J.W., An investigation of direct condensation of steam jet in subcooled water, International Communications in Heat and Mass Transfer **23** (1996) 947–958.

[3.7-6] KIM, Y.S., PARK, J.W., SONG, C.H., Investigation of the steam-water direct contact condensation heat transfer coefficients using interfacial transport models, International Communications in Heat and Mass Transfer **31** n3 (2004) 397–408.

[3.7-7] SONG, C.H., et al., "Characterization of direct contact condensation of steam jets discharge into a subcooled water", IAEA-TECDOC-1149 (2000) 21–37, IAEA TCM, PSI, Villigen (1998).

[3.7-8] CHAN, C.K., LEE., C.K.B., A regime map for direct contact condensation, Int. J. Multiphase Flow **8** No. 1 (1982) 11–20.

[3.7-9] PETROVIC DE WITH, A., CALAY, R.K., DE WITH, G., Three-dimensional condensation regime diagram for direct contact condensation of steam injected into water, International Journal of Heat and Mass Transfer **50** (2007) 1762–1770.

[3.7-10] FUKUDA, S., SAITO, S., Pressure variation due to vapor condensation in liquid (I), J. Atomic Energy Soc. Jpn. **24** (1982) 58–66.

[3.7-11] NARIAI, H., AYA, I., Fluid and pressure oscillations occuring at direct contact condensation of steam flow with cold water, Nuclear Engineering and Design **95** (1986) 35–45.

[3.7-12] LIANG, K.-S., Experimental and analytical study of direct contact condensation of steam in water, Ph. D. MIT May (1991).
[3.7-13] LAHEY, R.T., MOODY, F.J., The Thermohydraulics of a Boiling Water Reactor, 2ºEd. American Nuclear Society, Illinois (1993) 582.
[3.7-14] LEE, S.I., NO, H.C., Gravity-driven injection experiments and direct-contact condensation regime map for passive high-pressure injection system, Nuclear Engineering and Design **183** (1998) 213–234.
[3.7-15] CHO, S., et al., "Experimental study on dynamic pressure pulse in direct contact condensation of steam jets discharging into subcooled water", 1st Korea–Japan Symposium on Nuclear Thermohydraulics and Safety, Pusan, October (1998) 291–298.
[3.7-16] YOUN, D.H., et al., The direct contact condensation of steam in a pool at low mass flux, Journal of Nuclear Science and Technology **40** No. 10 (2003) 881–885.
[3.7-17] CHO, S., CHUN, S.-Y., BAEK, W.P., KIM, Y., Effect of multiple holes on the performance of sparger during direct contact condensation of steam, Experimental Thermal and Fluid Science **28** (2004) 629–638.
[3.7-18] PARK, C.K., SONG, C.H., JUN, H.G., Experimental investigation of the steam condensation phenomena due to a multi-hole sparger, Journal of Nuclear Science and Technology **44** No. 4 (2007) 548–557.
[3.7-19] PARK, C.K., SONG, C.H., JUN, H.G., YOUN, Y.J., Experimental investigation of steam condensation phenomena using a multihole sparger with a bottom hole, Journal of Nuclear Science and Technology **45** No. 9 (2008) 951–961.
[3.7-20] CHENG, L., WOO, K.S., ISHII, M., LIM, J., HAN, J., "Suppression pool mixing and condensation tests in PUMA facility", paper ICONE14-89348, Int. Conf. on Nuclear Engineering, ICONE14, Miami, Florida, USA, July (2006).
[3.7-21] VARZALY, A.M., et al., Mark III, Confirmatory test program, 1:3 scale condensation and stratification phenomena-test series 5807, General Electric Report, NEDE-21596-P, March (1977).
[3.7-22] VARZALY, A.M., GRAFTON, W.A., SEELY, D.S., Mark III, Confirmatory test program, full scale condensation and stratification phenomena-test series 5707, General Electric Report, NEDE-21853-P, August (1978).
[3.7-23] VARZALY, A.M., YU, K.P., KERINENEN, J.A., Mark III, Confirmatory test program, 1:9 area scale multicell condensation and stratification phenomena-test series 6003. General Electric Report, NEDE-24720-P, January (1980).
[3.7-24] GAMBLE, R.E., et al., Pressure suppression pool mixing in passive advanced BWR Plants, Nuclear Engineering and Design **204** (2001) 321–336.
[3.7-25] THOMAS, R.M., Condensation of steam on water in turbulent motion, Int. J. Multiphase Flow **5** No. 1 (1979) 1–15.
[3.7-26] SONIN, A.A., SHIMKO, M.A., CHUN, J., The steady condensation rate as a function of liquid-side turbulences, Int. J. Heat and Mass Transfer **29** No.9 (1986) 1319–1332.
[3.7-27] LEE, S.I., NO, H.C., Assessment of RELAP5/MOD3.1 for direct-contact condensation in the core makeup tank of the CARR passive reactor, Annals of Nuclear Energy **24** No. 7 (1997) 553–562.
[3.7-28] TIMPERI, A., PÄTTIKANGAS, T., NIEMI, J., Analysis of Loads and Fluid–Structure Interactions in a Condensation Pool, NKS-154, Electronic report, April (2007).
[3.7-29] KANG, H.S., SONG, C.H., CFD analysis for thermal mising in a subcooled water tank under a high steam mass flux discharge condition, Nuclear Engineering and Design **238** (2008) 492–501.
[3.7-30] DAVIS, J., YADIGAROGLU, G., Direct contact condensation in Hiemenz flow boundary layers, International Journal of Heat and Mass Transfer **47** Issues 8–9 (2004) 1863–1875.

3.8. GRAVITY DRIVEN COOLING AND ACCUMULATOR BEHAVIOUR

3.8.1. Introduction

Gravity driven cooling provides emergency core cooling water by gravity draining, in events with loss of coolant. This system requires a large volume of water above the core, plus additional depressurization capacity, so that the primary coolant system can be depressurized to allow for gravity flow from the elevated suppression pool. Since there are no large reactor vessel pipes at or below the core elevation, this design ensures that the core will remain covered by water during all design basis accidents. In general, gravity driven cooling concept is mainly based on the depressurization of the reactor pressure vessel to sufficiently low pressures to enable reflood of the core by gravity feed from an elevated pool. When the gravity driven cooling operates, the gravity drain flow rate to the reactor pressure vessel depends on the piping geometry, the state of the fluid, and the pressure conditions in both the water pool and the reactor pressure vessel. Flow entering the reactor pressure vessel during the later stages of blowdown during a postulated LOCA must be sufficient to keep the nuclear core flooded. The system which provides gravity driven cooling is a simple and economical safety system.

3.8.2. Examples and occurrence of gravity driven cooling and accumulator behaviour

Examples of gravity driven cooling system include the gravity driven cooling system (GDCS) of the Economic Simplified Boiling Water Reactor (ESBWR), and the passive core flooding system (HA-1 hydraulic accumulators of the first stage and HA-2 hydraulic accumulators of the second stage) of the WWER-1000/392. Passive safety systems which are incorporated in AHWR are also discussed.

3.8.2.1. Gravity driven cooling system in ESBWR

In the ESBWR design, the major system to insure core cooling at lower pressures is the Gravity Driven Cooling System (GDCS) which is a passive safety system and uses gravity to inject water into the reactor from the suppression pool (Fig. 3.8-1). The GDCS, in conjunction with the Automatic Depressurization System (ADS), comprises the emergency Core cooling System (ECCS) for the ESBWR. It provides a simple approach to Emergency Core Cooling eliminating the need for pumps or diesels, and does not need short term (three days) operator action. It requires more water in the reactor vessel above the core and additional depressurization capacity, so the reactor can be depressurized to very low pressures and gravity flow from the elevated suppression pool can keep the core covered. The additional water can also reduce pressure rates for transients and substantially more time before the core uncovers in multiple failure scenarios. Because ESBWR is a natural-circulation design, there are no large pipes attached to the vessel near or below core elevation, the design insures full core coverage for all design basis events.

The GDCS consists of an annular pressure suppression pool in the containment located at an elevation above the reactor core. The GDCS suppression pool is passively cooled and connected to the reactor pressure vessel (RPV) by piping and isolated by pyrotechnic-type ECCS injection valves, which open on a low RPV level signal and remain open after initial actuation. During a LOCA, the RPV would be depressurized by the ADS or by the LOCA itself, if it is a large break. Under such a circumstance the gravity head of the GDCS would then provide enough pressure to cause the pyrothecnic-type ECCS injection valves to open and large amounts of water to flow to the core. Because of the relative elevation of the core, suppression pool provides water injection in the long term when water from the GDCS pools is depleted. Once this cooling circuit is established, energy is removed from the core over long times by the passive containment cooling system (PCCS). The PCCS is the name given to passive containment coolers, which are placed in a large water pool, and associated piping that connects the drywell (DW) and wet well (WW) volumes to the coolers for eventual heat transport to the environment. It is designed in such a way that no matter where the fuel may reside (in-vessel or ex-vessel) an energy removal path is provided to the ultimate heat sink. Any steam generated by the blowdown or water evaporation due to the heating would be transported by natural convection upward to the passive containment coolers with the containment atmosphere. It then passes through the PCC condenser tube banks where the steam is condensed and the water condensate drains back to the

GDCS pools and the noncondensible gases are returned to the wet well suppression pool. A plant design using the GDCS feature has the potential to be more economical to design, construct, and operate due to the reduction in safety system equipment and the resulting reduction in supporting systems.

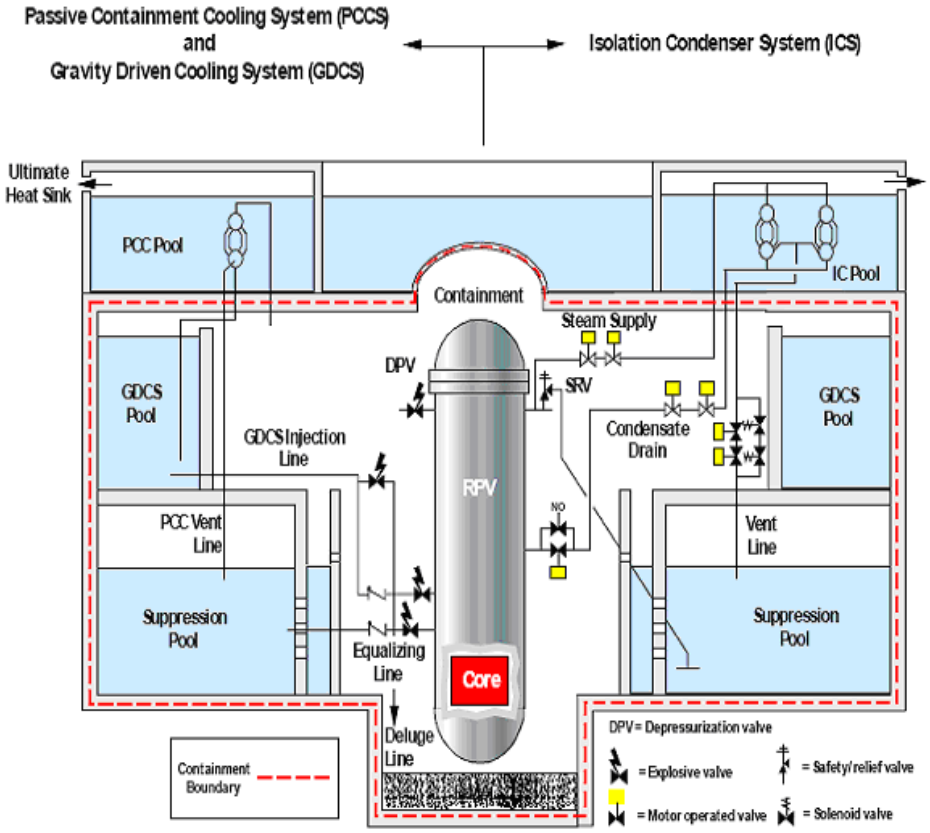

FIG. 3.8-1. ESBWR with its passive safety features.

3.8.2.2. Experimental basis for the gravity driven cooling system

PANDA is a large scale facility (Fig. 3.8-2), which has been constructed at the Paul Scherrer Institute (PSI), Switzerland, for the investigation of both overall dynamic response and the key phenomena of passive containment systems during the long term heat removal phase for Advanced Light Water Reactors (ALWRs). The facility has been configured to simulate the containment of a passive BWR, but the phenomena, which are taking place, are of a more generic character and of interest to LWR containment's in general. Using a modular concept with a basic set of cylindrical vessels (typical diameter 4m) which are interconnected by piping, the facility can be adapted to simulate different passive containment designs. In the PANDA test facility, ISP-42 tests including six different phases were performed. The summary and overview of these tests and selected results of the analysis are given in Section 4.6 of this report. Further details for ISP-42 PANDA tests are available in Refs [3.8-1 and 3.8-2]. The facility configuration used for ISP-42 tests is a scaled down model of the Economic Simplified BWR (ESBWR) containment and safety systems, as summarized in Section 4.6.

In this section, overview and some of the results of the second phase (phase B) of ISP-42 PANDA tests is summarized. This test simulated gravity driven cooling in ESBWR with the objective to investigate the discharge of cold water into a saturated RPV and to observe induced phenomena and the resulting system behaviour.

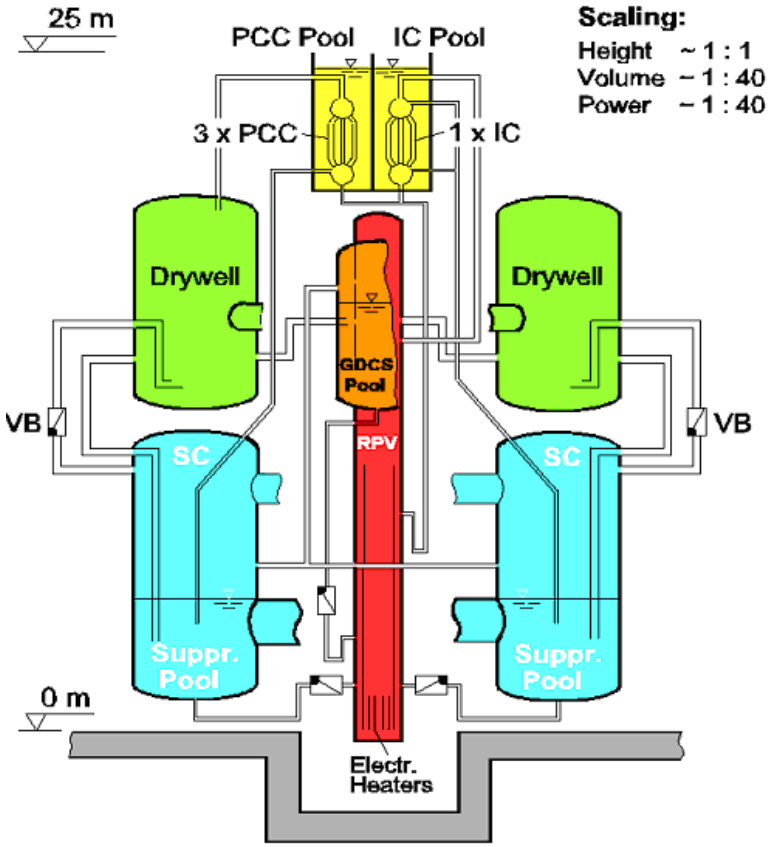

FIG. 3.8-2. Schematic of the PANDA test facility for the ESBWR configuration.

A sketch of the setup used for this test phase is shown in Fig. 3.8-3, which also represents the initial conditions of the test. Included in this sketch are the different initial conditions of the drywell and the wet well vessels as well as the liquid levels in the different vessels. All three PCCs are operational and there is no interconnection between the different PCC pools. The GDCS is filled with water whereas the water level in the RPV is well below the downcomer (DC) entrance/ riser exit. The main vent lines are not operational for this test and, therefore, are not depicted in the scheme. The two drywells were initially filled with steam.

The ISP-42 Phase-B test has been performed as follows:

Turning on the power of the electrical heater rods in RPV marked the time at zero, which was the start of the test. Because the two main steam valves on the connecting lines from RPV to DW1 and DW2 were opened simultaneously, steam was injected into the two drywells and to the PCC primary sides where condensation of the steam started instantaneously. Also the PCC feed valves were opened at 29s to allow startup of the three operational PCCs.

GDCS drain line valve connecting to RPV was opened at 48 s in the experiment. A large amount of cold water immediately flooded the lower part of the RPV, causing a collapse of voids, condensation of steam and suppression of boiling. The water level inside the RPV increased slowly. At the same time and for the following 300 s to 400 s, the three PCCs were filled with air and, consequently, condensation was terminated. This decrease of gas content (steam) in the RPV/drywell gas space resulted in a decrease of the drywell pressure. After the first surge ceased and all the cold water in the GDCS tank had been injected into the RPV, steam flow in the main steam line as well as in the PCC feed lines came to a halt and PCC power stayed low. For the next few thousand seconds, water in the RPV was heated up again until boiling resumed and steam flow in the main steam lines started. PCC primary sides were supplied with steam, initiating PCCs startup and eventually the system reached

stationary conditions again. The experiment was terminated when boiling in the PCC pools resumed. Further details on the description of the ISP-42 Phase-B can be obtained from Refs [3.8-1–3.8-3].

The phenomena which were observed during this phase are:

- Gravity driven cooling system tank discharge. This includes:
  - Subcooled water injection into the downcomer of the RPV
  - Collapse of voids in RPV
  - Wet well depressurization
  - Excess condensation in the system causes drywell pressure to decrease
- Non-condensible gas return from wet well to drywell (due to vacuum breaker openings)
- Resumption of boiling in the RPV
- Passive containment cooler startup

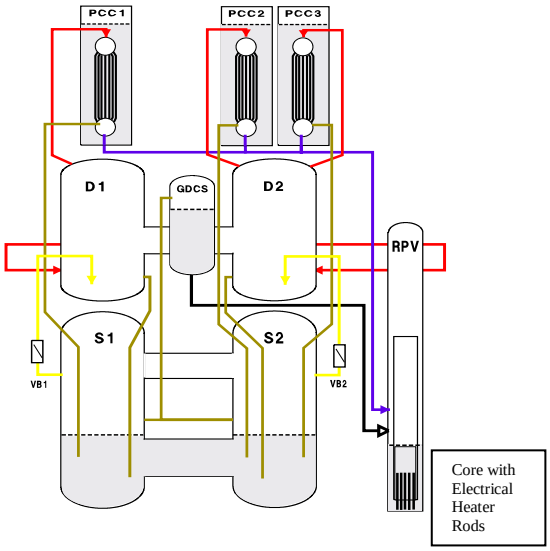

FIG. 3.8-3. ISP-42 Phase B: Gravity driven cooling system tank discharge.

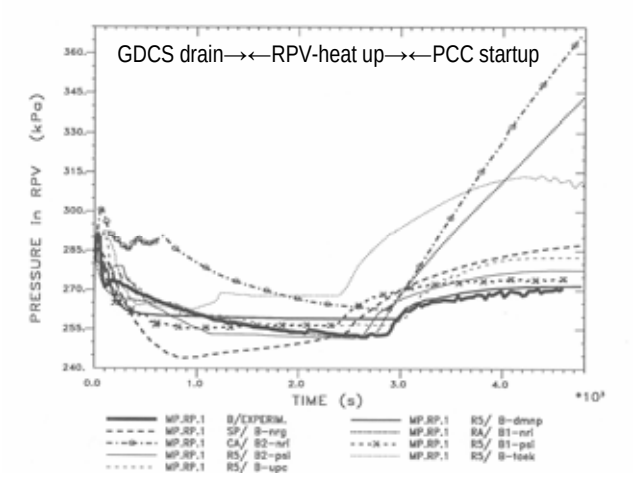

FIG. 3.8-4. Comparison of RPV pressure calculations with experimental data for Phase B of ISP-42.

The time behaviour of the pressures defines the response of the whole system to the specific transient and it is the first item of the phenomena to be investigated as well as the main parameter with respect to safety issues. The time behaviour of the pressure is characterized by a rapid decrease during GDCS drain at the beginning of the transient as a result of the inflow of cold water into the RPV causing collapse of voids and steam condensation in the RPV, as well as the continuing PCC heat removal due to steam condensation (Fig. 3.8-4). Both effects significantly reduced the amount of gas in the gas space of the RPV, drywell and the primary sides of the three PCCs thus reducing the system pressure. This phase is followed by a mild pressure decrease during RPV heat-up for the next 2500 s into the transient until boiling resumed in the RPV and finally an increase of pressure after 3000 s when first steam production in the RPV and later condensation in the PCCs started (PCC startup) (Figs 3.8-8 and 3.8-9). PCC power was nearly zero before PCC startup (Fig. 3.8-10), i.e. the time period between 400 s and 3000 s because the primary sides of the PCCs were filled with air after all the steam was condensed during the first 100 s of the transient and no additional steam was supplied afterwards (main steam line mass flows nearly zero, because of no steam production in the RPV) (Fig. 3.8-5). After GDCS injection by gravity was terminated at about 1260 s, subcooled water in the RPV was heated up to saturation and again started boiling. The increase of system pressure at 3000 s coincided with the start of significant mass flow in the two main steam lines as a result of steam production in the RPV (Fig. 3.8-6).

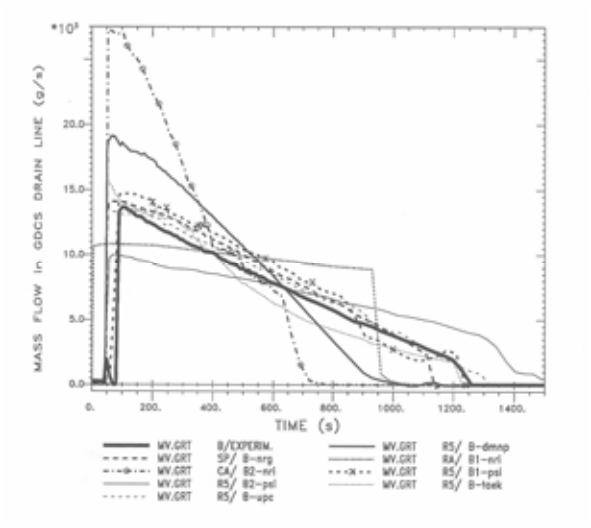

FIG. 3.8-5. Comparison of GDCS drain line mass flow calculations with experimental data for Phase B of ISP-42.

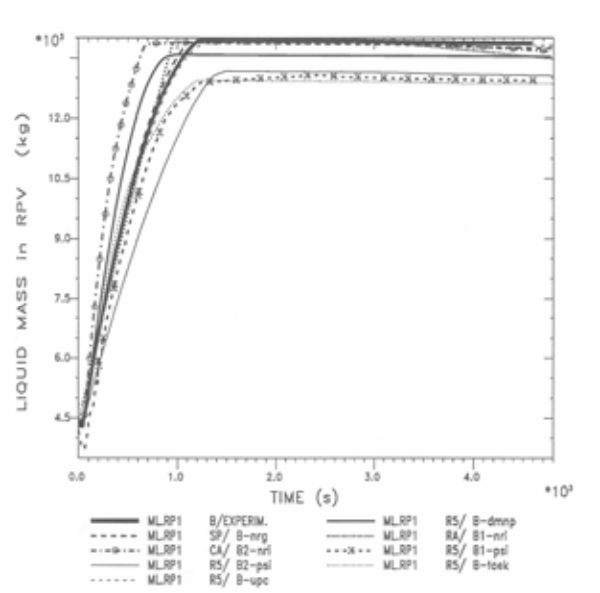

FIG.3.8-6. Comparison of liquid mass in RPV calculations with experimental data for Phase B of ISP-42.

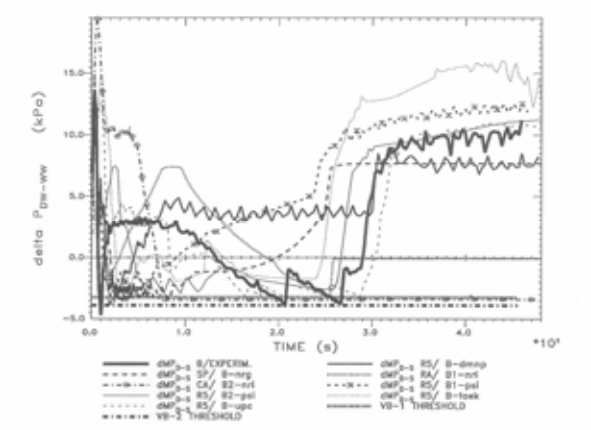

FIG.. 3.8-7. Comparison of pressure difference between drywell and wet well pressures as calculated by different participants and measured for the ISP-42 Phase B.

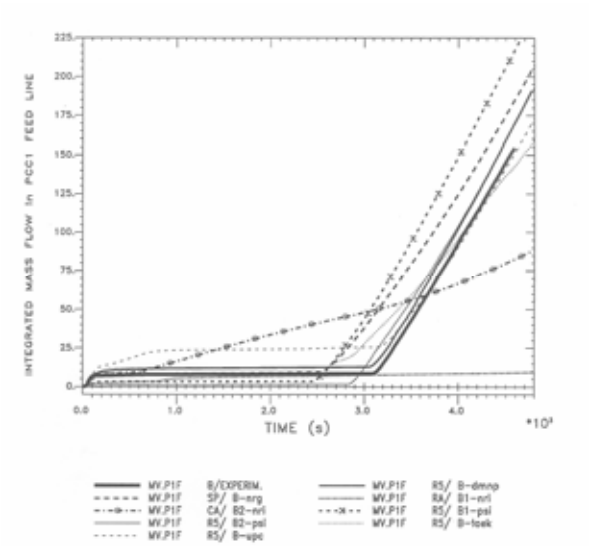

FIG. 3.8-8. Comparison of time integrated PCC-1 feed line mass flow calculations with experimental data for Phase B of ISP-42.

As it can be seen in Fig. 3.8-4, most of the ISP-42 phase-B test participants predicted the correct time behaviour for the system pressure, i.e. a rapid pressure decrease during the first 300 to 400 s of the transient followed by a mild decrease for the next 2500 s and its final increase after 3000 s. Two of the participants predicted a continuous pressurization which has not ended until the end of the simulation time. The calculated results for the GDCS discharge showed differences in the GDCS drain flow and few of the differences in the results are significant and manifest themselves in the decrease of the liquid mass (level) in the GDCS tank, in the increase of the RPV liquid level mass and in the pressure suppression due to condensation in the RPV. SPECTRUM (SP), which is lumped parameter containment code, and RELAP5 (R5), which is a system code and not designed to perform low pressure containment calculations, produced rather good and acceptable results. These results also indicate that the extendibility of the application area for RELAP5 code to this assessment area of gravity driven cooling is viable. The results of the comparison also show that most of the participants

did succeed in predicting vacuum breaker openings within the first 500 s of the transient as in the experiment, but the time of their occurrence and their duration differed considerably (Fig. 3.8-7). The resumption of boiling in the RPV was predicted by most of the participants and this phenomenon manifested itself by a sudden increase in the main steam lines as well as in the PCC feed lines (Fig. 3.8-8). PCC startup, at approximately 3100 s in the transient, and performance was predicted again by most of the participants within an error band of 500 s (Figs 3.8-8 and 3.8-9).

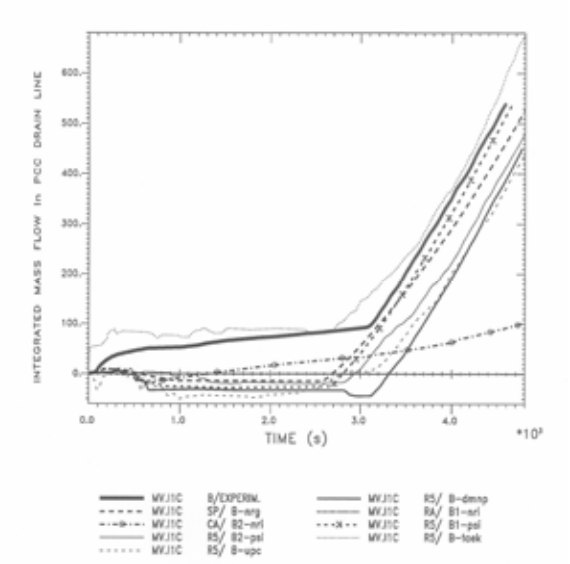

FIG. 3.8-9. Comparison of time integrated PCC drain mass flow calculations with experimental data for Phase B of ISP-42.

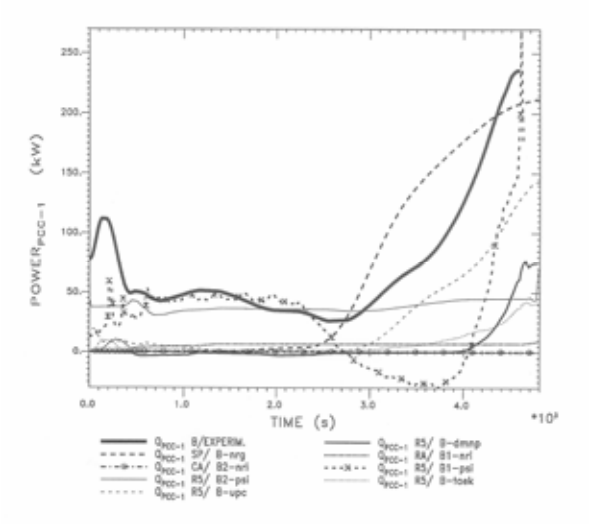

FIG. 3.8.10. Comparison of PCC-1 power calculated from the gradient of the pool mass as calculations and experimental data for Phase B of ISP-42.

3.8.2.3. Gravity driven cooling system in WWER 1000/392

Another example of gravity driven cooling systems is the passive subsystem for reactor core flooding and it is named HA-2 (hydroaccumulators of second stage) in WWER 1000/392. This system is a typical example of gravity driven cooling hydroaccumulator. It has been developed as an additional passive core flooding system. The system is intended for the possibility of providing a long term residual heat removal in case of primary LOCA accompanied by a station blackout. On the first stage of such an accident, the emergency core cooling is provided by traditional hydroaccumulators with nitrogen under pressure (HA-1). When the primary pressure decreases less than 1.5 MPa during the accident, the hydroaccumulators of the second stage are connected to the primary system. The design basis of the HA-2 is the removal of the residual heat at the last stage of a LOCA for at least 24 hours. The systems consist of four channels. The schematic drawing of one channel of the HA-2 system is presented in Fig. 3.8-11.

The upper part of the hydroaccumulators is connected to the cold leg of the primary circuit through special spring-type valves. These valves are intended to be opened when the primary pressure decreases below 1.5 MPa. The HA-2 are connected to the discharge lines of the traditional HA-1 through check valves intended for preventing HA-2 pressure increase and automatically open when the primary pressure decreases below 1.5 MPa.

The development project of the HA-2 was implemented using numerical optimization and was also tested by a number of support experiments.

For investigating the additional core flooding system, a full-scale facility with full scale layout of pipelines was designed and developed [3.8-4]. This facility comprised two tanks simulating the HA-2, which were connected with the help of surge lines by steam and water. Both accumulators were connected to the common collector with four discharge tubes which provided a step-wise variation of the flow rate. Two lower tanks simulating vapour space of inlet and outlet chambers were also connected with the help of surge lines by steam and water. Two series of experiments with cold water and with hot water were performed in this facility.

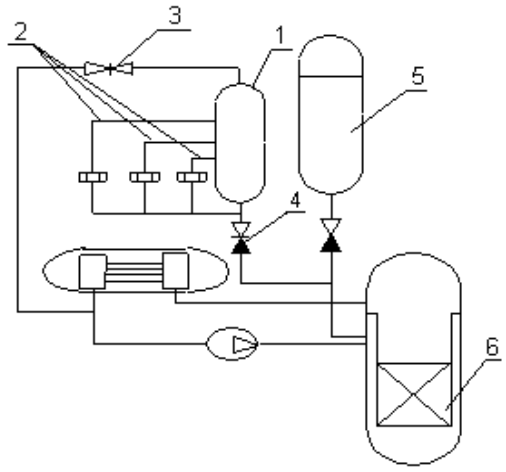

1 - hydroaccumulator of second stage (2 units)
2 - discharge line of HA-2 (with restrictive diaphragms)
3 - spring-type valve
4 - check valve
5 - traditional HA-1
6 - reactor

FIG. 3.8-11. Principle schema of one channel of HA-1 and HA-2.

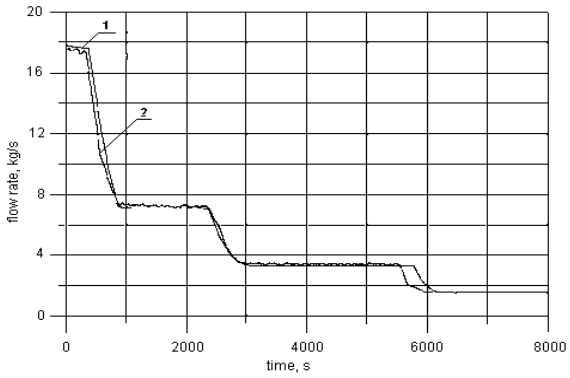

1 - calculation (design flow rate characteristic)
2 - experiment

FIG. 3.8-12. Flow rate characteristic of HA-2 test facility under cold conditions.

Figure 3.8-12 shows the comparison of the calculated design flow rate with the flow rate characteristic of the HA-2 test facility, which was obtained with cold water.

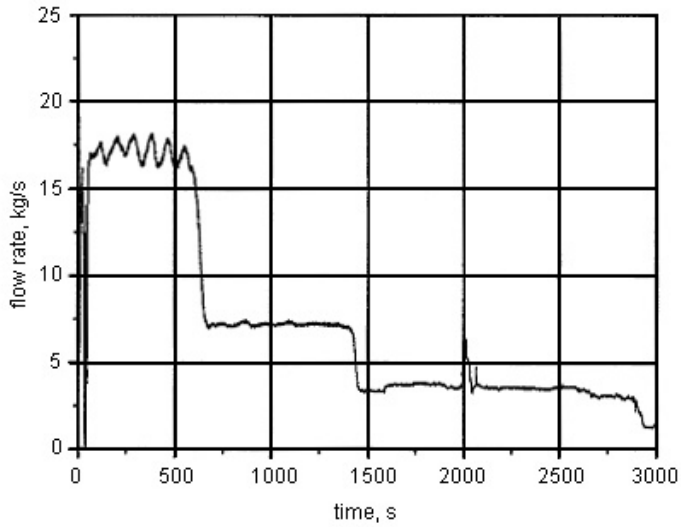

FIG. 3.8-13. Flow rate characteristic with the use of one upper tank.

The purpose of experiments was to adjust the discharge lines and optimize their operation. During these experiments, after some modernization of the test facility and with the use of only one upper tank, an experiment was conducted in which a flow rate with hot water was obtained and the results are presented in Fig. 3.8-13.

From a comparison of Figs 3.8-12 and 3.8-13, it is clearly seen that the test flow characteristic was close to the design characteristic. More details about these experiments can be obtained from Refs [3.8-5 and 3.8-6].

3.8.2.4. Gravity driven cooling system in AHWR

The Advanced Heavy Water Reactor (AHWR) [3.8-7] is a light water cooled and heavy water moderated pressure tube type boiling water reactor. In AHWR, it is proposed to remove the core heat by natural circulation during startup, power raising, normal operation, transients and accidental conditions. AHWR uses several passive concepts with a view to simplify the design and to enhance safety. The following passive systems are incorporated in AHWR

- Advanced accumulator using a fluidic device to inject emergency coolant during the initial stages of LOCA;
- Gravity driven cooling system (GDCS) for uninterrupted core cooling for at least 3 days after the accumulators are exhausted;
- Passive decay heat removal system with isolation condensers.

An integral test facility (Fig. 3.8-14 shows the building housing this facility) simulating main heat transport system (MHTS) and safety systems of AHWR has been set up at BARC, India, to investigate the overall system behaviour under different operating conditions, transients and accidents such as LOCA. In addition to MHTS, the Integral Test Loop (ITL) simulates the ECCS, Isolation Condenser (IC) system and GDCS of AHWR (Fig. 3.8-15). One of the objectives of this facility is to generate a database for the performance evaluation of the GDCS in the plant environment, in addition to other transient and accident aspects.

The ECCS in the AHWR essentially consists of the advanced accumulator and the GDCS which is designed to provide long term core cooling for 72 hours after a reactor trip following the occurrence of LOCA. The operation of the GDCS depends solely on the system pressure. In the event of any depressurization in the PHT system, water enters the core under gravity. The system consists mainly of a water pool known as gravity driven water pool (GDWP) and associated piping and components.

The GDWP in the ITL is scaled down by a factor 452, which results in a volume of 14.705 m3. Due to elevation constraints in the existing building, it is not possible to locate the GDWP at the same elevation as in the prototype. Hence, the GDWP is pressurized by nitrogen gas to compensate for the lower relative elevation in ITL. In addition, due to space constraints, the GDWP volume is sufficient to represent less than 24 hours instead of 72 hours. Some details of the scaling studies for the ITL facility in relation to AHWR can be found in Section 4.3 of this report and also in Ref. [3.8-9].

The first initial tests, which were performed in this facility during 2008, were the steady state and stability tests. Future tests in ITL facility will also include investigations on the GDCS behaviour. The steady state and stability performance has been predicted for the facility as well as the prototype reactor. The steady state data generated in the loop are in good agreement with the predictions of the in-house developed generalized correlation which is included in TINFLO-S code [3.8-8] and [3.8-9] as well as computer codes like RELAP5/MOD3.2. The stability data obtained also showed good agreement with the predictions of the in-house developed stability code. In addition, test data on the proposed startup procedure has been presented along with simulations using the RELAP5/MOD3.2 code. The code is found to reproduce all the essential trends of the observed transients. For further details, see Section 4.3 of this report.

FIG. 3.8-14. Photograph of ITL building.

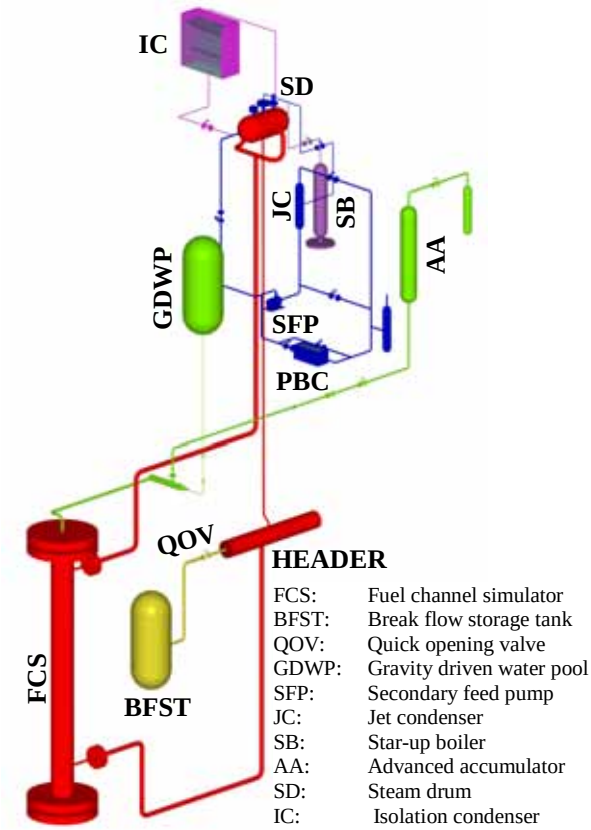

FIG. 3.8-15. 3-D view of ITL.

LIST OF ABBREVIATIONS

ADS	Automatic depressurization system
AHWR	Advanced heavy water reactor
ALWR	Advanced light water reactor
BARC	Bhabha Atomic Research Centre
BWR	Boiling water reactor
CA	CATHARE 2 Thermal-H-hydraulics system code
DC	Down-comer
DW	Drywell
ECCS	Emergency core cooling system
ESBWR	European simplified boiling water reactor
GDCS	Gravity driven cooling system
GDWP	Gravity driven water pool
HA-1	Hydraulic accumulator 1st Stage
HA-2	Hydraulic accumulator 2nd Stage
ITL	Integral test loop
IC	Isolation condenser
ISP	International standard problem
LOCA	Loss of coolant accident
LWR	Light water reactor
MHTS	Main heat transport system

MVL	Main vent line
NEA	Nuclear Energy Agency
OECD	Organization for Economic Cooperation and Development
PANDA	Passive Nachwärmeabfuhr- und Druckabbau-Testanlage (Passive decay heat removal and depressurization test facility)
PCC	Passive containment cooling
PCCS	Passive containment cooling system
PHT	Primary heat transport
PSI	Paul Scherrer Institut
R5	RELAP5/Mod3 Thermohydraulics system code
RA	RALOC/Mod4.0 Containment code for design basis and severe accidents
RPV	Reactor pressure vessel
SP	SPECTRUM Lump parameter containment code
VB	Vacuum breaker
WW	Wet well
WWER	Water cooled water-moderated energy reactor

REFERENCES FOR SECTION 3.8

[3.8-1] AKSAN, N., LUEBBESMEYER, D., ISP-42 PANDA tests: behaviour of passive containment systems during the long-term heat removal phase in advanced light water reactors; blind phase comparison report, OECD/NEA Report NEA/CSNI/R(2003) 6, May (2003) CD-ROM.

[3.8-2] AKSAN, N., LUEBBESMEYER, D., ISP-42 PANDA tests: behaviour of passive containment systems during the long-term heat removal phase in advanced light water reactors; open phase comparison report, OECD/NEA Report NEA/CSNI/R(2003) 7, May (2003) CD-ROM.

[3.8-3] AKSAN, N., "Gravity Driven Cooling in ISP-42 (PANDA) Phase-B", 2nd Research Coordination Meeting (RCM) of the Coordinated Research Program (CRP) on Natural Circulation Phenomena, Modelling, and Reliability of Passive Systems that Utilize Natural Circulation, Corvalis, Oregon, USA, August 29–September 2, 2005 (2005) CD-ROM.

[3.8-4] EFANOV, A.D., et al., "Large scale full-level thermal-hydraulic facility GE-2M to study joint operation of safety passive systems in WWER-1000 reactor plant", collection of papers of the 3rd Scientific and Technical Conference on Safety Assurance of NPP with WWER, Podolsk, Russia, May 26–30, 2003 (2003) CD-ROM.

[3.8-5] BERKOVICH, V.M., et al., "Experimental justification of hydraulic accumulator-2 system and optimization of hydraulic accumulators technological scheme", collection of papers of the 3rd Scientific and Technical Conference on "Safety Assurance of NPP with WWER". Podolsk, Russia, May 26–30, 2003 (2003) CD-ROM.

[3.8-6] EFANOV, A.D., et al., "Substantiation of design function of the 2nd step passive flooding system on large-scale facility", collection of papers of the 2nd Scientific and Technical Conference on "Safety Assurance of NPP with WWER". Podolsk, Russia, November 19–23, 2001 (2001) CD-ROM.

[3.8-7] SINHA, R.K., KAKODKAR, A., Advanced heavy water reactor, INS NEWS **15** Nos. 2–4 (2002) **16**, No.1 (2003).

[3.8-8] NAYAK, A.K., VIJAYAN, P.K., SAHA, D., VENKAT, RAJ, V., ARITOMI, M., Linear analysis of thermodynamic instabilities of the advanced heavy water reactor (AHWR), J. Nucl. Sci. Tech. **35** (1998) 768–778.

[3.8-9] SAHA, D., "Integral system tests in ITL simulating AHWR", 5th Research Coordination Meeting (RCM) of the Coordinated Research Project (CRP) on Natural Circulation Phenomena, Modelling, and Reliability of Passive Systems that Utilize Natural Circulation, Vienna, Austria, November 3–6, 2008 (2008) CD-ROM.

3.9. LIQUID TEMPERATURE STRATIFICATION

This section will provide an overview of the current understanding for experimentation, analytical models, and computational models with regard to the subject of natural circulation focusing on liquid temperature stratification experienced in the lower plenum, downcomer and horizontal/vertical piping.

3.9.1. Experimental data and facilities

Extensive research has been conducted in order to visualize and model the phenomenon of thermal stratification. Thermal stratification represents a significant concern for all water cooled reactors due to subsequent "slug" development as well as the consequences of thermal stresses on reactor components. In the event that a slug is formed the integrity of all pipes, valves, pumps and plant components involved is significantly compromised. Research to date has been an international effort. The following section outlines the most recent research regarding thermal stratification in both operating water cooled reactors and laboratory studies.

In 1985, Miksch, Lenz, and Lohberg [3.9-1] published results of testing investigating the formation of cracks on internal surfaces of horizontal piping. Research was performed at Kraftwerk Union AG in Erlangen, Germany. Cracking was occurring in a number of pressurized and boiling water reactors (PWR and BWR, respectively) in feedwater piping upstream of the steam generators and reactor pressure vessels. It had been observed in operating PWR and BWR plants, as well as laboratory studies, that slight fluctuations in flow rate cause separating layers to be raised and lowered. The phenomenon has been attributed to the density differences resulting from a temperature difference of the working fluid. Only slight flow resistances must be overcome in order for thermal stratification to occur. A minimum layer height of approximately 10% of the pipe's diameter is necessary. The stratified flow changes into "slug-flow" at approximately 6% of the full-load flow. Preceding this transformation the layer height reaches approximately 90% of the pipe's diameter. Pipe loadings from stratified flow cause increased overall bending stresses and create local stresses in the pipe cross section due to a non-linear circumferential metal temperature distribution. Further research led to the conclusion that thermal stratification causes a stress distribution in the pipe which is comparable to a bimetallic strip. In the hot upper region compressive stresses (membrane stresses in the axial direction) develop as a result of constrained expansion. The flexible nature of the piping gives rise to a bending stress which is superimposed on the membrane stresses. Results indicated that cracks formed as a result of cyclic stressing in the axial direction due to thermal stratification.

3.9.1.1. Overview of experiments conducted at the Young Gwang nuclear power plant

The Young Gwang Nuclear Power Plant (YGN) is an operating light water reactor (LWR) located in Korea. Research was conducted in the 1990's and findings were published in 1997. The brief description below has been assembled using the published findings of Yu, Park, Sohn and Bak [3.9-2].

Experiments were limited to the surge line connecting the pressurizer and one hot leg. The surge line runs primarily horizontally with vertical runs to the bottom of the pressurizer and top of the hot leg. The surge line is a 12-in schedule 160 (SA312 TP347) stainless steel pipe. Surge line temperature and displacement measurements were taken as the plant progressed through heat-up and cooldown. Thermocouples were placed at nine positions along the surge line piping, five were placed axially (designated A1–A5) and four were placed circumferentially (B1–B4). A schematic of the thermocouple placement along the surge line can be seen in Fig. 3.9-1.

The YGN test data indicate that the flow becomes stratified early during heat-up and remains stratified up to and including all operating conditions. All significant temperature differentials could be attributed to changes within the pressurizer; these changes are the result of normal plant operation. Top to bottom temperature difference and the resulting differential thermal expansion between the top and bottom of the pipe cross section induce overall bending moments and deflections in the surge line. Experimental data revealed that vertical thermal displacements due to stratified flow are directly related to the top-to–bottom temperature differentials. Using experimental data, an analytical heat

transfer model with various fluid conditions was developed in order to simulate the stratified flow condition. This model is discussed in Section 3.9.2.1.

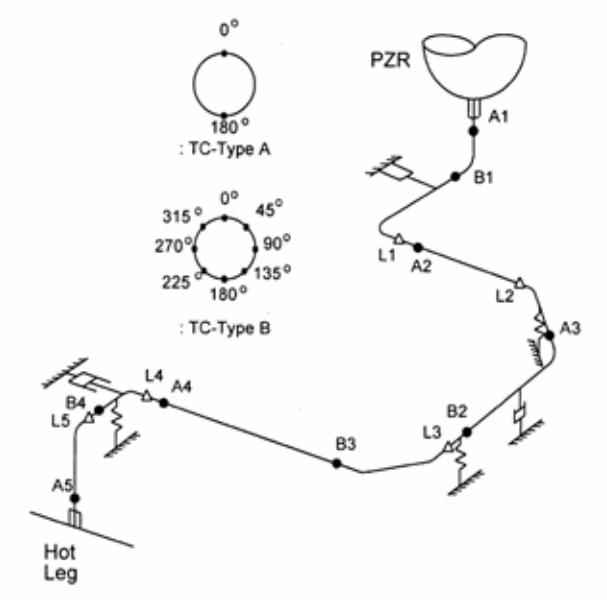

FIG. 3.9-1. Type A and B thermocouple placement along the surge line of the Young Gwangnuclear power plant [3.9-2].

3.9.1.2. Experiments conducted at Idaho State University

Research conducted at Idaho State University's (ISU) Thermal Fluids Laboratory was initiated in 2006 and is currently ongoing [3.9-3]. A schematic diagram of the test facility is shown in Fig. 3.9-2. The focus of this research is an evaluation of the Generation III Westinghouse AP600 advanced light water reactor performance during a loss of coolant accident. Passive emergency core cooling systems (ECCS) operate in a much different manner than their pump-driven counter parts. Flow in AP600 is driven by density gradients and the passive ECCS are designed to inject over a prolonged period of time using gravitational forces as the driving head to keep the core covered and cool.

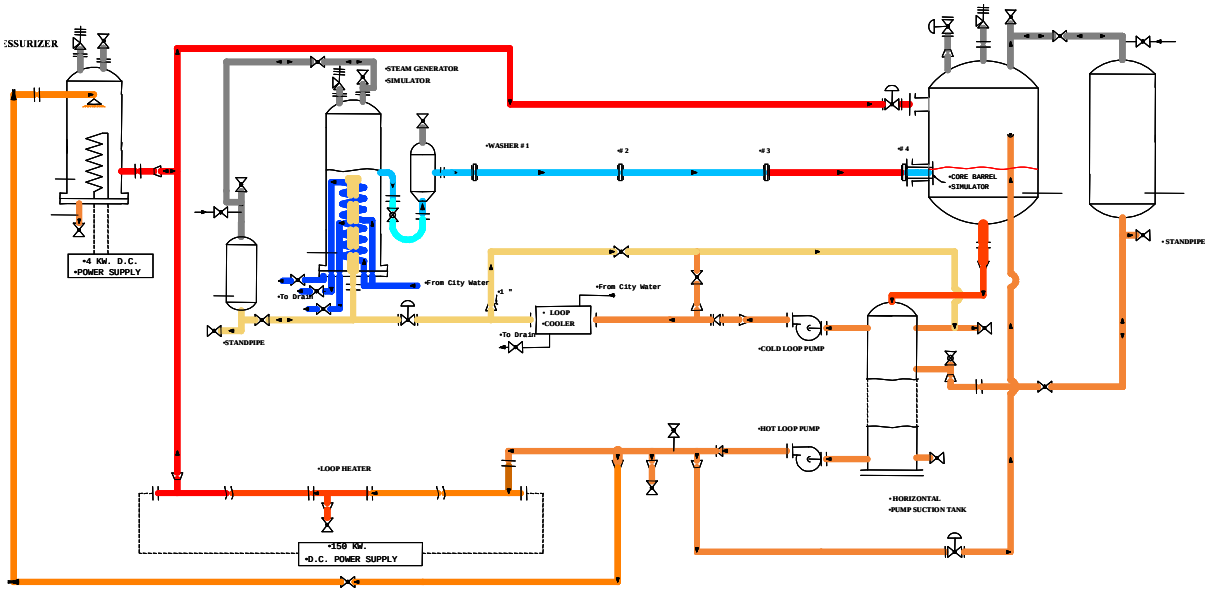

FIG. 3.9-2. Schematic diagram of the ISU steam-water two phase flow loop.

When passive ECCS injection begins, highly subcooled water enters horizontal piping and stratified flows of water with a density variation across the depth may occur. Because of the density variations, there are several flow features that are unseen in non-stratified single phase flows or even shallow steam over saturated water two phase flows. Research conducted at the ROSA-AP600 (Japan Atomic Energy Research Institute) have shown the formation of a stationary wedge, the intrusion of a heavier liquid from below, and the intrusion of a lighter liquid from above in the cold leg of a Generation III system with passive cooling for SBLOCAs.

An integral component of passive ECCS are horizontal pipe runs (usually the cold legs) either fully filled (Case I, see Fig. 3.9-3a) or partially-filled (Case II, see Fig. 3.9-3b) with stratified water. Generally the water used in the ECCS is at room-temperature, while the reactor vessel water inventory is often near plant operational temperatures. Due to this temperature difference interactions between high temperature saturated water, saturated steam, and highly subcooled water are virtually guaranteed. Whether the liquid behaviour is Case I or Case II is dependent on a number of variables including the conditions downstream of the horizontal pipe run (in the reactor downcomer) and the passive system flow rate. Generally speaking, if the downcomer water level is above the top of the horizontal pipe section and if the passive system flow is not critical (Froude number = 1) at the pipe exit, then the stratified flow condition shown in Fig. 3.9-3a occurs. On the other hand, if the downcomer water level is within the diameter of the cold leg, but above the ECCS flow stream free surface in the cold leg, then Case II condition occurs (Fig. 3.9-3b).

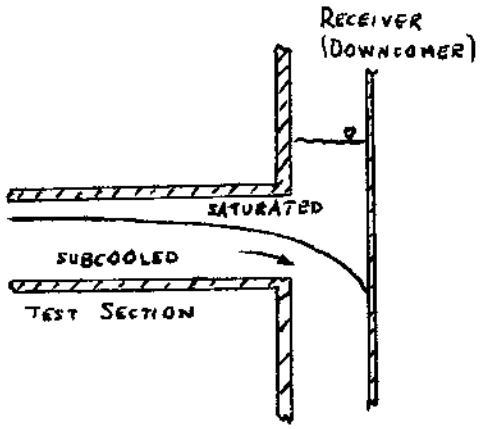

FIG. 3.9-3a. Case I, Downcomer water level above cold leg.

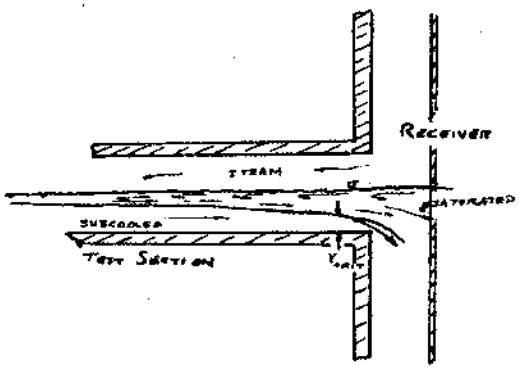

FIG.3.9-3b Case II Downcomer water level inside cold leg.

Potential problems associated with Case I and Case II flow behaviour are:

a. Very large temperature gradients will be present as measured in the ROSA-AP600 experiments [3.9-4]. The temperature gradients may easily exceed 200 K (gradients as large as 250 K have been measured) and thus lead to conditions that are conducive to thermal shock.

b. The Case II conditions, for large subcooling, are the precursors for condensation-induced water hammer (CIWH) events that may cause unexpected structural damage to the reactor system pressure boundary. Indeed, condensation induced water hammer was experienced during the ROSA-AP600 experiments and the APEX experiments.

Being able to accurately calculate the behaviour of the horizontally-stratified flow from passive ECCS is quite important because:

a. The injection flow rate determines the behaviour of the cold water plumes that move into the downcomer and provide cooling to the core. The movement and mixing of the cold water plumes determine whether the core is uniformly cooled or has preferential cooling at selected locations inside the core shroud. The geometry and dynamics of the pipe flow vis-à-vis the downcomer water level, with its saturated interface, are instrumental in defining the characteristics of the plume behaviour.

b. Thermal gradients, imposed on the reactor system pressure boundary under various accident conditions, should be minimized.

c. The quantity of free-surface area corresponding to subcooled water will determine, in part, the importance of CIWH to the reactor design.

Further research of CIWH was conducted using Idaho State University's test facilities. CIWH was observed within a horizontal section of the test facility; this section of the facility can be observed in Fig. 3.9-4.

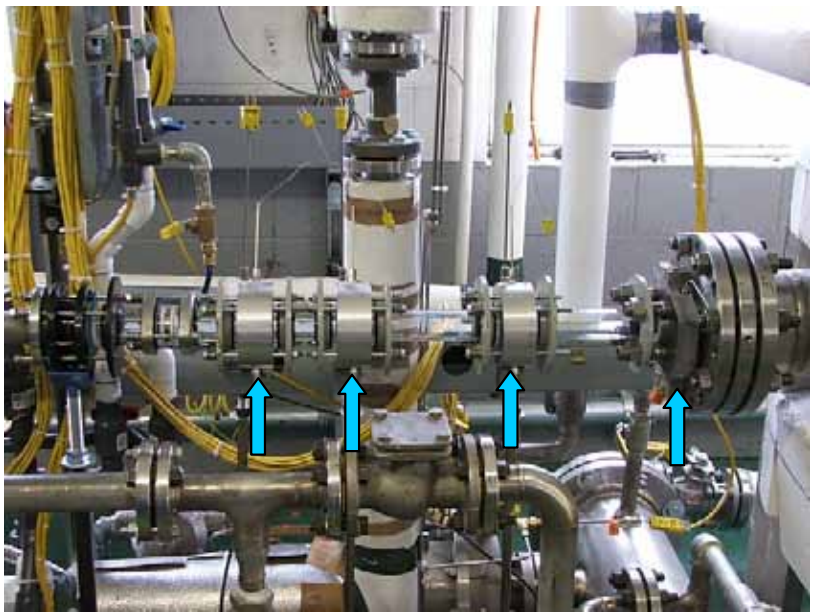

FIG.3.9-4. Photograph of the glass test section installed in the ISU two phase flow loop. Arrows indicate the location of the instrumented washers.

ISU researchers have found that the following conditions are required in order to initiate CIWH. Initially, steam overlaying a subcooled liquid forms the stratified layer. Both the steam and subcooled liquid have the ability to move in a concurrent or current direction relative to one another. A wave is then formed. This wave bridges the area between the steam–liquid interface and the top of the pipe. This wave acts as a barrier, preventing additional steam from moving and isolating it from the rest of the system. Rapid condensation of the trapped bubble occurs. The bubble becomes a void at steam vapour pressure. In response to the pressure gradient the plug begins to move with increasing mass. The acceleration of this plug, combined with its increasing mass, forms a slug. The slug will strike whatever barrier is in its path. When the slug abruptly comes to a halt a pressure pulse is created and begins to move through the system at the speed of sound of the fluid medium. Peak pressures and impact forces can be modelled analytically and have been reviewed at length [3.9-5]. Figure 3.9-5 shows the formation of the slug.

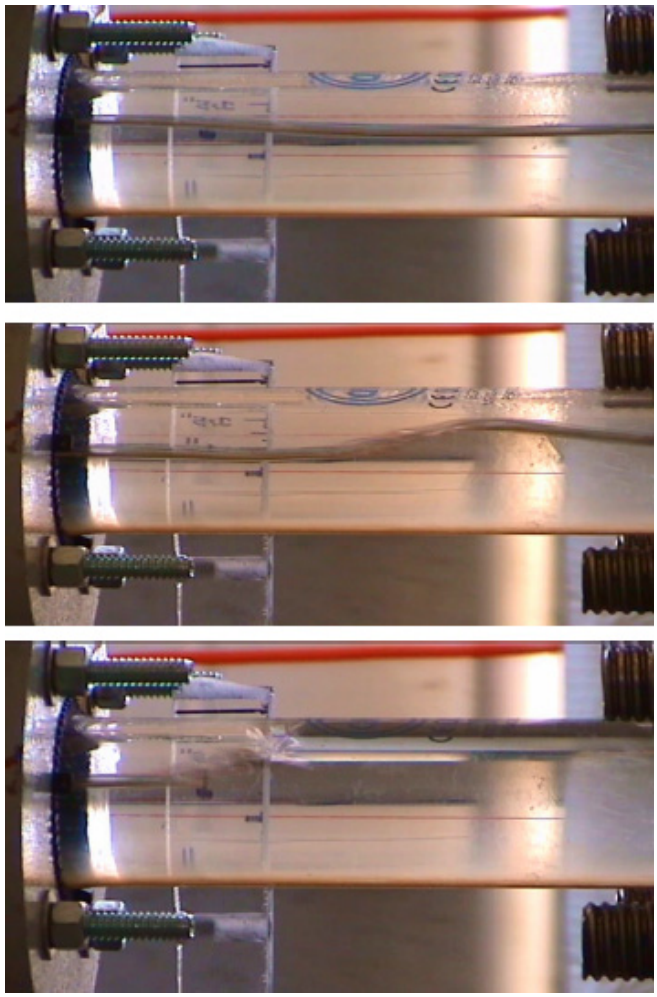

FIG.3.9-5. Pictures taken of the slug formation as it occurs in ISU's two phase flow loop.

3.9.1.3. Experiments conducted at the OSU APEX test facility

Extensive research has also been conducted at the APEX facility operated by Oregon State University. The OSU APEX Test Facility was constructed to model the Westinghouse AP600. It is a ¼-scale facility and includes the entire primary system and the passive safety systems including the residual natural circulation systems (RNCS). The incorporation of these elements has made the APEX facility one of the most useful in observing and modelling thermal stratification. A schematic of the APEX facility can be seen in Fig. 3.9-6.

The motivation for the studies conducted at the APEX facilities was centred around concern regarding Pressurized Thermal Shock (PTS). In the event of an emergency resulting in a significant loss in system pressure, cold water is injected into the system via the cold legs. If the flow rate in the primary legs is significant, the cold injected fluid will mix thoroughly with the hot water in the primary loop. However, at low flow rates, the cold injected water will stratify in the loops and form cold plumes in the downcomer. This situation could result in a "through wall" crack in the event that a pre-existing deformation in the vessel interacts with the cold plume for an extended period of time [3.9-7].

By simulating a SBLOCA thermal stratification was observed in the cold legs and downcomer. In the event of a SBLOCA cold water used for emergency cooling is injected into an operating (heated) system. Within the APEX facility, cooling water is injected into the steam generator lower plenum. This type of emergency core cooling is intended to model the passive cooling systems proposed in advanced light water reactor designs [3.9-7].

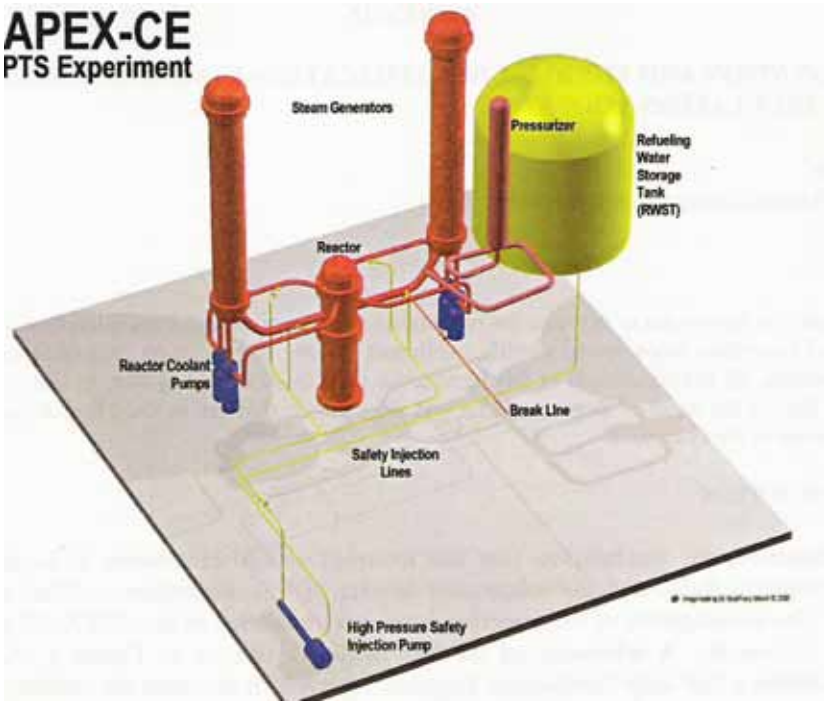

FIG. 3.9-6. Schematic diagram of the APEX test facility at Oregon State University [3.9-6].

Using analytical models discussed in Section 3.9.2.2, flow rates that would induce thermal stratification were quantified. This model did accurately calculate the flow rate necessary to observe stratification in the APEX facility. During a SBLOCA it was observed that the temperature in the lower downcomer steadily decreases throughout the LOCA, while the temperature in the upper downcomer quickly becomes saturated. Eventually vapour fills the upper downcomer and saturated steam is drawn into the cold leg. This marks the onset of thermal stratification in the cold legs [3.9-6].

3.9.1.4. Experiments conducted at the University of Idaho

Testing was conducted using an instrumented air-water-brine flow test loop. The test loop has a 38.1 mm (1.5 inch) internal diameter pipe attached to a 143 mm (45 inch) long clear glass pipe which connects the left-side reservoir the right-side reservoir (see Fig. 3.9-7). The pipe is aligned horizontally by adjusting the screw-footings of the reservoirs. The left reservoir is open to the atmosphere. The right reservoir has a lid. Pressurized air can be introduced into the air space to create air flow countercurrent to the brine flow. Prior to a test, the reservoirs are filled with water and brine in a layered-cake fashion with the brine at the bottom. The volume ratio between brine and water is about 30 to 1. The water is coloured with food dye so the brine–water interface is visible. At a stagnant condition the brine–water interface is slightly above the centre line of the pipe and the water–air interface is slightly below the crown of the pipe.

During tests, brine is pumped out from the bottom of the right reservoir and discharged to the bottom of the left reservoir. The pump is shown in the foreground of Fig. 3.9-7. This pumping action sets up a head differential that drives the brine at the surface of the left reservoir to the right reservoir via the pipe. The brine flow rate is adjustable by a regulating valve so that a wedge of water with various lengths forms in the pipe. The volumetric brine flow rate is measured by a Venturi meter. The length of the wedge is measured within 25 mm (1 inch). This seemly large uncertainty is caused by two difficulties. First, the thickness of the leading edge of the wedge is too thin and hence the colouring is too faint to discern the “water’s edge”. Secondly, due to non-uniform transverse velocity distribution

of the brine across the interface and surface tension between water and pipe wall, the “water’s edge” is V-shaped. The bottom of the V was taken as the “leading edge” of the wedge.

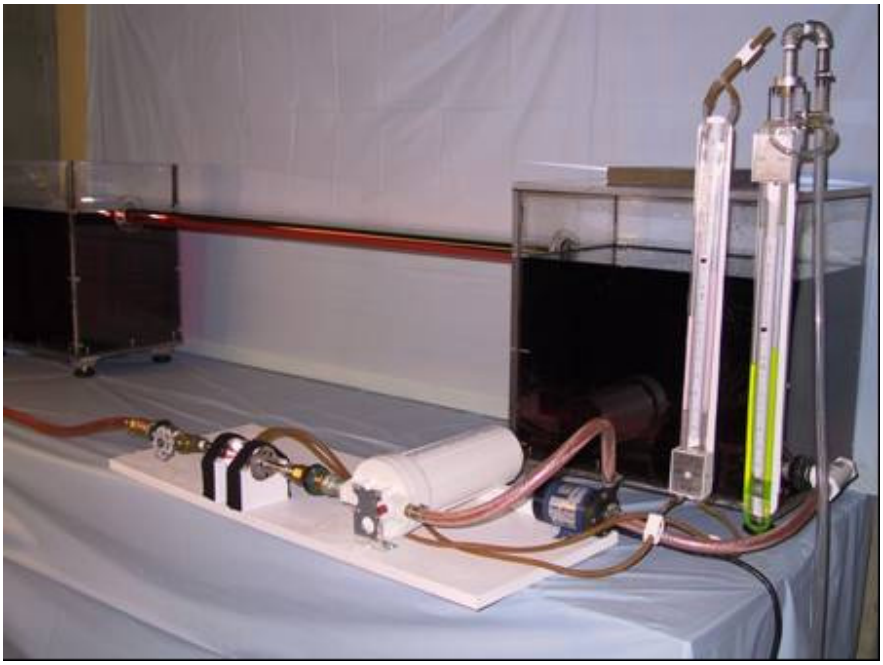

FIG. 3.9-7. University of Idaho portable air-water-brine system that demonstrates stratified flows.

Because water and brine are miscible, partial mixing occurred in the right reservoir during tests. This caused the mass density of the water to increase over time. At the beginning of each test, the specific weight of water was determined from the weight of a fixed volume (300 cc) of water collected at the surface of the right reservoir. Weights were measured by a balance with a resolution of 0.1 gram. The uncertainty in the calculated specific weight is estimated to be less than 0.05%.

The photographs shown in Fig. 3.9-8 were taken during a test and one can clearly see the stratified flow.

FIG. 3.9-8. Pictures of the stationary wedge (fresh water dyed red) overlying brine flow(clear).

3.9.1.5. Experiments conducted at the large scale test facility

The large scale test facility (LSTF) is operated by the Japan Atomic Energy Research Institute [3.9-4]. It was modified to simulate the Westinghouse AP600 and to provide data for comparison to the OSU APEX test facility [3.9-6]. The LSTF is more commonly known as the ROSA facility. The ROSA configuration has been used to study the thermohydraulics of advanced reactor systems under various conditions following a scram. While conducting research at the LSTF, thermal stratification and subsequent wedge formation were experienced. This phenomenon was experienced in a loop void of a heat exchanger when warm liquid moving from the steam generator U-tubes met with colder liquid in the downcommer. Thermal stratification was also seen in the loop containing a heat exchanger. Wedge formation was formed under the following condition: water from the U-tubes mixed with the discharge from the heat exchanger. In both loops, warm water flowed in the countercurrent direction to cold liquid to form stratified flow systems. The stratified flow pattern was stable and little mixing occurred.

3.9.1.6. Experiments conducted at the Imatran Voima Oy (IVO) test facility

Tests examining downcomer plume behaviour were obtained from the 2/5 scale, multiloop, transparent test facility [3.9-8] at Imatran Voima Oy (IVO) located in Helsinki, Finland. Fig. 3.9-9 presents two snapshot of IVO Test #2 showing plume penetration into the downcomer and the resulting thermal stratification. Dense high pressure injection fluid flows through the cold leg while the loop on the right experiences a flow rate 10 times greater.

FIG. 3.9-9. Photographs of the IVO transparent test loop [3.9-8].

3.9.2. Empirical approach

Several empirical models have been developed and validated using the research conducted by the facilities discussed in the "*Experimental Data and Facilities*" section (Section 3.9.1). These models are briefly discussed in the following section. The reader is encouraged to examine the reference material for more details. Table 3.9-1 provides a summary of the analytical models presented in this section.

TABLE 3.9-1. FACILITIES WHOSE RESEARCH UTILIZED ANALYTICAL MODELS

Test Facility	Affiliation	Location	Year	Reference
Young Gwang	Korea Atomic Energy Institute	South Korea	1997	[3.9-2]
APEX	Oregon State University	United States	2007	[3.9-6, 3.9-7]
LSTF/ROSA	Japan Atomic Energy Research Institute	Japan	1995	[3.9-4]

3.9.2.1. Empirical models developed at the Young Gwang nuclear power plant

Research conducted by Yu, Park, Sohn and Bak using the Young Gwang Nuclear Power Plant (previously discussed in Section 3.9.1.1) resulted in the following empirical model. As previously stated, stratified flow was defined by hot fluid in the upper portion of the pipe and cold fluid in the lower half with a sharp interface between them. During an outsurge (flow moving from the pressurizer to the hot leg) it was assumed that the upper (hotter) fluid is moving and the lower (colder) layer was stationary. The opposite flow regime was assumed for an insurge. For the moving layer, the Reynolds number (Re) was calculated based on the expected flow rate; the value of Re dictated whether or not the flow was laminar or turbulent, and hence the corresponding relationship for the Nusselt number (Nu). For laminar flow (Re < 2300), the relationship for Nu is given by:

$$Nu = 3.6 \tag{3.9-1}$$

For turbulent flow (Re > 2300), the classical Dittus-Boelter equation was used to calculate Nu:

$$Nu = 0.23 \cdot \mathrm{Re}^{0.8} \cdot \mathrm{Pr}^{0.33} \tag{3.9-2}$$

where Pr is the Prandtl number. For the stationary layer, it was assumed that the flow was laminar. The average heat transfer coefficients ($\overline{h}$) on the inside of the pipe were then calculated from the standard relationship involving Nusselt number, thermal conductivity of the fluid (k), and the pipe's hydraulic diameter (D_h):

$$\overline{h} = \frac{Nu \cdot k}{D_h} \tag{3.9-3}$$

The Reynolds number was calculated based on half of the fluid in the piping having the measured flow rate and the other half of the fluid being stationary. The properties of each fluid were taken at their respective temperatures and were considered to be saturated water.

A heat transfer analysis was performed to calculate the pipe wall temperature distributions for selected time points during heat up and cool down. The surge line was assumed to be uninsulated and accommodations were made to account for the radiation and natural convection effects experienced on the outer surface of the pipe. To account for the radiation heat loss from the pipe, the standard linearized radiation heat flux (q_r) equation was used:

$$q_r = h_r (T_2 - T_1) \tag{3.9-4}$$

where h_r was the radiation heat transfer coefficient, T_2 was the outside surface temperature of the pipe, and T_1 was the free stream air temperature. The value for h_r was found from the relationship:

$$h_r = \varepsilon \cdot \sigma (T_2^2 + T_1^2)(T_2 + T_1) \tag{3.9-5}$$

where ε was the emissivity of the outer pipe surface and σ was the Stefan-Boltzmann constant, given as:

$$\sigma = 5.67x10^{-8} \quad \frac{W}{m^2 \cdot K} \tag{3.9-6}$$

For the influence of natural convection heat losses outside of the pipe, the Grashof number (Gr) was found from:

$$Gr = \frac{g\beta(T_2 - T_1)D^3}{\nu^2} \tag{3.9-7}$$

where g was the acceleration of gravity (9.81 m/s^2), β was the volumetric coefficient of thermal expansion of the fluid medium (often given as the inverse of the absolute temperature for an ideal gas), D was the outside diameter of the pipe, and ν was the kinematic viscosity of the fluid.

In natural convection, the Grashof number is used in conjunction with the Prandtl number, instead of the Reynolds number, to calculate the Nusselt number value (shown in the following equation):

$$Nu = 0.14 \cdot (Gr \cdot \mathrm{Pr})^{1/3} \tag{3.9-8}$$

where the product of Gr·Pr must meet the following criteria:

$$6.52x10^7 < Gr \cdot \mathrm{Pr} < 3x10^{10} \tag{3.9-9}$$

The natural convection heat transfer coefficient (h_c) can then be found from Eq. 3.9-3. The combined heat transfer coefficient, including both natural convection and radiation, was then found from the relationship:

$$h = h_c + h_r \tag{3.9-10}$$

The emissivity for the surge line pipe was assumed to be 0.6 and the ambient air temperature was assumed to be 38 °C (100 °F). A comparison of calculated circumferential temperature distributions to measured values indicated that the circumferential temperature distributions due to stratified flow were conservatively predicted using the thermohydraulic model developed.

3.9.2.2. Empirical models developed at OSU's APEX facility

The onset of thermal stratification in the horizontal cold legs was accurately predicted using the equations given below. The correlations shown were developed by Theofanous [3.9-8]. The subscript "*HPI*" refers to *high pressure injection* and the subscript "*CL*" refers to the *cold leg*. This method was based on analysis performed only at the cold leg exit and can therefore be applied with equal validity by substituting the primary residual heat removal system with the HPI used with these equations. The boundary for onset of stratification was expressed by:

$$Fr_{HPI/CL} = \left\{1 + \frac{Q_{CL}}{Q_{HPI}}\right\}^{-7/5} \tag{3.9-11}$$

where Q_{CL} was the volumetric flow rate through a cold leg, Q_{HPI} was the volumetric flow rate through a single injection nozzle, and $Fr_{HPI/CL}$ was a modified superficial Froude number defined in the cold legs by:

$$Fr_{HPI/CL} = \frac{Q_{HPI}}{A_{CL}} \left\{ g \cdot D_{CL} + \frac{\rho_{HPI} - \rho_{CL}}{\rho_{HPI}} \right\}^{-1/2} \tag{3.9-12}$$

where A_{CL} and D_{CL} are the area and diameter of the cold leg, respectively; and ρ_{HPI} and ρ_{CL} are the fluid densities in the high pressure injection and cold legs, respectively. Reyes [3.9-7] also developed a criterion using a hydraulic jump analysis:

$$Fr_{HPI/CL} = \left[1 + \frac{\rho_L \cdot Q_{HPI}}{\rho_{HPI} \cdot Q_L} \right]^{-1/2} \left[1 + \frac{Q_L}{Q_{HPI}} \right]^{-3/2} \tag{3.9-13}$$

The values of the two criteria given by Eqs 3.9-11 and 3.9-13 are similar at high ratios of loop flow to injection flow (Q_{CL}/Q_{HPI}) but diverge significantly as this ratio approaches unity.

The results generated using the analytical model were compared to those found experimentally under three different cold leg conditions. These three cold leg conditions analysed were natural circulation injection, a stagnant loop condition, and the transition from mixed to stratified flow. The analytical models mimicked those found during operation of the APEX facility. Additional analytical models were developed and reviewed by Reyes [3.9-7].

3.9.2.3. Empirical models integrated into research conducted at the LSTF

Experiments conducted at the LSTF in Japan required the incorporation and development of several analytical models depicting the hydraulics of the stationary wedge, criterion of wedge formation, and the shape of the wedge [3.9-4]. Only the hydraulics of the stationary wedge will be presented here; additional information can be found in Ref. [3.9-4].

The following analysis of the hydraulics of a stationary wedge are applicable to most fluid slabs spanning the pipe cross section except for those that are vertically positioned near or at the side wall.

Let Δ be a dimensionless density differential defined as:

$$\Delta = \frac{\rho_1 - \rho_2}{\rho_2} \tag{3.9-14}$$

where the subscripts "1" designate the upper (or warmer) layer and "2" the lower (or colder) layer. Again, the symbol ρ designates a fluid's density. It was then assumed that the slope of the interface was sufficiently small so that the vertical component of the interfacial shear stress (τ) was negligible. A control volume enclosing a vertical slice of fluid beneath the interface was then considered. The x-momentum equation yields:

$$\tau = y_2 \frac{dP}{dx} \tag{3.9-15}$$

where x and y are the Cartesian coordinates and P represents the pressure in the cold layer. The x-gradient of pressure in the cold layer is caused by the slope of the interface and the pressure drop in the flow direction due to the pipe wall. Thus:

$$\frac{dP}{dx} = \rho_2 \cdot g\left[(1-\Delta)\frac{dy_1}{dx} + \frac{dy_2}{dx}\right] + \left(\frac{dP}{dx}\right)_w = -\rho_2 \cdot g\Delta\frac{dy_1}{dx} + \left(\frac{dP}{dx}\right)_w \tag{3.9-16}$$

where the subscript "w" designates at the wall surface. Combining Eqs 3.9-15 and 3.9-16 produces a new expression for τ:

$$\tau = -\rho_2 \cdot g \cdot y_2 \cdot \Delta\frac{dy_1}{dx} + y_2\left(\frac{dP}{dx}\right)_w \tag{3.9-17}$$

The upper layer can now be visualized as a converging conduit with its top horizontal. The slope (S) of the energy grade line for the cold layer was simply:

$$S = -\frac{1}{2g}\frac{dV^2}{dx} - \frac{1}{g \cdot \rho_2(1-\Delta)}\left(\frac{dP}{dx}\right)_w = F_1^2\frac{dy_1}{dx} - \frac{1}{g \cdot \rho_2(1-\Delta)}\left(\frac{dP}{dx}\right)_w \tag{3.9-18}$$

where V is fluid velocity and F_1 is the Froude number of the warm layer. Equations 3.9-17 and 3.9-18 were then combined to yield:

$$S + \frac{\tau}{\rho_2 \cdot g \cdot y_2} = -(\Delta - F_1^2)\frac{dy_1}{dx} - \frac{\Delta}{g \cdot \rho_2(1-\Delta)}\left(\frac{dP}{dx}\right)_w \tag{3.9-19}$$

The equation of motion was then applied to the warmer layer, noting that y_1 can be interpreted as the hydraulic radius of the flow areas:

$$\tau + \tau_w = \rho_2(1-\Delta)g \cdot y_1 \cdot S \tag{3.9-20}$$

where τ_w is the wall shear stress defined by:

$$\tau_w = \frac{\rho_2(1-\Delta) f_w V^2}{8} \tag{3.9-21}$$

where f_w is the wall's Darcy-Weisbach friction factor. Similar to the wall shear stress, the interfacial shear stress can be expressed in terms of a Darcy-Weisbach friction factor f and the mean velocity of the warm water layer V:

$$\tau = \frac{\rho_2(1-\Delta) f V^2}{8} \tag{3.9-22}$$

From Eqs 3.9-20, 3.9-21 and 3.9-22, it was shown that:

$$\frac{S}{\Delta} = \frac{f + f_w}{8}\frac{V^2}{\Delta g y_1} = \frac{f + f_w}{8}F_{ud}^2\left(\frac{D}{y_1}\right)^3 \tag{3.9-23}$$

in which F_{ud} is the upstream densimetric Froude number defined by:

$$F_{ud} = \frac{V}{\sqrt{\Delta g D}} \tag{3.9-24}$$

Since the pressure head along the top of the pipe can be expressed as the height of the warm water column:

$$\left(\frac{dP}{dx}\right)_w = \frac{-\rho_2(1-\Delta) f_w V^2}{8y_1} \tag{3.9-25}$$

Combining Eqs 3.9-19, 3.9-23 and 3.9-25, along with the assumption that $h=y_1/D$ and $S=x/D$, the differential equation for the profile of the wedge was obtained:

$$\frac{dh}{dx} = \frac{F_{ud}^2[\, f_w(1-\Delta)(h-1) - f(1-\Delta h)]}{8(1-h)(h^3 - F_{ud}^2)} \tag{3.9-26}$$

This differential equation defines the shape of the wedge. It was observed that dh/dx becomes very large at the toe of the wedge where h approaches unity and the heel of the wedge where h approaches $F_{ud}^{2/3}$. The latter signifies that the location of the critical flow section (y_{ic}) was governed by the following equation:

$$y_{ic} = DF_{ud}^{2/3} \tag{3.9-27}$$

3.9.3. Computer modelling

The most common computational fluid dynamic (CFD) codes used to model natural circulation and more specifically thermal stratification are CFX-4, FLOW-3D, and FLUENT, to name a few. CFD has been hailed as a very powerful tool in the modelling and analysis of many thermohydraulic phenomena, including:

- Mixing of cold and hot water in the event of a SBLOCA
- Pressurized thermal shock (PTS)
- Thermal fatigue
- Natural circulation in LWRs
- Flow in lower plenum of ABWR
- Thermal loading on structures.

However, CFD is not without flaws. Local phenomena are not always taken into account which leads to increased uncertainty, large factors of safety, and more expense. General concerns related to CFD in this subject area are similar to the concerns described in Section 3.1.

REFERENCES FOR SECTION 3.9

[3.9-1] MIKSCH, M., LENZ, E., LOHBERG, R., Loading conditions in horizontal feedwater pipes of LWRs influenced by thermal shock and thermal stratification effects, Nuclear Engineering and Design **84** (1985) 179–187.

[3.9-2] YU, Y.J., PARK, S.H., SOHN, G.H., BAK, W.J., Structural evaluation of thermal stratification for PWR surge line, Nuclear Engineering and Design **178** (1997) 211–220.

[3.9-3] WILLIAMS, B.G., SCHULTZ, R.R., PHOENIX, B., KADAKIA, H., LIOU, J.C.P., Final Report for "LWR Passive Safety – Providing the Basis for Innovative Improvements in Advanced LWR Reactor Passive Systems Design: An Educational R&D Project", for period July 16, 2003 – July 15, 2006, Department of Energy (DOE) Nuclear Engineering Education Research (NEER) Program Award Number DE-FG07-03ID14500 (2007).

[3.9-4] LIOU, J.C.P., SCHULTZ, R.R., KUKITA, Y., "Stably stratified flows in closed conduits", Proceedings of ICONE-5, Nice, France (1997).

[3.9-5] CHEN, C.J., RODI, W., Vertical Turbulent Buoyant Jets-A Review of Experimental Data, Pergamon Press, New York (1980).
[3.9-6] WACHS, D.M., REYES, J.N. JR., DAVIS, L.R., A study of thermal stratification in the cold legs during the subcooled blowdown phase of a loss of coolant accident in the OSU APEX thermal hydraulic testing facility, submitted at the American Nuclear Society Winter Meeting, Washington, D.C. (1998).
[3.9-7] REYES, J.N., "Flow stagnation and thermal stratification in single and two-phase natural circulation loops", in IAEA-TECDOC-1474, November (2005) 433–458.
[3.9-8] THEOFANOUS, T.G., et al., Decay of Buoyancy Driven Stratified Layers with Applications to Pressurized Thermal Shock (PTS), Purdue University, West Lafayette, Indiana, May (1984).

3.10. BEHAVIOUR OF EMERGENCY HEAT EXCHANGERS AND ISOLATION CONDENSERS

Current designs of ALWRs rely on passive, gravity driven supplies of cooling water and passive heat exchangers to remove decay heat during various transients such as SBLOCA events. Passive heat exchangers are also effective during transients where there is a loss of the normal heat sink with an intact primary system such as a station blackout event. With an intact primary system no energy can be removed from the primary system via mass transfer through a break. Therefore, a passive heat exchanger is connected to the primary system to allow for primary decay heat removal [3.10-1].

For some designs, this emergency heat exchanger is located in a pool inside of containment (Fig. 3.1-2). In these cases, the emergency heat exchanger consists of a closed loop with a heat exchanger immersed in an elevated pool. The elevation difference between the heat source and heat sink create a buoyancy-driven natural circulation. This force is often referred to as the thermal driving head. Heat is transferred to the pool by convection to the inside surface of the heat exchanger tubes, heat conduction through the tube walls, and nucleate boiling in the pool. The cooler liquid flows down the return line connected to the reactor vessel. It has a valve that remains closed until heat removal is needed in the core.

In the AP600/1000 there is a C-Tube type heat exchanger that resides in the IRWST which is called the PRHR heat exchanger. The PRHR heat exchanger is connected to one of the hot legs and can be used to remove decay heat. The IRWST is filled with cold borated water and is open to the containment. In the WWER-1000/V-392 a PRHR system from the core via steam generators to the atmosphere removes the residual heat. These heat exchangers are cooled by atmospheric air. In the WWER-640/V-407, a PRHR system via steam generators is also used to remove the decay heat. However, in this case, the heat exchangers are immersed in emergency heat removal tanks installed outside the containment. In the AC600 the PRHR system is mainly used to remove the residual reactor power. These heat exchangers are cooled by atmospheric air [3.10-1–3.10-5].

3.10.1. PRHR phenomena

The following phenomena are important to PRHR system performance and reliability:

- Buoyancy force
- Emergency heat exchanger loop flow resistance
- Single phase convective heat transfer
- Shell-side nucleate boiling heat transfer

These phenomena, models and experiments used to assess overall heat transfer from a PRHR are discussed in the following sections.

3.10.1.1. Buoyancy force

The primary driving force in a natural circulation system is the fluid density difference imposed over an elevation. This difference in density between the hot and cold legs of the PRHR creates a buoyancy force. In order to maximize the driving force and reduce the friction loss, large tubes could be used and the heat sink put at a higher elevation. If the heat sink is put at a higher location, cold pockets of water tend to form and create a change in the flow rate and density of the fluid at the heat source. This process will eventually lead to a flow reversal. Welander [3.10-8] was the first to observe the oscillatory nature of natural circulation. Keller [3.10-9] suggested that these oscillations could be periodic.

A majority of the research that has taken place since has been devoted to studying and observing these flow oscillations. These flow oscillations can occur in both single and two phase flow. The majority of the experiments that have been performed address the nature of a rectangular loop similar to Fig. 3.10-1.

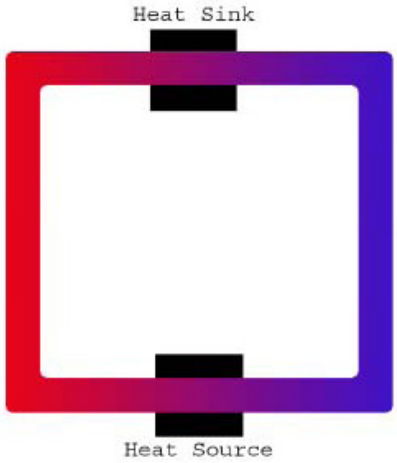

FIG. 3.10-1. Single phase natural circulation loop.

3.10.1.2. Emergency heat exchanger loop flow resistance

The total pressure loss in single or two phase flow consists of three components which are skin friction, form friction, and acceleration. The irreversible component of pressure loss caused by the wall shear stress can be seen in Eq. 3.10-1. Vijayan and Austregesilo observed that wall friction constitutive laws derived on the basis of forced flow may not be good estimators of natural circulation friction factors [3.10-10]. They derived non-dimensional groups with a modified Grashoff number and a new geometrical number. Tests were used as a benchmark to verify their data. The results were found to be reasonably accurate [3.10-11].

$$\Delta P = \frac{fL}{D_h}\frac{\dot{m}^2}{2\rho A^2} \tag{3.10-1}$$

The pressure loss of the system is dependent on the density of the fluid. The fluid density will be changing in this loop. Multiple studies have been conducted and the distance of separation from the heat sink and the heat source play a critical role in the frequency of flow instabilities. For single phase liquid, the density of the fluid can be predicted reasonably well using thermo-physical properties of the fluid.

3.10.1.3. Single phase convective heat transfer

Heat transfer by convection is more difficult to analyse compared to conduction heat transfer. Conduction heat transfer uses a single property of the heat transfer medium, thermal conductivity, to determine the heat transfer rate. The basic relationship for heat transfer by convection can be seen in Eq. 3.10-2:

$$\dot{Q} = hA_S\Delta T \tag{3.10-2}$$

Single phase liquid convective heat transfer is typically determined using the well-known Dittus-Boelter correlation.

3.10.1.4. Shell side heat transfer

Pool boiling will occur in the pool of water surrounding the heat exchanger. When the surface temperature of the heat exchanger exceeds the saturation temperature of the liquid, vapour bubbles will begin to form on the surface. The bubbles will grow very fast until they depart into the pool. These bubbles will either collapse or continue to grow. This process will create complex fluid motion around the heat exchanger tubes. In order to understand the fluid motion around the heat exchanger tubes we need to understand the thermodynamics of a single bubble and the hydrodynamics of the flow pattern from multiple bubbles.

Pool boiling is mostly convection driven with a small amount of latent heat transport at the surface. Over time many correlations have been developed to calculate the heat transfer coefficients in pool boiling. Generally the nucleate pool-boiling heat transfer coefficient is proportional to the heat flux. Pioro et al. performed an analysis of the most commonly used nucleate boiling heat transfer correlations. He found that the Rohsenow and Pioro correlations, given by Eqs 3.10-3 and 3.10-4 respectively are more accurate than other correlations [3.10-12].

$$\frac{c_L\left(T_w - T_{sat}\right)}{H_{fg}} = C_{sf}\left[\frac{q''}{\mu_L H_{fg}}\sqrt{\frac{\sigma}{g\left(\rho_L - \rho_g\right)}}\right]^{0.33}\left(\frac{c_L\mu_L}{k_L}\right)^n \tag{3.10-3}$$

$$Nu = C_{sf}K^{\frac{2}{3}}Pr^m \quad or \quad \frac{h_b l}{k} = C_{sf}\left[\frac{q''}{H_{fg}\rho_g^{0.5}\left(\sigma\left(\rho_L - \rho_g\right)\right)^{0.25}}\right]^{\frac{2}{3}}Pr^m \tag{3.10-4}$$

The variation of the local heat transfer coefficients in the tubes is a major problem in the accurate prediction of heat exchanger performance. The effects of flow patterns inside the IRWST may impact local heat transfer coefficients. Furthermore, the type of fluid affects the location where the maximum heat transfer takes place along the tube. The maximum heat transfer coefficient moves towards the sides of the tube as the fluid flow through the tube increases. Cornwell and Houston [3.10-13] claimed that differences in local heat transfer coefficients are caused by sliding bubbles on the outside of the tubes. Kang claimed that the differences were caused by liquid agitation and bubble coalescence [3.10-14]. Kang has performed several experiments to gather pool boiling data, which can be used in the design of passive heat exchangers [3.10-14].

Cornwell and Houston concluded that there are dangers in recommending a general heat transfer correlation, even when the area of application is clearly defined [3.10-13]. The fluctuations of the heat transfer vary greatly depending on fluid, temperature, pressure, and tube design. However, the design of heat exchangers, require a core correlation that can be used. Cornwell presented the best correlation they could find, shown in Eq. 3.10-5, for fully developed nucleate boiling of water or refrigerant. For water the correlation is valid from 22 kPa to 17.5 MPa.

$$Nu = AF(p)Re_b^{0.67}Pr^{0.4} \quad (3.10\text{-}5)$$

In Eq. 3.10-5, A and F are given by the following equations.

$$A = 9.7\,p_c^{0.5}$$

$$F = 1.8\,p_r^{0.17} + 4\,p_r^{1.2} + 10\,p_r^{10}$$

Chun and Kang performed experiments for the design of the PRHR System. Similar conclusions could be applied to the design of an isolation condenser and passive residual heat exchanger. They concluded that an increase in surface roughness increases heat transfer in both horizontal and vertical tubes. During nucleate boiling conditions the heat transfer is greater in vertical tubes. They also concluded that the heat transfer rate decreases as the tube diameter increases [3.10-15].

3.10.2. PRHR experiments

The following section will examine a number of experimental programs that have been undertaken for ALWRs utilizing a PRHR system.

3.10.2.1. Experimental activity related to the AP600/1000 PRHR

Tests of a C-Shell type PRHR Exchanger were conducted in the APEX, a one-fourth height scaled, integral system test facility at Oregon State University. The testing was conducted as part of the certification of the Westinghouse AP600 design and USNRC confirmatory testing. Figure 3.10-2 shows the inlet of the PRHR heat exchanger immersed in the IRWST in the APEX test facility. It consists of 88 stainless tubes attached to tube sheet headers connected to the IRWST.

FIG. 3.10-2. Photograph of the PRHR heat exchanger in the APEX IRWST.

One of the main purposes of the APEX facility was to examine the low pressure, longer term cooling behaviour of the AP600/1000 during the SBLOCA. Upon a primary system break, the system pressure and pressurizer level will drop. This will trigger a reactor trip which will cause a further reduction in pressurizer level and pressure as the reactor power drops and the fluid volume shrinks. Eventually, a safety injection signal will be generated on low pressurizer pressure which will actuate the CMTs and the PRHR along with tripping the RCPs.

At this stage of the transient the heat removal mechanisms include the energy release through the break, CMT recirculation, PRHR heat transfer and SG heat transfer. A continued drop in the primary inventory and pressure will cause the primary pressure to drop below the secondary side pressure which will cause a reversal in the SG heat transfer.

Typically, the PRHR is able to provide cooling in excess of the decay heat being produced. As the pressure continues to drop due to the mass and energy release, the pressure will drop low enough to cause accumulator injection. This accumulator injection will allow for nitrogen to be released into the primary system causing the PRHR tube bundles to be blanketed in non-condensable gas effectively disrupting heat transfer at the PRHR heat exchanger tubes. Further reduction in pressure will cause the primary to reach saturation conditions which will allow for two phase flow to begin making its way into the PBL and the CMT effectively ending CMT recirculation [3.10-6].

There are a number of phenomena of interest that have been explored in the APEX facility. The following will be examined below.

- PRHR-induced asymmetries
- PRHR heat exchanger performance and IRWST thermal stratification
- Cold leg thermal stratification

3.10.2.1.1. PRHR-induced asymmetries

During the early phases of the SBLOCA, there are two important phenomena occurring. The first is the depressurization of the system as the result of CMT and PRHR energy removal. The second is the cooling of the cold legs due to the natural circulation processes present in the primary loop. Both of these phenomena affect on another.

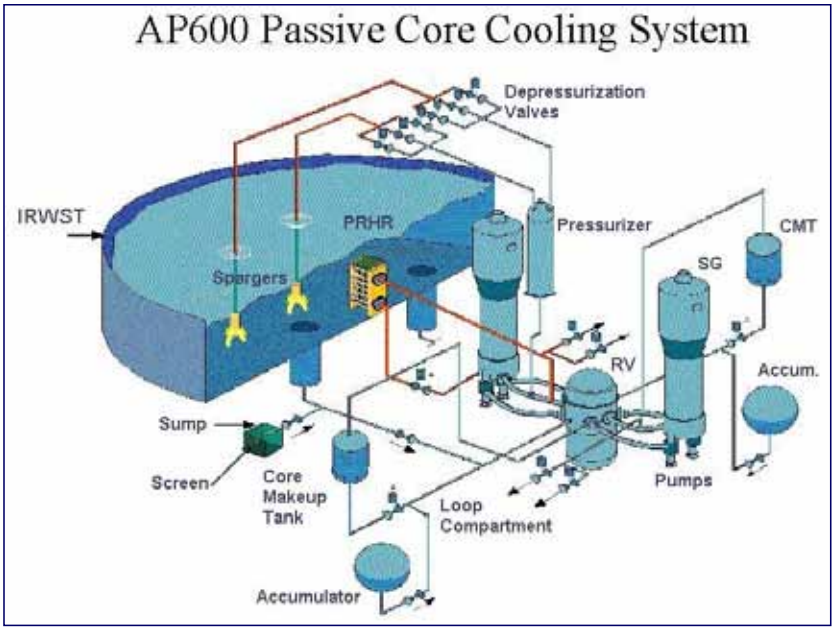

FIG.3.10-3. Passive safety systems used in the AP600 design.

In the AP600, both CMTs are located on the non-pressurizer loop as shown in Fig. 3.10-3. For the CMT side of the system, cold water returns to the cold legs via the downcomer. The PRHR is located on the pressurizer loop. For the PRHR side of the system, cold water returns to the cold legs via the SG outlet plenum. The cold legs on the PRHR side of the system tend to be somewhat cooler than the cold legs on the CMT side due to their different sources of water. This may lead to asymmetries in the cold leg cooling [3.10-6].

3.10.2.1.2. PRHR heat exchanger performance and IRWST thermal stratification

OSU conducted a series of tests for the NRC to assess the impact that thermal stratification in the IRWST has on PRHR heat exchanger performance. In particular, NRC-5002 and 5102, the Station Blackout Tests, produced long term heat-ups of the IRWST and significant thermal stratification [3.10-7]. These tests simulated a loss of all AC power to all reactor systems. Decay heat was removed by the PRHR using the PRHR heat exchanger.

Both station blackout tests were performed at a core power level of 425 kW. The only difference between the two tests was the test duration. Test 5002 was performed for five hours and test 5102 for seven hours. The primary coolant was initially at a pressure of 2.76 MPa and a hot leg temperature of 204°C. During the tests, heat was transferred from the core to the IRWST liquid. Fluid temperature measurements along the vertical axis of the IRWST indicated that the fluid became thermally stratified. Eventually the liquid at the top of the IRWST reached saturation conditions. As the test progressed, the saturation layer grew towards the bottom of the IRWST altering the PRHR heat exchanger's heat rejection process. Eventually, all of the IRWST liquid, except the liquid layer below the heat exchanger, reached saturation conditions [3.10-16]. The overall heat rejected by the PRHR was determined using the measured inlet mass flow rate and the tube thermocouples. A simple energy balance was performed for each of the four PRHR zones.

Zone one is the upper horizontal section from inlet to just before the U tube bend (Fig. 3.10-4). Zone two is the upper vertical section including the upper bend down to the PRHR heat exchanger midpoint. Zone three is the mirror image of zone two including the vertical tube running from the PRHR heat exchanger midpoint down to and including the bend. Zone four is the lower horizontal section from the end of the bend to the PRHR heat exchanger outlet. During the tests approximately 60% of the heat was rejected through zone 1. Another 20% of the heat was rejected through zone 2. The other zones become more and more important as thermal stratification occurs in the IRWST. In these tests the PRHR heat exchanger demonstrated the ability to remove core decay heat in a stable manner for a prolonged period without the use of active systems.

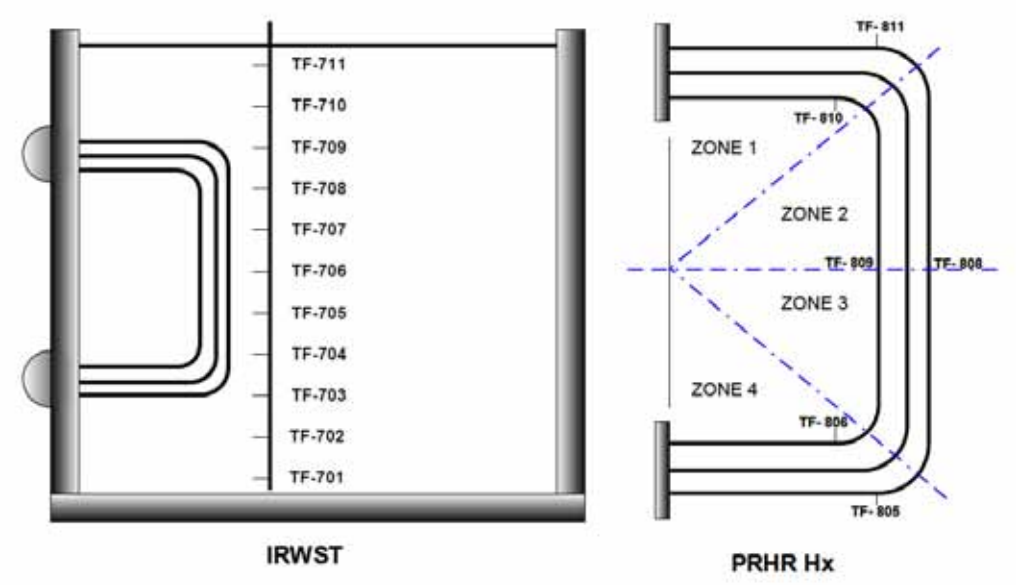

FIG. 3.10-4. Fluid temperature measurements in IRWST and PRHR tubes.

Models were developed using CFX 4.1, a computational fluid dynamics code. CFX was able to predict the thermal stratification in the IRWST. From experimental observations and the CFX modeling several points can be made concerning the flow behaviour in the IRWST. Firstly, the flow below the top portion of the PRHR is virtually motionless. Secondly, above the PRHR a flow recirculation

pattern establishes itself. Finally, the modeling of two phase flows in the IRWST is difficult using a CFD code [3.10-7].

3.10.2.1.3. Cold leg thermal stratification

The stratification of the coolant in the cold legs has been noted in tests conducted at the APEX and ROSA-AP600 facilities. Thermal stratification is characterized by a large difference in coolant temperature between the top and bottom of the cold legs [3.10-7].

In tests conducted at the APEX facility, thermal stratification has been observed. For larger break tests, thermal stratification is noted on both the PRHR and the CMT sides of the system. Nominally, the stratification measured on the PRHR side of the system is much larger than that measured in the CMT side cold legs. The stratification difference between the PRHR and CMT sides can be as large as 38°C (100°F). To some extent, this difference is to be expected as the PRHR side has a colder source of water in the PRHR heat exchanger than the CMT side cold legs whose water source is the downcomer.

After a RCP trip, the flow through the primary system is driven by natural circulation. Natural circulation flow represents a reduced flow rate when compared against pump-driven forced circulation but it still is in excess of the PRHR natural circulation flow. Therefore, the PRHR flow that enters the outlet plenum of the SG will be completely mixed with the loop natural circulation flow before it travels into the cold legs.

With a significant enough level drop due to a SBLOCA, SG tube voiding will occur and loop natural circulation will cease. When this happens a countercurrent flow situation will develop in the cold legs with the colder PRHR fluid running into the cold legs on the bottom and the hotter loop fluid moving into the SG outlet plenum along the top of the cold leg. Results at APEX indicate that there may even be a thin vapour layer running along the top of the cold leg.

As the coolant level continues to fall, steam will fill the upper portions of the RPV and cause an interruption of the PRHR flow. The PRHR tubes will drain and once drained PRHR injection will cease.

The Theofanous model [3.10-17] developed for HPSI flow induced cold leg stratification can be used in the situation of PRHR injection to determine the onset of thermal stratification. The boundary for the onset of thermal stratification is described using Eq. 3.10-6 where the superficial Froude number can be calculated using Eq. 3.10-7 [3.10-7].

$$Fr_{PRHR,CL} \cong \left(1 - \frac{Q_{NC}}{Q_{PRHR}}\right)^{-\frac{7}{5}} \tag{3.10-6}$$

$$Fr_{PRHR,CL} = \frac{Q_{PRHR}}{A_{CL}} \left(gD_{CL} \frac{\rho_{PRHR} - \rho_h}{\rho_{PRHR}}\right)^{-\frac{1}{2}} \tag{3.10-7}$$

CFX calculations were conducted and compared against the results collected in the APEX facility. CFX is a computational fluid dynamics code. CFX has a very limited ability to effectively model two phase flow and the presence of a thin vapour layer during the stratified flow phase in the cold legs make the use of CFX difficult.

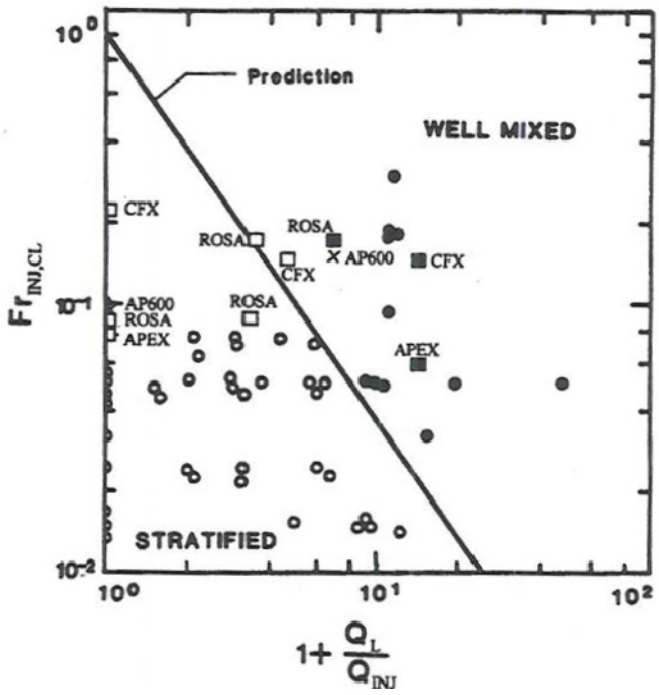

FIG. 3.10-5. Comparison of Theofanus thermal stratification onset criterion to data from APEX, ROSA-AP600, and CFX 4.1 results [3.10-7].

A plot comparing the results collected from APEX, ROSA-AP600 and CFX calculations has been compared against the onset of thermal stratification boundary developed using the Theofanous model and is shown in Fig. 3.10-5. It is noted in this figure that the primary natural circulation phase data lies on the well mixed side of the boundary while the stagnant loop flow data lies on the stratified side of the boundary [3.10-7].

3.10.2.2. Experimental activity related to the Chinese advanced PWR PRHR

The Chinese advanced PWR design contains passive safety features including a PRHR system. When actuated, the EFWT isolation valves open. This allows water to flow into the SG secondary side by gravity where it removes heat from the primary by changing phase into steam. The steam produced in the SGs is then condensed by a series of air coolers. These air coolers rely on the natural circulation of air through a chimney to cool and condense the incoming steam. The condensed steam will return to the SG through gravity.

The NPIC conducted a number of tests at the AC600 PRHR experimental test facility in order to demonstrate the operation of the PRHR system. In total, 166 steady state and 46 transient tests were conducted. The results of these tests indicate that the PRHR system is indeed effective at removing decay heat from the advanced Chinese PWR designs. The code MISAP 2.0 was also used to analyse the steady state and transient behaviour in the test facility [3.10-4].

3.10.2.3. Experimental activity related to the WWER PRHR

The SPOT system is the passive heat removal system for the WWER-1000 reactor design. SPOT consists of four groups of natural circulation loops corresponding to each primary system loop. Each group contains four heat exchangers which are located outside of containment. In these heat exchangers, steam extracted from the SGs is condensed. The condensed steam then flows via gravity back to the SG (See Section 4.10 for further details).

A number of experiments were conducted by OKB Gidropress. Thirty tests focused on defining heat losses in hot standby. Thirty tests focused on determining the power removed from the system as a

function of external air temperature and pressure. Two tests were conducted to explore the impact of non-condensable gases on the operation of the heat exchanger [3.10-3].

3.10.3. Isolation condenser phenomena

ICs have been developed to remove the decay heat from a nuclear core in the event of sudden reactor isolation, reactor hot standby, and safe shutdown conditions [3.10-18]. ICs have been used in many early BWR designs to control the reactor pressure automatically without removing coolant from the core. The IC consists of a shell and tube heat exchanger immersed in a large suppression pool located above the core. Steam condenses inside the heat exchanger creating a low pressure region which draws in more steam. The condensate returns by gravity to the reactor vessel. The primary driving force in this system is the condensation of steam.

Heat is transferred from the steam through the emergency heat exchanger tubes into the pool by three mechanisms: two phase convective heat transfer and condensation at the tube inside surface, heat conduction through the tube walls, and convective heat transfer at the tube outside surface.

The following phenomena can impact the performance and reliability of the IC:

- IC loop flow resistance
- Low pressure steam condensation
- Condensation heat transfer in the presence of non-condensable gases
- Shell-side convection heat transfer

These phenomena are discussed in the sections that follow.

3.10.3.1. IC loop flow resistance

In two phase natural circulation systems the flow rate is determined by a balance between the buoyancy force and the loop flow resistance. The buoyancy force is created by the density and elevation difference between the heat source and heat sink. The loop flow resistance is caused by friction and form pressure losses, flow acceleration and elevation differences. The behaviour of two phase fluids in loops is particularly complicated. The pressure drop and the heat transfer coefficients inside the condenser tubes are dependent on the two phase flow pattern. For example, slug flow can cause larger pressure drops in natural circulation loops than a homogeneous bubbly flow. Furthermore, slug flow behaviour is unsteady. Therefore, the local axial pressure drop is time dependent. Dukler and Hubbard demonstrated that there are two pressure loss contributions from slug flow. The first is the pressure drop from the slow moving liquid film compared to the slug velocity. The second is the pressure drop required to overcome the wall friction [3.10-19].

The equation for total pressure drop is given by Eq. 3.10-8. It includes a friction and form loss term, a momentum change term, and a gravitational pressure drop term.

$$\left(\frac{\partial p}{\partial z}\right)_{tot} = \left(\frac{\partial p}{\partial z}\right)_{fric} + \left(\frac{\partial p}{\partial z}\right)_{mom} + \left(\frac{\partial p}{\partial z}\right)_{elev} \tag{3.10-8}$$

A variety of pressure drop models have been developed to calculate the friction and form pressure losses in two phase flow. The basic approach is to modify a single phase fluid pressure drop calculation using a two phase fluid multiplier.

The following two phase friction factor multipliers are commonly used:

- Homogeneous model
- Lockhart-Martinelli (1949)

- Martinelli and Nelson (1948)
- Chrisholm and Sutherland (1969)

A detailed description of two phase pressure drop models is presented by Saha [3.10-20]. Nayak showed the influence of different two phase friction factor multiplier models on steady state natural circulation. From his experiment he concluded that all the different friction factor models overestimate the natural circulation flow rate [3.10-21].

3.10.3.2. Low pressure steam condensation

Much of the condensation behaviour of interest to IC operation occurs at relatively low pressure conditions. Condensation occurs when a vapour is cooled below the saturation temperature to induce the nucleation of droplets. This can occur in one of two ways. This may occur homogeneously within the vapour or heterogeneously on particulate matter. The isolation condenser cooling walls drive heterogeneous nucleation in the system. The two types of heterogeneous condensation that occur in the isolation condenser are drop-wise and film-wise. Collier's textbook provides a variety of theoretical condensation models developed to predict the local heat transfer coefficients for both vertical and horizontal tubes [3.10-22]. However, a reliable theory of drop-wise condensation has not been established.

3.10.3.3. Condensation heat transfer in the presence of non-condensable gases

This section provides an overview of experiments, models and code calculations related to condensation heat transfer in the presence of non-condensable gases. Of particular interest to isolation condensers is steam condensation in the presence of air and/or hydrogen.

IC heat transfer to the pool is accomplished by convection and steam condensation on the inside surface of the heat exchanger tubes. The heat transfer across the condensate layer controls the heat transfer rate to the pool. During IC operation, non-condensable gases are carried with the steam to the tube interior surfaces where the steam is condensed. A non-condensable gas boundary layer develops inside the condenser tube which acts as a resistance for further steam condensation. The build up of non-condensable gases on the tube walls of the isolation condenser will limit the heat transfer to the pool. It will force the heat to diffuse through the non-condensable gases which is a relatively slow process compared to convection. Several researchers have claimed that a small amount of non-condensable gas can greatly reduce heat transfer rates. Wang and Tu concluded that 5% non-condensable gas build up can reduce heat transfer by 50% [3.10-23].

3.10.3.3.1. Experiments

Many experiments for steam condensation in the presence of non-condensable gases were performed prior to 1988. A compilation of heat transfer correlations and experiments from that period can be found in Heat Transfer Equipment Design [3.10-24]. Table 3.10-1 lists several recent studies that have application to IC behaviour. Several tests have been conducted using either pure steam or mixtures of steam and air, steam and helium, and steam, air and helium. Helium is typically used as the working fluid instead of hydrogen which would be prototypic under accident conditions. Single tube tests have produced useful heat transfer data and have received extensive use in model development as shall be shown in the next section. Only a few multiple tube bundle tests have been conducted thus far. The most prototypic IC assessment tests were performed in the PANDA test facility at the Paul Scherrer Institute in Switzerland. A useful description of their ISP-42 tests and code comparisons to the test results are provided in Section 3.4.6 and Ref. [3.10-25].

TABLE 3.10-1. LIST OF EXPERIMENTS ON STEAM CONDENSATION IN TUBES (1988–PRESENT)

Experiment	Tubes	Pressure (MPa)	NC Mass Fraction	Codes
MIT, USA Steam/Helium [3.10-23]	1 tube 46 mm ID 2.54 m Length	0.1-.6	0.02-0.2 He	
MIT, USA Steam/Helium/Air [3.10-27]	1 tube 46 mm ID 2.54 m Length	0.1-.6	0.02-0.2 He 0.045-0.2 Air	
UC-Berkeley, USA [3.10-28] Steam	1 tube 47.5 mm ID 2.4 m Length	0.1-0.5	Pure Steam	
UC-Berkeley, USA [3.10-28] Steam/Air	1 tube 47.5 mm ID 2.4 m Length	0.1-0.5	0.01-0.4 Air	
UC-Berkeley, USA [3.10-28] Steam/Helium	1 tube 47.5 mm ID 2.4 m Length	0.40	0.003-0.15 He	
METU-CF [3.10-26] Middle East Technical University, Turkey Steam/Air	1 tube 33.0 mm ID 2.158 m Length	0.23-0.28	0.0-1.0 Air	RELAP5-MOD3.2 RELAP5-MOD3.3
UMCP [3.10-26] University of Maryland, USA Steam/Air	28 tubes 30 mm ID 3.9 m Length	0.41	0.0-1.0 Air	RELAP5-MOD3.2 RELAP5-MOD 3.3
PIPER-ONE [3.10-18] Steam	12 tubes 20 mm ID 0.4 m Length	0.4-0.5	Pure Steam	RELAP5-MOD2 RELAP5-MOD3
PANDA – PSI [3.10-25] (ISP-42) Steam/Air	20 tubes 50.8 mm 1.778 m Short Tubes 2.066 m Long Tubes	0.1-0.3	Steam-Air	RELAP5 CATHARE GOTHIC

Recently, the USNRC issued an International Agreement report, NUREG/IA-0210, describing steam/air condensation tests and code comparisons conducted in the METU-CF test facility at the Middle East Technical University in Turkey [3.10-26]. These tests exhibited similar behaviour to bundle tests conducted in the UMCP 2x4 test facility at the University of Maryland in the USA. Although the effort was aimed at understanding once-through steam generator heat transfer during the boiling condensing mode of operation, important insights were gained regarding transient heat transfer in tubes filled with steam and air mixtures. The METU-CF test facility consists of a boiler with an air inlet that produces a saturated steam/air mixture. This steam/air mixture flows downward through a single tube countercurrent heat exchanger.

That is, cooling water flows upward through a cooling jacket that surrounds the tube while the steam/air mixture flows downward through the tube. Axial temperature measurements provide for a heat balance used to determine the axial heat flux through the tube walls. The METU-CF tests show, in Fig. 3.10-6, that temperatures in the lower section of the condenser tube increase with time. It is postulated that the reason for this behaviour is that as steam condenses, air concentration increases at the bottom of the tube. Axial measurements of air concentration were not made for these tests. However, RELAP5 calculations of the METU-CF test, one of which is shown in Fig. 3.10-7, strongly supports this idea.

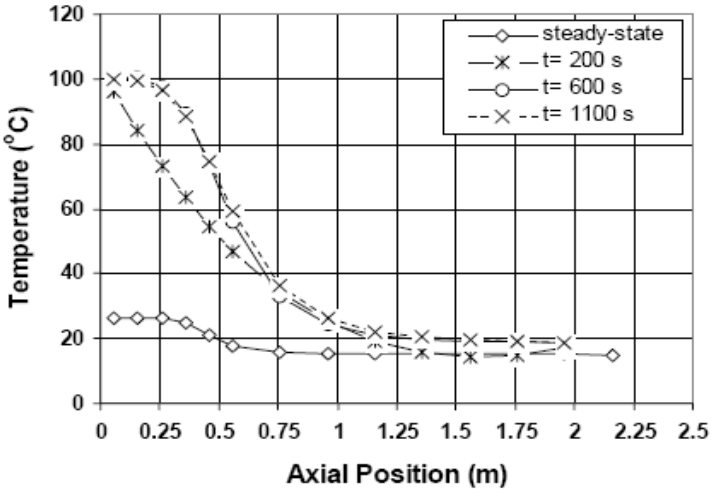

FIG. 3.10-6. METU-CF Test show that temperatures in the lower section of the condenser tube increase with time [3.10-26].

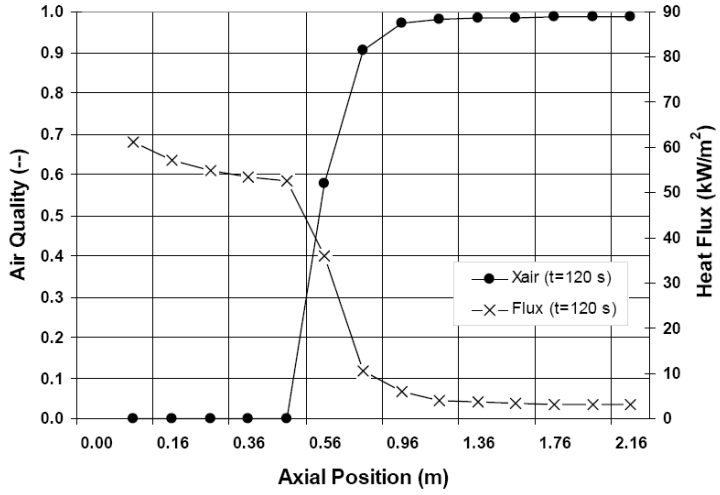

FIG. 3.10-7. RELAP5 Prediction of air mass fraction inside tubes for METU-CF test [3.10-26].

3.10.3.3.2. Models

This section presents several condensation heat transfer models for application to IC operation. They have been assessed against a variety of single-tube experiments involving steam condensation in the presence of non-condensable gases. Hasanein et al. [3.10-27] provides a brief introduction of the approaches used to analyse forced convective condensation of steam in the presence of non-condensable gases. They include a) boundary layer models which includes similarity solutions, integral methods and finite difference techniques, b) heat and mass transfer models, and c) numerical analyses. The approach used by Siddique et al. [3.10-29] and Hasanein et al. [3.10-27] was to develop semi-empirical correlations based on experimental data. They use mixture Nusselt, Schmidt, Reynolds and Jakob numbers to include the effects of high mass transfer, developing flow, film roughness and property variations.

The mixture Nusselt Number, Nu(x), as a function of axial position, x, in a tube is defined by Eq. 3.10-9. The Nusselt number is represented by the local convective heat transfer coefficient, h(x), times the tube diameter, d, divided by the thermal conductivity, k_{mix}, of the mixture. It is apparent, that

a decrease in the heat transfer coefficient due to the presence of a non-condensable gas will cause a decrease in the Nusselt Number.

$$Nu(x) = \frac{h(x)d}{k_{mix}} \tag{3.10-9}$$

The mixture Schmidt number is given by Eq. 3.10-10.

$$Sc(x) = \frac{\mu_{mix}}{\rho_{mix} D_v} \tag{3.10-10}$$

In this equation, D_v is the mass diffusion coefficient of the vapour in the non-condensable gas. The mixture Reynolds number is given by:

$$\mathrm{Re}(x) = \frac{4\dot{m}_{mix}}{\pi d \mu_{mix}} \tag{3.10-11}$$

The Jakob number for the mixture is given by:

$$Ja(x) = \frac{C_{p,mix}}{H_{fg}}\left[T_{sat}(x) - T_i(x)\right] \tag{3.10-12}$$

The mass flow rate fraction, W_i, at the inlet is also used in some correlations. It is given by:

$$W_i(x) = \frac{\dot{m}_{nc}}{\dot{m}_{mix}} \tag{3.10-13}$$

The following correlations were found to be in good agreement with experimental data over the ranges given. For steam-helium mixtures, the local Nusselt number was predicted by Siddique et al. using the following correlation [3.10-29].

$$Nu = 0.537\,\mathrm{Re}^{0.433} W_h^{-1.249} Ja^{-0.624} \tag{3.10-14}$$

In this correlation, W_h is the helium mass fraction at the inlet. This correlation is applicable to the following ranges:

$$0.02 < W_h < 0.52$$
$$300 < \mathrm{Re} < 11,400$$
$$0.004 < Ja < 0.07$$

A similar correlation is proposed by Hasanein et al. [3.10-27] in terms of the Schmidt number.

$$Nu = 0.199\,\mathrm{Re}^{0.327} Sc^{-2.715} Ja^{-1.058} \tag{3.10-15}$$

For the following range of conditions:

$$0.314 < Sc < 0.864$$
$$846 < \mathrm{Re} < 26,537$$
$$0.007 < Ja < 0.102$$

Hasanein et al. [3.10-27] also developed a correlation for mixtures of steam, air and helium. It is given as follows:

$$Nu = 1.279\,\mathrm{Re}^{0.256}\left(1-1.68W_a\right)W_h^{-0.741}Ja^{-0.952} \tag{3.10-16}$$

In this correlation, W_a is the air mass fraction at the inlet. This correlation is applicable to the following ranges:

$$0.023 < W_h < 0.405$$
$$0.0 < W_a < 0.574$$
$$846 < \mathrm{Re} < 26,537$$
$$0.007 < Ja < 0.102$$

As shown in Table 3.10-1, several code assessments have been conducted against experimental data. The most comprehensive assessment, in terms of conditions applicable to IC operation, was documented in ISP-42, for the PANDA facility. In general, code predictions for overall heat transfer in the IC heat exchangers can be reasonably predicted by some codes. Bovalini [3.10-18] performed an evaluation of the effects of using RELAP5/MOD2 and RELAP5/MOD3 to evaluate the effectiveness of heat transfer in the isolation condenser. He concluded that some of the variables such as pressure drop needed to be fine tuned for the models to adequately model the phenomena in the isolation condenser. The predicted local values of the condensation coefficient and flow regimes appear not to be consistent with the experimental data but the overall heat transfer was correct.

ABBREVIATIONS

ALWR	Advanced light water reactor
AP600	Advanced plant 600 MWe
AP1000	Advanced plant 1000 MWe
APEX	Advanced plant experiment
BWR	Boiling water reactors
CATHARE	Code avancé de thermohydraulique pour les accidents des réacteurs à eau
CFD	Computational fluid dynamics
CMT	Core make-up tank
EFWT	Emergency feed water tank
IAEA	International Atomic Energy Agency
IC	Isolation condenser
IRWST	In-containment refueling water storage tank
NPIC	Nuclear Power Institute of China
OSU	Oregon State University
PANDA	Passive Nachwärmeabfuhr- und Druckabbau-Testanlage (Passive decay heat Removal and depressurization test facility)
PBL	Pressure balance line
PRHR	Passive residual heat removal
PWR	Pressurized water reactor
RCP	Reactor coolant pump
RELAP	Reactor excursion and leak analysis package
ROSA	Rig of safety assessment
ROSA-AP600	Rig of safety assessment AP 600 configuration
RPV	Reactor pressure vessel
SBLOCA	Small break loss of coolant accident
SG	Steam generator
USNRC	United States Nuclear Regulatory Commission
WWER	Water moderated, water cooled energy reactor

NOMENCLATURE

A	Flow area (m^2)
A_S	Surface area (m^2)
c_L	Specific heat of liquid (J/kg-K)
D_h	Hydraulic diameter (m)
D_v	Mass diffusion coefficient
d	Diameter (m)
f	Friction factor
g	Acceleration of gravity (m/s^2)
H_{fg}	latent heat of vaporization (J/kg)
h	Heat transfer coefficient (W/m^2-K)
h_b	Nucleate pool boiling heat transfer coefficient (W/m^2-K)
k_L	Thermal conductivity of liquid (W/m-K)
L	Length (m)
l	Pool boiling characteristic dimension (m)
$\dot{m}$	Mass flow rate (kg/s)
p_c	Critical pressure (Pa)
p_r	Pressure ratio
$\dot{Q}$	Heat transfer rate (W)
q''	Heat flux (W/m^2)
T_w	Wall temperature (K)
T_{sat}	Saturation temperature (K)
W	Gas mass fraction
Fr	Froude umber
Ja	Jakob number
Nu	Nusselt number
Pr	Prandtl number
Re	Reynolds number
Sc	Schmidt Number

Greek symbols

ΔP	Pressure difference (Pa)
ΔT	Temperature difference (K)
ρ_g	Gas density (kg/m^3)
ρ_L	Liquid density (kg/m^3)
μ	Dynamic viscosity (Pa-s)
σ	Surface tension (N/m)

REFERENCES FOR SECTION 3.10

[3.10-1] INTERNATIONAL ATOMIC ENERGY AGENCY, Natural Circulation in Water Cooled Nuclear Power Plants, IAEA-TECDOC-1474, IAEA, Vienna (2005).

[3.10-2] INTERNATIONAL ATOMIC ENERGY AGENCY, Status of Advanced Light Water Reactor Designs 2004, IAEA-TECDOC-1391, IAEA, Vienna (2004).

[3.10-3] KURAKOV, Y.A., et al., "Development and validation of natural circulation based systems for new WWER designs", Natural Circulation Data and Methods for Advanced Water Cooled Nuclear Power Plant Design, IAEA-TECDOC-1281, IAEA, Vienna (2002).

[3.10-4] XIAO ZEJUN, et al., Experimental research progress on passive safety systems of Chinese advanced PWR, Nuclear Engineering and Design **225** (2003) 305–313.

[3.10-5] JUNLI GOU, SUIZHENG QIU, GUANGHUI SU, DOUNA JIA, Thermohydraulic Analysis of a Passive Residual Heat Removal System for an Integral Pressurized Water Reactor, Hindawi Publishing Corporation, Science and Technology of Nuclear Installations, Volume 2009, Article ID 473795, 12 pages, doi: 10.1155/2009/473795.

[3.10-6] BESETTE, D., DI MARZO, M., GRIFFITH, P., Phenomenology observed in the AP600 integral systems test programs conducted in the ROSA-AP600, APEX and SPES-2 facilities, April 1998, Office of Nuclear Regulatory Research, Reactor and Plant Systems Branch, RPSB-98-04 (1998).

[3.10-7] REYES, J. N., JR., et al., Final Report of NRC AP600 Research Conducted at Oregon State University, NUREG/CR-6641, August (1999).

[3.10-8] WELANDER, P., On the oscillatory instability of a differentially heated loop, J. Fluid Mech. **29** (1967) 17–30.

[3.10-9] KELLER, J.B., "Periodic Oscillations in a Model of Thermal Convection," J. Fluid Mech. **26** (1966) 599–606.

[3.10-10] VIJAYAN, P.K., AUSTREGESILO, H., Scaling laws for single phase natural circulation loops, Nuclear Engineering and Design **152** (1-3) (1994) 331–347.

[3.10-11] VIJAYAN, P.K., Experimental observations on the general trends of the steady state and stability behaviour of single phase natural circulation loops, Nuclear Engineering and Design **215** (1-2) (2002) 139–152.

[3.10-12] PIORO, I.L, ROHSENOW, W., DOERFFER, S.S., Nucleate pool-boiling heat transfer. Assessment of prediction methods, International Journal of Heat and Mass Transfer **47** (23) (2004) 5045–5057.

[3.10-13] CORNWELL, K., HOUSTON, S.D., Nucleate pool boiling on horizontal tubes: A convection-based correlation. International Journal of Heat and Mass Transfer **37**(SUPPL 1) (1994) 303–309.

[3.10-14] KANG, M., Local pool boiling coefficients on the outside surface of a horizontal tube. Journal of Heat Transfer **127** (8) (2005) 949–953.

[3.10-15] CHUN, M., KANG, M., Effects of heat exchanger tube geometries on nucleate pool boiling heat transfer in a scaled in-containment refueling water storage tank, International Communications in Heat and Mass Transfer **23** (1) (1996) 23–34.

[3.10-16] STEVENS, O.L., Characterization of the advanced plant experiment (apex) passive residual heat removal system heat exchanger. Master's thesis, Oregon State University (1996).

[3.10-17] THEOFANOUS, T.G., et al., Decay of Buoyancy Driven Stratified Layers with Applications to Pressurized Thermal Shock (PTS), Purdue University, West Lafayette, Indiana, May (1984).

[3.10-18] BOVALINI, R., D'AURIA, F., AND GALASSI, G.M., Application of RELAP5/MOD2 and RELAP5/MOD3 codes to isolation condenser related experiments. Nuclear Technology and Radiation Protection (1993) 138–145.

[3.10-19] DUKLER, A.E. AND HUBBARD, M.G., A model for gas-liquid slug flow in horizontal and near horizontal tubes, Industrial & Engineering Chemistry Fundamentals **14**(4) (1975) 337–347.

[3.10-20] SAHA, D., "Local phenomena associated with natural circulation", Annex 5 of Natural Circulation in Water Cooled Nuclear Power Plants, IAEA-TECDOC-1474, IAEA, Vienna (2005).

[3.10-21] NAYAK, A.K., DUBEY, P., CHAVAN, D.N., VIJAYAN, P.K., Study on the stability behaviour of two phase natural circulation systems using a four-equation drift flux model, Nuclear Engineering and Design **237** (4) (2007) 386–398.
[3.10-22] COLLIER, J.R., THOME, J.G., Convective Boiling And Condensation. Oxford University Press (1996).
[3.10-23] WANG, C., TU, C., Effect of non-condensable gas on forced convection condensation along a horizontal plate in a porous medium, International Journal of Heat and Mass Transfer **32** (10) (1989) 1847–1852.
[3.10-24] SHAH, R.K., Heat Transfer Equipment Design. Taylor & Francis (1988).
[3.10-25] AKSAN, N., "Overview on Panda test facility and ISP-42 PANDA tests data base", Annex 14 of Natural Circulation in Water Cooled Nuclear Power Plants, IAEA-TECDOC-1474, IAEA, Vienna (2005).
[3.10-26] TANRIKUT, A., YESIN, O., In-Tube Steam Condensation in the Presence of Air Under Transient Conditions, U.S. Nuclear Regulatory Commission, NUREG/IA-0210, May (2007).
[3.10-27] HASANEIN, H.A., KAZIMI, M.S., GOLAY, M.W., Forced convection in-tube steam condensation in the presence of non-condensable gases, International Journal of Heat and Mass Transfer **39** (13) (1996) 2625–2639.
[3.10-28] KUHN, S.Z., SCHROCK, V.E., PETERSON, P.F., An investigation of condensation from steam-gas mixtures flow downward inside a vertical tube, Nuclear Engineering and Design **177** (1997) 53–69.
[3.10-29] SIDDIQUE, M., GOLAY, M.W., KAZIMI, M.S., Theoretical modeling of forced convection condensation of steam in a vertical tube in the presence of a non-condensable gas, Nuclear Technology **106** (2) (1994) 202–215.

3.11. STRATIFICATION AND MIXING OF BORON

3.11.1. Introduction

In several reactor designs elevated tanks filled with borated water are designed to flood the core by gravity under emergency situations. The operation of the system requires that the isolation valve be open and that the driving head of the fluid exceed the system pressure plus a small amount to overcome the cracking pressure of the check valve. A precondition of the functionality of the system is the well mixed of the borated water. Disturbances of this state can occur during the filling procedure of the tank.

There exist only few experiments and theoretical investigations directed on this particular application. A broader experimental and theoretical background was elaborated on the boron mixing and stratification phenomena in the primary circuit of a nuclear reactor. The knowledge gained in this field concerning the capability of codes can also be applied on the actual plant application cases.

CFD codes for solving of lots of connected questions can be successful for momentum driven flow situations. Deficiencies are found in simulating a density driven flow situation. The flow type can be identified by the Froude Number.

3.11.2. Relevant scenarios

The main issues relating to the boron mixing and stratification phenomena in the primary circuit are;

- the formation of boron diluted slugs
- the onset of slug motion
- and the slug mixing and transport

Boron diluted slugs can be formed by external dilution at flow stagnation in the loop. Inherent dilution can occur at boiler-condenser operation or at back flow from the secondary side of the steam generator

during the primary-to-secondary leakage accidents. The slug can be transported into the core by restart of the main coolant pump or by re-establishment of natural circulation in a loop.

The main issues relevant for slug of diluted boron mixing and transport are:

- turbulent mixing in forced flow
- buoyancy induced turbulent mixing and stratification
- significance of large scale swirls
- turbulence under accelerating and Low-Re (Reynolds number) flow conditions
- flow distribution to the idle loops
- influence of the geometry and of internal structures (sieve plates, etc.)

Turbulent mixing in forced flow is fully determined by transport due to the liquid motion and molecular diffusion.

Buoyancy induced turbulent mixing can play an important role during natural circulation conditions. Density differences existing between the deborated slug and the ambient coolant determine the mixing. Due to the preceding scenario, the diluted slug can be heavier or lighter than the coolant with normal boron content. One of the main effects introduced by the density differences is the stratification of the coolant flow. The relation of momentum and density controlled forces (described by the Froude-Number) determines the importance of the stratification.

The Froude-Number is defined by

$$Fr = \frac{V_{in}}{\sqrt{gH \frac{\rho_{in} - \rho_a}{\rho_{in}}}}$$

with the inlet velocity V_{in}, the gravity acceleration g, the height extension H and the fluid densities of injected fluid (ρ_{in}) and initial available fluid (ρ_a). For Fr>>1 the flow is momentum driven whereas for Fr<<1 the flow can be considered as buoyancy driven.

For high Froude-Numbers, an almost ideal mixing of the injected borated water with the loop coolant can be expected and the density effects are negligible. Stratification is not expected for inherently created de-borated slugs. It is assumed (and substantiated by experiments) that no density differences exist over the cross section of the main coolant pipe.

For low Froude-Numbers the flow is driven by density differences, where stratification may occur. Similar modelling deficiencies are to be expected like for the simulation of temperature differences in large pools.

3.11.3. The EU-project FLOMIX-R

The EU project FLOMIX-R was aimed at describing the mixing phenomena relevant for both safety analysis, particularly in steam line break and boron dilution scenarios, and mixing phenomena of interest for economical operation and the structural integrity [3.11-1]. Coolant mixing inside the nuclear reactor is the most important inherent safety mechanism against boron dilution or overcooling transients and in the case of pressurized thermal shock scenarios. In pressurized water reactors (PWRs), boron acid is added to the water coolant to compensate the excess reactivity of fresh fuel loadings. Due to different mechanisms or system failures, slugs of low borated water can accumulate in the primary cooling system. This can happen e.g. as a consequence of a SBLOCA, when coolant circulation is interrupted, steam produced in the reactor core is condensed in the steam generator, and a slug of low-boron condensate will accumulate at the cold leg of the primary circuit. During startup of coolant circulation after refilling the primary circuit with emergency cooling water or by switching on

the first main coolant pump, this slug will be transported into the reactor core causing a significant reactivity insertion by decreasing the amount of neutron absorber. The mixing of the deborated condensate with borated water in the reactor pressure vessel is in that case the only mitigation mechanism to prevent severe accident consequences [3.11-2]. The mixing is also relevant in overcooling transients, when the coolant temperature in one or more loops decreases e.g. due to a leak in the secondary side steam system [3.11-3]. A strong decrease of the coolant temperature does also cause a reactivity insertion due to the enhanced moderation of neutrons.

In this project, slug mixing and flow distribution in the reactor primary vessel has been comprehensively investigated experimentally and simulated by using computational fluid dynamics (CFD) tools. Within this project, a comprehensive data base on coolant mixing inside the RPV was created [3.11-4]. Slug mixing experiments have been performed with several 1:5 scaled facilities representing different European reactor types: The Rossendorf coolant mixing model ROCOM and the VATTENFALL test facility, modelling a German Konvoi type and a Westinghouse type three-loop PWR, respectively [3.11-2, 5 and 6]. Additional data on slug mixing in a VVER-1000 type reactor gained at a 1:5 scaled metal mock-up at EDO Gidropress are provided [3.11-7]. Experimental results on mixing of fluids with density differences obtained at ROCOM and the FORTUM PTS test facilities are made available [3.11-2, 4, and 8]. Data from steady state mixing experiments at ROCOM [3.11-2] and plant commissioning test data from the NPP Paks and Loviisa [3.11-9, 10] were gained and used to contribute to the validation of CFD codes for the analysis of turbulent mixing problems. The commercial CFD codes CFX4, CFX5 and FLUENT6 have been used. The main objective was to investigate how well mixing during boron dilution transients in PWRs can be modelled by CFD codes.

3.11.3.1. Experimental basis

In some of the thermohydraulic integral test facilities, experiments for the investigation of boron mixing and stratification phenomena were performed The facilities, which are designed particularly for this purpose are the Vattenfall mixing test facility, the ROCOM facility in the Forschungszentrum Dresden-Rossendorf, the VVER-1000 mixing test facility at EDO Gidropress and the Fortum test facility on PTS.

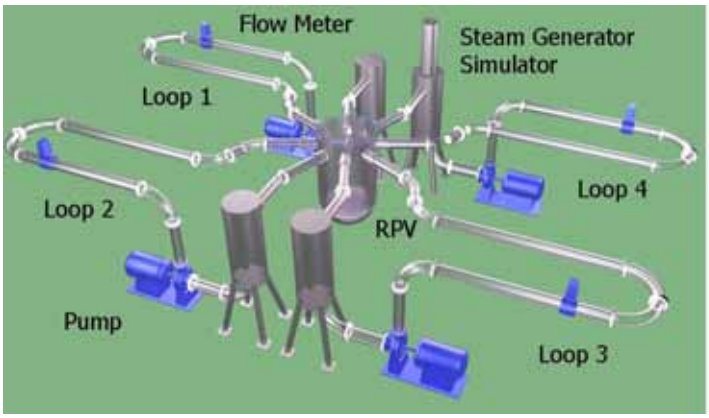

FIG.3.11-1. Scheme of ROCOM.

Figure 3.11-1 shows the schematic of the ROCOM facility (Rossendorf Coolant Mixing Model) which was erected for the investigation of coolant mixing in the reactor pressure vessel of a PWR. The test facility was designed for the investigation of a wide spectrum of mixing scenarios. Experiments are carried out to measure the time dependent distribution of the transport variables, coolant temperature, and boron concentration inside the reactor pressure vessel. The leading input variables are the time history of the flow rates in the four loops of the primary circuit as well as the coolant temperature or boron concentration in the inlet nozzles, respectively. The differences in either boron concentration or coolant temperature are modeled by means of a salt tracer solution, which influences the electrical

conductivity. The test facility is equipped with wire mesh measurement instrumentation on all essential positions, which allows a high resolution measurement of the transient tracer concentration in space and time.

3.11.3.2. CFD calculations

Different CFD codes were used and sensitivity tests for the following aspects were considered:

- Grid size
- Convergence criteria
- Round-off error
- Time step size
- Turbulence model
- Inlet boundary position and inlet boundary condition
- Outlet boundary position
- Internal geometry

Figure 3.11-2 shows examples for computational grid and time step sensitivity using the CFX-5 code. The number of mesh points for the discretization of the solution area has to be increased until convergence of the solution has been achieved (mesh with about 750.000 elements using the Upwind Discretization Scheme UDS). The same procedure has to be applied concerning time step refinement.

However, in practical applications with complicated geometry and complex flow phenomena like the mixing problems considered, a grid and time step independent solution cannot often be reached due to computing capacity limitation. In these cases, so called production meshes were used in the calculations. The production mesh is an optimum between maximum possible refined grid on the one hand, but with omitting parts of the flow domain, which were found to be of small impact on the results, e.g. the cold leg loops, and neglecting or simplifying some geometrical details e.g. by modelling complicated structures as porous body domain. In general, the choice of the production mesh is dependent from the process to be simulated. The production mesh for momentum driven mixing calculations might be different from that one for the analysis of buoyancy controlled mixing. The production mesh for the CFX-5 calculations was an unstructured grid with about 7 million elements (see Fig. 3.11-4).

Concerning numerical solution schemes, higher order schemes are preferred due to higher accuracy. Figure 3.11-3 shows the velocity distribution (vertical component) in the core inlet plane calculated with the FLUENT code for steady state conditions with one running pump in the Vattenfall facility by applying first order and second order scheme. Using the first order scheme, the solution is well converging, but physically wrong. The position of the maximum velocity observed in the experiment is not met in the first order solution. The reason is to be seen in the influence of inlet boundary conditions. The bend in the cold leg pipe not far from the RPV inlet nozzle causes an asymmetric velocity profile and turbulence parameters distribution at the RPV inlet. This impact of the bend is not well reproduced in the more diffusive first order scheme calculation. The disturbance caused by the bend is not “transported” to the core inlet plane, the diffusive scheme “forgets” about it.

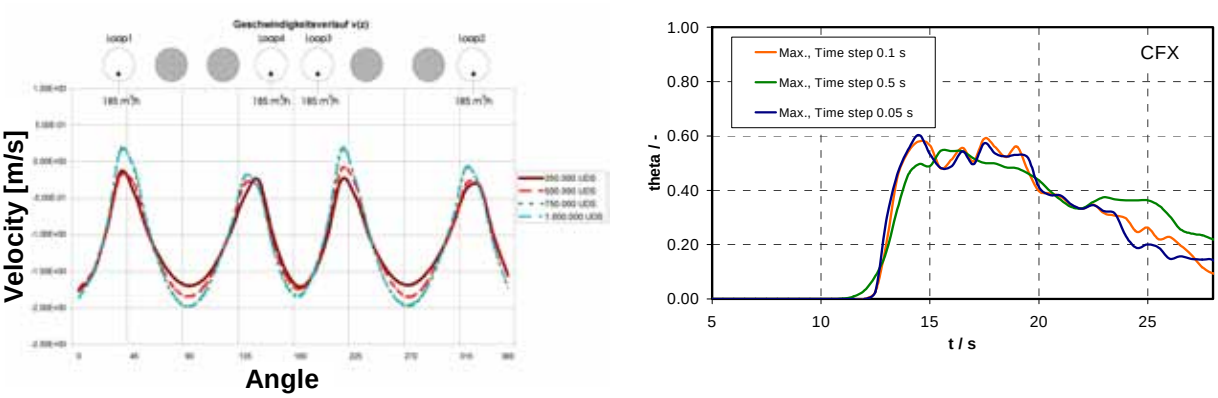

FIG. 3.11-2. Mesh and time step refinement to obtain converged numerical solutions — velocity distribution in the downcomer (upper) and time dependent global maximum of the mixing scalar at the core inlet (lower).

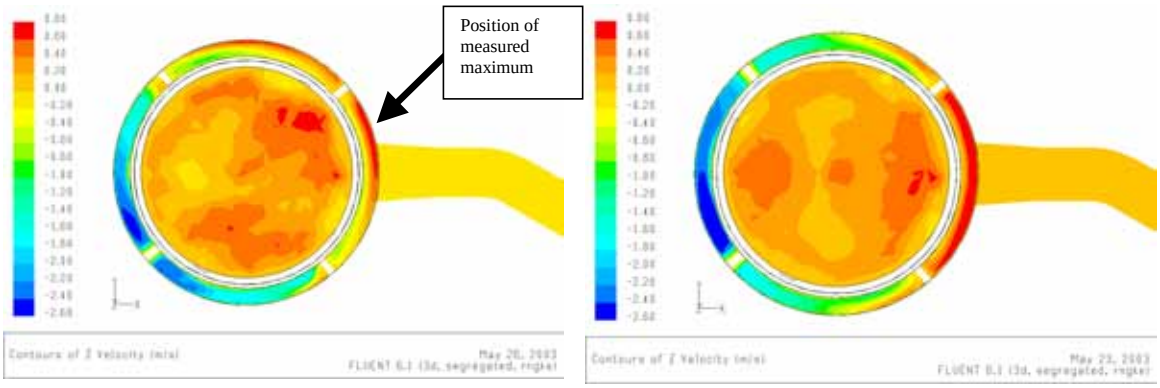

FIG.3.11-3. Calculated velocity distribution in the core inlet plane (in m/s) — at the second order (left) and first order (right) solution.

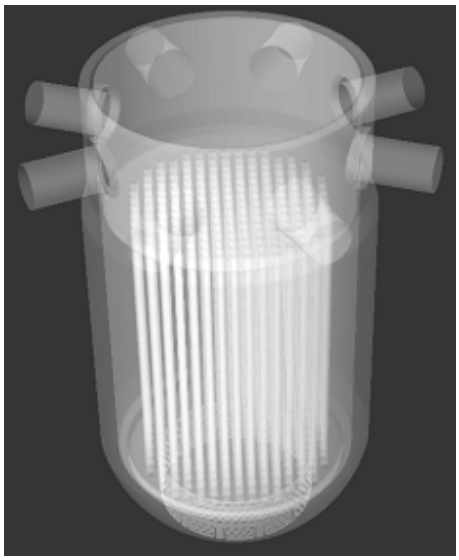

FIG.3.11-4. Visualization of the ROCOM production mesh for the CFX-5 calculations.

Figure 3.11-5 shows a comparison between CFD solutions and experiment for the steady state mixing test ROCOM-stat01 with four running pumps. The sector formation and the high maximum mixing scalar values are well reproduced in the calculation. The best agreement was achieved, when a transient calculation for the steady state conditions was performed, because the velocity field in the flow domain is not really time independent even with steady state boundary conditions. Macroscopic fluctuations occur, which are averaged from the transient solution.

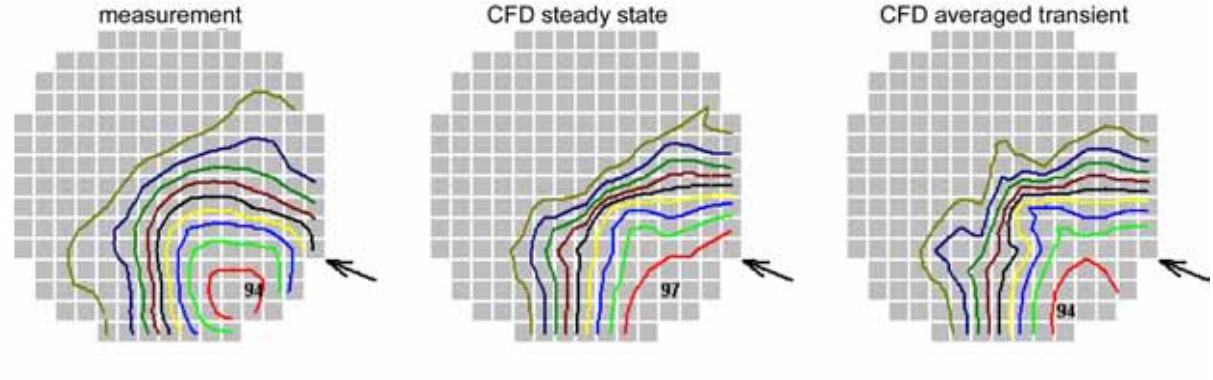

FIG.3.11-5. Comparison of the results from the steady state mixing test ROCOM_stat01.

3.11.3.3. CFD calculations for non-buoyant slug mixing tests

A detailed quantitative comparison of the results of CFD-calculations with measurements in the complex geometry of the model of a pressure vessel was performed. Different steady state and transient experiments and calculations were considered. The comparison was mainly concentrated on the core inlet plane. Additionally, the velocity distribution in the downcomer was compared.

In the steady state experiments, the different codes show the same global tendencies. The quantitative analysis demonstrated, that the spreading of the tracer in radial direction is underestimated in all presented calculations. The transient calculation with constant velocity in time shows the best agreement in the shape of the distribution of the mixing scalar in the core inlet plane and in the calculated maximum value. Further, the comparison of measurement positions, for which the coolant should flow through the sieve drum or around the sieve drum revealed great differences.

The pump startup experiment ROCOM-02 was calculated by the codes CFX-4 und CFX-5. The time behaviour of the maximum and the average perturbation calculated by both codes is inside the confidence interval of 2 σ during the main part of the considered time interval.

3.11.3.4. CFD calculations for buoyancy driven mixing experiments

The experiment was performed at the ROCOM facility with injection of water with 10% increased density into the cold leg with 5% of nominal flow rate. The computational grid includes detailed models of the sieve barrel, the core support plate and the rods modelling the core in the ROCOM test facility. The cold leg with the ECC-injection nozzle was added in order to capture the flow stratification in the cold leg which also influences mixing in the downcomer. The injection of water with higher density was performed from 5 to 15 s. Calculations were made using second order discretization schemes in space and time. Two constant time steps (0.1 s and 0.05 s) were used in combination with the SST turbulence model and scalable wall functions.

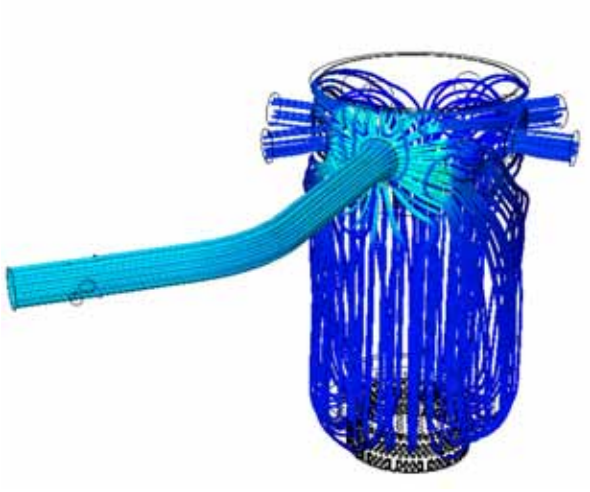

Streamlines representing the fluid flow
before the injection takes place (4 s)

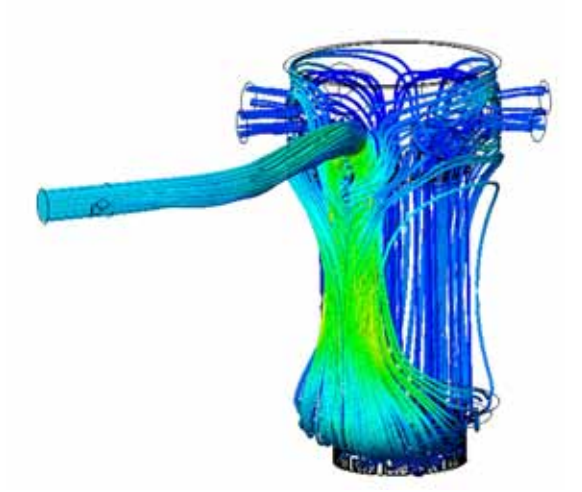

Streamlines representing the fluid flow
after the injection took place (23 s)

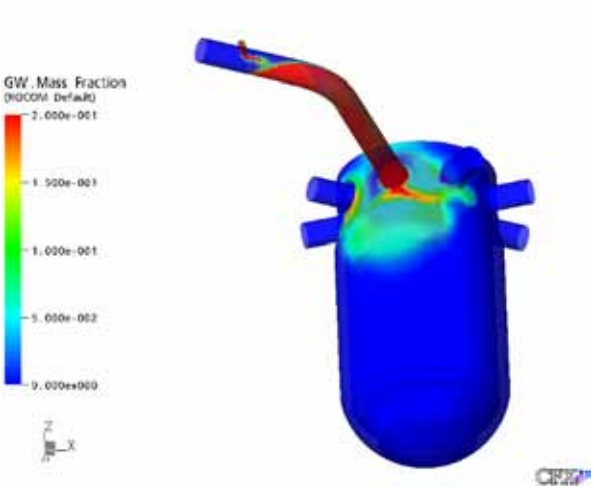

Tracer distribution (16 s)
zoomed mixing scalar Θ (0.0-0.2)

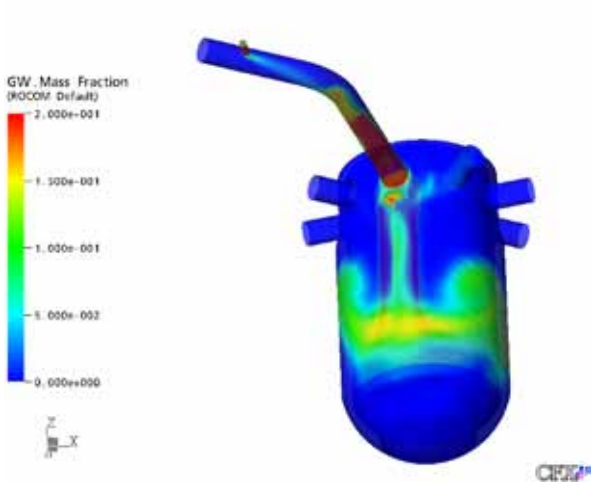

Tracer distribution in the downcomer (23 s)
zoomed mixing scalar Θ (0.0-0.2)

FIG. 3.11-6. Streamlines representing the fluid flow and tracer concentration in cold leg and RPV at different times.

Figure 3.11-6 (upper) shows the flow in the cold leg during and after the injection of the glucose solution. There is evidence of strong stratification with a higher concentration of glucose on the bottom of the cold leg. The glucose solution flows downwards directly below the inlet pipe (see Fig. 3.11-6, lower). A similar behaviour was also observed in the experiment.

Investigations on the influence of the turbulence model were performed by using a Reynolds Stress model (RST), based on the omega equation. The RST model, although calculated with the larger time step (due to higher computer resources requirements), shows better agreement with the measured data. However, quantitative comparison between measurement and calculation is difficult especially for the buoyancy driven mixing cases because of the fluctuating nature of the flow field and mixing pattern. It might be more useful to compare some averaged or integral parameters. This was done e.g. for the Fortum PTS experiments.

The buoyancy driven turbulent flow with stratification and mixing in selected Fortum mixing tests was modelled using the commercial CFD code FLUENT. The comparison was mainly based on the temperature/concentration data from the thermocouple locations near the pressure vessel wall and in the main (middle one) cold leg. The stratification and mixing in the main loop was studied using backflow ratio $Q^* = Q_h/Q_{HPI}$. Where Q_{HPI} is the cold water injection flow rate and Q_h is the flow rate from the downcomer to the main loop. The mixing of the cold water plume in the downcomer was studied using time dependent maximum and average injection water concentrations at RPV wall at different vertical levels.

The main features of flow and mixing were quite well simulated; stratification in the main cold leg and the downcomer, backflow from the downcomer and side loops to the main loops and the flow field in the downcomer. However, the mixing of the cold water plume was not as effective in simulations as in the experiments. More grid size tests with transient simulations are needed to test the grid-independency of simulations.

Preliminary turbulence models tests with Realizable k-ε and RNG k-ε models did not identify any significant differences between models.

3.11.3.5. CFD simulation mixing tests at Paks NPP (WWER-440 reactor)

Additional test data were made available by Paks NPP and AEKI for the FLOMIX-R project [3.11-9] and Rohde [3.11-4]). The data have been gained from commissioning tests of Paks NPP performed in years 1987–1989. The tests addressed mixing among coolant loop flows in the downcomer and up to the core inlet in forced flow conditions. The goal of the tests was to investigate potential loop temperature asymmetry that might occur and significantly affect power distribution in the core. Paks mixing experiments were simulated by VUJE (FLUENT), AEKI (FLUENT) and TU Budapest (CFX5). The calculations were performed for actual plant geometry. More detailed descriptions of the CFD analyses are given in Ref. [3.11-11].

Comprehensive computer models of VVER 440 reactor vessel were developed. They include all 6 loops with inlet nozzles and three baffles, whose purpose is to deflect the coolant injected into the reactor vessel from the safety injection tanks. Eight support consoles for the core barrel alignment were modelled as well. The mesh sensitivity tests showed that the calculational meshes did not meet the grid-independency criteria, in spite of the large node number. It was concluded that hybrid tetrahedral-hexahedral meshing which is available in modern CFD codes seems to be more suitable for the pressure vessel geometry because of the possible optimization between necessary number of mesh elements, adequate spatial resolution and the required effort for the mesh generation.

The performed calculations showed that the downward flow of the coolant in the downcomer shows clear distinct sectors. These sectors remain also at the core inlet. The maximum of the mixing scalar is not located directly below the inlet nozzle, but an azimuthal shift of the maximums can be observed because of the asymmetric location of the inlet nozzles and because of the hydro-accumulator baffles. The effect of the baffles can be observed even at the core inlet.

The results show qualitatively good agreement with the measured data. However, the mixing is underestimated in the predictions (the calculated maximums of the mixing scalars are larger than the measured ones). Following conclusions on the CFD modelling of the flow distribution in the RPV of a VVER-440 type reactor were drawn:

- Good numerical convergence was achieved with basic solver and solver settings based on residuals of continuity and momentum equations (using first order upwind discretization scheme and k-ε or RSM turbulence model).
- Some numerical fluctuations of the flow field were observed below the ECC baffles in the downcomer, possibly due to some unsteadiness of the flow field.
- Modelling of detailed internal geometry (e.g. flow baffles) may have a noticeable influence on results.

- ECC water baffles guide the main flow and generate turbulence effects in the downcomer.
- The alignment drifts have only local effect.
- Accurate model of the perforated elliptical bottom (modelling the elliptical perforated bottom as solid structure rather than using a porous medium) provides more realistic flow pattern and improves the accuracy of the calculation.
- Using pressure outlet boundary condition gives better numerical convergence than outflow boundary.
- Boundary layer at the walls of downcomer should be less then 3 mm, to keep y+ parameter less than 1000.
- High order methods decrease the numerical stability of the solution.

3.11.4. KAERI activities on APR-1400

The core bypass phenomenon of borated water injected through direct vessel injection nozzles in APR1400 (Advanced Power Reactor 1400MWe) during main steam line break (MSLB) accidents with a reactor coolant pump (RCP) running mode (see Fig. 3.11-14) has been simulated using a two channel and one dimensional system analysis model code (MARS), and a three dimensional CFD code (FLUENT) [3.11-12].

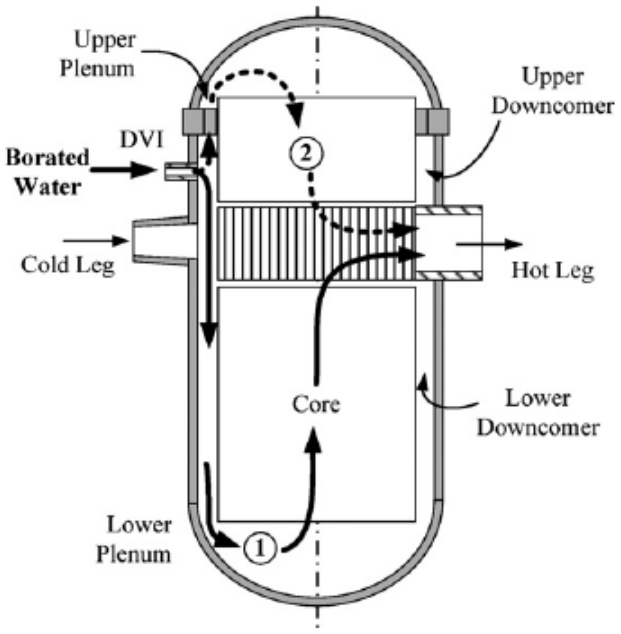

FIG.3.11-14. Flow paths of borated water in the APR1400.

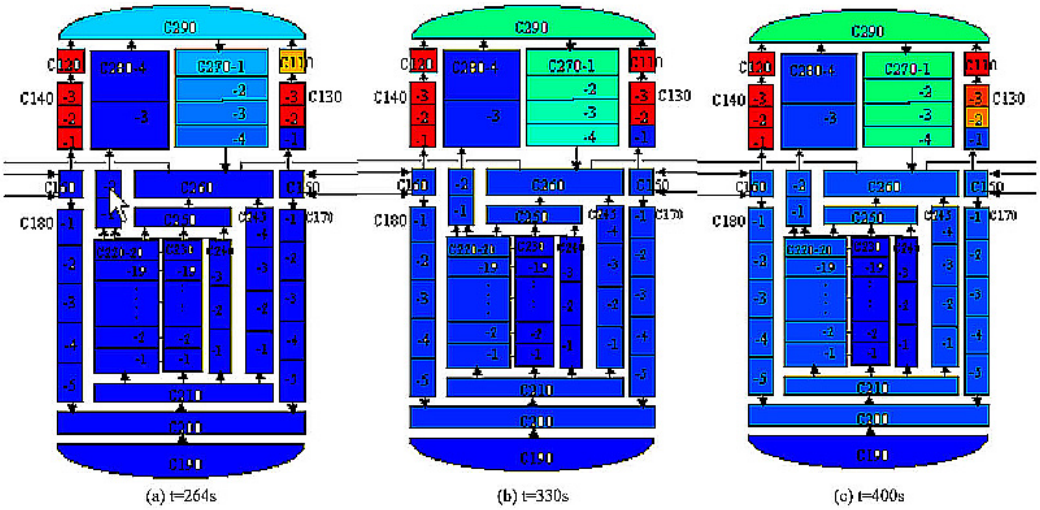

FIG.3.11-15. Propagation of borated water injected by DVI (calculated by the MARS code).

The results obtained from the two channel system analysis model of MARS have revealed that most of the borated water injected through the direct vessel injection nozzle flows mainly from the upper downcomer to the upper head of the reactor vessel and finally flows out through the upper plenum and the hot legs, and a small amount of borated water flows into the lower downcomer due to the high RCP flows during the HPSI mode of MSLB accidents.

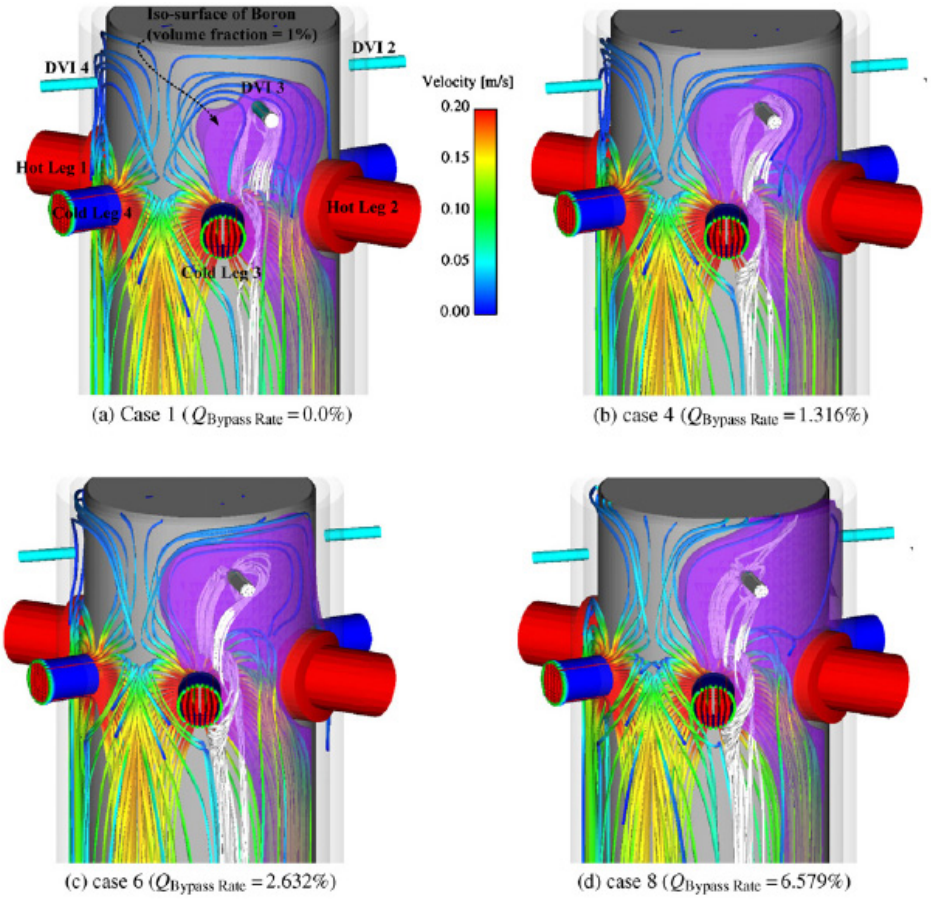

FIG.3.11-16. Flow pattern (pathlines) of ECC water and borated water, and iso-surface of volume fraction of borated water calculated using FLUENT.

MARS analysis using a two-channel and one dimensional system analysis model code predicted a serious core bypass phenomenon of borated water (see Fig. 3.11-15, Choi et al. 2007) [3.11-12], while three dimensional CFD analysis using FLUENT has shown results opposite to the MARS results (see Fig. 3.11-16). The CFD analysis has noted that the flow pattern in the downcomer is fully three dimensional and a vortex column formed near the cold legs due to impinging jets helps borated water to run downwards to the lower downcomer and core.

Although the CFD analysis predicted that core bypass phenomenon of borated water may occur through upper plenum when the ratio of total bypass flow rate through the upper plenum is increased, the degree of the core bypass phenomenon of borated water was not as much as with the MARS results. Visualization experiments performed using a scaled-down model of the APR1400 have also shown that borated water flows well to the lower plenum, as in the CFD analysis. The overall flow patterns of borated water observed during the visualization experiment are very similar to those with the CFD analysis. Both the CFD analysis and the visualization experiment have shown that a significant core bypass of borated water might not happen in the APR1400.

3.11.5. FZD Experiments and CFD calculations on the VeMix facility

A description of the facility is needed at an early stage. Extended turbulence models have been developed [3.11-13] by introducing additional balance equations for the turbulent quantities “turbulent mass flow” and “density variance”. The models have been implemented into the computational fluid dynamics code ANSYS-CFX. The validation of the models was performed against tests at a special experimental set-up, the VeMix facility (Fig. 3.11-17), where fluid of higher density was injected into a vertical test section filled with lighter fluid. As validation criteria the switching-over between a momentum controlled mixing pattern with a horizontal jet and buoyancy driven mixing with vertical sinking down of the heavier fluid was used. These two flow patterns are shown on Fig. 3.11-18. For the investigation of the mixing processes an especially developed conductivity wire mesh sensor was used [3.11-14]. The sensor is shown on Fig. 3.11-19.

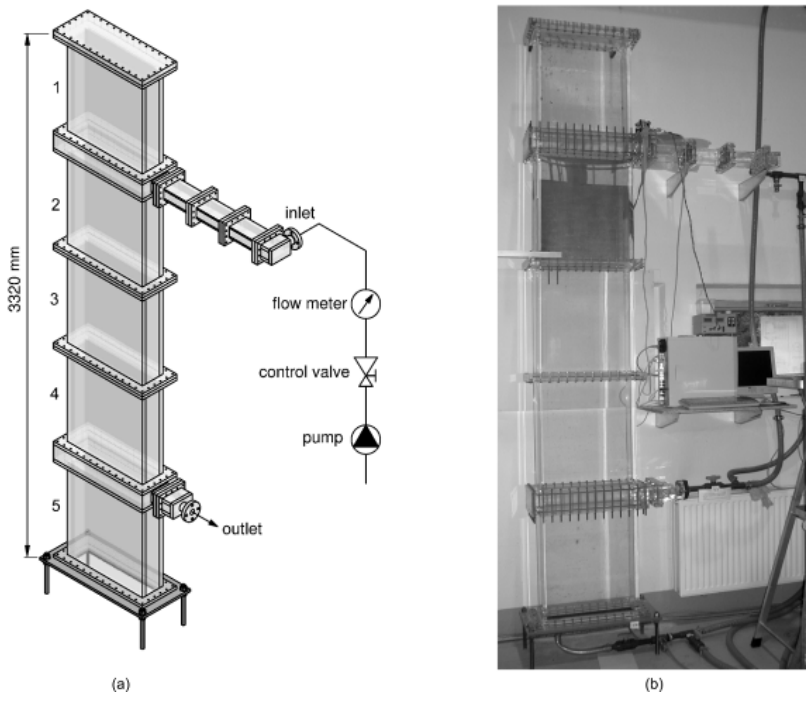

FIG.3.11-17. Schematic diagram (a) and photograph (b) of the test facility used in the buoyancy-driven flow experiment.

However, an improvement of the modelling of buoyancy driven mixing by use of the extended models could not be shown, because the calculated differences applying the different models were not relevant. Fig. 3.11-20 shows the calculated density distribution in one of the VeMix experiments with and without additional source terms in the balance equations for the turbulent quantities (middle and left figure) in comparison with measurement data from the wire mesh sensor (left).

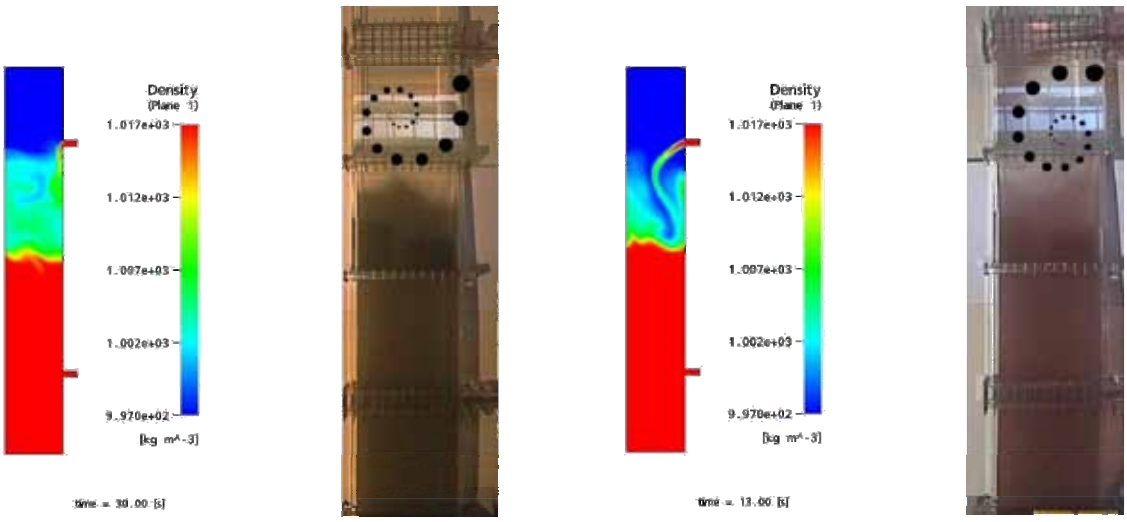

(a) falling down regime: flow rate = 0.4 l/s, Ri = 2.12

(b) horizontal jet regime: flow rate = 0.7 l/s, Ri = 0.69

FIG.3.11-18. Richardson Number (Ri) dependent flow regime for the flow condition $\Delta\rho$ = 2%, L = 0.83 m .

On the other hand, the modelling of the stratification of fluids with different density in the cold leg of a reactor primary circuit could be significantly improved when the profiles of the velocity and turbulence intensity over the cross section of the cold leg are correctly set at the location of the injection of heavier water. This can be achieved only if sufficient large parts of the cold legs are included in the modelling.

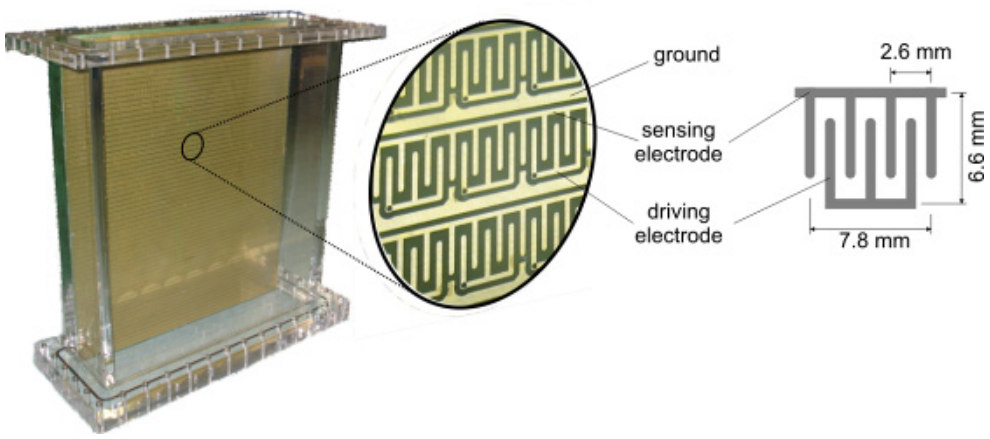

FIG.3.11-19. Surface wire mesh sensor with 64 x 64 measurement positions at the inner wall of a vertical test section of the VeMix facility (da Silva 2008).

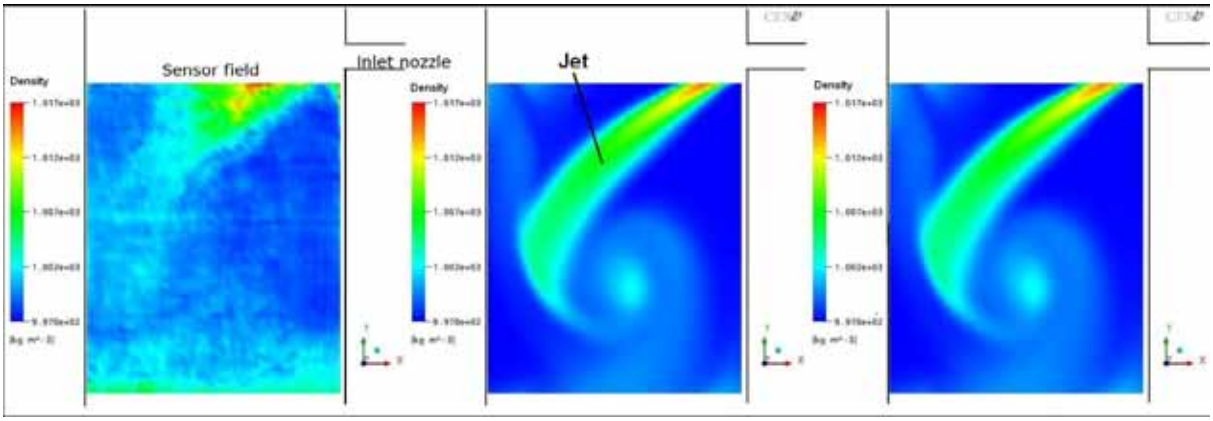

FIG.3.11-20. Calculated density distribution in a vertical section of the VeMix facility with use of different turbulence models (middle and right) in comparison with measured data (left).

3.11.6. Code capabilities

The capabilities of CFD codes are continuously growing due the rapid developments in computer technology. However, computer capacity is still, and will be for a foreseeable future, a limiting factor for the capacity for CFD calculations to produce completely accurate results. Simplified models for describing turbulence therefore have to be used and the computer capacity put restrictions on the resolution in space and time that one can use in a CFD calculation. This leads to modelling and numerical errors that could potentially give inaccurate results. Validation of the quality and trust of different approaches in CFD calculations are therefore needed. The Best Practice Guidelines (BPG) were used for quality assurance of the validation calculations. The ERCOFTAC BPG [3.11-15], have been specified for nuclear reactor safety calculations [3.11-16]. The BPG are built on the concept of an error hierarchy. The different types of errors in CFD simulations are divided into the two main categories:

- Numerical errors, caused by the discretization of the flow geometry and the model equations, and by their numerical solution
- Model errors, which arise from the approximation of physical processes by empirical mathematical models

This concept implies that numerical errors are quantified and reduced to an acceptable level, before comparison with experimental data is made. That means the CFD solution has to be shown to be grid-independent, i.e. results that do not change when the grid is refined further. A grid-independent solution can be defined as a solution that has a solution error that is within a range that can be accepted by the end-user, in view of the purpose of the calculations.

Developments in computer technology will make these quantifications of solution errors possible within a few years. The number of cells required for grid-independency can only be guessed. Several million cells are probably needed for most of the transient test cases in the shown examples of FLOMIX-R.

In most cases for the correct simulation of Boron mixing phenomena, a CFD model approach is necessary. Different analyses of corresponding experiments by CFD calculations have shown that the improvement of standard models has an only limited effect on the agreement of calculated to measured data. The correct simulation of all relevant boundary condition however plays a significant role. It has been demonstrated on calculations of experiments at the ROCOM mixing test facility, that e.g. the stratification in the cold leg is relevant as a boundary condition for the mixing process inside the reactor pressure vessel [3.11-17].

REFERENCES FOR SECTION 3.11

[3.11-1] ROHDE, U., et al., Fluid mixing and flow distribution in a primary circuit of a nuclear pressurized water reactor — validation of CFD codes, Nuclear Engineering and Design **237** 15-17 (2007) 1639–1655.

[3.11-2] KLIEM, S., ROHDE, U., WEISS, F.-P., Core response of a PWR to a slug of under-borated water, Nuclear Engineering and Design **230** (2004) 121–132.

[3.11-3] KLIEM, S., HÖHNE, T., ROHDE, U., WEISS, F. P., Main steam line break analysis of a VVER-440 reactor using the coupled thermohydraulics system/3D-neutron kinetics code DYN3D/ATHLET in combination with the CFD code CFX-4, 9th International Topical Meeting on Nuclear Reactor Thermal Hydraulics (NURETH-9), San Francisco, CA, October 3–8 (1999).

[3.11-4] ROHDE, U., et al., Fluid mixing and flow distribution in the reactor circuit measurement data base, Nuclear Engineering and Design **235** (2005) 421–443.

[3.11-5] ALAVYOON, F., HEMSTRÖM, B., ANDERSSON, N.G., KARLSSON, R.I., Experimental and computational approach to investigating rapid boron dilution transients in PWRs, Report No. US 95:4, presented at the OECD Specialist Meeting on Boron Dilution Reactivity Transients, State Collage, PA, U.S.A., 18–20 October (1995).

[3.11-6] PRASSER, H.-M., GRUNWALD, G., HÖHNE, T., KLIEM, S., ROHDE, U., WEISS, F.-P., Coolant mixing in a pressurised water reactor: deboration transients, steam-line breaks, and emergency core cooling injection, Nuclear Technology **143** July (2003) 37–56.

[3.11-7] BEZRUKOV, Y., et al., Documentation of Slug Mixing Experiments of OKB Gidropress, EU/FP5 FLOMIX-R-D16, Podolsk, Russian Federation (2002).

[3.11-8] TUOMISTO, H., Thermal-hydraulics of the Loviisa reactor pressure vessel overcooling transients, Imatran Voima Oy, Research Report IVO-A-01/87 (1987).

[3.11-9] ELTER, J., Experiment summary report, experimental investigation of thermal mixing phenomena in a six loop VVER type reactor, Paks Nuclear Power Plant Ltd., Safety Assessment Group, Flomix-R Project (2002).

[3.11-10] TSIMBALOV, S., et al., Coolant temperature distribution at VVER-440 core inlet, Atomnaya Energiya **52** (5) (1982) 304–308.

[3.11-11] HEMSTRÖM, B., HÖHNE, T., et al., Validation of CFD codes based on mixing experiments (final report on WP4), EU/FP5 FLOMIX-R Report, FLOMIX-R-D11. Vattenfall Utveckling, Sweden (2005).

[3.11-12] CHOI, C.R., KWON, T.S., SONG, C.H., Numerical analysis and visualization experiment on behaviour of borated water during MSLB with RCP running mode in an advanced reactor, Nuclear Engineering and Design **237** (2007) 778–790.

[3.11-13] VAIBAR, R., ROHDE, U., HÖHNE, T., CFD-Modellierung von Vermischungsvorgängen in Druckwasserreaktoren in Anwesenheit von Dichtegradienten (CFD modelling of mixing phenomena on PWR influenced by density gradients) (in German), Scientific-technical report FZD-500, Research Centre Dresden-Rossendorf, Rossendorf, July 2008, ISSN 1437-322X (2008).

[3.11-14] DA SILVA, M.J., THIELE, S., HÖHNE, T., VAIBAR, R., HAMPEL, U., Experimental studies and CFD calculations for buoyancy driven mixing phenomena, XCFD4NRS — Experiments and CFD Code Applications to Nuclear Reactor Safety, 10.-12.09.2008, Grenoble, France (2008).

[3.11-15] CASEY, M., WINTERGERSTE, T., Best Practice Guidelines, ERCOFTAC Special Interest Group on Quality and Trust in Industrial CFD, Report (2000).

[3.11-16] MAHAFFY, J., et al., Best practice guidelines for the use of CFD in nuclear reactor safety applications, NEA/CSNI/R(2007)5 (2007).

[3.11-17] HÖHNE, T., KLIEM, S.; VAIBAR, R., Experimental and numerical modeling of transition matrix from momentum to buoyancy-driven flow in a pressurized water reactor, 16th International Conference on Nuclear Engineering ICONE-16, 11.-15.05.2008, Orlando, USA, CD_ROM, 48490 (2008).

3.12. BEHAVIOUR OF CORE MAKE-UP TANK

In ALWR designs, gravity driven safety injection systems replace many of pump driven injection systems. One such system is the CMT. CMTs are used to replace the high pressure safety injection system in PWRs. The CMTs are nominally filled with cold borated water and are connected to the primary system by the PBL to the cold leg and the injection line to the downcomer. The outlet valve on the injection line is normally closed and will open on a safety injection signal to allow for flow into the primary system. CMTs are included in such ALWR designs as the AP600/1000 and the AC600/1000.

In the AP600, during a SBLOCA, the pressure and coolant inventory will decrease as mass and energy are lost out of the break. Following a sufficient reduction in pressure, a safety signal will be generated by the reactor protection system, the reactor will scram and the RCPs will trip. In addition, PRHR valves and the CMT outlet valves will open. Following the RCP trip, the plant will transition from forced convection to a single phase natural circulation cooling mechanism. Single phase natural circulation will remain effective until the SG tubes begin to void.

With the opening of the CMT outlet valve, cold borated water inside the CMT will begin to move by gravity into the downcomer through the DVI line. Concurrently, hot water will flow from the cold leg into the CMT to replace the cold water leaving the CMT. This natural circulation through the CMT is driven by the small density differences between the PBL and the injection line. Initially, there will be a sharp interface between the cold and hot coolant in the CMT. As the transient progresses mixing will occur at this interface making the interface less pronounced. This phase is often referred to as the recirculation phase. During the recirculation phase wall heat transfer through the CMT walls and mixing within the CMT are important phenomena to consider.

The next phase describing CMT behaviour during the SBLOCA is the oscillation phase. As the water level continues to drop in the primary system, two phase flow begins to enter the CMT through the PBL. In addition, the drop in pressure of the system may lead to steam flashing in the CMT. These mechanisms will lead to steam collecting in the CMT and the beginning of CMT draining. Condensation of steam on the CMT walls may lead to partial refills during the transient.

Continued release of primary coolant from the system will eventually lead to a situation where there is only steam entering the CMT through the PBL. At this point the CMT has entered the injection phase which is characterized by continued CMT draining. Although steam flow through the PBL is important during this phase, steam flashing in the CMT may still be occurring.

Eventually, the CMT level will drop sufficiently to trip an opening of the ADS1-3 valves. The drop in pressure due to the ADS blowdown will cause an injection of the accumulators. Accumulator injection may interrupt the draining of the CMT. However, upon completion of the accumulator injection CMT draining will resume. The CMT may drain to a point that triggers an opening of the ADS4 valves and a further blowdown of the primary system to near atmospheric pressure and an actuation of IRWST draining [3.12-1–3.12-6].

3.12.1 Core make-up tank phenomena

Several phenomena can arise during the operation of the CMT system. This includes

- Natural circulation flow
- CMT thermal stratification
- CMT draining

3.12.1.1. Natural circulation flow and CMT thermal stratification

During the natural circulation phase of a transient, cold borated water flows into the reactor downcomer while hot primary coolant flows into the head of the CMT. The flow rate is determined by

a balance between the CMT loop resistance and the buoyancy force created by the elevation and density differences of the CMT and reactor coolants. As natural circulation progresses, thermal layers will begin to form within the CMT. As the thermal layers grow in the upper portion of the CMT, the driving head for natural circulation is reduced. For prolonged operation at constant pressure, the entire volume of water inside of the CMT will reach equilibrium temperature with the primary fluid and natural circulation will stop or behave in an oscillatory manner. Single phase fluid natural circulation is reasonably well understood and predicted. IAEA-TECDOC-1474 describes a wide range of studies, models, and code comparisons for single phase natural circulation behaviour. The challenge is predicting the thermal layer growth in the CMT [3.12-5].

Flow oscillations can also occur when the water level in the cold leg is close to the height of the connection of the flow injection line. Tuunanen et al. performed experiments with different break sizes in the primary loop. For small breaks, Tuunanen et al. observed oscillating flow in the CMT lines through the entire experiment. The liquid in the CMT and the connected lines will become full of hot water before the CMT begins to inject water removing the driving force for natural circulation [3.12-6].

3.12.1.2. CMT draining

The phenomena of primary interest to CMT operation occurs during CMT draining. During this phase of operation, the balance line that connects the reactor cold leg to the CMT begins to void either by flashing or draining. When this occurs, natural circulation is interrupted and the fluid level in CMT begins to decrease. The CMT head is filled with saturated steam. Heat transfer from the CMT walls to the surrounding air at ambient temperature can result in steam condensation. Rapid condensation can occur inside the CMT if the thermal layer inside of the CMT is broken. Condensation and convective heat transfer takes place on the inside walls of the CMT. Flashing at the surface of the water can also occur causing an interruption of natural circulation.

3.12.2. Predictive models for CMT behaviour

This section presents predictive models for CMT gravity draining and convective heat transfer.

3.12.2.1. CMT draining model

Figure 3.12-1 shows a schematic of a simple tank that can be used to help understand the governing equations of the CMT's. The pressure at the liquid free surface is denoted by P_{FS}. The pressure at the injection line exit is denoted by P_E. The CMT's are filled with cold borated water. Hence, it is reasonable to assume that the working fluid is incompressible. The cross-sectional area of the tank, A_{Tank}, is assumed constant for this analysis. The injection flow area is denoted by A_E. The injection lines usually include multiple check valves, isolation valves and bends. As a result, the form loss coefficient, K, typically dominates the pressure drop in the line. The injection mass flow rate is denoted by $\dot{m}_{inj}$ and the time dependent liquid level by L(t). The governing equations for the CMT are provided in Table 3.12-1.

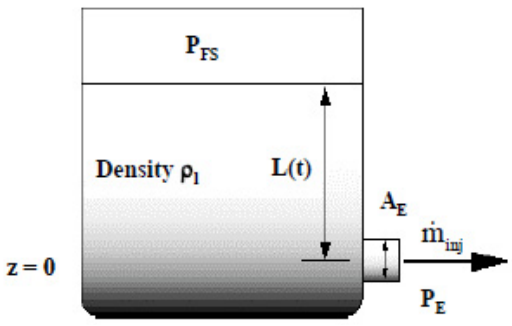

FIG. 3.12-1. CMT control volume for draining process.

TABLE 3.12-1. CMT GOVERNING EQUATIONS

Governing Equations

Mass Conservation:

$$\rho_l A_{Tank} \frac{dL}{dt} = -\dot{m}_{inj} \tag{3.12-1}$$

Bernoulli Equation:

$$\frac{P_{FS}}{\rho_l g} + z_{FS} + \frac{v_{FS}^2}{2g} = \frac{P_E}{\rho_l g} + z_E + \frac{v_E^2}{2g} + h_l \tag{3.12-2}$$

Darcy Formula:

$$h_l = \frac{v_E^2}{2g}\left(\frac{fl}{d} + K\right) = \frac{v_E^2}{2g}\Pi_{FE} \tag{3.12-3}$$

Governing Differential Equation

$$\rho_l A_{Tank} \frac{dL}{dt} = -\dot{m}_0 \left[\frac{\Delta P + \rho_l g L}{\Delta P_0 + \rho_l g L_0}\right]^{1/2} \tag{3.12-4}$$

Where:

$$\dot{m}_0 = A_E \left\{\frac{2\rho_l\left(\Delta P_0 + \rho_l g L_0\right)}{1+\Pi_{FE}}\right\}^{1/2} \tag{3.12-5}$$

The primary driving force for the CMT is gravity. It is assumed that the static pressure at the free surface equals that at the injection line exit. Thus the governing differential equation is given by Eq. (3.12-6) in Table 3.12-2. Using the initial conditions described by Eqs (3.12-7) and (3.12-8), the governing differential equation can be written in dimensionless form as given by Eq. (3.12-9). Equation (3.12-11) defines a characteristic residence time, τ, as the ratio of the initial liquid mass in the tank and the initial injection flow rate. Equation (3.12-9) can be integrated to obtain a very simple expression for the liquid level as a function of time.

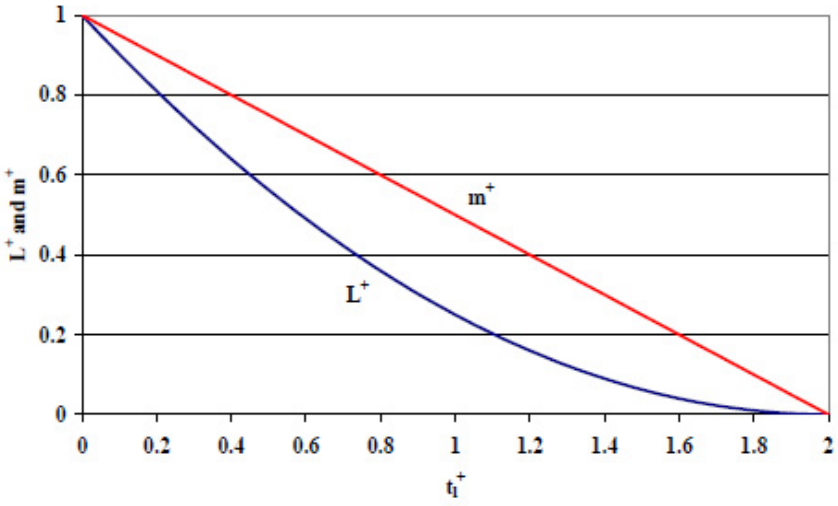

FIG. 3.12-2. Gravity draining curve.

Figure 3.12-2 presents a universal curve for gravity draining for the case of a tank with constant cross-sectional area with an incompressible working fluid and an exit line pressure drop that is dominated by form losses.

TABLE 3.12-2. GOVERNING DIFFERENTIAL EQUATIONS FOR GRAVITY DRAIN TANK

Governing Differential Equation

$$\rho_l A_{Tank} \frac{dL}{dt} = -\rho_l A_E \left\{ \frac{2gL}{1+\Pi_{FE}} \right\}^{1/2} \quad (3.12\text{-}6)$$

Initial Conditions

$$M_0 = \rho_l A_{Tank} L_0 \quad (3.12\text{-}7)$$

$$\dot{m}_0 = \rho_l A_E \left\{ \frac{2gL_0}{1+\Pi_{FE}} \right\}^{1/2} \quad (3.12\text{-}8)$$

Dimensionless Equation

$$\frac{dL^+}{dt^+} = -\left(L^+\right)^{1/2} \quad (3.12\text{-}9)$$

Where

$$L^+ = \frac{L}{L_0} \quad (3.12\text{-}10)$$

$$\dot{m}^+ = \frac{\dot{m}}{\dot{m}_0} \quad (3.12\text{-}11)$$

$$t^+ = \frac{t}{\tau} = \frac{t}{\left(M_0/\dot{m}_0\right)} \quad (3.12\text{-}12)$$

Analytical Solutions

$$L^+ = \left(1 - \frac{t^+}{2}\right)^2 \quad (3.12\text{-}13)$$

$$\dot{m}^+ = \left(1 - \frac{t^+}{2}\right) \quad (3.12\text{-}14)$$

Ranges:

$$0 \le L^+ \le 1$$

$$0 \le t^+ \le 2$$

$$0 \le \dot{m}^+ \le 1$$

3.12.2.2. Heat transfer coefficients

Tuunanen et al. suggested that the McAdams natural convection heat transfer correlation, Eq. (3.12-15), is appropriate for calculating the heat transfer from the fluid to the CMT wall [3.12-7].

$$\bar{h} = 0.13 \frac{k_f}{L} \left[G_R Pr_f \right]^{\frac{1}{3}} \quad (3.12\text{-}15)$$

The Grashoff number is given as:

$$G_R = g \frac{\beta \left(T_w - T_b\right) L^3 \rho_f^2}{\mu_f^2} \quad (3.12\text{-}16)$$

During the condensation phase, Cunningham suggested the Nusselt film condensation model.

$$\bar{h}_f = 0.925\left[\frac{4\rho_f\left(\rho_f-\rho_g\right)gk_f^3}{\mu_f^2 Re_\Gamma}\right]^{\frac{1}{3}} \quad (3.12\text{-}17)$$

Tuunanen et al. [3.12-7] observed that this correlation gave higher values than the experimental data.

3.12.3. CMT experiments

As mentioned above, the CMTs replace the high pressure safety injection in the AP600/1000 reactor design. In addition to the CMTs, the AP600/1000 passive safety injection systems include a passive residual heat removal system which can serve as a heat sink for the primary system in the event that the SGs are unavailable to perform this function. The PRHR system includes a C-tube heat exchanger located in the IRWST. Additional sources of injection coolant are provided by the accumulators and the IRWST. The accumulator tanks are pressured by nitrogen which provides the motive force for the injection. IRWST injection provides long term cooling through isolation check valves located on the injection line.

In an effort to certify and confirm the adequacy of the AP600/1000 passive safety injection system, a large database for the performance of the system components was commissioned by the US NRC and the US DOE. This database was collected using a combination of integral and separate effects test facilities. Much of the data collected by these various test programs remains proprietary due to their value to and application in a number of commercial concerns. Table 3.12-3 shows a listing of the major integral test programs conducted that can be related to the behaviour of the CMT. Specifically, three integral type test facilities were used in the certification and confirmation of the passive safety system for the AP-600/1000: ROSA-AP-600, APEX-600/1000 and SPES-2 [3.12-4].

TABLE 3.12-3. EXPERIMENTS INVOLVING CMTs RELATED AT THE DEVELOPMENT OF THE AP600

Experiment	Test Number and Types	Codes
PACTEL VTT Energy, Finland	15- SBLOCA	APROS 4.02 CATHARE RELAP5/MOD3.3
APEX AP600 OSU, USA	30 NRC Tests and 30 DOE/W Tests - SBLOCA, DEDVI, Station Blackout, Inadvertent ADS	RELAP5/MOD3.3
APEX1000 OSU, USA	11 NRC Tests and 11 DOE/W Tests - SBLOCA, DEDVI, Station Blackout	RELAP5/MOD3.3
SPES-2 Esperienze Termoidrauliche (SIET) laboratories in Piacenza, Italy	13 DOE/W Tests — SBLOCA, DEDVI	RELAP5/MOD3.3
ROSA-V, AP600 JAERI Japan	24 NRC Tests — SBLOCA, DEDVI	RELAP5/MOD3.3

ROSA-AP600 is located at the ROSA Large Scale Test facility which is operated under JAERI. ROSA has the ability to simulate SBLOCAs in PWRs. The prototypical PWR which the test facility design is based on is the 3423 MWt 4 loop Westinghouse PWR. The ROSA facility is scaled 1:48 by volume. It includes two loops instead of the prototypical 4 loops. In this case each loop in the test facility simulates two loops in the prototypical plant.

APEX is located at and operated by Oregon State University. It was originally constructed to simulate the low pressure and long term cooling phases of the Westinghouse AP600. It is scaled at 1:4 by height and 1:196 by volume. From 1995 to 2000, OSU performed more than 80 integral system experiments to obtain data to benchmark AP600 and AP1000 safety evaluation codes.

SPES-2 is a full-height, full-pressure, 1:395 power scale and volume scale simulation of the AP600 nuclear steam supply system and passive safety features. A series of thirteen design-basis events were simulated at SPES-2 to obtain data for verification and validation of the computer models used for the safety analysis of the AP600. The modeled initiating events included a series of SBLOCAs, single SG tube ruptures, and a main steam-line break.

3.12.3.1. CMT draining

For large breaks (breaks greater than 2 inches), a description of the CMT draining phenomena is relatively straightforward. In this case the recirculation phase is short and the system moves into the draining phase quickly. For small breaks (breaks less than 1 inch), the progression into the CMT draining phase is much harder to predict consistently.

The three facilities mentioned above allow us to look at various aspects of the CMT draining phenomena. As discussed above, draining by flashing occurs in the CMTs to create vapour. In this case the PBLs are still filled with liquid water. In the ROSA-AP600 facility, draining by flashing is the exclusive mechanism demonstrated. Draining by inflow occurs with the inflow of vapour through the PBLs into the CMTs. This mechanism is demonstrated in the SPES-2 facility. APEX has the advantage of being able to demonstrate both draining mechanisms during an individual test. In addition, due to the design of the APEX facility, asymmetrical CMT behaviour can be demonstrated which depends largely on break location [3.12-4].

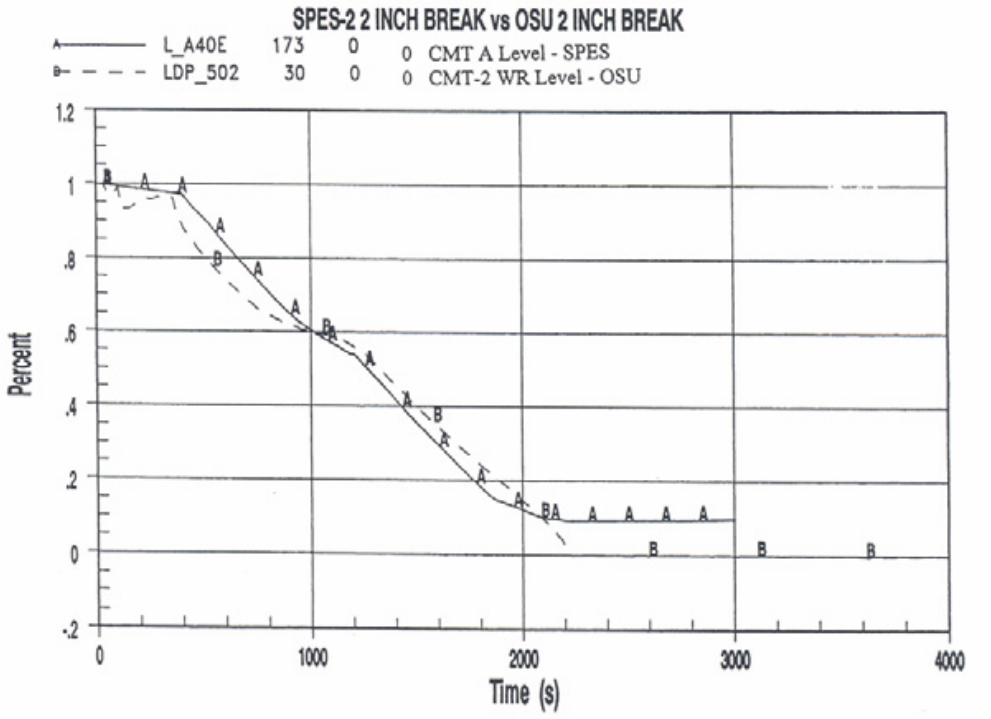

FIG. 3.12-3. CMT levels during a SPES-2 and APEX-600 5 cm cold leg break.

Counterpart SBLOCA tests were conducted in SPES-2 and APEX-600. Both facilities show that the CMT liquid draining rate was continuous. Figure 3.12-3 shows the CMT liquid levels during a 5 cm cold leg break test performed at SPES-2 and in APEX-600. It was observed that the draining rate was affected by interaction with the accumulator injection flow (~1000s) [3.12-8]. Figure 3.12-4 shows the CMT flow rate during the same test.

Details of the AP600 and AP1000 test programs are not available in the open literature because it involves Westinghouse business proprietary data that cannot be openly published.

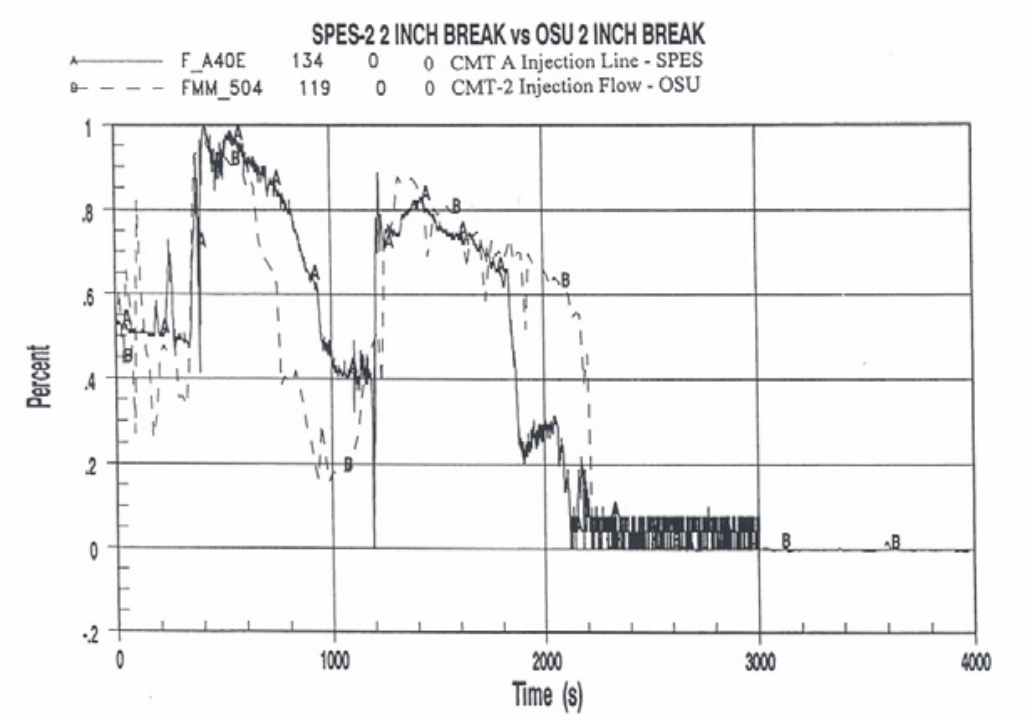

FIG. 3.12-4. CMT flow rates during a SPES-2 and APEX-600 5 cm cold leg break.

3.12.3.2. CMT refill

During the IRWST injection phase, refill of the CMTs was observed in the APEX facility. IRWST injection can cause the coolant level in the facility to rise to the level of and fill the cold legs. In this case, the PBLs may become blocked preventing the inflow of any additional vapour into the CMTs. Steam condensation will continue in the CMTs which causes a vacuum to develop; this in turn draws fluid up the PBLs into the CMTs. The presence of liquid water in the CMTs allows direct contact condensation of the CMT steam to occur. The enhanced condensation and the inflow of liquid water into the CMTs lead to CMT refill. Depending on the further progression of the transient a second CMT draining may take place after refill. CMT refill was only observed in the APEX facility and was not seen in ROSA-AP600 [3.12-4].

CMT refill is more likely to occur in the APEX facility versus the prototypical AP600 plant due to the differences in height between the two. However, the probability of refill occurring in the prototype cannot be eliminated entirely [3.12-1].

3.12.3.3. PACTEL experiments

PACTEL in Finland is another facility that has been used to explore the operation of PWR passive safety injection systems during a SBLOCA. PACTEL is a full height model of the six-loop VVER-400 plant. PACTEL is scaled at 1:305 by volume and contains three loops. Each model loop corresponds to two loops in the prototypical plant. Since PACTEL is based on the VVER-440 plant, its operation has not been specifically designed to model the AP-600 plant. However, PACTEL is able to model CMT behaviour along with behaviour in the PBLs and the injections lines which are applicable to AP600 passive safety injection system operation.

The objectives of the PACTEL facility are to (1) add to the database of collected experimental data describing the phenomena and performance of passive safety injection systems for ALWRs, and (2) provide high fidelity data which can be used to validate nuclear reactor system codes which can in turn be used for design and safety analyses application in relation to ALWRs [3.12-6].

Fifteen tests were conducted at PACTEL divided into three test series. The first series looked at the effects of break size. The second looked at the effects of break location. The third series looked at the effect of various CMT positions on CMT performance. Reference [3.12-6] discusses five such experiments conducted at the PACTEL facility. These five experiments are designed to assist in the validation of nuclear reactor system computer codes and look at the effects of break size on passive safety injection system behaviour.

From the data collected in these experiments, several conclusions regarding break size effects were made. Firstly, for smaller break sizes the recirculation phase and the oscillation phase (between recirculation and injection) lasted longer than seen with larger breaks. In addition it was observed that the hot liquid layer in the CMT tended to be thicker in the smaller break tests. Finally, local wall heat fluxes to the CMT wall were lower in the smaller break tests.

A number of additional observations were made during these tests. For instance, rapid condensation within the CMT was not seen. Potential mechanisms for the stoppage of flow to the CMT were also observed. It is known that the density difference between the PBL and the injection lines provide the motive force for the CMT flow. Therefore, CMT flow may stop if the density difference between the two becomes negligible. Some situations where this might occur include the filling of the CMT with hot water before the injection phase commences, or the entrance of cold water into the PBL during the injection phase.

PACTEL experiments were analysed using APROS, CATHARE and RELAP5. Out of the total fifteen PACTEL tests, three were selected for analysis - one from each test series. In general, the codes did an adequate job in modeling the experiments. Some areas for improvement were noted. Specifically, the modeling of thermal stratification and condensation in the CMT, and calculating the injection flow when the driving force is small [3.12-6, 3.12-7].

3.12.3.4. AC600/1000 experiments

Experiments were conducted by the Nuclear Power Institute of China (NPIC) to support the design effort for the AC600/1000. This test program included five test specifically designed to explore the behaviour of the CMT with a variety of break sizes [3.12-2].

ABBREVIATIONS

ADS	Automatic depressurization system
ALWR	Advanced light water reactor
AP600	Advanced plant 600 MWe
AP1000	Advanced plant 1000 MWe
APEX	Advanced plant experiment
APROS	Advanced process simulator
CATHARE	Code avancé de thermohydraulique pour les accidents des réacteurs à eau
CMT	Core make-up tank
DVI	Direct vessel injection
IRWST	In-containment refueling water storage tank
JAERI	Japan Atomic Energy Research Institute
OSU	Oregon State University
PACTEL	Parallel channel test loop
PBL	Pressure balance line
PRHR	Passive residual heat removal system
PWR	Pressurized water reactor
RCP	Reactor coolant pump
RELAP	Reactor excursion and leak analysis package
ROSA	Rig of safety assessment
ROSA-AP600	Rig of safety assessment AP 600 configuration
SBLOCA	Small break loss of coolant accident
SG	Steam generator
SPES	Simulatore per esperienze di sicurezza (Simulator for safety experimental analysis)
USNRC	United States Nuclear Regulatory Commission
USDOE	United States Department of Energy
VTT	Technical Research Centre of Finland
VVER	Russian pressurized water type reactor

NOMENCLATURE

g	acceleration of gravity
G_R	Grashoff Number
$\bar{h}$	average heat transfer coefficient
k_f	fluid thermal conductivity
L	mixing thickness of the hot liquid layer
Pr_f	fluid Prandtl number
Re_Γ	film flow Reynolds number
T_w	wall temperature
T_b	bulk fluid temperature

Greek symbols

β	thermal expansion coefficient of the fluid
μ_f	viscosity of the fluid
ρ_f	density of fluid
ρ_g	density of steam

REFERENCES FOR SECTION 3.12

[3.12-1] REYES, JR., J.N., GROOME, G.T., LAFI, A.Y., FRANZ, S.C., RUSHER, C., STROHECKER, M., WACHS, D., COLPO, S., BINNEY, S., Final Report of NRC AP600 Research Conducted at Oregon State University, NUREG/CR-6641 (1999).

[3.12-2] ZHANG, S., "Experiment research and calculation method of natural circulation flow for AC 600/1000", Natural Circulation Data and Methods for Advanced Water Cooled Nuclear Power Plant Designs, IAEA-TECDOC-1281, IAEA, Vienna (2002).

[3.12-3] XIAO ZEJUN, et al., Experimental research progress on passive safety systems of Chinese advanced PWR, Nuclear Engineering and Design **225** (2003) 305–313.

[3.12-4] BESSETTE, D., DI MARZO, M., GRIFFITH, P., "Phenomenology observed in the AP600 integral systems test programs conducted in the ROSA-AP600, APEX, and SPES-2 facilities", Office of Nuclear Regulatory Research, Reactor and Plant Systems Branch, RPSB-98-04

[3.12-5] REYES, JR, J.N., "AP 600 and AP 1000 passive safety system design and testing in APEX", Natural Circulation in Water Cooled Nuclear Power Plants, IAEA-TECDOD-1474, IAEA, Vienna (2005).

[3.12-6] TUUNANEN, J., RIIKONEN, V., KOUHIA, J., VIHAVAINEN, J., Analyses of PACTEL passive safety injection experiments GDE-21 through GDE-25, Nuclear Engineering and Design **180** (1998) 67–91.

[3.12-7] TUUNANEN, J., et al., Analyses of PACTEL passive safety system injection experiments with APROS, CATHARE and RELAP5 codes, Nuclear Engineering and Design **198** (2000) 261–286.

[3.12-8] REYES, JR., J.N., HOCHREITER, L.E., "Scaling Analysis for the OSU AP600 Test Facility (APEX)", Nuclear Engineering and Design **186** (1998) 53–109.

4. INTEGRAL TESTS AND PLANT ANALYSES, EXAMPLE CASES

Passive safety systems are becoming an important component in advanced reactor designs. This has led to an international interest in examining natural circulation phenomena as this may play an important role in the operation of these passive safety systems. Understanding reactor system behaviour is a challenging process due to the complex interactions between components and associated phenomena. Properly scaled integral test facilities can be used to explore these complex interactions. In addition, system analysis computer codes can be used as predictive tools in understaning the complex reactor system behaviour. However, before a system analysis computer code is used in a predictive capacity for a reactor design, it's efficacy in making predictions needs to be validated against data from a properly scaled integral test facility.

This chapter describes representative international integral test facilities that can be used for data collection for reactor types in which natural circulation may play an important role. Example experiments are described along with the analyses of these example cases in order to examine the ability of codes to model the phenomena that are occuring in the test facilities. As mentioned above, the data from these test facilities may be used to help assess the predictive capabilities of these models in relation to natural circulation phenomena. The goal of the information presented in this chapter is to survey the available international test facilities and the representative data that they can yield.

Each section of this chapter will address a particular test facility and prototypical plant design that the facility is modelling. In general each section will include a description of the test facility and example data sets collected during the operation of the facility. In some instances the sections will also include an analysis of the subject test with a comparison between the test data and the code results.

This chapter includes a wide variety of prototypical plant designs, test facilities and codes used for analysis. This makes this chapter an excellent resource for understanding the general capabilities of test facilities and codes that can be used for the examination of natural circulation phenomena.

The following prototypical reactor types are examined in this chapter:

- CANDU
- CAREM
- Advanced Heavy Water Reactor (AHWR)
- AP-600
- Multi-application Small Light Water Reactor (MASLWR)
- Simplified Boiling Water Reactor (SBWR)
- System Integrated Modular Advanced Reactor (SMART)
- WWER-1000
- WWER-440

The following international test facilities are described and representative data sets presented:

- CAPCN (CAREM)
- ITL (AHWR)
- ROSA/LSTF (AP-600)
- OSUMTF (MASLWR)
- PUMA (SBWR)

The use of the following system analysis computer codes is explored in a number of the sections in this chapter:

- RELAP5-3D
- RELAP5/Mod3.2
- CATHENA
- TASS/SMR
- ATHLET-1.2A
- DINAMIKA-97
- TECH-M-97
- KORSAR-V1

4.1. EXPERIMENTS AND SIMULATIONS IN SUPPORT OF NATURAL CIRCULATION COOLING FOR THE GEN-IV CANDU SCWR

One of the unique features of CANDU[1®] reactors is the separation between the low pressure moderator and the high-pressure coolant (Fig. 4.1-1). This feature makes it possible to use the moderator as a backup heat sink for emergency heat removal. Current CANDU reactors use a pumped loop to remove heat deposited in the moderator during normal operation. A passive moderator cooling system has advantages in terms of cost reduction and improved passive safety. AECL is studying methods of enhancing moderator effectiveness as a passive heat sink by designing and testing passive moderator cooling systems (PMCS) for heat rejection. The most promising of these designs is a flashing-driven moderator cooling system that is being developed for the GenIV CANDU-SCWR concept. In this concept, the heavy-water moderator exits the reactor calandria at a temperature close to saturation (slightly subcooled) so that vapour is generated in a riser connecting the calandria to a heat exchanger (Fig. 4.1-2). The two phase flow in the riser results in a significant increase in driving force (over that from single phase natural circulation), and makes it possible to reject the moderator heat load in a passive manner. This concept can be used to reject moderator heat under normal and emergency conditions using the same passive loop; this is desirable since it ensures the availability and functionality of the passive heat removal system. Operating the moderator close to saturation requires changes to the fuel channel design to remove restrictions associated with operating CANDU reactors that require the moderator to operate with a certain degree of subcooling [4.1-1][2]. The development of an advanced fuel channel design is a parallel activity that is part of the CANDU-SCWR development program at AECL [4.1-2].

[1] CANDU is a registered trademark of AECL

[2] This is necessary to avoid film boiling on the calandria tube if the pressure tube balloons into contact with the calandria tube following a loss of coolant accident (LOCA) combined with loss of Class IV power.

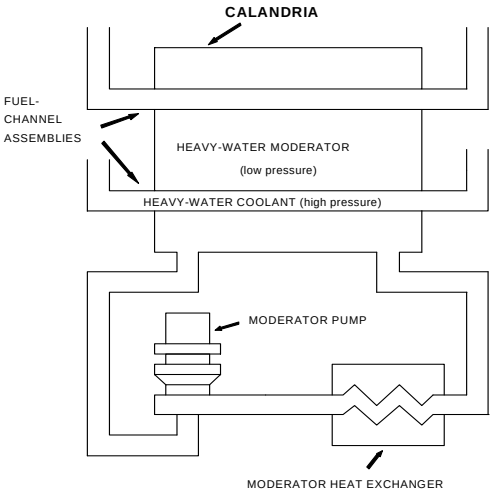

FIG. 4.1-1. CANDU calandria schematic.

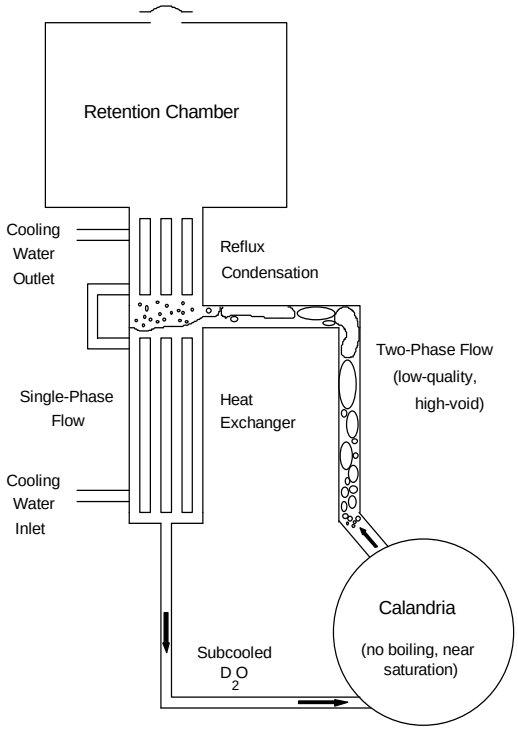

FIG. 4.1-2. Flashing-driven PMCS concept.

An important objective in the CANDU-SCWR design is to achieve significant safety enhancements so that the possibility of core damage is practically eliminated. This can be achieved by ensuring that the passive cooling loop is operational at all times for normal moderator heat removal as well as for emergency cooling. The advanced fuel channel design provides for controlled heat rejection to the moderator during normal and emergency heat removal [4.1-3]. This Section focuses on R&D activities that support the development of the natural circulation cooling concept.

4.1.1. Preliminary simulations and tests

The initial studies consisted of steady state simulations to examine the feasibility of rejecting the moderator heat load (~5% of reactor thermal power) using a natural circulation loop. The results showed that a single phase loop was not practically feasible. A two phase natural circulation system was necessary with the restriction that the moderator inside the calandria should remain in the liquid state. This restriction makes it necessary to design a loop where two phase is generated by flashing in the riser. Further simulations showed that a loop with a reasonable height (~8.5 m) would be able to remove moderator heat during normal operation. Furthermore, since the moderator heat during normal operation is comparable to decay heat following reactor shutdown, this loop could also be used for emergency heat removal if the emergency core cooling system fails.

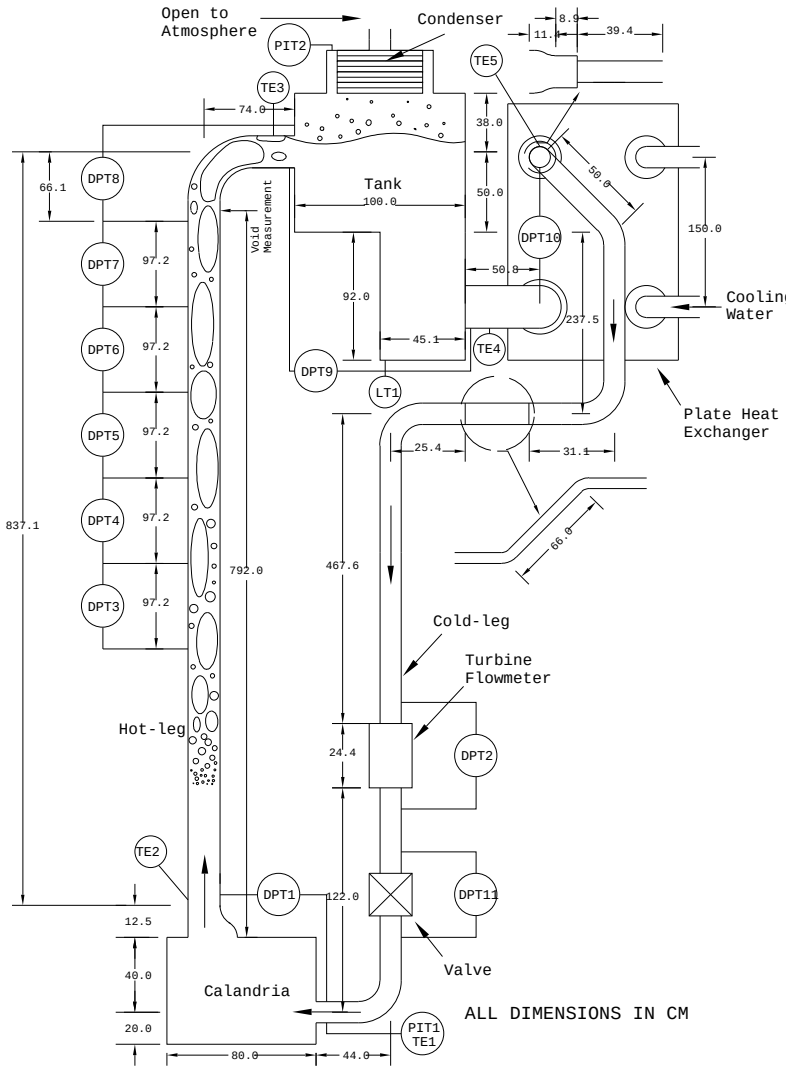

FIG. 4.1-3. Schematic of test loop for concept verification tests.

The next step was to evaluate the stability of the system. This was done through simulations using the CATHENA [4.1-4, 5] thermohydraulics code, and through tests using a full-height test loop. The volume of the full-height test loop was scaled by factor of 60. The riser was constructed using glass piping to allow flow visualization. A schematic of the scaled loop is shown in Fig. 4.1-3 [4.1-6].

Pre-test simulations of the scaled loop showed oscillatory behaviour at low powers caused by periodic transition from single phase to two phase flow. This is expected since the increase in flow resulting from void generation in the riser leads to a decrease in the calandria outlet temperature below the saturation value at the riser outlet pressure. However, as the power was increased to the point where flashing was sustained (~25% of full power), the flow stabilized (Fig. 4.1-4).

This behaviour was verified experimentally, where the results showed good qualitative agreement with the CATHENA simulations (Fig. 4.1-5). The flow remained stable as the power was increased to the simulated maximum heat load of ~1 MW [4.1-6].

The oscillations at low powers will be encountered during startup and are not expected to be problematic. However, it is desirable to eliminate or reduce the duration of these oscillations as the power increases to values that result in stable flow rates. A systematic investigation through separate-

effects tests was carried out to provide a better understanding of the phenomena leading to the low power flow oscillations.

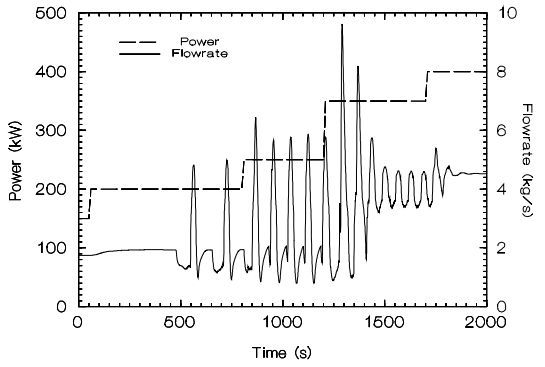

FIG. 4.1-4. Pre-test CATHENA simulations [4.1-6].

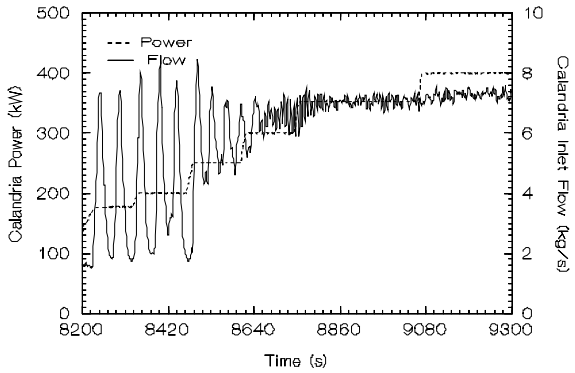

FIG. 4.1-5. Sample test results [4.1-6].

4.1.2. Separate-effects tests

The results obtained from the initial simulations and tests indicate that a stable behaviour can be obtained if flashing can be sustained in the hot leg. Flashing can be sustained in the hot leg by ensuring that the calandria inlet temperature is close to saturation at the outlet riser pressure. Preliminary simulations showed that this was indeed the case. The loop was modified by removing the heat exchanger (that functioned as a subcooler) and retaining the elevated condenser and accumulator tank [4.1-7] (Fig. 4.1-6).

Initial results from the separate effects tests showed that oscillations were still present at low powers (Fig. 4.1-7). This was inconsistent with pre-test simulations that indicated stable behaviour at all powers with a calandria inlet temperature close to saturation at the riser outlet pressure. Close examination of the results showed that two factors contributed to the low power oscillations: 1) flow and temperature distribution inside the calandria, and 2) preferential void generation at the discontinuities between the glass riser pipe segments. The effects of these factors were eliminated by introducing a mixing loop (to reduce temperature fluctuations at the calandria outlet) and by introducing a rough surface (rough wire inserted in the center of the top glass pipe segment) in the riser [4.1-7] to provide a continuous surface for void formation. The experimental results following these modifications showed significant improvement in loop stability at all power levels (Fig. 4.1-8).

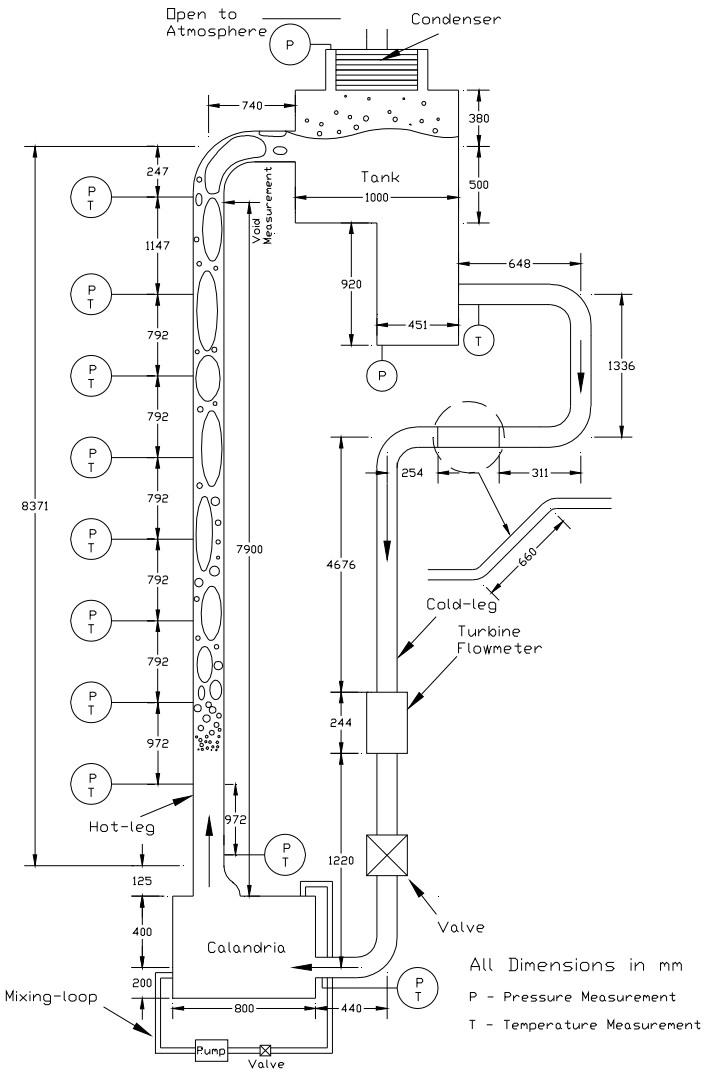

FIG. 4.1-6. Schematic of separate-effects test loop [4.1-7].

Subsequent comparison between CATHENA and the experimental results showed that CATHENA predicted significantly higher flow rates (Fig. 4.1-9). The reason is that CATHENA assumes thermodynamic equilibrium between the vapour and liquid phases where in reality a certain amount of superheat is required to initiate flashing. This results in a longer two phase section in the riser and larger flow rates in CATHENA simulations. The experimental results showed that between 2 and 3^{o}C of superheat was required to initiate flashing. Another CATHENA simulation was carried out with an artificially increased pressure at the riser outlet in attempt to match the flashing locations with those observed in the experiment. The results are shown in Fig. 4.1-10 where significant improvement can be seen. The remaining discrepancies can be attributed to uncertainties in the parameters used in the simulations, and to reduced void generation in the experiment away from the rough wire insert.

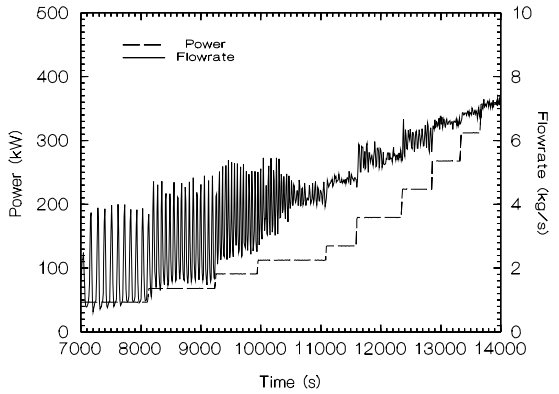

FIG. 4.1-7. Separate-effects tests (mixing loop off).

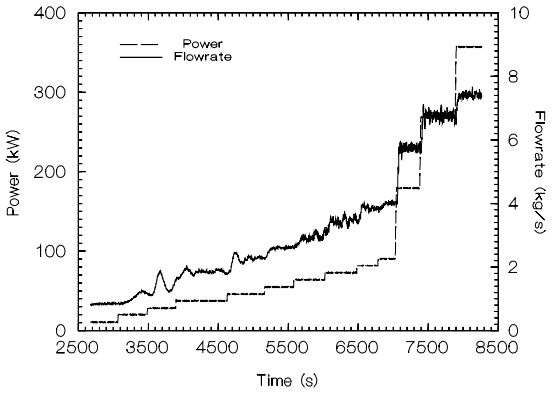

FIG. 4.1-8. Separate-effects tests (mixing loop on).

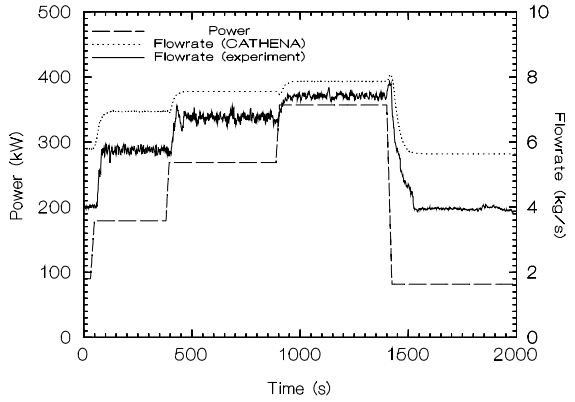

FIG. 4.1-9. Comparison with CATHENA using experimental condenser pressure.

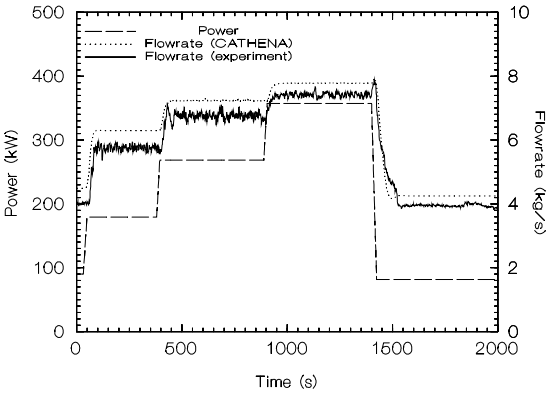

FIG. 4.1-10. Comparison with CATHENA using a higher condenser pressure.

The other separate-effects test studied the flow and temperature distributions inside the calandria. The objective was to investigate a suitable inlet/outlet configuration that would result in better mixing and in accumulation of higher temperature fluid close to the calandria outlet at all expected flow rates. An obvious choice is to locate the inlet at the bottom of the calandria vessel. However, another configuration that was used for certain CANDU designs was found to be superior [4.1-8]. This configuration is shown in Fig. 4.1-11 where it can be seen that the inlet consists of a number of nozzles located in the upper portion of the calandria and pointing downwards. This configuration was tested in a ¼-scale calandria simulator [4.1-8] with detailed velocity and temperature distribution measurements using a range of flow rates expected at low and full power operation. A typical result is shown in Figs 4.1-12 and 4.1-13 where it can be seen that the flow and temperature distributions are consistent with the requirements of the passive loop. Transient tests were also conducted to simulate changing power levels (using temperature measurements only) and the same temperature distribution was maintained. This means that the flow configuration in Fig. 4.1-11 can be used in the passive loop design to avoid any temperature variations at the calandria outlet that could be caused by three dimensional effects within the calandria vessel.

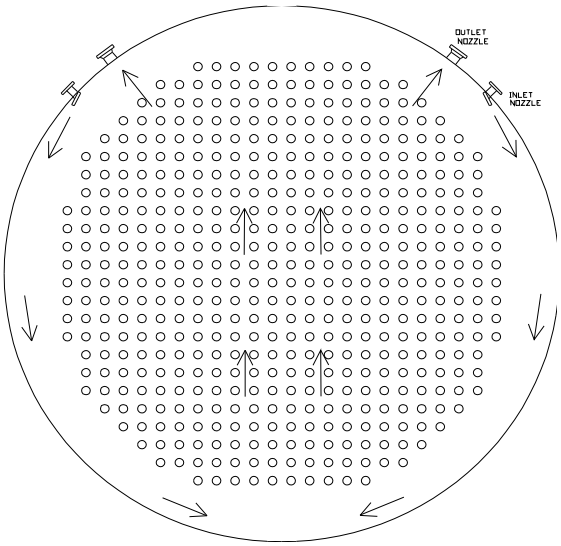

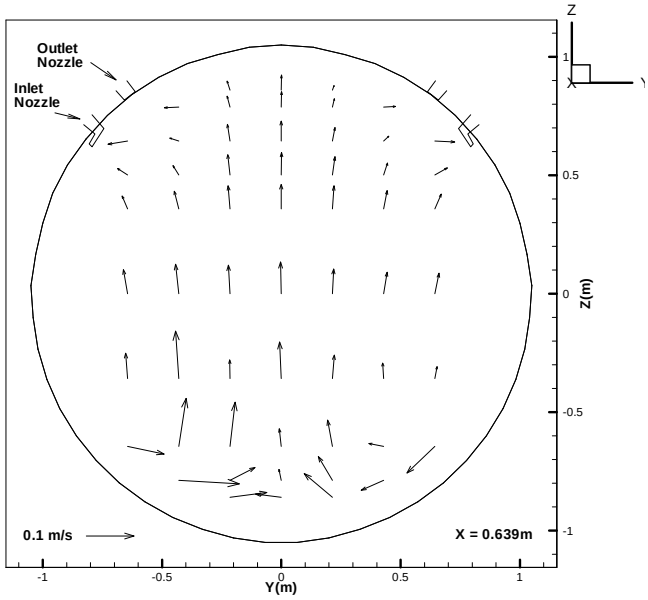

FIG. 4.1-11. Moderator flow configuration tested [4.1-8].

FIG. 4.1-12. Measured velocity profile [4.1-8].

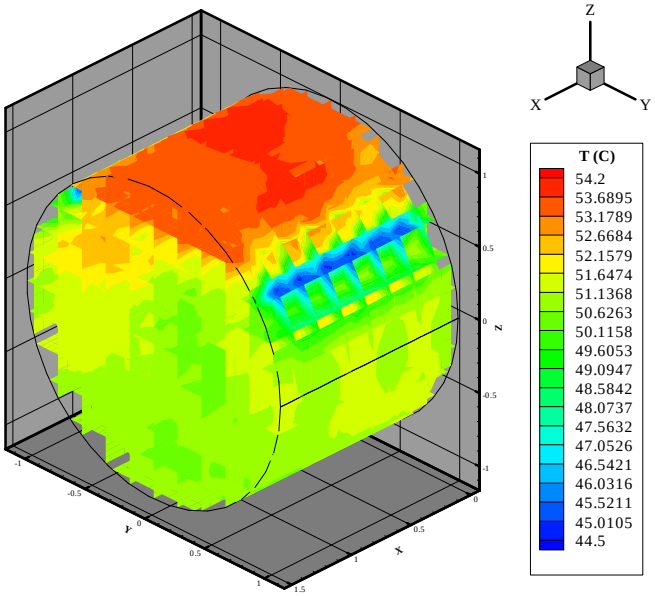

FIG. 4.1-13. Measured temperature distribution [4.1-8].

4.1.3. Modified loop

Results from the above tests were used to design and construct another loop with a different scale, and more representative calandria vessel geometry and flow configuration. The loop scale was chosen so that the calandria vessel linear dimensions were reduced by a factor of 10, and the loop height was smaller than the previous loop. Construction of this loop was completed recently and is currently undergoing commissioning (Fig. 4.1-14). This loop will be used to provide more validation data and can be re-configured relatively easily to add more components (e.g., another passive loop above the heat exchanger to reject heat to an ultimate heat sink).

4.1.4. Future plans

The larger (1/4-scale) calandria vessel that was used to study flow and temperature distributions will be used at a later stage to study the behaviour of a larger flashing-driven loop. Results from the smaller scale loop will provide input to the design of the larger loop components. The two loops are expected to provide more validation data, including data on scaling effects that can be used to design the actual reactor loop.

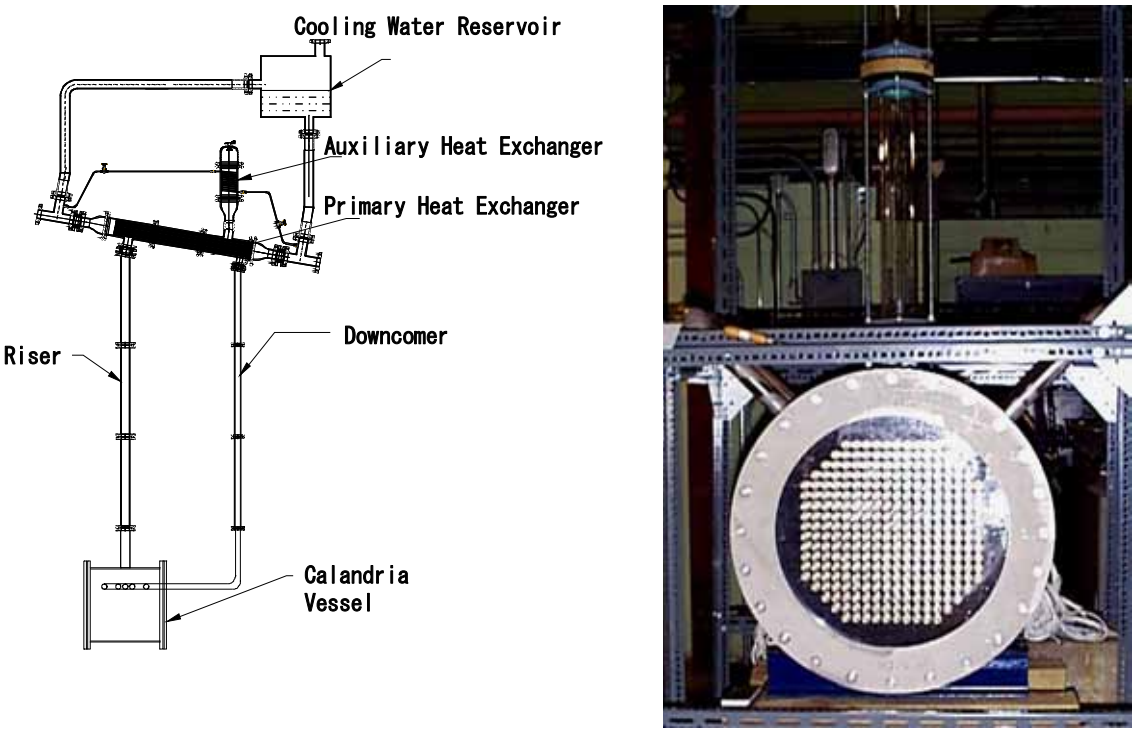

FIG. 4.1-14. Modified loop.

4.1.5. Summary

The separation between the high pressure coolant and low pressure moderator in CANDU reactors makes it possible to use the moderator as an additional heat sink to supplement the emergency core cooling system during some postulated accidents. A flashing-driven moderator cooling concept that can be used to remove moderator heat under normal conditions and decay heat under emergency conditions in advanced CANDU reactors is under development. In this concept, a sufficiently high moderator flow rate can be obtained due to the large density difference between the hot and cold-legs.

The research program so far has demonstrated the feasibility of employing a flashing-driven loop that can be used under normal and emergency conditions. Flow oscillations observed in earlier tests were found to occur at conditions where flashing cannot be sustained due to a combination of low calandria inlet temperature and low power. These flow oscillations could be encountered during startup and are not expected to be problematic. However, it is possible to avoid these oscillations by manipulating the calandria inlet temperature during startup so that flashing is sustained.

Another factor that could lead to flow oscillations is variations in the calandria outlet temperature that are caused by three dimensional effects within the calandria vessel. Designing and testing a suitable calandria flow configuration resolved this issue.

A new loop was designed and built recently that incorporates lessons learnt from the early tests. This loop has sufficient flexibility to allow re-configuration and further testing. A larger loop is planned to provide supplementary data and to study scaling effects.

REFERENCES FOR SECTION 4.1

[4.1-1] GILLESPIE, G.E., et al., "Moderator boiling on the external surface of a calandria tube in a CANDU reactor during a loss-of-coolant accident", Proceedings, International Meeting on Thermal Nuclear Reactor Safety, Chicago (1982).

[4.1-2] BUSHBY, S.J., et al., "Conceptual designs for advanced, high-temperature CANDU reactors", Proceedings, 8th International Conference on Nuclear Engineering, ICONE-8470, Baltimore (2000).

[4.1-3] KHARTABIL, H.F., "Enhanced passive safety for pressure tube reactors cooled with supercritical water", Proceedings of Global 2003, ANS/ENS International Winter Meeting, New Orleans, November 16–20 (2003).

[4.1-4] HANNA, B.N., CATHENA — a thermalhydraulic code for CANDU analysis, Nucl. Eng. Des., **180**, No. 2 (1998).

[4.1-5] BAEK, W.P., SPINKS, N.J., "CANDU Passive heat rejection using the moderator", International Conference on New Trends in Nuclear System Thermalhydraulics, Vol. 1, Paper No. C22.1, Pisa, Italy (1994).

[4.1-6] KHARTABIL, H.F., SPINKS, N.J., "An experimental study of a flashing-driven CANDU moderator cooling system", 16th Annual Conference, Canadian Nuclear Society, Saskatoon, Canada (1995).

[4.1-7] KHARTABIL, H.F., "A flashing-driven moderator cooling system for CANDU reactors: experimental and computational results", presented at the IAEA Technical Committee Meeting on Experimental Tests and Qualification of Analytical Methods to Address Thermohydraulic Phenomena in Advanced Water Cooled Reactors", PSI, Switzerland (1998).

[4.1-8] KHARTABIL, H.F., DUFFEY, R.B., "Velocity and temperature distribution measurements inside a scaled calandria in support of CANDU X passive moderator cooling system design", GENES4 /ANP2003, Kyoto, Japan (2003).

4.2. CAPCN: CAREM HIGH PRESSURE NATURAL CIRCULATION RIG

The High Pressure Natural Circulation Rig (the acronyms in Spanish CAPCN) was built in the 90´s to study natural circulation and self-pressurization, and to assess the CAREM primary circuit numerical modelling. CAPCN resembles CAREM prototype [4.2-1] in the primary loop and steam generators (helical once-through), while the secondary loop is designed just to produce adequate boundary conditions for the heat exchanger. Several tests were performed to obtain knowledge regarding thermohydraulics behaviour and control techniques around the nominal operational point.

4.2.1. Introduction

In the present section, CAPCN is described and RELAP5 calculations are compared with experimental data from three tests performed in the High Pressure Natural Circulation Rig: a) a temporal opening of the relief valve, b) temporal increase in the removed power, and c) temporal decrease in the generated power. The dominant physical phenomena are: two phase flow natural circulation, self-pressurization, steam condensation and flashing. Regarding self-pressurization (no active control of the pressure), it should be pointed out that it is the result of liquid-vapour equilibrium in the steam dome which in turns requires that the bulk temperature at core outlet to be close to the saturation value. In order to compensate for vapour condensation caused by thermal losses in the dome, two phase flow (which is generated in the heaters) comes from the riser into the dome. The large volume of the steam dome and the amount of saturated coolant (dome and riser) also contribute to damp pressure perturbations.

Figure 4.2-1 shows a simplified diagram of the CAPCN facility. The riser, the steam dome, the steam generator helicoids (located inside the pressure vessel), the down comer, the lower plenum and heaters zone can be observed. Figure 4.2-2 presents a view of the upper part of the CAPCN circuit.

CAPCN primary circuit has a lower plenum (12” diameter), a heating zone, a riser, a dome or upper plenum, a steam generator and a downcomer. The major part of the circuit is built with tubes of 3” diameter. There are 18 electrical heaters. Heat removal is done by natural circulation. Water enters into the heated section from the lower plenum. The coolant, now near saturation, flows upwards along the riser to the upper plenum. The water level is located in the dome, near the flanges. The water exits this plenum towards the steam generator, flowing downwards. The subcooled water flows into the downcomer or cold leg to the lower plenum. A valve in the cold leg can be used to adjust the natural circulation flow. The primary loop can be pressurized with nitrogen.

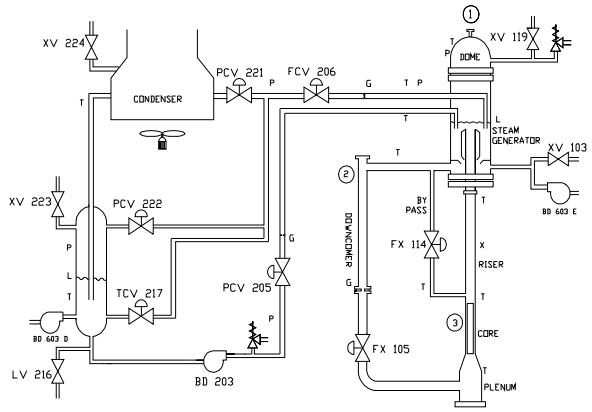

FIG. 4.2-1. Flow diagram of the CAPCN.

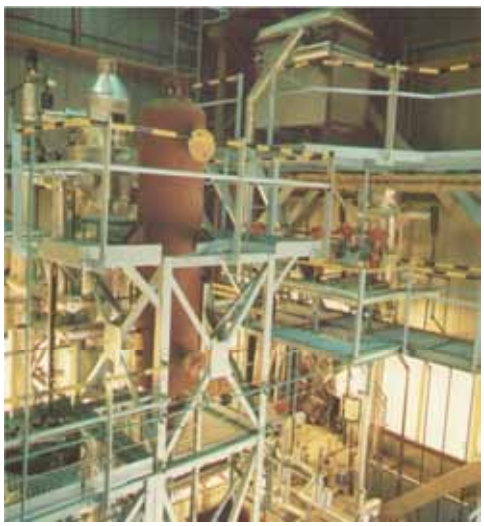

FIG. 4.2-2. CAPCN general view.

The steam generator consists of two helicoids that surround the uppermost part of the riser. The secondary system coolant flows inside the tubes. The secondary system is quite different from the CAREM one, but the boundary conditions to the steam generators are similar for the intensive quantities (pressure, temperature and velocity). The secondary loop pressure and cold leg temperatures are controlled through feedback loops operating valves. The pump allows the regulation of the flow. The condenser is an air cooled type with flow control.

CAPCN is a full-height facility with a nominal pressure of 115 bars. The primary loop may operate in saturated or subcooled (adding nitrogen) regimes, with a heating power of up to 300 kW and different hydraulic resistance. The electrical power can be manually or automatically regulated in order to generate power imbalances in the circuit and to set the pressure to the reference value.

Primary and secondary circuit mass flow rate measurements are taken in the cold leg and in SG feed-water line, respectively. In order to filter background noise, all the pressure and mass flow rate measurements have a lag (damped or smoothed) of a few seconds. Generally this is not problematic in slow transients; however, sharp mass flow rate or pressure peaks may be filtered by the instrument in the case of abrupt transients. The measurement uncertainties are ±1 °C (temperature), ±1 bar (pressure), and ±4% (mass flowrate). There is no measurement of void fraction in the riser.

4.2.2. CAPCN tests

It was of interest to simulate the dynamic response of the primary circuit due to perturbations in the generated and removed powers, and to a temporal loss of coolant. Furthermore, it was of interest to simulate the influence of some engineering parameters on system dynamics, like the water level in the dome, the hydraulic resistance, and the steam generators feed water temperature, etc. The following test groups were performed:

1. Preliminary tests to characterize components and equipment;
2. Thermal balance test, instrumentation calibration and evaluation of their accuracy;
3. Dynamic test around the operational nominal point without control: thermohydraulic response evaluation;
4. Dynamic test with the control loops (power-pressure).

Some examples of the transients performed (group 3) in the facility with approximately the same initial conditions but with different perturbations are listed in Table 4.2-1. Neither active nor control actions were performed during the tests, allowing the system to evolve naturally or intrinsically following the perturbation. Tests 1, 2 and 4 were selected as representative of the facility behaviour and for comparison with the RELAP5 MOD3.3 code.

TABLE 4.2-1. PERTURBATION CHARACTERISTICS OF THE SELECTED TRANSIENTS

Test	Perturbation	Length of the pulse [sec]	Pulse magnitude [%]
1	Relief valve opening	49	-
2	Secondary system mass flow increment	151	11
3	Secondary system mass flow decrease	152	-17
4	Heaters power increment	156	5
5	Heaters power decrease	152	-15

4.2.3. CAPCN nodalization

The present subsection describes the nodalization of CAPCN for RELAP5/MOD3.3. In order to develop the nodalization, attention was focused on the following thermohydraulic phenomena that occur during the transients in order to represent them properly:

- heat transfer in the steam generator
- self-pressurization in the dome
- steam condensation in the dome
- two phase flow in the riser
- natural circulation
- chocked flow in the relief valve
- heat transfer with the structures and heat losses

Considering the particular characteristics of CAPCN (the variables are strongly coupled due to natural circulation and self-pressurization), it is not possible to match all the process variables for steady state condition. For CAPCN simulation, the methodology to obtain the steady state was very similar to that used during the loop operation.

The independent parameters that are fixed by input are:

- Heat generation in the heaters
- Steam generator feed water temperature (secondary side)
- Steam generator feed water mass flow rate (adjusted to match the primary circuit experimental value)
- Primary circuit water level (by means of control loop adding or removing water depending on a reference level error)
- Hydraulic resistance in the primary circuit (adding a friction coefficient in the cold leg to match the mass flow rate. In CAPCN the nominal mass flow rate was adjusted by changing the area of the valve located in the cold leg: valve FX_105)
- Heat losses from the primary circuit and their distribution (estimated from experimental thermal balances)

And the dependent parameters are:

- Primary circuit pressure: depends on the power balance (the steady state pressure value is such that the heat removed by the steam generator and by the heat losses equals the heaters power)
- Primary circuit mass flow
- Secondary system steam temperature
- Primary system temperatures

The primary and secondary circuits nodalization consist of 267 hydraulic volumes which are connected with 268 junctions and 233 heat structures. The total number of RELAP5 hydrodynamic components is 25 and RELAP5 heat structures components is 11. The nodalization diagram is presented in Fig. 4.2-3.

Enough detail is provided in the nodalization to represent the geometry and to enhance the proper numerical modelling of the transport of enthalpy fronts along the riser and down-comer, as natural circulation flow depends on buoyancy forces. There are also zones where 3 dimensional effects could be important and in some way this would make difficult to capture the actual phenomenology and to interpret the results. In particular this applies to the dome, the steam generators lower plenum and circuit lower plenum at core inlet. In order to represent properly steam circulation in the dome, an array of two connected pipes was used.

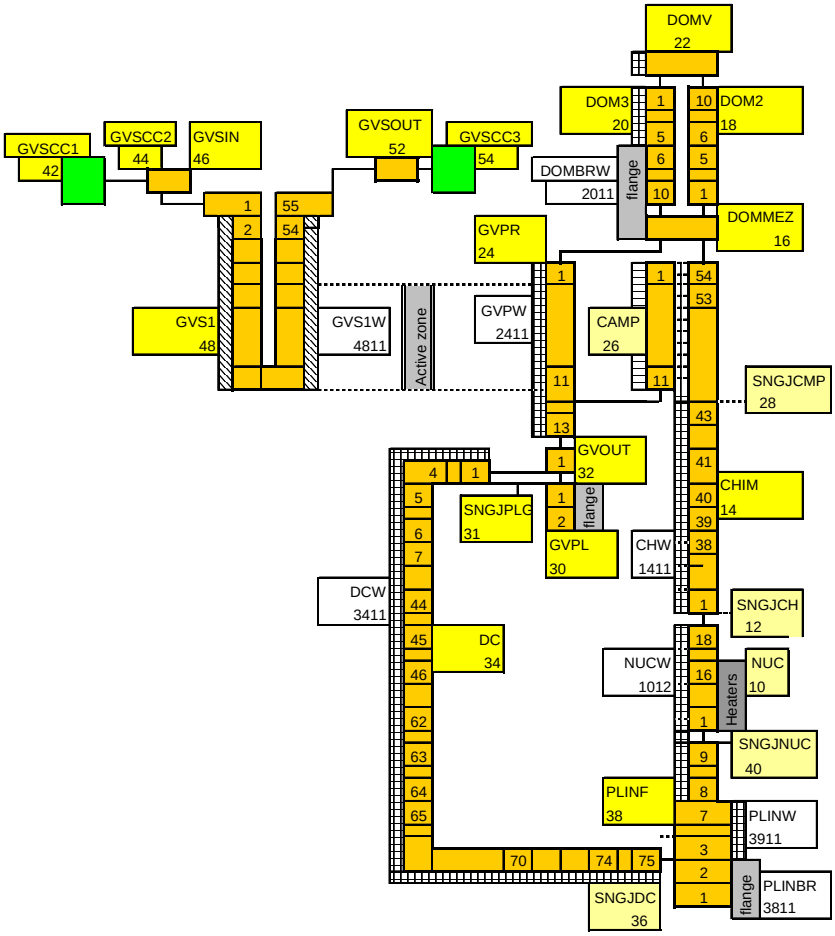

FIG. 4.2-3. Diagram of the primary circuit and steam generators tubes nodalization.

4.2.4. TEST 1: Relief valve temporal opening

The initial conditions prior to run Test 1 (steady state values) are compared with RELAP5 results in Table 4.2-2. From the comparison of the RELAP5 results with the measured values we can say that the agreement is very good.

This test begins with the opening of the relief valve, which is kept open for approximately 50 seconds, and then closed. The opening time was assumed to be one second; however, a value as high as 10 seconds does not change the results significantly. As consequence of the loss of coolant (steam) (Fig. 4.2-4), the system pressure drops sharply, as shown in Fig. 4.2-5. When the valve is closed, the pressure begins to increase slowly towards a new steady state value as the total energy accumulated in the system is changed. It can be seen from the results that the pressure predicted by RELAP5 is higher than the measured pressure.

The recorded primary circuit mass flow rate is shown in Fig. 4.2-6. A sharp increase is observed when the valve was opened then it diminished slowly when the valve was closed. The measured peak was interrupted because the measurement was out of range (1.62 kg/s). This abrupt increment is produced because of void fraction generation in the riser during the depressurization (the riser is near saturation and flashing occurs). When the valve is closed, the mass flow rate decreases because the bubbles collapse along the riser due to the pressure increment. A new steady state value can be observed.

TABLE 4.2-2: TEST 1 STEADY STATE: COMPARISON BETWEEN MEASUREMENT AND RELAP5 RESULTS

Variable	Measurement Mean value	RELAP5
Thermal power [kW]	239.73	239.74 (*)
Primary circuit mass flow rate [kg/s]	1.48	1.49 (***)
Steam dome pressure [MPa]	10.997	11.00 (***)
Water level (from riser outlet) [m]	0.437	0.434
Cold leg temperature [°C]	290.7	290.6
Secondary circuit mass flow rate [kg/s]	0.107	0.109 (**)
Steam generators feed water temperature [°C]	199.8	199.8 (*)
Steam generators outlet temperature (steam) [°C]	304.74	305.4

(*) Input value, fixed as boundary condition.
(**) Obtained value to match pressure in the primary circuit.
(***) Values obtained to match the experimental data as a result of the steady state calculation procedure.

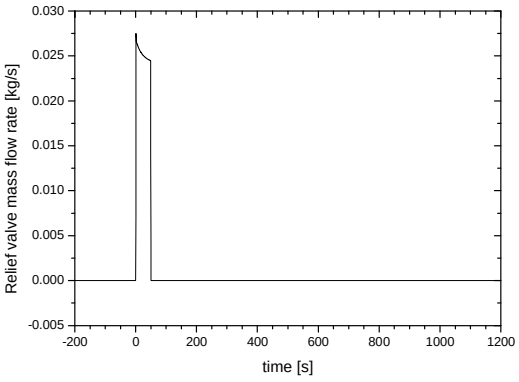

FIG. 4.2-4. Test 1: mass flow rate in the relief valve.

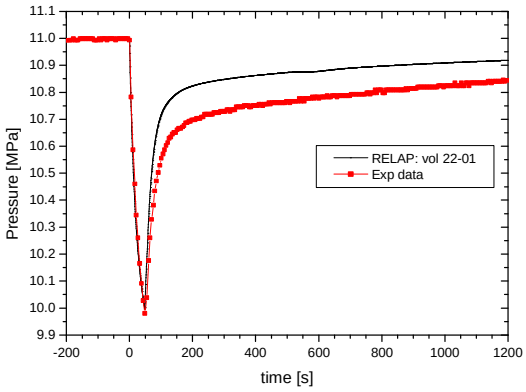

FIG. 4.2-5. Test 1: primary circuit pressure.

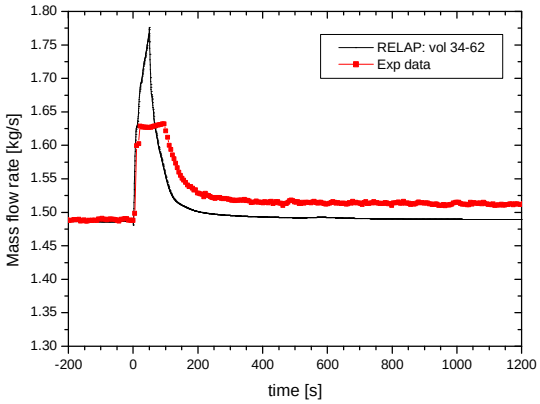

FIG. 4.2-6. Test 1: primary circuit mass flow rate.

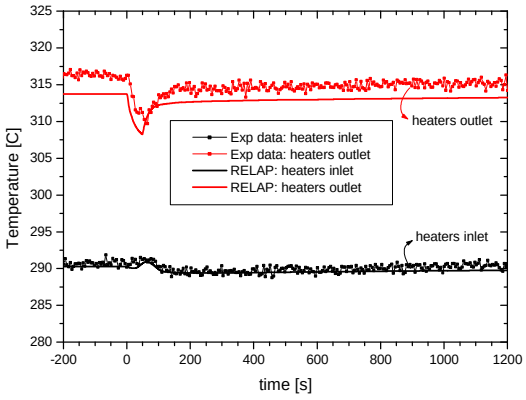

FIG. 4.2-7. Test 1: PCS temperatures.

Temperatures evolution at core inlet and outlet are compared in Fig. 4.2-7. A decrease in heaters outlet temperature is observed, this could be due to combination of two effects: 1) the increase of the mass flow rate, and 2) the decrease in the saturation temperature, following the pressure evolution. Heaters inlet temperatures initially increase because the SG outlet temperature increases as the fluid residence time decreases. And then it starts to decrease with a delay corresponding to the circuit transport time. The agreement between the cold leg temperatures is excellent; this parameter is an output of RELAP5 and is a consequence of a good matching of the mass flow rate, heat losses and steam generator modelling.

4.2.5. TEST 2: Secondary system mass flow increment

The steady state values are compared with RELAP5 results in Table 4.2-3. From the comparison of the RELAP5 results with the measured values we can say that the agreement is very good.

TABLE 4.2-3. TEST 2 STEADY STATE: COMPARISON BETWEEN MEASUREMENT AND RELAP5 RESULTS

Variable	Measurement Mean value	RELAP5
Thermal power [kW]	238.0	238.0 (*)
Primary circuit mass flow rate [kg/s]	1.49	1.495 (***)
Steam dome pressure [MPa]	11.02	11.02 (***)
Water level (from riser outlet) [m]	0.405	0.404
Cold leg temperature [°C]	291.6	291.2
Secondary circuit mass flow rate [kg/s]	0.107	0.108 (**)
Steam generators feed water temperature [°C]	208.2	208.2 (*)
Steam generators outlet temperature (steam) [°C]	305.10	306.3

(*) Input value, fixed as boundary condition.
(**) Obtained value to match pressure in the primary circuit.
(***) Values obtained to match the experimental data as a result of the steady state calculation procedure.

In this test, the feed water to the steam generators is increased approximately by 11% over 151 seconds. The mass flow rate is then decreased approximately to the initial value. Fig. 4.2-8 shows the steam mass flow rate at steam generator (SG) exit. The mass flow rate measurement shows some fluctuations, which are probably caused by the positive displacement pump (used because of the low flow and the required pump head).

When the secondary circuit mass flow rate is increased, heat removal in the SG is enhanced and the temperature of the cold leg decreases (see Fig. 4.2-9) leading to an increase in the primary circuit mass flow rate (see Fig. 4.2-10). When the lower temperature front arrives to the hot leg, the buoyancy force decreases and so does the mass flow, approaching a new steady state value after some damped oscillations caused by the thermal front transit along the circuit. When the secondary mass flow rate is decreased to the original value the same type of coupling is observed. It is observed that RELAP5 results match very well the heaters inlet temperature, while there is a shift in the outlet temperature, perhaps due to a different prediction in the void fraction generation. Nevertheless the difference is accepted taking into account the measurement error. The heat removal increment (that generates an energy imbalance in the system) causes the temperature in the down comer to decrease, and, therefore, the density increases. The water level and pressure decrease as a consequence (see Fig. 4.2-11). When the SG feed water is reduced to the original value, the removed power tends to balance the generated power, and the pressure begins to increase to a new steady state value. The initial decrease of water level is predicted faster than the experimental data. Nevertheless, the trends of the predicted parameters are consistent with the experimental observations.

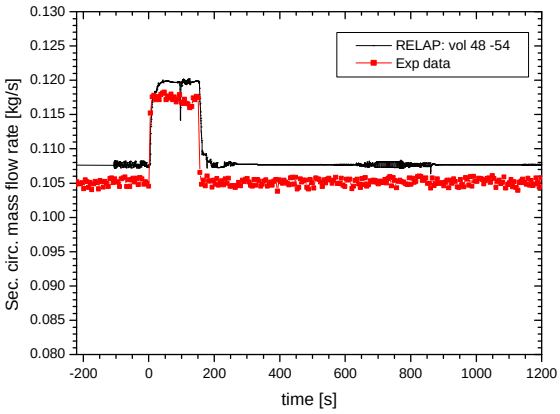

FIG. 4.2-8. Test 2: steam mass flow rate at SG exit.

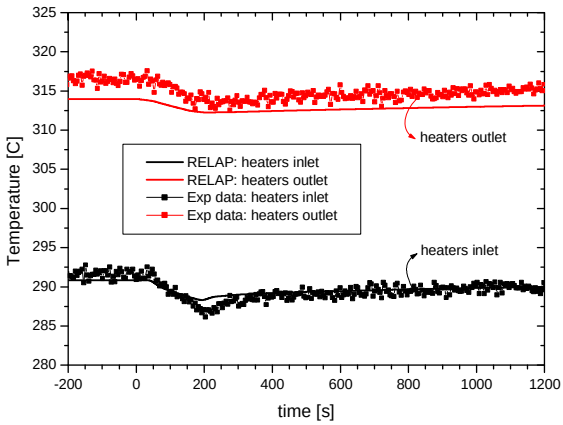

FIG. 4.2-9. Test 2: PCS temperatures.

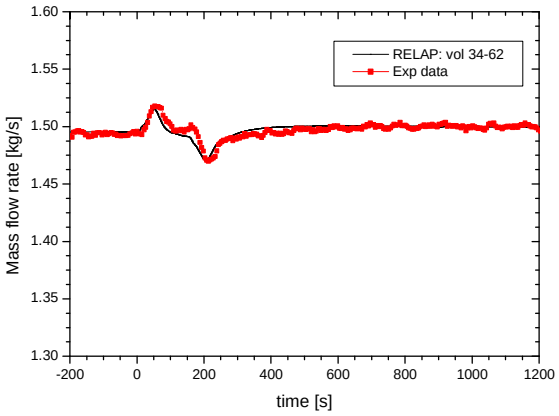

FIG. 4.2-10. Test 2: primary circuit mass flow rate.

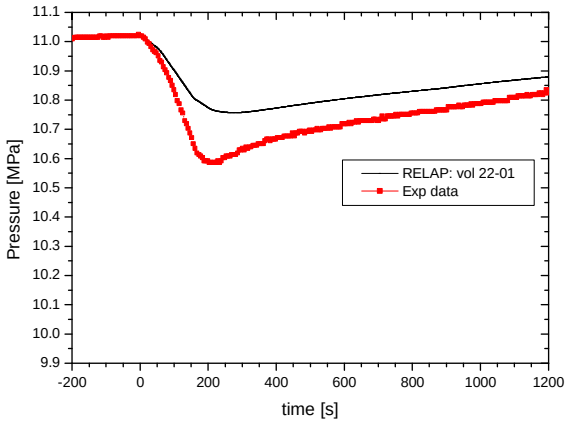

FIG. 4.2-11. Test 2: primary circuit pressure.

4.2.6. TEST 4: Heaters power increase

The initial conditions prior to run Test 4 are compared with RELAP5 results in Table 4. From the comparison of the RELAP5 results with the measured values we can say that the agreement is very good.

In this test, the thermal power is increased by 12 KW (about 5% of full power) over 150 seconds, as can be seen in Fig. 4.2-12. The pressure of the primary circuit and the circulated flow evolved mildly, with increments below 2 and 3% respectively, as shown in Figs 4.2-13 and 14. The primary circuit temperature measurements indicate some fluctuations as shown in Fig. 4.2-15, nevertheless the variation is small.

As the hot leg is close to saturation temperature, the power rise produces an abrupt increment in the void generation; for this reason the buoyancy force and the mass flow rate increase. Moreover, the hot leg would be expanded due to this increase of void fraction, increasing pressure and therefore the saturation temperature. This in turns generates a feedback on the void generation, tending to limit it.

TABLE 4.2-4. TESt 4 STEADY STATE:
COMPARISON BETWEEN MEASUREMENT AND RELAP5 RESULTS

Variable	Measurement Mean value	RELAP5
Thermal power [kW]	238.0	238.0 (*)
Primary circuit mass flow rate [kg/s]	1.51	1.51 (***)
Steam dome pressure [MPa]	10.99	10.98 (***)
Water level (from riser outlet) [m]	0.40	0.40
Cold leg temperature [°C]	291.9	290.9
Secondary circuit mass flow rate [kg/s]	10.55	0.1054 (**)
Steam generators feed water temperature [°C]	200.2	198.0 (*)
Steam generators outlet temperature (steam) [°C]	306.3	306.0

(*) Input value, fixed as boundary condition.
(**) Obtained value to match pressure in the primary circuit.
(***) Values obtained to match the experimental data as a result of the steady state calculation procedure.

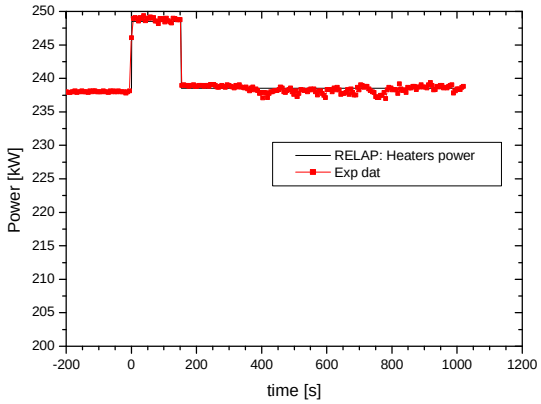

FIG. 4.2-12. Test 4: Heaters power evolution (boundary condition).

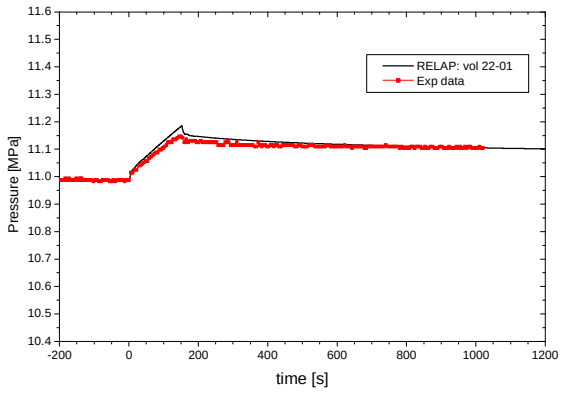

FIG. 4.2-13. Test 4: Primary circuit pressure.

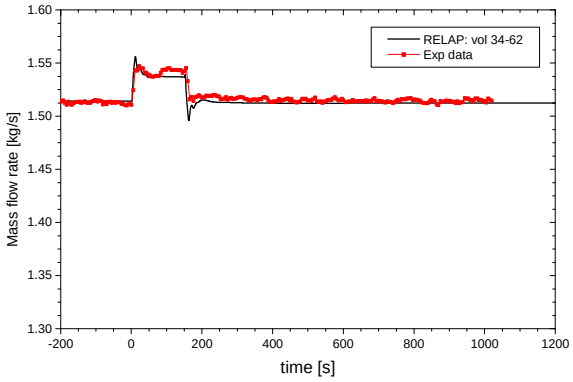

FIG. 4.2-14. Test 4: Primary circuit temperatures evolution.

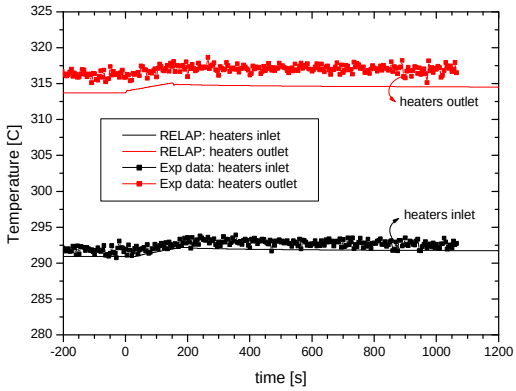

FIG. 4.2-15. Test 4: Primary circuit temperatures evolution.

In conclusion, it was found that all the trends and values are well reproduced by the code in the analysed transients, where power imbalance and a limited loss of coolant were introduced as perturbations into the system.

REFERENCES FOR SECTION 4.2

[4.2-1] INTERNATIONAL ATOMIC ENERGY AGENCY, Passive Safety Systems and Natural Circulation in Water Cooled Nuclear Power Plants, IAEA-TECDOC-1624, IAEA, Vienna (2009) Annex XIV, CAREM.

4.3. INTEGRAL SYSTEM TESTS IN INTEGRAL TEST LOOP SIMULATING ADVANCED HEAVY WATER REACTOR

The Advanced Heavy Water Reactor (AHWR) [4.3-1, and 4.3-2] is a light water cooled and heavy water moderated pressure tube type boiling water reactor. In the AHWR, it is proposed to remove the core heat by natural circulation during startup, power raising, normal operation, transients and accidental conditions. AHWR uses several passive concepts with a view to simplify the design and to enhance safety. An integral test facility (Fig. 4.3-1 shows the building housing of this facility) simulating the Main Heat Transport (MHT) and safety systems of AHWR has been set up at Bhabha Atomic Research Centre to investigate the overall system behaviour under different operating conditions, transients and accidents like loss of coolant accident. In addition to Main Heat Transport System (MHTS), the Integral Test Loop (ITL) simulates the Emergency Core Cooling System (ECCS), Isolation Condenser (IC) system and Gravity Driven Cooling System (GDCS) of the AHWR. The main objectives of the test facility are:

- Generation of database for
  - Plant transients
  - Accidental scenarios like LOCA;
- Evolution and validation of a startup procedure;
- Generation of database for the performance evaluation of the following in the plant environment:
  - Natural circulation in the MHT loop, including parallel channel behaviour,
  - Steam separation process in the steam drum,
  - Fluidic device in the advanced accumulator,
  - Gravity Driven Cooling System;
- Investigations of asymmetric behaviour like operation with one steam drum at a higher pressure or break in a steam line connected to one steam drum.

The scaling philosophy adopted for ITL is based on a three level approach [4.3-2]. At the system level, power-to-volume scaling philosophy is used. Boundary flows such as feed water flow rate, steam flow rate, safety injection etc. which can affect the integral behaviours are also scaled. In addition, important local phenomena which can influence the integral system behaviour such as Critical Heat Flux (CHF), steam-water separation in the steam drum, flow pattern transition etc. are also preserved.

4.3.1. AHWR MHTS and decay heat removal system

In the Main Heat Transport System (MHTS) (Fig. 4.3-2), the subcooled water flows from the Reactor Inlet Header (RIH) to the core through 452 feeder pipes. The subcooled water gets heated up as it rises through the 452 fuel assemblies. Boiling takes place in the fuel assemblies and steam-water two phase mixture comes out of the channels. Low quality steam-water mixture flows from the core outlet to 4 horizontal steam drums through 452 tail pipes. In the steam drum, steam gets separated from water by gravity. Under normal operating conditions, steam flows to the turbine, which is returned to steam drum as feed water at 130ºC. The feed water, after mixing with the saturated water flows through downcomers to the inlet header and the cycle repeats itself.

Besides core heat removal by natural circulation under normal operating conditions, a number of passive systems are incorporated in the AHWR in order to simplify the design and to enhance safety. The following passive systems are incorporated in the AHWR.

- Advanced accumulator using a fluidic device to inject emergency coolant during the initial stages of LOCA;
- Gravity driven cooling system (GDCS) for uninterrupted core cooling for at least 3 days after the accumulators are exhausted;
- Passive decay heat removal system with isolation condensers.

FIG. 4.3-1. Photograph of ITL building.

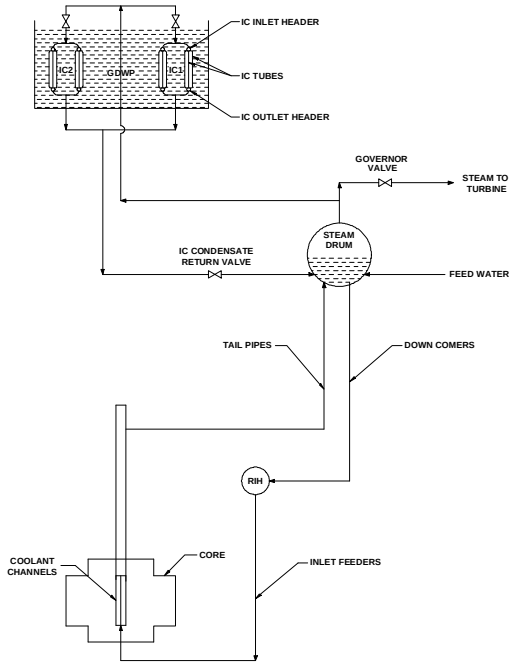

FIG. 4.3-2. MHT and isolation condenser systems of AHWR..

4.3.2. Scaling philosophy

The scaling philosophy adopted for ITL is based on a three level approach [4.3-3, 4.3-4 and 4.3-5]. At the global level (commonly known as integral scaling), power-to-volume scaling philosophy [4.3-6 and 4.3-7] is used. Boundary flows such as feed water flow rate, steam flow rate, safety injection etc. which can affect the integral behaviours, are also scaled. In addition, important local phenomena which can influence the integral system behaviour such as Critical Heat Flux (CHF), steam-water separation in the steam drum, flow pattern transition etc. are also preserved [4.3-8]. The details of the scaling philosophy are presented in following sections.

4.3.2.1. Power to volume scaling philosophy

For scaling, the primary heat transport system of nuclear reactors is assumed to consist of a large number of pipe sections, which are either vertical or horizontal. One dimensional homogenous two phase flow (EVET model) through a vertical pipe can be represented by the following governing equations:

Conservation of mass:
$$\frac{\partial \rho}{\partial t} + \frac{\partial (\rho v)}{\partial z} = 0 \qquad (4.3\text{-}1)$$

Conservation of momentum:
$$\rho \frac{\partial v}{\partial t} + \rho v \frac{\partial v}{\partial z} = -\frac{\partial p}{\partial z} - \frac{\zeta_w \tau}{A_c} - g\rho \qquad (4.3\text{-}2)$$

Conservation of energy:
$$\rho\frac{\partial \mathrm{h}}{\partial \mathrm{t}}+\rho \mathrm{v}\frac{\partial \mathrm{h}}{\partial \mathrm{z}}=\frac{\mathrm{q}\zeta_{\mathrm{h}}}{\mathrm{A_c}}+\frac{\partial \mathrm{p}}{\partial \mathrm{t}}+\mathrm{v}\frac{\partial \mathrm{p}}{\partial \mathrm{z}} \tag{4.3-3}$$

These equations are non-dimensionalized using the following substitutions:

$$t^{+}=\frac{t}{t_0};\quad z^{+}=\frac{z}{z_0};\quad \rho^{+}=\frac{\rho}{\rho_0};\quad v^{+}=\frac{v}{v_0};\quad p^{+}=\frac{p}{p_0}; \tag{4.3-4a}$$

$$\tau^{+}=\frac{\tau}{f\rho_0 v_0^{\,2}};\quad h^{+}=\frac{h}{h_0};\quad q^{+}=\frac{q}{q_0};\quad \zeta^{+}=\frac{\zeta}{\zeta_0};\quad A_c=\frac{A}{A_0}; \tag{4.3-4b}$$

Where, the quantities having subscript '0' are known reference values. The non-dimensional governing equations are:

$$\frac{\partial \rho^{+}}{\partial \mathrm{t}^{+}}+\left[\frac{\mathrm{v_0 t_0}}{\mathrm{l_0}}\right]\frac{\partial(\rho^{+}\mathrm{v}^{+})}{\partial \mathrm{z}^{+}}=0 \tag{4.3-5}$$

$$\rho^{+}\frac{\partial \mathrm{v}^{+}}{\partial \mathrm{t}^{+}}+\left[\frac{\mathrm{v_0 t_0}}{\mathrm{l_0}}\right]\rho^{+}\mathrm{v}^{+}\frac{\partial \mathrm{v}^{+}}{\partial \mathrm{z}^{+}}=\left[\frac{\mathrm{p_0 t_0}}{\mathrm{l_0}\rho_0\mathrm{v_0}}\right]\frac{\partial \mathrm{p}^{+}}{\partial \mathrm{z}^{+}}-\left[\frac{\zeta_0}{\mathrm{A_{c0}}}\mathrm{f\ v_0 t_0}\right]\frac{\zeta^{+}{}_{\mathrm{w}}\tau^{+}}{\mathrm{A_c}^{+}}-\left[\frac{\mathrm{g t_0}}{\mathrm{v_0}}\right]\rho^{+} \tag{4.3-6}$$

$$\rho^{+}\frac{\partial \mathrm{h}^{+}}{\partial \mathrm{t}^{+}}+\left[\frac{\mathrm{v_0 t_0}}{\mathrm{l_0}}\right]\rho^{+}\mathrm{v}^{+}\frac{\partial \mathrm{h}^{+}}{\partial \mathrm{z}^{+}}=\left[\frac{\zeta_0 \mathrm{q_0 t_0}}{\mathrm{A_{c0}}\rho_0\mathrm{h_0}}\right]\left(\frac{\zeta_{\mathrm{h}}{}^{+}\mathrm{q}^{+}}{\mathrm{A_c}^{+}}\right)+\left[\frac{\mathrm{p_0}}{\rho_0\mathrm{h_0}}\right]\frac{\partial \mathrm{p}^{+}}{\partial \mathrm{t}^{+}}+\left[\frac{\mathrm{v_0 t_0 p_0}}{\mathrm{l_0}\rho_0\mathrm{h_0}}\right]\mathrm{v}^{+}\frac{\partial \mathrm{p}^{+}}{\partial \mathrm{z}^{+}} \tag{4.3-7}$$

From Eqs (4.3-5)–(4.3-7), we can say that for similarity to be achieved between processes observed in a model (denoted by subscript 'm') and in the prototype (denoted by subscript 'p'), the following equalities must be satisfied:

$$\left[\frac{\mathrm{vt}}{\mathrm{l}}\right]_{\mathrm{m}}=\left[\frac{\mathrm{vt}}{\mathrm{l}}\right]_{\mathrm{p}} \tag{4.3-8a}$$

$$\left[\frac{\mathrm{p}}{\rho}\frac{\mathrm{t}}{\mathrm{lv}}\right]_{\mathrm{m}}=\left[\frac{\mathrm{p}}{\rho}\frac{\mathrm{t}}{\mathrm{lv}}\right]_{\mathrm{p}} \tag{4.3-8b}$$

$$\left[\frac{\zeta_{\mathrm{w}}}{\mathrm{A_c}}\mathrm{fvt}\right]_{\mathrm{m}}=\left[\frac{\zeta_{\mathrm{w}}}{\mathrm{A_c}}\mathrm{fvt}\right]_{\mathrm{p}} \tag{4.3-8c}$$

$$\left[\frac{\mathrm{gt}}{\mathrm{v}}\right]_{\mathrm{m}}=\left[\frac{\mathrm{gt}}{\mathrm{v}}\right]_{\mathrm{p}} \tag{4.3-8d}$$

$$\left[\frac{\zeta_{\mathrm{h}}}{\mathrm{A_c}}\frac{\mathrm{qt}}{\rho\mathrm{h}}\right]_{\mathrm{m}}=\left[\frac{\zeta_{\mathrm{h}}}{\mathrm{A_c}}\frac{\mathrm{qt}}{\rho\mathrm{h}}\right]_{\mathrm{p}} \tag{4.3-8e}$$

$$\left[\frac{p}{\rho h}\right]_m = \left[\frac{p}{\rho h}\right]_p \tag{4.3-8f}$$

The subscript '0' has been omitted from the above equations for convenience. Assuming that the same fluid is going to be used in the model and prototype and imposing the conditions of isochronicity and equality of pressures and temperature (and hence properties), then Eq. (4.3-8e) can be written as:

$$\left[\frac{\zeta_h q}{A_c}\right]_m = \left[\frac{\zeta_h q}{A_c}\right]_p$$

Multiplying both sides by l,

$$\left[\frac{l\zeta_h q}{lA_c}\right]_m = \left[\frac{l\zeta_h q}{lA_c}\right]_p$$

Since $l\zeta_h$ is heat transfer area, $l\zeta_h q$ is the power (ϕ). Similarly, lA_c is the volume (V). In other words, Eq. (4.3-8e) can be expressed as

$$\frac{\phi_p}{\phi_m} = \frac{V_p}{V_m} \tag{4.3-9}$$

where, V is the volume. Similarly, Eq. (4.3-8a) can be expressed as

$$\left(\frac{v}{l}\right)_m = \left(\frac{v}{l}\right)_p \qquad \text{or} \qquad \left(\frac{A_c v}{A_c l}\right)_m = \left(\frac{A_c v}{A_c l}\right)_p$$

This can be expressed as, $\frac{Q_p}{Q_m} = \frac{V_p}{V_m}$

Since the properties are the same in the model and prototype, this can be expressed as

$$\frac{Q_p}{Q_m} = \frac{W_p}{W_m} = \frac{V_p}{V_m} \tag{4.3-10}$$

From Eq. (4.3-8d) we get:

$$\frac{v_m}{v_p} = 1 \tag{4.3-11}$$

From Eq. (4.3-8b) we get:

$$\frac{(vl)_m}{(vl)_p} = 1 \tag{4.3-12}$$

Equations (4.3-11) and (4.3-12) can be satisfied only if elevations (in case of horizontal pipes, length) are preserved between model and prototype, i.e.,

$$\frac{l_m}{l_p} = 1$$

This also implies that

$$\frac{(A_c)_p}{(A_c)_m} = \frac{V_p}{V_m} \tag{4.3-13}$$

i.e., the flow areas are scaled by the volume scale ratio and hence the diameters are scaled by the square root of the volume scale ratio.

From Eq. (4.3-8c) we get:

$$\left(\frac{\zeta_w f}{A_c}\right)_m = \left(\frac{\zeta_w f}{A_c}\right)_p \Rightarrow \left(\frac{\zeta_w f}{V}\right)_m = \left(\frac{\zeta_w f}{V}\right)_p \Rightarrow \frac{(\zeta_w f)_p}{(\zeta_w f)_m} = \frac{V_p}{V_m} \tag{4.3-14}$$

Thus, the power to volume scaling relations can be expressed as

(1) Equal pressures and properties i.e.:

$$\frac{p_p}{p_m} = \frac{\rho_p}{\rho_m} = \frac{h_p}{h_m} = 1 \tag{4.3-15}$$

(2) Power to volume scaling relation:

$$\frac{\phi_p}{\phi_m} = \frac{W_p}{W_m} = \frac{Q_p}{Q_m} = \frac{V_p}{V_m} = S \tag{4.3-16}$$

Which also implies isochronicity i.e., $\frac{t_p}{t_m} = 1$

(3) Equal elevations:

$$\frac{l_p}{l_m} = 1, \text{ which also implies } \frac{(A_c)_p}{(A_c)_m} = \frac{V_p}{V_m} = S \tag{4.3-17}$$

(4) Equal frictional effects:

$$\left[\frac{\zeta_w f}{A_c}\right]_m = \left[\frac{\zeta_w f}{A_C}\right]_p \quad \text{or} \quad \frac{(\zeta_w f)_p}{(\zeta_w f)_m} = \frac{V_p}{V_m} = S \tag{4.3-18}$$

Thus, once the power to volume scaling ratio ‘S’ is fixed, all other quantities are automatically fixed. Hence, this method of scaling is known as ‘power to volume scaling.

Since the full size, full length components are proposed to be used for most components in ITL, allthe ratios expressed by Eqs (4.3-15)–(4.3-18) can be met in ITL. However, some components like the header, downcomer and steam drum have to be downsized because it is difficult to preserve the relationship expressed by Eq. (4.3-18).

4.3.2.2. Local phenomena scaling

Important local phenomena that can affect the integral system performance need to be scaled appropriately. The local phenomenon to be simulated depends on the component of the loop. The following local phenomena are considered.

- Critical Heat Flux (CHF): CHF is the most important local phenomena to be simulated in the core simulator. Use of full scale, full power and full pressure fuel channel simulator ensures that CHF can be simulated in ITL.
- Flashing: Flashing can occur in the riser due to decrease in the static head. It can cause instability during startup. Since full size, full height tail pipes (risers) are used in ITL, flashing can be simulated.
- Geysering: Geysering can occur due to the condensation of large slug bubbles that are generated in the core when they mix with subcooled water in the riser pipes. This phenomenon depends on size of slug bubble formed in the core, flow velocity, pressure and temperature in the riser. It also depends on subcooled boiling. Geysering is a highly thermal non-equilibrium phenomenon by nature. Since full scale core and riser pipe are simulated along with the operating conditions, Geysering can be simulated in ITL.
- Flow Stratification: Flow stratification occurs in horizontal pipes/large pipe sections at low steaming rates and hence is expected to occur at low power. To simulate flow stratification in ITL, the Froude number needs to be scaled.
- Flow pattern transition: Flow pattern transition can occur in the two phase regions of the loop. It can cause instability generally known as flow pattern transition instability. Again since full size, full height and operating conditions are simulated in ITL, flow pattern transition instability can be simulated in ITL.
- Steam-Water Separation: Steam-water separation (including carryover and carry under) is the most important local phenomena to be simulated in the steam drum. Steam-water separation at the interface depends on the interface area. Carryover depends on the steam velocity above the interface and carry under depends on the water velocity in the downcomer section of the steam drum. Since the steam drum is downsized the interface area is larger than required and since the steam velocity and downcomer velocity in the steam drum are not scaled, steam-water separation phenomenon is not exactly scaled.

4.3.2.3. Boundary flow scaling

For simulating the effect of certain components or systems on the integral system performance, it is sufficient to simulate only the boundary flow of mass and energy.

- Feed water flow: The feed water temperature needs to be maintained in the ITL at the same values as that of the AHWR. The feed water mass flow rate at normal operating condition has to be scaled in the same ratio as the volume scale.
- Accumulator Injection: For the accumulator, the following need to be simulated:
  - Transient non-dimensional injection flow rate;
  - Loss coefficient of the fluidic device and pressure loss in the injection pipe;
  - Water temperature and nitrogen pressure in the accumulator.
- Gravity Driven Cooling System (GDCS) Injection: Simulation of GDCS injection in ITL requires the same transient non-dimensional injection flow rate as that of AHWR. ITL maintains an initial nitrogen pressure in the GDCS tank to compensate for the difference of elevation. The temperature of the GDCS liquid in the model and prototype is maintained the same.

- Critical Flow: Critical flow simulation is important for LOCA following a pipe break. It depends on break size, upstream conditions (P, h), etc.

4.3.3. Description of ITL

4.3.3.1. Systems included in ITL

The integral test loop consists of the following systems:

- PHT system with all its components
- ECCS system including advanced accumulator and Gravity Driven Water Pool (GDWP)
- Secondary system up to turbine stop valve (CIES valve)
- Feed water system (flow rate and inlet temperature)
- Isolation condenser
- Control systems for
    - PHT pressure
    - Steam drum level
    - Power
        - Normal power raising
        - Step back/Set back
        - Trip
        - Decay power simulation
    - Feed water temperature and flow rate
    - Steam pressure and flow along with associated control and safety valves

Brief descriptions of the various systems of ITL are given below.

4.3.3.2. Primary heat transport (PHT) system

Overall scaling parameters

The prototype loop is scaled down by a factor of 452. Figure 4.3-3 shows a 3-D view of the test facility. It consists of a full size, 54-rod cluster with full size feeder and tail pipe. The components like steam drum; downcomer and header are scaled down in volume by a factor of 452. All primary loop piping is SS 316L and is designed for 304 ^{0}C temperature and 100 bar pressure. Overall scaling parameters are as below

- Pressure scaling: 1:1 (70 bar)
- Temperature scaling: 1:1 (285 ºC)
- Power scaling: 1:452
- Elevation scaling: 1: 1 (only for PHT Loop)
- Volume scaling: 1:452
- Maximum power to the test section: 3 MW

Steam drum

ITL consists of a horizontal steam drum (Fig. 4.3-4) wherein steam and water are separated by gravity. While scaling the steam drum, the important local phenomenon to be scaled is the steam-water separation by gravity, simulation of which requires the scaling of the carry-over and carry-under phenomena. The following parameters are considered to be important in scaling carry-over and carry-under.

- Steam and water velocity above the interface
- Interface area per unit of power
- Level in the steam drum (height of interface) and height of steam space above the interface
- Froude number (Fr) simulation

The above parameters are interrelated and generally accepted non-dimensional groups for the steam separation process are not available. Hence, a dimensional analysis was carried out to obtain the relevant non-dimensional groups. However, due to the adoption of power to volume scaling and geometrical constraints, the Froude number could not be simulated.

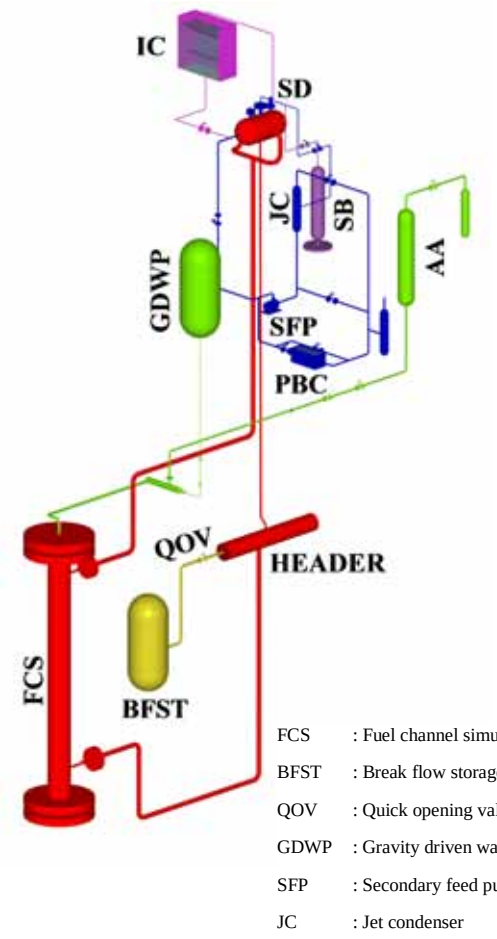

FIG. 4.3-3. 3-D view of ITL.

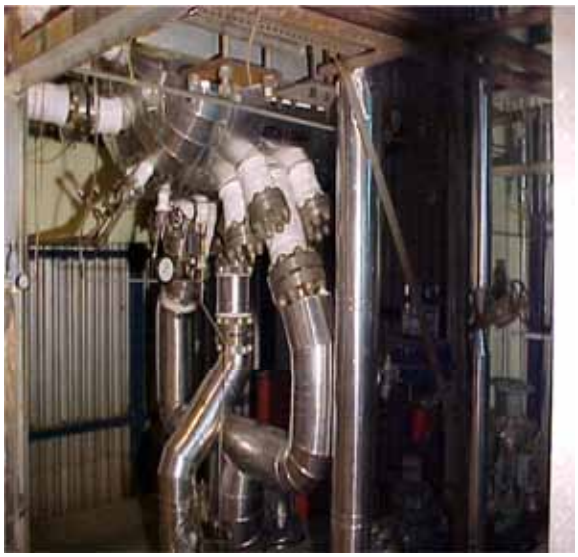

FIG. 4.3-4. Steam drum as installed in ITL.

Downcomer

In the AHWR, each steam drum is connected to the header by means of four downcomers. In ITL, a single downcomer pipe of full height and reduced diameter replaces all these 16 pipes. The downcomer diameter is arrived at by scaling down the flow area in the volume scale ratio, which will also simulate the velocities and preserve the time scale.

Header & feeder pipe

The header in the AHWR is connected to all the sixteen downcomers and 452 parallel feeder lines emerge from the header with 113 tail pipe lines connected to each steam drum. The dimensions of the header are obtained by volume scaling.

The feeder in the ITL is a pipe with reduced length due to space constraints in the existing building. To simulate the volume, the pipe diameter has been increased. However, the desired flow resistance can be simulated by placing an orifice plate in the flow path.

Core simulator

A directly heated 54-rod full scale fuel cluster simulator with central water rod for ECC injection is installed in ITL. The fuel cluster simulator, as fabricated, is shown in Fig. 4.3-5. The power of the test section during integral experiments is 2.03 MW, which corresponds to 1/452 of the reactor nominal power (920 MWth). A cross sectional view of Fuel Cluster Simulator and assembly drawing is depicted in Fig. 4.3-6.

FIG. 4.3-5. Photograph of fuel cluster simulator as installed in the facility.

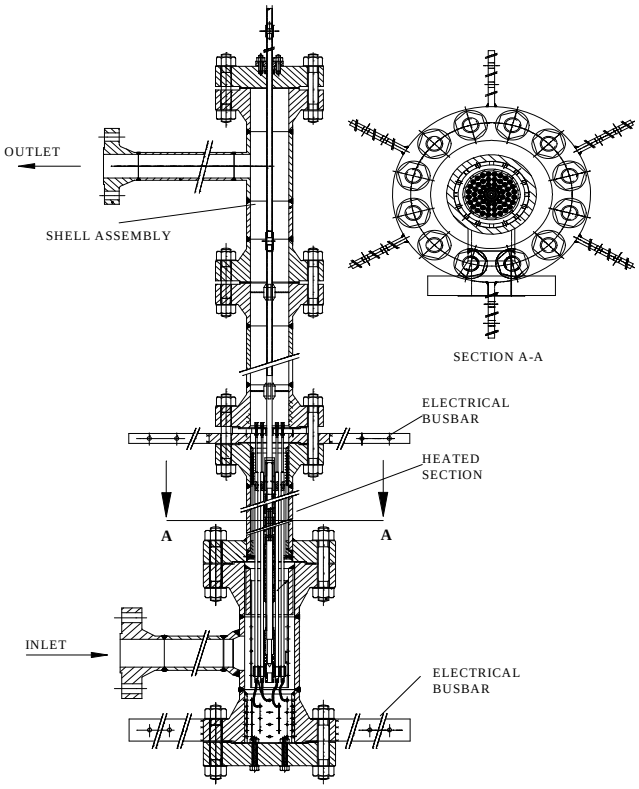

FIG. 4.3-6. Fuel rod cluster simulator set-up.

4.3.3.3. Steam and feed water system

The steam supply system to the turbine up to the governor valve will be simulated. All the controls on steam pressure including steam discharge, safety relief valve, dump valves and CIES valve will be simulated as per the plant. The steam produced in the facility will be condensed using a Jet condenser and a pool boiling cooler. The condensed steam will be supplied as feed water at the required temperature (130 ^{0}C) to the steam drum.

Jet condenser

The saturated steam coming from the steam drum is at 285 ^{0}C and 70 bar. This steam is to be condensed and recirculated to the steam drum at 130 ^{0}C under nominal power operation. The jet condenser is used to simulate these conditions by condensing the steam in a jet of cold water. The cold water for this jet is supplied by the pool boiling cooler. This spray of cold-water jet is maintained with the help of a secondary feed water pump.

Pool boiling cooler

The pool boiling cooler (PBC) is included in the circuit as the ultimate heat sink and to provide cold water at the required temperature to the jet condenser. Part of the feed pump discharge, at temperature of 130 ^{0}C, is sent through the pool boiling cooler, which in turn cools the water to be sent to the jet condenser. The cooling water for the pool boiling cooler is supplied from the service water system, which is normally at room temperature. The service water boils and the steam is released to the atmosphere. The level of water in the PBC is maintained manually. However, a level alarm is provided to alert the operator to commence water make-up.

4.3.3.4. Emergency core cooling system (ECCS)

The ECCS essentially consists of the advanced accumulator and the GDCS.

Advanced accumulator

The advanced accumulator is designed for core cooling in a passive manner in the event of LOCA in the AHWR. The accumulator is provided with a passive fluidic flow control device known as “vortex chamber”. It allows a large flow rate at the initial stage of the LOCA. As time elapses, the requirement for a large flow rate decreases and the fluidic device allows only a smaller flow rate.

As the primary system is scaled down in volume by a factor of 452, the accumulator volume is also scaled by the same ratio (a photograph of the advanced accumulator is shown in Fig.4.3-7). The initial pressure of nitrogen gas is maintained the same as in the prototype plant. The fluidic flow control device is geometrically simulated. The proportion of water volume above and below the standpipe is kept the same as in the plant. The pressure drop in the line from the accumulator to the PHT system injection point is also simulated.

FIG. 4.3-7. Advanced accumulator of ITL.

Gravity driven water pool (GDWP)

The gravity driven cooling system (GDCS) in the AHWR is designed to provide long term core cooling for 72 hours after a reactor trip following the occurrence of LOCA. The operation of the GDCS depends solely on the system pressure. In the event of any depressurization in the PHT system, water enters the core under gravity. The system mainly consists of a water pool known as GDWP and associated piping and components.

The total inventory of GDWP is 6000 m^3 and the level of water in the pool is 5.1 m. The GDWP in the ITL is scaled down by a factor 452 which results in a volume of 13.274 m^3. Due to elevation constraints in the existing building, it is not possible to locate the GDWP at the same elevation as in the prototype. Hence, the GDWP is pressurized by nitrogen gas to compensate for the lower relative elevation in ITL. Due to space constraints, the GDWP volume in the present facility is only 5 m^3. However, the volume required as per power-to-volume scaling philosophy is 13.274 m^3. Hence, the GDWP volume is sufficient to provide long term cooling of 27.12 hours instead of 72 hours.

4.3.3.5. Isolation condenser system

In the prototype AHWR, during normal shutdown the main steam line valve to the turbine is closed and decay heat is removed in four isolation condensers. Each isolation condenser is coupled to one steam drum and each steam drum is connected to 113 channels. For simulating IC water pool a separate water tank is installed at an elevation of 44.05 m that is on the terrace of the building which houses the facility.

4.3.3.6. Break simulation system

To simulate LOCA in the event of a break in the PHT system, a break simulation system is employed. The system consists of a quick opening valve (QOV), break simulating orifice and a tank to collect the break flow (known as break flow storage tank (BF-ST). To avoid the effect of backpressure on the critical flow rate at the break location, the pipeline after the break simulating orifice is made sufficiently large. Also, the distance between the QOV and the break-simulating orifice is kept to the minimum possible value. Break is simulated for header and feeder in ITL.

4.3.4. Extent of simulation of AHWR by ITL

If Eqs. (4.3-15)–(4.3-18) are satisfied then the simulated facility will have the same temporal variation of pressure, temperature and velocity in dimensional form as in the prototype plant, whereas mass flow rate and volumetric flow rates will be simulated in non-dimensional form. Looking at those equations, it is evident that no scaled facility can preserve all the above parameters, as some distortions are inherent in the scaling methodology itself. The frictional term i.e. (ζ f) cannot be simulated for a down sized pipe. If pipe length is maintained the same in the model and in the prototype, the pipe area in the model has to be reduced by a factor of S as compared to prototype to achieve volume scaling (Vp/Vm = S). Therefore, frictional effects ((ζ f)p/(ζ f)m = S) cannot be simulated. The scale distortions due to frictional effects cannot be compensated in the model except in the cases where the local pressure losses due to orifice, valves etc. are dominant over pipe frictional losses. In cases, where pipe friction is dominant, (ζ f)p/(ζ f)m is given by

$$\frac{(\zeta_w f)_p}{(\zeta_w f)_m} = \frac{(\zeta_w)_p}{(\zeta_w)_m}\frac{(f)_p}{(f)_m} = \frac{(\zeta_w)_p}{(\zeta_w)_m}\left[\frac{(A_c)_p}{(A_c)_m}\right]^b\left[\frac{(D)_m}{(D)_p}\right]^b = \left[\frac{(A_c)_p}{(A_c)_m}\right]^b\left[\frac{(D)_p}{(D)_m}\right]^{1-b} \quad (4.3\text{-}19)$$

Where

$$f = \frac{a}{Re^b}$$

Assuming Blasius equation to be valid for friction factor f and using Eq. (4.3-17), Eq. (4.3-19) is written as

$$\frac{(\zeta_w f)_p}{(\zeta_w f)_m} = S^{0.5(1+b)} = S^{0.625} \tag{4.3-20}$$

This is not equal to S as required by Eq. (4.3-18). The surface heat losses cannot be simulated for a down sized pipe as the surface area per unit volume changes with the pipe size. In addition distortions also occur because of space constraints and nonavailability of scaled down pipe sizes commercially.

However, power to volume scaling philosophy is adopted for pressure tube type of reactor because the diameters of most of the pipes are retained the same in the model as well as in the prototype. Only down sized components are the header, downcomer and the steam drum which can cause scale distortion to some extent. Therefore, it is important to investigate the adequacy of power to volume scaling by comparing the prototype and model behaviour using the same analytical tool.

A comparison of AHWR and ITL steady state behaviour predicted using the in-house developed code, TINFLO-S [4.3-9], is shown in Fig. 4.3-8. TINFLO-S is a linear stability analysis code based on homogeneous equilibrium model. A comparison for system stability of ITL and AHWR predicted using computer code, TINFLO-S, is shown in Fig. 4.3-9. Figures 4.3-8 and 4.3-9 show that the scaled test facility, ITL, closely matches the steady state and stability behaviour of AHWR.

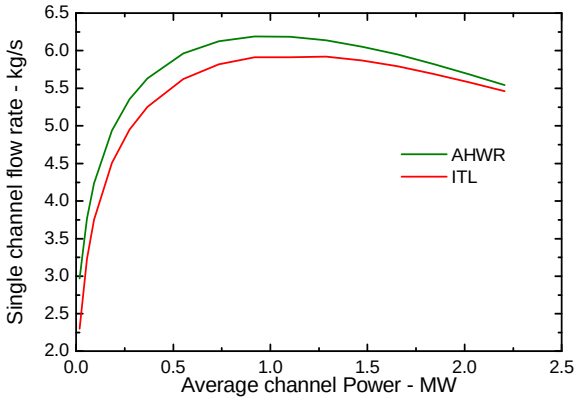

FIG. 4.3-8. Comparison of predicted steady state flowrates using TINFLO-S.

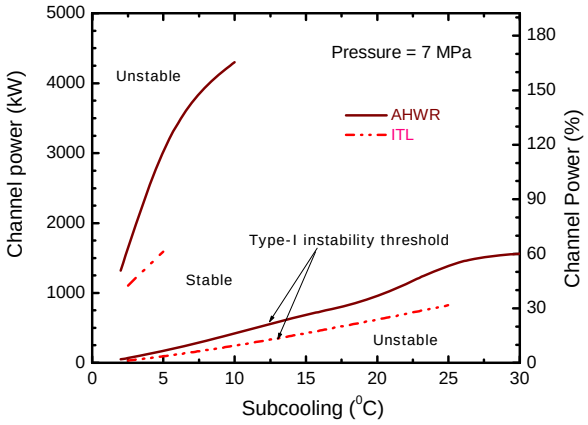

FIG. 4.3-9. Stability Map predicted by TINFLO-S for AHWR and ITL.

4.3.5. Experiments conducted in ITL

4.3.5.1. Steady state performance

Steady state experiments were conducted in ITL to study natural circulation behaviour. The Loop was operated at different pressures and channel inlet subcooling over a wide range of powers. Figures 4.3-10 and 4.3-11 show the comparison of measured and predicted steady state loop flow. A comparison of test data against some of the analytical tools is also shown. A comparison with generalized flow correlation developed by Gartia et al. [4.3-10] has also been made. Generalized correlations for steady state flow prediction in two phase natural circulation loops consider the steady state governing equations for the homogeneous equilibrium model. These equations are then solved to obtain the dimensionless flow rate as a function of a modified Grashof number and a geometric number.
Figure 4.3-12 shows a comparison of the measured and predicted flows in dimensionless form.

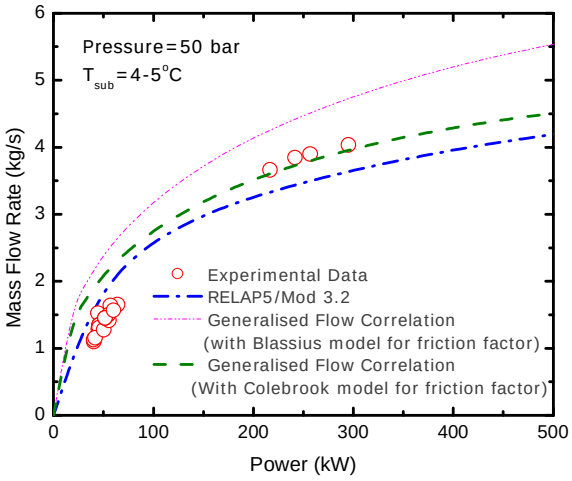

FIG. 4.3-10. Comparison of experimental steady state loop flow rate at 50 bar.

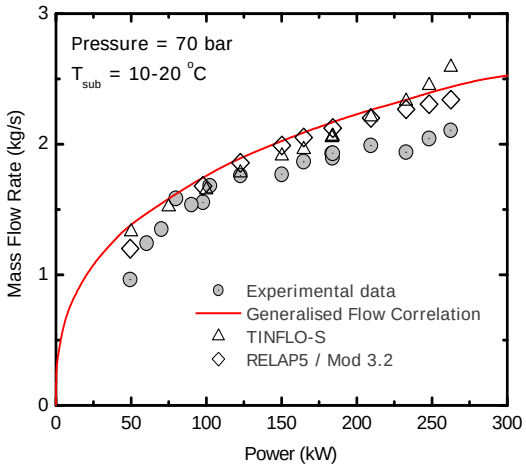

FIG. 4.3-11. Comparison of experimental steady state loop flow rate at 70 bar.

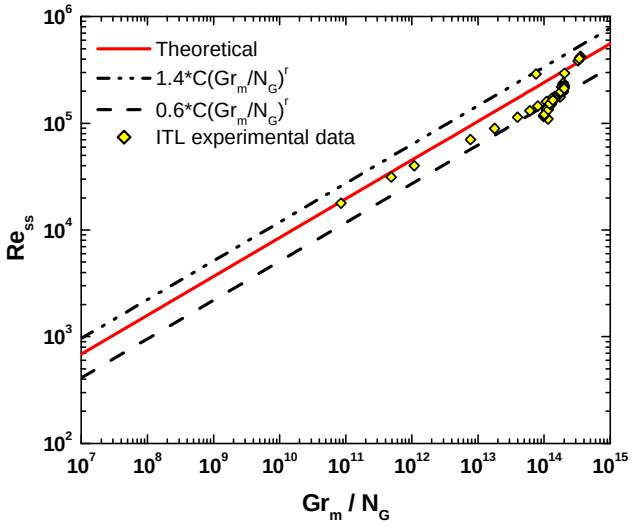

FIG. 4.3-12. Comparison of experimental and predicted flow in dimensionless form.

4.3.5.2. Startup experiments

Reactor startup is a procedure in which the pressure and temperature of the main heat transport system are raised from initial ambient conditions to nominal operating pressure and temperature. In the proposed startup procedure, the reactor is made critical at cold condition and the system is kept in single phase by external pressurization with steam until the system temperature and pressure reach 285ºC and 70 bar, respectively. During this period the system pressure is varied in such a way that cold pressurization is avoided. Also, the reactor power is maintained low enough to prevent fast and uneven structural heating, but at the same time high enough to have a reasonably fast startup. The external pressurization with steam keeps the system in single phase thereby suppressing the low pressure low power two phase instabilities. This phase of startup is termed as cold startup.

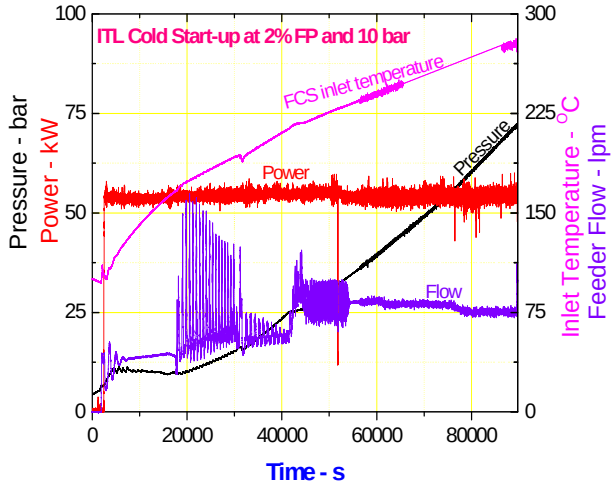

FIG. 4.3-13 (a). ITL startup at 10 bar – experimental data.

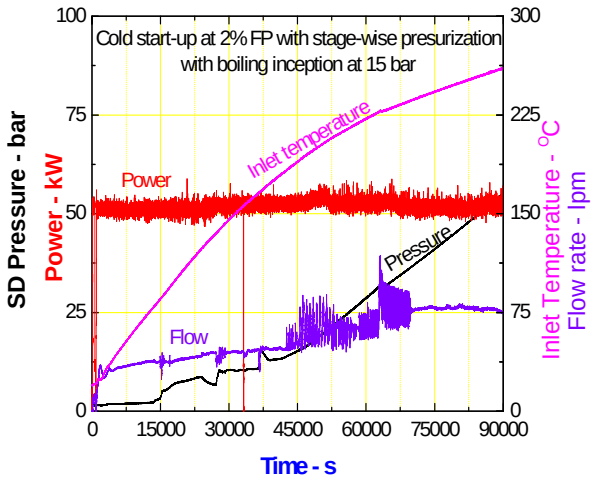

FIG. 4.3-13 (b). ITL startup at 15 bar – experimental data.

Experiments have been conducted in ITL to study the startup and stability of two phase natural circulation at low pressures. Figure 4.3-13 (a) shows the variation of thermohydraulic parameters during a typical cold startup experiment. During the test, the test section power was maintained at 2% of full power. Steam from an external boiler was supplied to maintain the system pressure at 10 bar until PHT fluid reached the saturation temperature. Initially, at the start of transient, single phase natural circulation oscillations are observed; these can be attributed to the inertia effect of flow. As system temperature reaches saturation, boiling is initiated. The boiling inception is accompanied by flow oscillations due to flashing. Effect of initial steam drum pressure is also studied during startup and it is found that external pressurization reduces the two phase oscillations at the transition to two phase natural circulation, Fig. 4.3-13 (b). The flow oscillations continue until the system pressure reaches a sufficiently high value (about 30 bar). At high pressures the oscillations are suppressed.

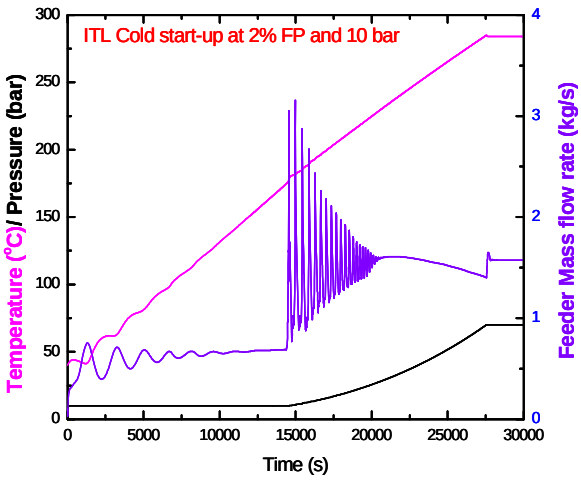

FIG. 4.3-14 (a). Simulation of ITL startup at 10 bar, using RELAP5/M3.2 without pipe heat loss.

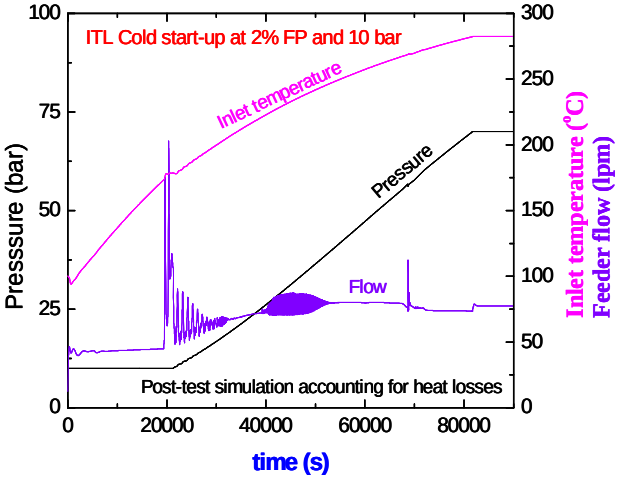

FIG. 4.3-14 (b). Simulation of ITL startup at 10 bar, using RELAP5/M3.2 with pipe heat loss.

The transient was simulated using numerical code RELAP5/MOD3.2, Fig. 4.3-14 (a). It was observed that the boiling inception takes place close to the steam drum, indicating the flashing effects that are characteristics of systems having tall risers. The results predicted by the model were fairly acceptable qualitatively. Analysis was also carried out considering the heat losses from piping, Fig. 4.3-14 (b).

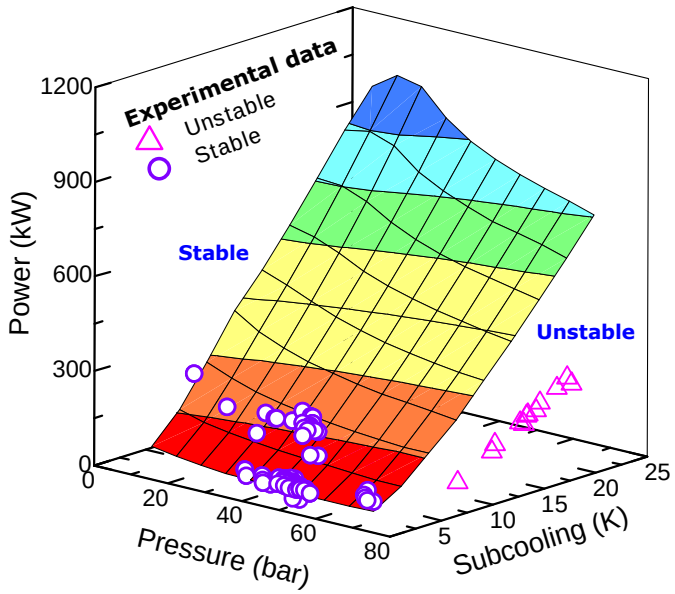

FIG. 4.3-15. Experimental data plotted on theoretically obtained stability map.

Figure 4.3-15 shows the startup data plotted on stability map. The stable and unstable points are successfully characterised by the theoretical stability map.

NOMENCLATURE

A	area (m^2)
D	diameter (m)
f	friction factor
Fr	v/(gL)1/2
g	acceleration due to gravity (m/s^2)
h	enthalpy (kJ/kg)
l	length (m)
L	characteristics length (m)
p	pressure (bar or Pa)
q	heat flux (W/m^2)
Q	volume flow rate (m^3/s)
S	scale ratio
t	time (s)
v	velocity (m/s)
V	volume (m^3)
W	mass flow rate (kg/s)
Z	elevation (m)

Greek symbols

ρ	density (kg/m^3)
ζ	perimeter (m)
ϕ	power factor
τ	shear stress (Pa)

Subscripts

c	cross section
h	heated
M	model
0	reference value
p	prototype
s	surface
W	wetted

Superscripts

+	non-dimensional

REFERENCES FOR SECTION 4.3

[4.3-1] SINHA, R.K., KAKODKAR, A., Advanced heavy water reactor, INS NEWS **15** 2–4 (2002), **16** 1 (2003).

[4.3-2] INTERNATIONAL ATOMIC ENERGY AGENCY, Passive Safety Systems and Natural Circulation in Water Cooled Nuclear Power Plants, IAEA-TECDOC-1624, IAEA, Vienna (2009) Annex III.

[4.3-3] ISHII, M., et al., "Scientific design of Purdue University Multi-Dimensional Integral Test Assembly (PUMA) for GE SBWR", NUREG/CR-6309, PU-NE 94/1 (1996).

[4.3-4] LOOMIS, G.G., SODA, K., "Results of the semiscale Mod-2A natural circulation experiments", NUREG/CR-2335 (1982).
[4.3-5] Multi-Loop Integral Test Facility (MIST) Specifications, NRC-04-83-168 (1983).
[4.3-6] D'AURIA, F., et al., Scaling of natural circulation in PWR systems, Nuclear Engineering and Design **132** (1991) 187–205.
[4.3-7] ZUBER, N., "Problems in modeling small break LOCA", NUREG-0724 (1980).
[4.3-8] RAO, G.S.S.P., et al., "Experimental and theoretical investigations in a two phase natural circulation loop", ISME-2003, XIII National Conference of Indian Society of Mechanical Engineers, December 30-31, 2003, IIT Roorkee (2003).
[4.3-9] NAYAK, A.K., et al., Linear analysis of thermodynamic instabilities of the advanced heavy water reactor (AHWR), J. Nucl. Sci. Tech. **35** (1998) 768–778.
[4.3-10] GARTIA, M.R., VIJAYAN, P.K., PILKHWAL, D.S., A generalized flow correlation for two phase natural circulation loops, Nuclear Engineering and Design **236** (2006) 1800–1809.

4.4. SUMMARY ON NATURAL CIRCULATION PHENOMENA OBSERVED IN ROSA-AP600 TESTS

Thermohydraulic integral experiments were conducted jointly by the Japan Atomic Energy Research Institute and the US NRC in support of the NRC review of the Westinghouse AP600 design. Experiments were conducted for various break location/size and different levels of assumed components failure using the Large Scale Test Facility (LSTF). The test results showed that the AP600 passive safety components performed satisfactorily in maintaining adequate core cooling and decay heat removal even for the cases including component failure.

The passive residual heat removal (PRHR) system and the core make-up tanks (CMTs) are the passive components unique to the AP600 design. The PRHR consists of a C-shaped heat exchanger tube bundle submerged in the in-containment refueling water storage tank (IRWST). The IRWST water inventory is of the same temperature as the containment atmosphere during normal operation of the reactor. Because of the relatively large height of the bundle and the large temperature difference across the heat exchanger tubes, high-Grashof-number natural convection would occur along the tube outer surfaces. The CMTs provide borated cold water supply, driven by gravity, to the core. Once it starts draining, the CMT liquid level signal is used to trip the actuation of ADS. Therefore, understanding the thermohydraulic behaviour in the CMT, including its interaction with other passive safety system, is essential for the safety analysis of the AP600 design.

This Section describes the test results focusing on the PRHR response and CMT behaviour. The PRHR heat transfer performance was numerically analysed by applying existing correlations to the PRHR tube bundle in the IRWST. The CMT behaviour can be divided into two phases: firstly, natural circulation phase and secondly the drain phase. Interactions between the CMT and the other safety components are also observed. The discharge rate is decreased by accumulator injection and is increased by the ADS actuation. When the pressure balance line (PBL) becomes empty, the CMT flow rate can be estimated by the free gravitational drain model.

4.4.1. Facility description

The LSTF was originally built as a 1/48 volumetrically scaled, full-height, full-pressure model of a Westinghouse-type four loop [3423 MWth] PWR of the current generation. The facility was modified by installing volumetrically scaled (1/30.5) AP600 passive safety components including two CMTs, a PRHR, a four-stage ADS, and an IRWST (see Fig. 4.4-1) [4.4-1]. The relative elevations of these components were preserved as closely as possible.

The simulated CMTs have a cylindrical configuration with hemispherical top and bottom heads. The bottom head is connected to the downcomer through a direct vessel injection (DVI) line, and the top head to the cold leg through a PBL. The tank is initially filled with water of ambient temperature

(typically 300 K) at the same pressure as the primary. The discharge line includes an isolation valve and a check valve. The isolation valve is tripped open in emergency situations. The check valve prevents reverse flow from the downcomer to the CMT.

The PRHR was constructed using approximately full-size heat exchanger tubes (19 mm outer diameter and 1.6 mm thickness) arranged in a 7 × 7 square array and built in a "C" shaped configuration as shown in Fig. 4.4-2. The number of the tubes was scaled based on the conservation of the power to volume ratio. The inlet plenum, located at the top of the C-section, is connected to the hot leg of the loop with a pressurizer. The outlet plenum, located at the bottom of the C-section, is connected to the cold leg near the outlet of the steam generator (SG). The IRWST is modeled by a cylindrical tank whose top is open to atmosphere. The tank internal space is divided into two regions by a separation plate (see Fig. 4.4-2), which extends the entire height of the tank. The PRHR heat exchanger tubes are located in one of these two regions and the ADS sparger in the other. Such a separation plate in the IRWST does not exist in the AP600 design, but was installed in the LSTF to avoid atypical interactions between the PRHR heat exchanger tubes and the ADS sparger caused by the much smaller distance between these components than in the full-size plant. The separation plate, however, may affect natural circulation flow which would take place around the heat exchanger tubes when the PRHR is put into operation. The effects of this atypical geometry on the heat transfer behaviour was evaluated numerically and is summarized in one of the later subsections.

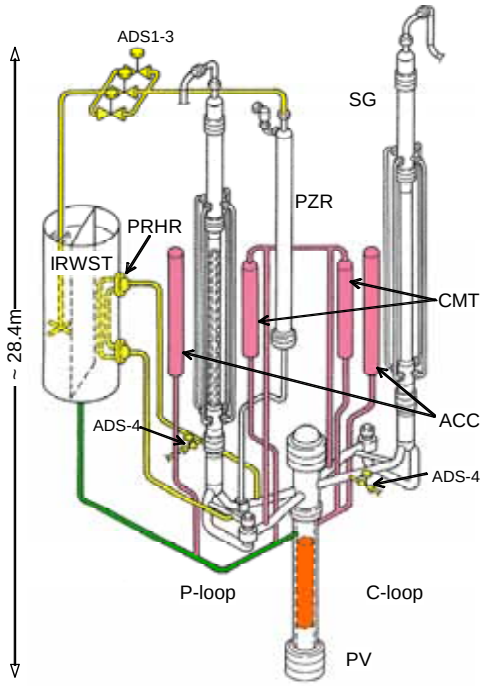

FIG. 4.4-1. The ROSA-V/LSTF modified for ROSA-AP600 project; PV stands for pressure vessel and PZR for pressurizer.

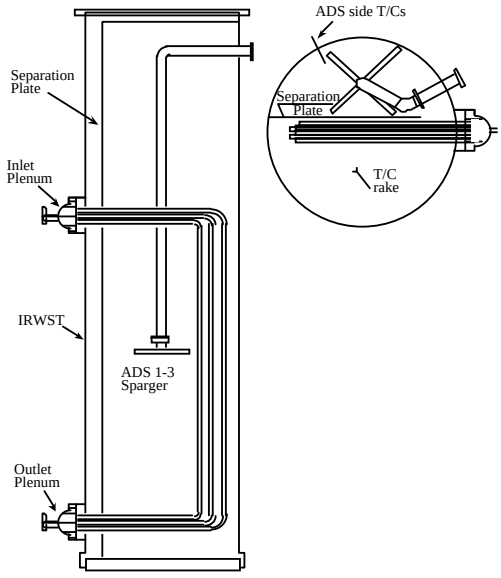

FIG. 4.4-2. The PRHR tube bundle and ADS sparger in the IRWST.

4.4.2. Experimental conditions

The conditions for ROSA-AP600 experiments are summarized in Table 4.4-1. The tests simulated various scenarios including: loss of coolant accidents (LOCAs) with a break in the cold leg, the PBL, the SG tubes, and the DVI lines; a main steam line break followed by SG tube ruptures; an inadvertent actuation of ADS; and a station blackout. The break size ranged from 1/2 to 2 inch. The break

orientation for the cold leg break and the ADS failure modes were also varied. The tests were initiated from a primary pressure of 15.5 MPa, a secondary pressure of 6.0 MPa, and hot- and cold-leg temperatures of 590 K and 550 K, respectively. The initial core flow rate was set at 16% of the scaled AP600 flow rate to obtain prototypical temperature distribution in the primary with a maximum available core power (10 MW) which was 16% of the scaled rated power.

The two CMTs were connected either with a common PBL to the same cold leg (C-loop cold leg), or with separate PBLs to the individual cold legs, depending on the type of experiment, as shown in Fig. 4.4-3. The separate-PBL configuration was used for the cases where the break directly affected the performance of one CMT, i.e., for the PBL breaks (Tests PB1 and PB2) and the double-ended guillotine break of the DVI line (Test DV1). Both CMTs were used in all the tests except for Test PB2 where the CMT connected to the intact PBL was assumed to fail.

This experiment also focuses on the PRHR behaviour found during studies of the 1-inch SBLOCA data (CL3 and CL7). However, work was also done to evaluate the PRHR behaviour when it was used for extended transients, for example during the 1/2-inch SBLOCA and the station blackout transients (CL4 and SB1 respectively). The number of the PRHR heat exchanger tubes was 45 for Tests CL3 and CL4, and 21 for CL7 and SB1.

TABLE 4.4-1. ROSA-AP600 TESTS CONDITIONS

Run ID	Test Conditions
SB1	Station Blackout
CL4	0.5-in. cold-leg break
CL3	1-in. cold-leg break
CL6	1-in. cold-leg break (top oriented break)
CL7	1-in. cold-leg break with 25% ADS-4
CL5	1-in. cold-leg break without ADS-1 to 3 actuation
PB2	1-in. PBL break (no actuation for one CMT connected to intact PBL)
SG1	U-tube rupture
DV1	DVI double-ended break
CL8	2-in. cold leg break
PB1	2-in. PBL break
AD1	Inadvertent actuation of ADS
SG2	100% MSLB with U-tube rupture

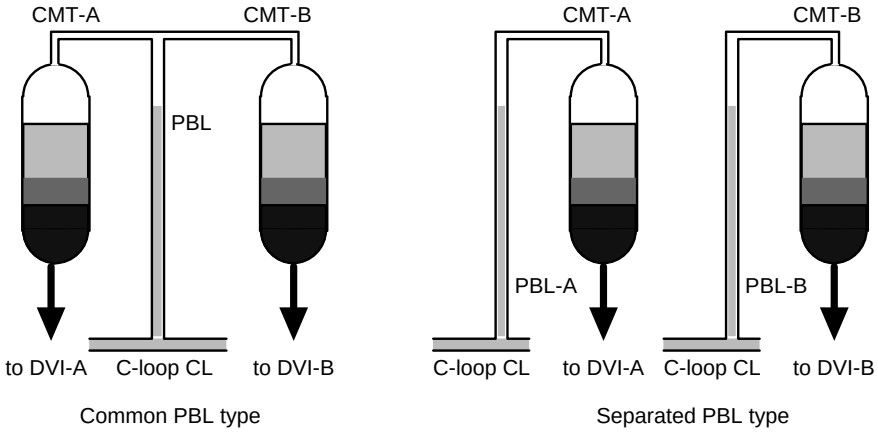

FIG. 4.4-3. Two CMT configurations.

4.4.3. Experimental results

4.4.3.1. Typical system pressure responses

The system pressure responses during the 1-inch cold leg break test CL3 (base case test) are shown in Fig. 4.4-4. The PRHR was actuated at 159 s after break. This was done by opening the return line valve after the low-pressurizer-pressure set point was reached. Immediately, natural circulation started through the PRHR and continued until it was interrupted at ~3600 s by the ingress of non-condensable gas into the heat exchanger tubes which occurred after the ADS opened.

The primary system pressure decreased continuously even after it became lower than the secondary side pressure as shown in Fig. 4.4-4. This continuous depressurization was caused by steam condensation on the steam–water interface which formed in the vessel upper plenum as a result of flashing of the upper vessel inventory. The PRHR operation replaced the warm liquid beneath the interface with cooler liquid while it preserved the interface in an undisturbed state. Meanwhile, there was no steam condensation in the PRHR itself until the ADS opened. Except during a short time period immediately after ADS actuation, the flow into the PRHR was single phase liquid.

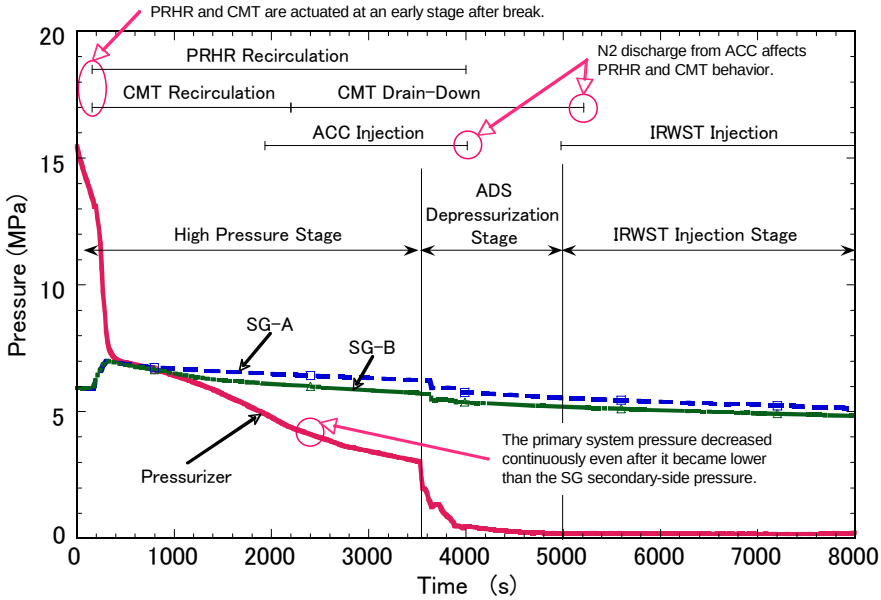

FIG. 4.4-4. System pressure response (CL3, base case test): the P-loop and the C-loop are the loops with and without pressurizer, respectively. Break is located at the cold leg of C-loop.

4.4.3.2. PRHR response

4.4.3.2.1. Heat removal by natural circulation

The PRHR heat removal rate became greater than the core decay power soon after the actuation of the PRHR, and remained so until the PRHR flow was terminated, as shown in Fig. 4.4-5. The heat transfer rates were higher for the half-inch break test (CL4) than for the 1-inch break tests (CL3 and CL7). This difference occurred because the PRHR inlet temperature was higher for Test CL4 due mainly to a delayed core power trip. The CL4 core scram was delayed after the pump trip by about 740 s because the control logic did not include any power trip logic linked to either the pump trip or low loop flow. Trip logic was modified for both the ROSA-AP600 experiments and the AP600 facility thereafter (the core was also tripped on low pressurizer level).

The total heat removal rate for Test CL7 was only 10 to 20% less than that for Test CL3, as shown in Fig. 4.4-5, even though the number of heat exchanger tubes was reduced from 45 to 21 between Tests CL3 and CL7. This result is obtained because the flow rate $\dot{m}$ due to natural circulation varies with the sum of loss coefficients divided by their cross-section areas squared - all raised to the 1/3-power, as explained by Zvirin [4.4-2]:

$$\dot{m} = \left[\frac{2\beta g Q L_H}{\rho C_p \sum_i \frac{K_i}{a_i^2}} \right]^{1/3} \qquad (4.4\text{-}1)$$

Hence, increasing the flow resistance of the PRHR heat exchanger loop by more than a factor of four increases the total flow resistance of the loop by only approximately 30%, and decreases the flow rate by only approximately 10%. At the same time, increased heat transfer due to the increased velocity in the tubes (primary side convection coefficient varies with velocity to the 0.8 power in the Dittus-Boelter correlation) and increased wall superheat (boiling heat flux varies with wall superheat between approximately the third and fourth power) nearly makes up for the reduction in heat transfer area when going from 45 to 21 heat exchanger tubes.

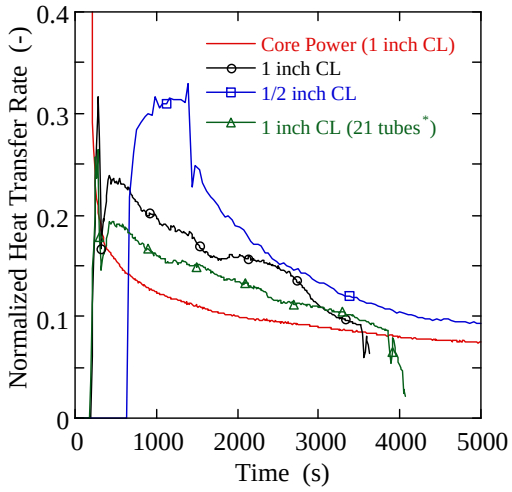

FIG. 4.4-5. Normalized heat transfer rate at PRHR; heat transfer rate is normalized by the initial core power.

4.4.3.2.2. Thermal stratification

The PRHR return flow temperature (~330 K) was close to the water temperature in the bottom of the IRWST. This cold return flow caused thermal stratification to occur in the cold leg of the P-loop (the loop to which the PRHR was connected) after natural circulation through the SG stopped due to boiling in the U-tubes caused by reverse heat transfer from the secondary side. Temperature differences up to about 200 K were observed between the top and the bottom of this leg. Thermal stratification was also observed in the pressure vessel due to the PRHR return flow and also the flow from the CMTs and the accumulators through the DVI line nozzles. Because of these cold liquid flows into the vessel, the fluid in the core region was kept subcooled until the ADS actuation as shown in Fig. 4.4-6. Because natural circulation through the SGs stopped soon after break, the flow in the core was driven mainly by natural circulation through the PRHR, although CMT recirculation also contributed.

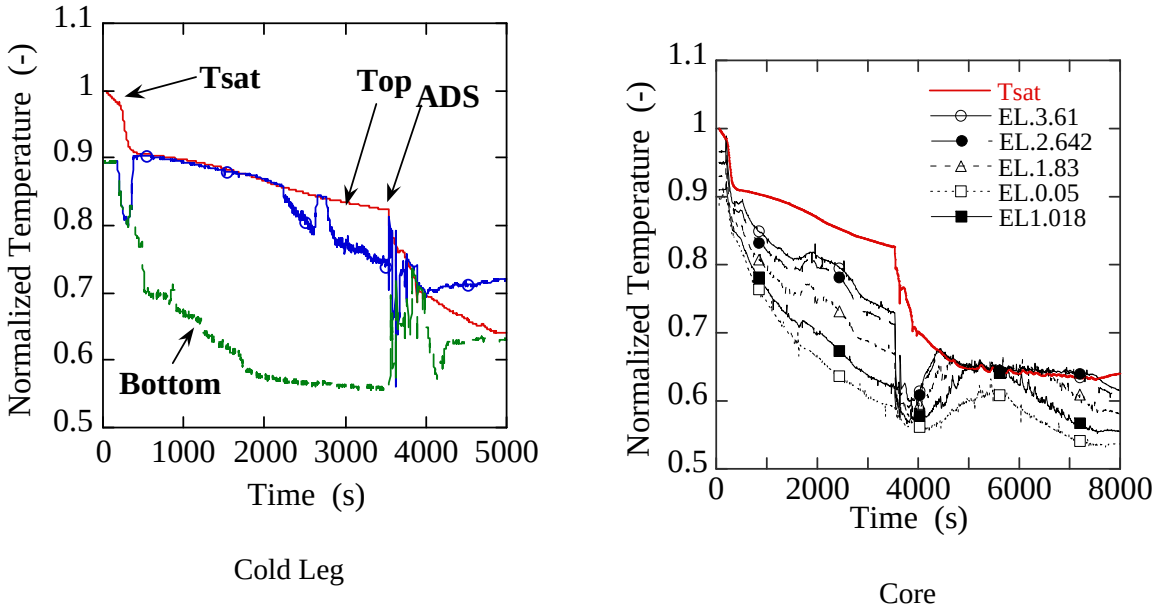

FIG. 4.4-6. Normalized fluid temperature in the cold-leg and core for test CL3.

4.4.3.2.3. Heat transfer analysis

The PRHR heat transfer analyses was simulated numerically by calculating the heat transfer on the inner and outer surface of the tube, the thermal conduction through the tube wall, and the thermal decay in the tube internal flow caused by the heat transfer to the IRWST. The heat exchanger tubes were lumped into a single model tube. That is, uniform distributions of flow and heat transfer among the heat exchanger tubes were assumed. The calculation was run for the boundary conditions obtained from the experimental data. The measured values of the return line mass flow rate, the inlet plenum pressure and temperature, and the IRWST fluid temperatures were used. The IRWST temperatures were given in terms of linear functions that interpolated the fluid temperatures measured near the center tube.

Several correlations were employed to predict the heat transfer coefficients (HTC) on the tube outer and inner surfaces. Since the details of HTC package used for calculation were described in the literature [4.4-9], the outline is briefly mentioned here. Firstly for the inner surface HTC, the Reynolds numbers of the tube internal flow were in the fully turbulent range (Re > 6000) according to the measured flow rates and fluid temperature. The heat transfer on the inner surface was therefore calculated by using the Colburn correlation [4.4-4] for turbulent forced convection flow:

$$h_{in} = 0.023 \frac{k}{d} \mathrm{Re}^{0.8}\, \mathrm{Pr}^{1/3} \tag{4.4-2}$$

The fluid properties were evaluated for the film temperature. Secondly for the outer surface HTC, the possible heat transfer modes on the tube outer surface were natural convection and nucleate boiling. The boiling onset temperature on the tube outer surface was predicted by using the Bergles-Rohsenow correlation [4.4-5]

$$T_{onset} = T_{sat} + 0.556 \left(\frac{556.3q}{P^{1.156}} \right)^{0.3538 P^{0.0234}} \tag{4.4-3}$$

The nucleation boiling heat transfer coefficient was predicted by using the Jens-Lottes correlation [4.4-6]

$$h_{out} = \Delta T_w^3 \left[1.22 e^{1.619 \times 10^{-7} P} \right]^4 \tag{4.4-4}$$

Finally for the natural convection HTC for single phase flow around the HX tube, the correlation of Lagmuir [4.4-7] and of Churchill-Chu [4.4-8] were used along the horizontal and the vertical part section of the tubes, respectively. The actual heat transfer rate on the outer surface was calculated by interpolating the boiling and convection heat transfer rates using Rohsenow's scheme [4.4-5]

$$q = q_c \left[1 + \left\{ \frac{q_n}{q_c} \left(1 - \frac{q_i}{q_c} \right) \right\}^2 \right]^{1/2} \tag{4.4-5}$$

where q is the heat flux. The subscripts c, n, and i denote convection, nucleate boiling, and the initiation of boiling, respectively. The heat flux q_i is obtained by multiplying the wall superheat for the boiling onset by the heat transfer coefficient calculated from the natural convection heat transfer correlation. The uncertainty in the estimated value of the HTC was also evaluated using the measurement uncertainties for the temperature (±3 K) and for the flow rate (±0.0057kg/s or 5% of full range).

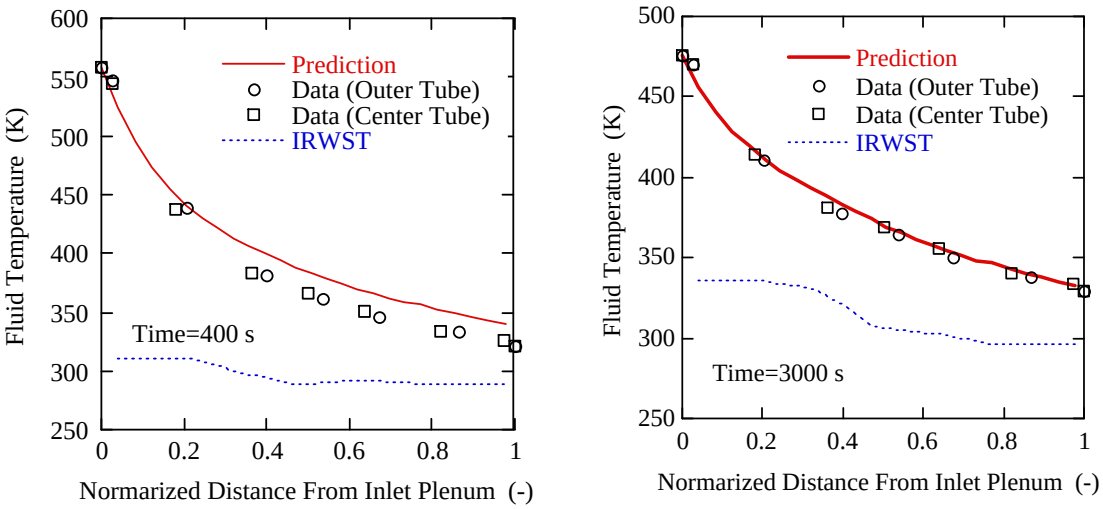

FIG. 4.4-7. Comparison of PRHR fluid temperature at 400 and 3000 s for CL3.

Figure 4.4-7 shows the comparisons of the predicted and measured fluid temperatures inside the heat exchanger tube at 400 s and 3000 s in Test CL3. The heat transfer mode on the tube outer surface was predicted to be subcooled boiling for the upper horizontal section and natural convection for the rest. The Grashof number along the vertical section ranged from $8x10^{11}$ to $2x10^{13}$. This range appears to be beyond most of the existing data bases available for natural circulation heat transfer. The data shown in this figure suggest that the heat transfer rates along the tube were generally well-predicted, although the fluid temperatures were slightly overpredicted indicating that the heat transfer rates were underpredicted. The total heat transfer rate of the PRHR was underpredicted by ~5% as shown in Fig.4.4-8.

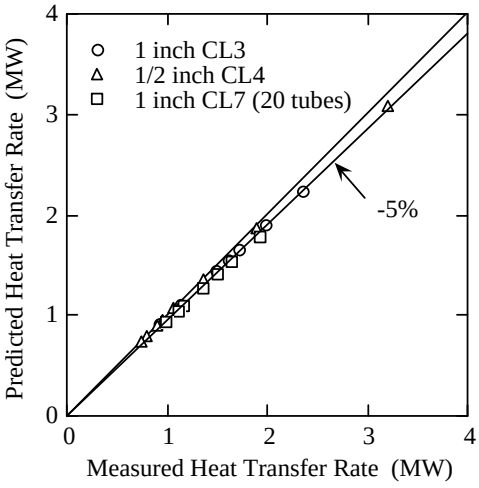

FIG. 4.4-8: Comparison of PRHR total heat transfer rates for tests.

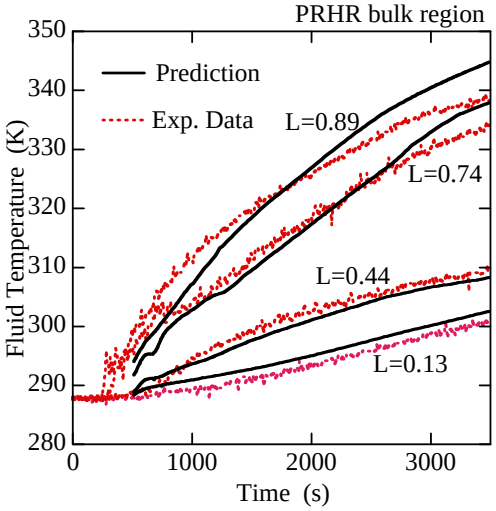

FIG. 4.4-9. Comparison of the IRWST fluid temperatures as a function of time for test CL3. L = Elevation / Initial Liquid Level.

The fluid temperature in the upper horizontal region, where nucleate boiling was calculated, was predicted well as shown in Fig. 4.4-7. The thermal resistance for this region was dominated by the convection inside the tube and the thermal conduction across the tube. The calculated fluid temperature decay was not greatly affected by the uncertainties in the predicted boiling heat transfer correlations. The data shown in Fig. 4.4-7, on the other hand, suggest underpredictions of the heat transfer rate in the vertical section. The outer tube, which was located in the peripheral region of the vertical bundle, had better cooling than the center tube which was located in the middle of the bundle.

4.4.3.2.4. IRWST natural circulation analysis

A numerical analysis of the three dimensional natural circulation flow in the IRWST was conducted using the FLUENT [4.4-3] code to gain insight into the effects of the atypical IRWST configuration (in particular the presence of the separation plate) used in the tests. The FLUENT code uses a $k-\varepsilon$ turbulence model. The IRWST was modeled using 23x20x34 control volumes. The tube bundle was represented as a porous medium. The bundle-to-liquid heat transfer rates estimated from the experimental data were imposed on the porous medium as a boundary condition.

The 1-inch cold leg break test (CL3) was analysed. The code, however, had difficulties calculating the energy balance in the IRWST for the first 500s after actuation of the PRHR for the aforementioned input model and the boundary conditions. To cope with this problem, the calculation was reinitialized at 500s. This was done by calculating a steady state temperature distribution in the IRWST that satisfies the energy balance at 500s with the velocity distribution fixed to that obtained at the end of the initial 0- and 500-s transient calculations. The calculation was then restarted from 500s and continued to 3500s. From several sensitivity calculations, the effects of the initial temperature and

velocity distributions disappear in 200s after the re-initiation of the transient calculations. Figure 4.4-9 compares the predicted and measured fluid temperatures versus time at four elevations in the PRHR side of the IRWST. The calculated temperatures agree with the experimental data within ~5K.

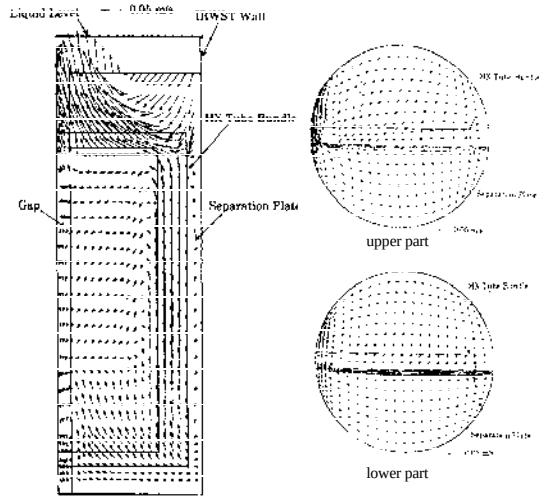

FIG. 4.4-10. Calculated IRWST velocity distribution in vertical and horizontal cross-section.

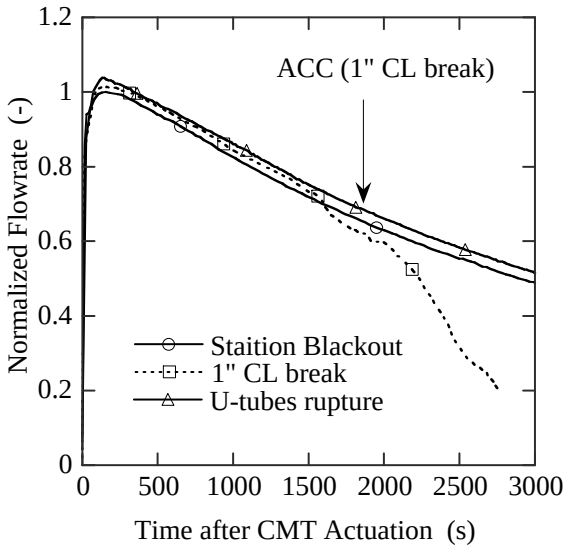

FIG. 4.4-11: CMT-A discharge line flow rates during NC phase for test SB1, CL6, SG1. The data are normalized with the maximum flow rate of SB1.

The calculated flow distribution at t = 1500s in the vertical cross-section of the tube bundle is shown in Fig. 4.4-10. The flow distributions at the elevations of the upper and lower horizontal sections of the bundle are also shown in this figure. The maximum flow velocity in the tank was calculated to be ~0.1 m/s, and the typical velocity was of the order of 0.01 m/s. Generally, the horizontal velocities were much smaller than the vertical ones. These numerical results are helpful to discuss the effect of the atypical IRWST geometry in the LSTF, due to the presence of a separation plate, on the flow and temperature distributions around the PRHR HX tubes. The most obvious effect of the separation plate was the presence of a horizontal flow across the inlet portion of the HX upper horizontal section as shown in the horizontal cross-sectional view in Fig. 4.4-10. This flow was caused by the fluid circulation through the gap between the separation plate and the inner wall from the ADS-sparger side toward the PRHR side of the IRWST. The cross flow velocities, however, were less than ~0.1 m/s and were not high to cause significant effects on the boiling heat transfer along this part of the HX.

Along the vertical section of the HX, the horizontal components of the fluid flow was generally much smaller than the vertical upward components. It is therefore unlikely that the proximity of the separation plate to the heat exchanger bundle greatly affected the natural convection heat transfer in this region. The lower horizontal section of the heat exchanger, on the other hand, contributed little to the total heat transfer through the PRHR. Atypical flow effect on this portion of the heat exchanger, if it exists, is not therefore of concern for the experimental simulation of the PRHR performance in the LSTF.

4.4.3.3. CMT response

The transient response of the CMTs can be described in terms of two distinct time intervals, i.e., a natural circulation phase and a drain phase. The former was characterized by single phase (liquid) natural circulation in each CMT loop. The circulation was established immediately after the opening of the discharge valve in the discharge line, and ended when either flashing occurred in the CMT

warm-water layer or the PBL inlet in the cold leg uncovered. The CMT then started to drain. The behaviour of the two CMTs was nearly the same except for Tests PB1 and DV1 where the break flow directly affected one of the CMTs.

4.4.3.3.1. Natural circulation phase

Figure 4.4-11 compares the natural circulation flow rates for tests with 1 inch break or less (CL6, SG1 and SB01) as a function of elapsed time after the initiation of natural circulation in each test. The flow rates were almost the same among the three tests, despite the difference in break diameter, until 2100 s when the accumulator injection initiated for test CL6. The accumulator flow into the DVI line increased the frictional pressure drop in the CMT loop, causing the CMT flow rate to decrease.

For tests with break diameter of 1 inch or less, the natural circulation flow through the PBL stopped when the CMT top head started to flash, or when equilibrium was reached between the temperatures in the PBL and CMTs. The former was the case for the small break LOCA experiments, and the latter was the case for tests SB1 and SG1. For SB1, the natural circulation ceased at ~12000 s. For SG1, the C-loop cold leg cooled rapidly due to the depressurization of the affected SG, and thus the temperature difference between the PBL and CMTs decreased.

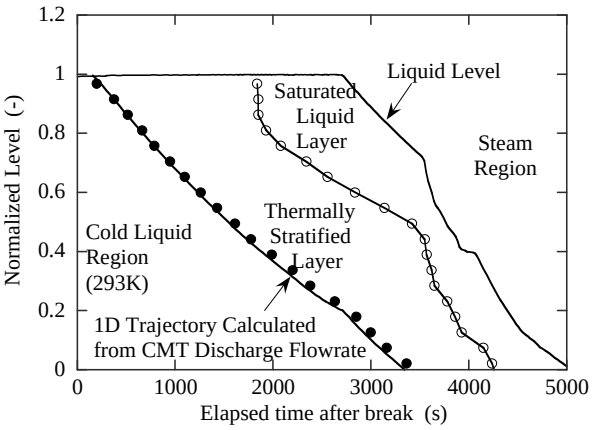

FIG. 4.4-12. Thermal stratification behaviour in CMT-A for test CL3.

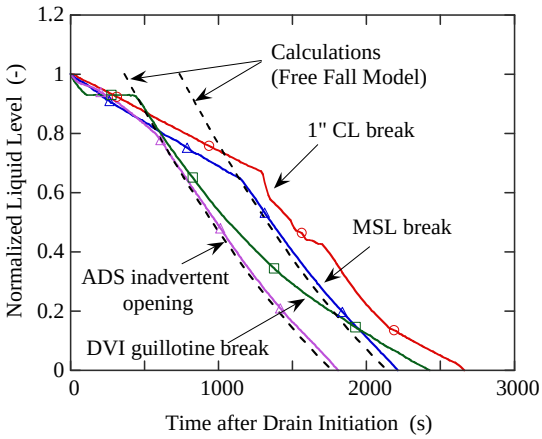

FIG. 4.4-13. Comparison of liquid levels measured for tests DV1, AD1, CL6, and SG2 and calculations.

During the single phase natural circulation period, the hot water from the cold leg accumulated in the upper part of the CMT by replacing the initial cold water inventory. This resulted in a clear thermal stratification as shown in Fig. 4.4-12 for test CL3. The bottom edge of stratification, as given by the measured temperature distribution, agreed with the one dimensional fluid trajectory that was calculated from the measured CMT discharge flow rate. Agreement between the two indicates axial conduction and diffusion in the CMT were insignificant. The radial temperature difference in the liquid, between the tank centerline and the mid-radius measurements, was visible only when the PBL flow became colder than the fluid in the CMT top head.

The thickness of the saturated liquid layer and that of the entire thermally-stratified layer had grown to ~2.2 and ~4.4 m, respectively, by the time of drain initiation in test CL6. Since the AD1 test had a much shorter natural circulation period than CL6, its saturated and warm stratified layers were less than 0.2 m (or even less than the measurable distance) and ~0.5 m thick, respectively. The temperature

of water coming through the PBL decreased continuously, because the cold legs cooled down due to the cold flow from the PRHR, CMTs and accumulators into the downcomer. For the break diameter less than 1 in., the duration of the natural circulation phase was so long that the PBL flow eventually became colder than the hottest water in the top of the CMTs. For these tests, the CMTs started flashing before the cold leg (and PBL) reached saturation.

4.4.3.3.2. Drain phase

The CMT drains were governed by one of two different mechanisms: flashing in the CMT (Mode I) for break diameter of 1 in. or less, and convection of gaseous flow to the CMT from the cold leg (Mode II) for break diameters greater than 2 inches. Each mode may be further broken down according to the magnitude of flashing for Mode I and the composition of the PBL flow (pure steam, or steam-nitrogen mixture) for Mode II. Interactions between the CMT and the other safety components were observed: the CMT discharge rate was decreased by the accumulator injection, and was increased by the actuation of the ADS. Refer to the literature by Yonomoto et al. [4.4-10] for details of these modes including the discussion for the effect of non-condensable gas, ADS failure and break location on the CMT behaviour.

The intensive flashing-induced drain (Mode I) and the cold leg voiding-induced drain (Mode II) involve two phase flow phenomena in the PBL and the cold leg. However, the measured level decrease rates in these modes were roughly the same irrespective of various differences in flow conditions. This may imply that the drain rates in these modes were only little affected by the dynamic pressure drop in the PBL and the cold leg. Also, for the breaks located in the cold leg or PBL, the measured downcomer level was close to the cold leg elevation for most of the transient. If the frictional pressure drop in the PBL can be neglected, the CMT level drop is simply represented by a free gravitational drain of a tank. Assuming that the liquid density can be represented by a constant value and that the downcomer liquid level can be represented by the cold leg elevation, we obtain

$$H = H_0 - \frac{1}{A}\left(\frac{H_0}{R}t\right)^{1/2} + \frac{t^2}{4RA^2} \tag{4.4-6}$$

R is the flow resistance in the CMT discharge line

$$R = \frac{\rho \Delta P}{g\dot{m}^2} \tag{4.4-7}$$

where $\dot{m}$ is the mass flow rate through the CMT discharge line.

The level change calculated with this equation is compared in Fig. 4.4-13 with Tests CL6, SG1, DV1 and AD1 results. The agreement is excellent for Tests AD1 and SG1 for the time periods after the CMT flow became unaffected by the ACC flow. For Tests DV1 and CL6, the measured level change rates were smaller than the calculated rates especially when the liquid level fell into the lower part of the tank. This was probably caused by depressurization in the gaseous space of the CMT due to condensation on the wall in the lower part of the tank, where the wall temperature was relatively low when it was exposed to the gas phase. This depressurization caused increase of the steam flow into the CMT and thus, increase of the frictional pressure loss along the PBL, which was detected by the DP measurement. The wall condensation was probably suppressed by the existence of nitrogen gas for tests AD1 and SG1.

4.4.4. Summary

The response of PRHR and CMT in ROSA-AP600 experiments were summarized and roughly discussed in this section. The summary obtained from the present study are as follows:

- The energy removal by the PRHR exceeded the core decay power soon after the actuation of the PRHR. This caused the pressures and temperatures in the primary side to decrease continuously. Furthermore, the core fluid was kept subcooled for the tests with the break diameter smaller than one inch until the ADS was actuated.
- The total heat transfer rate in the PRHR was predicted within 5% using heat transfer correlations available in the literature, although the correlations were applied beyond the range of the Grashof number or the heat exchanger geometry for which the correlations were developed.
- Single phase (liquid) natural circulation established in a loop formed by the CMT, the DVI line, a part of the vessel downcomer, a part of the cold leg and the PBL, immediately after the opening of the isolation valve in the CMT discharge line.
- The drain rates were predicted well by taking into account only the liquid head in the CMT and flow resistance in the discharge line, indicating no adverse effects of condensation on draining.

NOMENCLATURE

A: CMT tank flow area
a_i: Cross-sectional area of component i
C_p: Specific heat at constant pressure
g: Acceleration due to gravity
h: Heat transfer coefficient
H: CMT liquid level above the cold leg elevation
H_0: Initial CMT liquid at t = 0
k: Fluid thermal conductivity
K_i: Loss coefficient of component i (based on flow area)
L_H: Vertical distance between the thermal centers of the core and heat exchanger
$\dot{m}$: Mass flow rate
P: Pressure
Pr: Prandtl number
q: Heat flux
Q: Core power
R: Flow resistance in the CMT discharge line
Re: Reynolds number
T_{sat}: saturation temperature

Greek symbols

ΔP: Pressure drop
ΔT_w: Wall superheat
β: Thermal expansion coefficient
ρ: Liquid density

REFERENCES FOR SECTION 4.4

[4.4-1] KUKITA, Y., et al., ROSA/AP600 testing: facility modifications and initial test results, J. Nucl. Sci. Technol. **33** (1996) 259–265.

[4.4-2] ZVIRIN, T., Experimental and analytical investigation of a PWR natural circulation loop, EPRI-NP-1364-SR (1980).

[4.4-3] FLUENT User's Guide, Version 4.3 (1995).

[4.4-4] ROHSENOW, W.M., HARTNETT, J.P., Handbook of Heat Transfer, 7-32, McGraw-Hill Book Co. (1973).

[4.4-5] BERGLES, A.E., ROHSENOW, W.M., The determination of forced convection surface boiling heat transfer, J. Heat Transfer **86C** (1964) 365.

[4.4-6] JENS, W.H., LOTTES, P.A., Analysis of heat transfer burnout, pressure drop and density data for high pressure water, ANL-4672 (1951).

[4.4-7] LANGMUIR, I., Convection and conduction of heat in gases, Phys. Rev. Series I **34** (1912) 401.

[4.4-8] CURCHILL, S.W., CHU, H.H.S., Correlating equation for laminar and turbulent free convection from a vertical plates. Int. J. Heat Mass Transfer **18** 1323 (1975).

[4.4-9] YONOMOTO, T., KUKITA, Y., SCHULTZ, R.R., Heat transfer analysis of the passive residual heat removal system in ROSA/AP600 experiments, Nucl. Technol. **124** (1998) 18–30.

[4.4-10] YONOMOTO, T., et al., Core makeup tank behaviour observed during the ROSA-AP600 experiments, Nucl. Technol. **119** (1997) 112–122.

4.5. TESTING OF THE MULTI-APPLICATION SMALL LIGHT WATER REACTOR (MASLWR) PASSIVE SAFETY SYSTEMS

Experimental thermohydraulic research has been conducted at Oregon State University (OSU) for the purpose of assessing the performance of a new reactor design concept, the Multi-application Small Light Water Reactor (MASLWR). As currently conceived, the MASLWR design is a pressurized light water reactor relying on natural circulation during both steady state and transient operation.

MASLWR's Nuclear Steam Supply System (NSSS) is contained within the reactor vessel and the core flow is driven by natural circulation. The steam generators are located in the upper region of the vessel outside of the hot leg chimney and consist of banks of vertical, helical tubes. MASLWR's safety systems are designed to operate passively. There are no emergency cooling pumps and offsite power is not required for safety system operation.

The reactor vessel is surrounded by a cylindrical containment partially filled with water. This containment provides pressure suppression and liquid make-up capabilities. The reactor vessel can be depressurized using the Automatic Depressurization System (ADS) valves consisting of six valves discharging into various locations within containment. The entire containment vessel is submerged in a pool of water that acts as the ultimate heat sink. A schematic of the currently conceived MASLWR design is shown in Fig. 4.5-1[4.5-1].

OSU's MASLWR Test Facility is an integral test facility, which is scaled to model the steady state and transient operation of the prototypical MASLWR facility. It is scaled at 1:3 length scale, 1:254 volume scale and 1:1 time scale. It is designed for full pressure (114 bar) and full temperature (590 K) prototype operation and is constructed of stainless steel components [4.5-2].

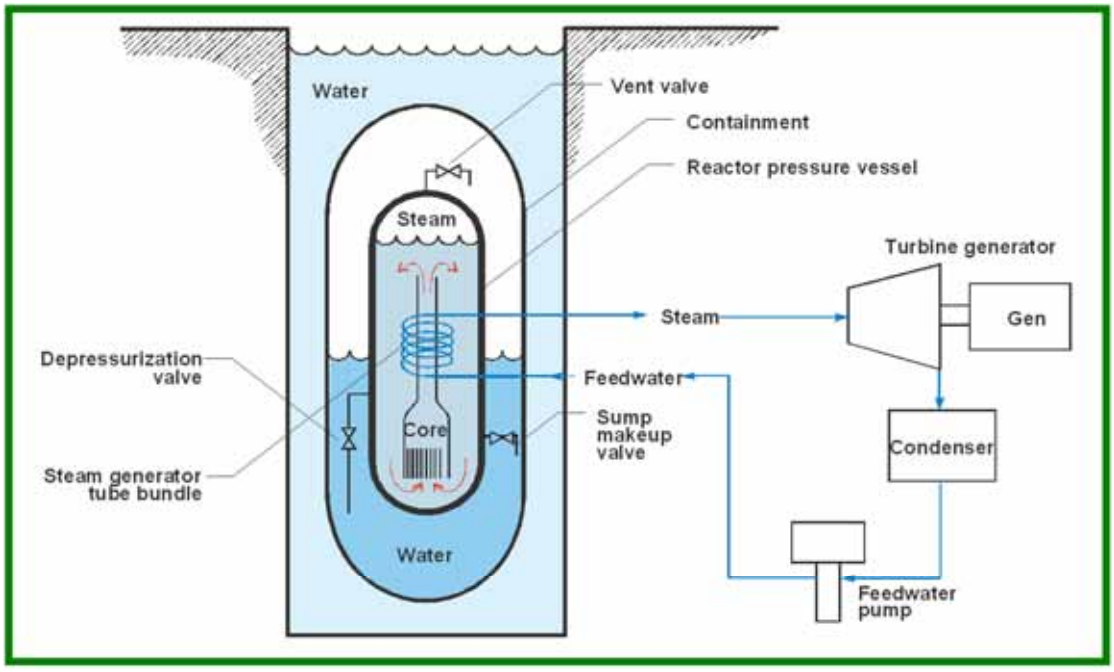

FIG. 4.5-1. MASLWR baseline design concept.

The test facility includes three major component packages. The first is the primary circuit which includes the reactor pressure vessel with its internal components (core, hot leg riser, steam generators, pressurizer, ADS lines, vent lines and sump recirculation lines). The second is the secondary circuit which includes the steam generators (internal to vessel), feed water pumps and associated feed water and steam valves. The third is the containment structure. OSU's test facility models the containment structure in which the pressure vessel sits as well as the cavity within which the containment structure is located. In addition to the physical structures of which the test facility is comprised there is an instrumentation and control system [4.5-1].

The purpose of the OSU MASLWR Test Facility is to assess the operation of the MASLWR under normal full pressure and full temperature conditions and to assess the passive safety systems under transient conditions. The data generated by the test program will be used to assess computer code calculations and to provide a better understanding of the thermohydraulic phenomena in the design of the MASLWR NSSS.

4.5.1. Facility description

The primary circuit of the test facility models the self-contained integrated reactor core and steam generator system. The core is comprised of electric heaters. The steam generator is comprised of helical coils that are located in the vessel, above the core and outside of the hot leg chimmney. This relative placement of core and steam generator allows for sufficient natural circulation flow under normal steady state and transient operating conditions. The primary circuit of the test facility has been designed with limits for operation at a primary side pressure of 11.4 MPa and a primary side temperature of 590 K. A detailed description of the test facility is contained in the test facility description report [4.5-3].

Primary coolant flow is upwards through the core and hot leg riser. This hot fluid is then cooled by the steam generator in the upper portion of the vessel. The cooler fluid flows downward around the outside of the hot leg riser into the lower plenum. From the lower plenum the fluid is drawn back into the core and heated once more. Figure 4.5-2 shows a schematic of the primary circuit components.

The test facility core consists of 56 electric heaters distributed in a square array with a maximum core power of 398 kW. The core geometry and thermal characteristics (flow areas, hydraulic diameters and local heat flux) have been preserved on a scaled basis.

The steam generator (SG) is a helical coil, once through heat exchanger located within the pressure vessel in the annular space between the hot leg riser and the inside surface of the pressure vessel shell. Feed water is provided from the city water supply and, after de-ionization and chemical treatment, is pumped into the SG from a feedwater storage tank by a positive displacement pump. This pump uses a variable speed controller to allow for precise control of the feed water mass flow rate. The steam produced is vented to atmosphere.

The SG consists of three separate parallel helical coil tube sections. The outer and middle coils consist of five tubes each while the inner coil consists of four tubes. Each coil is separate from the others but the tubes within a coil are joined at a common inlet header to ensure pressure equilibrium. Cold feedwater enters at the bottom of the SG and boils off after traveling a certain length in the SG tubes. This boil off length is a function of both core power and feed water flow rate. Nominally, this boil off length is approximately 40% shorter than the actual length of the steam generator tubes so the steam will leave the SG superheated. Each SG coil exhausts the superheated steam into a common steam drum from where it is subsequently exhausted to atmosphere.

The MASLWR containment vessel and the surrounding containment pool are modeled in the OSU MASLWR test facility as two separate vessels. One vessel models the suppression pool volume, vapour bubble volume and the condensation surface inside of the containment vessel. The second vessel models the heat capacity of the water pool within which the containment vessel is held. The two vessels are separated by a stainless steel plate. This plate models the scaled heat transfer surface between the containment vessel and the surrounding vessel pool. Figure 4.5-3 is a photograph of the test facility containment, taken during facility construction, which identifies these two vessels.

The containment vessel is connected to the reactor pressure vessel (RPV) by six independent automatic depressurization system (ADS) lines. There are two blowdown lines, two vent lines and two sump recirculation (core make-up) lines. Flow through each of these lines is via an independent automatically operated valve controlled through the test facility control system. The containment vessel is capable of prolonged operation at 2.07 MPa and 477.6 K.

The test facility is instrumented to capture the behaviour of the facility during steady state and transient operation. The following information can be obtained by the test facility data acquisition system:

- Feed water—mass flow rate and temperature,
- Feed water through each SG coil—mass flow rate, temperature and pressure,
- Main steam—volumetric flow rate and pressure,
- Differential pressure—across core, hot leg chimney, SG, and annulus below SG,
- Pressurizer—coolant level, pressure and temperature,
- Temperatures—core inlet, core exit, primary loop at SG.

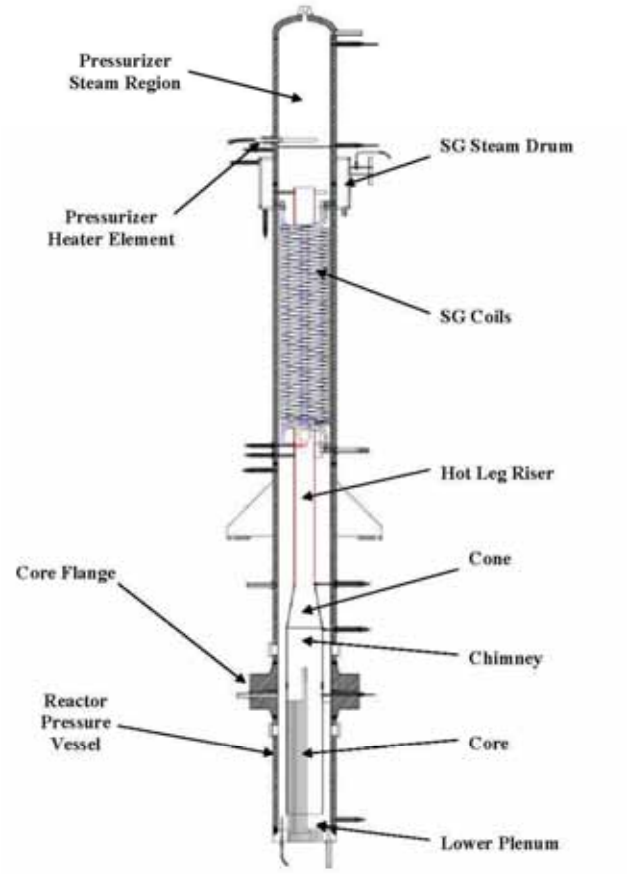

FIG. 4.5-2. OSU MASLWR test facility reactor pressure vessel key areas.

FIG. 4.5-3. OSU MASLWRtest facility containment and cooling pool.

The test facility control system accomplishes two tasks. The first is to process input signals from the various facility instrumentation (thermocouples, pressure meters, flow meters, valve and relay positions). The second is to generate control signals determined by the system logic (valve and relay control signals, heater and pump control signals). The following systems can be regulated by the test facility control system:

- Core heaters (including decay power modelling),
- Main feed water pump,
- Pressurizer heaters,
- Feedwater storage tank level,
- Pressurizer water level (draining during system heat-up only),
- Containment heaters (used to maintain an adiabatic boundary condition on all walls of containment except for the prescribed condensation wall ensuring that heat transfer only takes place between the containment pool vessel and the high pressure containment vessel).

4.5.2. Testing program

The purpose of the OSU MASLWR Test Facility is to assess the operation of the prototypical MASLWR under normal full pressure and full temperature conditions and to assess the passive safety systems under transient conditions. To this end, four tests were conducted at the OSU MASLWR Test Facility. These tests included 1 design basis accident and 1 beyond design basis accident. Table 4.5-1 presents a brief description of the four tests [4.5-4].

TABLE 4.5-1. SUMMARY OF OSU MASLWR TESTING PROGRAM

Test #	Simulation	Low ADS 1 (%)	Low ADS 2 (%)	High ADS 1 (%)	High ADS 2 (%)	Sump Recirc 1 (%)	Sump Recirc 2 (%)
OSU-MASLWR-001	Inadvertent actuation of 1 submerged ADS valve	Failed Shut	100	100	100	100	100
OSU-MASLWR-002	Natural circulation at core power up to 210 kW	N/A	N/A	N/A	N/A	N/A	N/A
OSU-MASLWR-003A	Natural circulation at core power up to 210 kW (Continuation of test 002)	Failed Shut	N/A	N/A	N/A	N/A	N/A
OSU-MASLWR-003B	Inadvertent actuation of 1 high containment ADS valve	Failed Shut	100	Failed Shut	100	100	100

4.5.2.1. Inadvertent actuation of 1 submerged ADS valve (OSU_MASLWR-001)

The purpose of this test is to determine the pressure behaviour of the pressure vessel and containment following an inadvertent actuation of one of the submerged ADS valves and the subsequent vessel depressurization. In this test it is assumed that the second ADS valve would fail in the closed position. Both of these ADS lines are located below the vessel coolant level and below the water level in containment upon initiation of the transient.

Upon actuation of one of these ADS valves, the primary system blows down into containment through the open line. Initially, the blowdown is subcooled due to the location of the ADS lines and the high system pressure. Eventually, the subcooled blowdown flow will give way to choked two phase flow in the ADS line. This transition occurs when the system pressure has dropped sufficiently so that the differential pressure at the break location results in flashing of the coolant. This two phase blowdown period is characterized by decreasing depressurization rates and the paralleling of the primary system pressure and the saturation pressure. Eventually, the system pressure will equal the saturation pressure and break flow will become single phase. This single phase flow regime is characterized by an increase in depressurization rate over the two phase flow phase. The water level in the primary vessel continues to drop. When the ADS line gets uncovered the break flow will still be single phase but will consist of vapour instead of fluid. Figure 4.5-4 shows the pressure history of the primary system and containment during OSU-MASLWR-001.

When the pressure between the vessel and containment reaches 0.517 MPa the two valves high in containment open in succession. This results in an equalization of the pressure between the vessel and containment. After the pressure difference between containment and the vessel reaches approximately 35 kPa, the sump recirculation valves open. This allows for the vessel to refill due to the higher water level in containment. The water level in the vessel never falls below the top of the core. Figure 4.5-5 shows the vessel coolant level during the transient.

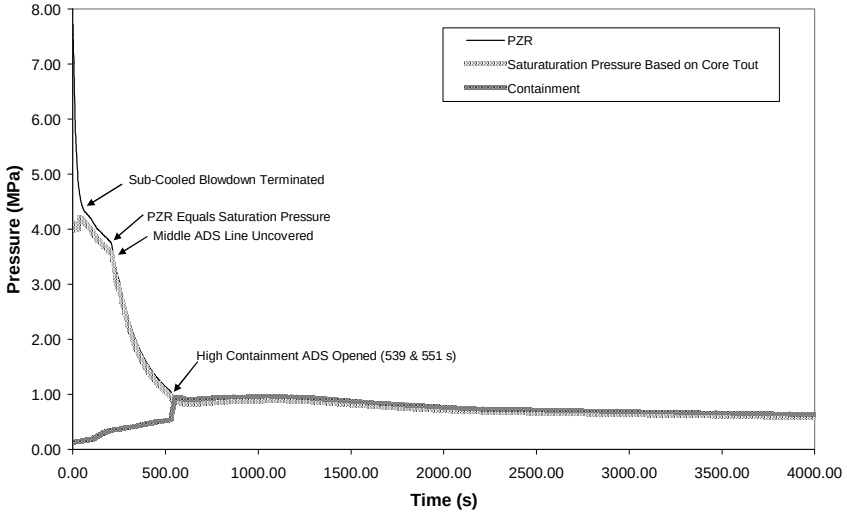

FIG. 4.5-4. Pressure history of primary system and containment for test OSU-MASLWR-001.

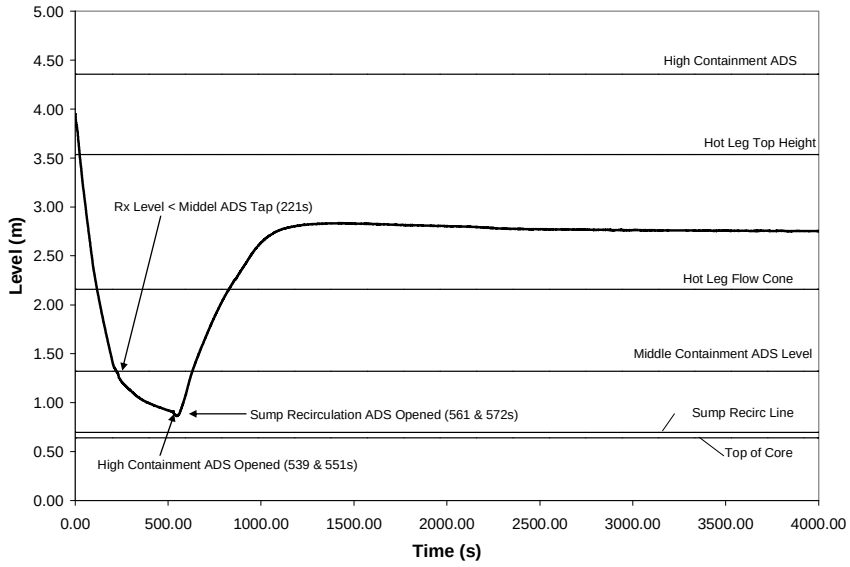

FIG. 4.5-5. Vessel coolant level during test OSU-MASLWR-001.

4.5.2.2. Natural circulation with core power up to 210 kW (OSU-MASLWR-002 & 003A)

The purpose of these tests is to get primary system flow rates and secondary side steam superheat for a variety of core powers and feed water flow rates. MASLWR is controlled by varying the degree of main steam superheat. Main steam superheat can be adjusted by varying core power, feedwater flow rate or both. During these two tests, 7 different core powers were used as well as 9 different feed water mass flow rates. Table 4.5-2 shows the core power and the feed water flow rate for each of the subject tests.

TABLE 4.5-2. CORE POWER AND FEED WATER FLOW RATES
FOR TESTS OSU-MASLWR-002&003A

Test	Period #	Start time (s)	End time (s)	Core Power (kW)	Feed Water (kg/min)
MASLWR OSU-002	1	0	127	80.0	1.13
	2	250	550	100.0	1.81
	3	750	1200	100.0	2.14
	4	1380	1570	100.0	2.50
	5	1670	1920	110.0	2.49
	6	2060	2250	125.0	2.50
	7	2450	2600	160.0	3.85
	8	2700	2930	165.0	3.83
MASLWR OSU-003A	9	0	450	210.0	4.14
	10	550	1000	210.0	4.56

Figures 4.5-6 and 4.5-7 show the volumetric flow rate across the core for the subject tests. As the core power is increased in tests OSU-MASLWR-002 & 003A from 80 kW to 210 kW there is a subsequent increase in the temperature difference across the core as well as an increase in the coolant flow rate through the core.

The main steam superheat is a function of the core power and the feed water flow rate. The main steam superheat is calculated using the difference between the main steam saturation temperature and the measured main steam temperature. An increase in core power increases the slope in the main steam superheat graph. An increase in the feed water flow rate tends to decrease the slope of the main steam superheat graph. The main steam superheat for tests OSU-MASLWR-002 & 003B are shown in Figs 4.5-8 and 4.5-9. The main steam superheat varies from approximately 12 K to a maximum around 38 K.

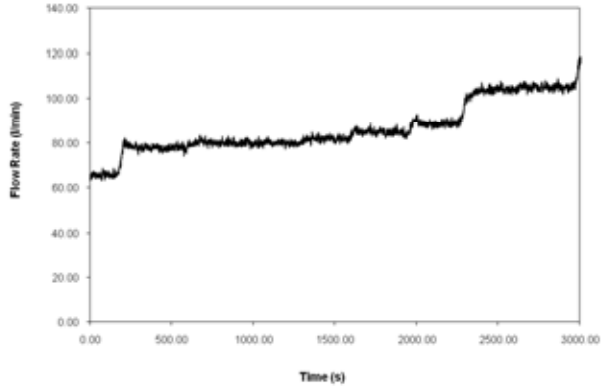

FIG. 4.5-6. Core volumetric flow for test OSU-MASLWR-002.

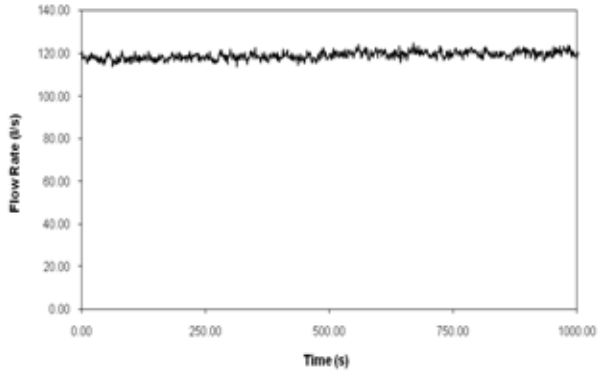

FIG. 4.5-7. Core volumetric flow for test OSU-MASLWR-003A.

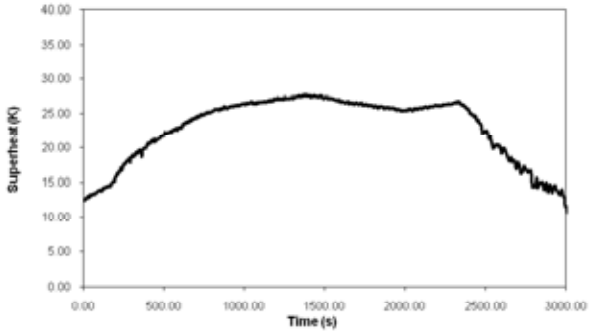

FIG. 4.5-8. Steam superheat for test OSU-MASLWR-002.

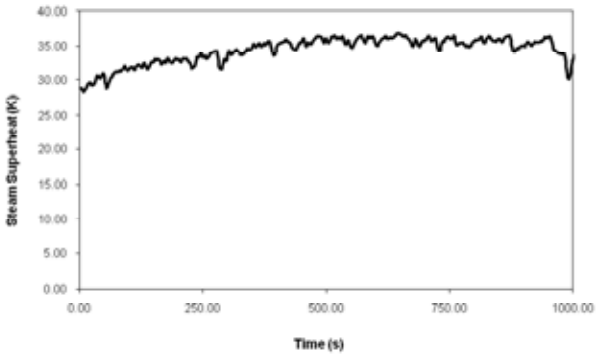

FIG. 4.5-9. Steam superheat for test OSU-MASLWR-003A.

4.5.2.3. Inadvertent high containment ADS vent line actuation (OSU-MASLWR-003B)

The purpose of this test is to acquire the pressure transient in the containment and the primary system during inadvertent actuation of the high containment ADS vent line. This represents a beyond design basis accident scenario for MASLWR. During this test there is no core heating. Additionally, there is no pre-heating of the containment non-condensation surfaces.

The normal sequence of ADS actuation in MASLWR is (1) submerged ADS lines, (2) high containment ADS lines, and (3) sump recirculation lines. This sequence minimizes the rise in containment pressure due to the large amount of energy transferred to the subcooled containment coolant. When the high containment lines are actuated first, the choked flow in the high containment line will limit the rate at which the containment and vessel pressures equalize. The containment pressure will thus be determined by the difference between the steam flow rate through the high containment lines and the condensation rate in the containment. Containment and system pressure during the test are shown in Fig. 4.5-10.

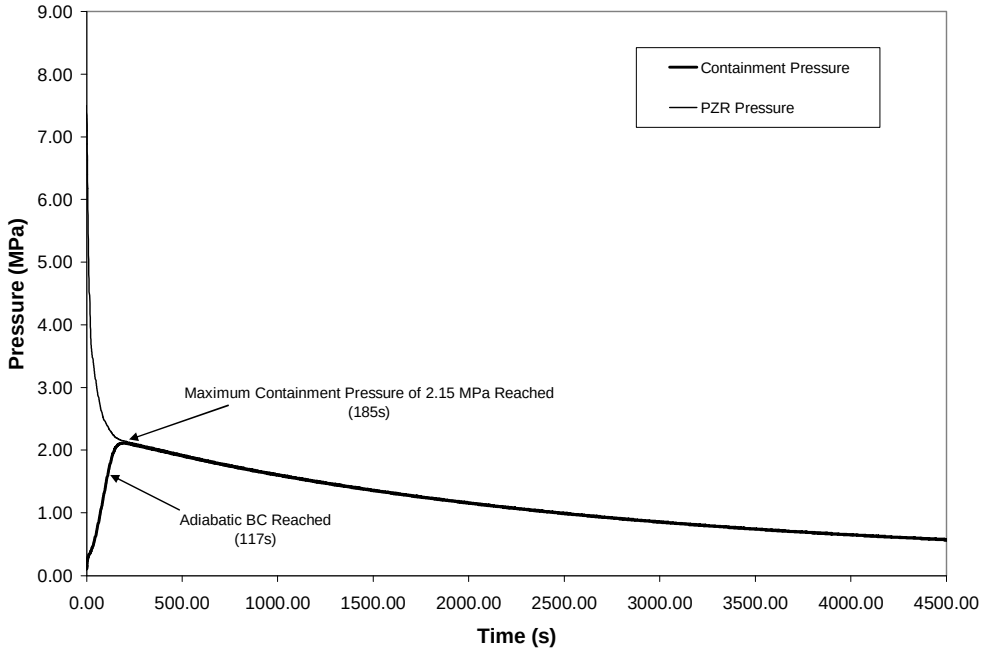

FIG. 4.5-10. Containment and system pressure for test OSU-MASLWR-003B.

As mentioned, there is no pre-heating of the containment non-condensation surfaces as part of this test. Therefore, an adiabatic wall boundary condition has not been provided on the non-condensation surfaces in containment. This introduces a small distortion at the initiation of the transient. However, after the initial transient the containment non-condensation surfaces reach the saturation temperature inside containment and stay within 5% of the saturation temperature for the duration of the transient.

Thermocouples located a few millimeters off of the surface of the condensation surface between the vessel and containment show similar trends. Temperatures quickly matched the saturation temperature, and as the thermocouple level was surpassed by the containment coolant surface level, the temperature measurements dropped to the liquid temperature as shown in Fig 4.5-11.

The liquid level in the containment never reached a level greater than 3.77 m (291s). As a result, only the lower two thermocouples became submerged. The wall temperature at the elevation of 4.08 m after the initial heat up stays well below the saturation temperature. The wall temperature at the elevation of 5.61 m exceeded the saturation temperature at approximately 62 s, and elevation 5.11 m exceeded saturation at approximately 995 seconds. Both of these locations remained above saturation temperature once it was exceeded.

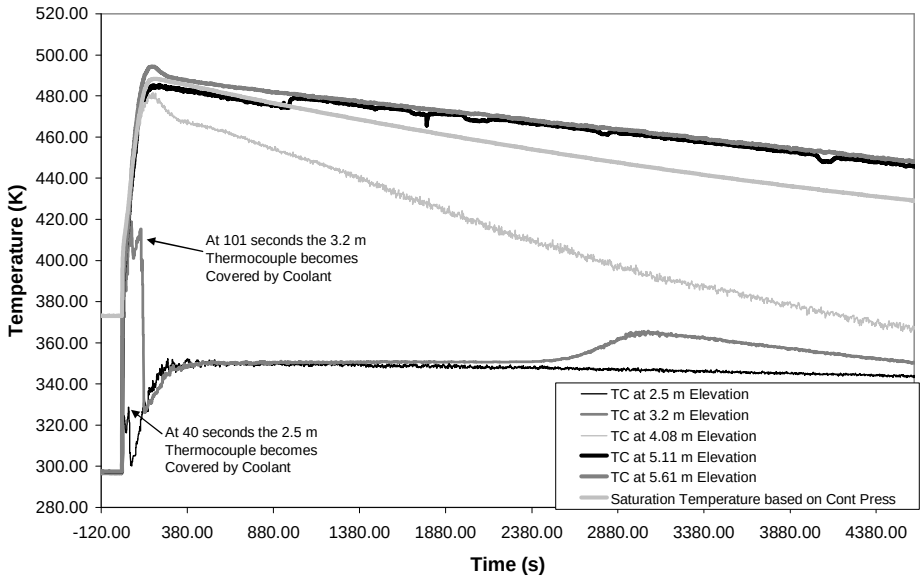

FIG. 4.5-11. Containment condensation plate wall temperatures for test OSU-MASLWR-003B.

4.5.3. RELAP5-3D model of MASLWR test facility

A RELAP5-3D model of the OSU MASLWR Test Facility has been constructed. RELAP5-3D is a general thermohydraulic code developed and maintained by the Idaho National Laboratory. Version 2.4.2 was used in developing the OSU MASLWR Test Facility model. The model of the OSU MASLWR test facility has been developed using only one dimensional components. Figure 4.5-12 shows a schematic of the RELAP5-3D model of the OSU MASLWR Test Facility.

The RELAP5-3D model was constructed in order to examine the ability of the code to accurately predict the behaviour of the MASLWR Test Facility under a variety of steady state and transient conditions. Three model scenarios were developed. The first models the steady state behaviour of the test facility under a variety of core power and feed water flow rates. The second scenario looks at the inadvertent actuation of the ADS valve/line and the subsequent vessel blowdown into the containment vessel. The third scenario looks at the inadvertent actuation of the vent valve/line and the subsequent vessel blowdown into the containment vessel.

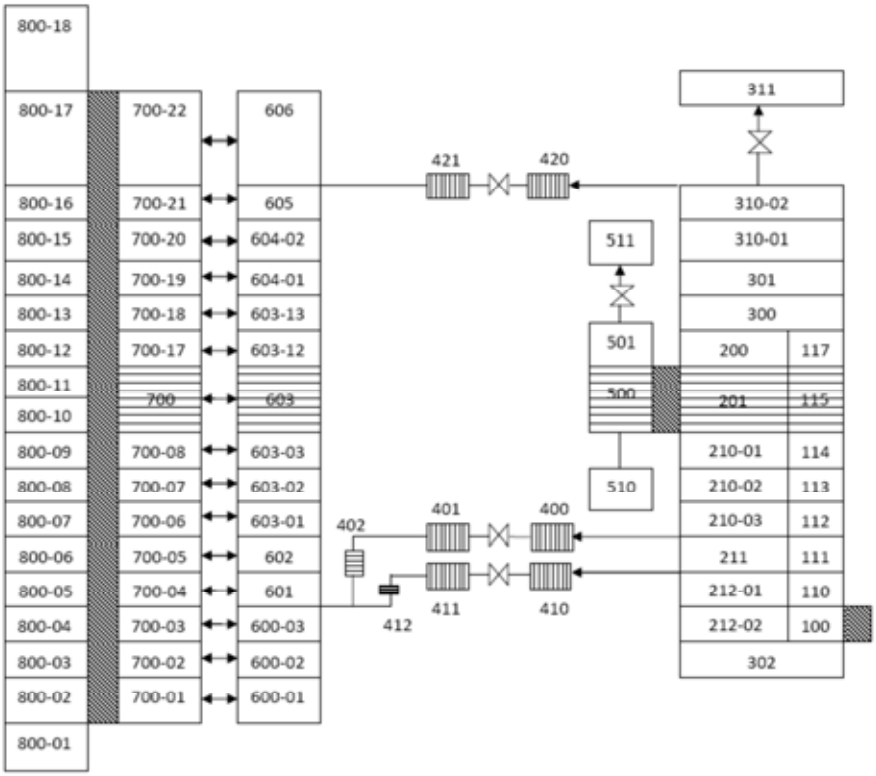

FIG 4.5-12. RELAP5-3D model of OSU MASLWR test facility.

4.5.3.1. Natural circulation with core power up to 210kW (tests OSU-MASLWR-002/003A)

Figures 4.5-13 and 4.5-14 show comparisons between the primary flow rates for the actual test facility and the RELAP5 model in tests -002 and -003A. With the exception of the first step (power = 80 kW and feed water Flow = 1.13 kg/min) RELAP5 underestimates the primary flow rate. This underestimation is less than 10% for all the lower flow rates (steps 1-6). At the higher flow rates (steps 7–10) the discrepancies between the RELAP5 and actual primary flow rates are more pronounced. The difference in steps 7 through 10 are approximately a 12% underestimation using RELAP5.

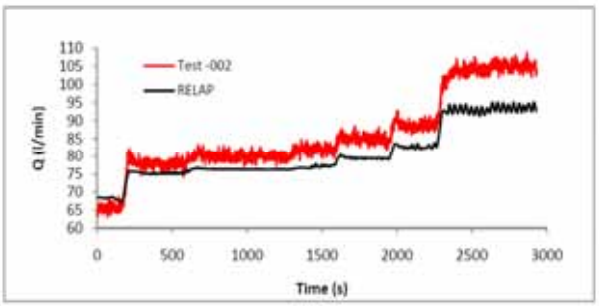

FIG. 4.5-13. Primary system flow rates for test facility and RELAP model for Test-002.

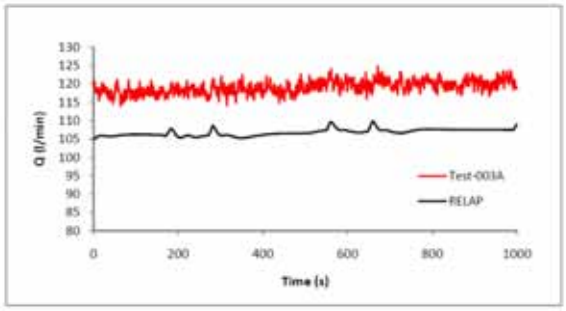

FIG. 4.5-14. Primary system flow rates for test facility and RELAP model for Test-003A.

Figures 4.5-15 and 4.5-16 show a comparison between the core inlet and core outlet temperatures for the actual test facility and the RELAP5 model. The lower temperature is the core inlet temperature and the higher temperature is the core outlet temperature. The average coolant temperatures in the RELAP model are generally higher than in the actual test facility. Since the same amount of energy is being

deposited into the system in both RELAP5 and the test facility, there is a likelihood that the test facility RELAP model may be underestimating either the heat storage of the vessel components or the heat transfer from the vessel itself into the environment.

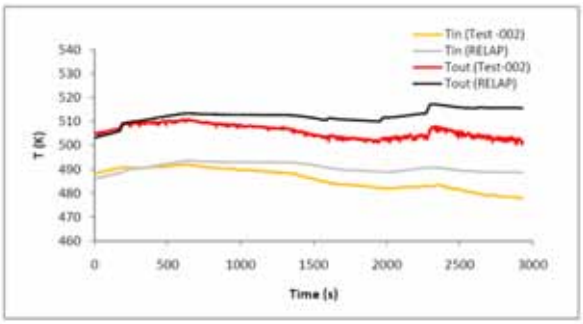

FIG. 4.5-15. Core temperatures for tes facility and RELAP model in Test-002.

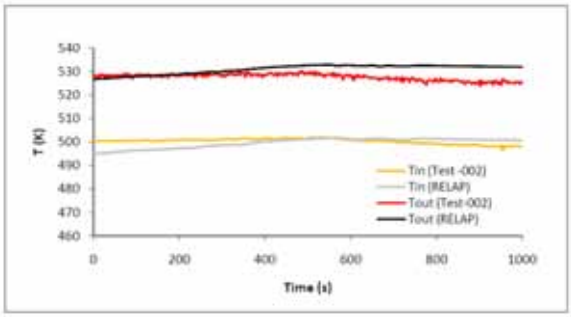

FIG. 4.5-16. Core temperatures for test facility and RELAP model for Test -003A.

4.5.3.2. Inadvertent actuation of one submerged ADS valve (Test OSU-MASLWR-001)

Figure 4.5-17 shows the pressure history of the primary system and containment for the actual test facility transient and the RELAP model of the transient. The RELAP model blows down more rapidly than the test facility with the subsequent more rapid decrease in primary pressure and more rapid rise in containment pressure. The increased speed of the transient in RELAP also caused an earlier actuation of the vent valves and the sump recirculation valves since these valves are actuated on the pressure difference between containment and the primary system. The general behaviour of the transient including the identification of the choked flow regimes noted above was similar between the RELAP model and the test facility results. Note that the RELAP model utilized the Ransom-Trapp choking model at the ADS line discharge. The subcooled, two phase and superheated choking discharge coefficients were maintained at the default values of 1.0.

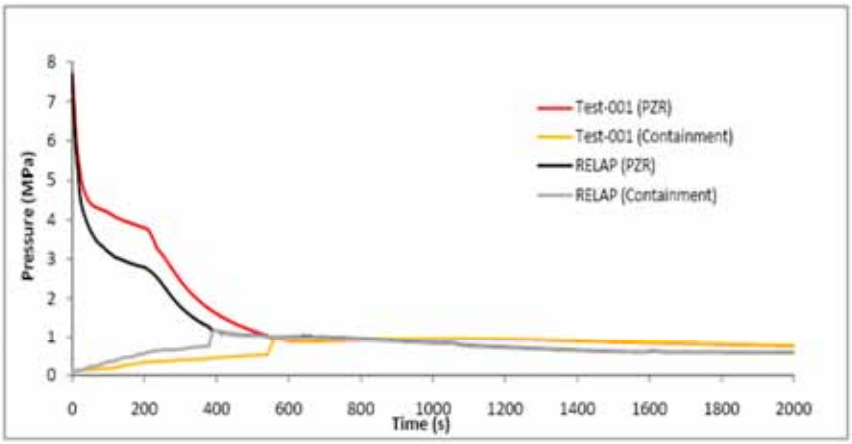

FIG. 4.5-17. Primary and containment pressure during MASLWR ADS blowdown.

4.5.4. Summary

The OSU MASLWR test facility is a scaled model of the prototypical MASLWR that has been used to conduct proof of concept testing for MASLWR. Testing was completed demonstrating normal startup, operation and shutdown. Control of the facility using the core power, feed water flow and main steam superheat was also explored. In addition to normal operations, one design basis accident and one beyond design basis accident scenario were investigated. During these accident scenarios, the containment-vessel behaviour/coupling was examined as well as condensation behaviour within containment. A linear stability anslysis completed for the prototypical MASLWR indicates that the natural circulation will remain stable within the bounds of the stability study.

REFERENCES FOR SECTION 4.5

[4.5-1] MODRO, S.M., et al., Multi-application small light water reactor, DOE Nuclear Energy Research Initiative Final Report, Idaho National Engineering and Environmental Laboratory (2003).

[4.5-2] REYES, J.N., KING, J., "Scaling analysis for the OSU integral test facility", OSU-NE-2003-01, Oregon State University, Corvallis, OR (2003).

[4.5-3] DEMICK, N.T., GALVIN, M.R., GROOME, J.T., WOODS, B.G., OSU MASLWR Test Facility Description Report, OSU-MASLWR-07001 (2007).

[4.5-4] REYES, J.N., et al., Testing of the multi-application small light reactor (MASLWR) passive safety systems, Nuclear Engineering and Design **237** (2007) 1999–2005.

4.6. OVERVIEW ON THE PANDA TEST FACILITY AND ISP-42 PANDA TESTS DATA BASE

PANDA (Passive Nachwärmeabfuhr- und Druckabbau-Testanlage) is a large scale facility, which has been constructed at the Paul Scherrer Institute (PSI), Switzerland, for the investigation of both overall dynamic response and the key phenomena of passive containment systems during the long term heat removal phase for Advanced Light Water Reactors (ALWRs). Using a modular concept with a basic set of cylindrical vessels (typical diameter 4m), which are interconnected by piping, the facility can be adapted to simulate different passive containment designs (Fig. 4.6-1).

Since early 1990's, there has been number of projects related to the use of PANDA test facility for various evolutionary reactor designs, e.g., SBWR, ESBWR, SWR-1000, etc. Different PCCS concepts were experimentally investigated in the PANDA test facility with some minor modifications in the facility for each program. This is being a confirmation of its flexibility, due to the modular construction, in use of various applications. The earlier investigations in the PANDA test facility, in addition to the current and future investigations, will be briefly provided in coming sections.

In PANDA test facility some tests were also performed for use as the basis of International Standard Problem number 42 (ISP-42). The OECD/NEA Committee on the Safety of Nuclear Installations (CSNI) approved, at its meeting on December 3–5, 1997, an International Standard Problem (ISP) involving a test in the PANDA facility, based on a recommendation from the Principal Working Group 2 (PWG2) on System Behaviour. The main interest for this ISP is code validation in relation to a range of LWR and advanced LWR (ALWR) (mainly) containment issues that have been designated as important and involving thermohydraulic phenomena. The ISP-42 test was subdivided in six well-defined sequential phases, restricting the phenomena, which are taking place in each test phase, to a reasonable number and separating them as much as possible. This gives the ISP-42 participants the choice to calculate one, several, or all of the six test phases, depending on the type of transient and the phenomena that they are interested in. For each test phase, the initial and boundary conditions are defined separately so that if there are code model deficiencies in the preceding test phase the calculations for the next phase can be started and performed independently. Overview on the ISP-42 PANDA test with a sample result obtained from Phase-A and summary of the major conclusions from the ISP-42 exercise are also presented in this section.

4.6.1. Summary of PANDA facility description

PANDA is a large scale facility, which has been constructed at PSI for the investigation of both overall dynamic response and the key phenomena of passive containment systems during the long term heat removal phase for Advanced Light Water Reactors (ALWRs). The facility has been configured to simulate the containment of a passive BWR, but the phenomena, which are taking place, are of a more generic character and of interest to LWR containment's in general. Using a modular concept with a basic set of cylindrical vessels (typical diameter 4m) which are interconnected by piping, the facility can be adapted to simulate different passive containment designs. The facility configuration used for ISP-42 tests is a scaled down model of European Simplified BWR containment

and safety systems. After a detailed scaling analysis, power and volumes are scaled 1:40, and pressure, relevant heights and pressure drops are 1:1. Detailed scaling analysis which was applied to the design of the PANDA facility can be found in Ref. [4.6-1].

As can be seen from the 3-dimensional drawing of Fig. 4.6-1 and it is illustrated in the schematic sketch of Fig. 4.6-2, the PANDA facility mainly consists of six large pressure vessels, simulating the various containment volumes. One of these vessels represents the Reactor Pressure Vessel (RPV), which acts as the steam source during a transient. RPV contains at its bottom a core simulator consisting of 115 electrically heated heater elements, which are located in a shroud acting as a riser/down-comer configuration and thus enabling natural circulation in the lower two thirds of the RPV. Electrical heater rods simulate the history of core decay heat generation with programmable power generation, maximum being 1.5 MW. The RPV is connected to the PANDA facility via the two Main Steam Lines (steam supply to the system), the PCC drain line (liquid return of the condensed steam in the PCCs) and the GDCS drain line. At the top of the RPV, an additional flange may be used for helium injection.

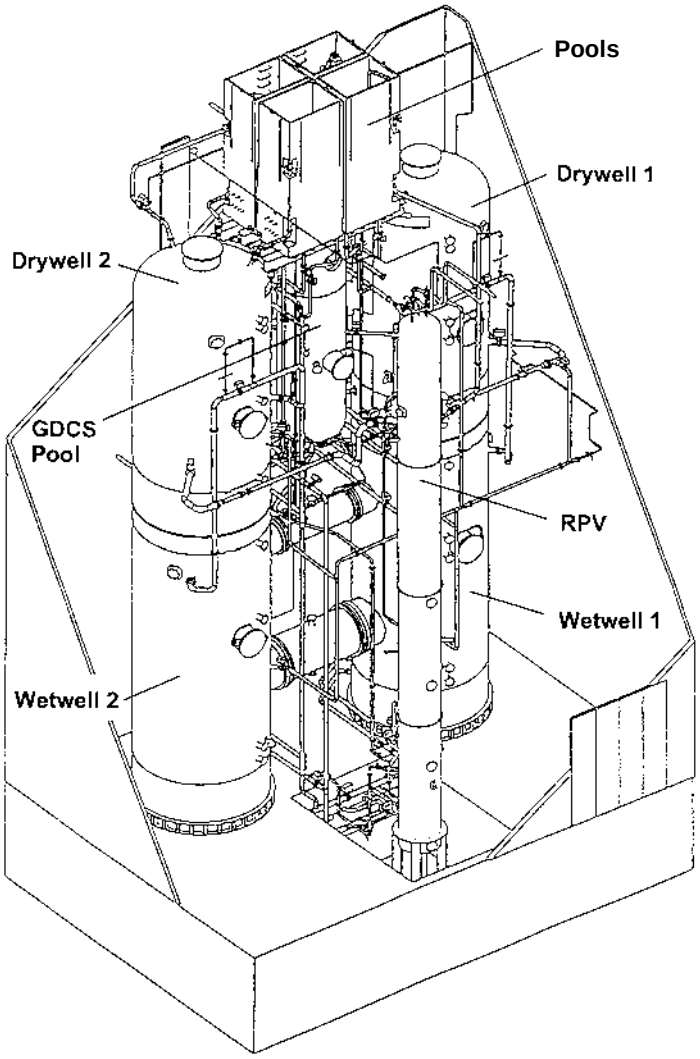

FIG. 4.6-1. 3-D view of the PANDA test facility.

Two other large cylindrical vessels of an inner height 8.0 m and an inner volume of 89.9 m^3 each, represent the Drywell (DW), connected each other with a large diameter dry-well connection pipe (outer diameter of 1.0 m). The dry-well as a whole is connected to the rest of the system via the two Main Steam Lines (steam supply to the system and input from RPV), the PCC feed lines (output of dry-well), the Main Vent Lines (output of dry-well) and the Vacuum Breaker Lines (input to dry-well,

in case the wet well pressure exceeds the dry-well pressure). At the top of the dry-well-1, air may be injected to simulate a sudden release of trapped air into the system. The two DW vessels are filled with gas. Except under startup conditions, this is more or less pure steam (air fraction is quite small).

The other two large cylindrical vessels, of inner volume of 115.9 m^3 each and an inner height of 10.11 m, filled with water at a level of approximately 4m, represent the Wet well (WW, also called suppression chamber). The two WW vessels are connected each other by two large diameter pipes of 4m length each, one in the liquid section of the wet well (1.5 m diameter), and the other one in the gas space of the wet well (1.0 m diameter). The wet well as a whole is connected to the PANDA facility via the two Main Vent Lines (input), the three PCC vent lines (input), the two pressure equalization lines and the Vacuum Breaker Lines (output, in case the wet well pressure exceeds the dry-well pressure significantly).

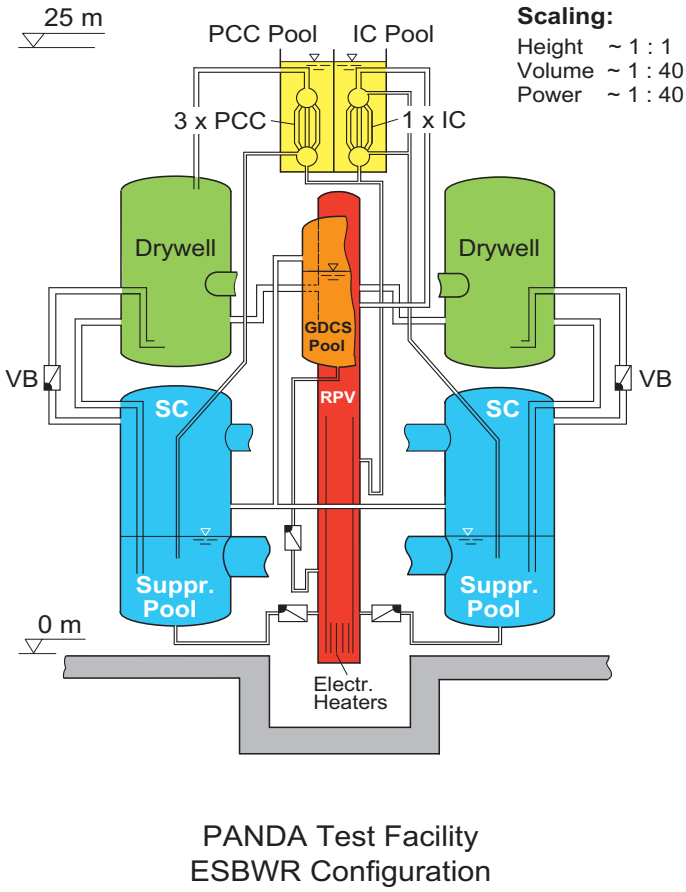

FIG. 4.6-2. Schematic of the PANDA test facility for the ESBWR configuration.

The last vessel primarily represents a Gravity Driven Cooling System (GDCS) pool with a volume of 17.6 m^3 and inner height of 6.06m, and it can function as additional containment volume for wet well gas space. The GDCS tank is connected to the rest of the facility via the GDCS drain line to RPV (output) and the pressure equalization line to the wet well vessels. GDCS drain line connects the inside bottom of the GDCS tank with the lower part of the downcomer of the RPV. A check valve allows only one directional flow from the tank to the RPV. To establish similar pressure in the gas spaces of GDCS tank and wet well, the pressure equalization line connects GDCS tank with the gas space of the two wet wells.

In addition, four rectangular pools open to the atmosphere are located on top of the facility. These pools may be equipped with immersed heat exchangers and used as heat sinks outside the containment, or as cooling storage pools in other configuration. As mentioned earlier, the modular facility arrangement provides the flexibility needed to investigate a variety of containment design. For the ISP-42 tests, these pools contain three Passive Containment Coolers (PCCs) connected to dry-well. Each of the three PCCs consists of a PCC unit, which is submerged in a separate water pool, where the bottom of the pool is located 19.8 m above the ground floor. The PCC unit is a heat exchanger and is made of an upper drum, a tube bundle (20 tubes, diameter of 0.0508 m and length of between 1.778 m and 2.066 m), and a lower collector drum. Each PCC unit is submerged into the secondary side water inside the PCC pool tank and is connected to the drywell and the rest of the system via the PCC feed line (input) at the top of the upper drum, whereas the PCC lower drum has two connections, one of them is the PCC vent line (non-condensable output) on the right side of the lower drum and the other one is the PCC drain line (output) at the bottom of the lower drum. Steam/air mixture enters from the top of the PCC unit, and then the steam part is condensed in the tube bundle and drained out of the PCCs via the drain line to the RPV, whereas non-condensable may be vented via the vent line to the wet well. The two PCC units are connected to one of the drywell, the third unit is connected to the other drywell. The fact that the three PCC units are connected to two drywell vessels allows asymmetric behaviour and creates flows between these vessels. Such an asymmetric flow also occurs with equal flow resistance from the RPV to two of the drywell vessels when all three PCCs are in operation.

The different vessels and the primary side of the PCCs are connected to each other by means of different pipes. The major system lines are: Main Steam Lines (MSLs), which connect the upper part of the RPV with dry-well-1 and dry-well-2, respectively; Main Vent Lines (MVLs) connect the lower part of the dry-well with the wet well pool, approximately 1.6m below the surface of the pool. Each MVL enters its respective wet well vessel nearly at the top and is then led inside the vessel to the pool. The exit of the MVL pipe is submerged in the pool water.

In general, BWR containment concepts rely on Vacuum Breaker (VB) installed between the drywell and wet well. Their function is not to allow the wet well pressure to exceed drywell pressure by a certain margin. There are two vacuum breakers connecting the upper part of the two wet wells to the lower part of the two dry-wells by VB lines (VBLs) in the PANDA facility. The operation of the actual vacuum breaker is simulated in PANDA by control valves. These are opened and closed by the facility control system when the measured differential pressure between the wet well and the dry-well exceeds an upper and a lower limit, respectively. Therefore, under normal conditions, the lines are closed by the VB valves. Additional auxiliary lines are available to establish the desired stationary conditions at the beginning of each of the sequences of the experiment. These lines are not shown in Figs 4.6-1 and 4.6-2.

The system line pressure losses were carefully scaled using orifices and the theoretical line resistances were measured and verified by system characterization tests. In addition all vessels and system lines were carefully insulated using rock-wool and the heat losses were determined and provided, separately. The facility is instrumented with over 500 sensors and axial distributions of temperatures and non-condensable concentrations in the vessels can be obtained from thermocouple, pressure and (a limited number) of oxygen (air) probe measurements. Further detailed description of the PANDA test facility for ISP-42 test series can be found in Ref. [4.6-2], and the boundary and initial conditions with the list of measurement locations for each phases of the ISP-42 are provided in Ref. [4.6-3].

4.6.2. Earlier investigations in PANDA test facility

In early 1990's, the Simplified Boiling Water Reactor (SBWR) design was used as reference design for the PANDA test facility (Fig. 4.6-3), and the main goal of the project were the experimental and analytical investigation of the startup and long term operation of the passive containment cooling system of the SBWR and related aspects [4.6-4] and [4.6-5]. In a first test series, the steady state characteristics of the PCCS condenser units were investigated. In addition, ten integral system tests were performed addressing specific topics of concept demonstration, asymmetric steam injection,

reduced condenser capacity, isolation condenser and PCC system interaction, and vacuum breaker leakage.

European SBWR (ESBWR) was also simulated in PANDA test facility using different scaling as in SBWR simulation and some component modifications were done (Fig. 4.6-2). Series of transient system tests were carried out in the PANDA facility to investigate the performance of the passive containment cooling system of the ESBWR [4.6-6]. Eight system tests in PANDA with challenging conditions were performed to explore the real PCCS limitations, e.g., low water level in PCC pool, deferred release of "trapped air" in drywell. During one of the tests, helium was injected (as simulation of hydrogen) to simulate beyond design basis accident conditions.

Further, different PCCS concepts were experimentally investigated in the existing PANDA test facility (Fig. 4.6-4). In this specific case SWR-1000 Building condenser was simulated and tested by using different scaling and also some specific limited modifications in the facility (confirming the flexibility of the modular construction of the PANDA test facility) [4.6-7].

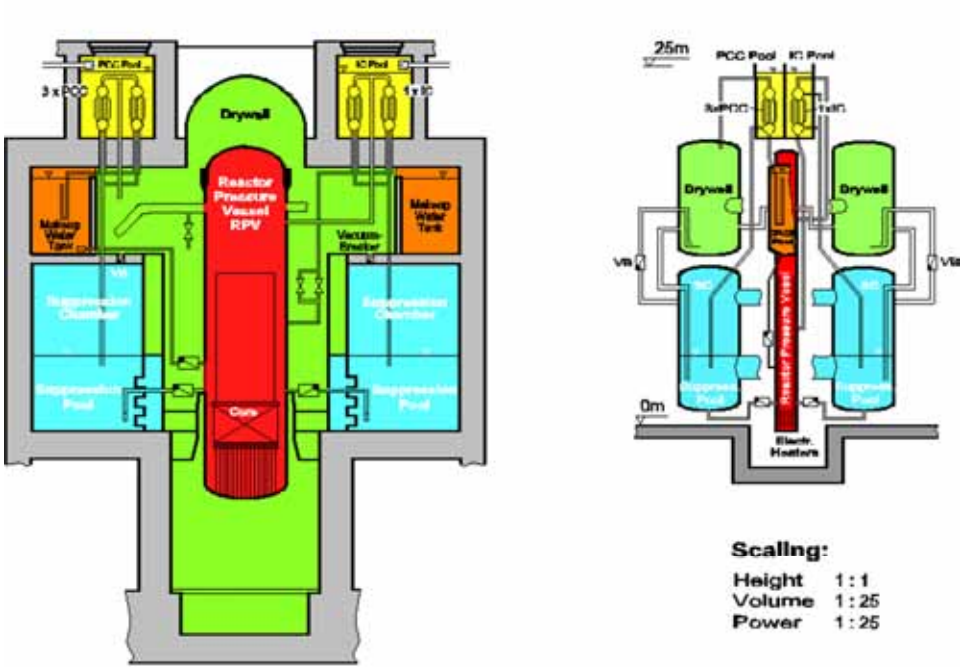

FIG. 4.6-3. SBWR versus PANDA test facilty.

On the basis of the ESBWR configuration for the PANDA test facility, ISP-42 tests were performed. Further details on ISP-42 exercise are provided in the next sections.

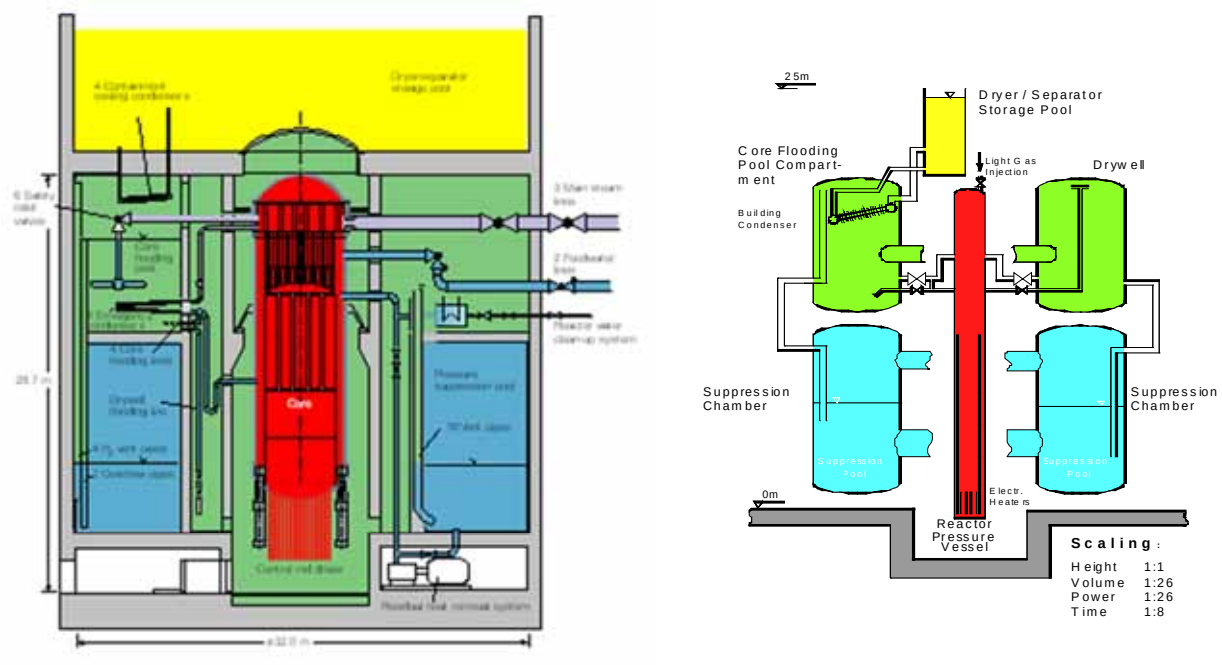

FIG. 4.6-4. SWR 1000 versus PANDA test facility.

4.6.3. ISP-42 PANDA test outline and overview

Following a proposal, the OECD/NEA Committee on the Safety of Nuclear Installations approved, at its meeting on December 3–5, 1997, a new International Standard Problem (ISP) involving a test in the PANDA facility, based on a recommendation from the Principal Working Group 2 (PWG2) on System Behaviour. The main interest for this ISP is code validation in relation to a range of LWR and advanced LWR (ALWR) (mainly) containment issues that have been designated as important and involving thermohydraulic phenomena. This ISP on PANDA test is also financially supported by the research foundation of the Swiss Utilities (Project- und Studienfonds der Elektrizitätswirtschaft, PSEL).

A preparatory meeting in March 1998 was called to discuss the scenario of the proposed ISP with some representatives from the OECD member countries. The ISP-test scenario has been defined taking into account the recommendations received from the representatives who attended this meeting and also comments received from other organizations. The ISP-PANDA test was performed on 21–22 April 1998, taking about 14 hours. Since the first phase of ISP-42 was going to be conducted as a “double-blind” or “blind” exercise, the experimental data was locked. In the second phase, the “open” exercise has been conducted by providing the ISP-42 PANDA test data to the participants and by performing post-test analysis.

ISP-42 PANDA test scenario was established to cover many typical LWR and ALWR containment and primary system phenomena. The test was subdivided in six well-defined sequential phases, restricting the phenomena, which are taking place in each test phase, to a reasonable number and separating them as much as possible. This gives the ISP-42 participants the choice to calculate one, several, or all of the six test phases, depending on the type of transient and the phenomena that they are interested in. For each test phase, the initial and boundary conditions are defined separately so that if there are code model deficiencies in the preceding test phase the calculations for the next phase can be started and performed independently.

The main issues and phenomena covered in the ISP-42 PANDA test are the following:

- Transient and quasi steady state operation of a passive containment cooling system (condenser immersed in pool),
- Coupled primary system and containment behaviour and phenomena,
- Reactor Pressure Vessel (RPV) operation at low power and low pressure under natural circulation conditions,
- Gravity driven ECCS injection in an initially saturated RPV,
- Venting of a steam/non-condensable gas mixture (through an immersed vent pipe into a wet well compartment),
- Steam condensation in the presence of non-condensable gases in tubes,
- Mixing and stratification of light (helium) and/or heavy (air) gases with steam in large volumes (3D effects, steam jets, air or helium release),
- Mixing and stratification in large water pools.

The ISP-42 PANDA departs to some degree from the traditional procedures in that it has to some extent an exploratory character: it is partly designed to answer certain interesting questions with respect to how far can system or containment codes go in addressing the classes of phenomena investigated and what could be expected either from available “commercial” CFD codes or "large mesh" codes suitable for containment analysis. Thus one of the outcomes of the ISP could be the clarification of certain development needs in relation to the calculational precision needed and the safety relevance of considering in detail certain particular phenomena.

The first part of the ISP-42 was “blind” or “double blind” for the organizations that have no previous familiarity with the facility, as noted above. Only the system description and the phase initial and boundary conditions were given to the participants for the blind part of the ISP. After completing the “blind” part, an open part was initiated by providing all the ISP-PANDA test data to the interested organizations. It should be emphasized again that the various phases of the test are clearly defined by providing simple initial and boundary conditions; thus participants were not forced to do the entire ISP but were able to choose the phases of interest to their organizations. Different sets of codes were also used for the various phases, as appropriate.

The configuration used for ISP-42 was corresponding to the European Simplified Boiling Water Reactor (ESBWR) containment and passive decay heat removal system at about 1:40 volumetric and power scale, and full scale for time and thermodynamic state (Fig. 4.6-2). The actual test took over ten hours, including all conditioning and test phases. The ISP-42 PANDA test consists of six phases, A through F. These phases represent a sequence of operating modes or processes as used for the simulation and study of the behaviour of ALWR containment’s with passive safety systems. Each of these phases in fact a separate experiment, with its own initial and boundary conditions. The six different test phases are listed as below:

Phase A: Passive Containment Cooling System Startup

Phase B: Gravity-Driven Cooling System Discharge

Phase C: Long Term Passive Decay Heat Removal

Phase D: Overload at Pure-Steam Conditions

Phase E: Release of Hidden Air

Phase F: Release of Light Gas in Reactor Pressure Vessel

The ISP-42 participants in the exercise chose the number of test phases they wished to calculate. Ten organisations from nine countries did participate in the "blind" phase pre-test calculations. Forty-nine submitted calculational results are included in the "blind" phase comparisons report [4.6-8]. A large number of physical parameters were selected for comparison. In general, most of the predicted results were in quite good agreement with the test results; however, some prediction cases differed significantly and the reasons for these differences were in detail discussed.

The experimental data was distributed to all ISP-42 participants for their post-test calculations by June 2000. There were 27 new submissions for different phases of "open" phase analyses of ISP-42 by some of the participants, 8 organizations from 8 countries. "Open" phase submissions, comparisons, and analyses for ISP-42 are based on the outcome of the results presented in the "blind" phase report of ISP-42 [4.6-8]. It is to be noted that as outcome of the good results obtained in the "blind" phase comparisons, some ISP-42 participants decided not to submit "open" phase calculations. Consequently, the number of submissions for "open" phase was less than "blind" phase and they were mostly dealing with improvements of system modelling (re-nodalization) or the modifications of the code physical models. One of the submissions using GOTHIC code, in relation to test phase E, was a new submission. The detailed comparisons and analyses of the "open" phase of the ISP-42 were issued as a separate report [4.6-9]. Improvements on the cases submitted were observed with the recent versions of the codes, use of some other physical models and re-nodalization of the system depending on the specific phenomenon observed in the six phases of the ISP-42. In addition to the good results obtained in the "blind" phase, these improvements also provided additional good agreements with the test results. Some of the prediction cases still differed significantly, for these cases the reasons of differences were identified to some limited degree.

4.6.4. Short description of ISP-42 Phase-A test and some results as example case

The objective of the first test phase (Phase A) of ISP-42 was to investigate the startup of a passive cooling system when steam is injected into a cold vessel filled with air and to observe the resulting gas mixing and system behaviour.

A sketch of the setup used for this phase is shown in Fig. 4.6-5. Here, the parts of the system filled with water are slightly darker than those filled with steam, air, or a steam/air mixture. As it can be seen from Fig. 4.6-5, all three PCCs are operational, and there is no interconnection between the different PCC pools. The GDCS is filled with water whereas the water level in the RPV is much below the downcomer entrance/riser exit. The main vent lines and the vacuum breaker lines are not operational for this test and therefore are not depicted in this scheme.

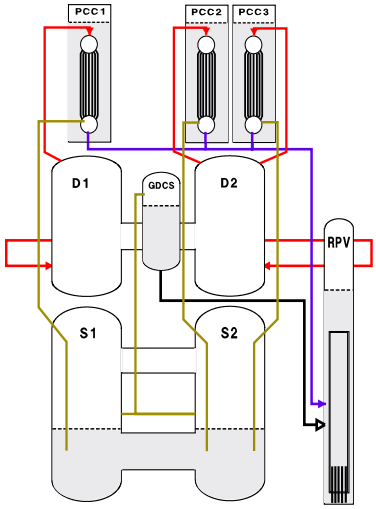

FIG. 4.6-5. ISP-42 Phase A: passive containment cooling system startup.

At zero seconds, RPV power has been switched on thus allowing steam to flow into the two drywell vessels. There, the steam slowly diluted the gas content of the drywell, which initially consisted of pure cold air and was also partially condensed at the cold vessel walls. Due to the inflow of additional gas (steam) into the drywell, pressure in the drywell as well as in the PCCs increased until it exceeded wet well pressure approximately 10 kPa, the hydrostatic head at the outlet of the PCC vent lines. Then, drywell content partially was pushed through the PCC primary sides into the two wet well pools via the PCC vent lines; the rest of the steam was stored in the drywells or has been condensed on the drywell walls. As long as the feed flow is small (due to a high condensation rate at the drywell walls) or/and the steam content of the flow mixture is low, no condensation has taken place in the PCCs. Instead, the mixture has been vented into the wet wells where the steam content has been condensed and the air content was separated into the gas space. Here, the separated air increased the amount of gas in the gas space thus increasing the system pressure. After some time into the transient, the dilution of the initial air content by the steam has been progressed and steam condensation started in the PCC tubes removing significant amounts of steam out of the vent flow, thus decreasing the inflow of air into the wet well gas space, which resulted in a decrease of the pressure increase. The condensed steam has flown through the drain lines back into the RPV whereas a reduced gas flow is vented into the wet wells. During the final almost stationary part of the experiment, nearly the whole gas flow consisted of steam, which was condensed in the PCC tubes removing steam in the same order of magnitude than produced in the RPV, which resulted in ceasing the inflow of air into the wet well gas space and consequently the pressure increase in the primary system. Further details on the description of phase -A- can be obtained from Refs [4.6-8] and [4.6-9].

The phenomena, which may be expected during this test, are:

- System pressurization due to a delayed startup of the passive containment coolers (PCCs);
- Injection of a hot steam jet into the cold air atmosphere of both drywell vessels. This includes:
  - Gas mixing and/or stratification in the drywell vessels and in the gas spaces of the two wet well vessels;
  - Steam condensation on walls for a wide range of gas flow rates and non-condensable gas (air) fractions;
- PCC performance. This includes:
  - Steam condensation in tubes for a wide range of gas flow rates and non-condensable gas (air) fractions;
  - Air/steam venting from drywell to wet well pools, gas plumes in the wet well pools.

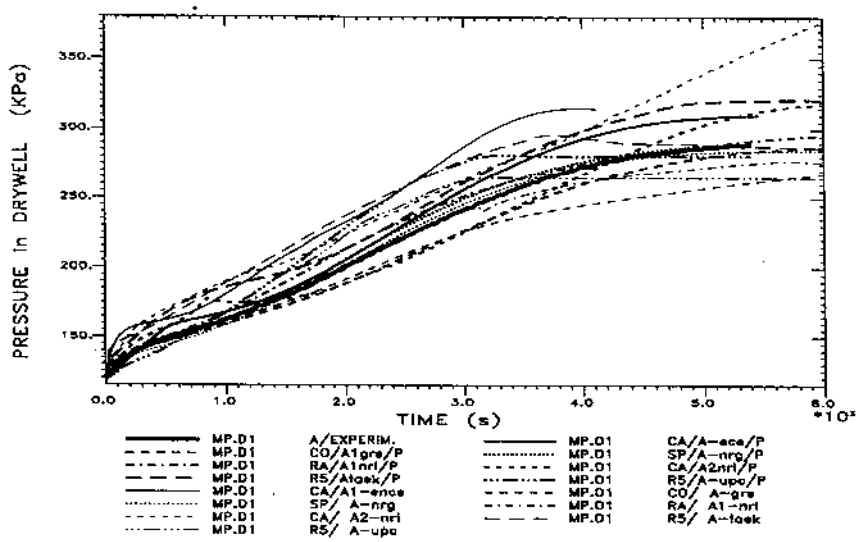

FIG.. 4.6-6. Comparison of drywell pressure calculations (blind and open phases) with experimental data for Phase A of ISP-42.

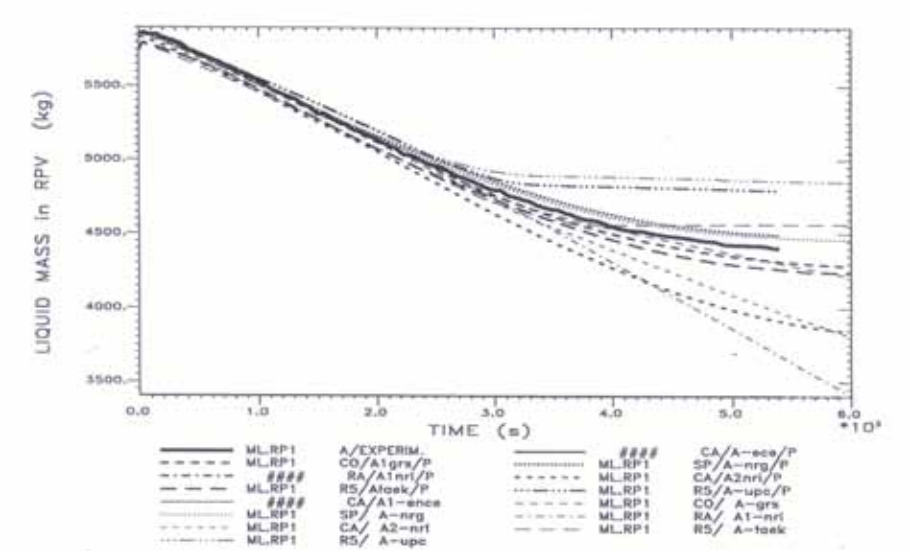

FIG. 4.6-7. Comparison of liquid mass inventory predictions (blind and open phases) with experimental data (Reactor Pressure Vessel) for Phase A of ISP-42.

The time behaviour of the pressures defines the response of the whole system to the specific transient and it is the first item of the phenomena to be investigated as well as the main parameter with respect to safety issues. As may be seen in Fig. 4.6-6, all ISP-42 phase-A test participants except one predicted the right time behaviour for the system pressure (i.e. a steady increase followed by a turn into a approximately stationary phase when the energy balance has become close to zero). The decrease of the liquid mass inventory in the RPV determines the production of steam, which is injected into the two drywells. The injected steam partly condenses in the drywells (at least at the beginning of the transient) and afterwards mostly condenses on the primary sides of the PCCs. Fig. 4.6-7 shows the comparison of the liquid mass inventory predictions in the RPV to the experimental data. The three Passive Containment Coolers (PCCs) on top of the PANDA building remove the heat out of the primary system by condensing the steam on the primary side and evaporating the water on the secondary side water pools. The amount of steam removed out of the gas space of the primary system (which includes wet well, drywell and GDCS gas spaces) either by

condensing in the PCCs or in the wet well pools, which controls the final system pressure. Therefore, correctly predicting the performance of the three PCCs was one of the key issues for the correct simulation of the whole system, assuming that the influence of air transport to the wet well gas space was correctly modelled and the effect of stratification/mixing in the wet well pool was negligible which is shown as comparison of calculated to experimental data in Figs 4.6-9 and 4.6-10 as axial temperature distribution at 500 s and 4000s of the transient. In addition, Fig. 4.6-8 for the drywell pressure provides some indication of the "User Effect". The same code used by different organizations, in this case RELAP5 and CATHARE codes, produced quite different results as seen in this figure. For further detailed analysis of the comparisons of the calculated and experimental data for ISP-42 Phase-A, interested reader can refer to the Refs [4.6-8] and [4.6-9].

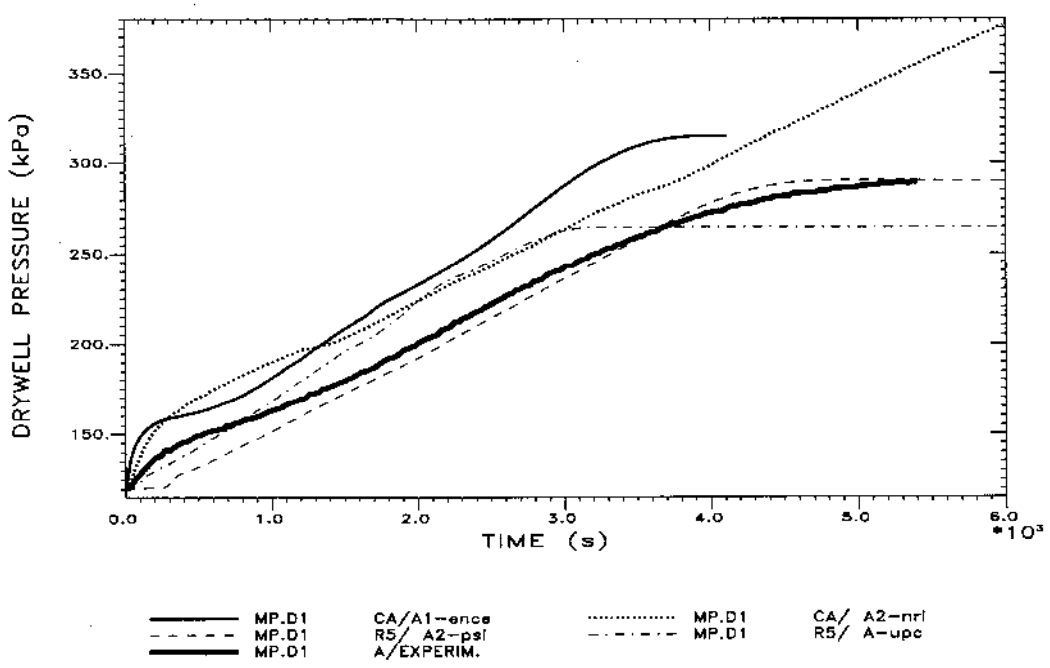

FIG. 4.6-8. Drywell pressure RELAP5/Mod3 and CATHARE code calculations compared to experimental data for Phase A of ISP-42.

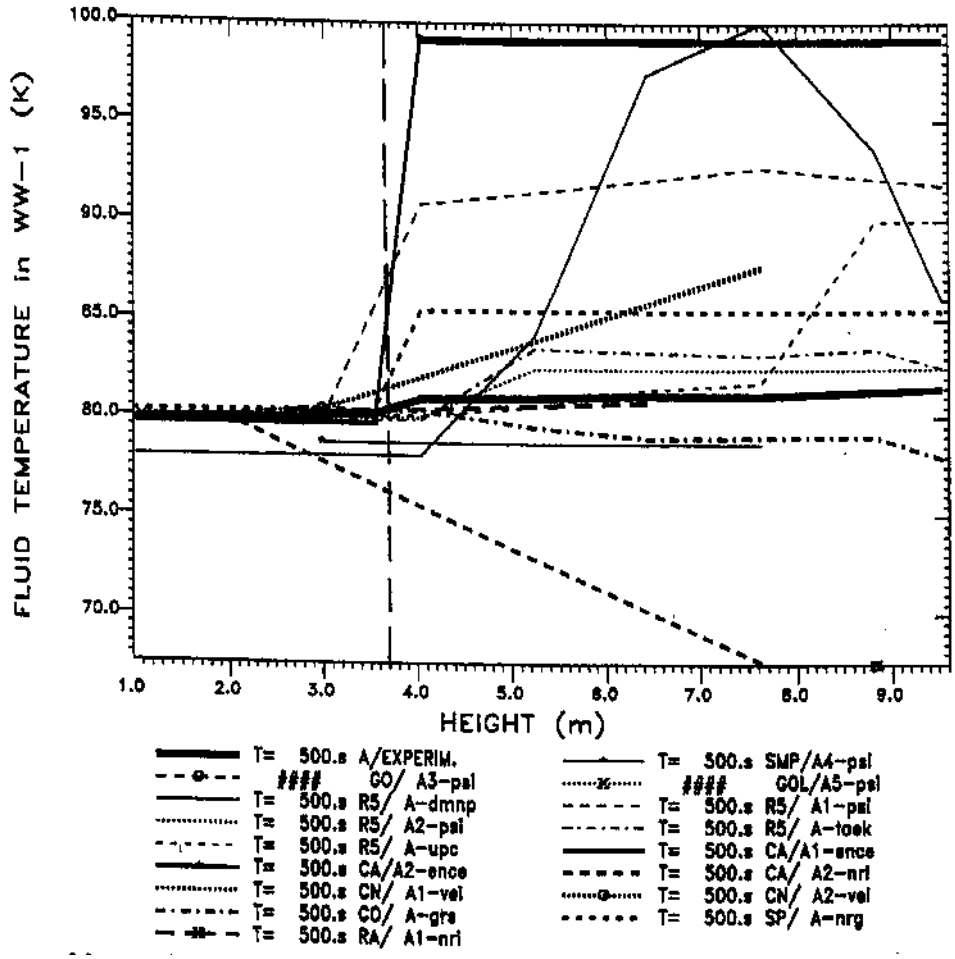

FIG. 4.6-9. Measured and predicted axial temperature distribution in wet well-1 at 500s for Phase A of ISP-42.

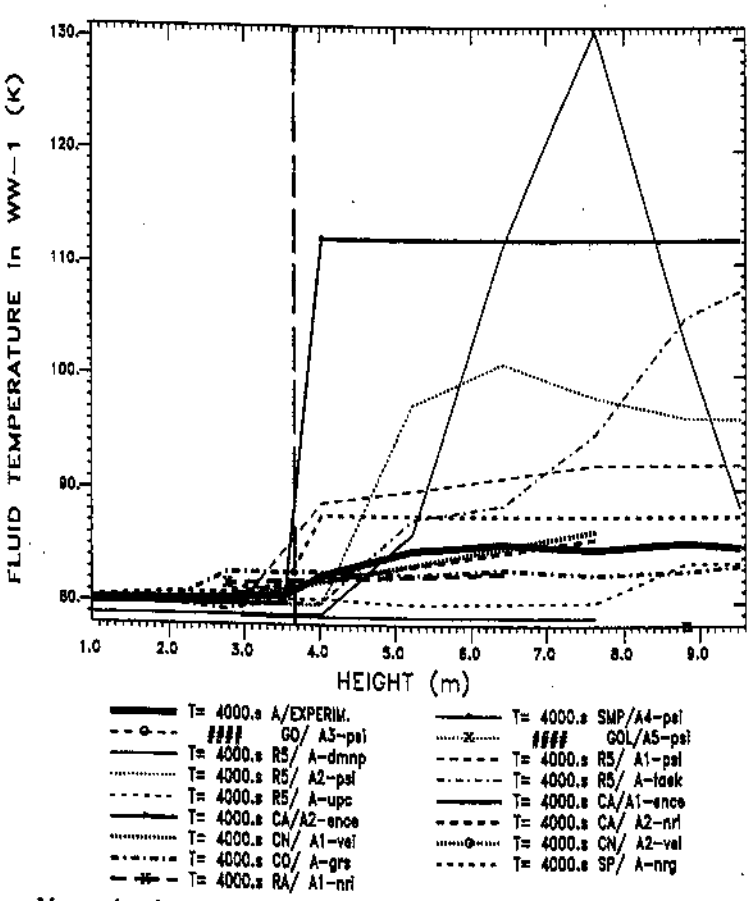

FIG. 4.6-10. Measured and predicted axial temperature distribution in wet well-1 at 4000s for Phase A of ISP-42.

4.6.5. Summary of the major conclusions from ISP-42 PANDA tests

Some of the major conclusions drawn on the basis of the six phases of the ISP-42 post test cases and also covering the "blind" phase results can be summarized as follows (Interested readers should refer to Refs [4.6-8] and [4.6-9] for more detailed information):

- Objectives set at the beginning of this ISP-42 activity have been achieved, even though very demanding efforts needed for such multiple exercises with six different phases.
- Most important parameter in relation to reactor safety, the containment pressure history has been calculated sufficiently correct for most of the ISP-42 participants for all six phases of ISP-42.
- The overall best results were obtained by the lumped parameter code SPECTRA.
- Although system codes like CATHARE or RELAP5 were not designed to calculate typical containment problems in low pressure environments in the presence of large amounts of non-condensibles, they produced acceptable results. Containment code COCOSYS also produced globally acceptable results.
- Some codes (like GOTHIC) had problems to model specific equipment (e.g. PCCs) properly, some tuning of physical models, which needed some knowledge of the facility behaviour, were introduced. The RELAP5 or CATHARE codes were superior with respect to the higher

flexibility to simulate special components and, in this case, specifically the modelling of the PCCs.

- Most of the major deviations could be attributed to problems with the nodalization or simply input errors rather than deficiencies of the specific codes. For example, in the case of RELAP5 and CATHARE, the same code used by different organizations produced quite different results ("user effect" and also different level of experience of the code users).
- It was observed that major attention should be given to provide the appropriate input parameters, which are used in the analysis. As an example, use of loss coefficients and their distribution, especially for low power, low pressure transients as in ISP-42, is a very important factor. Even though experimentally measured data are provided to the code users, due to modelling necessities specific to the computer code used, there could be substantial deviations in the input data. In order to ensure the appropriateness of these types of parameters, every input model could be reviewed as carefully as possible. An important factor is the computer code user's discipline. This discipline cannot be forced, or substituted by Quality Assurance (QA) procedures. But it may help to reduce inappropriate use of some input parameters.
- For simple physical situations (e.g., well-mixed conditions in phase A), choice of a lumped parameter approach is permitted. In such cases, little gain in predictive capability is achieved at the cost of very large computation time for 3-D simulation and detailed nodalizations. Sensitivity studies can help to select the appropriate detailed nodalization and needed sophistication of physical models, and determine criteria for reasonable compromises between accuracy and computing time or costs.
- 3-D models such as in GOTHIC code include right physical representation of phenomena but number of difficulties currently prevents to take full advantage of these capabilities, e.g., accurate calculation of stratified conditions and its effect on system pressure (global parameter). Consequently, further assessment of 3-D models and advanced modelling features (e.g., turbulence) are necessary using well defined separate effects experiments for specific phenomena related to containment multicompartment geometries.
- The use of CFD codes still exploratory, as they usually lack built-in physical models, interfaces (boundary conditions) with other components are difficult to set, and they occasionally show problems with respect to convergence. Consequently, there was no submission with CFD codes.
- The knowledge gained in ISP-42 and other PANDA tests indicated the need to improve and upgrade some of the instrumentation, e.g., improved measurement of injected medium, improved measurement of local concentration of air, helium and steam in the gas spaces of the different PANDA compartments.
- The data set produced for the six phases of the ISP-42 PANDA tests will be used as the basis of assessment of computer codes in relation to the passive containment cooling systems in the next future, at least next ten years. These data will be available to the requesting organizations through NEA-Data Bank and European Community Project CERTA.

4.6.6. Recent and future investigations in PANDA test facility

In this section, the test programs, which are performed in the recent years together with the investigations planned for the future, are provided in brief form. These programs are being TEMPEST, NACUSP, and SETH/PANDA. TEMPEST and NACUSP are performed within the 5th Frame Work Program of EU and SETH/PANDA was performed within a cooperative program of OECD/NEA. Presently a new project called SETH-2 is in progress in cooperation with OECD/NEA.

The primary objective of TEMPEST (Testing and Enhanced Modelling of Passive Evolutionary Systems Technology for Containment Cooling) was to validate and improve advanced modelling methods, with emphasis on CFD and other tools with 3-D capabilities [4.6-10]. It included experimental investigations of the effect of light gases on containment behaviour and of new design

features for accident mitigation, as well as evaluation of the performance of CFD codes and containment codes. The objectives of the PANDA tests in the TEMPEST project were:

- to assess effects of light gases on PCCs and containment performance,
- to investigate new accident mitigating design feature (Drywell Gas Recirculation System, DGRS),
- to provide a database for assessing the capabilities of CFD and other 3-D codes. For this purpose, improved instrumentation (including concentration measurements by means of a mass spectrometer) was installed in the PANDA test facility.

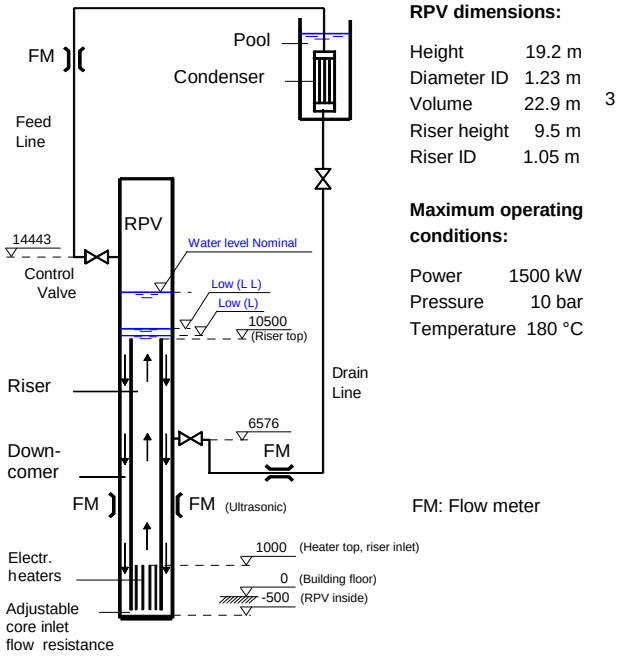

FIG. 4.6-11. PANDA experimental facility, natural-circulation loop and condensation/cooling loop (NACUSP) configuration.

The configuration of the system was similar to that used for the ESBWR tests (Fig. 4.6-2). The DGRS consisted of a fan blower, sucking gas from the vent lines of the PCCs and re-injecting the gas into the Drywell. Total of five tests were performed (including symmetric and asymmetric injection conditions).

The NACUSP project offers the opportunity to validate the codes in relation to the capability to simulate natural circulation behaviour at low pressure [4.6-11]. In the PANDA test facility, 25 tests have been carried out in order to investigate natural circulation and stability, at low pressure and low power conditions. The test configuration (Fig. 4.6-11) includes the Reactor Pressure Vessel (RPV) with core simulator, riser and down-comer and a condenser submerged in a pool, which is used as a heat sink. The configuration used for the NACUSP tests (not using any of the large vessels used for containment tests) demonstrates again the flexibility of the facility, and its multipurpose feature. The tests were performed at a constant power, balanced by a specific condenser heat removal capacity (which was kept constant all over the test period). The test matrix allowed for varying the RPV power and pressure, and also other parameters influencing the natural circulation such as water level in the RPV and the core inlet hydraulic resistance.

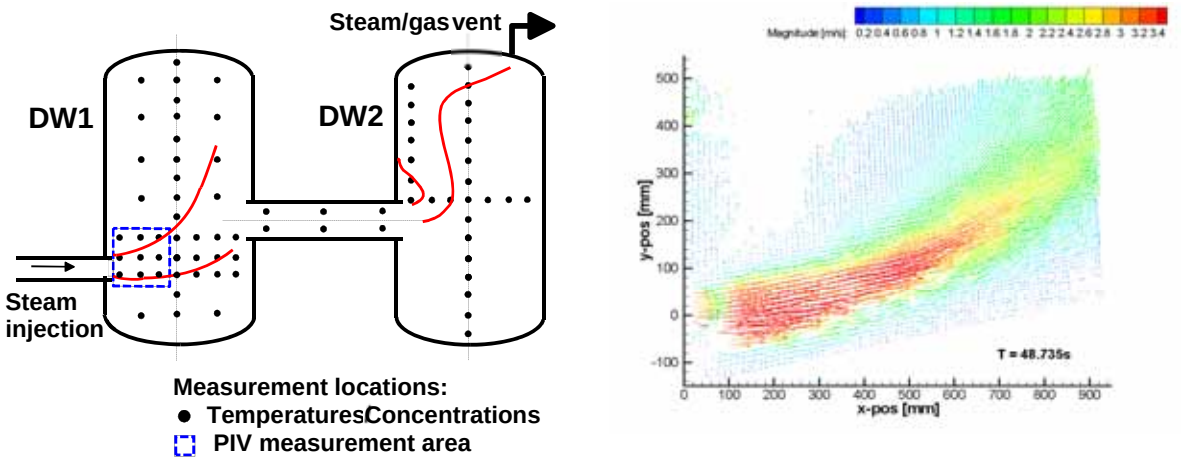

FIG. 4.6-12. OECD/NEA, SETH/PANDA schematic for wall plume test configuration and sample test data.

The OECD/NEA SETH project was an international cooperation project. It had also a component SETH/PANDA and it utilized the PANDA test facility. The program addressed relevant safety issues in both PWR and BWR containment gas spaces with steam and air (or helium to simulate hydrogen) as working fluids. The PANDA facility was used for this purpose with relatively minor hardware changes and several instrumentation improvements. The objective of SETH/PANDA was to provide a better understanding of 3D phenomena and the database needed for the validation of advanced codes through a set of experiments. The experiments aimed to study the mixing and distribution of steam and non-condensable gas (air or helium) in multidimensional, well-defined geometry configurations, at scales approaching those of actual containment buildings or compartments, under a variety of well-established initial and boundary conditions. The tests revealed the nature of mixing and stratification phenomena under accident conditions of interest to current and advanced power reactors and produced data for field code development and validation. The investigations included three series of tests characterized by wall plumes (Fig. 4.6-12), free plumes and horizontal high-momentum jet [4.6-12]. In addition to these series of tests, one specific three-gas test, which is identified in the SETH project as Test 25, with air, steam and helium has been carried out. Analytical activities performed by the project participants aimed at the assessment of strengths and drawbacks of different codes in analysing the phenomena occurring in these PANDA tests. The analytical activities revealed a number of simulation challenges in relation to: gas transport and stratification for the case of high flow exit elevations, prediction of peak gas temperature (mainly in the near-wall plume test series), stratification disruption and erosion for the case of the three gas test, condensation and condensate transport and re-evaporation phenomena. While the SETH/PANDA tests were designed to produce the conditions for stratification buildup, the test program related to the second phase of the project (i.e. SETH-2) the PANDA investigations will deal with stratification break-up. In the SETH-2 project, tests will be made also in the MISTRA Facility (France). The main phenomena studied in the PANDA SETH-2 tests are gas mixing/stratification (Fig. 4.6-13), natural/forced convection, direct-contact/wall condensation, occurring inside LWR containment compartments. Thus, these test series complement the data produced in PANDA SETH, where conditions leading to buildup of stratification were studied. The total number of tests to be performed in the PANDA facility in the frame of the SETH-2 project is 24.

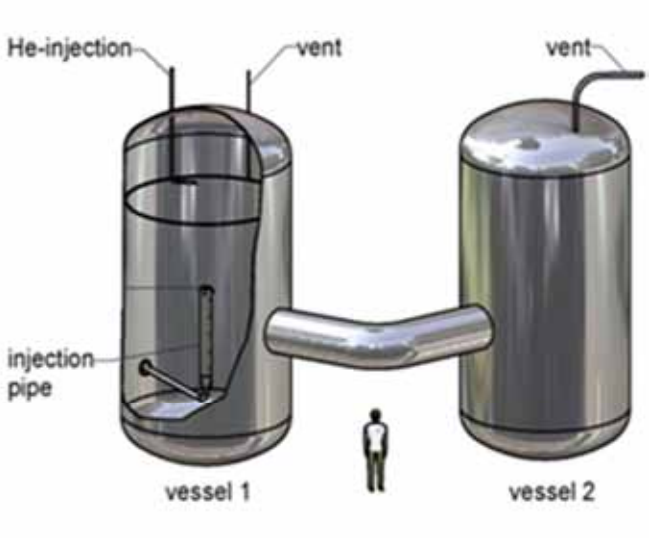

FIG. 4.6-13. OECD/NEA, SETH-2/PANDA schematic for the vertical jet series.

The extensive database established using the PANDA test facility contributes, for the years to come, to further improve containment cooling systems and containment design of passive plants; and allow for system code, containment code and CFD code assessment in a wide parameter range and also for different phenomena.

ABBREVIATIONS

ABWR	Advanced boiling water reactor
ALWR	Advanced light water reactor
CSNI	Committee on the Safety of Nuclear Installations
AP600	Advanced pressurized reactor, 600MWe
BWR	Boiling water reactor
CFD	Computational fluid dynamics
DW	Drywell
ESBWR	European simplified boiling water reactor
EU	European Union
GDCS	Gravity driven cooling system
IC	Isolation condenser
ISP	International standard problem
LOCA	Loss of coolant accident
LWR	Light water reactor
MVL	Main vent line
NEA	Nuclear Energy Agency
OECD	Orgnization for Economic Cooperation and Development
PANDA	Passive Nachwärmeabfuhr- und Druckabbau-Testanlage (Passive decay heat removal and depressurization test facility)
PCC	Passive containment cooling
PCCS	Passive containment cooling system
PWG2	Principal Working Group No.2 on System Behaviour
PWR	Pressurized water reactor
RPV	Reactor pressure vessel
SBWR	Simplified boiling water reactor
SETH	SESAR (Senior group of experts of CSNI) thermal hydraulics
SWR1000	Siedewasserreaktor, 1000MWe
VB	Vacuum breaker
WW	Wet well

REFERENCES FOR SECTION 4.6

[4.6-1] YADIGAROGLU, G., "Derivation of general scaling criteria for BWR containment tests", Proceedings of the ASME-JSME 4th International Conference on Nuclear Engineering (ICONE-IV), New Orleans, Louisiana, USA, 10–14 March (1996) 547–558.

[4.6-2] LUEBBESMEYER, D., et al., "ISP-42 description of the PANDA-facility", PSI Internal Report, TM-42-98-41, January (1999).

[4.6-3] AUBERT, C., DREIER, J., "ISP-42 PANDA test phases: history of events, boundary and initial conditions, calculational parameters", PSI Internal Report, TM-42-98-40, January (1999).

[4.6-4] DREIER, J., et al., The PANDA facility and first test results, Kerntechnik **61** (1996) 214–222.

[4.6-5] DREIER, J., et al., "PANDA test results and code assessment for investigation of passive decay heat removal from the core of a BWR", Proceedings of the 6th International Conference on Nuclear Engineering (ICONE-6), Paper No. ICONE-6463, 10–14 May (1998).

[4.6-6] HUGGENBERGER, M., et al., "TEPSS related PANDA tests (ESBWR)", Proceedings of a IAEA Technical Committee Meeting on Experimental Tests and Qualification of Analytical Methods to Address Thermohydraulic Phenomena in Advanced Water Cooled Reactors, 14–17 September 1998, Villigen, Switzerland, IAEA-TECDOC-1149, IAEA, Vienna (2000) 267–276.

[4.6-7] DREIER, J., et al., "SWR 100 related containment cooling system tests in PANDA", Proceedings of a IAEA Technical Committee Meeting on Experimental Tests and Qualification of Analytical Methods to Address Thermohydraulic Phenomena in Advanced Water Cooled Reactors, 14–17 September 1998, Villigen, Switzerland, IAEA-TECDOC-1149, IAEA, Vienna (2000) 277–286.

[4.6-8] LUEBBESMEYER, D., AKSAN, N., ISP-42 PANDA tests: behaviour of passive containment systems during the long term heat removal phase in advanced light water reactors; blind phase comparison report, OECD/NEA Report, NEA/CSNI/R(2003) 6 (2003) CD-ROM.

[4.6-9] LUEBBESMEYER, D., AKSAN, N., ISP-42 PANDA tests: behaviour of passive containment systems during the long term heat removal phase in advanced light water reactors; open phase comparison report, OECD/NEA Report, NEA/CSNI/R(2003) 7, May (2003) CD-ROM.

[4.6-10] WICHERS, V.A., et al., Testing and enhanced modelling of passive evolutionary systems technology for containment cooling (TEMPEST), FISA 2001, EU Research in Reactor Safety, Luxembourg, November (2001) 514–526.

[4.6-11] KETELAAR, K.C.J., et al., Natural circulation and stability performance of BWRs (NACUSP), FISA 2001, EU Research in Reactor Safety, Luxembourg, November (2001) 535–546.

[4.6-12] PALADINO, D., et al., "LWR containment safety research in PANDA", Proceedings of the 2008 International Congress on Advances on Nuclear Power Plants (ICAPP'08), Anaheim, CA, USA, Paper no. ICAPP'08-8303, 8–12 June (2008).

4.7. PURDUE UNIVERSITY MULTIDIMENSIONAL INTEGRAL TEST ASSEMBLY (PUMA)

4.7.1. Introduction

The General Electric (GE) Nuclear Energy developed a new boiling water reactor called the Simplified Boiling Water Reactor (SBWR). Major differences between the current Boiling Water Reactors (BWRs) and the SBWR are in the simplification of the coolant circulation system and implementation of passive emergency cooling systems. There is no recirculation pump to drive the coolant in the vessel of the SBWR. The emergency core cooling and containment cooling systems do not have active pump-injected flows. The schematic of the SBWR is shown in FIG. 4.7-1.

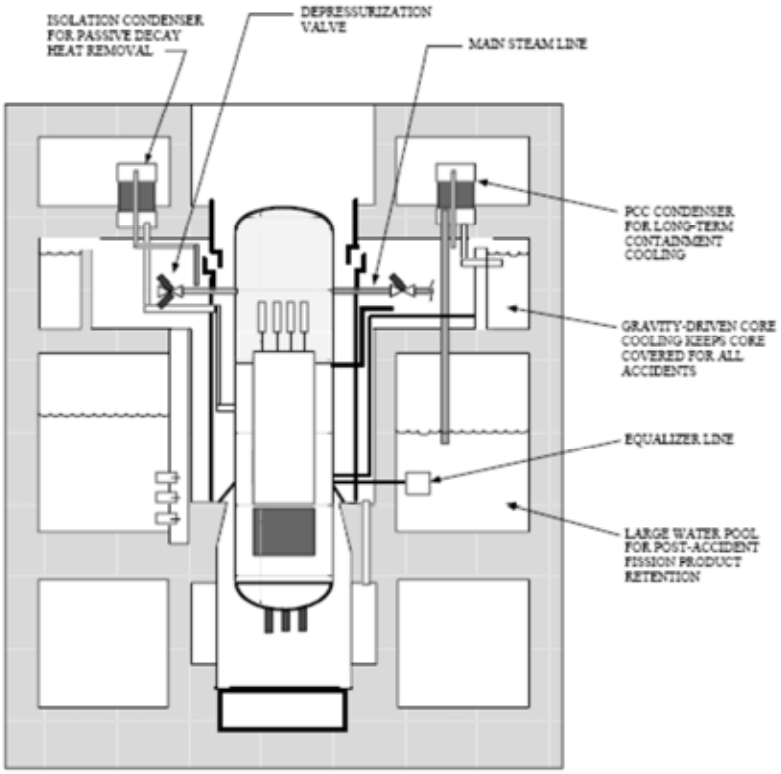

FIG. 4.7-1. Schematic of the SBWR safety system.

There are several engineered safety systems and safety-grade systems in the SBWR which are directly related to the relevant issues and objectives of the PUMA program: (1) the Automatic Depressurization System (ADS), (2) the Gravity-Driven Cooling System (GDCS), (3) the Passive Containment Cooling System (PCCS), and (4) the Isolation Condenser System (ICS). The GDCS and PCCS are new designs unique to the SBWR and do not exist in operating BWRs. The ICS is functionally similar to those in some operating BWRs. Both GDCS and PCCS are designed for low pressure operation (less than 1.03 MPa or 150 psia), but the ICS is capable of high pressure operation as well (up to 7.58 MPa or 1100 psia).

The ADS will be actuated at a prescribed vessel condition and depressurizes the reactor vessel so that the GDCS can be activated to lead to water injection. The goal is to maintain adequate core and containment cooling by preventing core uncovery and dryout of the fuel pins.

The performance of these safety systems under loss of coolant accident (LOCA) and other important transients is a major concern. Since the emergency cooling systems are driven by gravitational head, interactions among the ADS, GDCS, PCCS and other auxiliary systems are important. The emergency cooling systems depend not only on the gravitational head but also on the relative static pressure

differences among the vessel, drywell (DW) and wet well (WW). The phenomena encountered after the initial vessel depressurization in the SBWR are somewhat different from those studied by the nuclear community in existing commercial nuclear reactors.

PUMA facility was initially built to obtain integral test data for the analysis of design basis accidents of GE SBWR for the US Nuclear Regulatory Commission (NRC). The first series of the integral test data were taken for the various LOCA scenarios simulating the SBWR accident transients. The second series of the data were obtained for the design study of the Purdue 200 MWe and 1200 MWe SBWRs under the sponsorship of the US Departments of Energy (DOE). Some results of these tests are presented in this section. Later the facility was modified to simulate the new GE design ESBWR (Economic Simplified Boiling Water Reactor) and the new facility is called PUMA-E (PUMA for ESBWR Application), however in this section only the design of PUMA is presented.

4.7.2. Objectives

The major objectives of the PUMA program are to:

(1) provide integral test data for assessment of the safety analysis code for SBWR or other passively safe BWRs applications,

(2) assess the integral performance of GDCS and PCCS,

(3) assess relevant SBWR phenomena important to LOCAs and other transients.

The focus of the PUMA integral test program during DOE sponsored period is to obtain experimental data of the important phenomena expected in the SBWR design, which can be used for the assessment of the safety analysis code. The objective of the scaling study is to provide a facility design that can reproduce the phenomena which occur during both the later stages of depressurization of the SBWR Reactor Pressure Vessel (RPV) and during the functioning of the gravity-driven safety systems.

The particular focus of the integral experiments is to obtain data on the performance and interaction of the GDCS and PCCS, the maintenance of the coolant level in the RPV, containment integrity, maintenance of the natural circulation, possible occurrence of two phase natural circulation instabilities, the effect of non-condensable gases on PCCS performance and potential impact on the core cooling.

4.7.3. Scaling method for PUMA design

The three-level scaling approach was developed for the scientific design of an integral test facility and then it was applied to the design of the PUMA (Ishii et al. [4.7-1] and [4.7-2]). The present method consists of integral system scaling, whose components comprise the first two levels, and the phenomenological scaling constitutes the third level of scaling. More specifically, the scaling is considered as follows: (1) the integral response function scaling, (2) control volume and boundary flow scaling, (3) local phenomena scaling. The first two levels are termed the top-down approach while the third level is the bottom-up approach. This scheme provides a scaling methodology that is practical and yields technically justifiable results. The basis of the scaling criteria is the conservation principles and constitutive laws.

The scaling laws for forced convection single phase flow are well established. The natural circulation single phase problem was investigated by Heisler and Singer [4.7-3] and Heisler [4.7-4]. The similarity analysis in this case is very complex since there is a coupling of the driving force and heat transfer process. Two phase flow similarity criteria were developed by Ishii [4.7-5], Ishii and Jones [4.7-6], Ishii and Kataoka [4.7-7], and Kocamustafaogullari and Ishii [4.7-8]. The method used in the two phase flow scaling was a perturbation technique along with the steady state solution using the drift-flux model and constitutive relations. The resulting transfer functions were non-dimensionalized, and then the system scaling criteria were obtained. This presents the development of a systematic scaling method for the design of a thermohydraulic integral test facility and for the analysis of experimental data relative to the prototypic conditions. The detailed scaling method is described in FIG. 4.7-2.

Integral system scaling (1st level)

The prototype system consists of multiple interconnected components. The first level of the scaling method focuses on the development of scaling criteria for each component using the response function scaling (Ishii et al. [4.7-1] and [4.7-2]). It is assumed that each component can be mathematically described as one dimensional system. A combination of the single phase formulation and the drift-flux two phase flow formulation is used to express the conservation principles of mass, momentum and energy.

The system conservation equations are solved under a transient condition using a linear small-perturbation analysis. The solution yields various transfer functions between variables, for example between the inlet flow, void fraction, enthalpy, and pressure. It is noted that these transfer functions describe the system dynamic responses. The similarity criteria are developed by non-dimensionalizing the transfer functions and then by identifying the conditions to make the non-dimensional transfer functions to be identical between the prototype and an integral test facility. Therefore, it can be said that first level of the scaling preserves the integral response similarity of the whole component system.

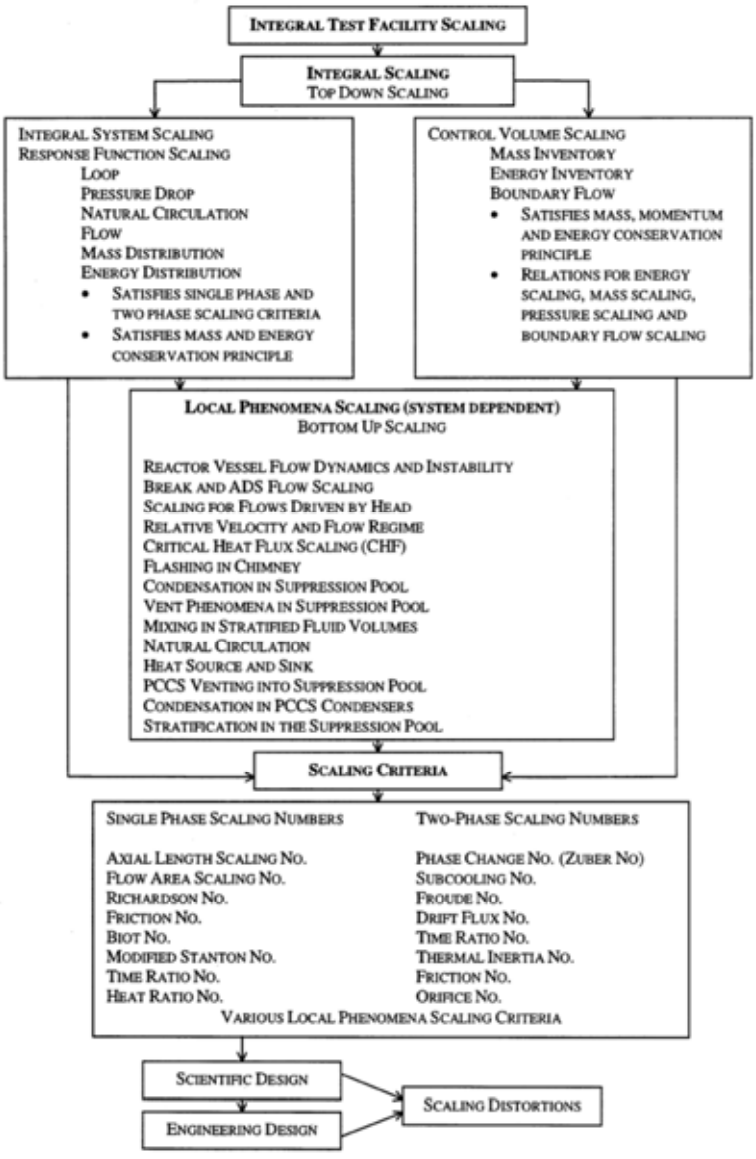

FIG. 4.7-2. Integral test facility scaling methodology flow chart (Ishii et al. [4.7-1] and [4.7-2]).

Mass and energy inventory and boundary flow scaling (2nd level)

A nuclear reactor system such as the SBWR consists of several interconnected components. Therefore, it is essential to simulate the thermohydraulic interactions between these components. The second level of the scaling analysis focuses on the mass and energy inventory of each component and the intercomponent mass and energy transfers (Ishii et al. [4.7-1] and [4.7-2]). This is accomplished by introducing a scaling method based on the control volume balance equations of mass, momentum and energy. The first and second level scaling analyses are, therefore, based on the conservation principles of mass, momentum and energy.

Local phenomena scaling (3rd level)

Although the global scaling criteria satisfy the system response similarity, the local phenomena similarity may not be satisfied. This is due to the fact that in two phase flow various local phenomena have their own internal length scales and the microscale physical phenomena that affect various transfer mechanisms may not be fully represented by a simple one dimensional drift-flux formulation. Therefore, it is necessary to evaluate the key local phenomena and various constitutive relations in terms of scaling. The third level of scaling analyses focuses on the various local phenomena, constitutive laws, and their impact on the overall scaling strategy.

PUMA scaling

At the prototypic pressure simulation, the following relations are obtained from the integral system scaling and the boundary flow scaling results:

$$p_R = 1 \tag{4.7-1}$$

$$a_{iR} = \left(\frac{a_i}{a_o} \right)_R = 1 \tag{4.7-2}$$

$$l_{iR} = \left(\frac{l_i}{l_o} \right)_R = 1 \tag{4.7-3}$$

$$u_R = l_R^{1/2} \tag{4.7-4}$$

$$q'''_R = \frac{1}{l_R^{1/2}} \tag{4.7-5}$$

According to Eqs (4.7-2) and (4.7-3), the major geometric configurations of the scaled model are determined by $a_{iR} = 1$ and $l_{iR} = 1$. This leaves some freedom in choosing the height ratio, l_R, and area ratio, a_R. The overall cost of the facility is reflected by the volume ratio, $v_R = l_R a_R$ and height ratio, l_R.

By examining the previous GE facility and cost, the height of model is scaled by

$$l_R = \frac{1}{4} \tag{4.7-6}$$

and then the volume is scaled by

$$v_R = \frac{1}{400} \tag{4.7-7}$$

The previous GE integral facilities for the SBWR are all full height. The GIST facility is a low pressure, full-height facility with $l_R = 1$ and $a_R = \frac{1}{508}$. The GIRAFFE facility in Japan has $l_R = 1$ and $a_R = \frac{1}{400}$. The PANDA facility has $l_R = 1$ and $a_R = \frac{1}{25}$. The aspect ratio l_R / d_R, for these facilities are 22.5, 20 and 5, respectively. In view of the overall cost, the volume scale of these facilities, friction and structural heat similarities, a PUMA facility at the volume of scale of $\sim \frac{1}{400}$ appears to be optimal.

Since the previous facilities are full height, the impact of the actual total height on various phenomena was evaluated sufficiently. However, the previous facilities fell into the category of thin and tall systems, which have some shortcomings. The reduction in flow area increases the frictional resistance significantly. A flow area ratio of less than 1/200 can have a significant impact on the total frictional resistance. Decreasing l_R for a fixed volume scale can increase d_R. Hence, the reduction in height can effectively eliminate the significant problem in the simulation of the friction number.

The three-level scaling analysis indicates that the reduction in the height does not necessarily distort the natural circulation phenomena because the balance between the driving head and the loop frictional resistance determines the circulation rate. In order to preserve the kinematic and energy similarity, the system velocity and time scales should be reduced by the specified factors in a reduced height system. Under these conditions, the driving head and loop frictional resistance can be matched. The second advantage of using the reduced height system is that the aspect ratio becomes much closer to the prototypical system. The detailed scaling ratios for PUMA to SBWR are given in TABLE 4.7-1.

TABLE 4.7-1. SCALING RATIOS BETWEEN PROTOTYPE AND PUMA

Description	Parameter	Numerical Value
Pressure Ratio	p_R	1
Area Ratio	a_R	1/100
Length Ratio	l_R	1/4
Velocity Ratio	u_R	1/2
Volume Ratio	v_R	1/400
Power Density Ratio	q'''_R	2
Time Ratio	t_R	1/2

4.7.4. Description of PUMA facility

The PUMA facility was constructed based on the detailed scaling analysis (Ishii et al. [4.7-1]). The PUMA facility contains all of the thermohydraulic components of the SBWR. It can be applied over the range of conditions required for the assessment of the response of the passive safety system. It also addresses the integral system response by simulating the interactions between the different components. The detailed description of PUMA facility is shown in Fig. 4.7-3.

Reactor pressure vessel (RPV)

The RPV is the most vital component in the scaling, design and experiment. This observation is based on the fact that nearly all SBWR safety systems are designed to prevent core uncovery and dryout for

design basis accidents, and that the RPV is the main source of steam/energy inventory in the integral facility. The PUMA RPV is composed of vessel, lower plenum, core plate, core, chimney, separators, dryers and downcomer. The overall height and diameter of the RPV are 6.126 m and 0.597 m, respectively. A schematic of the RPV is shown in Fig. 4.7-4 with the major internal components and their corresponding heights.

The core inlet plate in PUMA is designed not only to match the scaled pressure drop across the core plate, but also to account for the area distortion in the core. The core is composed of (1) core heater rods and (2) bypass. The core accommodates thirty eight heater rods that are placed in three concentric rings. The PUMA chimney has nine partitions at the lower part of the chimney to simulate partitions in the prototypic chimney. The downcomer area extends from the top of the chimney to the lower plenum. The steam separator assembly is located directly above the chimney shroud to simulate the prototypic separator in SBWR.

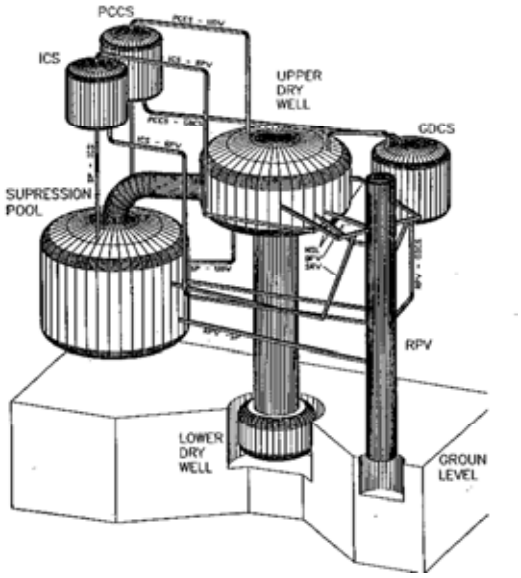

FIG. 4.7-3. Schematic of PUMA facility.

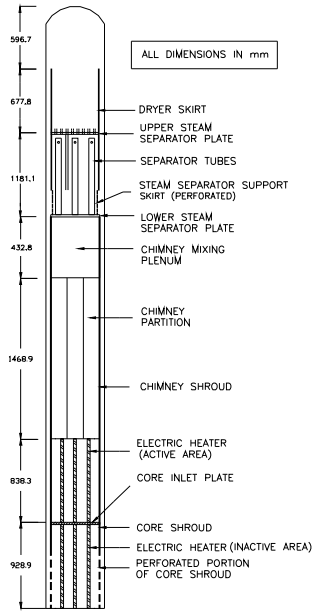

FIG. 4.7-4. Schematic of the RPV in PUMA.

Drywell

The SBWR containment, as shown in FIG. 4.7-1, is a reinforced concrete cylindrical structure which houses the RPV, GDCS, SP, ADS and their related components. The containment structure is divided into a drywell and a SP which are interconnected through vent lines. The prototype drywell consists of an upper drywell volume and a lower drywell volume, which are separated by the vessel support skirt and connected by an open flow area to allow for pressure equalization. The upper drywell surrounds the upper portion of the RPV and houses the ADS, PCCS/ICS piping, GDCS and other related systems.

From the geometrical scaling criteria, the volume of the drywell is scaled by 1/400 and the height is scaled by 1/4. In the present model, the annular geometry of the drywell around the RPV is modeled as a single cylinder. There are two reasons in choosing this design concept. First, if the annular geometry of the drywell were to be scaled as an annulus, the width of the annulus would be scaled by 1/10 due to the geometric scaling consideration. This substantially increases frictional losses due to the reduced hydraulic diameter. Second, construction of a single cylinder is simpler as compared to an annulus. FIG. 4.7-5 shows a schematic of the PUMA drywell and SP.

Suppression pool (SP)

The wet well (WW) consists of the suppression pool (SP) and gas space located above the pool. The SP is a large water reservoir capable of absorbing a large amount of energy by condensing the steam discharged from the drywell during the LOCA or the steam discharged from the RPV due to the SRV actuation. The water serves as an additional source of reactor water make-up through three GDCS equalization lines that connect the SP to the RPV. The SP is connected to the drywell through the vent system, which is composed of eight vertical/horizontal vent modules. In the event of LOCA, the increased pressure inside the drywell forces a mixture of steam, water and non-condensable gases into the SP through vent system. The steam quickly condenses in the pool, and non-condensable gases rise and are collected in the gas space volume in the WW.

The SRV also discharges steam into the SP through discharging piping connected to spargers near the bottom of the pool. The non-condensable gas vent lines from the PCCS and ICS are also routed into the SP.

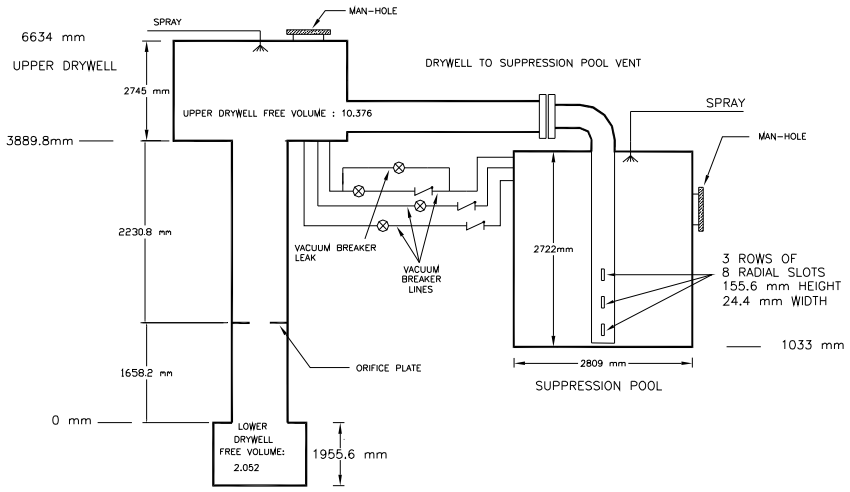

FIG. 4.7-5. Design of the drywell and SP in PUMA.

Similar to the drywell design, the SP in PUMA was designed as single cylinder instead of the annulus as shown in FIG. 4.7-5. A single vertical vent line is centered in the SP with 8 openings at three levels on the perimeter of the submerged line. This simulates the eight prototype vertical vents and the vent openings into the suppression pool. Three vacuum breakers, located on top of the suppression chamber, are connected to the drywell region. The SRV lines, PCCS and ICS vent lines are also submerged in the pool.

Gravity-driven cooling system (GDCS)

As a part of ECCS, the GDCS plays a major role in the SBWR safety mechanisms. The GDCS can be considered as two separate systems: a short term safety system and long term safety system.

The former is designed to provide short term water make-up to the reactor vessel for maintaining fuel cladding temperatures below safety limits. Three separate water pools, located within the upper drywell at an elevation above the active core region, provide gravity-driven water make-up to the reactor vessel.

The long term GDCS safety system is designed to provide the long term vessel cooling by keeping the core region covered with water through gravity-driven flow. This is accomplished through three GDCS equalization lines connecting the SP to the RPV.

For PUMA, the volume and elevation of each of the GDCS pools is scaled using volume and height scaling ratio. Due to the reduced diameter and height of the PUMA RPV, it is also necessary to reduce the number of the GDCS penetrations into the vessel in order to maintain some similarity to the SBWR in the degree of mixing occurring in the downcomer region.

In order to conserve space and simplify construction procedure, three PUMA GDCS pools are designed to fit into a single cylindrical tank. As shown in FIG. 4.7-6, the tank is vertically partitioned into three independent pools, simulating each of three GDCS pools in the prototype. In PUMA, a single line connects the gas space at the top of the GDCS tank to the upper drywell.

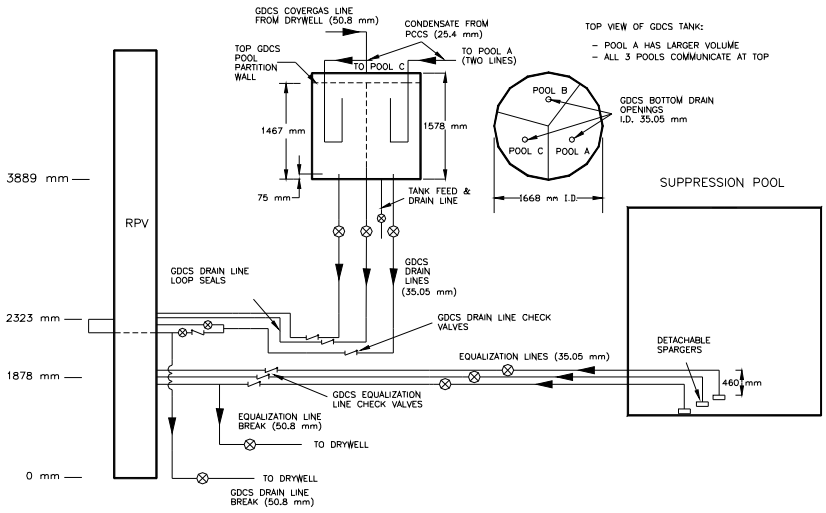

FIG. 4.7-6. GDCS design in PUMA.

Passive containment cooling system (PCCS) and isolation condenser system (ICS)

The PCCS is designed to remove the core decay that is rejected to the containment after a LOCA, whereas the ICS is designed to remove the decay heat from the RPV after any reactor isolation following interruption in normal reactor operation. In the SBWR, a total of three PCCS condensers and three ICS condensers are submerged in a large pool which is located outside and above the containment. The design of the PCCS and ICS condensers is shown in FIG. 4.7-7.

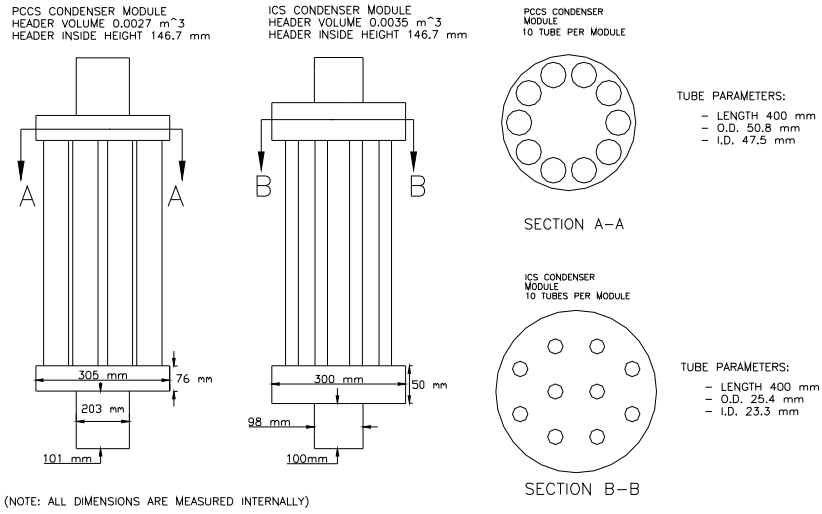

FIG. 4.7-7. Design of PCCS and ICS condensers in PUMA.

In the PUMA, there are three PCCS condensers that are scaled using the power ratio for heat transfer surface area and using the prototypic diameter for the tubes. However, three ICS condensers in the PUMA are scaled using the volume ratio and surface area ratio, but not using the prototypic diameter for tubes, since the ICS condensers are filled with water when it functions. The inlet for each PCCS condenser is connected to the upper drywell. The detailed PCCS design is shown in FIG. 4.7-8.

The inlet of ICS is connected to the RPV via the DPV lines. Since there are two DPV lines in PUMA, one line from the DPV is branched into two lines to allow for a total of three ICS supply lines. The diameter of the ICS steam supply lines is determined by boundary flow scaling.

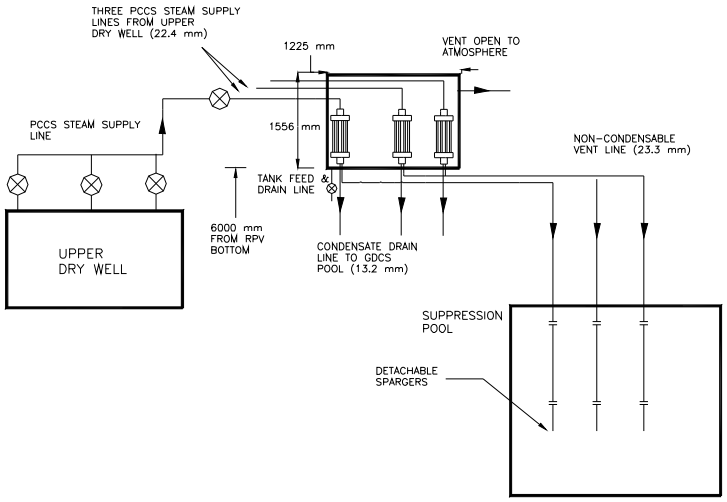

FIG. 4.7-8. Schematic of the PCCS in PUMA.

Automatic depressurization system (ADS)

The ADS is a part of the SBWR ECCS. Its function is to depressurize the reactor so that the gravity-driven GDCS water can be injected into the reactor. The ADS consists of eight Safety Relief Valves (SRVs), six Depressurization Valves (DPVs), and their associated instrumentation and control.

The DPV and SRV lines are connected to the upper drywell and SP, respectively. Full port ball valves with electrical actuators are used for the opening and closing of the SRVs and DPVs in PUMA. These ball valves have response times of 2–5 s. Each of the SRVs and DPVs are instrumented with flow rate, temperature, and pressure measurement devices.

4.7.5. Purdue 200 MWe SBWR design

A new compact modular 200 MWe SBWR was developed by Purdue University (Zheng [[4.7-9]]) under the DOE project. The design involved identification of the principal design criteria dictated by the safe operation of the reactor, identification of coolant requirements, design of reactor system, and design of the engineered safety systems based on passive systems.

The most important feature of the SBWR is the elimination of the re-circulation loop and pumps. Natural circulation cooling is provided in place of pumps. Natural circulation results in an extremely reliable and simple system to produce the steam needed to drive the turbine and generator. There are no active emergency core cooling systems. The reactor emergency core cooling systems are based on gravity-induced flow. Furthermore, the containment cooling is performed by a passive system. Elimination of the re-circulation pumps and loops, internal pumps, and active safety systems substantially reduces the number of piping and valve components and excludes the need for a large emergency AC power supply. These simplifications have considerable potential for reducing the cost of the reactor. In addition, the passive safety systems are more reliable by providing enhanced safety against LOCAs and other DBAs. However, it appears that the 600 MWe size SBWR may not have a large market demand.

In view of the above, some safety study was performed for this new design, namely a compact modular 200 MWe SBWR. This SBWR design has several advantages relative to the existing Light Water Reactor (LWR) systems. First, the BWR is a direct Rankine cycle, which eliminates the need for steam generators. Second, a compact modular SBWR with fully passive safety features is ideal for developing countries. The compact reactor, because of its modular construction approach, requires a shorter construction time, is transportable, can fit remote site application, and requires fewer infrastructures. Third, the significant reduction in the number of pumps and elimination of the requirement for an emergency AC power supply simplifies the plant design, operation and maintenance, as well as overall cost.

The scaling methodology for the design of the SBWR-200 is based on the three-level scaling approach developed by Ishii et al. [4.7-1]. Based on the scaling criteria obtained from the scaling analysis, the design of SBWR-200 has been performed. In this design it was assumed that the new design of the reactor operates at the same pressure as the reference reactor SBWR-600, and the heights of the reactor including reactor vessel, containment, suppression pool, emergency core cooling systems and the condenser systems are the same as the reference reactor design. In TABLE 4.7-2, the thermohydraulic characteristics, fuel characteristics and other reactor components are listed with the design parameters. The ratio of the component parameter with reference parameter is also given in this table to indicate the scaling criteria used in deriving the design parameters.

TABLE 4.7-2. DESIGN AND SCALING CHARACTERISTICS FOR SBWR-200

Design Characteristic	Units	GE-SBWR	SBWR-200	Ratio
Thermal and Hydraulic Reference design thermal power	MWt	2000	660	3.03
Steam flow rate	kg/h	3.89×10^6	1.2758×10^6	3.05
Core coolant flow rate	kg/h	27.2×10^6	8.922×10^6	3.05
Feed water flow rate	kg/h	3.876×10^6	1.2758×10^6	3.04
Absolute pressure, nominal in steam dome	MPa	7.171	7.171	1
Coolant saturation temperature at core	ºC	288.3	288.3	1
Average linear heat generation rate	kW/m	16.6	16.6	1
Coolant enthalpy at core inlet	kJkg	1228.3	1228.3	1
Core inlet temperature at 216.6ºC FFWT	ºC	278.5	278.5	1
Core average exit quality		14.3	14.3	1
Fuel Assembly				
Number of fuel assemblies		732	240	3.05
Fuel rod array size		8x8	8x8	-
Pitch of square rod array	mm	16.2	16.2	1
Fuel Rods				
Number of fuel rods per assembly		60	60	1
Outside diameter	mm	12.27	12.27	1
Core Assembly				
Core diameter	mm	4730	1577	3
Active fuel length	mm	2743	2750	1

The primary and associated cooling systems for the reactor under consideration are briefly discussed here. The containment boundary of the reactor includes the RPV, DW, WW, GDCS, ICS piping, PCCS piping and ADS. The condensers and pools for the ICS and PCCS are located outside and above the containment boundary. The reactor has a unique depressurization scheme in which the ADS system is activated when the RPV water level goes below certain specified value. The ADS, which consists of six DPVs and six SRVs, open in sequence when activated. SP provides pressure suppression during initial blowdown steam load by direct contact condensation. At the time of ADS activation, the injection valves of the GDCS are opened. When the RPV pressure levels with DW/GDCS pressure, the GDCS injects cold water directly into RPV. Any further decrease of water level in the RPV triggers the water injection from SP through the GDCS equalization lines. Thus core uncovery is totally

avoided. For long term cooling the PCCS condenses steam from the containment environment and returns the water to the RPV. All core-cooling mechanisms are based on gravitational head, and hence ensure safety and reliability. In FIG. 4.7-9, the design of the SBWR-200 reactor pressure vessel and containment system layouts are shown.

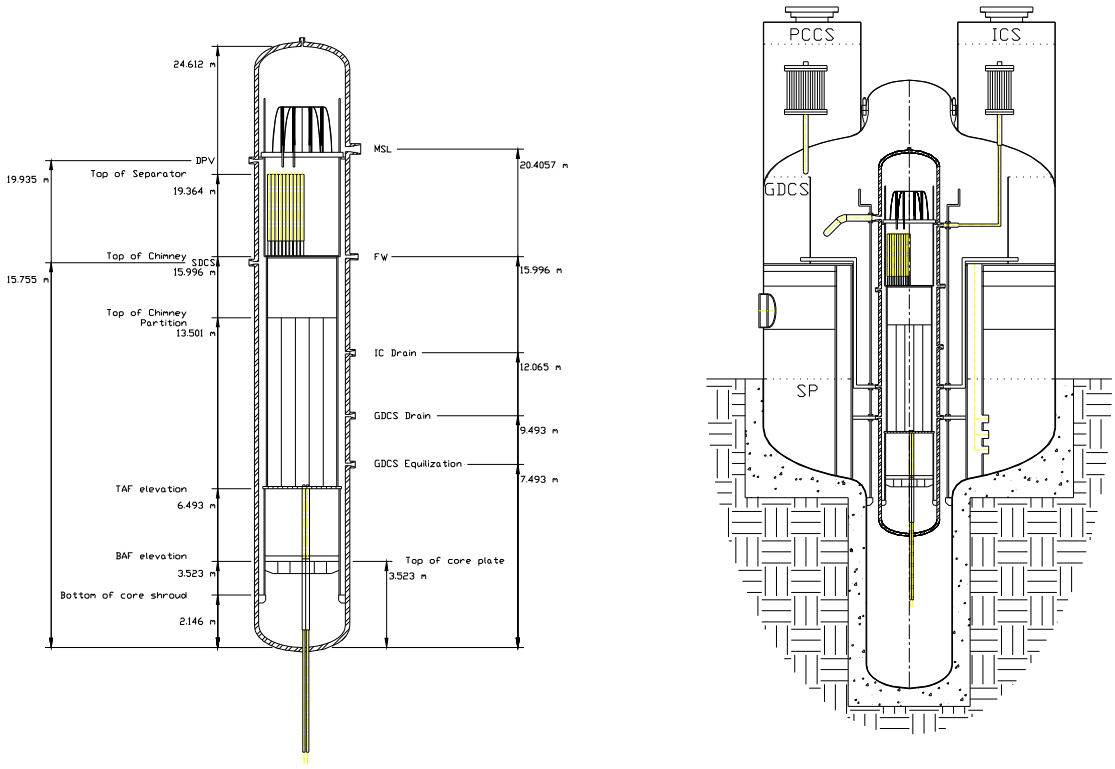

(a) Reactor Pressure Vessel (b) Containment

FIG. 4.7-9. SBWR-200 reactor pressure vessel and containment.

4.7.6. PUMA integral tests for SBWR-200 safety analysis

The SBWR-200 (Zheng [4.7-9]) and SBWR-1200 (Xu et al. [4.7-10]) transient response and safety component behaviours during anticipated reactor transients and accidents are studied through a set of pre-determined design basis accidents under the DOE NERI project. Three kinds of LOCA simulation tests have been conducted at PUMA in the late 90's – Main Steam Line Break (MSLB), GDCS Drain Line Break (GDLB), and Bottom Drain Line Break (BDLB). The MSLB is a well-known design basis accident to investigate the SBWR safety performance under a guillotine break on the main steam line during the plant normal operation. It is a large break LOCA which requires ADS discharging and full functioning of safety systems. The GDLB represents the typical intermediate line breaks inside containment. It is assumed that one out of the six GDCS drain lines undergoes a double ended pipe break. The BDLB represents the typical small line breaks inside containment. The accident is initiated by a break at the joint of the vessel bottom drain line and reactor water cleanup unit. The test matrix for SBWR-200 and SBWR-1200 is summarized in TABLE 4.7-3.

The PUMA facility can simulate a LOCA process below vessel pressure of 1.03 MPa (150 psia). The thermodynamic status of major facility components (RPV, DW, SP, GDCS pool, ICS and PCCS pool) at the test starting point can be predicted by the reactor thermohydraulic analysis code such as RELAP5, because this early blowdown phase of transients has been studied extensively and the code has been well benchmarked.

The RELAP5 input model for the SBWR-200/1200 is developed using plant geometries which are specified from the SBWR-200/1200 preliminary design report. The RELAP5 SBWR model is divided into several distinct sections according to the plant geometries and functions, such as the pressure

vessel, containment and engineered safety components. The primary system is modeled with great detail in order to perform mass and energy inventory analysis. The containment and safety components are modeled relatively simple to saving the computational time.

A steady state running at the normal operation condition is performed to ensure that the RELAP5 SBWR system model has correct initial conditions to match SBWR design. The transient running for the SBWR LOCA is terminated once the vessel pressure reaches 1.03 MPa. The PUMA test initial conditions then can be scaled down from the code predicted SBWR conditions. The facility was then prepared to match this initial condition at 1.03 MPa during the accident.

TABLE 4.7-3. PUMA SBWR-200/1200 INTEGRAL TEST MATRIX

Test Type	SBWR-200	SBWR-1200
Design basis accidents	MSLB	
	BDLB	BDLB
Beyond design basis accidents		BDLB with one PCCS disabled
		BDLB with one GDCS drain line blocked and one PCCS disabled

The objective of this task was to analyse the performance of the safety systems during a transient in the SBWR-200 reactors through code modelling and integral system testing. The focus of the research was the analysis of a major DBA such as a LOCA. The RELAP5/MOD3.2 best estimate system analysis code was used and its applicability to the SBWR-200 reactor safety system evaluation was examined.

Two types of LOCA analyses were performed using the PUMA integral test facilities. These LOCAs are MSLB and BDLB. The PUMA facility can handle transient of the accident from 1.03 MPa (150 psia) pressure to low pressures. Hence initial conditions at 1.03 MPa pressure are required to conduct integral tests. RELAP5/MOD3.2 code was used to obtain initial conditions for integral tests. The RELAP5 input decks for SBWR-200 were prepared and the MSLB and BDLB cases were simulated.

Main steam line break and bottom drain line break LOCAs

MSLB is a well-known DBA to investigate the SBWR-200 safety performance under the abnormal operation condition. It is a large break LOCA that requires ADS discharging and fully functioning of safety systems. Since one of the innovative SBWR-200 safety designs is to transfer most of the DBAs into a large break LOCA via ADS discharge, MSLB is a particular representative case for the SBWR-200 design safety analysis. The PUMA MSLB test schematic is shown in FIG. 4.7-10.

PUMA MSLB tests lasted 8 hours, which corresponded to 16 hours in the plant. After the break on the main steam line B was initiated, coolant inside the RPV quickly flashed and flowed out through the break line. Choking flow was quickly achieved at break section and the pressure on the RPV dropped rapidly under the control of the ADS. This RPV depressurization allowed the injection of the GDCS. The MSLB blowdown phase lasted between 200 and 300 seconds. Following the GDCS injection, highly subcooled GDCS water suppressed the boiling in the RPV. The GDCS drain time lasted for about 3500 seconds. The PCCS started working after the GDCS injection was terminated. The RPV started boiling again due to continued decay heat. The reactor primary system and containment reached a relatively stable pressure level for the remaining period of the test. No significant changes in the system temperature and pressure were observed during the long term cooling phase.

BDLB accident is a design basis small break LOCA in the SBWR-200. The PUMA BDLB test simulated the accident scenario in the SBWR-200 by introducing the break located at the junction between the bottom drain line (BDL) and the reactor water cleanup line (RWCU). The lowest break

elevation is considered to potentially be the most serious DBA in the SBWR-200 design. The PUMA BDLB test schematic is shown in FIG. 4.7-11.

PUMA BDLB test lasted 16 hours. Similar to MSLB, the PUMA BDLB test progression also showed three phases. The ADS actuated immediately after the break initiation. The choking flow occurred and RPV water level dropped below RWCU level. The blowdown phase lasted for approximately 100 s. At the end of the blowdown phase GDCS water started to drain after the DW and RPV pressures equalized and it lasted up to 2750 s. The PCCS and ICS started working immediately after the GDCS injection terminated. After the WW/RPV equalization line opened, the system pressure was stabilized and the long term cooling phase was achieved.

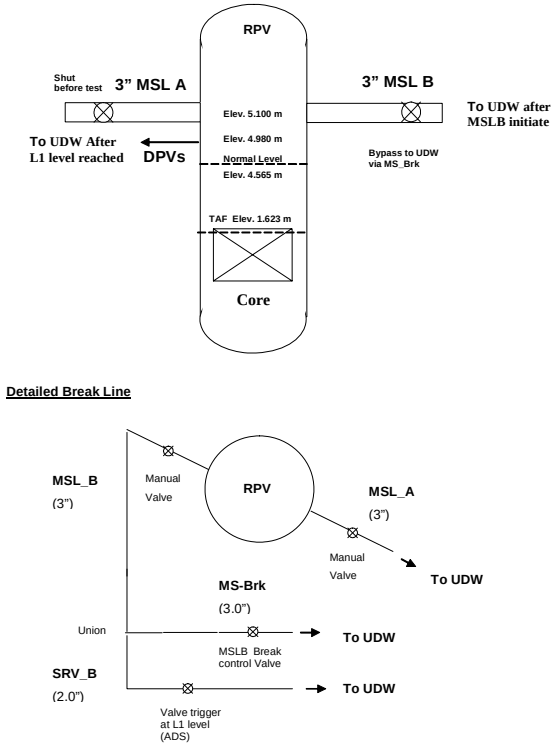

FIG. 4.7-10. PUMA main steam line break schematic.

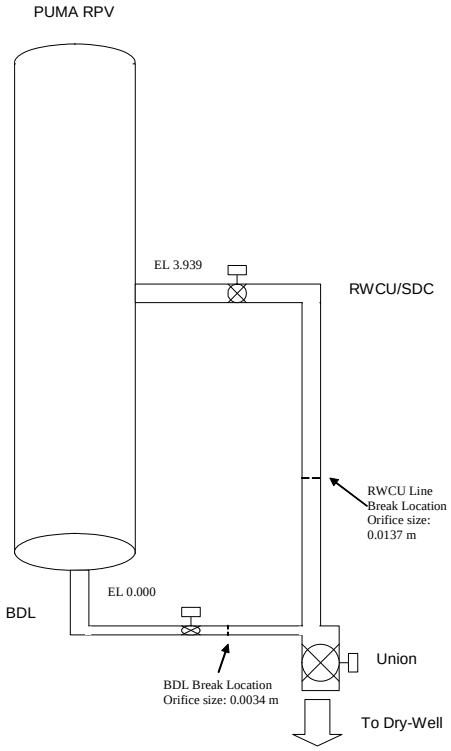

FIG. 4.7-11. PUMA bottom drain line break schematic.

4.7.7. Code applicability analysis for SBWR-200 main steam line break

The RELAP5 code applicability to the small and large break LOCA scenario was examined by comparing code predictions with the PUMA test data. There are three important SBWR-200 safety issues, i.e., the primary system water inventory, the containment integrity and the engineered safety system functionality. In this section, the comparisons between the RELAP5 simulation predictions and the counterpart integral test data are shown with respect to these key parameters.

PUMA MSLB transient calculation was carried out based on the system initial conditions at 1.03 MPa. A long term MSLB transient calculation, up to 30,000 seconds, was performed and the run-time ratio (CPU time to problem run time) of 3.34 was obtained. In the following section key representative test results are presented.

Downcomer collapsed water level

The downcomer collapsed water level, which is the measure of the RPV water inventory, is shown in Fig. 4.7-12. The code predicted downcomer collapsed water level agrees with the test data for all three accident phases reasonably well. In the early blowdown stage of the transient, the downcomer collapsed water level drops due to the break flow out of the RPV. It then increases due to the GDCS injection. The water levels in both test and code prediction show consistent trends in the blowdown stage. The minimum level in the figure corresponds to the starting time of the GDCS injection. It was higher than the Top of Active Fuel (TAF). Since the minimum downcomer collapsed water level was well above the TAF, the core remains covered during the entire transient. This result suggests that the SBWR-200 design is safe from core uncovery for MSLB accident. The agreement of the downcomer water level also shows the primary system mass inventory can be well modeled by REALP5. The general strategy of the SBWR-200 safety is to avoid core uncovery for the DBAs. This should significantly increase the probability of avoiding the core damage.

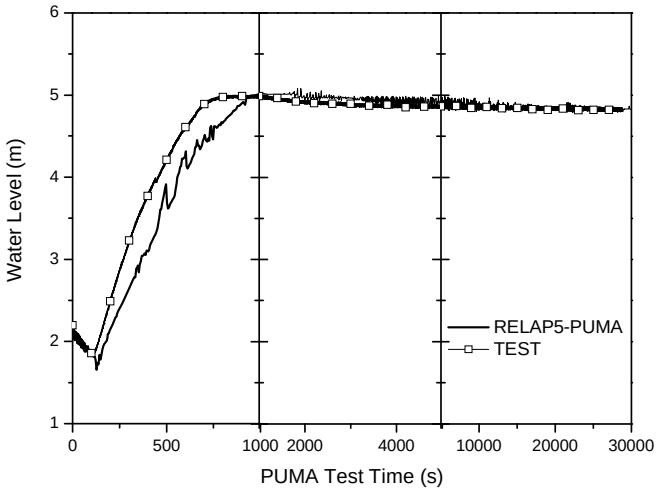

FIG. 4.7-12. PUMA MSLB for SBWR-200, downcomer collapsed water level.

DW pressure

The DW and WW make-up the SBWR-200 containment boundary. The containment integrity is secure whenever pressure inside DW and WW is below the design limit. In most period of the transient, the WW pressure follows the DW. The DW pressure trend is shown in Fig. 4.7-13. According to MSLB test analysis, the DW pressure rises quickly at the initial blowdown stage and equalizes with the RPV pressure. It then decreases because of the GDCS water injection into the core which collapses steam void in the core. The pressure increases again after the GDCS flow terminates and it stabilizes during the long term cooling phase. The code predicted DW pressure shows similar trend as the test data, confirming that the containment integrity is maintained for the entire MSLB transient. However, the predicted DW pressure is higher than the test data in the long term cooling phase. Though the RELAP5 containment pressure prediction is conservative, it may be necessary to improve the RELAP5 models for accurate containment phenomena analysis.

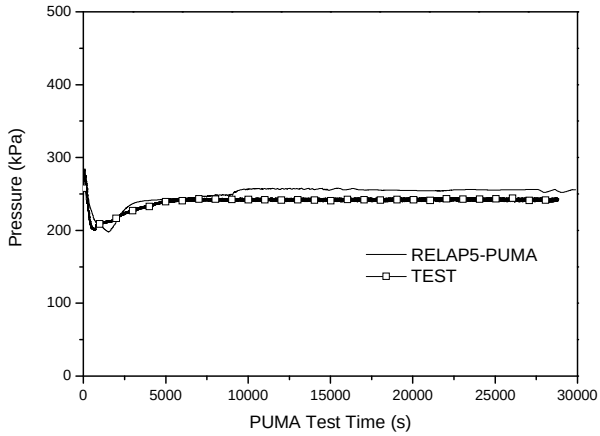

FIG. 4.7-13. PUMA MSLB for SBWR-200, DW pressure.

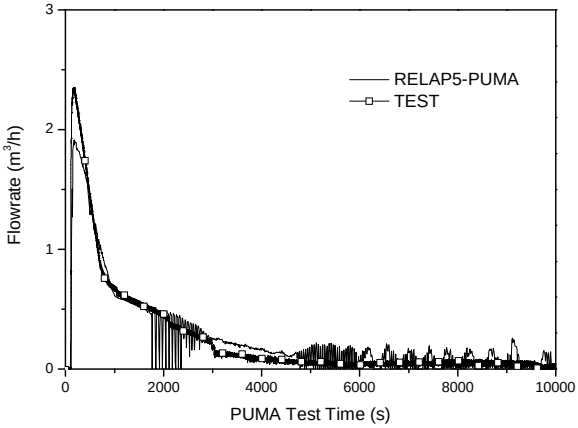

FIG. 4.7-14. PUMA MSLB for SBWR-200, GDCS-A drain injection flow rate.

GDCS drain flow

GDCS is designed as the main emergency core cooling system for the SBWR-200. The GDCS drain flow rate indicates the GDCS behaviour in the MSLB. Figure 4.7-14 shows that the code predicted GDCS flow rate agrees well with the test data. The GDCS starts to drain after the RPV pressure is equalized with the containment pressure. The flow rate change indicates the gravity head change during the drain process. The small flow rate after the main GDCS flow termination is due to the returning flow from the PCCS condensation line. This indicates that the GDCS functions properly as designed. It also indicates that the GDCS drain process is well represented by RELAP5/MOD3.2.

Decay heat removal

PCCS and ICS are two SBWR-200 safety components primarily responsible for decay heat removal in the transients. The PCCS and ICS heat removal rate are plotted with the decay power curve in FIG. 4.7-15. The predicted heat removal rates show that the ICS works primarily on the early blowdown stage while the PCCS functions at the later stage of the accident. The prediction of ICS performance confirms the test data. The comparison also shows that PCCS functions automatically after reboiling of the RPV water, revealing the passive PCCS performance as designed. The PCCS heat removal rate shows the correct trend since it follows the power decay trend. The code calculated PCCS heat removal rate approaches the decay power input at the later transient, which means that the PCCS is the primary heat removal component for SBWR-200 accidents in the long term cooling phase. The experimental data for PCCS show that for a certain period the instrumentation was unstable, but it recovered later.

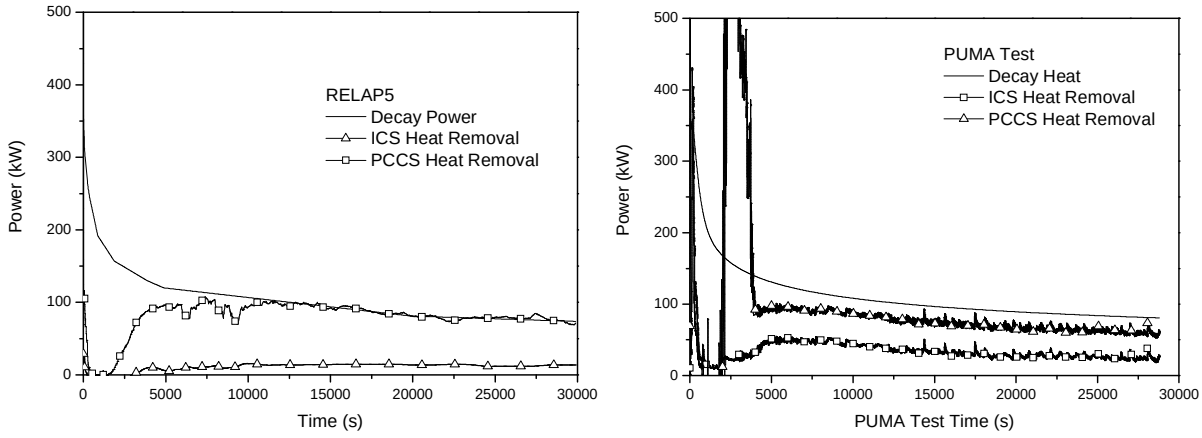

FIG. 4.7-15. PUMA MSLB for SBWR-200, decay heat removal.

4.7.8. PUMA BDLB test prediction

PUMA BDLB calculation simulates 58,500 seconds transient performance. The CPU to problem run time of 8.9 was achieved. The assessment of the RELAP5/MOD3.2 for the BDLB transient prediction was performed with the key parameter comparison similar to the MSLB case.

Downcomer collapsed water level

The downcomer collapsed water level is shown in Fig. 4.7-16. The BDLB is a small break LOCA, however, it is potentially the most challenging LOCA compared to other the larger break LOCAs such as MSLB. As illustrated in the blowdown stage of the transient, the downcomer collapsed water level dropped due to the break flow through the RWCU line. It then increased due to the GDCS water injection into the RPV. The minimum level in the figure is lower than the TAF. This means that possibility of core uncovery for a short period in BDLB LOCA. However, this is unlikely because the two phase level is higher than the collapsed water level. The result also implies that the break elevation is more dominant safety factor than the break size in the SBWR-200 reactor. The code predicted downcomer collapsed water level agreed with the test data for all three accident phases.

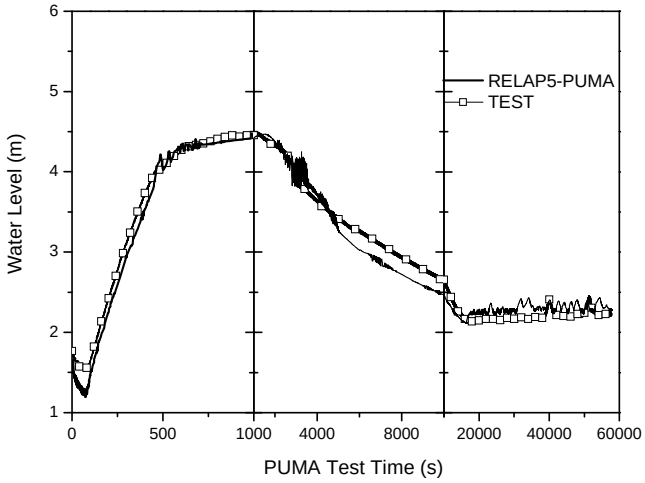

FIG. 4.7-16. PUMA BDLB for SBWR-200, downcomer collapsed water level.

DW pressure

The DW pressure in BDLB modelling result is not as good as the level prediction, though it still preserves the general trends (Fig. 4.7-17). The DW pressure as indicated by both code prediction and test data is well below the design limits confirming that the containment remains secure for the entire BDLB transient. However, the code underpredicts the pressure in the GDCS drain phase and overpredicts the pressure in the long term cooling phase. Though the prediction of the containment pressure in the BDLB case is conservative, it may be necessary to improve the RELAP5 models for accurate containment phenomena analysis.

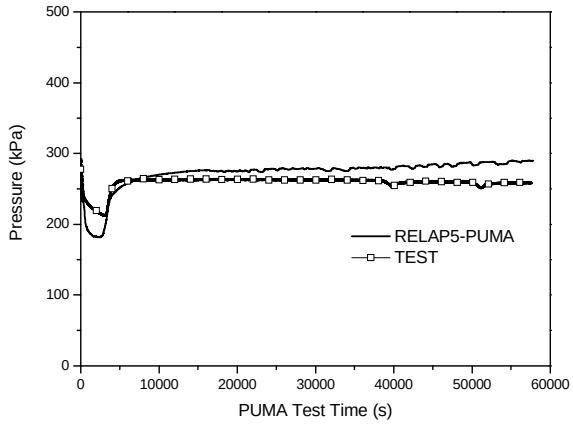

FIG. 4.7-17. PUMA BDLB for SBWR-200, DW pressure.

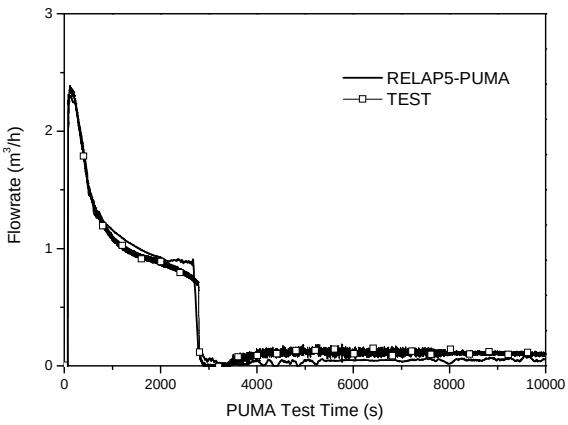

FIG. 4.7-18. PUMA BDLB for SBWR-200, GDCS-A drain injection flow rate.

GDCS drain flow

The GDCS drain flow rate calculated by PUMA BDLB prediction is shown in Fig. 4.7-18. The predicted GDCS behaviour shows good agreement with the test data. The GDCS starts to drain after the primary system pressure equalized with the containment pressure. The flow rate changes according to the gravity head. This indicates that the GDCS functions properly in BDLB case as designed. It also indicates that the GDCS drain process is well represented by RELAP5.

Decay heat removal

The SP functions as the primary heat sink for the initial RPV energy inventory. The PCCS and ICS heat removal rate are plotted with the decay power curve in FIG. 4.7-19. The predicted heat removal rate shows that the ICS works primarily during early blowdown stage while the PCCS functions at the later stage of accident. The prediction of ICS performance confirms the test data. The comparison also shows that PCCS functions automatically after the RPV water is reboiled, revealing the PCCS performance as designed. The PCCS heat removal rate follows the power decay trend. The code calculated PCCS heat removal rate approaches the decay power input at the later transient, indicating PCCS is the primary heat removal component for SBWR-200 accidents during the long term cooling phase.

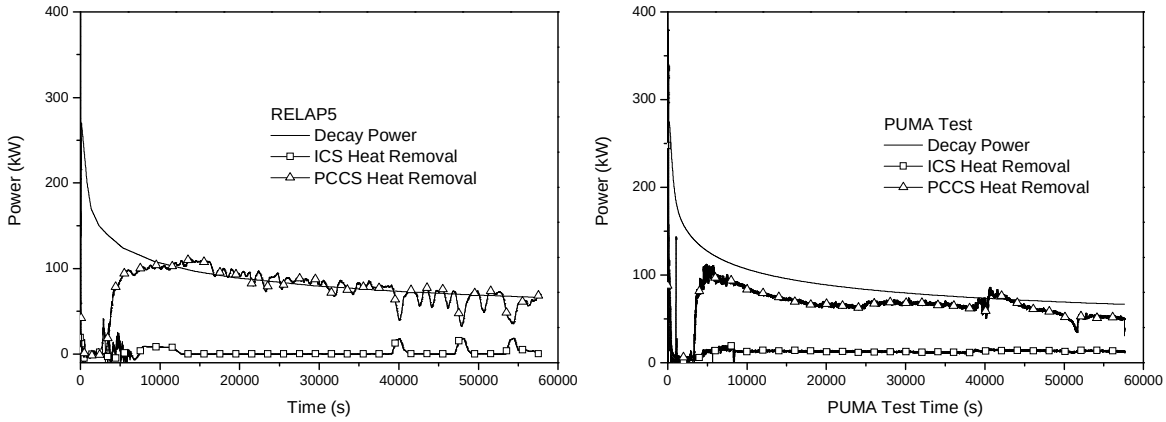

FIG. 4.7-19. PUMA BDLB for SBWR-200, decay heat removal.

4.7.9. Summary

For the proper design of the scaled-down SBWR integral facility, PUMA, the development of a well-balanced and justifiable scaling approach was essential. The PUMA scaling was based on the combination of the top-down approach, focusing on the integral system scaling, and the bottom-up approach, focusing on the scaling of key local phenomena. After the system scaling is completed, the scientific design of the system is performed. In this stage, various practical considerations, including the instrumentation, was considered. The scientific design was translated into an engineering design that meets requirement such as state and local licensing codes, manufacturability, operation and servicing of the test facility.

The study of both single and multiple failure accidents in the SBWR demonstrated the primary reactor safety, as the water level and the containment pressure were maintained below the safety limit. The comparisons of the code prediction by RELAP5 and the test with appropriate scaling considerations illustrated that the code was applicable to safety analysis of the SBWR and the PUMA test facility was well built to simulate the current accident scenarios such as the design basis accidents and some beyond design basis accidents. The scaling methodology applied to the PUMA is also proven to be scientifically justifiable.

NOMENCLATURE

Symbols

a_R	Area ratio
d_R	Diameter ratio
l_R	Length ratio
p_R	Pressure ratio
q'''_R	Power density ratio
t_R	Time ratio
u_R	Velocity ratio
v_R	Volume ratio

Subscripts

i	ith component
o	reference point/component
R	ratio of model over prototype

Abbreviations

AC	Alternating current
ADS	Automatic depressurization system
BDLB	Bottom drain line break
BWR	Boiling water reactor
DBA	Design basis accident
DOE	Department of Energy
DPV	Depressurization valve
DW	Drywell
ESBWR	Economic simplified boiling water reactor
GDCS	Gravity-driven cooling system
GDLB	GDCS drain line break
GE	General Electric

GIRAFFE	Gravity-driven integral full-height test for passive heat removal
GIST	GDCS integrated systems test
ICS	Isolation condenser system
LOCA	Loss of coolant accident
LWR	Light water reactor
MSLB	Main steam line break
PANDA	Passive Nachwärmeabfuhr- und Druckabbau-Testanlage (Passive decay heat removal and depressurization test facility)
PCCS	Passive containment cooling system
PUMA	Purdue University multidimensional integral test assembly
RPV	Reactor pressure vessel
PUMA-E	Purdue University multidimensional integral test assembly for ESBWR application
SBWR	Simplified boiling water reactor
SP	Suppression pool
SRV	Safety relief valve
TAF	Top of active fuel
WW	Wet well

REFERENCES FOR SECTION 4.7

[4.7-1] ISHII, M., et al., Scientific Design of Purdue University Multi-Dimensional Integral Test Assembly (PUMA) for GE SBWR, NUREG/CR-6309, PU-NE 94/1, Technical Report (1996).

[4.7-2] ISHII, M., et al., The three-level scaling approach with application to the Purdue University Multi-dimensional Integral Test Assembly (PUMA), Nuclear Engineering and Design **186** (1998) 177–211.

[4.7-3] HEISLER, M.P., SINGER, R.M., "Facility requirement for natural convection shutdown heat removal system testing", Hemisphere, Washington, DC (1981) 113.

[4.7-4] HEISLER, M.P., Development of scaling requirements for natural convection liquid-metal fast breeder reactor shutdown heat removal test facility, Nuclear Science and Engineering **80** (1982) 347.

[4.7-5] ISHII, M., Thermally Induced Flow Instabilities in Two phase Mixtures in Thermal Equilibrium, Ph.D. thesis, Georgia Institute of Technology (1971).

[4.7-6] ISHII, M., JONES, O. C., Derivation and Application of Scaling Criteria for Two phase Flows, Two phase Flows and Heat Transfer. Proc. NATO Advanced Studies Institute, Vol. 1, Istanbul, Turkey, 25 (1976) 163–185.

[4.7-7] ISHII, M., KATAOKA, I., Scaling laws for thermal-hydraulic system under single-phase and two phase natural circulation, Nuclear Engineering and Design **81** (1984) 411–425.

[4.7-8] KOCAMUSTAFAOGULLARI, G., ISHII, M., Scaling criteria for two phase flow natural and forced convection loop and their application to conceptual 2×4 simulation loop design, Tech. Rep. ANL-83-61, Argonne National Laboratory (1983).

[4.7-9] ZHENG, D., Natural Circulation Reactor Design Safety Analysis, Ph.D. Thesis, Purdue University (2001).

[4.7-10] XU, Y., ISHII, M., FELTUS, M.A., Safety analysis of multiple-failure of passive safety systems in SBWR-1200 SBLOCA, Nuclear Engineering and Design **230** (2004) 107–119.

4.8. NATURAL CIRCULATION CHARACTERISTICS WITH A PASSIVE COOLDOWN OPERATION IN AN INTEGRAL TYPE REACTOR, SMART

The System Integrated Modular Advanced ReacTor (SMART), with a thermal power capability of 330 MW, designed to generate 90 MW of electricity and to produce 40,000 m^3/day of potable water by using approximately 10% of the total energy produced [4.8-1]. The basic design of the SMART and its application system for seawater desalination was completed. Afterwards, a project to construct an integral type reactor, a 1/5 scaled pilot plant of the SMART (SMART pilot plant), was started to demonstrate the enhanced performance and safety features of its design [4.8-2]. The SMART pilot plant adopts inherent safety improving features such as a large volume of the reactor coolant, large negative moderator temperature coefficient, a low core power density, a self-controlled pressurizer (PZR) with N_2 gas, a canned motor main coolant pump (MCP) without a pump seal, and a modular helically coiled once-through steam generator (SG) cassette. In addition, the SMART pilot plant enhances its safety and reliability by incorporating passive design features into the major engineered safety systems such as the passive residual heat removal system (PRHRS), and the reactor overpressure protection system (ROPS).

4.8.1. SMART pilot plant system description

The schematic diagram of the SMART NSSS is shown in Fig. 4.8-1. The SMART pilot plant core design is characterized by an ultra long cycle operation with a single or modified single batch reload scheme, a low core power density, an enhanced safety with a large negative moderator temperature coefficient (MTC) at any time during a fuel cycle, a large thermal margin, inherently free from an xenon oscillation instability, and a minimum rod motion for a load follow with a coolant temperature control. Due to the soluble boron-free operation, a design requirement for the control element drive mechanism (CEDM) is a fine maneuvering capability to control excess core reactivity. A linear step motor type CEDM is employed for an easy maintenance.

Steam generator (SG) cassettes are located in the annulus between the reactor pressure vessel (RPV) and the core support barrel. Each SG cassette is a once-through type with helically coiled tubes wound around the inner shell. The primary coolant flows downward in the shell side of the SG tubes, while the secondary feedwater flows upward in the tube side.

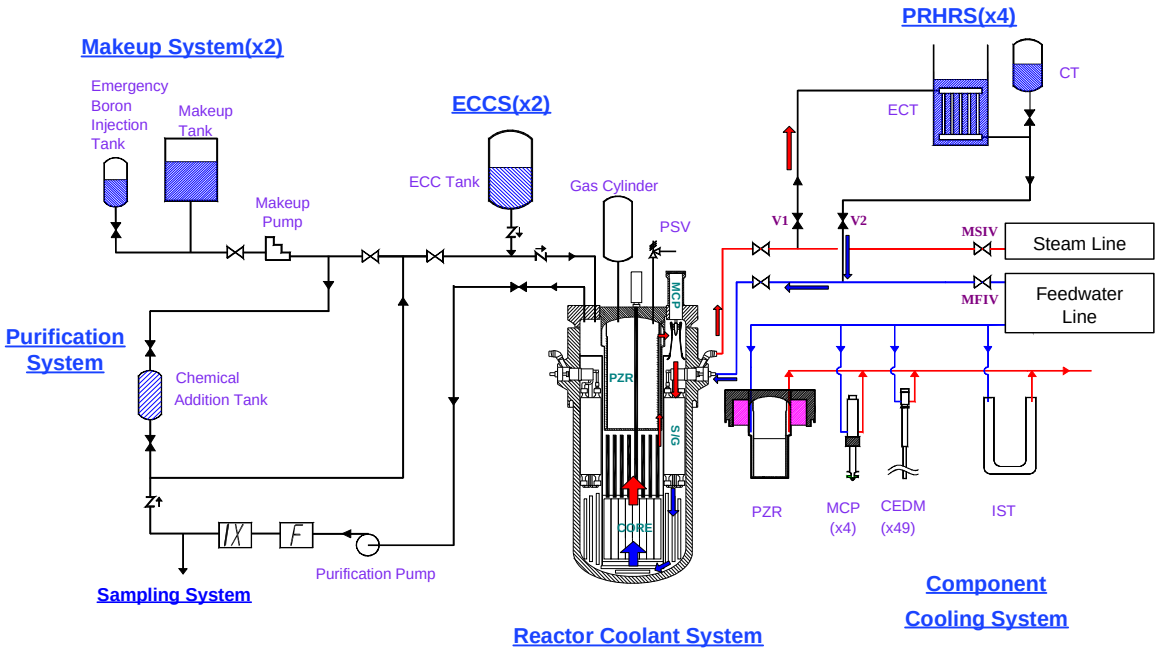

FIG. 4.8-1. Schematic diagram of the SMART NSSS.

The SMART pilot plant adopted an in-vessel self-controlled pressurizer located in the upper space of the RPV. The volume of the PZR is filled with water, steam and nitrogen gas. The self-pressurizing design eliminates a need of active mechanisms such as spray and heater. The system pressure is determined by a sum of the steam and nitrogen partial pressures.

The main coolant pump is installed vertically on the RPV annular cover. The MCP is an integral unit consisting of a canned asynchronous 3-phase motor and an axial flow single stage pump.

The safety systems are designed to meet the redundancy and independency design requirements to ensure a high reliability and safety. The PRHRS cools down a coolant in the reactor coolant system (RCS) by a natural circulation for emergency situations where a normal steam extraction or feedwater supply is unavailable. The safety injection system (SIS) compensates for a coolant inventory loss to ensure that the core is always covered with water in the case of a small break loss of coolant accident (SBLOCA).

The shutdown cooling system (SCS) is designed to remove normal heat and sensible heat in the reactor vessel from a hot shutdown to a refueling condition. When the reactor coolant system temperature reaches 473K and 2.3 MPa, the shutdown cooling system cools the reactor coolant system to a refueling condition.

4.8.2. Loss of feedwater flow transient for the SMART pilot plant

4.8.2.1. Cooldown characteristics

The cooldown capability of the SMART pilot plant is important for the shutdown operation, which needs to maintain a flow in the RCS and the PRHRS by a natural circulation. A cooldown operation period is dependent on the period from a power operation to a SCS entry condition because the system is cooled down by a forced circulation after it reaches the SCS entry condition. There are three kinds of natural circulation circuits in the cooldown operation;

1. A flow path for a natural circulation is established in the PRHRS due to a density difference after an automatic opening of the PRHR isolation valves and a closing of the main feedwater isolation valves (MFIVs)/main steam isolation valves (MSIVs). The refueling water tank (RWT) is located high enough above the SG to remove the heat transferred from the RCS by a natural convection.
2. A natural circulation path is established between the reactor core and the SG primary side in the primary system after the MCP stops. The decay heat generated in the reactor core is transported to the SG primary side by a natural circulation flow.
3. Third, a natural circulation path is established around the heat exchanger inside the RWT. The heat from the SG is transferred to the water in the RWT through the heat exchanger. A hot water which is transferred from the heat exchanger is located at a low part of the RWT and relatively cold water is located at a high position. Therefore, the water is circulated around the heat exchanger in the RWT by a natural circulation.

4.8.2.2. Analysis methods

The thermohydraulic response of the system during a natural circulation transient is analysed by TASS/SMR code which is a system analysis code based on six conservation equations related to a mixture mass, liquid mass, non-condensable gas mass, mixture energy, steam energy and a mixture momentum [4.8-3]. A number of the SMART pilot plant specific models reflecting its design characteristics, such as a helical tube SG, PZR with a non-condensable gas, and a critical flow with N_2 gas, have been addressed in the code. The TASS/SMR code has been developed at the KAERI. The code can incorporate slip effects by using empirical correlations at the flow-paths by means of a user's option. The core power is determined by a point kinetics model, which is used to describe the time dependent response of the core power to consider the reactivity feedbacks. The code has been verified by a comparison with the system analysis code, MARS [4.8-3, 4]. The MARS code, which has

a capability for an analysis of system responses for an integral type reactor, was also developed at KAERI. In addition, the verification work for the TASS/SMR is currently underway by using the experimental data of the VISTA facility. The VISTA facility is a thermohydraulic scaled down experimental facility to verify the performance and safety issues for the SMART pilot plant [4.8-5].

The analysis in this section is performed by the realistic initial/boundary conditions and assumptions summarized in Table 4.8-1. The initial core power and feedwater flow rate are assumed to be 100% of the nominal values. The initial pressures of the PZR and the SG steam are 14.7 MPa and 3.45 MPa, respectively. The primary system liquid temperature at the SG inlet and outlet is 583K and 545K, respectively. The secondary side of the steam generator maintains a steam temperature of 558K. The feedwater flow with 323K is controlled to maintain a constant power of 100%. A realistic set of the Doppler and the moderator density reactivity feedback is used to simulate a power change for a transient.

4.8.2.3. Analysis results

The volume of the SG secondary side of the SMART pilot plant is relatively small compared to that of the commercial pressurized water reactors. The pressure of the SG secondary side increases if the turbine stop valve closes. In addition, the feedwater flow decreases as the pressure of the SG secondary side increases. High SG secondary pressure and low feedwater flow signals are adopted in the trip functions in the design of the SMART pilot plant. In the case of a loss of feedwater flow transient, a trip signal occurs rapidly by a low feedwater flow, then the PRHRS isolation valve is opened and the MFIVs/MSIVs are closed by the low feedwater flow signal.

Assuming a loss of offsite power (LOOP), the MCP begins to coast down and the coolant in the RCS and PRHRS becomes a natural circulation flow from a forced circulation flow as shown in Figs 4.8-2 and 4.8-3. The natural circulation flow rate in the RCS reaches around 5% of the initial flow rate in the early stage and decreases gradually according to the calculation results. The natural circulation flow is stable within around 5 minutes and that in the primary system is similar to the decreasing ratio of the secondary system as shown in Fig. 4.8-3.

TABLE 4.8-4. INITIAL/BOUNDARY CONDITIONS FOR THE ANALYSIS

Parameter	Value
Initial Core Power (% of nominal value)	100 %
RCS Flow Rates (Core/Core Bypass/Total)	316.2/9.8/326 kg/s
PZR Pressure/Gas Temperature	14.7 MPa/384 K
Primary SG Inlet/Outlet Temperatures	583 K/545 K
Initial Feedwater Flow Rate per section	6.006 kg/s
Main Feedwater Pressure/Temperature	4.63 MPa/323 K
Main Steam Pressure/Temperature	3.45 MPa/558 K
Initial CT Pressure	4.5 MPa
Initial RWT Temperature/Water volume	323.0 K/ 300 m^3
Shutdown Reactivity	-8.83 %$\Delta\rho$

The initial feedwater flow rate is 24.02 kg/s and it decreases rapidly to 3.4 kg/s, which is 14% of the initial flow rate. A natural circulation loop is formed within a few minutes and then its flow rate gradually decreases. The PRHRS flow rate is maintained at a minimum of 7 % of its initial value until the RCS reaches the SCS entry condition. When the PRHRS is filled with a single phase liquid, the cooling capability of the PRHRS decreases because the two phase natural circulation changes to a single phase liquid natural circulation. So, the coolant in the RCS should remove the decay heat by a forced circulation through the SCS after it reaches the SCS entry condition.

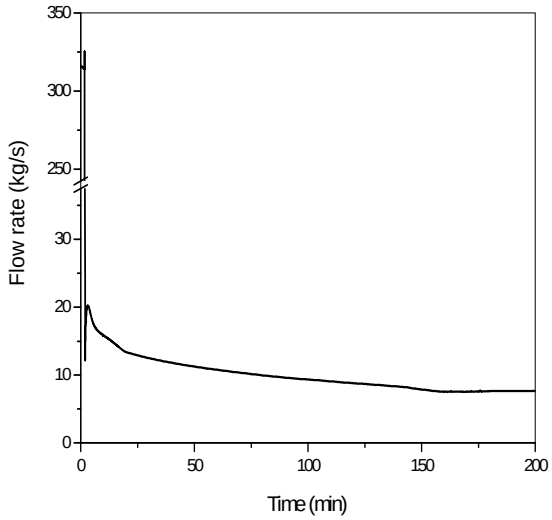

FIG. 4.8-2. Reactor coolant system flow rate.

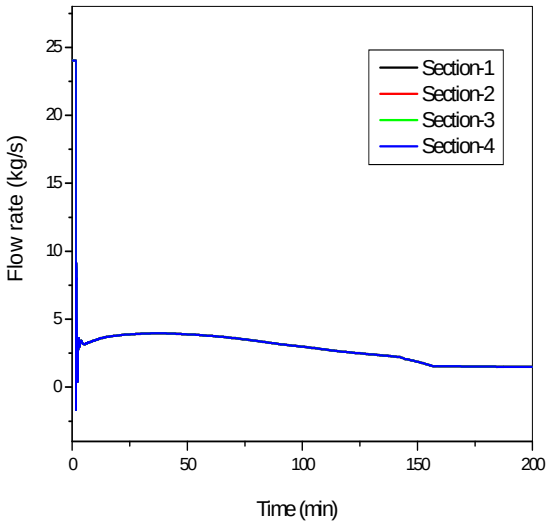

FIG. 4.8-3. PRHRS flow rate.

Figure 4.8-4 shows the coolant temperature at the SG inlet and outlet. The coolant temperature is above 30 K of the subcooling margin for a steady state and it maintains at least 20 K for the transient. The saturation temperature decreases rapidly due to a decreasing system pressure, which is depressurized by an operator's action using an operation of the reactor coolant gas vent system (RCGVS) when the coolant temperature reaches the SCS entry condition, which is 473 K of the coolant temperature at the SG inlet.

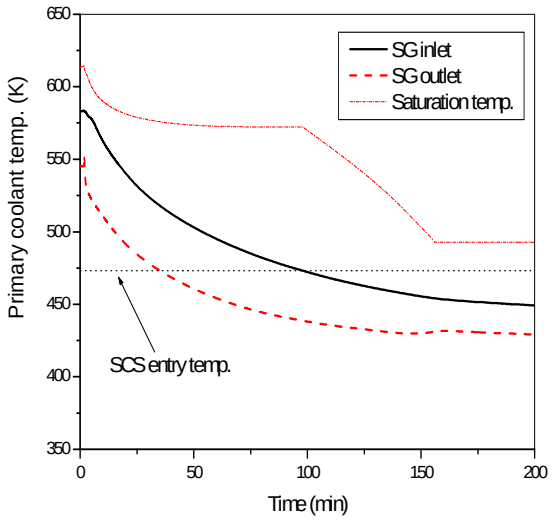

FIG. 4.8-4. Primary coolant temperature.

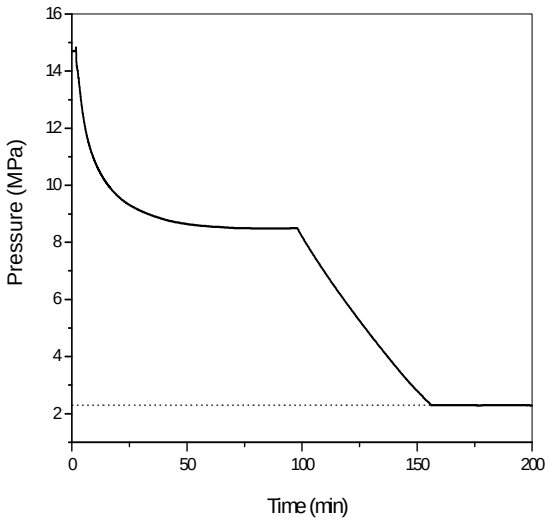

FIG. 4.8-5. Pressurizer pressure.

The pressurizer pressure begins to decrease with the transient and then, it stabilizes at 8.5 MPa as shown in Fig. 4.8-5. However, the system condition needs to be lower than 473 K and 2.3 MPa in order to connect the SCS. The RCGVS is operated to achieve these conditions when the coolant temperature reaches 473 K. Then, the system pressure decreases rapidly to 2.3 MPa.

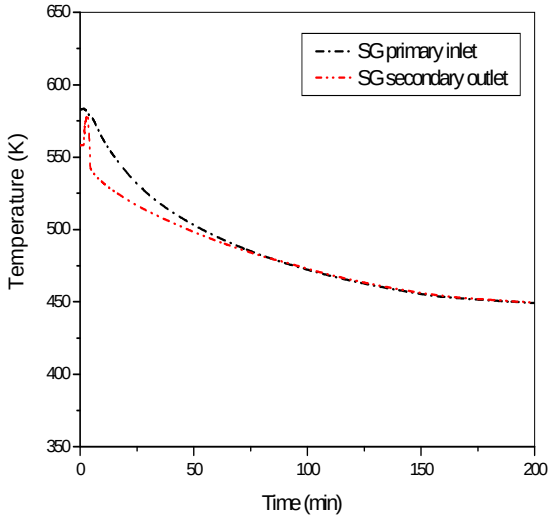

FIG. 4.8-6. Coolant temperature at the SG.

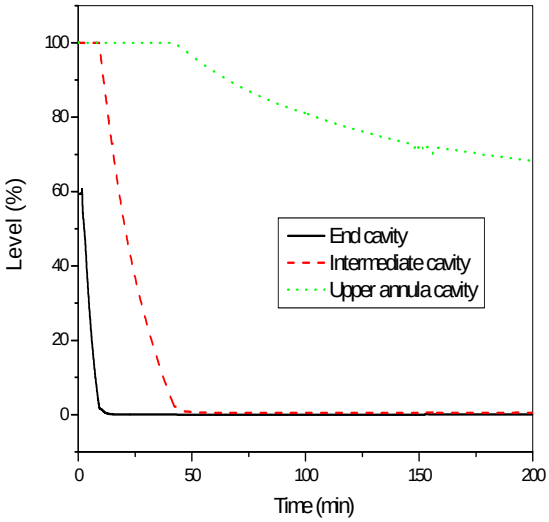

FIG. 4.8-7. Pressurizer water level.

In normal conditions, the SG secondary outlet temperature, which has 43 K of superheated steam, is 25 K lower than the SG primary inlet temperature as shown in Fig. 4.8-6. For the transient condition, the secondary outlet temperature is nearly the same as the primary inlet temperature at a low power. This is a typical behaviour for a helical type steam generator.

The water level at the pressurizer decreases as the RCS is cooled down by a natural circulation as shown in Fig. 4.8-7. The end cavity and intermediate cavity are empty at 8 minutes and 42 minutes, respectively.

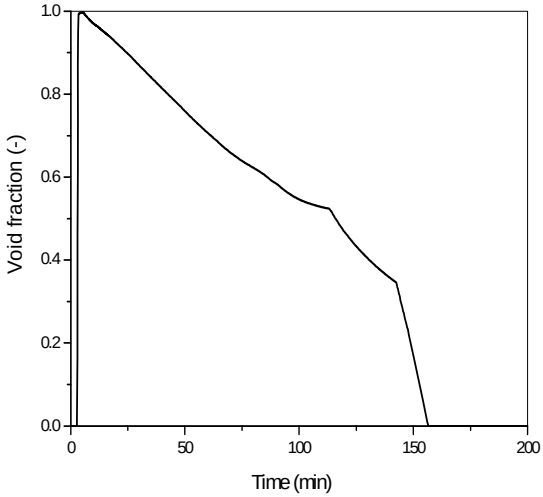

FIG.4.8-8. Void fraction at heat exchanger.

Finally, the water level reaches 70% of the upper annular cavity when the RCS reaches the SCS entry condition.

The PRHRS should perform its function well for a cooldown operation by a natural circulation. Therefore, it is important to maintain a two phase natural circulation to guarantee a suitable operation of the PRHRS. Figure 4.8-8 shows the void fraction at the inlet of the heat exchanger. It is found that a void exists in the PRHRS until the RCS reaches the SCS entry condition at 156 minutes. That is, the RCS is properly cooled down by a two phase natural circulation in the PRHRS. The water in the RWT is a final heat sink for the decay heat transferred through the SG and the heat exchanger. As a result of the transient, the water temperature increases or the water boils in the RWT. In this study, the initial water temperature and the volume are 323 K and 300 m^3, respectively. The liquid temperature increases by 20 K and no bulk boiling occurs. Therefore, the PRHRS can operate in the conditions where the water is not boiled as well as the heat exchanger is submerged in the water in the RWT.

4.8.3. General remarks

The cooldown characteristics and the natural circulation performance of the SMART pilot plant with a passive residual heat removal system have been investigated with realistic assumptions and initial conditions by the TASS/SMR code. A loss of feedwater flow was considered to evaluate the natural circulation characteristics of the SMART pilot plant.

The results of the natural circulation capability show that the RCS and the PRHRS adequately remove the core decay heat and assure an appropriate heat capacity in the reactor vessel by a natural circulation. For the design basis condition, the SMART pilot plant can cool down the coolant to the SCS entry condition within 150 minutes.

REFERENCES FOR SECTION 4.8

[4.8-1] CHANG, M.H., YEO, J.W., ZEE, S.Q., LEE, D.J., PARK, K.B., KOO, I.S., KIM, H.C., KIM, J.I., “Basic design report of SMART”, KAERI/TR-2142/2002, KAERI, Rep. of Korea (2002).

[4.8-2] KIM, S.-H., KIM, K.K., YEO, J.W., CHANG, M.H., ZEE, S.Q., “Design verification program of SMART”, Proc. GENES4/ANP2003, Kyoto, Japan, September 15–19 (2003).

[4.8-3] YANG, S.H., CHUNG, Y.-J., KIM, K.-K., Experimental validation of the TASS/SMR code for an integral type pressurized water reactor, Annals of Nuclear Energy **35** (2008) 1903–1911.

[4.8-4] JEONG, J.J., HA, K.S., CHUNG, B.D., LEE, W.J., Development of a multi-dimensional thermal hydraulic system code. MARS 1.3.1., Ann. Nucl. Energy **26** (1999) 1611.

[4.8-5] CHOI, K.-Y., et al., “VISTA: Thermohydraulic integral test facility for the SMART reactor”, The 10th International Topical Meeting on Nuclear Reactor Thermohydraulics (NURETH-10), Seoul, Korea, October 5–9 (2003).

4.9. MODELLING OF NATURAL CIRCULATION PHENOMENA IN WWER-440/V213 REACTORS

Natural circulation is an essential core cooling mechanism during normal as well as accidental plant operation. In accidental conditions with loss of coolant from primary system but with preserved secondary side heat sink, different modes of natural circulation may take place. Therefore, the dependence of natural circulation on the primary system inventory is of particular interest especially in small break LOCA scenarios, where core cooling at reduced coolant inventory should be ensured. In the particular case of WWER-440 geometry the natural circulation in primary system is influenced due to presence of loop seals in both hot and cold legs of the circulation loops. Furthermore, due to the horizontal steam generators the driving head for the natural circulation is rather small. The PArallel Channel TEst Loop (PACTEL) facility was designed and constructed in Finland to study experimentally thermohydraulic characteristics of WWER-440 reactors. In 1992–1993, the OECD/CSNI standard problem ISP-33 was conducted on the PACTEL facility with the aim to study experimentally natural circulation in VVER-440 over a range of primary side inventory levels as well as to test the ability of thermohydraulic computer codes to analyse this kind of phenomena.

The post-test calculation of the ISP-33 experiment is presented here. This analysis was performed using RELAP5-3D code (version 2.2.4). Taking into account the character of PACTEL facility and ISP-33 experiment, only 1-D capabilities of RELAP5-3D were used. In parallel, an analysis of full scale case was performed for the standard WWER-440/V213 plant following the scenario of counterpart experiment. The analysis of both, scaled-down facility as well as full scale WWER-440/V213 NPP are compared and conclusions are drawn.

TABLE 4.9-1. CHARACTERISTICS OF THE PACTEL FACILITY AND THEIR COMPARISON WITH REFERENCE PLANT

Parameter	PACTEL	VVER-440/V213
Volumetric scaling ratio	1:305	-
Scaling factor of component heights and elevations	1:1	-
Number of primary loops	3	6
Maximum heating /thermal power	1 MW	1375 MW
Number of fuel rods	144	39438
Outer diameter of fuel rod	9.1 mm	9.1 mm
Heated length of fuel rod simulators	2.42 m	2.42 m
Maximum operating primary pressure	8.0 MPa	12.3 MPa
Maximum operating primary temperature	300°C	300°C
Maximum operating secondary pressure	5.0 MPa	5.0 MPa
Maximum operating secondary temperature	260°C	260°C

4.9.1. Description of PACTEL facility

The PACTEL facility (Fig. 4.9-1) is a scaled down model of the 6-loop VVER-440 reactor with three separate loops and full length, electrically heated fuel rod simulators. The reference reactor of the PACTEL is Loviisa NPP. The volumetric scaling factor of the facility is 1:305; elevations are preserved in full height to match the natural circulation gravitational heads in the reference system. The facility was designed to simulate the major components of the primary system of WWER-440 reactors during small and medium LOCAs, natural circulation and operational transients. The reactor vessel model consists of U-tube construction, which includes downcomer, lower plenum, core and upper plenum. The rod bundle simulating the core consists of 144 fuel rod simulators with a chopped cosine axial power distribution and a maximum total power output of 1 MW (22% of scaled full

power). The fuel rod pitch (12.2 mm) and diameter (9.1 mm) are identical to those of reference reactor. Three loops with double capacity steam generators (SG) are used to model the six loops of reference plant. The horizontal U-tubes lengths and diameters of the PACTEL steam generators correspond to those of the full scale plant, but the overall height of tubing is smaller. Basic characteristics of PACTEL facility and reference plant are given in Table 4.9-1.

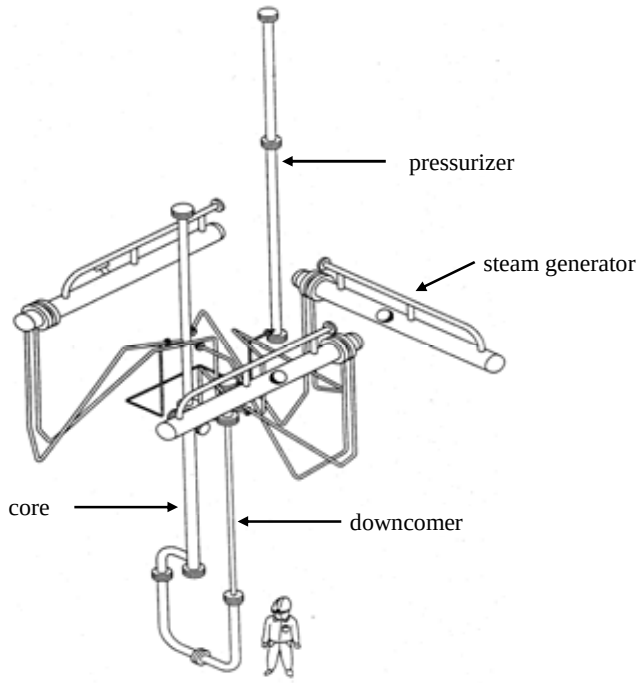

FIG.4.9-1. PACTEL facility – older ISP-33 configuration of the facility.

4.9.2. Differences between PACTEL and WWER-440/V213

Comparing to experimental facilities, which are reduced in scale and simplified, the NPP represents much more complex and complicated system. Main differences between experimental facility PACTEL and reference Loviisa NPP are as follows:

- Reduced volumetric scale (1:305);
- Reduced number of loops (3 instead of 6);
- Lower height of SG tubing (but the full length of SG tubes is preserved);
- Lower importance of 3-D effects than in real facility;
- Higher importance of heat losses and heat capacities, etc.

Besides the above differences there are also certain differences between the reference Loviisa NPP and standard WWER-440/V213 units (e.g. different shape of cold leg loop seals due to different design of reactor cooling pumps). It is obvious that due to above-mentioned differences the response of the scaled-down facility and full scale NPP will be different. A concrete example of such comparison between reduced and full scale results is given here for PACTEL ISP-33 test and its counterpart scenario analysed for full scale WWER-440/V213. For this purpose the initial and boundary conditions applied in NPP analysis were adjusted to ISP-33 experimental scenario as closely as possible — even if such adjustment does not comply with reference state of the NPP (e.g. considering draining valve at the bottom of reactor pressure vessel) or allowed operational regimes.

4.9.3. Description of ISP-33 experiment

The main goal of ISP-33 and the corresponding experiment was to study natural circulation in a VVER-440 primary system including several single and two phase natural circulation modes. Contrary to typical SBLOCA event without ECCS injection with continuous transitions between different natural circulation modes, the primary coolant mass was reduced stepwise in the liquid form from the bottom of reactor vessel and the amount of drained water was given as boundary condition. The heat generated in the core representing decay heat was transported by coolant to the steam generators. The amount of water drained in one step was about 9.5% of initial coolant inventory. The draining periods were very short in comparison with the stabilising period between the two subsequent drain downs (Fig. 4.9-4). That is why the different natural circulation mechanisms were clearly identified during the experiment. The expected periods during the experiment were:

- Single phase natural circulation.
- Two phase natural circulation with continuous liquid flow.
- Natural circulation of boiler-condenser type. Heat is transported by saturated steam to SGs and condensed there. The resulting water is then returned to the reactor pressure vessel via cold legs and the downcomer.
- Cooling of the core with partially superheated steam. The steam generators are still capable of removing the heat from primary system.

The PRZ heaters were switched off after first draining. The secondary side conditions in SGs were held constant; secondary side pressure was controlled by control valve (steam dump to atmosphere) and the SG water level was controlled by operation of feedwater (FW) pump. When the core temperature began to rise and maximum cladding temperature reached 350°C, secondary side was depressurized and the core heaters were switched off (termination of the experiment).

4.9.4. Modelling assumptions for RELAP5-3D

Due to the nature of the facility and ISP-33 experiment, only 1-D capabilities of RELAP-3D code were used for PACTEL nodalization. Similar approach was used also for full scale VVER-440/V213 nodalization.

TABLE 4.9-2. RELAP5-3D NODALIZATION OF THE PACTEL FACILITY

Number of control volumes	286
Number of junctions	308
Number of heat structures	317
Number of mesh points in heat structures	1921

The PACTEL nodalization (Fig. 4.9-2) consists of a pressure vessel and three-loop representation of the facility in which each loop is connected to separate steam generator. The core region is modelled by one single hydraulic channel (instead of three). Nine heated volumes were used in axial direction in order to reproduce chopped cosine axial power profile of the fuel rod simulators. Geometry of the individual loops was modelled precisely in order to enable simulation of asymmetrical behaviour of the loops during experiment (e.g. loop seal clearing). Steam generators heat exchange tubes were lumped into three horizontal layers. A recirculation model of the SG [4.9-3] was used on the secondary side. FW injection was modelled as boundary condition. Having in mind the importance of heat capacities and heat losses in phenomenology of natural circulation in scaled facilities, all important heat structures in primary system (vessel internals and walls) were modelled. Default control flags were used preferably. Basic information about the nodalization is summarized in Table 4.9-2.

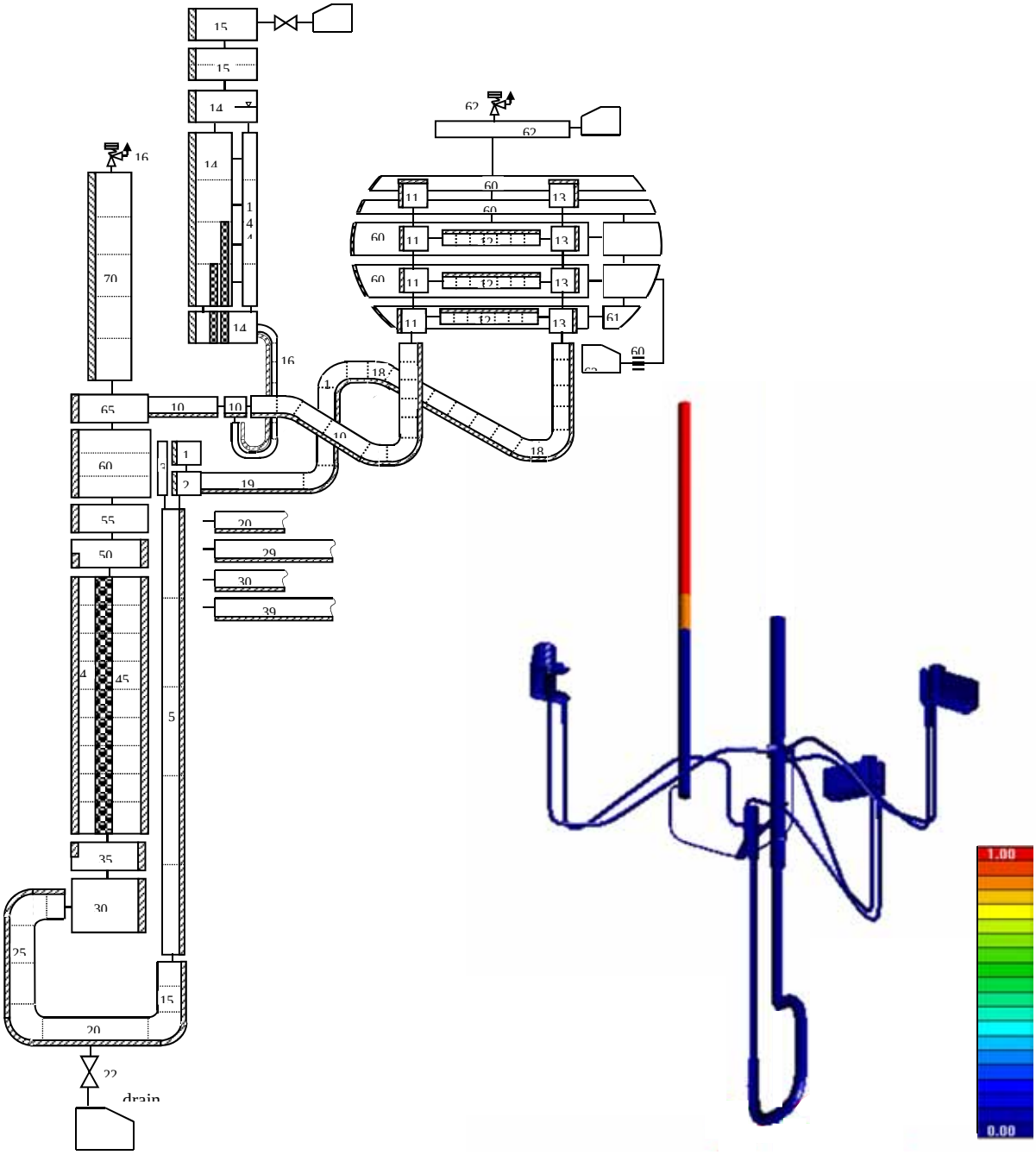

FIG. 4.9-2. PACTEL nodalization.

Model of VVER-440/V213 NPP (Fig. 4.9-3) consists of six-loop nodalization. Experience from experiments performed on PACTEL facility (mainly ISP-33, LOCAs, SG boil-off) was taken into account in nodalization development. The model should be applicable to broad range of applications. Therefore, besides detailed nodalization of the primary and secondary systems, significant attention was paid also to the modelling of core kinetics, ECCS, auxiliary systems, reactor protection system and plant controllers (make-up and let-down systems, PRZ heaters, PRZ spray, FW controller, reactor

power controller, turbine controller, steam dumps to condenser and atmosphere, etc.). Basic information about the nodalization is summarized in Table 4.9-3.

TABLE 4.9-3. RELAP5-3D NODALIZATION SCHEME OF THE VVER-440/V213 NPP

Number of control volumes	891
Number of junctions	995
Number of heat structures	826
Number of mesh points in heat structures	3604

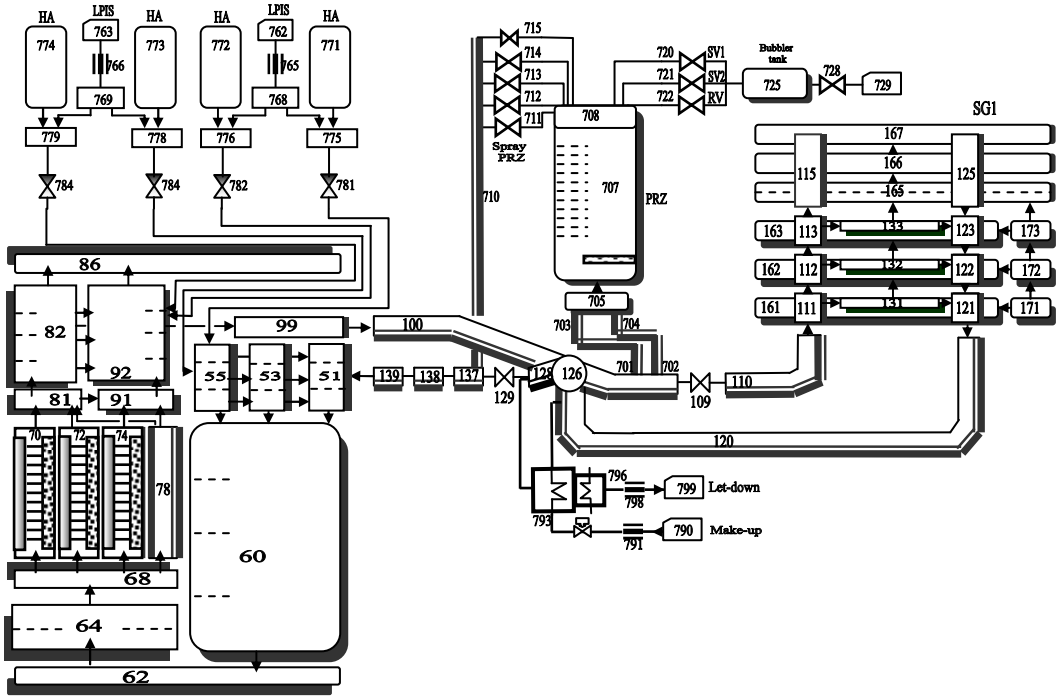

FIG. 4.9-3. WWER-440/V213 plant nodalization.

4.9.5. Results

Experimental results obtained in ISP-33 are described and illustrated e.g. in [4.9-1] and [4.9-2]. Only brief description is therefore given here. The effect of first draining was rapid decrease of the primary pressure (Fig. 4.9-7) until saturation conditions were reached at the core outlet. The flow in the downcomer (Fig. 4.9-5) remained single phase with almost constant flow rate.

During the second draining the amount of vapour in upper plenum increased rapidly. When the swell level in the upper plenum drops below the hot leg nozzles level, voiding also began in the hot legs. Consequently, the flow rate dropped and became stagnant. The hot leg loop seals prevented the vapour from upper plenum to reach the steam generators. Consequently, primary pressure rose sharply. When the pressure increased, water flowed back into pressurizer (Fig. 4.9-6). After short flow stagnation, loop seal clearing occurred. This was repeated two additional times. During the highest pressure spike the setpoint for safety valve leaking was reached and small amount of water (about 10 kg [4.9-2])

escaped through safety valve located on the top of upper plenum. During the 3rd draining pressure dropped and saturation temperature was reached in upper plenum. The PRZ was emptied again, and primary mass flow rate increased. Relatively stable two phase flow was established. The bulk of this flow took place through one loop, though any of the loops was totally stagnant. As the primary inventory was reduced further, the flow rates continued to decline, finally becoming nearly stagnant. The heat transfer mechanism from primary to secondary changed to boiler-condenser mode. Reflux condensation was not observed because of the horizontal SG tubes and loop seals geometry. The core heat-up takes place after seventh draining. As soon as the maximum cladding temperature reached 350°C, the depressurization of secondary side took place. Experiment was completed 140 seconds later in order to protect core heaters.

PACTEL analysis [4.9-3]: Up to the 6th draining, the overall behaviour of the PACTEL primary system was basically well predicted by RELAP5-3D calculation, including the effect of flow stagnation followed by multiple loop seal clearing after 2nd drainage. Since the 6th draining, the water level in reactor vessel predicted by the code is more than 1 m higher than the experimental value. Consequently, in the calculation the core heat up was predicted about 890 s later during the 8th draining (i.e. an additional draining was necessary comparing to experiment). Despite of the time delay, the drop of secondary pressure, the course of primary pressure and water level in reactor were well predicted by code.

Full scale VVER-440/V213 analysis [4.9-4]: The mass flow-rates on Figs. 4.9-4 and 4.9-5 were divided by volumetric scaling factor in order to enable the comparison with experimental results. Up to the 6th draining, the overall behaviour of VVER-440/V213 agrees reasonably with experimental results. The effect of flow stagnation followed by pressure rise and multiple loop seal clearing after 2nd drainage is well predicted, too. However, the maximum value of pressure peaks is lower and the number of pressure peaks is higher than in the experiment. This can be explained by higher (6 instead of 3) number of loops (i.e. higher number of loop seal clearings) in full scale NPP. Collapsed water level in RPV is predicted rather higher than in the experiment. This is due to differences in elevations between PACTEL and standard VVER-440/V213 NPP. Otherwise the course of collapsed water level in RPV, downcomer and PRZ is similar.

After the 6th draining, the water level in reactor vessel dropped deeper than in the experiment and, consequently, core heat up occurred shortly later. There was still relatively large amount of coolant in cold leg loop seals and in lowermost SG tubes at this time. In the experiment an additional 7th draining was necessary in order to initiate the core heat-up. This discrepancy is probably due to differences in geometrical arrangement of cold leg loop seals in Loviisa NPP (reference plant for PACTEL facility) and standard VVER-440/V213 units.

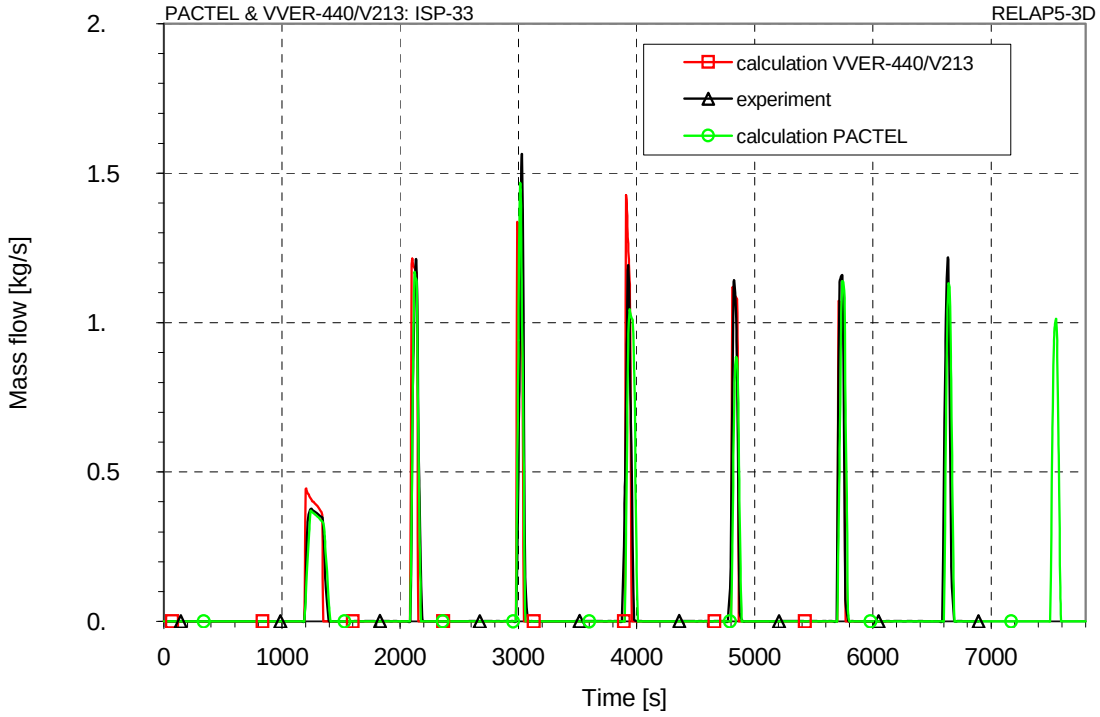

FIG. 4.9-4. Mass flow through the drainage valve.

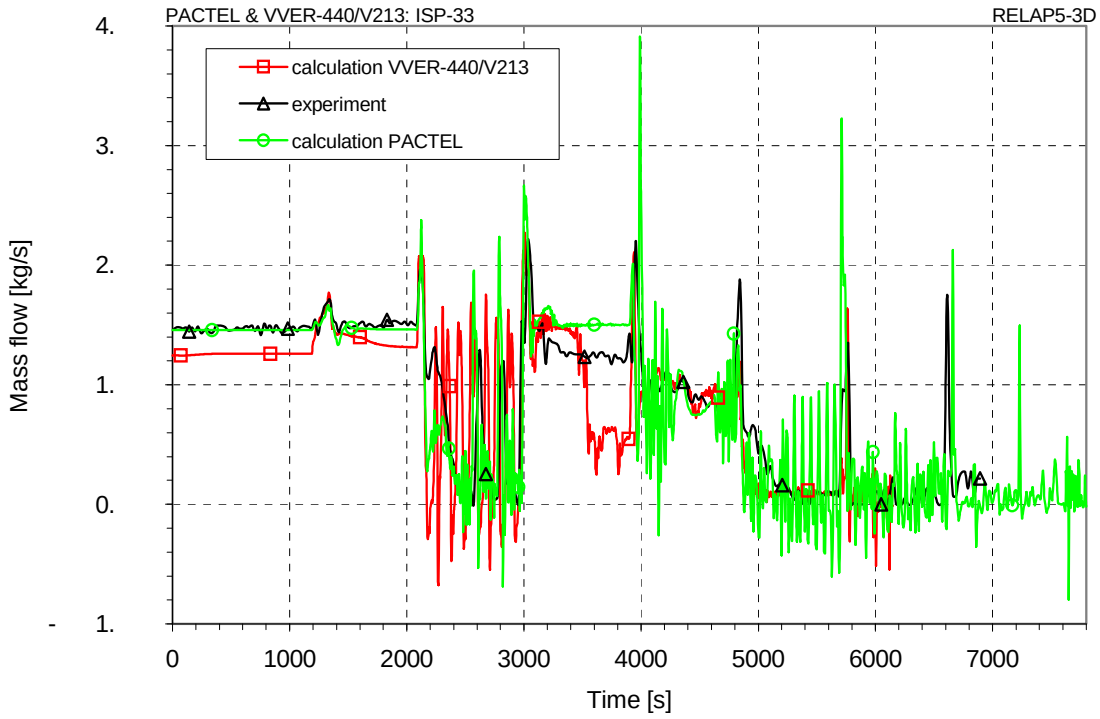

FIG. 4.9-5. Downcomer mass flow.

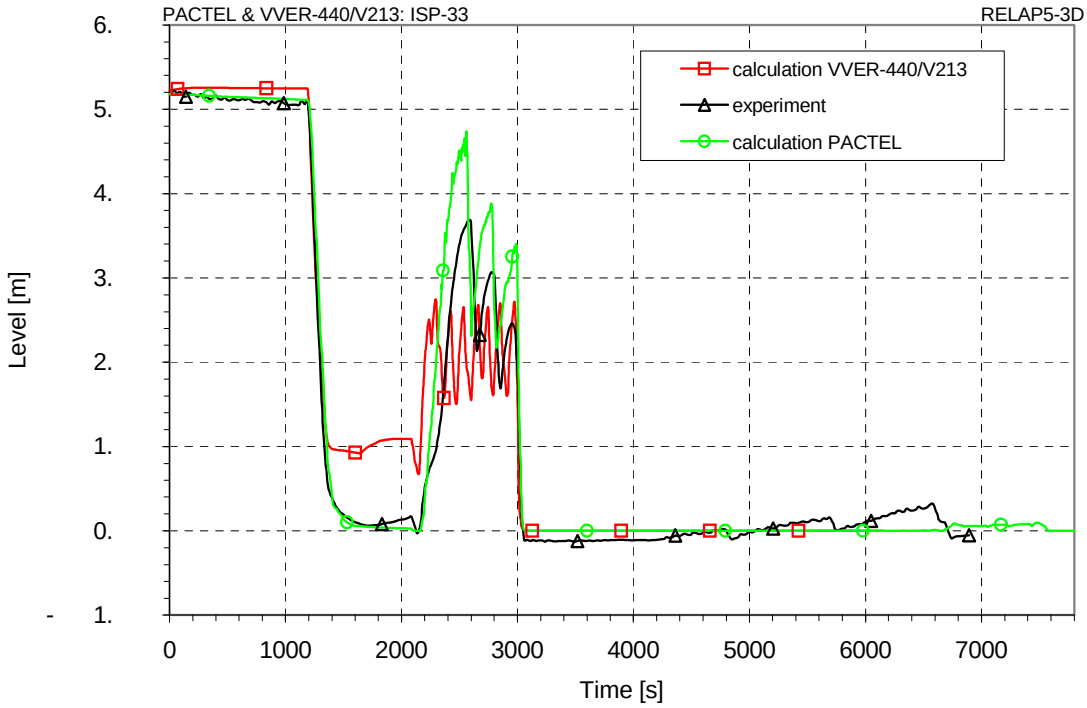

FIG. 4.9-6. Pressurizer collapsed level.

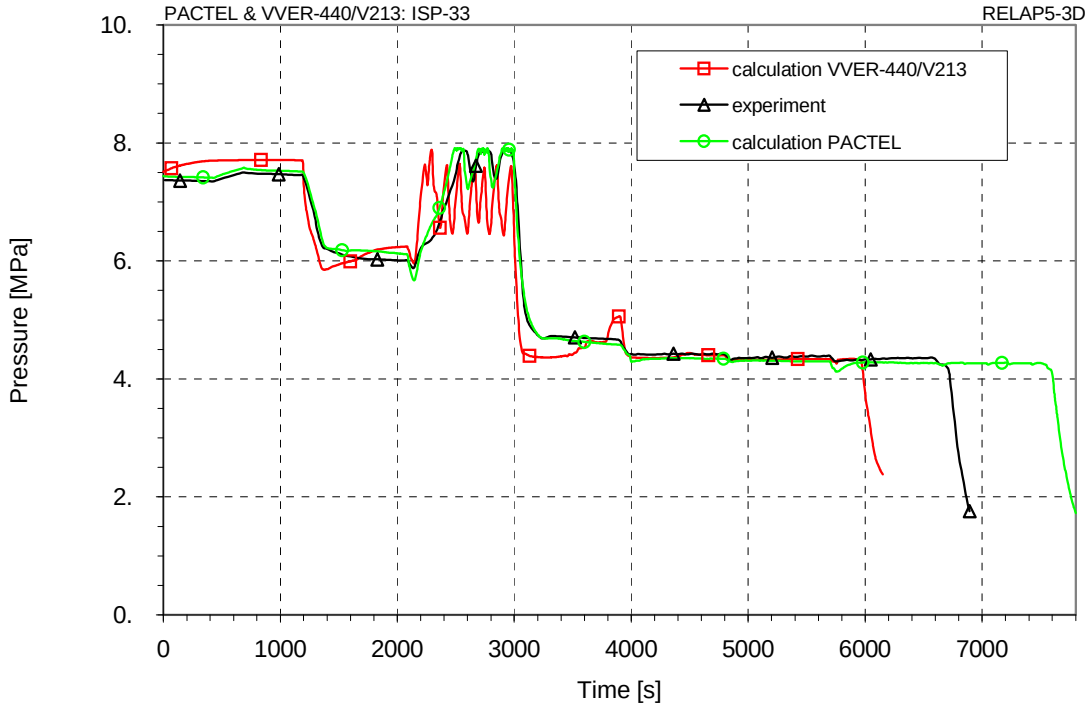

FIG. 4.9-7. Pressure in upper plenum.

4.9.6. General remarks

Main conclusions can be summarized as follows:

- For the primary mass inventories higher than ~ 50% of nominal value the overall behaviour agree well with experiment for both, PACTEL and plant calculation.
- Transition from single to two phase natural circulation is characterized by flow stagnation followed by multiple loop seals clearing. The number of corresponding pressure spikes in full scale VVER-440/V213 case is higher, but the magnitude of pressure spikes is lower than in the experiment. This is due to different number of circulation loops (6 versus 3 in PACTEL facility).
- The start of core heat-up is predicted in PACTEL analysis one drainage later than in experiment.
- The start of core heat-up is predicted for VVER-440/V213 one drainage earlier than in experiment. This is probably due to differences in geometrical arrangement of cold leg loop seals in Loviisa NPP (reference plant for PACTEL facility) and standard VVER-440/V213 units. There was still relatively large amount of coolant trapped in hot and cold leg loop seals after the 6^{th} draining. However, under the ISP-33 conditions this coolant was not available for core cooling.
- In the case of typical LOCAs the coolant would be lost in the form of steam-water mixture from loops whereas in the ISP-33 scenario the coolant was drained in water phase from RPV bottom. Such draining results in unfavourable residual coolant distribution within the primary system.

ABBREVIATIONS

ECCS	Emergency core cooling system
FW	Feedwater
LOCA	Loss of coolant accident
NPP	Nuclear power plant
PRZ	Pressurizer
RCP	Reactor coolant pump
RPV	Reactor pressure vessel
SB	Small break
SG	Steam generator
SV	Safety valve

REFERENCES FOR SECTION 4.9

[4.9-1] KOUHIA, J., et al., International Standard Problem ISP-33 at the PACTEL Facility for the Simulation of VVER-440 Type PWRs, European Two phase Flow Group Meeting, Hannover, Germany, 7–10 June (1993).

[4.9-2] OECD/NEA/CSNI, International Standard Problem No.33, PACTEL Natural Circulation Stepwise Coolant Inventory Reduction Experiment, Comparison Report, Vol. 1 and 2, NEA/CSNI/R(94)24, December (1994).

[4.9-3] MATEJOVIC, P., BACHRATY, M., VRANKA, L., “Analysis of ISP-33 using RELAP5-3D code”, Fifth International Information Exchange Forum on Safety Analysis for NPP’s of WWER and RBMK types Obninsk, Russian Federation, 16–20 October (2000).

[4.9-4] MATEJOVIC, P., BACHRATY, M., “Modeling of natural circulation phenomena in WWER-440 reactors”, IAEA research contract No. 12894/RBF (2006).

4.10. EFFECT OF HA-2 AND SPOT SYSTEMS ON SEVERE ACCIDENT PREVENTION IN WWER-1000/392 DESIGN

4.10.1. Introduction

The Russian safety standards require that consideration should be given to the beyond-design-basis accidents as the events and scenarios forming a certain part of the design basis. The target designs are the estimated frequency of the limiting radioactivity release less than 10^{-7} per reactor-year, and the estimated frequency of severe core damage less than 10^{-5} per reactor-year. Such regulatory approach results in development of special engineered safety features for effective prevention and mitigation of severe accidents.

The reactor plant WWER-1000/392 design is developed on the basis of standard reactor plant WWER-1000/320 being in operation at nuclear power plants in Russia, Ukraine, Czech Republic and Bulgaria. The reactor plant WWER-1000/392 is located in the double reinforced concrete containment that prevents release of the radioactive products into environment and protects the reactor plant from the external impacts (the design makes provision for protection against earthquake up to magnitude 8 as per scale MSK-64, air shock wave with pressure on the front up to 30 kPa, and aircraft crash).

In WWER-1000/392 project, an evolutionary approach to design is applied, i.e. the equipment and processes proved to be operable at existing NPPs are mainly used. At the same time, application of the advanced equipment and additional passive safety systems is directed to achievement of the higher safety level. Examples of improvements directed to safety enhancement are:

- Advanced reactor WWER-1000;
- Passive residual heat removal system (SPOT);
- Passive core flooding system (HA-2);
- Passive quick boron injection system;
- RCP with the seals excluding leaks from them during long term loss of power supply;
- Passive system to maintain rarefaction in the space between primary and secondary containments.

This section considers the role of the key WWER-1000/392 passive systems (SPOT and HA-2) dedicated to prevent or mitigate severe accidents resulting from the BDBA scenarios:

- Station blackout;
- LOCA with active ECCS (emergency core cooling system) failed.

These BDBA scenarios are essentially contributing to core damage frequency for existing WWER-1000/320 plants

4.10.2. HA-2 and SPOT systems

The safety function “fuel cooling during transients and accidents” is ensured by provision of sufficient coolant inventory, by coolant injection, sufficient heat transfer, by circulation of the coolant, and by provision of the ultimate heat sink. Depending on the type of transient/accident, a subset of these functions or all of them may be required. Various passive systems and components are proposed for WWER-1000/392 reactor concept to fulfil these functions.

The passive system for reactor flooding during loss of coolant accidents in WWER-1000/V-392 design comprises two groups of hydro accumulators as it is shown in Fig. 4.10-1. First group (so called HA-1 system) consists of four traditional emergency core cooling system accumulators being used at the operating WWER-1000 reactors; these accumulators are pressurized to about 6 MPa by nitrogen and connected in pairs to the upper plenum and downcomer through the special nozzles in the reactor pressure vessel. Second stage accumulators (HA-2 system) are the tanks (with boric acid solution of concentration 16 g/kg) connected to the reactor coolant system through the check valves and special spring-type valves. These valves are kept closed by the primary pressure; when the

primary pressure drops below 1.5 MPa, the spring opens the valve. Such configuration and valve design ensures continuity of hydrostatic head irrespective of the primary pressure change during an accident. Installation of hydraulic profiling of the outlet route ensures a step-wise limitation of the water flow rate from the tank when the water level in the tank is decreasing. The water inventory in the second stage accumulators (about 1000t) ensures the long term core cooling in case of a LOCA even if all active ECCS mechanisms are inoperable.

Passive residual heat removal system from the core via steam generators to the atmosphere (so called SPOT system) plays an important role in the core melt frequency reduction. Heat removal capacity of SPOT system under the worst external conditions amounts approximately 3% of nominal reactor power. The heat removal at the initial stage of the accident is performed due to partial water evaporation from the secondary side via steam generator relief valves to the atmosphere.

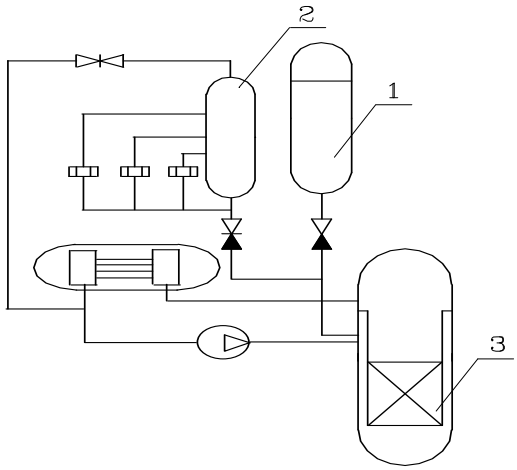

1 — HA-1 accumulator;
2 — HA-2 accumulator (2 per train); 3 — reactor

FIG. 4.10-1. Flow diagram of HA-1 and HA-2 (1 train of 4).

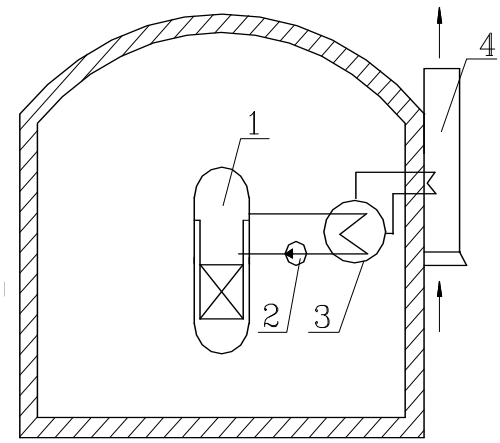

1 — reactor; 2 — reactor coolant pump;
3 — steam generator; 4 — air heat exchanger

FIG. 4.10-2. Flow diagram of SPOT (1 train of 4).

The SPOT system for WWER-1000/392 design (see Fig 4.10-2) consists of four groups (corresponding to the number of reactor coolant system loops) of closed natural circulation circuits. Steam extracted from the steam generator condenses in the ribbed tubular air-cooled heat exchanger, and the condensate flows by gravity to the steam generator. During normal operation the SPOT system is in standby mode, and all the SPOT circuits are in the warmed-up state. In case of plant blackout, the SPOT state changes from the standby to the operating condition. In addition to its main purpose (core decay heat removal in case of complete loss of a.c. power), the SPOT system can maintain the hot standby parameters of the reactor plant; for this purpose the SPOT has a special controller. The system is thermally insulated, so the heat losses in standby conditions are less than 0.1% of reactor rated power. Natural circulation within the SPOT system is provided by the corresponding layout of the steam generator, heat exchanger and draught air duct.

The steam circuit pipeline runs from fresh steam line to collector that distributes the steam by smaller tubes to four heat exchangers. The condensate from each heat exchanger is supplied by tubes to the collector and then by pipeline to the steam generator. Two isolation valves are installed at heat exchanging module inlet and outlet to isolate it in case of damage or maintenance. Small diameter pipelines with valves installed on them are provided for removal of air from heat exchanger when filling them with water during hydro-test and for periodical removal of non-condensables under standby conditions. Cooling air is taken from the atmosphere outside the reactor building. The air

takes the heat from the steam and leaves via the draught air ducts, which have the common outlet collector-deflector. Inlet and outlet gates and controller are installed on the airside of each heat-exchanging module. The gates open via switch on the heat-exchanging module to operation. The controller can be used to change the airflow rate to ensure additional SPOT system functions (for example, to maintain the reactor plant in the hot standby conditions or to cool it down).

4.10.3. Methodology of analysis

The following typical beyond-design accidents that essentially determine the design basis of the above passive systems are considered in this report:

- Station blackout, i.e. loss of off-site and on-site a.c. power with failure of all emergency diesel generators;
- Large break LOCA (double-ended cold leg break of 850 mm diameter) with station blackout.

These sequences essentially contribute to core melt frequency and limiting radioactive release frequency for operating WWER-1000/320 plants.

To demonstrate the effect of HA-2 and SPOT systems under the above BDBA conditions, the analysis of these sequences with and without operation of HA-2 and SPOT systems was performed. The analysis was of realistic type, i.e.:

- Initial plant conditions correspond to the normal operation at rated power without account for possible deviations and uncertainties in parameters, set-point values, etc.;
- Core characteristics (reactivity coefficients, power peaking factors, etc.) are assumed in accordance with neutron-physical calculations without account for the calculation uncertainties and errors;
- Failures of the equipment (other than assumed in the scenarios under consideration) and operator errors are not taken into account.

The domestic DINAMIKA-97 and TECH-M-97 codes developed by OKB “Gidropress” and certified by Russian regulatory body were used for the analysis. Besides, some supporting calculations have been performed by new domestic code KORSAR-V1 and other leading codes such as RELAP5/Mod3.2 and ATHLET-1.2A.

4.10.4. BDBA sequences without HA-2 and SPOT operation

4.10.4.1. Station blackout

Figures 4.10-3–4.10-6 show the calculation results of accident with station blackout without account for operation of new passive systems HA-2 and SPOT. As a result of initiating event all RCP are disconnected, the turbine generator stop valves are closed, the PRZ (pressurizer) systems are de-energized, the make-up-letdown system and BRU-K (dump valve to turbine condenser) are disconnected, feed water supply to SG (steam generator) is stopped. In addition failure of the diesel-generators results in failure of all active safety systems to operate.

After reactor scram (by the fact of disconnection of three and more RCP) the reactor power decreases to decay heat level. After termination of RCP coast-down, the natural circulation of primary coolant is established. With this, heat removal from the primary circuit is provided due to secondary side dumping devices (BRU-A — dump valve to atmosphere and SG SV — steam generator safety valve) operation that leads to decrease of water inventory in SG. Corresponding decrease of heat removal from the primary circuit leads to increase of the primary pressure resulting in periodical opening of the PRZ SV (pressurizer safety valve) and loss of primary coolant. Decrease in upper plenum level below the outlet reactor nozzle results in loss of natural circulation. Ongoing decrease of the reactor coolant level results in core top uncovering and in heating-up of the fuel rod claddings leading to severe core

damage. Table 4.10-1 presents the chronological sequence of some important events occurred during this accident.

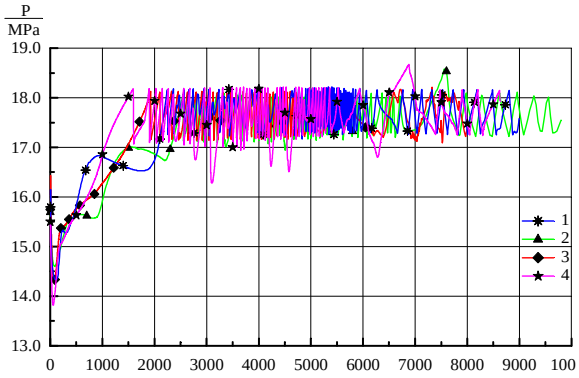

Core outlet pressure
1 – ATHLET; 2 – RELAP5;
3 – DINAMIKA; 4 – KORSAR

FIG. 4.10-3. Station blackout without SPOT.

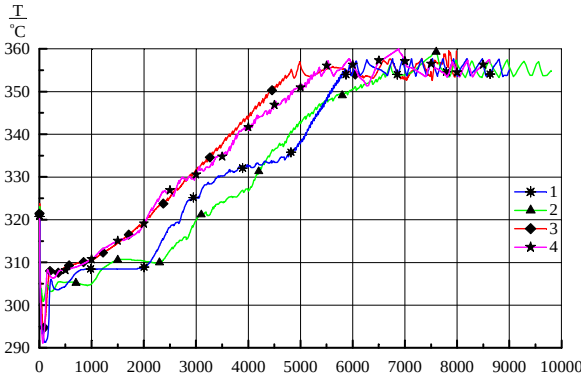

Coolant temperature at reactor outlet:
1 – ATHLET; 2 – RELAP5;
3 – DINAMIKA; 4 – KORSAR

FIG. 4.10-4. Station blackout without SPOT.

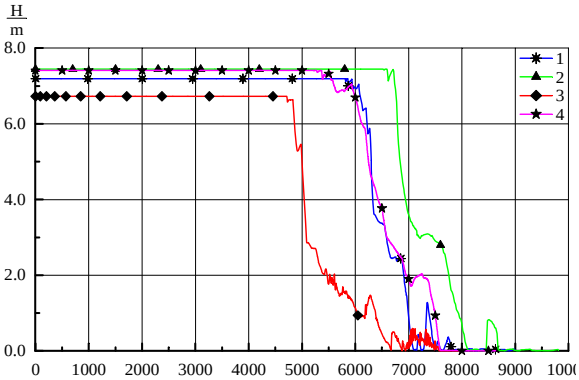

Collapsed level in upper plenum:
1 – ATHLET; 2 – RELAP5;
3 – DINAMIKA; 4 – KORSAR

FIG. 4.10-5. Station blackout without SPOT.

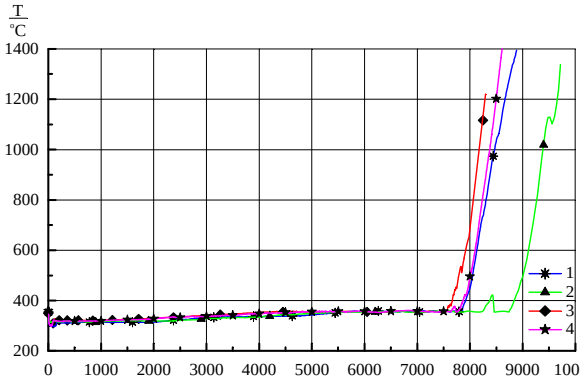

Peak cladding temperature
1 – ATHLET; 2 – RELAP5;
3 – DINAMIKA; 4 – KORSAR

FIG. 4.10-6. Station blackout without SPOT.

TABLE 4.10-1. SEQUENCE OF EVENTS

Event	Time (s)			
	DINAMIKA	RELAP5	ATHLET	KORSAR
PRZ SV first opening	1920	2550	2240	1590
Level in upper plenum appears	4830	6600	5900	5380
SG empty	7500	6400	6200	6270
Loss of natural circulation in RCS	6000	7200	6600	7000
PCT reaches 1200°C	8280	9500	8680	8500

The above results show that the accident scenario predicted by the different codes is, as a whole, practically the same. Violation of maximum design limit on fuel rod damage occurs already in 2–2.5 h after accident initiation.

4.10.4.2. Large break LOCA

Figures 4.10-7 and 4.10-8 show the calculation results for the accident with double-ended break of the main coolant pipeline at the reactor inlet with station blackout without account for operation of HA-2 system. These results have been obtained using TECH-M-97 code.

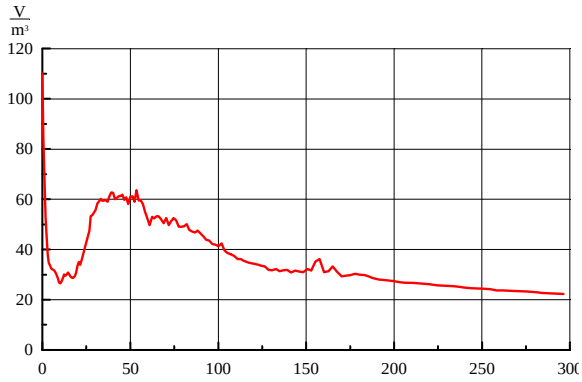

Coolant inventory in RPV

FIG. 4.10-7. Large break LOCA without HA-2 (TECH-M).

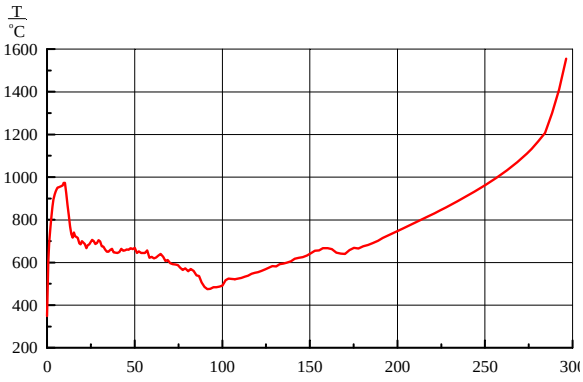

Peak cladding temperature

FIG. 4.10-8. Large break LOCA without HA-2 (TECH-M).

When the primary pressure decreases to 5.88 MPa, the traditional ECCS hydro accumulators (HA-1) are put into operation to restrict the reactor emptying and to refill the lower reactor plenum. Primary coolant inventory increases due to HA-1 operation thereby ensuring the core cooling within some period of time. Then water level decrease in the reactor results in deterioration of core heat removal and its subsequent heating-up of the fuel after 100 s. By 285 s since accident initiation the maximum cladding temperature exceeds 1200ºC (according to Russian safety regulations, this value is an indicator of severe core damage).

The same calculation was performed using RELAP5/MOD3.2 code. The calculation results are given in Figs 4.10-9 and 4.10-10. As one can see, the transient scenario is practically similar to that obtained by TECH-M-97 code. Heating-up of the fuel rod cladding begins at 100 s and the maximum clad temperature exceeds 1200ºC at 280 s.

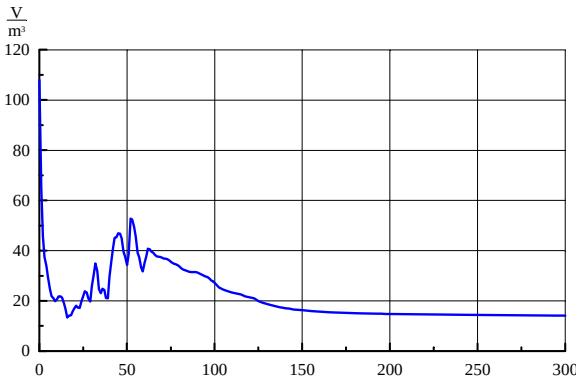

Coolant inventory in RPV

FIG. 4.10-9. Large break LOCA without HA-2 (RELAP5).

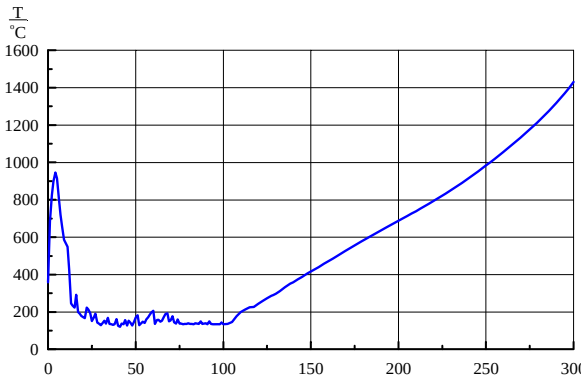

Peak cladding temperature

FIG. 4.10-10. Large break LOCA without HA-2 (RELAP5).

4.10.5. BDBA sequences with HA-2 and SPOT operation

4.10.5.1. Station blackout

Figures 4.10-11–4.10-14 show the calculation results of accident for station blackout with account of SPOT operation.

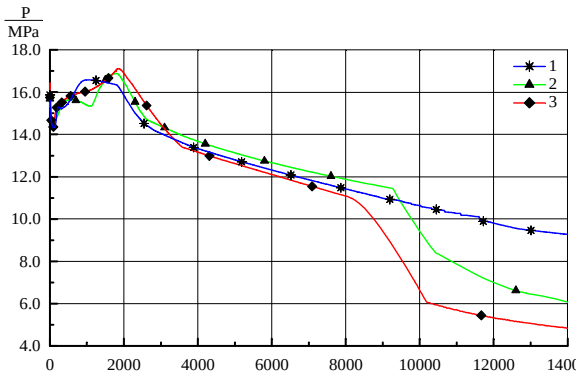

Core outlet pressure
1 – ATHLET; 2 – RELAP5;
3 – DINAMIKA

FIG. 4.10-11. Station blackout with SPOT.

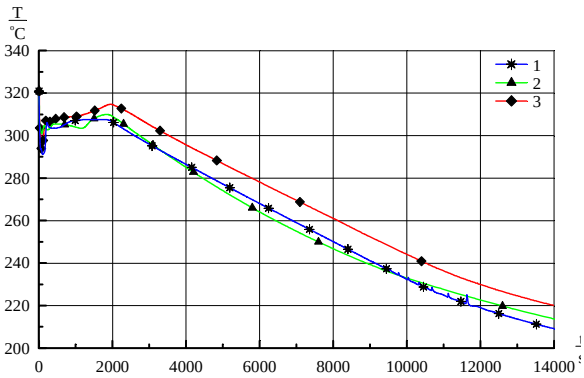

Coolant temperature at reactor outlet:
1 – ATHLET; 2 – RELAP5;
3 – DINAMIKA

FIG. 4.10-12. Station blackout with SPOT.

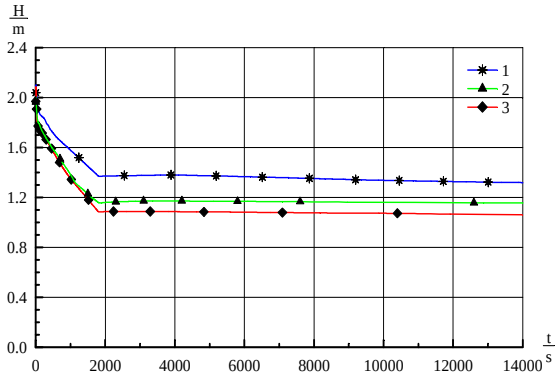

Collapsed level in SG:
1 – ATHLET; 2 – RELAP5;
3 – DINAMIKA

FIG. 4.10-13. Station blackout with SPOT.

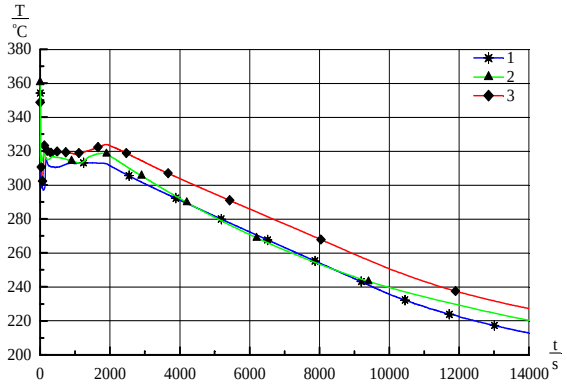

Maximum temperature of fuel rod cladding
1 – ATHL
ET; 2 – RELAP5;
3 – DINAMIKA

FIG. 4.10-14. Station blackout with SPOT.

Accident scenario at the first stage is similar to that considered in Section 4.10.4.1 above. However, as a result of SPOT operation, a portion of heat from the primary circuit is removed into environment, and the rest is removed due to BRU-A operations. After corresponding decrease of decay heat the steam dump devices of the secondary circuit are closed and loss of water from SG stops. Heat removal from the primary circuit is provided due to close-circuit operation of the SPOT (steam condensation in the heat-exchange modules, and condensate returns back into the SG). The primary parameters (primary pressure and temperature) begin to decrease, adequate core cooling is ensured at all the times.

Thus, the calculation results show that SPOT operation prevents any core damage during the beyond design-basis accident under consideration.

4.10.5.2. Large break LOCA

Figures 4.10-15–4.10-18 show the calculation results for this accident obtained by TECH-M-97 computer code. It was assumed for the SPOT operation that the operator switches it into cool down mode in 1800 s and from this moment the steam generators start cooling down. Duration of a stage of SG cool down amounts to 4800 s. After temperature in the secondary circuit decreases below the primary circuit temperature, the steam generators start to operate under the condition of steam condensation in the primary circuit with condensate reflux into the loops.

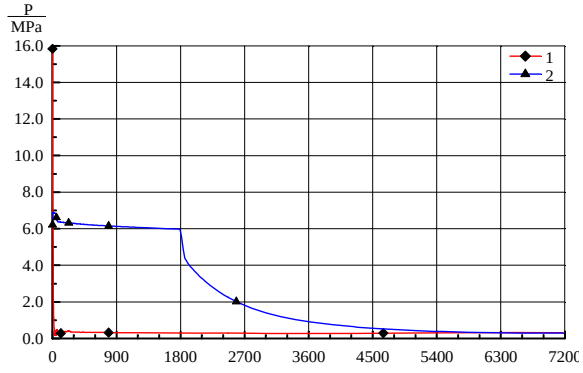

1 — Core outlet pressure; 2 — SG pressure

FIG. 4.10-15. Large break LOCA with HA-2 and SPOT (TECH-M).

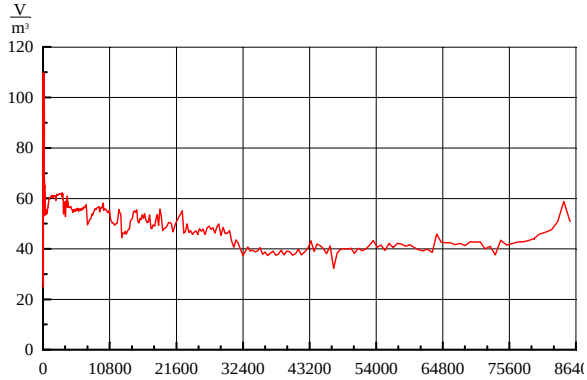

Coolant inventory in RPV

FIG. 4.10-16. Large break LOCA with HA-2 and SPOT (TECH-M).

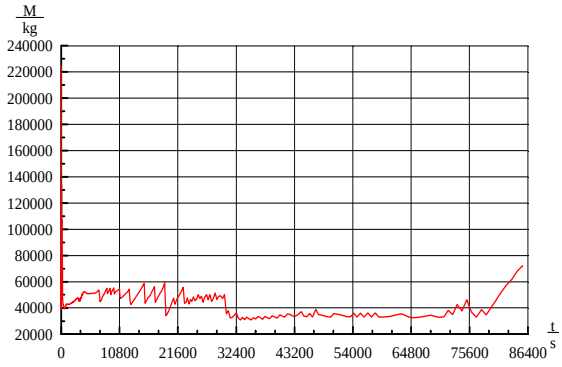

Coolant inventory in RCS

FIG. 4.10-17. Large break LOCA with HA-2 and SPOT (TECH-M).

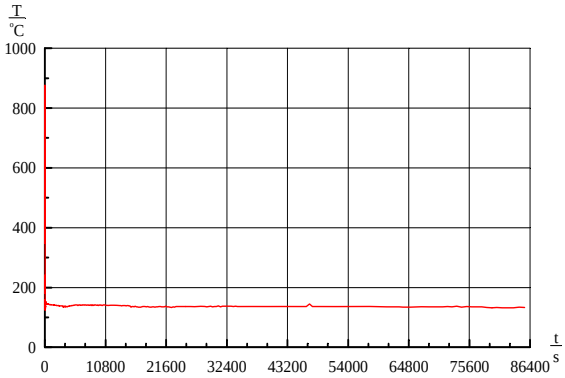

Peak cladding temperature

FIG. 4.10-18. Large break LOCA with HA-2 and SPOT (TECH-M).

The make-up from HA-2 keeps the water inventory in the primary circuit at about 50 t, and it ensures the adequate cooling of the fuel. Thus the most part of coolant inventory is concentrated within the reactor. After HA-2 transition for the last step of supply (at 30 000 s) there is decrease in the primary coolant inventory (approximately to 32 000 kg), however, no core heating-up is observed.

The same scenario was also analysed by RELAP5/MOD3.2 code. The calculation results are as a whole in good agreement with TECH-M-97 results and have demonstrated that adequate core cooling is provided throughout the time under consideration.

4.10.6. General remarks

The analysis of station blackout accident without operation of SPOT system has shown the exceeding of the maximum design limit of fuel rod damage already in 2–2.5 h after initiating event. Operation of SPOT system prevents any core damage during the BDBA under consideration.

The analysis of LBLOCA with active ECCS failed without operation of HA-2 system has shown the exceeding of the maximum design limit of fuel rod damage in a few minutes after initiation of accident. Operation of HA-2 system prevents core damage above DBA acceptance criteria during this BDBA.

The analysis has demonstrated that operation of new passive safety systems (SPOT and HA-2) in the considered BDBAs ensures the effective core cooling within required period of time.

New passive safety systems HA-2 and SPOT allowed significant improving of the plant safety. In particular, the estimated core melt frequency for WWER-1000/392 design is about three orders of magnitude less than for the operating power units of WWER-1000/320 design.

5. METHODOLOGY FOR EXAMINING PASSIVE SYSTEM RELIABILITY AND EXAMPLE APPLICATION

Innovative reactor concepts make use of passive safety systems to a large extent in combination with active safety systems. According to the IAEA definitions [5.1], a passive system does not need external input, especially energy to operate. That is why passive systems are expected to combine among others, the advantages of simplicity, a decrease in the need for human interaction and a reduction or avoidance of external electrical power or signals.

Besides the open feedback on economic competitiveness, special aspects like lack of data on some phenomena, missing operating experience over the wide range of conditions, and driving forces which are smaller — in most cases — than in active safety systems, must be taken into account.

This remark is especially applicable to the passive systems B or C (i.e. implementing moving working fluid, following the IAEA classification [5-1]) and in particular to the passive systems that utilize natural circulation. These passive safety systems in their designs rely on natural forces to perform their accident prevention and mitigation functions once actuated and started. These driving forces are not generated by external power sources (e.g., pumped systems), as is the case in operating and evolutionary reactor designs. Because the magnitude of the natural forces, which drive the operation of passive systems, is relatively small, counter-forces (e.g. friction) can be of comparable magnitude and cannot be ignored as it is generally the case of systems including pumps. Moreover, there are considerable uncertainties associated with factors on which the magnitude of these forces and counter forces depends (e.g. values of heat transfer coefficients and pressure losses). In addition, the magnitude of such natural driving forces depends on specific plant conditions and configurations which could exist at the time a system is called upon to perform its safety function. All these uncertainties affect the thermohydraulic (T-H) performance of the passive system. This particular aspect, inherent to these passive systems, was discussed extensively in an international workshop [5-2]. Previous work carried out by ENEA, University of Pisa and Polytechnic of Milan, led to the development of a procedure called Reliability of Passive Systems (REPAS), which helps evaluating the reliability of natural circulation systems under specific conditions [5-3, 5-4].

To assess the impact of uncertainties on the predicted performance of the passive system, a large number of calculations with best estimate T-H codes are needed. If all the sequences where the passive system studied is involved are considered, the number of calculations can be prohibitive. For all these reasons, it appeared necessary to create a specific methodology to assess the reliability of passive systems B or C. The methodology has been developed within the framework of a Project called Reliability Methods for Passive Safety Functions (RMPS), performed under the auspices of the European 5th Framework Programme [5-5]. The methodology addresses the following problems:

- Identification and quantification of the sources of uncertainties and determination of the important variables;
- Propagation of the uncertainties through T-H models and assessment of T-H passive system unreliability;
- Introduction of passive system unreliability in the accident sequence analysis.

In Section 5.1, each step of the methodology is described and commented and a diagram of the methodology is presented. Some improvements of this methodology, proposed after the end of the RMPS project (in early 2004) are highlighted in Section 5.2. Alternative methodologies are presented in Section 5.3. Finally the application of the RMPS methodology on the example of CAREM-like Passive Residual Heat Removal System (PRHRS), performed within the present IAEA Coordinated Research Project, is described in Section 5.4.

5.1. SYNTHESIS OF METHODOLOGIES DEVELOPED IN RMPS PROJECT

The methodology proposed consists of several steps, which are shown in Fig.5-1 and are detailed in the following paragraphs.

5.1.1. Definition of the accident scenario(s)

The first step of the methodology is the definition of the accident scenario(s) in which the passive system is expected to operate. Knowledge of each scenario helps identifying the specific failure criteria and relevant parameters and the specific quantification of uncertainties. The results obtained in the reliability and sensitivity analyses of the passive system are thus specific to each scenario. A global evaluation of the passive system is obtained by the integration of its unreliability in a Probabilistic Safety Assessment, in which all the sequences involving the passive system are considered (see section 5.1.9). This approach is preferred to conservative analyses consisting in evaluating the system reliability for the worst scenario considered or in integrating the larger variability of the uncertain parameters covering all the scenarios involving the system.

5.1.2. System characterisation

The purpose of this analysis is to obtain information on the behaviour of the passive system, in an accident scenario occurring during the life of the nuclear reactor and to identify the failure zones and conditions, if such exist. Therefore, the missions of the system, its failure modes and the failure criteria must be defined.

5.1.2.1. Mission(s) of the system

The missions of the system are the goals for which the passive system has been designed and located within the overall system. For instance, the mission of the passive system can be decay heat removal, vessel cooling, pressure decrease of the primary circuit, etc. In some cases, the passive system can be designed to fulfil several missions at the same time or different missions depending on the considered scenario.

5.1.2.2. Failure mode

Due to the complexity of thermohydraulic phenomena and to the interaction between the passive system and the overall system, it is not always obvious to associate a failure mode to the mission of the system. A qualitative analysis is often necessary so as to identify potential failure modes and their consequences, associated with the passive system operation. A hazard identification qualitative method such as the FMEA (Failure Mode and Effect Analysis) can be used to identify the parameters judged critical for the performance of the passive system and to help associate failure modes and corresponding indicators of the failure cause. This method can necessitate the introduction, in addition to mechanical components of the system (piping, drain valve, etc.), of a “virtual” component. This component is identified as natural circulation and is evaluated in terms of potential “phenomenological” factors (these include non-condensable gas build up, thermal stratification, surface oxidation, cracking, etc.), whose consequences can affect the passive system performance.

5.1.2.3. Success/failure criteria

Knowledge on the system missions and failure modes allows the evaluation of the failure criteria. The failure criteria can be established in terms of exceeding/not exceeding given thresholds set on relevant physical quantities over given time periods (e.g. mission times), as for example exceeding a limit pressure in the primary system during the first 24 hours after the beginning of the scenario, or not removing more than a given fraction of the residual energy produced during the same time period. In some cases, it is better to define a global failure criterion for the whole system instead of a specific criterion for the passive system. For instance, the failure criterion can be based on the peak cladding temperature during a specified period. In this case, it will be necessary to model the complete system and not only the passive system.

5.1.3. System modelling

Due to the lack of suitable experimental databases for passive systems in operation, the evaluation must rely on numerical modelling. The system analysis must be carried out with a qualified thermohydraulic system code and performing best estimate calculations. Indeed there is an increasing interest in computational reactor safety analysis to replace the conservative evaluation model calculations by best estimate calculations supplemented by a quantitative uncertainty analysis [5-6]. Particularly in the present methodology where the objective is the passive system reliability evaluation, it is important to simulate the passive system performance in a realistic and not conservative way. At this stage, calculations have to be carried out on the reference case with nominal values of the system characteristic parameters. The results have to be compared with experimental data if any exists. During the characterisation process, the modelling and the evaluation of the passive system, new failure modes can be identified (such as flow oscillations, plug phenomena due to non-condensable gases, etc.) which must also be taken into account.

5.1.4. Identification of uncertainty sources

First of all, the method requires the identification of the potentially important contributors to uncertainty. These contributors are

- Approximations in modelling physical process: for instance the treatment of a liquid-steam mixture as a homogeneous fluid, the use of empirical correlations, etc;
- Approximations in modelling system geometry: simplification of complex geometry features and approximation of three dimensional systems;
- The input variables: initial and boundary conditions, such as plant temperatures, pressures, water levels and reactor power, dimensions, physical properties, such as densities, conductivities, specific heats, and thermohydraulic parameters, such as heat transfer coefficients or friction factors.

This identification of the relevant parameters must be based on expert opinions. Different methodologies have been developed to evaluate the overall uncertainty in the physical model predictions and some efforts have been made for the internal uncertainty assessment capacity of thermohydraulic codes [5-7]. However, in the present study, model uncertainties are not accounted for, focusing the attention on the uncertainties relative to the system input parameters. This choice was made due to the limited resources of the project, but in real applications the reliability assessment should include also the other type of uncertainties.

5.1.5. Identification of the relevant parameters

The evaluation of the reliability of a passive system requires the identification of the relevant parameters which really affect system goal accomplishment. The tool chosen here for this task is the Analytic Hierarchy Process [5-8, 5-9]. This method consists of three major steps: the building of a hierarchy to decompose the problem at hand, the input of pairwise comparison judgments on the relevance of the considered parameters and the computation of priority vectors to obtain their ranking. The hierarchy is built in three steps:

- Accurately define the most important goal (i.e. the mission) of the passive system and place it at the top level;
- Build the hierarchy downward into different levels by putting in each level those factors directly influencing the elements of the level just above and directly influenced by the elements of the level just below;
- At the bottom of the hierarchy place the basic parameters.

Then for each element of each level a pairwise comparison matrix is build by expert elicitation to assess the influence of the relevant entries of the level below in relation to the element under analysis. The proper question in the pairwise comparison is on the form: "Considering entries *X* and *Y* of level *s-1*, how much more important is entry *X* compared to entry *Y* with respect to their influence on element *k* of level *s*?" The principal eigenvector of the comparison matrix provides the priority vector of the element under consideration. Once all the priority vectors are available, they are multiplied appropriately through the branches of the hierarchy in order to determine the overall weights of the bottom-level basic parameters with regards to the previously defined top goal. The major advantage of the pairwise comparison approach to quantification is the simple and intuitive way of expressing judgments on the relative importance of the different constituents of the hierarchy, and the possibility of checking for consistency in the judgment entries.

5.1.6. Uncertainty quantification

A key issue in this methodology is the selection of the distributions for the input parameters. The main objective is that the selected distribution for each input parameter must quantify the state of knowledge and express the reliable and available information about the parameter. The choice of distribution may highly affect the reliability evaluations of the passive system. Different points of view have to be considered for this quantification:

5.1.6.1. The amount of data

When the data on a parameter are abundant, statistical methods can be used such as the maximum likelihood method or the method of moments to adjust analytical density functions and different goodness-of-fit tests can be used (Chi square, Kolmogorov, etc.) to find the best analytical fit to the data. When the data are sparse or non-existent and this is generally the case when we consider the uncertainties affecting the passive system performance, the evaluation of the probability functions of the uncertain parameters must be based on expert judgement. Thus a subjective approach is used where the uncertainty is characterised as a probability density function that shows the range of values where the actual value of the parameter may be and what parts of the range the analyst considers more likely than others. In the case where no preferences can be justified, a uniform distribution can be specified, i.e. each value between minimum and maximum is equally likely. These distributions are quantitative expressions of the state of knowledge and can be modified if there is new evidence. If suitable observations become available, they can be used consistently to update the distributions.

5.1.6.2. Dependence between parameters

If parameters have common contributors to their uncertainty, the respective states of knowledge are dependent. As a consequence of this dependence, values of different parameters cannot be combined freely and independently. Instances of such limitations need to be identified and the dependencies need to be quantified, if judged to be potentially important. If the analyst knows of dependencies between parameters explicitly, multivariate distributions or conditional probability distributions may be used. The dependence between the parameters can be also introduced by covariance matrices or by functional relations between the parameters.

5.1.7. Sensitivity analysis

5.1.7.1. Objectives

An important feature of the methodology is to evaluate the sensitivity of reliability driving output variables (pressure, removed power, etc.) with respect to input uncertain parameters. The sensitivity measures give a ranking of input parameters. This information provides guidance as to where to improve the state of knowledge in order to reduce the output uncertainties most effectively. If experimental results are available to be compared with calculations, the sensitivity measures provide guidance as to where to improve the models of the computer code.

5.1.7.2. Qualitative sensitivity analysis

Sometimes the lack of operational experience and significant data concerning the passive system performance forces the analysis to be performed in a qualitative way aiming at the identification, for each failure mode, of both the level of uncertainty associated with the phenomenon and the sensitivity of failure probability to that phenomenon [5-10]. For example, even if a phenomenon is highly uncertain (because of deficiencies in the physical modelling) this may not be important for the overall failure probability. Conversely a phenomenon may be well understood (therefore the uncertainty is small) but the failure probability may be sensitive to small variation in this parameter. The worst case is characterized by "high" rankings relative to either sensitivity or uncertainty (e.g. presence of non-condensable gas or thermal stratification), making the corresponding phenomena evaluation a critical challenge.

5.1.7.3. Quantitative sensitivity analysis

The quantitative sensitivity analysis necessitates thermohydraulic calculations. It consists in ranking the parameters according to their relative contribution on the overall code response uncertainty and quantifying this contribution for each parameter. To apportion the variation in the output to the different input parameters, many techniques can be used [5-11], each yielding different measures of sensitivity.

A common approach is to base the sensitivity analysis on a linear regression method, which is based on the hypothesis of a linear relation between response and input parameters. This, in case of passive systems is obviously restrictive. However, the method is simple and quick, and provides useful insights in case of a restricted number of sampling, as will be often our case. Three different sensitivity coefficients have been considered, each one providing a slightly different information on the relevance of a parameter: Standardized Regression Coefficients (SRC), Partial Correlation Coefficients (PCC) and Correlation Coefficients (CC). Small differences between the different coefficients may be due to a certain degree of correlation between the inputs and to the system’s non-linearity. These occurrences should be analysed, the first one possibly through the examination of the correlation matrix and the second one by calculating the model coefficient of determination R2.

Depending on the nature of the model representing the passive system operation and calculating its performances, it can be more accurate to use sensitivity methods developed for non-monotonous or non-linear models.

In case of non-linear but monotonous models, we can perform rank transformations and calculate associated indices: standardized rank regression coefficients (SRRCs) and partial rank correlation coefficients (PRCCs). The rank transformation is a simple procedure, which involves replacing the data with their corresponding ranks. We can also calculate a determination coefficient based on the rank R^{2*}. The R^{2*} will be higher than the R^2 in case of non-linear models. The difference between R^2 and R^{2*} is a useful indicator of non-linearity of the model. For non-linear and non-monotonous models, two methods exist: *the Fourier Amplitude Sensitivity Test (FAST) and the Sobol method.*

The general idea of these methods is to decompose the total variance of the response, in terms corresponding to uncertainty on the input parameters taken independently, in terms corresponding to the interaction between two parameters, in terms corresponding to the interaction between three parameters, etc. The Sobol indices are calculated by Monte-Carlo simulation. The problem of these methods, and specially the Sobol method, is that a good estimation of these indices requires a great number of calculations (i.e. 10000 simulations). Thus, it is necessary first to calculate a response surface validated in the domain of variation of the random variables (see Section 5.1.8.4). Thus, if the model is really not linear, nor monotonous, we propose to:

- adjust non linear models on the data,
- test the validity of the model (e.g. in calculating R^2, residues, predictive robustness),
- use the model as a response surface in order to evaluate the Sobol or FAST indices.

5.1.8. Reliability evaluations

Different methods can be used to quantify the reliability of the passive system once a best estimate thermohydraulic code and a model of the system are given. The failure function of a passive system according to a specified mission is given by:

M = relevant output variable – threshold = g(X1, X2,…,Xn) (5-1)

in which the Xi (i=1,…,n) are the n basic random variables (input parameters), and g(.) is the functional relationship between the random variables and the failure of the system. The failure function can be defined in such a way that the limit state, or failure surface, is given by M = 0. The failure event is defined as the space where $M \leq 0$, and the success event is defined as the space where $M > 0$. Thus a probability of failure can be evaluated by the following integral:

$$P_f = \int\int ... \int f_X(x_1, x_2, ..., x_n) dx_1 dx_2 ... dx_n \quad (5\text{-}2)$$

where fX is the joint density function of X1 ,X2,…, Xn, and the integration is performed over the region where $M \leq 0$. Because each of the basic random variables has a unique distribution and because they interact, the integral (Eq. 5-2) cannot be easily evaluated. Two types of methods can be used to estimate the failure probability: the Monte Carlo simulation with or without variance reduction techniques and the First and Second Order Reliability Methods (FORM/SORM).

5.1.8.1. Direct Monte Carlo

Direct Monte Carlo simulation techniques [5-12] can be used to estimate the failure probability defined in Eqs. (1) (or its complement to 1, reliability). Monte Carlo simulations consist in drawing samples of the basic variables according to their probabilistic characteristics and then feeding them into the failure function. An estimate $\overline{P_f}$ of the probability of failure Pf can be found in dividing the number of simulation cycles in which $g(.) \leq 0$, by the total number of simulation cycles N. As N approaches infinity, $\overline{P_f}$ approaches the true failure probability. It is recommended to measure the statistical accuracy of the estimated failure probability by computing its variation coefficient (ratio of standard deviation to average of estimations). The smaller the variation coefficient, the better the

accuracy of the estimated failure probability. For a small number of simulation cycles, the variance of $\overline{P_f}$ can be quite large. Consequently, it may take a large number of simulation cycles to achieve a good accuracy. Then, the amount of computer time needed for the direct Monte Carlo method will be high, since each simulation cycle involves a long calculation (several hours) performed by a thermohydraulic code.

5.1.8.2. Variance reduction techniques

Variance reduction techniques offer an increase in the efficiency and accuracy of the simulation-based assessment of the passive system reliability for a relatively small number of simulation cycles [5.12, 5.13]. Different variance reduction techniques exist, such as: importance sampling, stratified sampling, Latin Hypercube Sampling (LHS), conditional expectation, directional simulation, etc.

5.1.8.3. FORM/SORM

An alternative to the Monte Carlo simulation is the use of First/Second Order Reliability Methods (FORM/SORM) [5-13 to 5-15]. They consist of 4 steps:

- Transformation of the space of the basic random variables $X_1, X_2,\ldots,X_n$ into a space of standard normal variables,
- Search for, in this transformed space, the point of minimum distance from the origin to the limit state surface (this point is called the design point),
- Approximation by a first/second order surface of the real failure surface near the design point,
- Computation of the failure probability corresponding to the approximated failure surface.

FORM and SORM apply only to problems where the set of basic variables are continuous. For small probabilities FORM/SORM are extremely efficient when compared to simulation methods. The calculation time is, for FORM approximately linear in the number of basic variables and independent from the probability level. The drawbacks of these methods come from the difficulty in identifying the design point when the failure surface is not sufficiently smooth, and from the fact that, contrary to Monte Carlo method, there is no direct way to estimate the accuracy of the provided estimation.

5.1.8.4. Response surface methods

To avoid the problem of long computer times in the previous methods, it can be interesting to approximate the response $Y=g(X)$ given by the T-H code, in the space of the input random variables, by a simple mathematical model $\tilde{g}(X)$ called response surface. Experiments are conducted with the basic random variables $X_1, X_2,\ldots,X_n$ a sufficient number of times to define the response surface to the level of accuracy desired. Each experiment can be represented by a point with coordinates $x_{1j}, x_{2j},\ldots,x_{nj}$ in an n-dimensional space. At each point, a value of y_j is calculated by the T-H code and the unknown coefficients of the response surface $\tilde{g}(X)$ are determined in such a way that the error is minimum in the region of interest. When a response surface has been determined, the passive system reliability can be easily assessed in using the Monte Carlo simulation. Different types of response surfaces can be fitted: polynomial, thin plate splines, neural networks, generalised linear model, Partial Least Squares regression, etc. The type of response surface will be chosen depending on the problem [5-16]. In any case, the response surface is just an approximation to the real model, and the error committed in such approximation should be taken into account in the final reliability estimate.

5.1.9. Integration of passive system reliability in PSA

The objective of this part of the methodology is the development of a consistent approach for introducing passive system reliability in an accident sequence in a Probabilistic Safety Assessments (PSA). So far, in existing innovative nuclear reactor projects PSA's , only passive system components failure probabilities are taken into account, disregarding the physical phenomena on which the system

is based, such as the natural circulation. In fact, the inclusion of this aspect of the passive system failure in the PSA models is a difficult and challenging task and no commonly accepted practices exist. In a first approach, we have chosen an Event Tree (ET) representation of the accident sequences. ET techniques allow the identification of all accident sequences deriving from an initiating event. The initiating event is an event (e.g. equipment failure, transient) that can lead to the accident if no protective action is taken by safety systems. Each sequence of the ET represents a certain combination of events corresponding to the failure or to the success of safety systems. Therefore, ET provides a set of alternative consequences. The consequences in the case of Level 1 PSA of nuclear reactors are usually defined as degrees of reactor core damage, including 'safe' state and 'severe'' accident state. These consequences are generally evaluated by T-H calculations carried out in a conservative way.

This choice of the event tree presentation might seem unsuitable because it does not appear to consider the dynamic aspects of the transient progression including dynamic system interactions, T-H induced failure, and operator actions in response to system dynamics. In fact, we have treated examples where the overall reactor, including the safety systems and in particular the passive system, is modeled by the T-H code. This results in the fact that the dynamic system interactions are taken into account by the T-H calculation itself. In addition, we have not considered human intervention during the studied sequences, which is coherent with the usual utilization of the passive systems in innovative reactors. So, for a first approach, the event tree presentation seems a good and simple representation for the assessment of accident sequences, including the passive systems.

For the sequences where the definition of envelope cases are impossible, events corresponding to the failure of the physical process are added to the event tree and uncertainty analyses are carried out to evaluate the corresponding failure probability. For this purpose, the T-H code is coupled to a Monte-Carlo simulation modulus. The failure probabilities obtained by these reliability analyses are fed into the corresponding sequences.

5.1.10. Conclusion and open questions

The developed methodology participates to the safety assessment of reactors equipped with T-H passive systems and is an indispensable tool for the designers who define the architecture of safety systems and for the regulatory authorities in the safety evaluation of passive system.

The RMPS methodology was successfully applied to several passive systems, such as the Isolation Condenser System of Boiling Water Reactor [5-17], the Hydro-Accumulators of the VVER. or the RP2 (Residual Passive heat Removal system on the Primary circuit) system [5-5]. In Section 5.4, a new example of application, performed within the present IAEA Coordinated Research Project and concerning the PRHRS of the CAREM-like reactor will be presented.

In conclusion, it should first of all be noted that the concept of intrinsic reliability of a component which exists for an active system or structural component is not directly applicable to a T-H passive system. Indeed, the probability or the frequency value associated with the T-H passive system is linked to a given scenario (state of the other systems on the circuit, environmental conditions, etc.). A methodology to incorporate these reliability data into a single characteristic value, representative of all the possible situations, has not been found to date.

The results of the analyses made show that, in spite of the inherent characteristics of passive systems, which are a priori considered as advantages (simplicity, decrease of the need for human interaction, reduction or avoidance of external electrical power or signals), the decision for the designers to replace an active safety system by a passive system is not easy from a safety point of view. Moreover before making a final decision on this selection, other points which have not been addressed within the framework of the RMPS project, due to limited time and resources, have to be studied in future work. In particular, a very important issue concerns the human factors, which play an important role in the inspection and the maintenance of the passive systems.

In addition to the improvement of different topics of the RMPS methodology and in order to answer to the question of the choice between active and passive systems, it is necessary to take into account other points of view than the reliability, such as the efficiency, the simplicity, the robustness, the human factor and economic evaluations, and to develop a tool for helping the systems design's optimisation.

- About the improvement of the RMPS methodology, two items of the methodology roadmap deserve closer attention: the identification of the relevant parameters and the quantification of uncertainties. In RMPS, the identification of the input parameters is not based on strict rules. Rules, which guarantee a rational approach to the problem and, which demonstrate that the procedure is based on realistic assumptions, would justify the choice of the uncertain parameters and moreover should convince the designer. In the selection of the relevant input parameters, a clear distinction for the various kinds of uncertainties should be introduced distinguishing between modelling uncertainties on one side and uncertainties dealing with the state of knowledge about the passive systems and their characteristic parameters on the other side.
- Another important item of improvement is the integration of the passive systems reliability in the PSAs. The first attempts performed within the framework of RMPS have taken into account the failures of the components of the passive system as well as the impairment of the physical process involved like basic events in static event trees. However in order to generalise the methodology, it is important to take into account the dynamic aspects differently than by their alone modelling into the T-H code. Indeed in complex situations where several safety systems are competing and where the human operation cannot be completely eliminated, this modelling should prove to be impossible or too expensive in computing times. It is thus interesting to explore other solutions already used in the dynamic PSA like the method of the dynamic event trees.
- Human factors are important, since they may affect deeply the reliability of a passive system. Indeed the periodic maintenance and inspection of such systems introduce particular constraints; unlike an active system that can be more easily isolated or inspected during the shutdown periods, a passive system requires to be tested under its real physical conditions of utilization and this can generate new specific implementation in the global architecture and safety problems. In addition, the question of whether it is an advantage or a disadvantage that passive systems do not allow operator intervention during its operation, should be investigated.
- Technical-economical evaluations of the systems must be carried out to provide information that is essential for the comparison between passive and active systems. Before comparing a passive and an active system on the same mission, it is necessary to make sure that the passive system design is optimised in terms of performance. Methods have to be developed to ensure the optimisation.

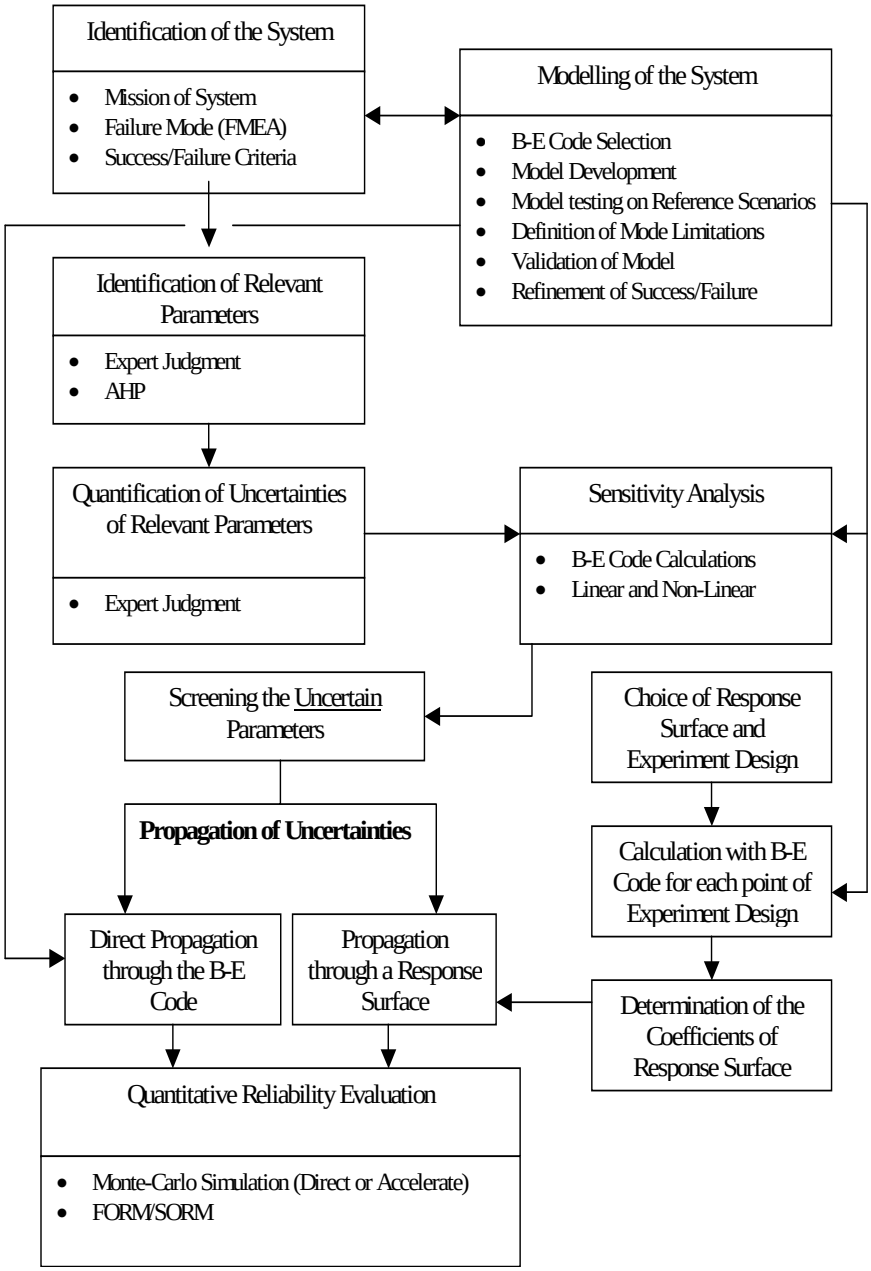

FIG. 5-1. RMPS methodology roadmap.

5.2. METHODOLOGY IMPROVEMENTS

Two steps were identified after the development of the methodology where an improvement was desirable: the inclusion of a formal expert judgment (EJ) protocol to estimate distributions for parameters whose values are either sparse or not available, and the use of efficient sensitivity analysis techniques to estimate the impact of changes in the input parameter distributions on the reliability estimates.

5.2.1. Expert judgment techniques

Based on a deep and thorough review of the available literature about EJ procedures and techniques and their application in different areas within the field of nuclear technology (see, for example, [5-18], [5-19], [5-20] and [5-21]), a protocol containing the following phases is proposed as an improvement of the RMPS methodology:

1. Selection of the project team
2. Definition of the questions to be studied
3. Selection of experts
4. Training
5. Tasks definition
6. Individual experts' work
7. Elicitation of experts' opinions
8. Analysis and aggregation of results
9. Documentation

5.2.1.1. Selection of the project team

The project team consists of analysts and generalists. Analysts are in charge of organising the steps of the protocol, so they should have a sound background in probability and statistics theory, in knowledge psychology and in elicitation techniques, and they should also be skilful at working with people, since they will have to extensively interact with experts. Generalists provide help to the analysts in all subjects related to the passive system studied. They should be able to help experts when decomposing a problem and they should be skilful at getting information sources as needed. So, they must have a good general knowledge about the system studied, though they do not need to be leading experts in that field. The organisation interested in the study usually provides the generalists. For this type of application (passive system related), usually one analyst and one generalist are enough to make the project team.

5.2.1.2. Definition of the questions to be studied

It is extremely important to arrive at an *accurate definition* of the parameters whose uncertain is going to be characterised. *Accurate definition* of a parameter means the full definition of the parameter, including any relevant underlying implicit hypothesis; there should be no ambiguity in the parameter definition. After this, a list including all relevant sources of information should be done. The list of references must show the actual state of knowledge about each parameter under study.

5.2.1.3. Selection of experts

The only objective of this phase is to select the most qualified experts to perform the assessment. Qualified Experts are those that: 1) have the necessary knowledge and experience to perform the assessment, 2) are willing to participate in the assessment, and 3) do not have important motivational biases (personal interests on getting specific results). The first step to get the final list of experts is to start with a large list of potential experts. That first list could be based on the opinion of the generalist plus a thorough search in the scientific literature about that area. A screening should be done checking the three points in the list above. If necessary, interviews should be done to check those conditions, mainly the third one. After performing the screening, a shorter list should be obtained, from which the final selection of experts will be done. In order to arrive at the final list, two criteria should be taken into account: the number of experts to assess each question should preferably be between three and five (based on Bayesian combination of opinions' criteria) and the experts should have as much diversity as possible (different background, different types of organisations, etc.).

5.2.1.4. Training

The objective of this phase is to acquaint experts with normative aspects of EJ elicitation processes. This main objective may be decomposed as the following sub-objectives: 1) motivate experts to provide rigorous assessments, 2) remind them basic concepts of probability and statistics, 3) provide them training in the assessment of Bayesian probabilities, and 4) acquaint them with basic issues related to knowledge biases.

During the motivation phase the experts must get information to point out the importance of the work they are going to do. Firstly, the project team explains to the experts the study frame where their opinions will be used, stressing the part of the study where their opinions are relevant. Secondly, the necessity of EJ will be explained. Thirdly, the project team will inform them that the key issue is not to predict a single value of each parameter under study, but characterising their uncertainty, allowing others to know the actual state of knowledge in that area.

After remembering basic probability and statistics concepts, the experts get some training about assessing Bayesian probabilities, which includes: accurate definition of questions to be assessed (making explicit implicit hypotheses, showing well and non-well posed questions), decomposition as a way to simplify assessments (use of influence diagrams, event trees and uncertainty propagation techniques) and adequate evaluation of different evidences in order to assess probabilities (use of Bayes' theorem and concepts of independence and reliability of information sources). The last part of the training session is dedicated to explain knowledge biases to the experts in order to teach them to provide more reliable opinions.

5.2.1.5. Tasks definition

This step is done through an interactive session of the project team and the experts. The issue at hand is to explain to the experts, in a detailed way, the questions to be assessed and to make a schedule of the activities to be developed by each expert. All the work developed by the team project during the *Definition of the Problem* phase should be used now. The session should start with a presentation by the generalist of the parameters to be assessed, including all relevant sources of information previously identified. Experts should provide their own view of the problem and the definition of the parameters, pointing out, if needed, further information sources, computations to be made, etc. The result of this session, eventually, would be a refined definition of the parameters under study. Common definitions to all the experts should be agreed.

The second step in this meeting is to study the possible ways to decompose each parameter. The team project should provide a seminal decomposition that should be discussed with the experts. The objective is to help the experts to develop their own decompositions. Decompositions could be quite different from one expert to another one. Experts will have to assess uncertainties of variables in the lowest levels. The analysts will do the aggregation.

5.2.1.6. Individual experts' work

Experts develop their analysis during this phase, according to the schedule agreed in the previous step. Each expert will write by the end of this period a report summarising the main hypotheses and procedures used during his/her work, the conclusions achieved and, if he/she wishes, a preliminary assessment of uncertainties. Whenever needed during this period, the project team should be available to each expert in order to provide statistical support or to solve any doubt about the parameters to be assessed. At the end of this phase, the project team organises a meeting with all the experts. Each expert presents his/her work and the conclusions achieved. This meeting allows each expert to get some hints about alternative ways to tackle the problem.

5.2.1.7. Elicitation of experts' opinions

The elicitation of each expert opinion's is individual and should be done in a quiet environment, if possible without interruptions. It is convenient to have the presence of a generalist, in addition to the expert and the analyst. In a systematic way, the analyst gets the opinion of the expert for each parameter, asking for supporting reasons whenever necessary. The role of the generalist in this session is to provide additional information when needed, to provide general support and to audit the session in order to avoid irregularities (bias induction, etc.). Whenever needed, the analyst could ask questions in a different way to check potential inconsistencies. The session must be recorded as much as possible (tape recorders, video or extensive hand annotations). The techniques used to help the expert when assessing uncertainties are quite standard: quantile assessment for continuous variables and probability estimations for discrete variables; in the case of experts with some skills in probability other techniques like direct parameter assessment or drawings are acceptable.

5.2.1.8. Analysis and aggregation of results

The objective of this phase is to check that there are not important biases and that the underlying rationale is correct. If biases and logic faults are not present in expert's assessments, the next step is to check if individual opinions may be aggregated to get a unique distribution for each parameter.

Before aggregating individual distributions, one condition should be checked. It is related to the overlap between distributions of different experts. If the distributions do not overlap or the overlap is very poor, it means that essentially the experts disagree. In that case aggregation should be avoided. Under these circumstances a reconciliation session could be of help. An analyst should lead the session and should organise it according to the following steps: 1) exposition of different opinions, 2) identification of differences, 3) discussion about the reasons for each original assessment, 4) discussion about the different sources of information used, and 5) re-elaboration of individual opinions in posterior elicitation sessions or joint assessment (through consensus) of a common distribution, if agreed by experts.

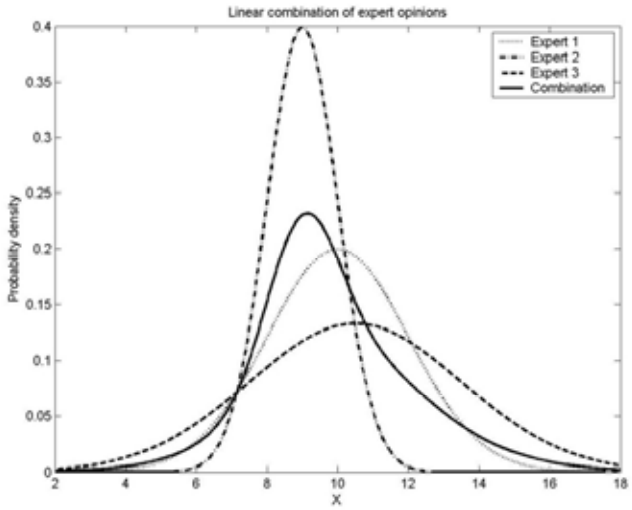

FIG. 5-2. Example of linear combination with equal weights of the opinion of three experts.

In the case that a consensus distribution is obtained, this is the final step (before documentation). If further elicitation sessions are needed, the consistency of the opinions is checked again and aggregation is done if acceptable overlap is achieved. Otherwise, the project team should choose which opinions could be aggregated as main opinion of the group, and which opinions should be left as an alternative to perform sensitivity analysis. The main strategies for aggregation are: 1) linear combination, 2) log-linear combination, and 3) Bayesian combination. The most popular aggregation technique is the linear combination with equal weights (all experts are considered equally credible). Figure 5-2 shows an example of linear combination with equal weights of the opinion of three experts. Opinions are given in terms of probability density functions (PDFs) in Fig. 5-2.

5.2.1.9. Documentation

The documentation of the application must be as complete as possible, including results and description of the ways to obtain them. The contents of the documentation should follow the order of application of the procedure, recording, in each step, *what* has been done, *why* it has been done, *how* it has been done and *who* has done it. In order to achieve this degree of documentation, a schedule of standardised documentation activities should be made for each phase. It should always be completely clear to the reader what is a result assessed by an expert and what results are the outcomes of an aggregation, sensitivity analysis or any other analysis not provided explicitly by an expert

5.2.2. Distribution sensitivity analysis

It is of real interest to check how much could change the distribution of the output (relevant output parameter) of the passive system, and consequently its reliability, when the distribution of the input parameters changes, say from $f_1(\mathbf{x})$ to $f_2(\mathbf{x})$. A method is available in the scientific literature to tackle this problem: the rejection method [5-22]. This method is also proposed to be included in the methodology.

There are two conditions for the application of this method: first, the support of $f_2(\mathbf{x})$, R_2, must be contained in the support of $f_1(\mathbf{x})$, R_1; and second, the quotient $f_2(\mathbf{x})/f_1(\mathbf{x})$ must be bounded. Let us assume that the bound is H; in other words, $(f_2(\mathbf{x})/f_1(\mathbf{x})) \leq H \ \ \forall \mathbf{x} \in R_2$. In the following lines are the steps to be followed:

- <u>*Step 1*</u>⇨ Obtain a sample of size n of the random input vector under the reference distribution: $\mathbf{x_1}, \mathbf{x_2}, \ldots, \mathbf{x_n}$
- <u>*Step 2*</u> ⇨ Run the code for those n sets of inputs and get the corresponding sample of the output variable: $y_1, y_2, \ldots, y_n$
- <u>*Step 3*</u>⇨ For each sample $\mathbf{x_i}$, take a sample of the uniform distribution V_i between 0 and $Hf_1(\mathbf{x_i})$
- <u>*Step 4*</u>⇨ Retain in the sample the corresponding output value $Y_i=y_i$ if the realisation v_i of V_i is less or equal to $f_2(\mathbf{x_i})$, otherwise reject it. This way a sample $y'_1, y'_2, \ldots, y'_k$ (subsample of the original sample $y_1, y_2, \ldots, y_n$) is obtained, which follows the distribution $f_2(\mathbf{x})$

This procedure for estimating the distribution function of Y under $f_2(\mathbf{x})$ produces an unbiased estimator (no systematic error is introduced in the estimation process).

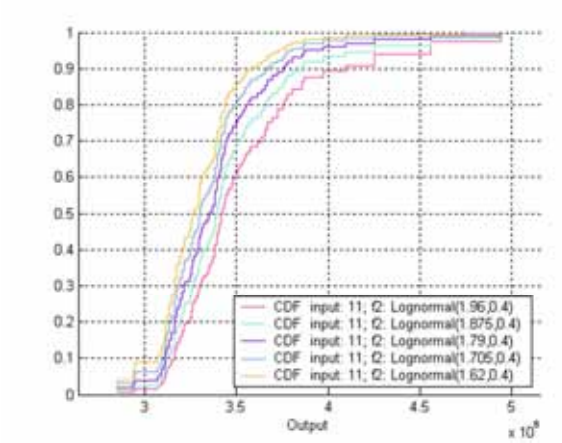

FIG. 5-3. Application of a distribution sensitivity technique to a passive system (important input parameter).

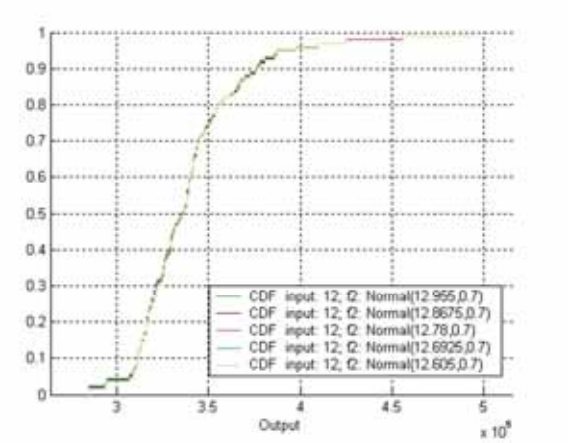

FIG. 5-4. Application of a distribution sensitivity technique to a passive system (irrelevant input parameter).

Figures 5-3 and 5-4 show the application of an extension of the rejection method (see [5-23]) to a passive system. In both figures, the y-axis represents cumulative relative frequency. The output is in both cases the peak pressure in the primary system, given in Pa (Pascal), The system is supposed to fail if the output exceeds 4 Mpa (value $4 \cdot 10^6$ on the plot). Figure 5-3 shows the results of applying this technique in the case of an important parameter. Results reported in this figure refer to the base case (intermediate line, input parameter following a log-normal distribution with geometric mean 1.79 and geometric standard deviation 0.4) and to four different alternatives for the geometric mean. The impact of changing the geometric mean of this input parameter on the output cumulative distribution function (CDF) is obvious and relevant. Watching the probability of exceeding the failure criterion, in the base case it is roughly 0.04, and it varies between 0.02 and 0.11 for the different alternatives. Figure 5-4 shows that changing the mean of the input normal parameter considered has no impact on the whole CDF and on the probability of system failure.

5.3. ALTERNATIVE METHODOLOGIES

In addition to the RMPS approach, a number of alternative methodologies have been investigated for the reliability assessment of T-H passive systems. This section provides a synthetic presentation of some of these methodologies.

5.3.1. ENEA methodologies

In this part, for completeness the three alternative methodologies proposed within the CRP by ENEA and currently available in the open literature for this task are reviewed [5-24, 5-25]. In the first methodology, the failure probability is evaluated as the probability of occurrence of different independent failure modes, a priori identified as leading to the violation of the boundary conditions and/or physical mechanisms needed for successful passive system operation. In the second, modelling of the passive system is simplified by linking to the modelling of the unreliability of the hardware components of the system: this is achieved by identifying the hardware failures that degrade the natural mechanisms upon which the passive system relies and associating the unreliability of the components designed to assure the best conditions for passive function performance. The third approach is based on the concept of functional failure, defined as the probability of the passive system failing to achieve its safety function as specified in terms of a given safety variable crossing a fixed safety threshold. In the following, these methods are presented and analysed.

5.3.1.1. Approach based on independent failure modes

In this approach, the reliability of a passive system is seen from two main perspectives: system/component reliability (e.g., valves, piping) and physical phenomena degradation. The former calls for soundly-engineered safety components with at least the same level of reliability of the active ones and can be treated in the classical way, i.e., in terms of failures of components. The latter perspective is concerned with the evaluation of the natural physical phenomena underpinning the passive safety function and the long term effects of the surroundings on its performance/stability; it addresses the critical failures that defeat or degrade the natural mechanisms which sustain the operation of the passive system.

In this view, the passive system failure probability is evaluated as the probability of occurrence of the different failure modes, considered independent, critical for the passive safety function, i.e. which would violate the boundary conditions and physical mechanisms necessary for the successful operation of the passive system. A detailed description of the approach is given in [5-26] together with an exploratory application to a typical natural circulation, two phase flow loop of an isolation condenser [5-10].

The operative steps of the procedure adopted are:

- Identify the failure modes affecting the natural circulation phenomenon: for this scope, well structured and commonly used qualitative hazard analyses may be adopted, e.g. FMEA and HAZOP, specifically tailored to considering the phenomenology of the natural circulation [5-27]. These analyses must concern both mechanical components and the natural circulation itself, treated as a "virtual component" whose operation may be disturbed by unexpected mechanical and thermal loads, plugging, non-condensable gas buildup and heat exchange process reduction which generate additional "physical" failure modes.
- Identify a set of n critical parameters $x = \{x_1, x_2, \ldots, x_i, \ldots, x_n\}$ as direct indicators of the failure modes identified in step 1. (e.g., non-condensable fraction, undetected leakage size, valve closure area, heat loss and piping layout).
- Assuming that all of the failure modes identified in step 1 are independent from each other, select proper probability distributions $\{f_1(x_1), f_2(x_2), \ldots, f_i(x_i), \ldots, f_n(x_n)\}$ over the ranges of variability of the corresponding critical parameters identified in step 2: the mean (or, alternatively, the median or mode) values can be taken equal to the expected values of the parameters in nominal conditions while the variances represent the uncertainty associated to each mode of failure.
- Identify the critical intervals $\{F_1, F_2, \ldots, F_i, \ldots, F_n\}$ defining the failure criteria for all the parameters: if at least one of the critical parameters lies in its critical interval, then the system is failed.
- Compute the failure probabilities, Q_i, $i = 1, 2, \ldots, n$, pertaining to each failure mode by integrating each probability density function, $f_i(x_i)$, over the corresponding range of failure, F_i:

$$Q_i = \int_{F_i} f_i(x_i)dx_i \, , i = 1,2,...,n \tag{5-3}$$

- Under the assumption of independence (step 3), calculate the overall probability of failure of the natural circulation system, Q, by combining all the failure probabilities for each failure mode, Q_i, as follows:

$$Q = 1 - \prod_{i=1}^{n}(1 - Q_i) \tag{5-4}$$

Thus, for a passive system with n mutually independent failure modes, the total failure probability is computed as for a series system with n critical elements, by summing-up all the single failure probabilities.

Once the probability distributions of the parameters are assigned, the failure probability of the system can be easily obtained from Eqs 5-3 and 5-4 if proper failure criteria are assigned in step 4. Unfortunately, difficulties arise in assigning the range and the probability density functions of the critical parameters defining the failure modes, as well as in defining proper failure criteria, i.e. the failure threshold, because of the unavailability of a consistent experimental and operating data base. This lack of experimental evidence forces to resort to expert/engineering judgments to a large extent, so that results depend strongly upon the expert judgment elicitation process [5-10, 5-26, 5-27].

5.3.1.2. Approach based on failure modes of passive system hardware components

In order to overcome the difficulties of the approach highlighted in the previous section, an effort could be made to try to associate to each natural circulation degradation mode a failure mode of a hardware component designed to ensure the corresponding conditions for successful passive safety function performance (e.g. vent valves opening for removal of non-condensable gases, piping integrity, heat exchanger for heat transfer process).

Thus, the probabilities of degraded physical mechanisms upon which the passive system relies are reduced to unreliability figures of the components whose failures challenge the successful passive system operation [5-10]. If, on the one hand, this approach may in theory represent a viable way to address the matter, on the other hand, some critical issues arise with respect to the effectiveness and completeness of the performance assessment over the entire range of possible failure modes that the system may potentially undergo and their association to corresponding hardware failures. In this simplified methodology, degradation of the natural circulation process is always related to failures of active and passive components, not acknowledging, for instance, any possibility of failure just because of unfavourable initial or boundary conditions.

In addition, the fault tree representing the physical process decomposition is used as a surrogate model to replace the complex T-H code that models the system behaviour. This decomposition is not appropriate to foresee interactions among physical phenomena and makes it extremely difficult to realistically assess the impact of parametric uncertainty on the performance of the system.

5.3.1.3 Functional failure approach

This approach exploits the concept of functional failure to define the probability of failing to successifuly carry out a given safety function (e.g., decay heat removal). The idea comes from the Resistance-Stress (R-S) interference model of fracture mechanics (Fig. 5-5).

In the framework of T-H passive systems reliability assessment, *R* and *S* express respectively the safety functional Requirement (*R*) on a safety physical parameter (for example, a minimum threshold value of water mass flow required to be circulating through the system for its successful performance) and system State (*S*) (i.e., the actual value of water mass flow circulating). Probability distributions are assigned to both *R* and *S* to reflect the uncertainties in both the safety thresholds for failure and the actual conditions of the system state. The function of the passive system defines the safety parameter values that define system failure, whose probability is obtained by comparing the state probability density function with that of the defined safety functional requirement [5-28, 5-29, 5-30].

Note that the analysis typically focus on the passive system process variables rather than on the reactor parameters, since these latter are not considered direct indicators of the performance of the system, despite the effect of the surroundings on the performance/stability of the natural circulation.

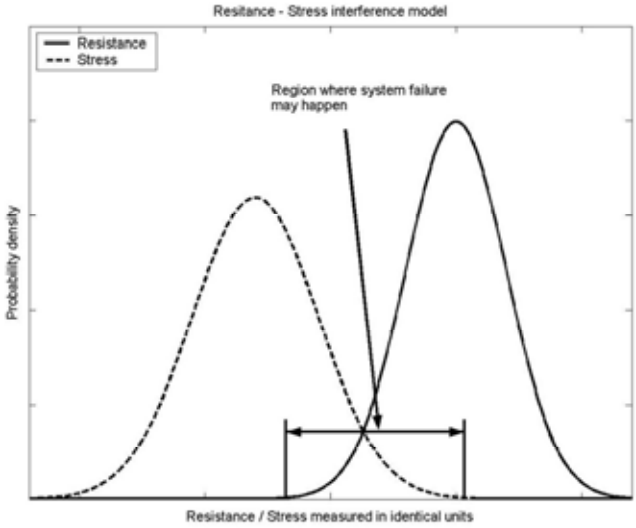

FIG. 5-5. Resistance-Stress (R-S) interference model.

In the analysis, the states of the system are divided into two sets, the failed and the safe states, separated by a limiting state of the safe set which identifies the safety functional requirement parameter *R*. Failure then corresponds to the crossing of the system parameter *S* through the limit state of the safe set [5-30]. Introducing the random variable Limit State Function (LSF) as $G = R - S$, one defines

$$G = R - S \quad \begin{cases} > 0 \text{ for function successfully performed} \\ = 0 \text{ at limit state} \\ < 0 \text{ for failure at performing the function} \end{cases} \tag{5-5}$$

Obviously, the difficulties lie in the definition of the probability distributions $f_R(r)$ and $f_S(s)$ of *R* and *S* respectively, from which the distribution $f_G(g)$ for *G* is derived. In lack of reliable data, engineering judgement must again be used to obtain such distributions. Then, the failure probability *Q* is computed as the probability that *S* is greater than *R*, i.e. the LSF in Eq. 5-5 is lower than 0:

$$Q = P(S > R) = \int_{-\infty}^{+\infty} \left[\int_{r}^{+\infty} f_S(s)ds \right] f_R(r)dr = P(G < 0) = \int_{-\infty}^{0} f_G(g)dg \tag{5-6}$$

An example of application of this approach can be found in Ref. [5-29], in which the uncertainty distribution of the peak cladding temperature (the stress or load on the cladding) is calculated by propagating the uncertainties in the performance of the passive cooling system through Monte Carlo (MC) importance sampling.

It is conceptually worth noting a subtle difference in the treatment of the variables *R* and *S* of the resistance-stress model for the reliability assessment of passive systems [5-28]. In fact, if for example *S* and *R* are the actual mass flow rate and its requirement threshold value below which natural convection fails, respectively, the conditions discriminating the safe state region from the failure region in (4) are reversed: the function is successfully realized when *S* is larger than *R* whereas, on the contrary, failure occurs when *S* is less than *R*. The same holds in case of consideration of other

physical variables as performance outputs, like the pressure differential driving force or the heat removal rate.

In a more general case, failure of the system may occur only when a system actual state parameter *S* falls below a minimum threshold value or above a maximum threshold; the probability of the two exclusive events of failure must then be summed to give the total probability of failure:

$$Q = Q_l + Q_u = \int_{-\infty}^{+\infty}\left[\int_{S}^{+\infty} f_R(r)dr\right] f_S(s)ds + \int_{-\infty}^{+\infty}\left[\int_{r}^{+\infty} f_S(s)ds\right] f_R(r)dr \qquad (5\text{-}7)$$

The application of the functional reliability approach in Ref. [5-28], where the two quantities *R* and *S* are considered independent, shows that the type of the probability distributions does not influence the estimated probability of failure of the system, which, conversely, is affected by the assigned parameter range.

Finally in Ref. [5-30], reliability analysis is of interest mainly as a tool in the design process, within a risk-informed framework. The reliability-based design approach for the T-H passive systems is introduced, by evaluating the *R-S* model of a characteristic parameter against the reliability targets and finally an analytical solution is obtained. The results of the analysis, in terms of minimal parameter requirement as a function of the desired reliability, help designer determine the allowable limits for the system performance parameters, within a risk-informed design process.

5.3.2. APSRA methodology

A different approach is followed in the APSRA (Assessment of Passive System Reliability) methodology developed at Bhabha Atomic Research Centre (BARC), India [5-31]. In this approach, a failure surface is generated by considering the deviation of all those critical parameters, which influence the system performance. Then, the causes of deviation of these parameters are found through root diagnosis. It is attributed that the deviation of such physical parameters occurs only due to a failure of mechanical components such as valves, control systems, etc. Then, the probability of failure of a system is evaluated from the failure probability of these mechanical components through classical PSA treatment. Moreover, to reduce the uncertainty in code predictions, APSRA methodology proposes to use experimental data from integral facilities as well as separate effect tests to reduce the uncertainty in best estimate codes for prediction of failure surface.

The different steps of the methodology are displayed on Fig. 5-6. Some steps of the methodology are classical such as identification of the critical parameters and definition of failure criteria. The originality of the method lies in the generation of a failure surface and its validation with test data (step V) and the use of root diagnosis to find deviation of key parameters which can cause the failure of the system (step VI).

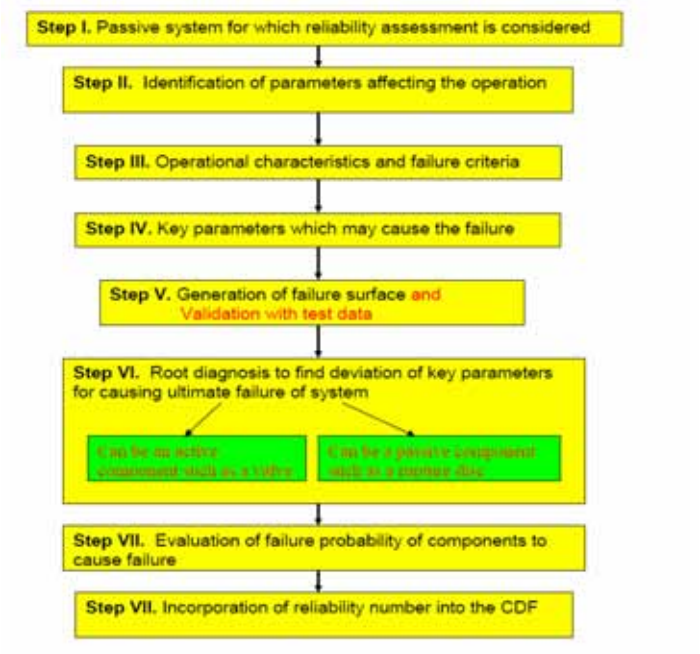

FIG. 5-6. The APSRA methodology.

The failure surface is produced in using a T-H code by parametric study, where each key parameter is deviated from its nominal value until the system fails. An example of failure surface obtained with 3 key parameters is given on Fig. 5-7. After establishing the failure surface, the task is to find out the cause of deviation of key parameters, which could produce the system failure.

The deviation of key parameters can be caused either by:

- Failure of active components: valves, external pumps, control systems,
- Failure of passive components: passive valves, relief valves.

For example, a high feed water temperature in natural circulation reactor, can be due to a low feed water flow rate. This can happen due to:

- malfunctioning of the feed pumps,
- malfunctioning of feed control valves or controller,
- malfunctioning of steam drum level control valves, etc.

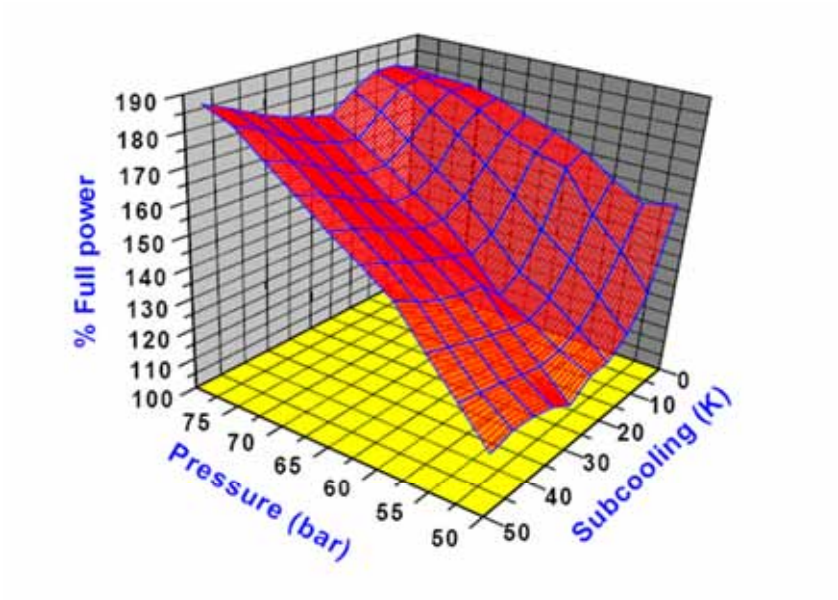

FIG. 5-7. Example of failure surface.

A fault tree is build based on this logic. And similar fault trees can be built for change of other key parameters. From these fault trees, the probability of deviation of key parameters can be calculated. Looking at the failure surface, the probability of failure for each point can be calculated by considering the probability of deviations of all those parameters which are responsible for causing the failure. The result obtained is a surface of failure probabilities (Fig. 5-8). This methodology has been applied to Main Heat Transport (MHT) system of the Indian AHWR concept.

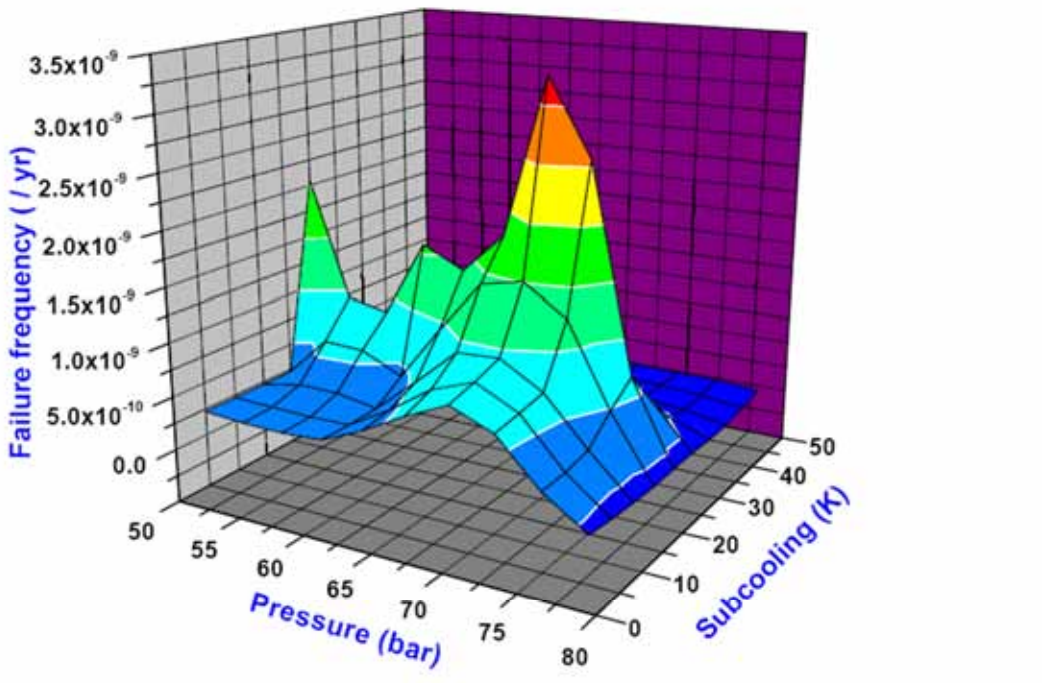

FIG. 5-8. Achievement of the probabilities of failure of the passive system.

5.3.3. Similarities and difference between methodologies RMPS, APSRA and ENEA

As highlighted above, all three methods devised by ENEA share with the main RMPS approach the issue related to the uncertainties affecting the system performance assessment process. With respect to the RMPS a greater simplicity is introduced, although detrimental to the relevance of the approaches themselves: this is particularly relevant as far as the approach based on hardware components failure is concerned. The approach based on independent failure modes introduces a high level of conservatism as it appears that the probability of failure of the system is relevantly high, because of the combination of various modes of failure, where a single fault is sufficient to challenge the system performance. The correspondent value of probability of failure can be conservatively assumed as the upper bound for the unavailability of the system, within a sort of "parts-count" reliability estimation. Finally the main drawback in the last ENEA method lies in the selection and definition of the probability distributions that describe the characteristic parameters, based mainly on subjective/engineering judgment.

Different approaches have been used in the RMPS and APSRA methodologies. RMPS proposes to take into account, in the PSA model, the failure of a physical process. This problem is treated in using a best estimate (T-H) code plus uncertainty approach. APSRA includes in the PSA model the failure of those components which cause a deviation of the key parameters from their nominal states resulting in a system failure. Hence, APSRA does not treat the deviation of key process parameters causing the failure of the passive system through a probability density function unlike that treated by RMPS. Besides, APSRA incorporates an important effort on qualification of the model and use of the experimental data to reduce the model uncertainty. On the other hand, RMPS treats the model uncertainties through probability density function (similar to that of variation of process parameters from their nominal states) which are allowed to propagate to evaluate the reliability of passive system.

5.4. RELIABILITY ANALYSIS OF "CAREM LIKE" PASSIVE RESIDUAL HEAT REMOVAL SYSTEM BY MEANS OF RMPS METHODOLOGY

5.4.1. Introduction

The present section deals with the application of RMPS methodology [5-5, 5-11, 5-32] to a Passive Residual Heat Removal System of a "CAREM Like" reactor. The aim of this work is to quantify the failure probability of the passive safety function associated with the system under analysis. The methodological steps performed can be separated into the following:

- Identification of the system mission, accident scenario and associated failure criterion,
- System modelling,
- Characterization of the TH phenomena (identification of relevant parameters and their correspondent uncertainties),
- Direct Monte Carlo simulation applied to TH code,
- Sensitivity analysis,
- Quantitative reliability estimation.

The system mission alludes to the safety function that the passive system has to perform (i.e. decay heat removal and primary pressure decrease); these are the goals for which the passive system has been designed and located within the overall system. Therefore, the system mission is related with some particular/s initiating event/s and allows the definition of design targets for passive system.

The failure criterion is established in terms of the non fulfillment of the mentioned design targets.

Once the system mission, accidental scenario and failure criterion are established, a system model has to be developed by means of a best-estimate TH code (e.g. RELAP5 Mod3.3).

According to the procedural steps, the relevant parameters connected with the TH phenomena have to be identified, associating to them adequate nominal values, range of variation and probability distributions concerning which parts or the range are more likely than others.

Direct Monte Carlo simulation involves the propagation of the uncertain selected parameters through the considered TH code obtaining a model response (i.e. output variable) which allows, by means of statistical techniques, to estimate the probability of failure of the passive function.

The model response is achieved through of the application of an adequate system performance indicator, strictly linked to the defined failure criterion.

In case the variance of the estimator is quite large, it may take an impractical number of simulations cycles to achieve a specific precision of the sought estimate. In this case, uncertain parameter can be propagated throughout a simplified computational model (i.e. response surface) in order to obtain the desired precision or at least a proper upper bound for the estimation of the failure probability.

5.4.2. CAREM reactor description

5.4.2.1. Primary system

The CAREM NPP design is based on a light water integral reactor. The whole high-energy primary system, core, steam generators, primary coolant and steam dome, is contained inside a single pressure vessel.

For low power modules (below 150MWe), the flow rate in the reactor primary systems is achieved by natural circulation (Fig. 5-9). Reactor coolant natural circulation is produced by the location of the steam generators above the core. The driving forces obtained by the differences in the density along the circuit are balanced by the friction and form losses, producing the adequate flow rate in the core in order to have the sufficient thermal margin to critical phenomena. Coolant acts also as neutron moderator.

Self-pressurization of the primary system in the steam dome is the result of the liquid-vapour equilibrium. The large volume of the integral pressurizer also contributes to the damping of eventual pressure perturbations. Due to self-pressurization, bulk temperature at core outlet is near saturation. Heaters and sprinkles typical of conventional PWR’s are thus eliminated [5-33, 5-34].

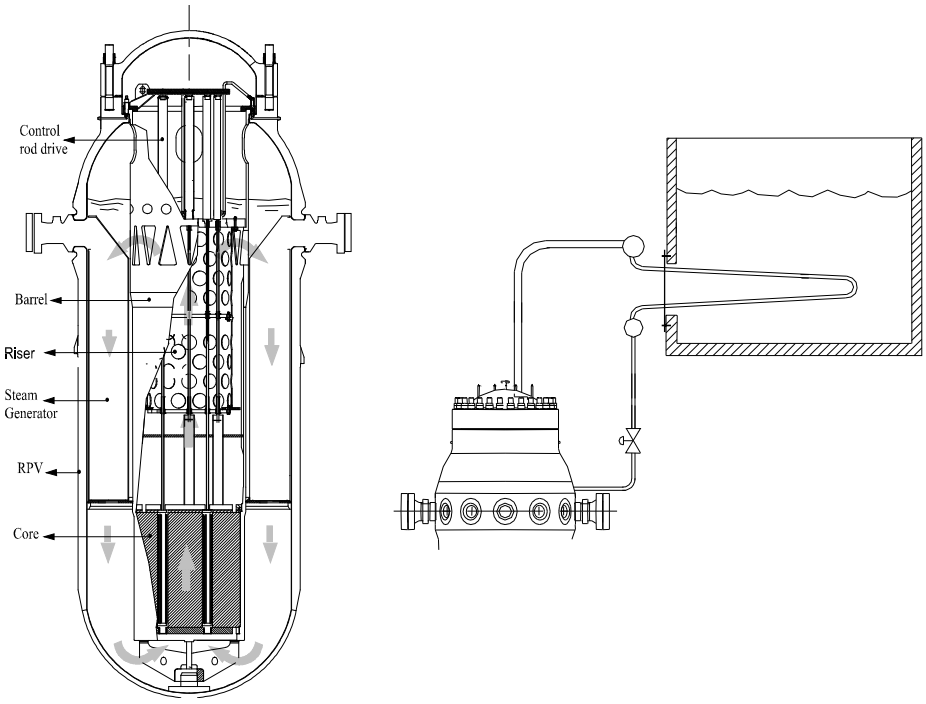

FIG. 5-9. CAREM primary system and passive residual heat removal system.

5.4.2.2. Passive residual heat removal system

The Passive Residual Heat Removal System (PRHRS) been designed to reduce the pressure on the primary system and to remove the decay heat in case of Loss of Heat Sink (LOHS). It is a simple system that operates condensing steam from the primary system in emergency condensers (Fig. 5-9). The inlet valves in the steam line are always open, while the outlet valves are normally closed, therefore the tube bundles are filled with condensate. When the system is triggered, the outlet valves open automatically. The water drains from the tubes and steam from primary system enters into the tube bundles, condensing over their cold surface. The condensate is returned to the reactor vessel establishing a natural circulation circuit. In this way, heat is removed from the reactor coolant. During the condensation process the heat is transferred to the water of the pool by a boiling process [5-34].

5.4.3. CAREM like integral reactor model

The integral system proposed is a CAREM-like reactor type being composed by a primary system and PRHR system.

The term CAREM-like implies that the model reported approximates the design characteristics of CAREM-25 (geometric values, systems layout, etc.) without being “actual” design values, and further simplifications has been taken into account in order to set up a definitive model for the development of the task reported here.

Despite the above, mentioned CAREM-like represents an accurate model for passive safety function evaluation purposes and for testing the capabilities of the methodology employed.

5.4.3.1. CAREM-like passive residual heat removal system (PRHRS) identification

Mission of the system: Given a Loss of Heat Sink transient, the safety function of the Passive Residual Heat Removal System (PRHRS) is to remove the decay heat, thus reducing the pressure on primary system until the hot shutdown condition is reached.

Accident scenario: In order to evaluate the system reliability it has been proposed as accident scenario a LOHS. The initiating event considered has the following characteristics:

- Loss of SG removed power with a 12.8 sec. ramp.
- No feed and bleed systems are taken into account.
- All safety systems involved: First Shutdown System (FSS), PRHRS and Safety Relief Valves) are triggered only by primary system pressure.

No feedback due to reactivity coefficients is accounted for (conservatively, core power remains constant until the SCRAM condition is reached).

Failure criterion: In terms of the system mission can be defined two design targets for the PRHRS. The first one is a short term design target and implies the avoidance of primary system overpressure, at or beyond the opening set-point of safety relief valves. The second one is a long term target and involves the system hot shutdown condition. For this study case, only the short term design target is regarded; therefore, the passive systems failure condition is achieved when the safety relief valves opening set-point is reached.

5.4.3.2. Description of CAREM-like RELAP5 model

In order to perform the calculations with RELAP5 Mod3.3 a one dimensional nodalisation of CAREM-like reactor has been developed (Figs 5-10 & 5-11). The model involves the Primary System and the PRHRS.

5.4.3.3. CAREM-like primary system nodalisation

The primary circuit nodalisation has been established dividing it into the most relevant components:

- RPV dome
- Steam Generators (SG)
- Down comer
- Riser
- Core
- Lower plenum

Special attention was paid to the dome nodalisation, in order to allow three dimensional fluid circulation in a one dimensional path [5-33]. For its description, the dome nodalisation can be divided into three parts (Fig. 5-11). The first part is the dome lower region (BR302, BR306, BR356 and BR352), which allows circulation of the fluid coming from riser to SG, also permitting the fluid movement in the liquid/vapour stratified zone. The second part is the upstream-downstream region (BR358, PIPE 360, PIPE314, BR309) implemented in order to model properly the physical process of fluid motion inside the dome. Finally, the third part is the upper vapour region (BR141), which represents the upper zone of the RPV that contains only vapour and where the connections of the PRHRS steam lines are located.

Condensation on control rods hydraulic feed tubes (which are located into the steam dome [5-29] and condensation on RPV wall due to thermal loss to exterior are modelled since they rule the vapour generated in the core, which travels along the riser up to the dome. The amount of vapour affects the hot leg density and the buoyancy forces that, together with the pressure losses, determine the primary circuit mass-flow rate.

The condensation on the RPV is also modelled by fixing a heat flux boundary condition, in this case, through heat structures HS364 and HS368.

The reactor down comer, riser and lower plenum are modelled as single hydronamic component (HC) (PIPE 110, PIPE 130 and BR 116). Down-comer and riser are divided into a suitable number of nodes in order to follow properly the thermal fronts. On the other hand lower plenum is modelled with a unique volume aiming to represent the water mixture effect before it comes into the core.

The SG primary side is modelled as a single HC (PIPE 162) regarding the above exposed criteria for the down-comer and riser nodalisation. The heat transfer is modelled through HS232 by imposing as boundary condition the SG removed power. The overall model represents the twelve SG with a primary flow and heat transfer areas equal to the sum of all of them.

The core active zone is modelled by the HC PIPE120 and HS120. The power generated in the core is imposed as boundary condition by HS120. The power source is obtained from point kinetics calculation, according to ANS79-3 model, without taking into account the feedback due to reactivity coefficients.

For the primary circuit there are also included RPV and Barrel passive heat structures. This heat structures has been modelled respecting the total masses and material heat capacity.

For the overall primary system sliced nodalisation and similar length between nodes of adjacent volumes criteria has been adopted.

5.4.3.4 CAREM-like passive residual heat removal system nodalisation

The PRHRS nodalisation includes the following system components:

- Steam line (steam line piping + in header)
- Condensers
- Return line (return line piping + out header)
- Pool

As for the primary system model, the sliced nodalisation criterion has been adopted in the steam and return lines regarding also the criterion of similar length between nodes of adjacent volumes.

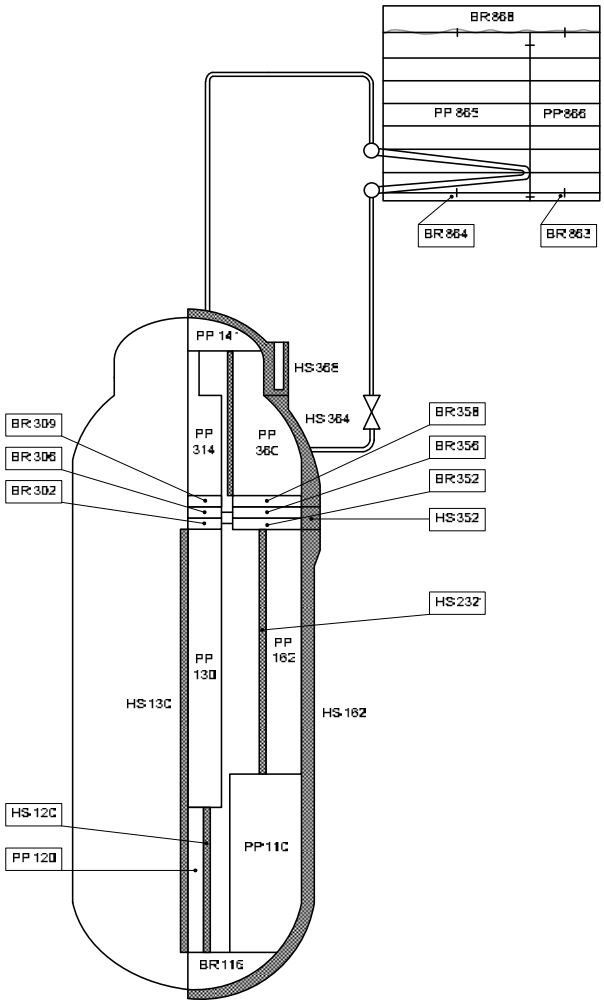

FIG. 5-10. CAREM-like nodalisation layout.

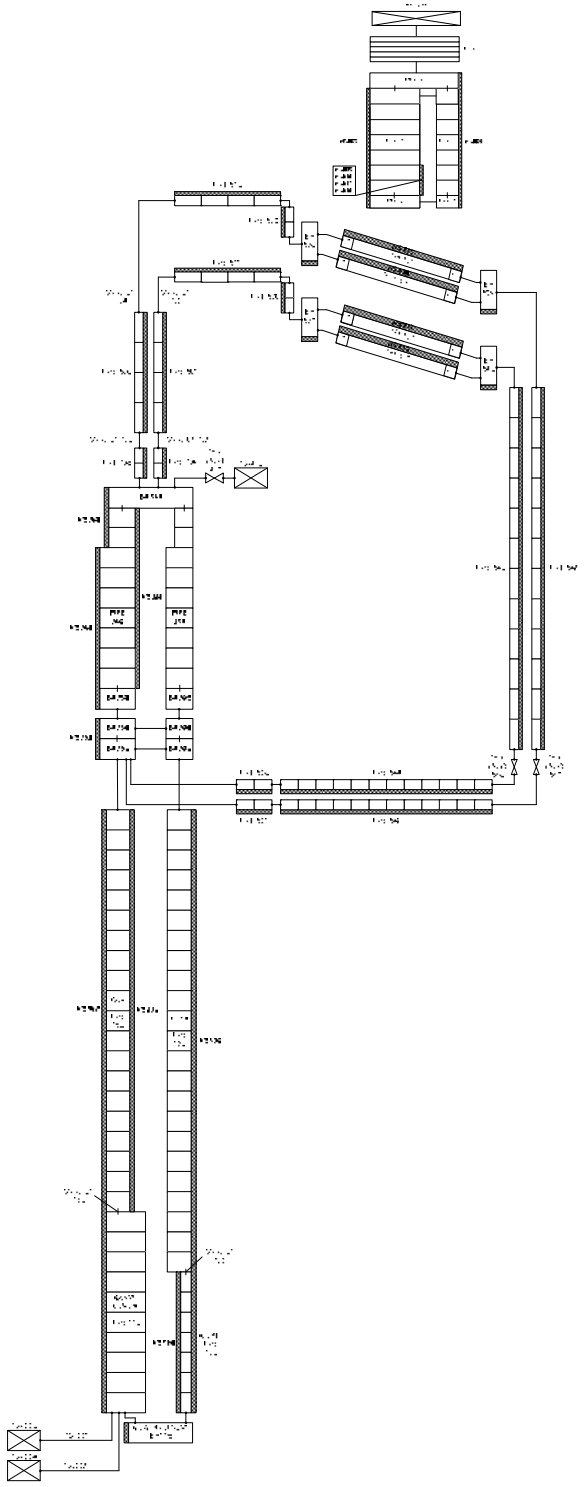

FIG. 5-11. CAREM-like nodalisation scheme.

Since the steam line valves are always open they were not considered in the present nodalisation (Fig. 5-11). A single valve has been added in the discharge line instead the complete set of two valves.

For all the system piping the correspondent heat structures has been taken into account. For the particular case of the heat structures associated to the steam line pipes (HS798/799 – HS800/801–

HS810/811) a heat flux boundary condition has been imposed aiming to simulate the system heat losses.

In order to simulate properly the natural circulation inside the pool a detailed open pool model has been adopted regarding an upstream branch representing the zone of the pool that is in contact with the condensers and above them, and a downstream branch representing the surrounding areas.

The atmospheric condition is fixed by a time dependent volume and a fictitious pipe connected to the top of the pool.

In order to improve the time in which the steady state condition is reached two fictitious controls have been added to the previously described model.

The first one is a dome water level control, which modifies the primary circuit mass inventory by adding/extracting water from the down-comer. Meanwhile the second one is a primary circuit pressure control.

All the mass flow rates through the junctions must verify to be close to zero before the transient beginning. Regarding the above mentioned and in order to assure a real steady state condition the system runs free of controls during several seconds before the start of the transient.

5.4.4. Results for reference case

5.4.4.1. Steady state verification for nominal case

Previous to the transient run, steady state verification has been performed in order to determine the acceptability of the obtained results for the steady state condition. Table 5-1 shows that the acceptability criteria are accomplished for reference case.

TABLE 5-1. STEADY STATE VERIFICATION

	PARAMETER	ERROR(3)	UNIT	ACCEPTABLE ERROR	UNIT
OP (1)	Power operational	0.00	%	-	-
P1	Reactor Nominal Pressure	0.00	%	-	-
L	RPV dome water level	0.04	m	0.05 (2)	m
M	PCS mass flow rate	0.3	%	2	%
HL (1)	RPV dome heat losses	0.0	%	10	%
C2 (1)	Heat losses piping — IC suction	0.4	%	10	%

(1) Imposed as boundary condition.
(2) This acceptable error is defined for the pressurizer collapsed level in a PWR reactor.
(3) The % error is defined as: $e[\%] = |\text{ref. value} - \text{calc. value}| / |\text{calc. value}|$

5.4.4.2. Description of the loss of heat sink (LOHS) transient

The dynamics of the primary system pressure, regarding a LOHS scenario, is described in this section. In order to clarify the explanation, three phases of the transient have been identified (Fig. 5-12).

Phase I: due to the LOHS, down-comer temperature increases leading to a decrease in the water density. Therefore, the steam in the dome is compressed increasing the system pressure. When primary system pressure reaches the correspondent set-point, the FSS is triggered. As a consequence of the power reduction core void generation stops. Thus, temporal pressures decrease is verified. Once finalized this brief depressurization stage, because there is no power removal, the temperature goes on increasing in the down-comer and in the whole circuit driving again to the primary circuit coolant expansion with the subsequent primary system pressure increase. During this pressurization phase, the whole primary system remains in a subcooled condition.

Phase II: when system's pressure reaches the PRHRS set-point, the system is activated by opening the return line valves. As it was explained before, the subcooled water drains from the tubes and steam coming from primary system enters into the tube bundles condensing on them. Immediately after the PRHRS actuation a first sharp depressurization phase takes place. This behaviour is mainly due to imbalance coming from the steam condensation in the dome without liquid boiling in the primary system. This condition is also accompanied, in a less extent, by the subcooled water (at pool temperature) coming into the RPV from condensers tubes immediately after the PRHRS actuation.

Phase III: once the system reaches again its saturation condition the depressurization ends and from this moment on, pressure begins to be ruled by steam reposition into the steam dome (generated in the core) and steam condensation in the PRHRS

The main phenomena associated to each one of its phases are summarized in Table 5-2.

TABLE 5-2. DESCRIPTION OF LOHS FOR REFERENCE (NOMINAL) TRANSIENT

Phase ID	Descriptor	Main phenomenological condition
I	Pressurization phase	Primary system subcooled condition
II	Sharp depressurization phase	Steam condensation in the dome without liquid boiling in the primary system
III	PRHRS operation phase	Primary system near equilibrium condition

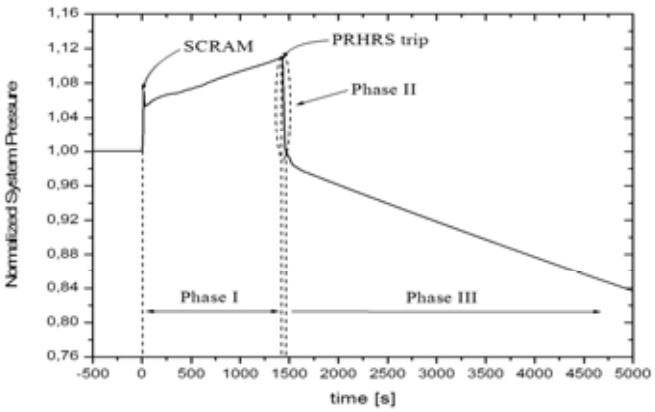

FIG. 5-12. Short term pressure evolution for reference (nominal) case. This evolution reflects the condition of higher power removed by PRHRS (in relationship with the core generated power) thus leading to a sustained depressurization after the ending of Phase II.

5.4.5. Definition of the performance indicator

The output observable characterizes the passive system behaviour regarding the design failure criterion (i.e. safety relief valves opening set-point). Considering this, the output observable must reflect the PRHRS operative margin (i.e. departure from the safety relief valves opening set-point) or eventually its failure condition. In this sense, the observable appears as a performance indicator [5-4] of the passive safety function.

For this application the following performance indicator (*PI*) is adopted:

$$PI = \frac{Qc_{psp}}{Qc} \tag{5-8}$$

where Qc = actual removed power by the PRHRS; and Qc_{psp}= minimum removed power needed to avoid safety relief valves opening condition. From its definition, PI represents a factor which affects the actual removed power by PRHRS. This factor, tells how much Qc has to be reduced (or eventually increased) in order that primary system pressure met the failure criterion (i.e. PI ≥ 1). The value of Qc_{psp} can be obtained through a parameterization of Qc; performing stepwise calculations. For this analysis it is assumed that Qc is independent of pressure (and consequently of time), which is a good approximation for high pressures. This allows defining the following constant which can be understood as a fictitious removed power:

$$Qc' = \xi \times Qc \tag{5-9}$$

where ξ is a factor that varies from one to zero. The maximum accumulated energy (for Qc') can be determined as:

$$E_{\max} = EI + \int_{t_0}^{t_1} Qnet(t)\,dt - Qc'\cdot(t_1 - td) \tag{5-10}$$

where *EI* = initial system energy; *Qnet* = net primary system power; t_0 = starting time of the transient; t_1 = time at which the system maximum accumulated energy is reached (intersection between *Qnet* and *Qc*); and *td* = PRHRS activation time. Providing that decay power is only function of time, the following dependency is verified:

$$E_{\max} = f(Qc', t1) = f(Qc', g(Qc')) \equiv f(Qc') \tag{5-11}$$

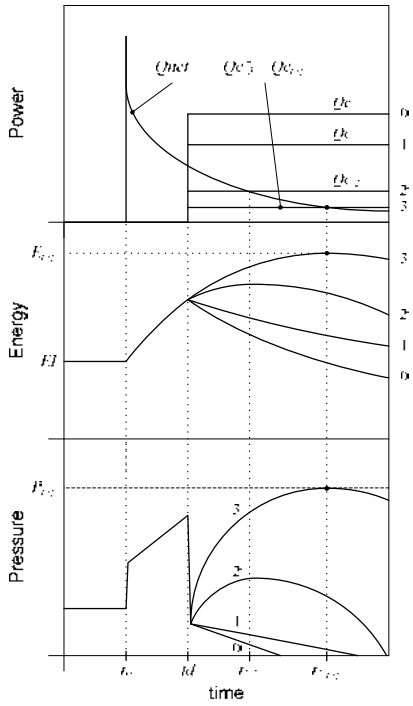

FIG. 5-13. Qualitative evolutions of net power, pressure and energy regarding for different conditions of removed power by the PRHRS. The stepwise process starts with condition 0 and ends at condition 3 when the safety relief valves set point is reached.

Moreover, during Phase III the system is near equilibrium condition and the energy calculated depends almost only of system pressure (given that the coolant total mass is constant), thus it fulfils:

$$E_{\max} = h(P_{\max}) \tag{5-12}$$

Therefore, the energy of the system corresponding to the pressure set point of the safety relief valves can be expressed as follows:

$$E_{psp} = h(P_{psp}) = f(Q_{psp}) \tag{5-13}$$

Taking into account Eqs 5-9 and 5-10; it can be seen that if ξ is reduced in each step of the calculation; *E* will gradually increment until it matches with E_{psp}. Once this condition is achieved, $Qc_{psp} = Qc'$ and the value of the parameter ξ will provide the sought *PI*.

A qualitative graphical view of this stepwise process is shown in Fig. 5-13; on each step only *Qc* is changed, keeping the rest of the system constant. Note that if $Qc \geq Qnet(td)$; E_{max} is independent of *Qc* and it occurs always at *td*.

5.4.6. Uncertainties of the relevant parameters

A key point of the methodology is the selection of relevant parameters and their uncertainty quantification (i.e. assignment of probability distribution functions, nominal values and range of variation). Relevant parameters are those related to the nominal system configuration (design parameters) and physical quantities (critical parameters) that may affect the mission of the passive system. The uncertainties pertaining to the code are not accounted for, focusing the attention on the uncertainties relative to the input parameters characteristic of the passive system or the overall system [5-5].

This entire methodological step was carried out by means of expert judgment. Some of the most important considerations are summarized below:

Nominal values: Despite the model adopted is a simplified and fairly accurate version of CAREM reactor geometry, the reference values considered for calculations approximates to nominal operational values of CAREM-25.

Range of variations: Upper and lower range limits of the parameters are established regarding realistic departures from their nominal values. This implies the consideration of operational procedures during the reactor commissioning (e.g. core inlet friction for setting up the nominal mass flow on the primary circuit) and control systems actions associated with those variables that are regulated.

Probabilities distributions: The probability distributions chosen satisfy the simplicity criteria while they reflect accurately the actual variables behaviour. Regarding what was stated in the previous paragraph, parameters distributions has been truncated since the sampling beyond the range limits could lead to unrealistic system configurations (overlapping of parameters ranges, non realistic values for regulated variables, etc.). Moreover, the parameters are considered to be statistically independent.

The uncertainty of the selected parameters is characterized by truncated NORMAL and LOGNORMAL distributions. The characteristic parameters of the distributions (μ and σ) have been derived regarding the following considerations[3]:

- The nominal value corresponds to the mode of the chosen distribution
- The sampling range has to have a fixed probability content of 95.5%

In Table 5-3, the full parameters table with the PDF characteristic values are reported.

[3] In case of log-normally distributed parameters, further expert criteria was needed in order to set up one range limit since the three equations obtained can not be simultaneously satisfied. In this sense, the expert criteria has been to fix the upper limit value.

TABLE 5-3. SELECTED PARAMETERS FOR THIS STUDY CASE. THE NOMINAL VALUES AND RANGE OF VARIATION ARE NORMALIZED AND DISTRIBUTIONS ARE TRUNCATED AT RANGE LIMITS

	Parameters		Nominal value	Range		Distribution
1	OP	Power operational	1.00	0.95	1.05	TNORMAL
2	SD1	SCRAM delay	1.00	0.68	1.60	TLOGNORMAL
3	SD2	SCRAM: safety rods total drop time	2.00	1.20	4.00	TLOGNORMAL
4	DF	Decay power factor (ANS79-3)	1.00	0.85	1.20	TLOGNORMAL
5	P1	Reactor nominal pressure	1.00	0.99	1.01	TNORMAL
6	SP	SCRAM: pressure set point	1.06	1.05	1.07	TNORMAL
7	P2	PRHRS: pressure set point	1.11	1.10	1.12	TNORMAL
8	L	RPV dome water level	1.00	0.75	1.25	TNORMAL
9	M	Primary circuit mass flow rate	1.00	0.96	1.04	TNORMAL
10	T2	PRHRS valves opening time + RPS delay	2.00	1.00	3.00	TNORMAL
11	PT	PRHRS pool temperature	1.00	0.55	2.38	TLOGNORMAL
12	TT	PRHRS tube thickness	1.00	0.89	1.11	TNORMAL
13	C2	Heat losses in vapour line	$5.00\ 10^{-5}$	0.00	$1.00\ 10^{-4}$	TNORMAL
14	W1	PRHRS tube thickness	$5.71\ 10^{-3}$	0.00	$5.71\ 10^{-2}$	TLOGNORMAL
15	HL	RPV dome (steam zone) heat losses	$1.00\ 10^{-3}$	$5.00\ 10^{-4}$	$1.50\ 10^{-3}$	TNORMAL
16	F	PRHRS inlet friction	1.00	0.50	1.50	TNORMAL

5.4.7. Direct propagation of uncertainties through B-E code

The aim of direct Monte Carlo simulation is to propagate the uncertain parameters through a TH code (RELAP5 Mod3.3) in order to obtain a model response (set of code run results) which will be evaluated regarding the failure criteria associated to the passive safety function under analysis.

In the following sections the first two steps of direct Monte Carlo simulation (i.e. sampling and B-E code run) are addressed, giving a description of the procedures employed and results obtained.

5.4.7.1. Sampling method

In order to obtain the parameters samples, Simple Random Sampling (SRS) method was adopted. In this method, every value of the sample is randomly generated from the correspondent parameters distributions. Simple Random Sampling provides a suitable option when no information of the system response is available having as main advantages the simplicity of samples generation, the availability of well know methods for estimation and statistical analysis and the capacity of aggregation.

5.4.7.2. Generation of input vectors

This selection has been made drawing samples of the sixteen (16) selected parameters (Table 5-5).

A hundred samples were obtained for each parameter implying the same number of code runs regarding that each input vector (or input set) was built in the following way:

$$S_1 = \left(P_{1,1}; P_{2,1}; .....; P_{16,1}\right)$$
$$S_2 = \left(P_{1,2}; P_{2,2}; .....; P_{16,2}\right)$$
...
$$S_{100} = \left(P_{1,100}; P_{2,100}; .....; P_{16,100}\right)$$

where S_j = set of parameters used to perform the j^{th} code run (with: j=1,2,…100); and $P_{i,j}$ = j^{th} sample value of parameter i (with: i=1,2…,16)

The number of code runs, thus, the sample size was selected aiming at satisfing the Wilks' formula. Based on the hypothesis that nothing is known about the output distribution function except that it is continuous; Wilks' formula gives the proper number of independent observations of the random output (Y) in order to fulfil for a one-sided tolerance interval

$$P\left[P\left(Y \le y_{MAX}\right) > \alpha\right] \ge \beta \tag{5-14}$$

were α = probability content; β = confidence level; and y_{MAX} = maximum output sample value.

The selection of one-side tolerance interval is justified since the problem addressed (concerning the failure criterion definition) can be understood as problem of excess from a given value, therefore it is not important what occurs in the left tail of the output distribution function.

The number of independent observations of the output variable (i.e. number of code runs) for the one-sided tolerance interval can be calculated by means of next equation:

$$1 - \alpha^N \ge \beta \tag{5-15}$$

where N = nearest higher integer to the calculated value.

The selected sample size (100 samples) satisfy the 95%/99% criteria (probability content = 95%, confidence level= 99%) for one-sided tolerance interval.

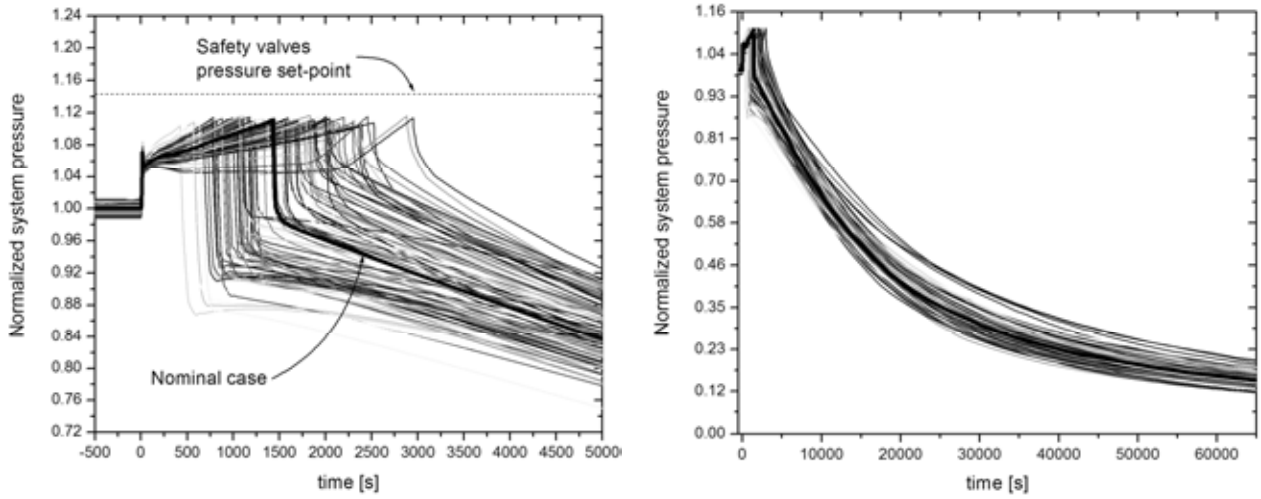

FIG. 5-14. Short term and long term system pressure evolution — normalized scale.

5.4.7.3. Direct Monte Carlo simulation results

In this section, the results obtained by Direct Monte Carlo simulation are presented. Each shown result corresponds to a B-E code run (RELAP5 Mod3.3) of the associated input vector. The main outcomes obtained are linked to the design failure criterion selected for the PRHR system. In this sense, the pressure evolution and system energy are reported.

A qualitative straightforward analysis of the pressure evolutions (Fig. 5-14) shows that none of the cases met the failure criterion (i.e. none of the cases exceed the safety valves pressure set point). The model response (i.e. output variable) reflects the same condition; but now, specifying for each one of the cases the departure from failure domain (Fig. 5-15).

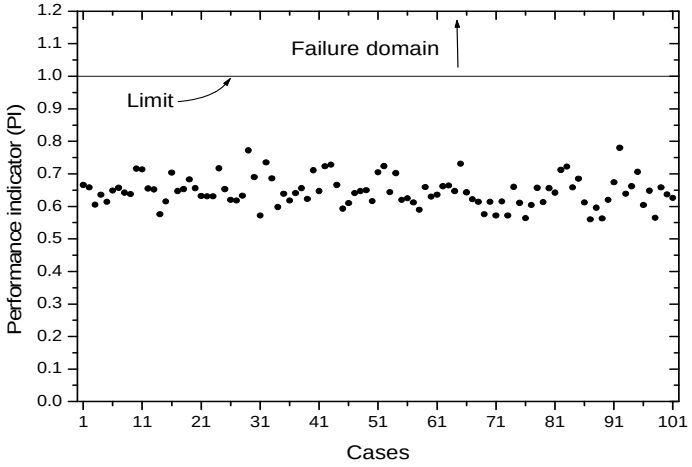

FIG. 5-15. Performance indicators obtained from direct Monte Carlo simulation.

5.4.8. Sensitivity analysis

For the present case study, sensitivity analysis is performed to determine those parameters whose uncertainty has a major impact on model response uncertainty and thus, the passive safety function. The assumption of linear relationship between the output observable ($Y = PI$) and the input parameters (X_i), is made:

$$Y = \beta_0 + \sum_{i=1}^{P} \beta_i X_i \tag{5-16}$$

where P = number of parameters; β_0 and β_i = regression coefficients; and X_i = selected parameters (i.e. 1-OP, 2-SD1, 3-SD2, etc.). This allows calculating the Standardized Regression Coefficients (SRC) and Partial Regression coefficients (PCC) sensitivity indices. The linear hypothesis has to be validated throughout the determination coefficient R^2. The coefficient R^2 represents the variance percentage of the output variable explained by the regression model. The more R^2 is close to one, the more the relation between the output and the inputs is linear. It can also be obtained a coefficient of determination based on the rank R^2*; the difference between R^2 and R^2* is a useful indicator of nonlinearity of the model (R^2* is higher than R^2 in case of non-linear models). Further theoretical aspects of sensitivity analysis based on regression techniques can be found in [5-5, 5-11, 5-35, 5-36].

It is important to remark that SRCs and PCCs provide related but not identical measures of variable importance. SRCs are sensitive to all distributions, this implies that they will not take into account the fact that a correlation between X_i and Y can be a consequence of a third parameter influence; however PCCs provide importance measures that tend to exclude the effect of the other variables. Nevertheless,

in case that the input variables are uncorrelated, the order of variable importance based either on SRCs or PCCs (in their absolute values) is exactly the same [5-11]; condition that corresponds to the present study case.

The results obtained are summarized in Table 5-4. The linear hypothesis is validated since $R^2 = 0.90$ and $R^2* = 0.88$.

TABLE 5-4. SRC AND PCC SENSITIVITY INDICES

Parameter ID	SRC	Rank	PCC	Rank
4-DF	0.632	1	0.879	1
8-L	-0.451	2	-0.776	2
15-HL	0.360	3	0.721	3
12-TT	0.315	4	0.674	4
14-W1	0.253	5	0.584	5
1-OP	0.205	6	0.527	6
13-C2	0.124	7	0.348	7
11-PT	0.109	8	0.295	8
5-P1	-0.070	9	-0.202	9
3-SD2	0.066	10	0.191	10
7-P2	0.051	11	0.147	11
9-M	-0.031	12	-0.087	12
10-T2	-0.017	13	-0.049	13
6-SP	-0.008	14	-0.025	14
2-SD1	-0.005	15	-0.016	15
16-F	-0.002	16	-0.006	16

According to the ranking; 4-DF (decay power factor), 8-L (RPV water level), 15-HL (RPV dome heat losses), 12-TT (PRHRS tube thickness) and 14-W1 (PRHRS tube thickness due to fouling); are the most important input parameters. This outcome has a straightforward connection with the dynamic behaviour of the CAREM-like model, since the parameters related with primary system (regarding the trend given by their sign) are those linked to higher accumulation of energy; meanwhile parameters related to PRHRS contributes to the impairment of heat transfer to the pool.

5.4.9. Quantitative passive safety function reliability evaluation

5.4.9.1. Reliability analysis from direct Monte Carlo simulation outcomes

The quantitative reliability associated to the passive safety function can be evaluated in terms of the following estimator:

$$p_f = \frac{m}{N} \tag{5-17}$$

where m = number of code runs in which the passive safety function fails; and N = total number of code runs. As it was previously shown, neither all stochastic selected cases (100) nor the nominal case provide PI values within the failure domain. Therefore, $m = 0$ (Eq. 5-17) allowing that failure probability estimator takes the value zero. This result comes from the inadequacy of direct Monte Carlo simulation for estimating very low probabilities. Moreover, direct Monte Carlo involves large computational time on each run (given the complexity of the physical problem to solve) allowing only

a limited number of output observables, which are not enough for achieving a proper upper bound of the probability of failure.

A further analysis can be performed considering the failure estimator definition:

$$p_f = \frac{X}{N} = \frac{\sum_{i=1}^{n} Xi}{N} \tag{5-18}$$

where X_i = Bernoulli random variable obtained from each code run (this variable can take only two values: *1*, in case of system failure with a probability *p* and *0*, in case of success, with a probability *1-p*).

Thus, $Z = \sum_{i=1}^{n} X_i$ is a binomial random variable and the probability to obtain *k* failures among n simulations is: $P(Z = k) = \binom{n}{k} p^k (1-p)^{n-k}$.

Then the likelihood of the evidence E (*k=0*, i.e. no failures among *n* simulations) is:

$$L(E|p) = P(p_f = 0|p) = (1-p)^n \tag{5-19}$$

We can estimate the probability distribution for *p*, $\pi(p|E)$ given the evidence E, in using Bayes' theorem:

$$\pi(p|E) = \frac{\pi_0(p) \cdot L(E|p)}{\int_0^1 L(E|p) \cdot \pi_0(p) dp} \tag{5-20}$$

where $\pi_0(p)$ = prior distribution function of *p*; and $L(E|p)$ = likelihood function shown in Eq. 5-19.

The prior distribution function characterizes a subjective degree of conviction on the occurrence of a certain event. In this study case, this degree of belief is represented regarding two alternatives which respectively are pessimistic [5-37] and uniform distribution functions. In aims of completeness, both equations are presented below:

Pessimistic: $\pi_0(p) = \varepsilon \cdot (1-p)^{\varepsilon - 1}$ ($\varepsilon << 1$)

Uniform: $\pi_0(p) = 1$

Through the Bayesian update, the following 'a posteriori' cumulative distributions were obtained:

$$_{\varepsilon}\Pi(p|E) = 1 - (1-p)^{N+\varepsilon} \tag{5-21}$$

$$_{1}\Pi(p|E) = 1 - (1-p)^{N+1} \tag{5-22}$$

In Eq. 5-21; ε can be neglected given that is very small compared to unity.

By definition, $\Pi(\gamma) = P(p \le \gamma)$ and if it is demanded that this probability exceeds a certain value β; it follows that:

$$1 - (1-\gamma)^k \ge \beta \tag{5-23}$$

where β expresses the "confidence" that p will be lower than γ; and k can alternatively take the values *N or N+1* accordingly to the prior distribution selected. It worth to notice that whether the pessimistic prior distribution function is selected ($k = N$), the result achieved is the same to the provided by Wilks' formula, derived from sampling theory (Eq. 5-15). Considering $\beta = 0.95$; and N = 100, it is obtained $\gamma = 0.03$ (for both prior distribution functions). This constitutes a very high upper bound for the probability of failure, according to passive systems capabilities. Therefore, the use of Monte Carlo method based on surrogate models was necessary in order to quantify a proper upper bound of the probability of failure.

5.4.9.2. Response surface calculation

Response surfaces consist in a simplified substitute model that fits the initial data, which has good prediction capacities and demands negligible time for one calculation. This feature allows, once the Response Surface has been determined, to assess the passive system reliability easily by using Monte Carlo simulation.

A first degree linear model based on multiple linear regression is adopted for constructing the response surface. A stepwise variable selection procedure has been performed and leads to the suppression of five useless parameters in the linear model. The parameters of the linear predictor are summarized in Table 5-5; meanwhile a few criteria that determine the quality of the approximation are summarized in Table 5-6.

TABLE 5-5. COEFFICIENTS ASSOCIATED TO THE EXPLANATORY VARIABLES

ID	βi	Rank
INTERCEPT	-6.0498e-01	
4-DF	3.5602e-01	1
8-L	-1.6496e-01	2
15-HL	7.3801e-01	3
12-TT	3.3504e-02	4
1-OP	4.3327e-03	6
13-C2	2.5559e-03	7
11-PT	4.2339e-04	8
5-P1	-4.4460e-02	9
3-SD2	5.3553e-03	10
7-P2	5.4902e-02	11

TABLE 5-6. VALUES OF THE MAIN QUALITY CRITERIA USED TO DETERMINE THE GOODNESS OF THE APPROXIMATION

Quality Criterion	Value
R	8.9696e-01
MSE	2.1533e-04
BIAS	3.3307e-16
Maximum residual	4.2245e-02

The Mean Square Error (MSE) is defined as the average of the squared differences between the observed outputs and the predicted outputs. It has to be compared to the variance of the observed outputs. The bias (BIAS) is defined as the average of the differences between the observed and the predicted outputs. Compared to the mean of the observed outputs, it shows if there is a problem with the regression model (non symmetric residuals). Here, it can be seen a perfect very small bias. Finally, the maximum residual, compared to the root mean square of MSE, allows detecting some anomaly as a very large residual of the regression model. No anomaly is present here.

In this study, all these criteria have also been computed in a prediction context using cross validation techniques. These results, not shown here, are similar to the approximation criteria. Therefore, it can be concluded that the determined response surface has also good predictive capabilities.

5.4.9.3. Monte Carlo simulation based on surrogate model and reliability calculation

Monte Carlo simulation was performed on a basis of the calculated response surface. A million runs were done obtaining no cases within the failure domain. Even though the number of simulations is highly increased, the very low probability of failure makes not possible to achieve a proper estimation using Monte Carlo simulation. Nevertheless, this new information allows, now, to estimate a conservative upper bound of the probability of failure by means of Eq. 5-23.

Regarding the result provided by the Bayesian update of the pessimistic prior distribution function (which is the same result achieved from Wilks' formula), $N = 10^6$ and a confidence level $\beta = 0.95$; the upper bound achieved for the probability of failure is: $\gamma = 3.10^{-6}$.

The uncertainty on the response surface has not been taken into account in this application, but it should have been in a real case. For this application, it is believed that the introduction of this uncertainty will not affect significantly the results.

5.4.10. Conclusions of this application

In the present work it has been obtained a conservative upper bound of 3.10^{-6} for the failure probability of the addressed passive safety function. This result has been achieved updating the evidence of no failure cases from 10^6 code runs performed over a first degree linear model (response surface). This simplified model fits the direct Monte Carlo simulation outcomes (i.e. performance indicators), obtained by means of a RELAP5 Mod3.3 model.

The small upper bound achieved shows the highly reliable performance of the passive system addressed in this study. The exhaustiveness in the parameters selection and their uncertainties quantification is essential, since the outcomes of the procedure are strongly dependent on them. In this sense, regarding further applications, structured methods as Analytical Hierarchy Process could be employed for the identification of the relevant parameters.

Another sensitive point in the methodology is the selection of the performance indicator (i.e. output observable). Its adequacy sustain the results from direct Monte Carlo simulations and the calculations based on surrogate model; therefore, the performance indicator must be strictly linked to the design failure criteria and its definition have to assure that the correct system's phenomenology is encompassed.

Through sensitivity analysis, strong dependences between high Performance Indicator values (worst system condition) and parameters: "decay power factor", "RPV water level", "RPV dome heat losses", "PRHRS tube thickness" and "PRHRS tube thickness due to fouling"; was found. This outcome has a straightforward connection with the dynamic behaviour of the CAREM-like model, since the parameters related with primary system (regarding the trend given by their sign) are those linked to higher accumulation of energy; meanwhile parameters related to PRHRS contributes to the impairment of heat transfer to the pool.

REFERENCES FOR CHAPTER 5

[5-1] INTERNATIONAL ATOMIC ENERGY AGENCY, Safety Related Terms for Advanced Nuclear Plants, IAEA TECDOC-626, IAEA, Vienna (1991).

[5-2] OECD/NEA/CSNI, Passive System Reliability. A Challenge to Reliability Engineering and Licensing of Advanced Nuclear Power Plants, Proceedings of an International Workshop, OECD/NEA/CSNI/R(2002)10, Cadarache, France, 4–6 March (2002).

[5-3] D'AURIA, F., GALASSI, G.M., Methodology for the evaluation of the reliability of passive systems, University of Pisa Report: DIMNP - NT 420(00)-rev. 1 (2000).

[5-4] JAFARI, J., D'AURIA, F., KAZEMINEJAD, H., DAVILU, H., Reliability evaluation of a natural circulation system, Nuclear Engineering and Design **224** (2003) 79–104.

[5-5] MARQUÈS, M., et al., Methodology for the evaluation of a passive system and its integration into a probabilistic safety assessment, Nuclear Engineering and Design **235** (2005) 2612–2631.

[5-6] GLÄSER, H., Experience in application of uncertainty methods and review of methods used in licensing, Exploratory OECD meeting of experts on best estimate calculations and uncertainty analysis, Aix-en-Provence, France, 13–14 May (2002).

[5-7] D'AURIA, F., GIANNOTTI, W., Development of a code with internal assessment of uncertainty, Nuclear Technology **131** (2000).

[5-8] SAATY, T., Mathematical Methods of Operations Research, Dover Publications, Inc. (1988).

[5-9] ZIO, E., CANTARELLA, M., CAMMI, A., The analytic hierarchy process as a systematic approach to the identification of important parameters for the reliability assessment of passive systems, Nuclear Engineering and Design **226** (2003) 311–336.

[5-10] BURGAZZI, L., Passive system reliability analysis: a study on the isolation condenser, Nuclear Technology **139** 1, July (2002) 3–9.

[5-11] SALTELLI, A., et al., Sensitivity Analysis, John Wiley & Sons (2000).

[5-12] RUBINSTEIN, R.Y., Simulations and Monte-Carlo method, Wiley Series in Probability and Mathematical Statistics, J. Wiley & Sons (1981).

[5-13] MADSEN, H., et al., Methods of structural safety, Prentice Hall (1986).

[5-14] RACKWITZ, R., et al., Structural reliability under combined random load sequences, Computers and Structures **9** (1979) 489–494.

[5-15] MELCHERS, R.E., Structural reliability analysis and prediction, J.Wiley & Sons (1999).

[5-16] DEVICTOR, N., "Advances in methods for uncertainty and sensitivity analysis", Proc. Workshop on Level 2 PSA and Severe Accident Management, OECD/NEA/CSNI/WGRISK, Köln, March (2004).

[5-17] MARQUÈS, M., et al., Reliability Methods for Passive Safety functions, Proc. Int. Conf. ICONE 10, Arlington, Virginia, USA April 14–18 (2002).

[5-18] USNRC, Severe Accident Risks: an Assessment for Five U.S. Nuclear Power plants. Final Summary Report. NUREG 1150, Vol. 1 (1991).

[5-19] COOKE, R.M., Experts in Uncertainty. Opinion and Subjective Probability in Science. Oxford University Press (1991).

[5-20] GARTHWAITE, P.H., KADANE, J.B., O'HAGAN, A., Statistical Methods for Eliciting Probability Distributions, JASA **100** 470 (2005) 680–700.

[5-21] SIMOLA, K., MENGOLINI, A., BOLADO, R., Formal Expert Judgement, An Overview, JRC technical report EUR 21772EN (2005).

[5-22] BECKMAN, R.J. , MCKAY, M.D., Monte Carlo Estimation under Different Distributions. Technometrics **29** 2 (1987) 153–160.

[5-23] BOLADO, R., VALERO, J., Distribution Sensitivity Analyses for Three Different Scenarios within the RP2 System Case Study, JRC technical report EUR 20980EN (2003).

[5-24] BURGAZZI, L., State of the art in reliability of thermohydraulic passive systems, Reliability Engineering and System Safety **92**, June (2007) 671–675.

[5-25] ZIO, E., PEDRONI, N., Building confidence in the reliability assessment of thermohydraulic passive systems, Reliability Engineering and System Safety **94** (2009) 268–281.

[5-26] BURGAZZI, L., Addressing the uncertainties related to passive system reliability, Progress in Nuclear Energy **49**, January (2007) 93–102.

[5-27] BURGAZZI, L., Evaluation of uncertainties related to passive systems performance, Nuclear Engineering and Design **230**, June (2004) 93–106.

[5-28] BURGAZZI, L., Reliability evaluation of passive systems through functional reliability assessment, Nuclear Technology **144** (2003) 145–151.

[5-29] PAGANI, L.P., APOSTOLAKIS, G.E., HEJZLAR, P., The impact of uncertainties on the performance of passive systems, Nuclear Technology **149** (2005) 129–140.

[5-30] BURGAZZI, L., Thermohydraulic passive system reliability-based design approach, Reliability Engineering and System Safety **92**, September (2007) 1250–1257.

[5-31] NAYAK, A.K., et al., Passive system reliability analysis using the ASPRA methodology, Nuclear Engineering and Design **238** 6 (2008) 1430–1440.

[5-32] MARQUÈS, M., "Reliability of passive systems that utilize natural circulation", IAEA Course on Natural Circulation in Water-Cooled Nuclear Power Plants, International Centre for Theoretical Physics (ICTP), Trieste, Italy, 28 June to 2 July 2004, Paper id: T23 and T24 (2004).

[5-33] ZANOCCO, P., GIMÉNEZ, M., DELMASTRO, D., D'AURIA, F., Self-pressurization behaviour in integrated reactors, Heat and Technology **21** 1 (2003) 149–158.

[5-34] INTERNATIONAL ATOMIC ENERGY AGENCY, Status of Innovative Small and Medium Sized Reactor Designs 2005: Reactors with Conventional Refuelling Schemes, IAEA-TECDOC-1485, IAEA, Vienna (2006).

[5-35] VOLKOVA, E., IOOSS, B., VAN DORPE, F., Global sensitivity analysis for a numerical model of radionuclide migration from RRC "Kurchatov Institute" radwaste disposal site, Stochastic Environmental Research and Risk Assessment **22** 1 (2008) 17–31.

[5-36] DEVICTOR, N., BOLADO LAVÍN, R., Uncertainty and sensitivity methods in support of PSA level 2, SARNET-PSA2-P06 Revision 0, SARNET report, European Commision (2006).

[5-37] WALLIS, G., Evaluating the probability that the outputs of a computer code with random inputs will meet a set of evaluation criteria, Reliability Engineering & System Safety **91** (2006) 820–827.

6. GENERAL SUMMARY AND CONCLUDING REMARKS

The content of this TECDOC is based on work done and related activities carried out by the institutes within the Member States contributing to the IAEA Coordinated Research Project (CRP), entitled Natural Circulation Phenomena, Modeling and Reliability of Passive Safety Systems that Utilize Natural Circulation. This CRP was performed from early 2004 to 2009 and focused on the use of passive safety systems to help meet the safety and economic goals of a new generation of nuclear power plants. The results of the CRP work have been published in three consecutive IAEA-TECDOC reports, including this TECDOC [6-1 to 6-2]. The major subject areas covered in these reports can be identified as:

- Establish an overview of the current understanding on Natural Circulation
- Identify and Describe Reference Systems
- Identify and characterize phenomena that influence natural circulation
- Examine application of data and codes to design and safety
- Examine the reliability of passive systems that utilize natural circulation

The conclusions, recommendations and future needs for the phenomena, experimental work, and analysis addressed in this TECDOC are provided in each of the related chapters in some detail and also within the context of the subject area dealt by each writing group. Therefore the reader should refer to the individual chapters for the details of the conclusions and recommendations for needs. In this chapter a short summary and some concluding remarks are provided in generic form. Detailed plans for future development are outside the purpose of the CRP.

The identification and definition of the phenomena for advanced water cooled reactors with emphasis to passive safety systems is also presented in the second chapter of this TECDOC in addition to [6-2]. Phenomena have been classified into two categories. These are being phenomena occurring during interaction between primary system and containment; and phenomena originated by the presence of new components and systems or special reactor configurations. Definitions and descriptions of the twelve “additional” phenomena, which are identified during the work of the CRP on Natural Circulation, are given in some detail. It is important to provide these descriptions and definitions in order to avoid some miss-understandings under the short titles of the phenomena. These descriptions are supplement to the definitions of phenomena which are developed for the current operational water cooled nuclear power plants.

6.1. SUMMARY AND CONCLUDING REMARKS FOR CHAPTER 3

Twelve phenomena identified within the Chapter 2 based on the overall road-map of the IAEA-CRP activity, are considered in Chapter 3. Namely, the characterization of ‘additional’ phenomena (i.e. the writing-up of Chapter 3) implied primarily a qualitative but also an accurate and quantitative as far as possible description of phenomena that has been done having in mind three key guidelines:

a) To distinguish the ‘additional’ phenomena here considered from the phenomena occurring or expected following transient behaviour in current generation of reactor (limited use of passive systems);

b) To distinguish among each other the ‘additional’ phenomena;

c) To contribute in providing a comprehensive picture of the transient performance of the class of innovative reactors here concerned where passive system features are exploited.

More than ten different specialists (IAEA CRP members) have been involved in setting up Chapter 3 and all in all contributed around 200 pages for the description of twelve phenomena.

Emphasis in the content for each chapter was given to the activities discussed during the IAEA CRP Research Coordination Meetings (RCMs). There were total of 5 RCMs during the CRP period. Therefore, the chapter reflects the current scientific and technological interests at the institutions of the

authors and should not be considered as a state of the art report although an effort has been made to cover the broadest range of conditions for each phenomenon, which establishes an overview of the current understanding. A few summary-conclusive remarks are given hereafter connected with each of the twelve phenomena descriptions.

Behaviour in large pools of liquid

The liquid pools constitute ultimate heat sinks for a wide variety of reactors and, per each reactor, for a wide variety of conditions, section 3.1. These range from surrounding heat exchanger, to providing condensation capability for relief valves, to providing reservoir coolant for gravity flooding, to provide a heat sink for the containment system. Sometimes different functions are ensured by the same pool. Typical volume also widely ranges from a few cubic meters to thousands cubic meters. Key facts for the thermohydraulic phenomena associated with pool behaviour are:

- Need of computational fluid-dynamics code for modelling phenomena like internal circulation and stratification;
- Need of experimental data specifically when two phase conditions are involved.

Effect of non-condensable gases on condensation heat transfer

The condensation constitutes a relevant thermohydraulic phenomenon for existing reactors. As such, this phenomenon is considered in reports dealing with current generation reactors. The tight coupling between primary system and containment makes the phenomenon of even greater importance in the case of innovative reactors subject of the present report. Therefore, a comprehensive (state of the art type) discussion is provided in section 3.2, encompassing situations relevant for current generation and innovative reactors.

Starting with the fundamental description of the phenomenon, containment and primary system conditions are distinguished. Mechanistic models are described together with system codes primarily dealing with containment situations. Emphasis is given to the role of non-condensable gases, as expected from the title of the section. An overview is given of the experimental data that are used for validation and selected experimental data are described.

Pointing out the importance of geometry for the model/correlation development and assessment constitutes an important outcome of the survey activity in section 3.2. “Intersection” of subjects and duplication of concepts in relation to section 3.3 (see below) could not be avoided and should be considered as a strength rather than a limitation of the present report, because they give to the reader the opportunity to look at the same subject from different viewpoints.

Condensation on the containment structures

A comprehensive, state of the art type description of condensation is provided in section 3.3 making reference to the containment.

The format and the level of detail in the description are similar as in the section 3.2. Furthermore, the following classifications constitute valuable outcomes from the section:

- Mechanistic models;
- Results from experimental data giving emphasis to the geometry and to overall values of the Heat Transfer Coefficient;
- Codes, discussing the qualification level of system type of codes and introducing the pioneering research of condensation in CFD type of codes.

Again, “intersection” of subjects and duplication of concepts in relation to section 3.2 could not be avoided and should be considered as a strength rather than a limitation of the present report (see the

last statement in the above paragraph dealing with the 'Effect of non condensable gases on condensation heat transfer').

Behaviour of containment emergency systems

As a difference from the content of sections 3.2 and 3.3, the attention is focused in section 3.4 to the system and component behaviour rather than to the phenomena, however keeping in mind that condensation with presence of non-condensable gases constitutes the key mechanism that characterizes the working conditions for the containment emergency systems.

The content of the section 3.4 deals with the detailed description of large research projects carried out in the institutions that are represented in the IAEA CRP with emphasis give to the innovative types of boiling and pressurized water reactors. In this connection system geometrical features are described together with relevant results from the experimental campaigns.

An added value for the section 3.4 is constituted by the discussion about the capability, primarily of current system codes, to predict the behaviour of containment emergency system. The key outcome is the demonstration of the capabilities of the considered codes in predicting the phenomena of interest in transient conditions, i.e. consistently with the safety needs for the design of such systems. However, recommendations are given for areas of the codes that need improvement.

Thermo-fluid dynamics and pressure drops in various geometrical configurations

The pressure drops concerned in section 3.5 are the local pressure drops originated by, typically abrupt, area changes. In this case, as is the case of section 3.2, the phenomenon is of interest to the current generation of reactors as well as to the innovative reactors. Therefore, suitable descriptions are available from other international documents. The peculiarities of innovative reactors that justified a specific section here are the geometric discontinuities introduced by the 'innovative' design and the small driving forces originated by the substitution, as far as possible, of active systems by passive systems.

The section 3.5 presents experimental data and correlations applicable for a wide variety of situations in a wide range of parameters. As result of the deep survey, the inadequacy of the database is emphasized for situations relevant to the containment and for a number of configurations that are specific of the innovative reactors.

An added value for the section 3.5 is constituted by the gathering and the description of the accuracy database derived by the comparison between experimental data and results of the application of correlations and models. This may be used to provide confidence in the application of the concerned correlations and models.

Natural circulation in closed loop

The natural circulation in closed loop constitutes a peculiarity of the innovative reactors exploited either in nominal working conditions or in accident conditions, section 3.6. As in some of the previous cases (e.g. local pressure drops, section 3.5), the natural circulation phenomenon is also relevant for the current generation of reactor. Thus, phenomenon information can also be found in different internationally recognized documents. Based on the above, an attempt has been made to set up a general enough content in section 3.6 to cover all aspects relevant to natural circulation with emphasis to conditions that are specific of the innovative reactors.

Simplified model approaches are described, together with the application of complex computational tools. A central role to understand the details of the involved phenomena is played by the experimental evidence and by the characteristics of the developed input decks (nodalization). This is testified by the consideration given in section 3.6 to the facilities, to the experimental database and to the process for demonstrating the quality of a nodalization.

The stability of the flow constitutes the main issue in natural circulation. Therefore, special emphasis is given to the stability and to the methods to predict stability.

Steam–liquid interaction

Typical conditions for steam–liquid interaction occur, section 3.7: a) in a pool where steam (or two phase mixture) is injected; b) following the injection of emergency systems where cold liquid stream may enter in a vapour zone; c) following the actuation of liquid sprays in a steam environment or, d) during high pressure break flow (typically superheated fluid with respect to the containment pressure) when two phase fluid enters into contact with the containment atmosphere including or not non-condensable gases. Under these conditions, so called direct contact condensation takes place .

The situations listed above are also foreseen in current generation reactors. However, the relevance may not be so high as in the innovative reactors where, owing to the small driving heads available, minor variations (e.g. in predicting) of key quantities that affect the phenomena may cause scenario evolutions toward noticeably different directions.

Emphasis is given to the direct contact condensation and condensation regime maps related are discussed in this section. Suppression pool mixing and condensation tests are summarized, together with the application of the thermohydraulic system codes and commercial CFD type of codes to the thermal mixing of condensed water and subcooled water in a containment suppression pool configuration.

Gravity driven cooling and accumulator behaviour

Passive injection of liquid into the primary system is involved by Gravity Driven Cooling and Accumulator Behaviour, section 3.8. The gravity force, i.e. the only force present in case of gravity tanks installed at an elevation typically higher than the core of the concerned reactors, is supplemented by the gas pressure in case of accumulators.

Only accumulators are installed in current generation reactors. In relation to accumulators, suitable description can be found in the document dealing with existing reactors. Therefore, the discussion in section 3.8 is mostly focused on the behaviour of the gravity tanks. Examples and application cases are given from Economic simplified Boiling Water Reactor (ESBWR), passive flooding system of WWER-1000/392, and the Advanced Heavy Water Reactor (AHWR) passive safety systems using gravity driven core cooling concept.

Liquid temperature stratification

The discussion related to liquid temperature stratification is also part of the phenomenon ‘Behaviour of Large Pools of Liquid’ and is discussed in section 3.1 in addition to section 3.9.

Extensive research has been conducted in order to visualize and model the phenomenon of thermal stratification. Thermal stratification represents a significant concern for all water cooled reactors due to subsequent “slug” development and also the consequences of the thermal stresses on reactor components. The most recent research regarding thermal stratification in both operating reactors and laboratory studies are summarized, e.g., the Young Gwan Nuclear Power Plant (YGN) in the Republic of Korea, experiments conducted at Idaho State University (ISU) for AP600 advanced light water reactor, Oregon State University (OSU) APEX test facility, experiments conducted in Large Scale Test Facility (LSTF) to simulate AP600 (providing data for comparison to OSU APEX test facility), etc.

Several empirical models which were developed and validated using the research conducted with the above mentioned facilities are also briefly discussed. Use of CFD codes for thermal stratification has

indicated that local phenomena are not always taken into account which leads to increased uncertainty, large factors of safety, and more expense.

Behaviour of emergency heat exchangers and isolation condensers

The prototype systems denominated Emergency Heat exchangers and Isolation Condenser, can be taken as systems that characterize the innovative reactors, section 3.10. Typical system configurations adopted in the reactor under design (or even under construction), are described.

Natural circulation with separate boiling and condensing regions in the loop characterize the system together with the high elevation (related to core) of the heat exchanger that is immersed in a pool constituting the ultimate heat sink.

The experimental database acquired so far and the capabilities of the current codes in predicting the relevant phenomena are discussed in the section 3.10. It is pointed out that research efforts, particularly in the area of steam condensation in complex geometries in the presence of non-condensable gases, should be continued.

CFD has a very limited ability to effectively model two phase flow and the presence of a thin vapour layer during the stratified flow phase in the cold legs make the use of CFD difficult. On the other side, use of CFD was rather successful in analysing the single phase stratification in large tanks, e.g. IRSWT.

Stratification and mixing of boron

The main topics of boron mixing and stratification phenomena in the primary circuit are, section 3.11: a) the formation of boron diluted slugs; b) the onset of slug motion; c) the slug mixing and transport. Boron diluted slugs can be formed by external dilution at flow stagnation in the loop. Inherent dilution can occur at boiler-condenser operation or at back flow from the secondary side of the steam generator during the primary-to-secondary leakage accidents. The slug can be transported into the core by restart of the main coolant pump or by re-establishment of natural circulation in a loop. Turbulence, mixing, diffusion and transport are key mechanisms involved with Stratification and Mixing of Boron that are discussed in the chapter.

The problems connected with boron (namely boron dilution) are relevant in either the current generation or the innovative generation. However, only the advent of CFD type of codes allowed a suitable treatment of the key mechanisms above mentioned. Therefore, the content of section 3.11 is equally applicable to all types of reactors and constitutes a complement to documents dealing with phenomena in current reactors.

Experimental database reproducing situations relevant to the reactors and suitability of CFD codes are discussed in the section. Computer capacity is still, and will be for a foreseeable future, a limiting factor for the capacity for CFD calculations to produce completely accurate results. Simplified models for describing turbulence therefore have to be used and the computer capacity put restrictions on the resolution in space and time that one can use in a CFD calculation. This leads to modelling and numerical errors that could potentially give inaccurate results. Validation of the quality and trust of different approaches in CFD calculations are therefore needed. In this connection the importance of using best practice guidelines when CFD code are applied is emphasized with main reference to showing the convergence of results with the reduction of mesh size down to suitable values.

Behaviour of core make-up tanks

As in the case of isolation condenser, it can be said that the core make-up tanks (CMT), section 3.12, characterize the innovative reactors. The idea at the basis of the design of the CMT is to have available water for core cooling without the need of pressurizing gas.

On the one hand the CMT feature adds reliability to the actuation of the system, on the other hand the much smaller driving forces available in comparison with the case of the accumulator, imposes a careful design of the piping connected with the primary loop.

The experimental database acquired so far and the capabilities of the current codes in predicting the relevant phenomena connected with the CMT operation are discussed in the section 3.12. It is pointed out that research efforts, particularly in the area of instability in the flow delivery also connected with steam condensation at the free surface inside the tanks should be continued.

6.2. SUMMARY AND CONCLUDING REMARKS FOR CHAPTER 4

The Chapter 4 provides an excellent overview of representative international integral test facilities that can be used for data collection for reactor types in which natural circulation may play an important role. It is clear that these facilities are providing high quality data that can be utilized for both phenomenological examination and the examination of the ability of nuclear reactor systems codes to model the phenomena that are occurring in the test facilities.

Each section of this chapter addressed a particular test facility and prototypical plant design that the facility is modelling. In general, each section includes a description of the test facility and example data sets collected during the operation of the facility. In some instances, an analysis of the subject test with a comparison between the test data and the code results was presented. In particular, the following information was presented in Chapter 4.

- A flashing-driven moderator cooling system being developed for the CANDU-SCWR concept was discussed along with current and future test loops as well as a comparison between AECL collected test data with reactor system code CATHENA.
- Experimental data collected in the CAREM High Pressure Natural Circulation Rig was presented for the following three transients: (a) opening of a relief valve, (b) an increase in heat removal, and (c) a decrease in core power. The experimental data was compared with results from RELAP5 simulations for the three subject transients.
- An integral test facility simulating Main Heat Transport and safety systems of the AHWR which can be used to investigate overall system behaviour under different operating conditions, transients and accidents has been described. Experiments examining (a) steady state natural circulation behaviour, and (b) reactor startup and stability of two phase natural circulation at low pressures were presented.
- Data collected from thermohydraulic integral experiments conducted at the Large Scale Test Facility in support of design reviews for the AP600 design were presented. These experiments were conducted for various break locations and sizes and component failures. The response of PRHR and CMT in these experiments was examined.
- The MASLWR Integral Test Facility was described. Experiments investigating the operation of the MASLWR under normal full pressure and full temperature conditions and the operation of the passive safety systems under transient conditions were conducted and described.
- International Standard Problem number 42 conducted at the PANDA Test Facility was described. ISP-42 test was subdivided in six well-defined sequential phases which allowed for collected data to be used for code validation in relation to a range of LWR and advanced LWR containment issues. Comparisons with a number of reactor system and containment codes such as RELAP5, CATHARE, SPECTRA, GOTHIC and COCOSYS were presented and analysed.
- The PUMA integral test program and the applicable scaling analyses for the experimental simulation of the important phenomena expected in the SBWR like reactor design was discussed. This program included the collection of test data that can be used for the study of both single and multiple failure accidents in the SBWR. Comparisons of the data with RELAP5 were also presented.

- The natural circulation characteristics of the System Integrated Modular Advanced ReacTor (SMART) during a loss of feedwater flow transient were analysed using the TASS/SMR code.
- The PArallel Channel TEst Loop (PACTEL) facility and its relation to a standard VVER-440/V213 unit were explored. Data collected in support of International Standard Problem 33 used to (a) experimentally examine natural circulation in the VVER-440 over a range of primary side inventory levels and (b) test the ability of thermohydraulic computer codes to analyse this kind of phenomena were presented.
- Passive safety systems (SPOT and HA-2) for the WWER-1000/392 reactor design have been analysed for the following scenarios: (a) station blackout; and (b) LOCA with active ECCS failed. This analysis was conducted with the ATHLET, RELAP5, DINAMIK and KORSAR system codes.

6.3. SUMMARY AND CONCLUDING REMARKS FOR CHAPTER 5

The Chapter 5 deals specifically with the methodology for examining passive system reliability and application of the methodology presented in this TECDOC to an example case. Due to the specificities of passive systems that utilize natural circulation (small driving force, large uncertainties in their performance, lack of data…), there is a strong need for the development and demonstration of consistent methodologies and approaches for evaluating their reliability. This is a crucial issue to be resolved for their extensive use in future nuclear power plants.

As a first step forward in this direction, the RMPS methodology was developed to address the following problems: 1) Identification and quantification of the design parameters that affect the performance of the system and determination of the important variables, 2) Consideration of the ranges of variation of the important variables in calculations performed by thermohydraulic (T-H) models and assessment of passive system unreliability and 3) Introduction of passive system unreliability in accident sequence analyses.

In this approach, the passive system is modelled by a qualified T-H code (e.g. CATHARE) and the reliability evaluation is based on results of code runs, whose inputs are sampled by Monte-Carlo (M-C) simulation. This approach provides realistic assessment of the passive system reliability, thanks to the flexibility of the M-C simulation, which adapts to T-H model complexity without resort to simplifying approximation. In order to limit the number of T-H code runs required by M-C simulation, alternative methods have been proposed such as variance reduction techniques, first and second order reliability methods and response surface methods. The RMPS methodology has been successfully applied to passive systems utilizing natural circulation in different types of reactors (BWR, PWR, and VVER). A complete example of application concerning the passive residual heat removal system of a CAREM like reactor has been presented within this document, including the conclusions drawn from the analysis of this application. The RMPS methodology tackles also an important problem, which is the integration of passive system reliability in a Probabilistic Safety Assessments (PSA). So far, in existing innovative nuclear reactor projects PSA's, only passive system components failure probabilities are taken into account, disregarding the physical phenomena on which the system is based, such as the natural circulation. The first attempts performed within the framework of RMPS have taken into account the failures of the components of the passive system as well as the impairment of the physical process involved like basic events in static event trees.

Two other steps were identified after the development of the RMPS methodology where an improvement was desirable: the inclusion of a formal expert judgment (EJ) protocol to estimate distributions for parameters whose values are either sparse or not available, and the use of efficient sensitivity analysis techniques to estimate the impact of changes in the input parameter distributions on the reliability estimates. The proposed techniques to solve these two problems have been described within this document.

In addition to the RMPS approach, a number of additional support methodologies have been investigated for the reliability assessment of T-H passive systems. The three support methodologies proposed by ENEA have been reviewed. In the first methodology, the failure probability is evaluated as the probability of occurrence of different independent failure modes, a priori identified as leading to the violation of the boundary conditions or physical mechanisms needed for successful passive system operation. In the second, modelling of the passive system is simplified by linking to the modelling of the unreliability of the hardware components of the system: this is achieved by identifying the hardware failures that degrade the natural mechanisms upon which the passive system relies and associating the unreliability of the components designed to assure the best conditions for passive function performance. The third approach is based on the concept of functional failure, defined as the probability of the passive system failing to achieve its safety function as specified in terms of a given safety variable crossing a fixed safety threshold. Finally an additional approach is followed in the APSRA (Assessment of Passive System ReliAbility) methodology developed by BARC. In this approach, a failure surface is generated by considering the deviation of all those critical parameters, which influence the system performance. Then, the causes of deviation of these parameters are found through root diagnosis. It is attributed that the deviation of such physical parameters occurs only due to a failure of mechanical components such as valves, control systems, etc. Then, the probability of failure of a system is evaluated from the failure probability of these mechanical components through classical PSA treatment. Moreover, to reduce the uncertainty in code predictions, BARC foresee to use in-house experimental data from integral facilities as well as separate effects tests.

6.4. OTHER REMARKS

In addition to the three TECDOCs published in this CRP, further activities have been initiated or support has been provided to perform following activities:

1) The IAEA training course on “Natural Circulation Phenomena and Passive System in Advanced Water Cooled Reactors”, which was established in 2004, with major contributions from some selected experts in the CRP. This course has been given annually since that time at different locations and organizations, International Centre of Theoretical Physics in Trieste (Italy), Idaho National Laboratories (Idaho Falls, Idaho, USA), and University of Pisa (Pisa, Italy).

2) During the course of this CRP, there has been extensive experimental data exchange. Some of these data have been used for code validation purposes by few of the CRP participants, e.g., International Standard Problem (ISP)-42, which is based on the tests performed in PANDA test facility (Switzerland).

3) An IAEA International Collaborative Standard Problem (ICSP) has been initiated and supported by the IAEA CRP on Natural Circulation Phenomena, Modelling, and Reliability of Passive Systems that Utilize Natural Circulation. In September 2006, the MASLWR (Multi-application Small light Water Reactor) Natural Circulation Standard Problem Working Group was formed within this CRP. The purpose of this IAEA ICSP is to provide experimental data on flow instability phenomena under natural circulation conditions and coupled containment/reactor vessel behaviour in integral-type reactors. The tests which are performed in MASLWR test facility at Oregon State University (OSU), USA will be used to assess computer codes for reactor system design and analysis. This IAEA ICSP is presently in execution and in progress.

4) A complete example of application concerning the passive residual heat removal system of a CAREM like reactor has been presented within this document, including the conclusions drawn from the analysis of this application. This activity was performed in co-operation by CNEA (Argentina), University of Pisa (Italy), and CEA (France) with the partial sponsorship of the IAEA.

5) A new IAEA CRP entitled “Development of Methodologies for Performance Assessment of Passive Safety Systems in Advanced Reactors” has been supported and partially activated by the members of the CRP on Natural Circulation. This CRP aims on development of a common approach to assess performance of passive safety systems. Such an approach could facilitate

design optimization and safety qualification of the future advanced reactor designs, contributing to their enhanced safety levels and improved economics. This CRP is taking place from 2009 to 2012.

Finally, it is to be emphasized that the knowledge and information collected in two TECDOCs [6-1 to 6-2] is an excellent form of presenting the recent research performed in a collected form on natural circulation for advanced water cooled reactors. And these also help to form a basis of a text book for young scientists and engineers in the field of nuclear technology.

REFERENCES FOR CHAPTER 6

[6-1] INTERNATIONAL ATOMIC ENERGY AGENCY, Natural Circulation in Water cooled Nuclear Power Plants: Phenomena, Models, and Methodology for System Reliability Assessments, IAEA-TECDOC-1474, IAEA, Vienna (2005).

[6-2] INTERNATIONAL ATOMIC ENERGY AGENCY, Passive Safety Systems and Natural Circulation in Water Cooled Nuclear Power Plants, IAEA-TECDOC-1624, IAEA, Vienna (2009).

CONTRIBUTORS TO DRAFTING AND REVIEW

Aksan, N.	Paul Scherrer Institut, Switzerland
Bolado, R.	European Commission, Netherlands
Burgazzi, L.	ENEA, Italy
Choi, J.-H.	International Atomic Energy Agency
Chung, Y.-J.	Korea Atomic Energy Research Institute, Republic of Korea
D'Auria, F.	University of Pisa, Italy
De La Rosa, F.C.	University of Valencia, Spain
Giménez, M.O.	Comisión Nacional de Energía Atómica, Argentina
Ishii, M.	Purdue University, USA
Khartabil, H.	Chalk River Laboratories, Atomic Energy of Canada Ltd., Canada
Korotaev, K.	OKB Gidropress, Russian Federation
Krepper, E.	Forschungszentrum Dresden-Rossendorf, Germany
Marques, M.	CEA, France
Matejovic, P.	IVS, Slovakia
Reyes, J.N.	Oregon State University, USA
Saha, D.	Bhabha Atomic Research Centre, India
Sibamoto, Y.	Japan Atomic Energy Agency, Japan
Tehrani, A.	HSE, UK
Williams, B.	Idaho State University, USA
Woods, B.	Oregon State University, USA

RESEARCH COORDINATION MEETINGS

2–5 November 2004, IAEA-HQ, Vienna, Austria

29 August–2 September 2005, Oregon State University, Corvallis, Oregon, USA

11–15 September 2006, Commissariat à l'Énergie Atomique (CEA), Cadarache, France

10–13 September 2007, IAEA-HQ, Vienna, Austria

3–6 November 2008, IAEA-HQ, Vienna, Austria

IAEA
International Atomic Energy Agency

Where to order IAEA publications

In the following countries IAEA publications may be purchased from the sources listed below, or from major local booksellers. Payment may be made in local currency or with UNESCO coupons.

AUSTRALIA
DA Information Services, 648 Whitehorse Road, MITCHAM 3132
Telephone: +61 3 9210 7777 • Fax: +61 3 9210 7788
Email: service@dadirect.com.au • Web site: http://www.dadirect.com.au

BELGIUM
Jean de Lannoy, avenue du Roi 202, B-1190 Brussels
Telephone: +32 2 538 43 08 • Fax: +32 2 538 08 41
Email: jean.de.lannoy@infoboard.be • Web site: http://www.jean-de-lannoy.be

CANADA
Bernan Associates, 4501 Forbes Blvd, Suite 200, Lanham, MD 20706-4346, USA
Telephone: 1-800-865-3457 • Fax: 1-800-865-3450
Email: customercare@bernan.com • Web site: http://www.bernan.com

Renouf Publishing Company Ltd., 1-5369 Canotek Rd., Ottawa, Ontario, K1J 9J3
Telephone: +613 745 2665 • Fax: +613 745 7660
Email: order.dept@renoufbooks.com • Web site: http://www.renoufbooks.com

CHINA
IAEA Publications in Chinese: China Nuclear Energy Industry Corporation, Translation Section, P.O. Box 2103, Beijing

CZECH REPUBLIC
Suweco CZ, S.R.O., Klecakova 347, 180 21 Praha 9
Telephone: +420 26603 5364 • Fax: +420 28482 1646
Email: nakup@suweco.cz • Web site: http://www.suweco.cz

FINLAND
Akateeminen Kirjakauppa, PO BOX 128 (Keskuskatu 1), FIN-00101 Helsinki
Telephone: +358 9 121 41 • Fax: +358 9 121 4450
Email: akatilaus@akateeminen.com • Web site: http://www.akateeminen.com

FRANCE
Form-Edit, 5, rue Janssen, P.O. Box 25, F-75921 Paris Cedex 19
Telephone: +33 1 42 01 49 49 • Fax: +33 1 42 01 90 90
Email: formedit@formedit.fr • Web site: http://www. formedit.fr

Lavoisier SAS, 145 rue de Provigny, 94236 Cachan Cedex
Telephone: + 33 1 47 40 67 02 • Fax +33 1 47 40 67 02
Email: romuald.verrier@lavoisier.fr • Web site: http://www.lavoisier.fr

GERMANY
UNO-Verlag, Vertriebs- und Verlags GmbH, Am Hofgarten 10, D-53113 Bonn
Telephone: + 49 228 94 90 20 • Fax: +49 228 94 90 20 or +49 228 94 90 222
Email: bestellung@uno-verlag.de • Web site: http://www.uno-verlag.de

HUNGARY
Librotrade Ltd., Book Import, P.O. Box 126, H-1656 Budapest
Telephone: +36 1 257 7777 • Fax: +36 1 257 7472 • Email: books@librotrade.hu

INDIA
Allied Publishers Group, 1st Floor, Dubash House, 15, J. N. Heredia Marg, Ballard Estate, Mumbai 400 001,
Telephone: +91 22 22617926/27 • Fax: +91 22 22617928
Email: alliedpl@vsnl.com • Web site: http://www.alliedpublishers.com

Bookwell, 2/72, Nirankari Colony, Delhi 110009
Telephone: +91 11 23268786, +91 11 23257264 • Fax: +91 11 23281315
Email: bookwell@vsnl.net

ITALY
Libreria Scientifica Dott. Lucio di Biasio “AEIOU”, Via Coronelli 6, I-20146 Milan
Telephone: +39 02 48 95 45 52 or 48 95 45 62 • Fax: +39 02 48 95 45 48
Email: info@libreriaaeiou.eu • Website: www.libreriaaeiou.eu

JAPAN
Maruzen Company, Ltd., 13-6 Nihonbashi, 3 chome, Chuo-ku, Tokyo 103-0027
Telephone: +81 3 3275 8582 • Fax: +81 3 3275 9072
Email: journal@maruzen.co.jp • Web site: http://www.maruzen.co.jp

REPUBLIC OF KOREA
KINS Inc., Information Business Dept. Samho Bldg. 2nd Floor, 275-1 Yang Jae-dong SeoCho-G, Seoul 137-130
Telephone: +02 589 1740 • Fax: +02 589 1746 • Web site: http://www.kins.re.kr

NETHERLANDS
De Lindeboom Internationale Publicaties B.V., M.A. de Ruyterstraat 20A, NL-7482 BZ Haaksbergen
Telephone: +31 (0) 53 5740004 • Fax: +31 (0) 53 5729296
Email: books@delindeboom.com • Web site: http://www.delindeboom.com

Martinus Nijhoff International, Koraalrood 50, P.O. Box 1853, 2700 CZ Zoetermeer
Telephone: +31 793 684 400 • Fax: +31 793 615 698
Email: info@nijhoff.nl • Web site: http://www.nijhoff.nl

Swets and Zeitlinger b.v., P.O. Box 830, 2160 SZ Lisse
Telephone: +31 252 435 111 • Fax: +31 252 415 888
Email: infoho@swets.nl • Web site: http://www.swets.nl

NEW ZEALAND
DA Information Services, 648 Whitehorse Road, MITCHAM 3132, Australia
Telephone: +61 3 9210 7777 • Fax: +61 3 9210 7788
Email: service@dadirect.com.au • Web site: http://www.dadirect.com.au

SLOVENIA
Cankarjeva Zalozba d.d., Kopitarjeva 2, SI-1512 Ljubljana
Telephone: +386 1 432 31 44 • Fax: +386 1 230 14 35
Email: import.books@cankarjeva-z.si • Web site: http://www.cankarjeva-z.si/uvoz

SPAIN
Díaz de Santos, S.A., c/ Juan Bravo, 3A, E-28006 Madrid
Telephone: +34 91 781 94 80 • Fax: +34 91 575 55 63
Email: compras@diazdesantos.es, carmela@diazdesantos.es, barcelona@diazdesantos.es, julio@diazdesantos.es
Web site: http://www.diazdesantos.es

UNITED KINGDOM
The Stationery Office Ltd, International Sales Agency, PO Box 29, Norwich, NR3 1 GN
Telephone (orders): +44 870 600 5552 • (enquiries): +44 207 873 8372 • Fax: +44 207 873 8203
Email (orders): book.orders@tso.co.uk • (enquiries): book.enquiries@tso.co.uk • Web site: http://www.tso.co.uk

On-line orders
DELTA Int. Book Wholesalers Ltd., 39 Alexandra Road, Addlestone, Surrey, KT15 2PQ
Email: info@profbooks.com • Web site: http://www.profbooks.com

Books on the Environment
Earthprint Ltd., P.O. Box 119, Stevenage SG1 4TP
Telephone: +44 1438748111 • Fax: +44 1438748844
Email: orders@earthprint.com • Web site: http://www.earthprint.com

UNITED NATIONS
Dept. I004, Room DC2-0853, First Avenue at 46th Street, New York, N.Y. 10017, USA
(UN) Telephone: +800 253-9646 or +212 963-8302 • Fax: +212 963-3489
Email: publications@un.org • Web site: http://www.un.org

UNITED STATES OF AMERICA
Bernan Associates, 4501 Forbes Blvd., Suite 200, Lanham, MD 20706-4346
Telephone: 1-800-865-3457 • Fax: 1-800-865-3450
Email: customercare@bernan.com · Web site: http://www.bernan.com

Renouf Publishing Company Ltd., 812 Proctor Ave., Ogdensburg, NY, 13669
Telephone: +888 551 7470 (toll-free) • Fax: +888 568 8546 (toll-free)
Email: order.dept@renoufbooks.com • Web site: http://www.renoufbooks.com

Orders and requests for information may also be addressed directly to:

Marketing and Sales Unit, International Atomic Energy Agency
Vienna International Centre, PO Box 100, 1400 Vienna, Austria
Telephone: +43 1 2600 22529 (or 22530) • Fax: +43 1 2600 29302
Email: sales.publications@iaea.org • Web site: http://www.iaea.org/books